A Probabilistic Safety Analysis on Fuel Subassembly Events of Monju

K. Haga[a], K. Koyama[b], H. Endo[a]

[a] Japan Nuclear Energy Safety Organization, 4-1-28 Toranomon, Minato-ku, Tokyo, 105-0001, Japan

[b] Mitsubishi FBR Systems, INC., 2-34-17, Jingumae, Shibuya-ku, Tokyo, 150-0001, Japan

Presented by T. Okawa

Abstract. Fast Breeder Reactor (FBR)'s fuel subassembly is characterized by a narrow pin gap and a high power density. Due to these characteristics, Japan Nuclear Energy Safety Organization performed Probabilistic Safety Analysis of Monju on fuel subassembly events as well as the whole-core initiating events such as anticipated transient without scram to check the safety of the reactor. Causes of the fuel subassembly events are the stochastic fuel pin failure and the local blockage by foreign materials. Here, at first the probability of a stochastic fuel pin failure was investigated from the operational experiences of world's FBRs and a fuel pin failure probability was obtained (1.2×10^{-4}). Then, Event tree (A) for a fuel pin failure to a molten pool formation in a fuel subassembly, and Event tree (B) for the failure propagation from the molten pool to outer fuel subassemblies were drawn. The responses of four-kinds of anomaly detection systems were considered. The obtained frequency of the molten pool formation in a fuel subassembly was 1.7×10^{-5}/ry and that of the failure propagation to 37 fuel subassemblies was 1.1×10^{-7}/ry. The frequency of subassembly to subassembly propagation was similar to the analysis of SNR-300. The subassembly failure frequency due to a pin failure was three orders larger than those from blockages by foreign materials.

1. Introduction

One of the characteristics of Fast Breeder Reactor (FBR)'s subassembly is a narrow pin gap and a high power density. Due to the characteristics, for the evaluation of safety of FBR, Probabilistic Safety Analysis (PSA) of fuel subassembly events will be unavoidable as well as those caused by any plant malfunction. Hence, Japan Nuclear Energy Safety Organization (JNES) performed PSA of Monju on fuel subassembly events besides on the whole-core initiating events such as Anticipated Transient Without Scram (ATWS). The causes of subassembly events are the stochastic fuel pin failure and the local blockage by foreign materials.

In this work, as the first step, the probability of stochastic fuel pin failure was obtained from operational experiences of world's FBRs. Then, an event tree from one pin failure to molten fuel pool formation in a fuel subassembly was drawn taking consideration of the responses of anomaly detection systems. Lastly, another event tree from the molten fuel pool formation to failure of 37 fuel subassemblies was derived to get the frequency of the whole code damage due to one pin failure.

2. PSA for the initiating event of stochastic fuel pin failure

2.1 Evaluation of frequency of the initiating event

In the beginning of this PSA work, the probability of stochastic fuel pin failure was evaluated from experiences of FBR operation in the world. Table 1 was reffered from a presentation by Japan Atomic Energy Agency[1] . Although the table does not cover all FBRs in the world, we used the data as an available one at present.

Table 1 shows that the total irradiated fuel pin was about 526,000 and the total fuel subassembly included the failed pins was 63. Because the number of failed pins in each subassembly is unknown, we assumed that 1.5 pins failed in each subassembly. Then, the fuel pin failure ratio is calculated as 1.8×10^{-4} (=1.5×63/526000). It was further assumed that all fuels were loaded in these reactors for 3 years. Thus, the fuel failure rate per reactor year (ry) is estimated to be 0.6×10^{-4} /ry/pin.

The reactor core of Monju consists of 198 fuel subassemblies and each fuel subassembly contains 169 pins. Hence, the stochastic fuel pin failure frequency of Monju results in 2.0 pins/ry (=0.6 $\times 10^{-4} \times 198 \times 169$).

2.2 Progress of the subassembly event and the responces of anomaly detection systems

Figure 1 shows the sensors used for the anomaly deteciton systems in Monju. There are three types of sensors. The first is the thermocouple at each fuel subassembly outlet. They observe the temperature rise due to flow blockage. For example, the subassembly flow rate reduction of about 4% corresponds to the outlet temperature rise of about 5 K, that is large enough to recognize the anomaly. The second is the cover gas monitor system that detects beta- and gamma-rays emitted from the gaseous and volatile fission products (FPs). The third is the delayed neutron (DN) detection system and the reactor is automatically scrammed once two sensors detected (2 out of 3). The DN system is installed in each primary coolant loop of 3. Besides these sensors, the reactor power meter (nuclear instrumentation system) which sensors are installed outside of the reactor vessel will supply some meaningful information at the stage of partial core melting.

Figure 2 shows an event sequence initiated by a stochastic pin failure [2] and responses of the anomaly detection systems. When a fuel pin failure occurs, FP gases and volatile FPs will be released into sodium and some parts of FPs will be transferred to the cover gas. Because the cover gas monitor system is designed to detect even one pin failure, we noted as the Detection step **1** to this detection stage. At the breached location of the failed pin, the fuel pellets contact with coolant and delayed neutron precursors, even fuel meat, may be released into coolant. This situation brings a chance that DN sensors detect the anomaly (Detection step **2**-1). The fuel/coolant contact will produce chemical reaction products called as sodium-uranate and the fuel pin will swell radially. These reaction products and the released fuel meat would form local blockages. Corresponding to the increase in the blocked flow area, the flow rate into the fuel subassembly is decreased and the temperature rise will be detected by the fuel subassembly outlet thermocouple (Detection step **2**-2). If the local temperature just behind the blockage eventually increases as to sodium boiling occurrences and the heat from the fuel is not fully removed by the coolant boiling, the clad and fuel themselves will melt. The tremendus increase in the realeased DN amount will make easier the fuel failure detection (Detection step **3**). Once the released meat adheres at the downstream in the pin bundle, the radial enlargement of the blockage will result in formation

of a molten fuel pool, and the anomaly would be detected even by the reactor power monitor (Detection step **4**).

2.3 Event tree of stochastic pin failure to subassembly failure

Figure 3 shows a derived event tree of subassembly event initiating from stochastic pin failure of Monju. Here, we define the word of "subassembly failure" to the situation that a molten fuel pool is formed in a fuel subassembly. The probability of each branching point was assigned by our technical judgement based on the probability ranking table shown in Table 2. Because in the case of pin failure, even if the defect is miner, there are chances that the pin failure is found anytime as shown in Fig.2. Thus, in the event tree, the probability of the detection and the following reactor trip was examined in every progress step. To assign the probability to each heading titled "Detection & reactor trip," an additional event tree to each heading was drawn (Fig.4-Fig.8). In the initial stage of the event progression, because the flow disturbance causing the temperature rise at the subassembly outlet and the DN release rate will be very small, the failure will be mainly detected only by the cover gas monitor system. There is no chance that the anomaly will effect the reactor power. The heading "Detection & reactor trip (1)" in Fig. 4 corresponds to such circumstances. It is considered that several days are needed for the probability of the heading to become near one. When the pin failure breach is enlarged, the amount of DN released will be increased.

The next step of the fault tree questions if the DN detection records exceeded the auto-scram level. Even in the case of low DN detection level, as the time passes on, the DN level may increase to the scram level and this situation is judged by the "Detection & reactor trip (2)." It is considered that a time period from some 10 minuts to some hours is needed for the probability to become near one. Figure 5 is an event tree for the heading when the ND record is less than the scram level, even if the fuel contacted with coolant. On the other hand, Figure 6 corresponds to the situation that the DN level exceeded the auto-scram level.

Then, the event tree of Fig. 3 continues to question if the molten fuel is released into the coolant, and if secondary blockages are formed by the fuel meat. Two pathes end in a molten fuel pool formation in the fuel subassembly. The process of these events is checked by the "Detection & reactor trip (3)" and the "Detection & reactor trip (4)." Figure 7 and Fig. 8 represent the event trees to them, respectively. It is considered that some minutes are needed for the probability to become near one to the former case and about 10 seconds to the latter case.

In Fig. 3, Fig.4 and Fig. 5, there are figures written in red. These figures correspond to the situation that the reactor is scrammed as soon as a fuel failure is detected. On the other hand, the figures written in black correspond to the situation that the "Run Beyond Clad Breach (RBCB)" is assumed. Figure 3 indicates that the derived probability of molten fuel pool formation from stochasitic one fuel pin failure is 8.47×10^{-6} ($=7.70\times10^{-6}+7.7\times10^{-7}$) to the RBCB case. When RBCB is not allowed, the probability decreases by one order as to 6.96×10^{-7} ($=6.55\times10^{-7}+4.1\times10^{-8}$).

2.4 Event tree for the whole core accident

Different from anomal plant events that directly lead to a whole core failure, in cases of subassembly events, there exists a process that one subassembly failure propagates to surrounding subassemblies and eventually to the whole core. Because of this process, to the subassembly event we considered that some definition is needed to represent the failure state corresponding to a whole core failure. Figure 9 shows an event tree of subassembly-to-subassembly failure propagation. The figure indicates that one subassembly failure propagates to the surrounding 6 subassemblies, then to the outer 12 subassemblies, and so on.

Because the progress time of subassembly-to-subassembly failure propagation would be short, such as 10 seconds, the manual operation by the outlet temperature monitor and the cover gas monitor becomes effective. If the function of the cover gas monitors was normal, the steep increase in the radioactivity caused by a large-scale fuel failure will surely monitored, however, due to the long time delay of the information transmission will be not in time to relieve the situation at this stage. Hence, the success probability of manual reactor scram was assumed only to following two cases; (1) alarm by the outlet temperature rise of the failed fuel subassembly, and (2) steep rise of the cover gas radioactivity.

Figures 10, 11, 12, 13 indicate the local event trees to the "Detection & reactor trip" (5)-1: following an large amount of molten fuel and clad release from the failed subassembly, the "Detection & reactor trip" (5)-2: following a small amount of molten fuel and clad release from the failed subassembly, the "Detection & reactor trip"(6), the "Detection & reactor trip"(7), respectively.

Figure 14 shows the probability that the subassembly-to-subassembly failure propagation ends during the process. For example, when a molten pool was formed in 37 fuel subassemblies, the failure would propagate to outer subassemblies with a probability of 6.7×10^{-3}. From the figure we see the ratio of (subassembly numbers outside of the failed subassemblies) / (failed subassembly numbers). The ratio decreases as the numbers of failed subassembly increases. When 37 subassemblies failed, the ratio become far less than one. In that situation, the failure propagation would be hard to terminate before reaching to almost all area of the core. Thus, the failure frequency of the whole core due to a stochastic pin failure would be close to 1.13×10^{-7} $(=2.0 \times 8.47 \times 10^{-6} \times 6.7 \times 10^{-3})$ /ry.

From the point of safety standard, the INSAG report [3] requires that the frequency of severe accident is less than 10^{-5}/ry to a new nuclear power plant. Above mentioned values are far less than the standard.

3. Disccusions

3.1 Comparison with probability of other causes on fuel subassembly events

There are other initiators of fuel subassembly events. Foreign materials, such as remained matters after the plant construction, loose parts, sodium oxide, oil or seal materials, have potentials to cause local blockage in fuel subassemblies. Previously we investigated the probability of a molten pool formation by these materials in Monju. The estimated value was 4.6×10^{-8}/ry [4]. The corresponding value to a stochastic fuel pin failure is 1.69×10^{-5} $(=2.0 \times 8.47 \times 10^{-6})$ /ry. Because it is three orders larger than that caused by blockage of foreign materials, it can be said that the investigation on only stochastic pin failure would be sufficient for the argument of subassembly events on reactor safety.

3.2 Comparison with PSAs to other plants

Some PSA activities on subassembly events of FBR have been reported. Schleisiek made PSA for SNR-300 on one fuel pin failure[5]. As the results, he estimated (1) 3×10^{-8} to the prompt or mechanical damege of 19 fuel subassemblies and (2) 7×10^{-8} to the thermal failure propagation to 19 fuel subassemblies assuming DN detector failure[4]. The total failure probalility of 19 fuel subassemblies is 1.0×10^{-7}/pin failure. The corresponding probalility obtained in our analsis is $2.0 \times 10^{-7} (= 8.47 \times 10^{-6} \times 0.024)$/ pin failure. Considering the uncertainty of PSA, both values would be substantially same.

Vaughan made PSA for CDFR, that was designed in UK, to all potential initiators of fuel subassembly events and evaluated the probability of melting of "substantial part" of a fuel subassembly [6]. The largest value was 1.92×10^{-6}/ry and it was caused by a random fuel pin failure. The failed fuel subassembly situation would be identical with that we call "molten pool formation in a fuel subassembly." The corresponding value in our study is 1.69×10^{-5} （ $= 2.0 \times 8.47 \times 10^{-6}$） /ry and this value is one order larger than his evaluation. However, in his paper enough information, such as probabilities of branching points in the event tree, is not given to find the reasons of this differeance. Konomura performed PSA for the subassembly event of Monju. Although the detailed data is not shown, it is concluded that "the frequency of failure propagation outside of the failed subassembly from one fuel pin failure is quite small, such as less than 10^{-7}/ry " [7]. The corresponding situation in our study will be the failure upto the outer 6 fuel subasssemblies. The frequency is 2.9×10^{-6} $(= 8.47 \times 10^{-6} \times 0.347)$/ry and it is again one order larger than his estimation. The reason of their one order smaller probability than us might come from that in their analysis they did not allow RBCB.

4. Conclusions

PSA for fuel sabassembly events of Monju has been performed. As the initiator, a stochastic fuel pin faliure was mainly discussed. At first, the experiences of stochastic fuel pin faliure of FBRs in the world were surveyed and the evaluated probability of pin failure was 1.8×10^{-4}. From the data, the fuel pin failure rate of Monju was estimated to be 2.0 pin/ry. From event tree analyses, the probability that one fuel pin failure proceeds to a molten fuel pool formation in the fuel subassembly was estimated to be 8.47×10^{-6}. Hence, the frequency of one fuel pin failure to reach a molten fuel pool formation in the fuel subassembly becomes 1.7×10^{-5}/ry. If the reactor was shutdown at the moment of the first detection, the situation that is called "without RBCB" in this study, the probability that one pin faiure causes the fuel subassembly failure will decrease by one order (6.96×10^{-7}).

The probability of proceeding from the molten pool formation in a fuel subassembly to 19 fuel subassemblies failure was estimated 0.024, and the probability to 37 fuel subassemblies failure was 6.7×10^{-3}. As the result, the frequency that one stochastic fuel pin failure causes 37 fuel subassemblies failure was estimated to be 1.1×10^{-7}/ry.

Whereas the calculated values in this study are substantially same as those derived to SNR-300 , one order larger than those obtained to CDFR.

Because the probalilities of other causes of fuel subassembly events, such as blockage by foreign materials, to bring a fuel fuel subassembly failure were three orders smaller than that by stochastic fuel pin failure, the obtained value to the stochastic fuel pin failure is enough

for considering the effect of the subassembly events to the reactor safety and the evaluated value in this study is two orders smaller than the standard of INSAG.

REFERENCES

[1] *"Failed fuel pin data of FBRs in the World" 4th Monju Safety Confirmation Commity Meeting, Paper 4-3 presented by JNC, Tokyo, March 2006.*

[2] *K. Haga, K. Yamaguchi, F. Namekawa, "Review and Future Needs of Experimental Studies on Local Faults," Int. Topical Mtg. on Science and Technology of Fast reactor Safety, Guernsey, pp. 513-518, May 1986.*

[3] *"Basic Safety Principles for Nuclear Plants," INSAG, March 1988.*

[4] *K. Haga, H. Endo, K.. Koyama, "PSA of FBR Fuel Subassembly Events(2) – Blockage with Foreign Materials," Atomic Energy Society of Japan 2010 Spring Mtg., Mito, F19, March 2010. (in Japanese)*

[5] *K. Schleisiek, "Risk Oriented Analysis of Subassembly Accident, Int. Topical Mtg. on Fast Reactor Safety, Knoxville, Vol. I, pp. 144-150, April 1985.*

[6] *G.J. Vaughan, "Event Tree Analysis of the Sub-assembly Accident, Int. Mtg. on Science and Techinology of Fast Reactor Safety," pp. 457-463, Guernsey, May 1985.*

[7] *M. Konomura, "Evaluation of Event Progress of FBR local Faults Appling the Probabilistic Analysis," Atomic Energy Society of Japan 1992 Spring Mtg., Hiratsuka, p. 547, March 1992. (in Japanese)*

Table 1   Stochastic fuel pin faiure data of FBRs in the world [1]

Reactor	Numbers of fuel subassembles including failed pins	Numbers of total irradiated pins	Irradiated period
FFTF	12	about 64,000	1980－1992
Phenix	29	about 179,000	1973－1993
Super Phenix	0	about 121,000	1985－1999
PFR	22	about 98,000	1974－1994
Joyo	0	about 64,000	1978－2005

Table 2 Probability ranking table

| Probability Rankings	Qualitative Expressions	Set Probabilities	Categories
1	Indeterminate	0.5	The probabilities of the occurrence and non-occurrence of the event are rated at much the same levels.
2	Unlikely	0.1	The occurrence of the event is technically rated as unlikely.
2	Likely	0.9	The occurrence of the event is technically rated as likely.
3	Highly unlikely	0.01	Occurrence is technically rated as highly unlikely.
3	Highly likely	0.99	Occurrence is technically rated as highly likely.
4	Extremely unlikely	<0.01	The occurrence of the event is technically rated as extremely unlikely. This branch is established because of its importance.
4	Extremely likely	>0.99	The occurrence of the event is technically rated as very likely.
5	Impossible	ε	The occurrence of the event is rated as impossible.
5	Certain	1-ε	The occurrence of the event is rated as certain or deemed certain.
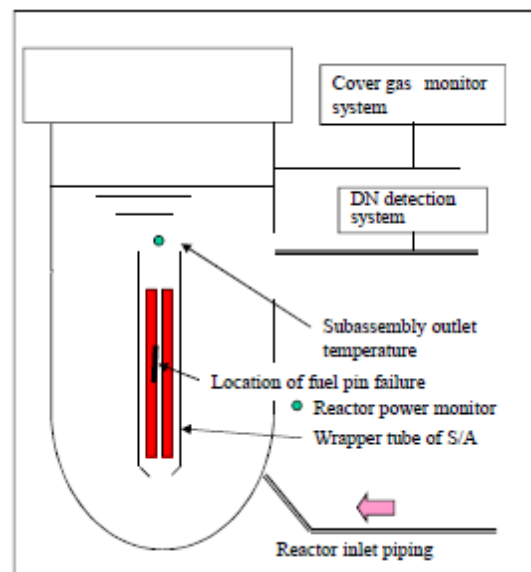
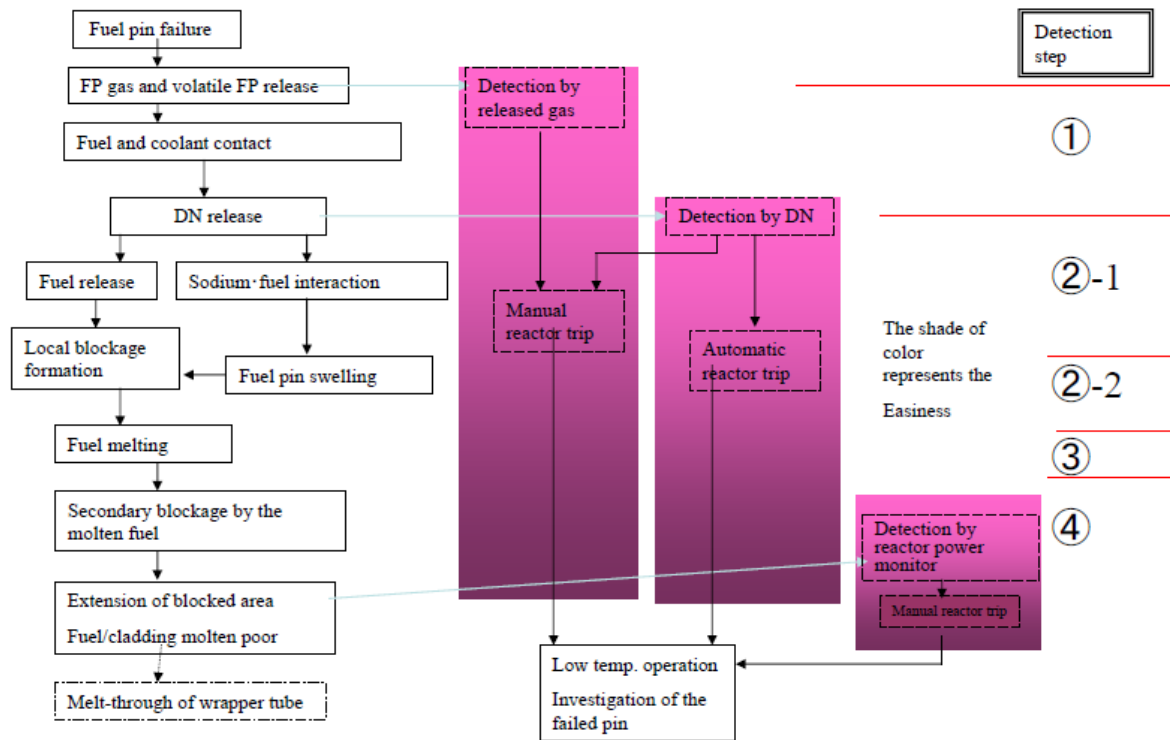Fig.1 Anomally detection systems of Monju

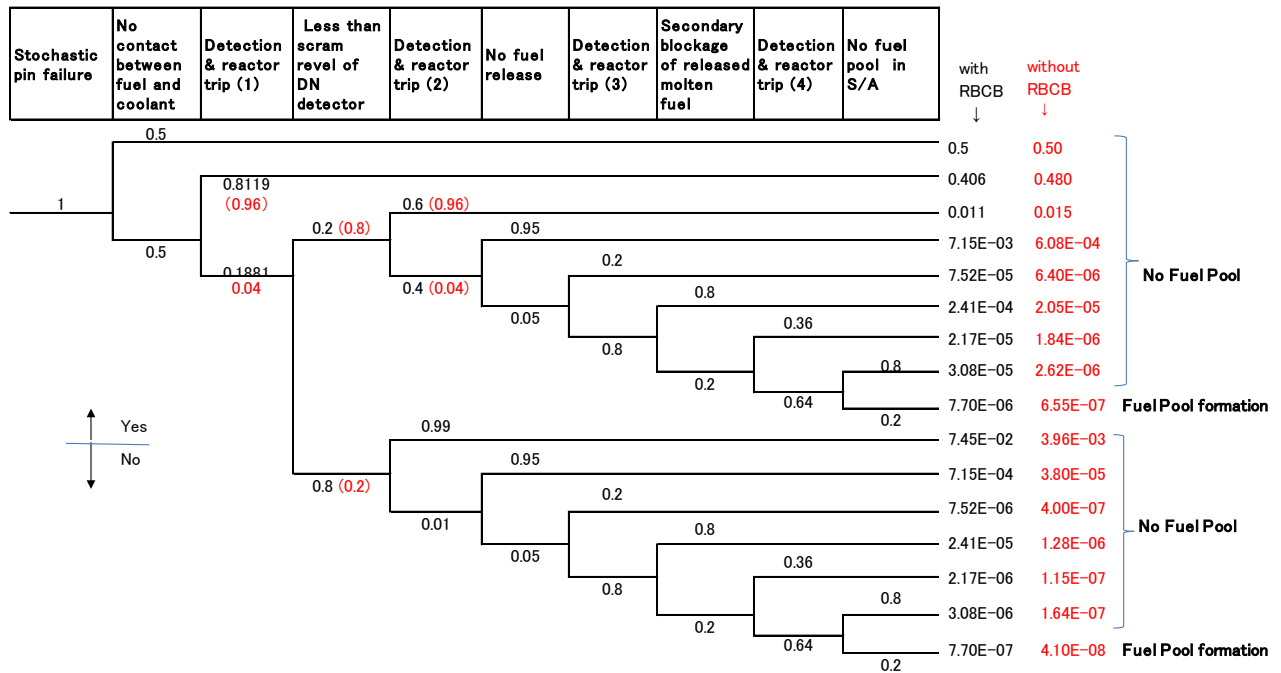Fig.2 Event scenario and corresponding anomally systems

Fig. 3 Event tree of stochastic fuel pin failure to molten pool formation in a fuel
subassembly (The effect of RBCB, run beyond clad breach, is compared)
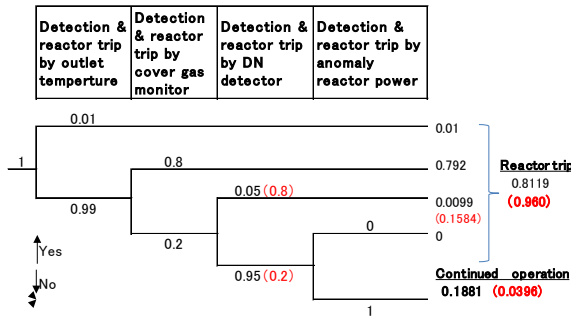
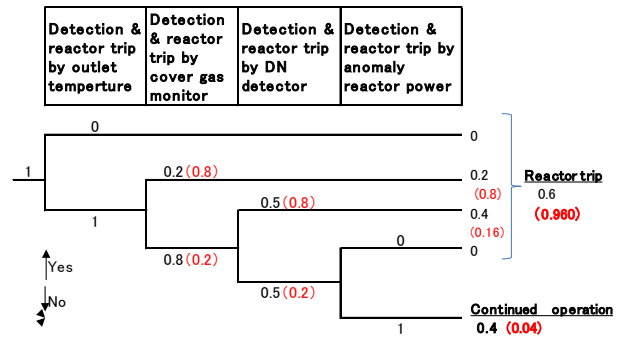Fig. 4 Event tree for the heading "Detection and reactor trip (1)" －before DN signal is observed

Fig. 5 Event tree for the heading "Detection and reactor trip (2)-1" －after DN signal is observed under the scram level
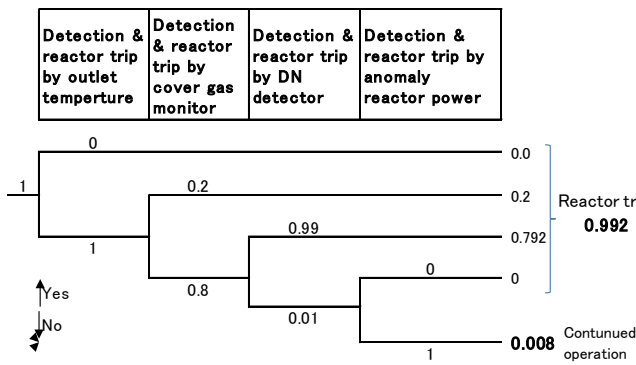

Fig. 6 Event tree for the heading "Detection and reactor trip (2)-2" － after DN signal is observed over the scram level
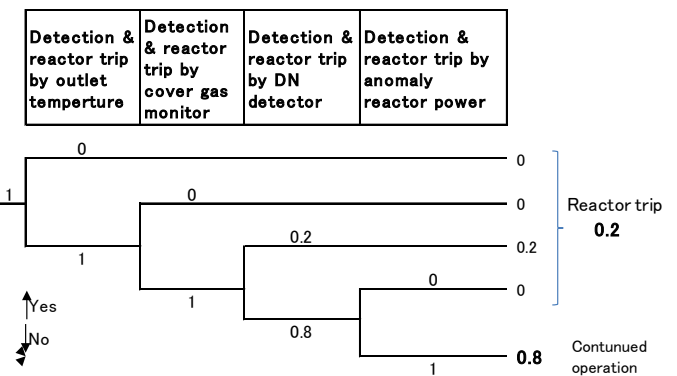

Fig. 7 Event tree for the heading "Detection and reactor trip (3)" － before secondary blockage formation
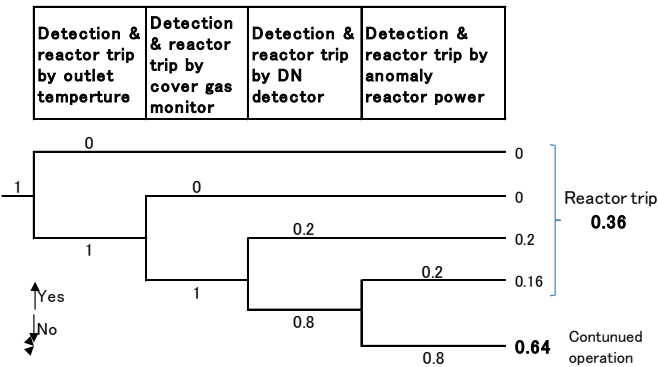

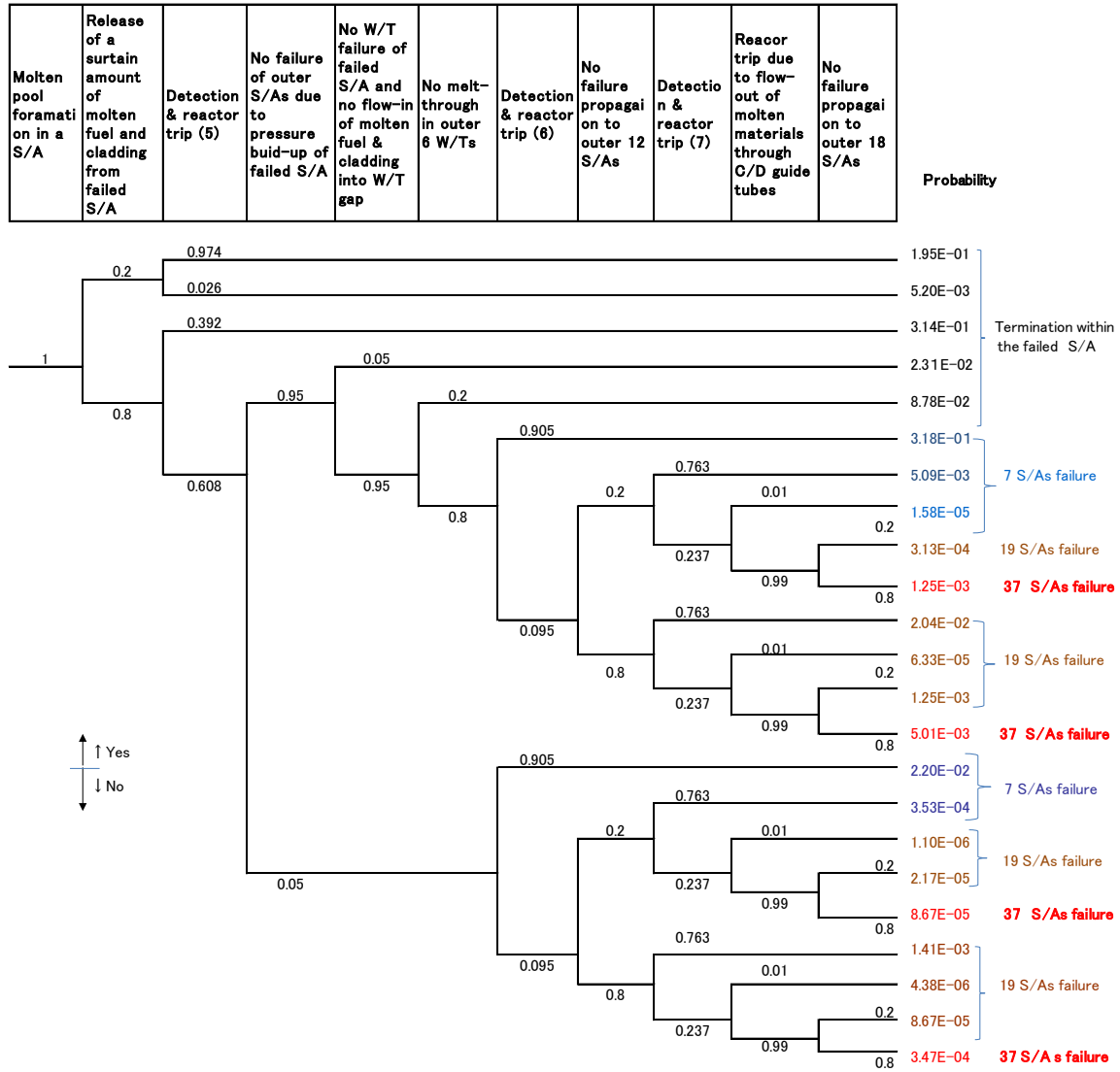Fig.8 Event tree for the heading "Detection and reactor trip (4)" －after secondary blockage formation

Molten pool foramation in a S/A	Release of a surtain amount of molten fuel and cladding from failed S/A	Detection & reactor trip (5)	No failure of outer S/As due to pressure buid-up of failed S/A	No W/T failure of failed S/A and no flow-in of molten fuel & cladding into W/T gap	No melt-through in outer 6 W/Ts	Detection & reactor trip (6)	No failure propagaion to outer 12 S/As	Detection & reactor trip (7)	Reacor trip due to flow-out of molten materials through C/D guide tubes	No failure propagaion to outer 18 S/As	Probability

Fig. 9 Event tree from molten pool formation to 37 fuel subassembly failure

Detection & reactor trip by outlet temperture	Detection & reactor trip by cover gas monitor	Detection & reactor trip by DN detector	Detection & reactor trip by anomaly reactor power

Fig. 10 Event tree for the heading "Detection & reactor trip (5)-1" in Fig.9

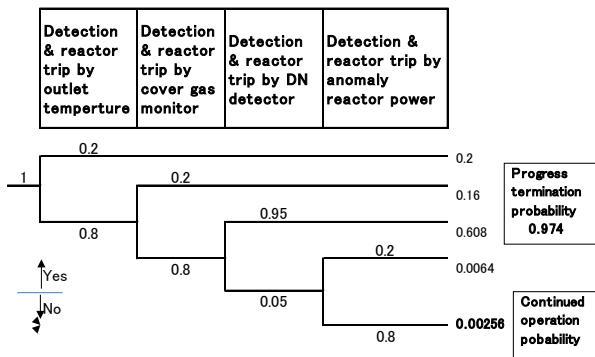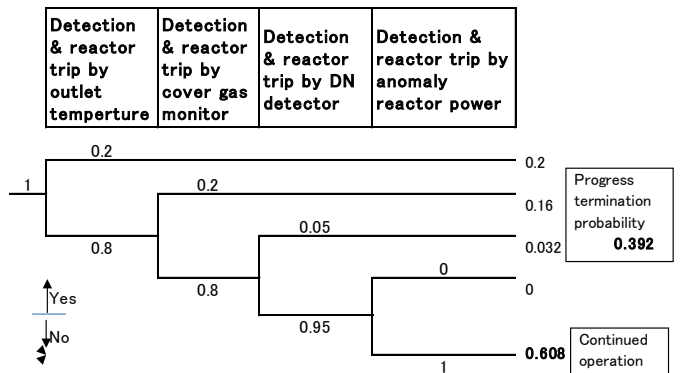| Detection & reactor trip by outlet temperture	Detection & reactor trip by cover gas monitor	Detection & reactor trip by DN detector	Detection & reactor trip by anomaly reactor power

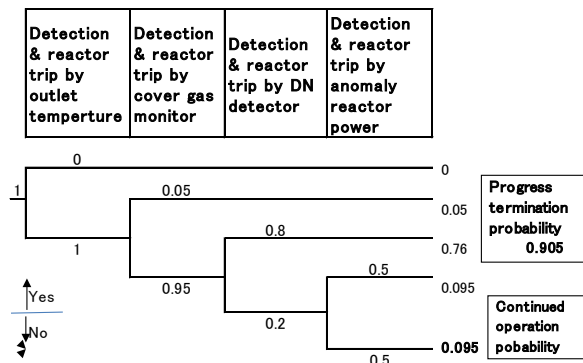Fig. 11 Event tree for the heading "Detection & reactor trip (5)-2" in Fig.9

9

Fig. 12   Event tree for the heading
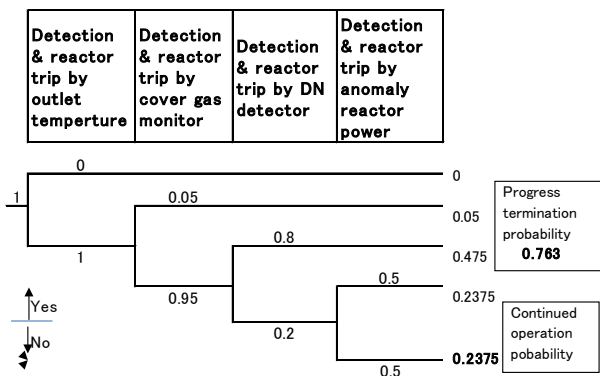"Detection & reactor trip (6)"
in Fig.9

Fig. 13 Event tree for the heading "Detection
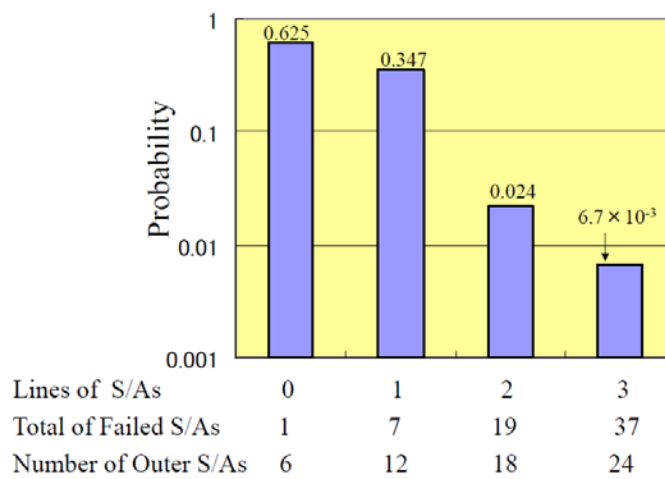& reactor trip (7)" in Fig.9

Fig. 14   Probability of S/A (subassembly) to
S/A failure propagation

High Temperature Thermochemistry of (U-Pu)O$_2$ MOX Fuel with B$_4$C absorber
Application to severe accidents in SFR

S. Gossé[a], **T. Alpettaz**[a], **C. Guéneau**[a], **P. Allegri**[b]

[a] CEA, DEN – Centre de Saclay, 91191 Gif-sur-Yvette, France

[b] CEA, DEN – Centre de Marcoule, 30207 Bagnols-sur-Cèze, France

Abstract. The fuel pins of the ASTRID Sodium cooled Fast Reactor prototype will be made of (U,Pu)O$_{2\pm x}$ mixed oxide (MOX) fuel pellets with a stainless steel cladding. In case of a core melting accident, MOX fuel and boron carbide (B$_4$C) from the absorber materials of the control rods and from the upper neutron shields shall react at high temperature. To study this interaction, an experimental program was carried-out using high temperature mass spectrometry. The measured partial pressure of the gaseous species released during the (UO$_{2\pm x}$ + B$_4$C) chemical interaction was compared with thermochemical calculations using the FUELBASE thermodynamic database. Post-test characterization of the sample have been performed by XRD, SEM and microprobe analyse. The impact of these results on the accidental behaviour of a MOX core will be discussed.

Introduction.

In the framework of the development of the Sodium cooled Fast Reactor (SFR), a safety study is being carried out to understand the consequences of a hypothetical core meltdown accident. The reference fuel materials for this reactor are (U,Pu)O$_2$ for the fissile pellets, stainless steel for the cladding and the vessel. In case of a core meltdown accident, a complex multiconstituent system (partially or fully melted) shall form. This so-called "corium" is mainly made of molten oxide fuel and liquid stainless steel coming from the structural materials and from the cladding.

In order to decrease the risk of recriticality of the corium, B$_4$C absorber is planned to be directly introduced in the core as complementary shutdown system. In case of temperature increase, B$_4$C shall strongly interact (if possible within the same phase) with the fissile atoms as a fusible neutron absorber [1]. Therefore, the interaction at high temperature between (U,Pu)O$_2$ and B$_4$C is a key issue to adress to predict the efficiency of this passive mitigation system.

This study focuses on the (UO$_{2\pm x}$-B$_4$C) chemical interaction at high temperature as well as thermodynamic properties on this complex system. Even if this sub-system enters the composition of the corium, it had been hardly ever studied [2].

Experimental Study by High Temperature Mass Spectrometry.

The High Temperature Mass Spectrometry (HTMS) method, often coupled with Knudsen effusion cells (KEMS), is a well established technique to measure partial pressures above samples heated at high temperature. When gaseous species are formed, Knudsen cells can also be used to investigate kinetics of chemical reactions that involve a gas release.

In this method, samples are placed in a Knudsen cell where the condensed phases are in equilibrium with the gaseous phase. In the lid of the Knudsen cell, a drilled hole with small dimensions with respect to the surface of the sample permits to sample a very small amount of the vapours released from the cell.

In this molecular beam, the mean free path of the molecules satisifies the conditions of a molecular beam *i.e.* without any collisions between the gaseous molecules during their sampling. This rarefied gas flow passes through a diaphragm directly in the ionization chamber of a mass spectrometer maintained under high vacuum. Then, the gaseous species are ionized by an electron beam. These ions are then extracted from the ionization chamber, accelerated by an electric field, and finally separated according to their mass/charge ratio by a high frequency electric field. More specific characteristics of this method were already described elsewhere [3] [4].

In case of the ($UO_2 + B_4C$) interaction, the composition of the equilibrium gaseous phase can be calculated using the FUELBASE thermodynamic database [5] [6] in which the thermodynamic modellings of the B-O [7], B-U [8] and B-C [9] systems were added to the database on U-Pu-O system (FIG. 1).

For an equimolar mixture (50% mol. of $UO_{2.02} + 50\%$ mol. B_4C) and in the 1250 K – 2500 K temperature range, the vapours are mainly made of CO(g) which pressure is about two order of magnitude higher than the other species $B_2O_{2(g)}$, $B_2O_{3(g)}$, $BO_{(g)}$, $CO_{2(g)}$ by descending order. Then, lower pressures of uranium species $UO_{2(g)}$, $UO_{(g)}$, $UO_{3(g)}$ and $U_{(g)}$ shall with values under 10^{-6} Bar at 2000 K. These pressures are too low to be measured by HTMS.

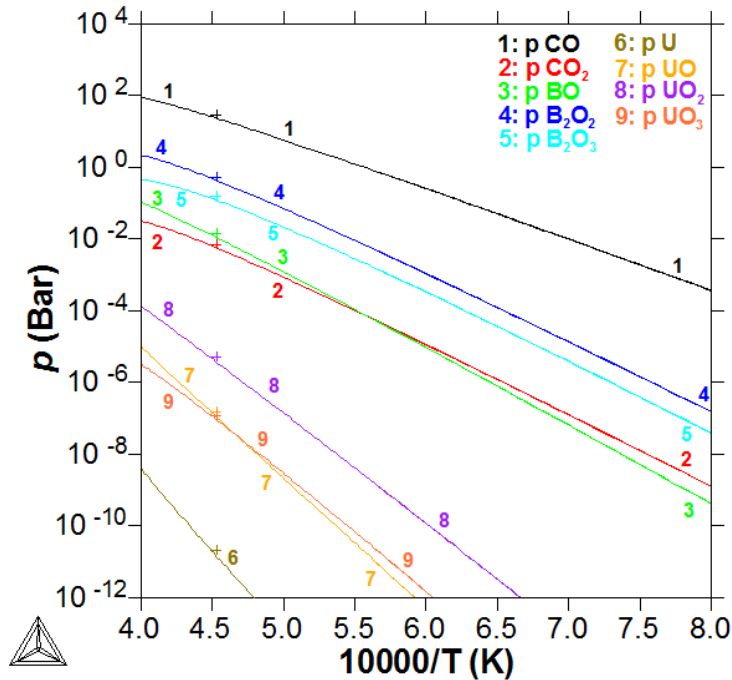*FIG. 1. Partial equilibrium pressures calculated for an equimolar $UO_{2.02} + B_4C$ mixture as a function of the inverse of temperature in K*

The gaseous flow of this complex gaseous mixture made of boron and carbon oxides can be measured from the ionic intensities of the ionized molecules. These measurements versus time lead to the kinetics of formation of the gaseous phase. Subsequently the evolution of the condensed phase composition is known versus time. From the total mass loss, the final overall composition of the sample at the end of the experiment can be determined in the B-C-O-U system and compared to the composition of the condensed phases measured using post-mortem analyses performed bySEM/EDS and XRD on mounted and polished cross sections.

The Use of Knudsen Cells in Mass Spectrometric Methods

Considering the high pressure of BO(g) compared to that of B_2O_2(g) during the experiment, in contradiction with the thermodynamic calculations, a possible fragmentation of the molecule (e.g. $B_2O_{2(g)} \rightarrow 2 BO_{(g)}$) is assumed in the ionization chamber of the mass spectrometer. This fragmentation phenomenom will not affect the calculation of the gaseous species flow. The total mass loss (Δm_{tot}) of

the sample which is directly correlated to the gas release of $CO_{(g)}$, $CO_{2(g)}$ and $B_2O_{2(g)}$, $B_2O_{3(g)}$, $BO_{(g)}$ is used to calibrate the mass spectrometer.

In equation (1), the Beer-Lambert law is applied to the absorption of the electrons in a diluted medium. This law leads to the basic mass spectrometric relation between the vapour pressures and the measured ionic intensities as a function of temperature [3]:

$$p_i S_i = I_i T \tag{1}$$

The flow of gaseous molecules, in moles per unit of time, is obtained by the Hertz-Knudsen relation [4]. Under isotropy condition, this gaseous flow released by the surface (S) of a sample is equal to the rarefied gas effusion flow through a hole with a smaller surface (s) with ($S/s \geq 100$). If the thickness of the lid is not ideally thin, a Clausing coefficient (C) is considered for the transmission of the aperture. The obtained relation (2) is effective as long as the mean free path of the molecules in the gas is longer than the dimensions of the lid orifice [3]:

$$\frac{dn_i}{dt} = \frac{p_i s C}{\sqrt{2\pi M_i R T}} \tag{2}$$

For each (i) gaseous species, it is possible to calculate the molecular flow by combining the mass spectrometric and the Knudsen-Hertz equations (1 & 2):

$$\frac{dn_i}{dt} = \frac{s C I_i \sqrt{T}}{S_i \sqrt{2\pi M_i R}} \tag{3}$$

For a given geometry and single vapour specie, all the fixed parameters can be considered as a single constant βi, specific to the specie and to the device (4).

$$\beta_i = \frac{s \cdot C}{S_i \sqrt{2\pi M_i R}} \tag{4}$$

In equation (3), the molecular flow of a gaseous species is proportional to the measured ionic intensities and the temperature squared root product. The time integral of this relation represents the amount of evaporated moles and so the mass loss of the sample due to the formation of the (i) specie. Then, the total amount of released gas (in moles) is determined by integration of the molecular flow with time.

$$n_i(t) = \beta_i \int_0^t I_i \sqrt{T} \, dt \tag{5}$$

Each value of βi can be determined from the total mass loss of the identified gaseous molecules using equation (6) and equation (7).

$$\Delta m_{tot} = \Delta m_{CO_{(g)}} + \Delta m_{CO_{2(g)}} + \Delta m_{BO_{(g)}} + \Delta m_{B_2O_{2(g)}} + \Delta m_{B_2O_{3(g)}} \tag{6}$$

With:

$$\beta_i = \frac{\Delta m_i}{M_i \int_0^{tf} I_i \sqrt{T} \, dt} \tag{7}$$

When several gaseous species enter the vapour composition, each sensitivity (S_i) is obtained by an appropriate calibration of the mass spectrometer. The mass spectrometer response is corrected by taking into account several parameters (8):

$$S_i = I_{e^-} \cdot G \cdot \eta_i \cdot \sigma_i \cdot \gamma_i \cdot f_i \tag{8}$$

I_{e^-} is the electron beam intensity, G is a geometric factor; both are independent of the ionized specie. Then, η_i is the mass spectrometer transmission, σ_i is the ionization cross section of the ionized molecule, f_i is the isotopic abundance ratio and γ_i is the detector yield. In the case of the $(UO_{2\pm x} + B_4C)$ system, the considered parameters are the ionization cross sections (σ_i) and an isotopic abundance (f_i) equal to 0.8 due to the ^{10}B and ^{11}B isotope relative amounts for the boron oxides.

For a 15 eV energy for the electrons, the ionization cross sections of the gaseous species come from the recommanded data by Drowart et al. [4]. The values for $CO_{(g)}$, $CO_{2(g)}$ and $BO_{(g)}$, $B_2O_{2(g)}$, $B_2O_{3(g)}$ are respectively equal to 0.669, 0.75 and 1.412, 2.824, 2.905. Using the previous corrections, the molecular flow (9) and the mass flow (10) can be defined by the following relations:

Molecular flow:

$$\Delta n_{tot} = \Delta n_{CO_{(g)}} + \Delta n_{CO_{2(g)}} + \Delta n_{BO_{(g)}} + \Delta n_{B_2O_{2(g)}} + \Delta n_{B_2O_{3(g)}}$$

$$\Delta n_{tot} = \frac{\int_0^t I_{CO} \sqrt{T} dt}{\sigma_{CO} \cdot f_{CO} \sqrt{M_{CO}}} + \frac{\int_0^t I_{CO_2} \sqrt{T} dt}{\sigma_{CO_2} \cdot f_{CO_2} \sqrt{M_{CO_2}}} + \frac{\int_0^t I_{BO} \sqrt{T} dt}{\sigma_{BO} \cdot f_{BO} \sqrt{M_{BO}}}$$

$$+ \frac{\int_0^t I_{B_2O_2} \sqrt{T} dt}{\sigma_{B_2O_2} \cdot f_{B_2O_2} \sqrt{M_{B_2O_2}}} + \frac{\int_0^t I_{B_2O_3} \sqrt{T} dt}{\sigma_{B_2O_3} \cdot f_{B_2O_3} \sqrt{M_{B_2O_3}}} \tag{9}$$

Mass flow:

$$\Delta m_{tot} = \Delta m_{CO_{(g)}} + \Delta m_{CO_{2(g)}} + \Delta m_{BO_{(g)}} + \Delta m_{B_2O_{2(g)}} + \Delta m_{B_2O_{3(g)}}$$

$$\Delta m_{tot} = \frac{\sqrt{M_{CO}} \int_0^t I_{CO} \sqrt{T} dt}{\sigma_{CO} \cdot f_{CO}} + \frac{\sqrt{M_{CO_2}} \int_0^t I_{CO_2} \sqrt{T} dt}{\sigma_{CO_2} \cdot f_{CO_2}} + \frac{\sqrt{M_{BO}} \int_0^t I_{BO} \sqrt{T} dt}{\sigma_{BO} \cdot f_{BO}}$$

$$+ \frac{\sqrt{M_{B_2O_2}} \int_0^t I_{B_2O_2} \sqrt{T} dt}{\sigma_{B_2O_2} \cdot f_{B_2O_2}} + \frac{\sqrt{M_{B_2O_3}} \int_0^t I_{B_2O_3} \sqrt{T} dt}{\sigma_{B_2O_3} \cdot f_{B_2O_3}} \tag{10}$$

Using these equations (9 & 10), the boron, carbon and oxygen elementary flows (11) are calculated by summing the molecular flows weighted by the stoichiometry of the gaseous molecules (*because no gaseous uranium oxide release was observed during the experiments, the uranium flow was not considered*).

From relations (11), it is possible to calculate both the gas release from the Knudsen cell and the evolution of the the sample versus time during the experiment.

$$n_B(t) = n_{BO}(t) + 2 \cdot n_{B_2O_2}(t) + 2 \cdot n_{B_2O_3}(t)$$

$$n_C(t) = n_{CO}(t) + n_{CO_2}(t) \tag{11}$$

$$n_O(t) = n_{CO}(t) + 2 \cdot n_{CO_2}(t) + n_{BO}(t) + 2 \cdot n_{B_2O_2}(t) + 3 \cdot n_{B_2O_3}(t)$$

Experimental results

The experiment was performed on a equimolar mixture of powders (50% mol. of $UO_{2.02}$ + 50% mol. B_4C) at 2073 K. In an assembly, This composition corresponds to the relative fractions of $UO_{2\pm x}$ and B_4C in a fuel assembly considering the complementary shutdown system. The starting O/U ratio of the

$UO_{2\pm x}$ powder is equal to 2.02. Even if the O/U ratio is slightly higher than in the fresh fuel, this oxide stoichiometry is representative for a very low burn-up fuel. Furthermore, a ppreliminary feasibility test performed with $UO_{2.10}$ hyper stoichiometric oxide showed a huge $CO_{(g)}$ release due to the fast reduction of $UO_{2\pm x}$ by the carbon of B_4C.

The samples were prepared in a glovebox from a mixture of $UO_{2.02}$ and B_4C powders. The total weight of the sample is about 1.5 g set in a tungsten crucible with a 13 mm inner diameter. The diameter of the lid aperture is 1.5 mm. The temperature ramp prior to the plateau approximately lasts after 100 minutes, then the duration of the stationnary at 2073 K plateau is about 300 minutes.

According to the $(I_i T)$ measurements for the gaseous species in FIG. 2 , a strong gas release was observed during heating. For all gas species, a peak begins to form when the temperature reaches 1273 K (FIG. 2).
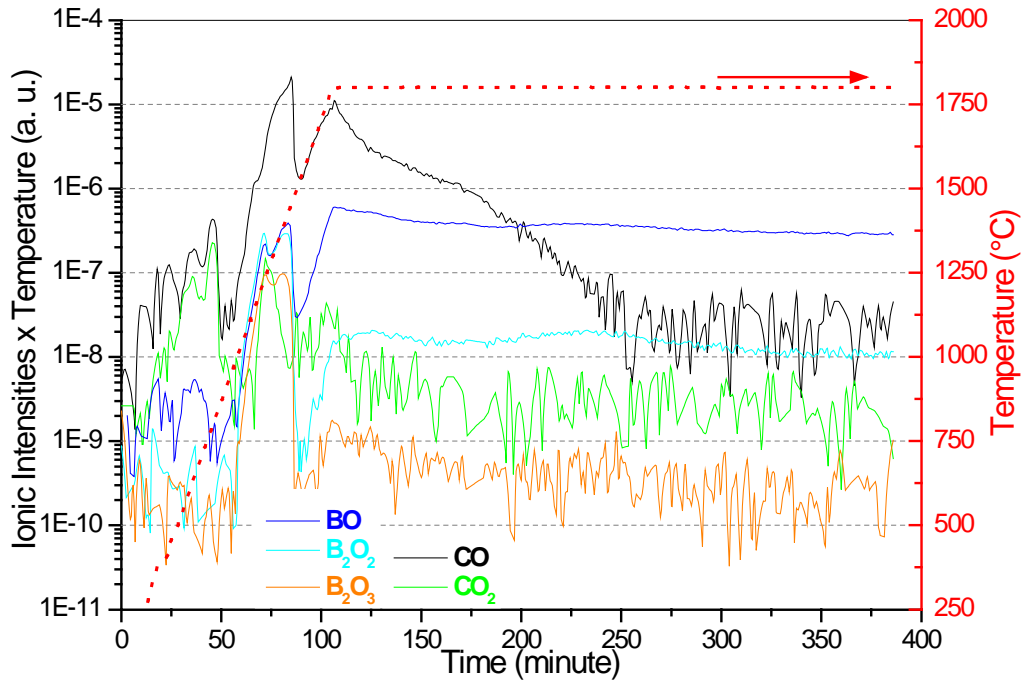

FIG. 2. Left axis: $I_i T$ product (related to partial pressures in the Knudsen cell) for $CO_{(g)}$, $CO_{2(g)}$ and $B_2O_{2(g)}$, $B_2O_{3(g)}$, $BO_{(g)}$ gaseous species as a function of time. Right axis: Temperature (°C) as a function of time during the HTMS experiment

As previously reported, the high response of $BO_{(g)}$ vs. $B_2O_{2(g)}$ is interpreted as a fragmentation phenomenon of $B_2O_{2(g)}$ into two molecules of $BO_{(g)}$.as confirmed by the thermodynamic calculations and by the measurement of the gaseous phase above $B_2O_{3(l)}$ under reducing conditions by Jacobson et al. [10].

Then, the molecular flows (3) released from the Knudsen cell are integrated according to (9) to assess the mass loss of the sample (FIG. 3). During the experiment, the main mass loss is due to the oxygen release from boron and carbon oxides. Therefore, the sample has a strong tendency to get reduced.
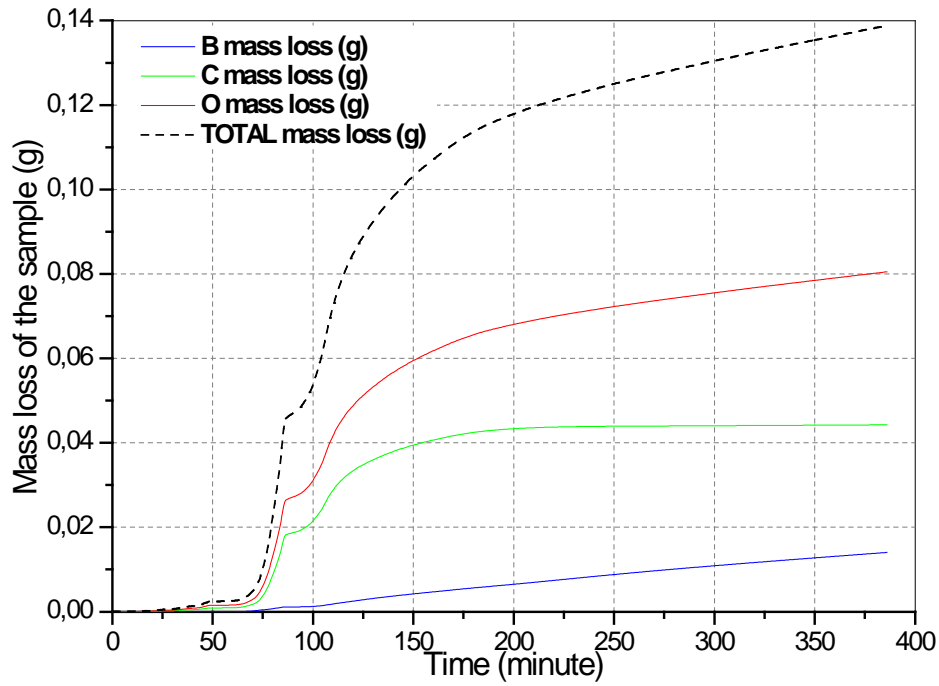
FIG. 3. Boron, carbon, oxygen and total (dashed line) mass loss of the sample as a function of time during the HTMS experiment

From the mass loss in B, C and O (FIG. 3), the elementary composition of the sample was determined versus time in FIG. 4. The number of moles of uranium remains constant because no significant uranium species ($U_{(g)}$, $UO_{(g)}$, $UO_{2(g)}$, $UO_{3(g)}$) were measured in the vapor, in agreement with their low pressures according to the thermodynamic calculations in FIG. 1.
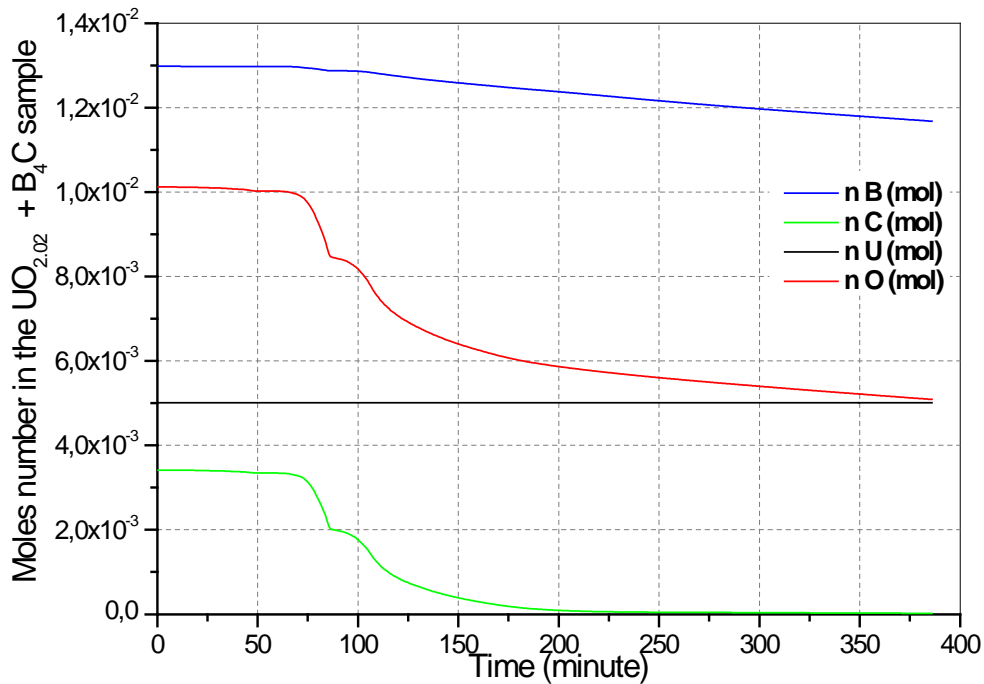
FIG. 4. Evolution of the elementary B-C-O-U composition as a function of time during the HTMS experiment

During the experiment, the $UO_{2.02}$ fuel is reduced by B_4C by forming mainly made of $CO_{(g)}$, $CO_{2(g)}$ and boron oxides in the gas phase (FIG. 5). Once the UO_{2+x} fuel is reduced to the minimum (O/U) ratio corresponding to UO_{2-x} at the phase boundary in the U-O phase diagram [6], metallic uranium enriched phases will tend to form.
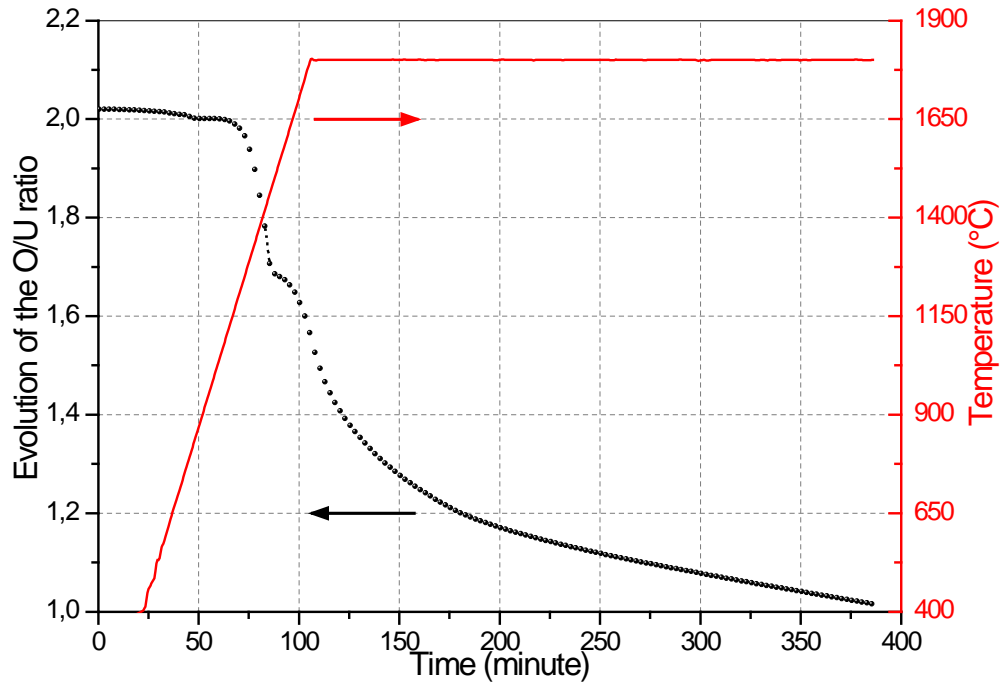
FIG. 5. Evolution of the O/U ratio in $UO_{2\pm x}$ as a function of time during the HTMS experiment

From the evolution of the sampel composition versus time, the mole fractions of the phases are calculated versus time in FIG. 6 using the FUELBASE database. The results show that the two major phases are $UO_{2\pm x}$ and UB_4 (FIG. 6).
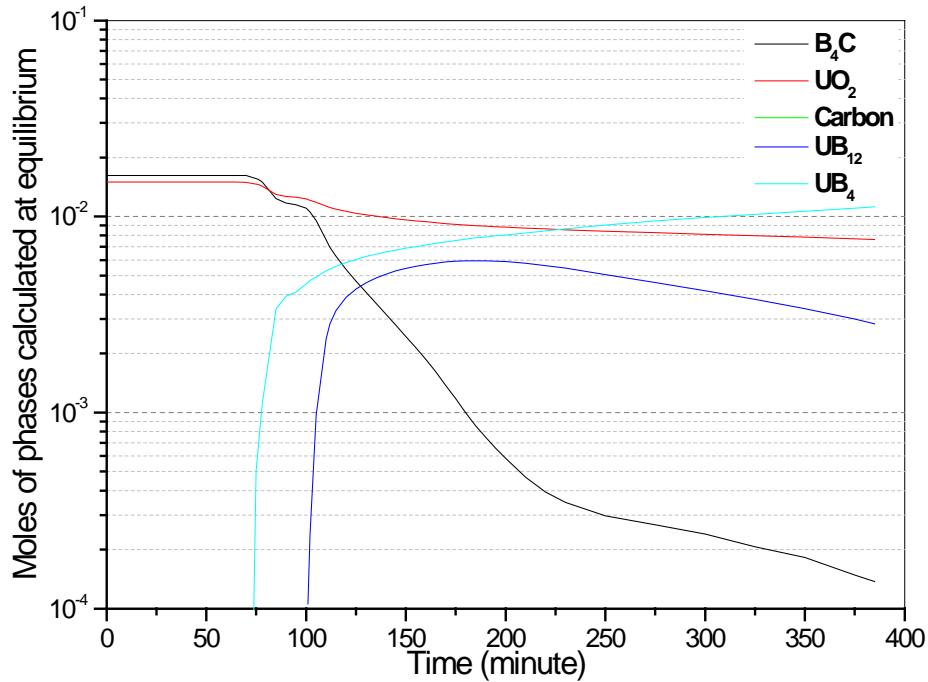
FIG. 6. Calculated moles of phases a function of time using the FUELBASE database during the experiment

At the end of the experiment, the calculated O/U ratio in $UO_{2\pm x}$ is equal to 1.992. The relative mole fractions of the main phases formed during the interaction are 51 % of UB_4, 36 % of $UO_{2\pm x}$ and 13 % of UB_{12}.

Micrographs of the sample after the experiment are presented in FIG. 7. In the mixed powders, elliptic aggregates surrounded by white precipitates are present. This phenomenon may be due to solid/gas reactions. In the vicinity of these aggregates, the powder density seems to be more disseminated too.
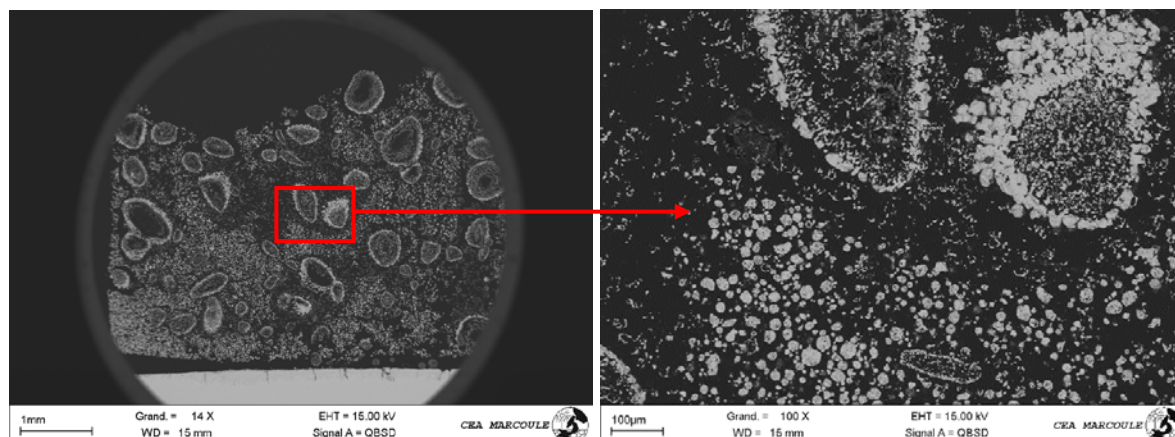
FIG. 7. SEM image of the 50% mol. $UO_{2.02}$ + 50% mol. B_4C sample after the HTMS experiment. The dark grey matrix is the resin. On the left hand side picture, the circle is a diaphragm

The semi-quantitative SEM/EDS analyses of the sample show that the composition of the particles surrounding the agregates correspond to the UB_4 compound (FIG. 8). No carbon was detected as calculated in FIG. 4.

Spectre	U %a	O %a	B %a
1	35.32	64.68	-
2	20.43	-	79.57
3	22.19	-	77.81
4	22.14	-	77.86
5	20.53	-	79.47
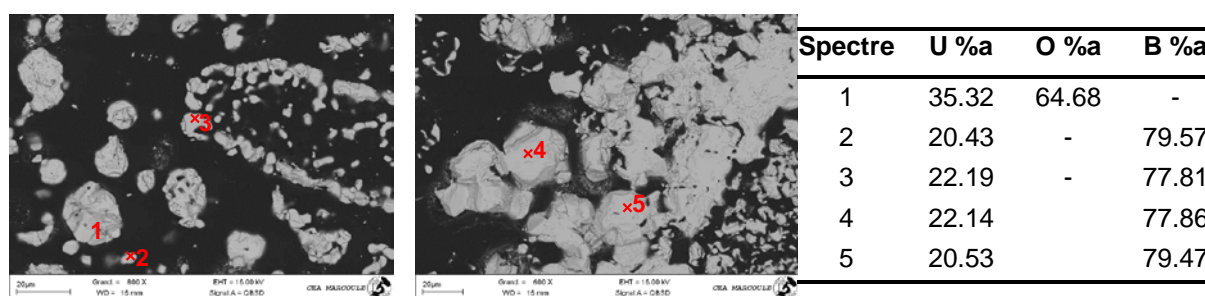
FIG. 8. EDS analyses of the sample. Formation of UB_4 clusters in the $UO_{2.02}$ + B_4C powder mixture

The X-Ray diffraction diagram is consistent with the EDS analyses (FIG. 9). It highlights the presence of $UO_{2\pm x}$ and the formation of UB_4. The possible presence of other uranium borides (UB_2, UB_{12}) could not be revealed. If the UB_{12} boride was formed, its fraction would be lower than the limit of detection of the method. The peaks indexed by tungsten are due to the response or contribution of the crucible.
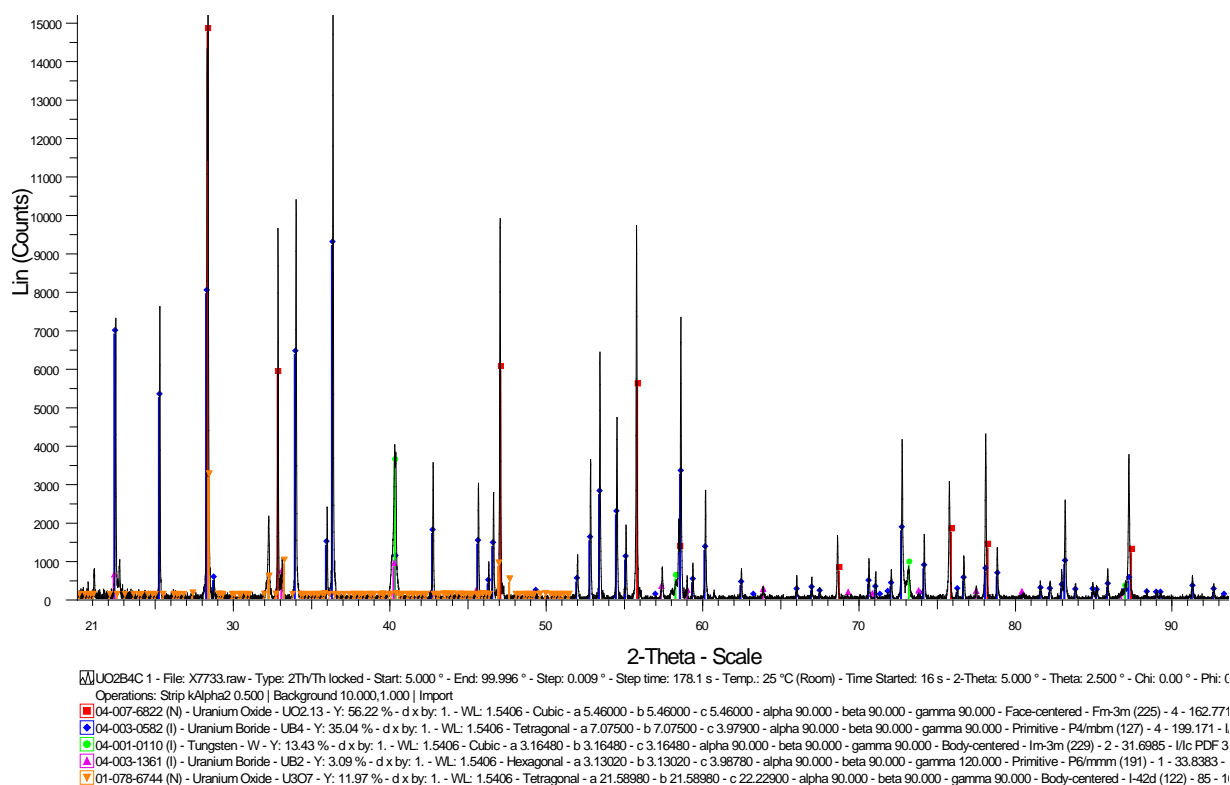
FIG. 9. X-Ray diffraction pattern of the sample, indexed peaks reveal $UO_{2\pm x}$ and UB_4. Colours are Red for UO_2, Blue for UB_4, Green for W, Pink for UB_2, Orange for U_3O_7

Conclusion

The chemical interaction between $UO_{2\pm x}$ and B_4C at 2073 K was studied by high temperature mass spectrometry (HTMS) . A sharp release of boron and carbon gaseous oxides, mainly CO(g) and in lower extents $B_2O_{2(g)}$, $B_2O_{3(g)}$, $BO_{(g)}$, $CO_{2(g)}$ was observed. After a five hour heat treatment, the resulting phases are the sub-stoichiometric UO_{2-x} and UB_4 formed by reduction of UO_{2+x} by B_4C. No carbon was found in the sample. Even if a small amount of UB_{12} was calculated, its formation could not be corroborated.

The measured molecular flows are consistent with the relative partial pressures calculated using the FUELBASE thermodynamic database. The final calculated composition of the sample is consistent with the analyses of the sample performed after the test, using XRD and SEM.

The B_4C absorber shows a good efficiency towards the risk of recriticality since only 10 % of the initial boron content is vaporised during the $(UO_{2\pm x} + B_4C)$ interaction. Furthermore, the main formed phase is the UB_4 compound in which the aborber / fissile atom ratio is equal to 4. Nevertheless, the fast reduction of the system due to the release of gaseous boron and carbon oxides has to be considered at higher temperature because it could lead to the formation of a metallic liquid phase.

REFERENCES

[1] Etude des matériaux sacrificiels absorbants et diluants pour le contrôle de la réactivité dans le cas d'un accident hypothétique de fusion du cœur de réacteurs de quatrième génération
Plevocova K.
Ph. D. Thesis, Université d'Orléans, 16th december 2010

[2] An experimental study of the effect of boron carbide on the SFR corium composition
Plevacova K., Journeau C., Piluso P., Poirier J., 2010
International Youth Nuclear Congress (IYNC 2010), Cape town, South Africa 114 p. 1- 9

[3] Kinetic study of the UO_2/C interaction by high-temperature mass spectrometry
S. Gossé, C. Guéneau, T. Alpettaz, et al.
Nuclear Engineering and Design, Volume: 238, Issue: 11 pp. 2866-2876

[4] High Temperature Mass Spectrometry: Instrumental Techniques, Ionization Cross-Sections, Pressure Measurements and Thermodynamic Data
Drowart J., Chatillon C., Hastie J., Bonnell D., 2005
Pure Applied Chemistry, 77, pp. 683-737

[5] A Thermodynamic Approach for Advanced Fuels of Gas Cooled Reactors
C. Guéneau, S. Chatain, S. Gossé, C. Rado, O. Rapaud, J. Lechelle, J.C. Dumas, 2005
Journal Nuclear Materials, Vol 344, pp 191-197

[6] Thermodynamic modelling of advanced oxide and carbide nuclear fuels: Description of the U–Pu–O–C systems
C. Guéneau, N. Dupin, B. Sundman, C. Martial, J-C Dumas, S. Gossé, S. Chatain, F. De Bruycker, D. Manara, R.J.M. Konings, 2011
Journal of Nuclear Materials, Vol 419, Issues 1–3, Pages 145–167

[7] SSUB4 Thermodynamic Database
P. Shi, 2006
http://www.thermocalc.se/TCDATA.htm

[8] Thermodynamic Modelling of the C-U and B-U Binary Systems
Chevalier P. Y., Fischer E., 2001
Journal of Nuclear Materials, 288, pp. 100-129

[9] Development of a thermodynamic data set for the system B-C-N-O-Si
B. Kasper, H. J. Seifert, A. Kussmaul, H. L. Lukas, F. Aldinger, 1997
Material-wissenschaftliche Grundlagen, Werkstowoche '96, Stuttgart, pp 623-628

[10] High-Temperature Vaporization of $B_2O_{3(l)}$ under Reducing Conditions
Jacobson N. S., Myers D. L., 2011
The Journal of Physical-Chemistry B, 115, 13253–13260

[11] Mass spectrometric study of UO_2–ZrO_2 pseudo-binary system
Baïchi M., Chatillon C., Guéneau C., Chatain S., 2001
Journal of Nuclear Materials, 294 (1-2), pp. 84-87

[12] The Knudsen Effusion Method. The Characterization of High Temperature Vapors
Carlson K. D., 1967
Ed. J.L. Margrave, J. Wiley, New York, Chap. 5, pp. 115-129

SODIUM EXPERIMENTS ON NATURAL CIRCULATION DECAY HEAT REMOVAL AND 3D SIMULATION OF PLENUM THERMAL HYDRAULICS

H. Kamide[a]**, A. Ono**[a]**, N. Kimura**[a]**, J. Endoh**[b]**, O. Watanabe**[b]

[a] Japan Atomic Energy Agency, Oarai, Ibaraki, Japan

[b] Mitsubishi FBR Systems, Inc., Shibuya, Tokyo, Japan

Abstract. Natural circulation decay heat removal is one of the significant issues for fast reactor safety, especially in long term station blackout events. Several sodium experiments were carried out using a 7-subassembly core model for core thermal hydraulics under natural circulation conditions and for onset transients of natural circulation in a decay heat removal system (DHRS) including natural draft. Significant heat removal via inter-wrapper flow was confirmed in the experiments. Solidification of sodium in an air cooler is one of key issues in loss of heat sink events. Natural circulation characteristics under long-term decay heat removal were also obtained. Multi-dimensional phenomena, e.g., thermal stratification and bypass flow in plenums and/or heat exchangers, may influence the natural circulation. Thus, 3D simulation method was developed for entire region in the primary loop. Comparison of temperature distributions in a DHRS heat exchanger between experiment and analysis was done.

1. INTRODUCTION

The natural circulation is a significant issue on passive features of a sodium cooled fast reactor especially in a total blackout event. Fully natural circulation system is adopted in a decay heat removal system (DHRS) of Japan Sodium Cooled Fast Reactor (JSFR) [1], which is developed by Japan Atomic Energy Agency in cooperation with Mitsubishi FBR Systems and Japanese electric power companies. The JSFR has two loops of the main heat transport systems. Then the DHRS of JSFR consists of two units of PRACS (primary reactor auxiliary cooling system), each of which has a heat exchanger in an inlet plenum of Intermediate Heat Exchanger (IHX), and further one unit of DRACS (direct reactor auxiliary cooling system), which has a dipped heat exchanger (DHX) in the reactor vessel. The decay heat after a reactor scram is removed solely by natural circulations in the primary loops and DHRS and also natural draft in the air coolers. Such natural circulation DHRS is a key issue of the JSFR development project. Start-up and long term natural circulations are of importance for the decay heat removal. Further, core thermal hydraulics, which is influenced by cold sodium provided by DHX, is also significant to evaluate the highest temperature in the core.

A large scale sodium experiment, ILONA [2], was carried out for the DHRS of European Fast Reactor (EFR) [3]. Heat removal capacity of the air cooler and transient behavior at the tube outlets during the start-up were confirmed to be within the permissible range. However, the experimental data is still limited, especially for the interactions among the loops and natural draft.

Increase of component size and heat exchangers installed in a component, i.e., PRACS may result in multi-dimensional flow, e.g., bypass flow and thermal stratification. Thus, a multi-dimensional simulation method of the primary and decay heat removal systems has been developed to take accounts of such phenomena.

Sodium experiments were carried out to study the core thermal hydraulics and transient behavior of natural circulation in the DHRS of JSFR including low temperature condition as the long-term behavior. A partial model of the straight tube type PRACS heat exchanger is installed in a sodium test loop named PLANDTL [4], which consists of a core model, a reactor upper plenum, the primary loop, and DHRS. Objectives of this study are to investigate the transient and long-term behavior of DHRS including the natural draft and to validate the multi-dimensional simulation method. The core thermal hydraulics is also discussed. When DRACS is operated, cold sodium is provided into the reactor upper plenum. This cold sodium can penetrate into the gap region between the subassemblies in a core barrel and make natural convection. Such gap flow is referred as inter-wrapper flow (IWF). Several sodium experiments [5] were carried out on IWF by authors. Here, extremely low core flow conditions are shown to reveal heat removal capability of IWF.

2. SODIUM TEST FACILITY

2.1. Test Loop

A sodium test loop, PLANDTL, was used to investigate the core thermal hydraulics and transient phenomena in the PRACS. Figure 1 shows schematic of the test loop. It consists of a simulated core, a reactor upper plenum, the primary loop, IHX, a lower plenum, the secondary loop, a main air cooler instead of a steam generator, a DHRS loop, and an air cooler of DHRS. A dipped heat exchanger (DHX) is installed in the reactor upper plenum. The PLANDTL loop was originally designed to simulate thermal hydraulics in the core during transition from forced to natural circulation. A partial and axially full-scale model of core fuel subassemblies was installed. The primary loop was designed to give appropriate boundary conditions to the core model.
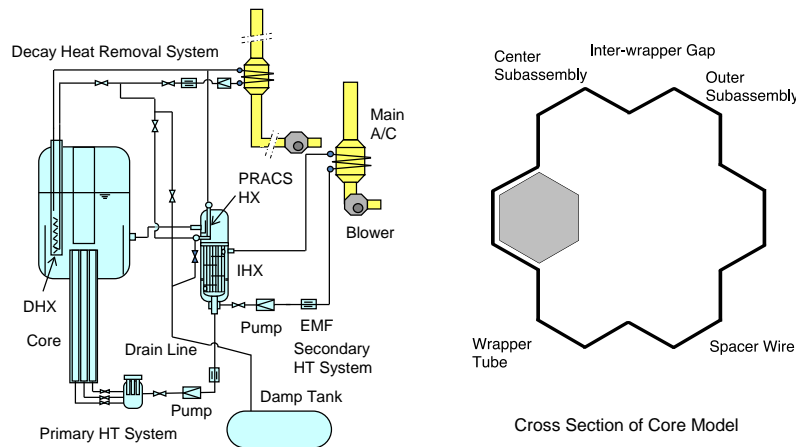
FIG. 1. Schematic of PLANDTL loop and Core Model.

The core model has 7 subassemblies and a 37-pin bundle in the center subassembly as shown in Fig. 1, where the surface heat flux on each the fuel pin is simulated by an electric heater. The pin diameter and pitch are modeled with nearly 1/1 scale of a reactor. The heated length is 1m and the same as in a reactor. The center subassembly is a full-scale partial model. Total power of the core is 1MW at the maximum. The pin surface heat flux in the central subassembly reaches around 12% of full power condition in a reactor core fuel subassembly.

A partial model of PHX was installed in the inlet plenum of IHX to simulate JSFR. The DHRS loop in the PLANDTL can select the DHX or PHX as the sodium heat exchanger. The height difference between the PHX and the air cooler in the DHRS loop is 1/7 of that in JSFR. The air stack height from

the DHRS air cooler is nearly 1/8 of that in JSFR. The pipe diameter of the DHRS loop is also 1/8 of that in JSFR. The IHX is a shell and tube type heat exchanger and the primary coolant flows through the inside of the tubes. The tube length is around 1/6 of that in JSFR. The scales of height differences among the core, the PHX, the DHRS air cooler, and the air stack are within a range of 1/6 to 1/8. Thus, it is believed that basic phenomena in the start-up of natural circulations from the air stack, the PRACS loop and the primary loop can be investigated in this sodium test facility.

2.2. PRACS Heat Exchanger (PHX) Model

Figure 2 shows schematic of the PHX model in the IHX. In order to evaluate heat transfer characteristics of PHX, the Pe number similarity is required. The PHX tube bundle is modeled by real dimensions, but in partial length and region. Two layers of the tubes are set near the inner shell wall. There is a wide flow area beside the tubes. The tube outer diameter is 27.2mm and only 15% smaller than that in JSFR. The ratios of tube pitch to diameter in circumferential and radial directions are nearly the same as those in JSFR. Local natural circulation in the IHX inlet plenum will develop along the PHX tubes. Thus longer tube length is desired. However, vertical tube length is 0.59m and nearly 1/3 of that in JSFR due to space limitation. This was considered in the experimental conditions.
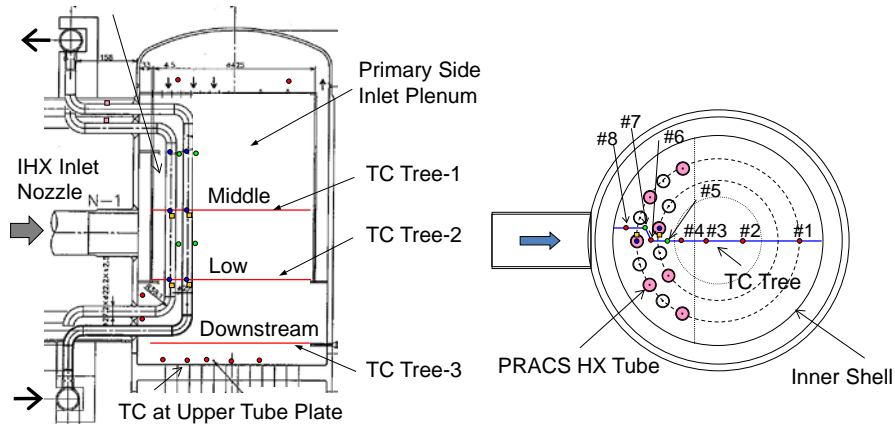

FIG. 2. Schematic of PRACS Heat Exchanger (PHX) in IHX Inlet Plenum.

As for the natural circulation through the DHRS loop, the head is governed by the height difference between the PHX and the air cooler. When the Ri number similarity is assumed in the DHRS loop, the power ratio is estimated under the same temperature condition as in JSFR. When the length scale is 1/8, the ratio of heat removal becomes 1/180. The heat removal capacity of the PHX should be 130kW in the model. The heat transfer area, i.e., tube number was set so as to obtain this heat removal capacity.

2.3. Measurement System

Temperatures in the IHX inlet plenum and the core model are measured by thermocouples of 0.5mm diameter (Chromel-Alumel type). The measurement positions are shown in Figs. 1 and 2. Transverse distributions across the PHX tubes and the flow area beside the tubes are measured at several heights. The measurement errors of the thermocouples were less than 0.2°C based on relative calibration in a temperature range between 300 and 500°C in IHX. Flow rates in the loops are measured by electromagnetic flow meters. The calibrations were done based on tank volume between two level meters and time differences during a sodium drain from the tank. The estimated standard deviations of error were 0.76 and 0.07 l/min in the primary loop and the DHRS loop, respectively. Typical flow rates of natural circulations were 40 and 25 l/min in the primary loop and the DHRS loop, respectively.

3. 3D SIMULATION METHOD

A three-dimensional numerical analysis method for whole of the primary system [6] has been developed to deal with phenomena such as local natural convections and thermal stratifications under decay heat removal conditions. The computational fluid dynamic analysis code, STAR-CD, is employed as the main frame of the three-dimensional simulation. A whole core thermal-hydraulic code, TREFOIL [7], and a flow network model for simulating the secondary side of PRACS, DRACS and IHX were incorporated into the three-dimensional method. TREFOIL code can analyze the core thermal-hydraulics taking into account of inter-subassembly heat transfer, inter- and intra-subassembly flow redistributions. RNG k-ε turbulent model [8][9] and a second order advection scheme named MARS (Monotone Advection and Reconstruction Scheme) [10] are applied to the three-dimensional method as a set of options in STAR-CD code, the pressure losses in the core subassemblies are calculated based on the empirical formulas by Cheng and Todreas [11] and that in the tube bundles of the heat exchangers and in the pumps are calculated based on design results of each component. The other pressure losses such as in pipes with elbows and in plenum are calculated based on the standard logarithmic law of wall friction in STAR-CD code.

This three-dimensional method was applied to the PLANDTL sodium test. The computational domain with mesh division simulating the geometry of the primary system is shown in Fig. 3. The total number of meshes is about 3,300,000. The one-dimensional flow network models simulating the secondary side of PRACS and IHX were also assembled. The PRACS model includes PHX, the secondary sodium piping and the air-cooler with the dumper and the air stack. The characteristics of the test apparatus such as the pressure losses in the core, the tube bundle of IHX, the baffle plate supporting PHX tubes and the secondary side of PRACS including the air cooler with the air stack, and the heat transfer coefficients in the core subassemblies, tube bundles of IHX and PHX and the air cooler, and the thermal-hydraulic properties of sodium were incorporated into the three-dimensional method as input data.
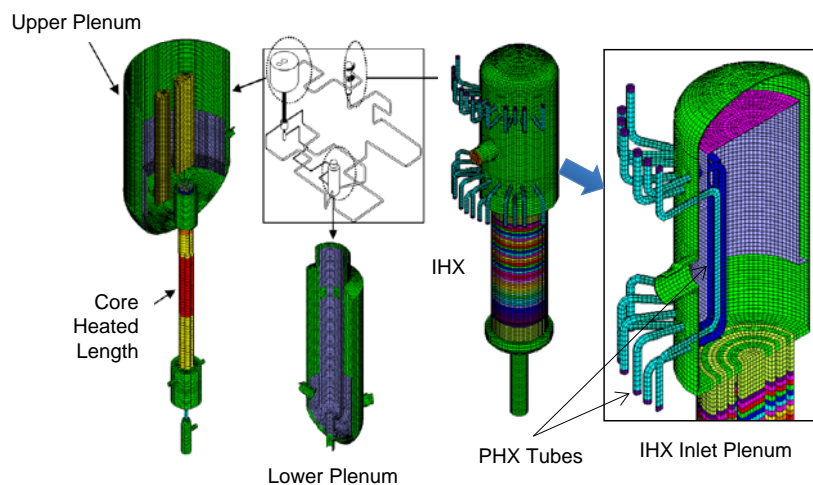
FIG. 3. Schematic of Computational Domain of 3D Simulation Method for PLANDTL.

4. EXPERIMENTAL RESULTS

4.1. Steady State Experiments on Inter-wrapper Flow

Inter-wrapper flow (IWF) is driven by buoyancy force between the hot core and the reactor upper plenum where DHX provides cold sodium. The cold sodium penetrates into gap region between the core subassemblies and natural convection is formed in the core gap region. Steady-state sodium

experiments, which simulate the natural circulation decay heat removal, were performed by using PLANDTL.

The heater power of the core was adjusted so that the heat flux at the pin surfaces in the center subassembly would be maintained at 1.5% of the full power conditions of a real reactor. The heater power and flow rate in the subassemblies were set at the same values for each of the seven subassemblies using flow control valves in the feed lines between the lower plenum and the core. In order to simplify the phenomena in the core model, the valve openings of these flow control valves were set at a small value, i.e., flow redistribution between the subassemblies was suppressed. The inlet temperature of the core was set at a constant value (300˚C) in all experimental cases except for zero flow rate case. The secondary circuit of the IHX was always closed by a valve. Steady-state condition was confirmed by noting a flat time trend in the upper plenum temperatures; typically, steady-state was attained in one day. The data of temperature and flow rate were recorded for 300s at time intervals of 0.096s. The time-averaged data are discussed in the following section.

In order to demonstrate the cooling potential of IWF, extremely low flow conditions in the subassemblies, including zero flow rate, were examined. The zero flow rate condition, in particular, simulates the situation where all primary circuits in a reactor are unavailable and decay heat is removed solely by in-vessel natural convection. Case name is identified as D#.#, where "#.#" indicates that the flow velocity in the 37-pin bundle is #.#% of the full power condition of a reactor. The Re number was defined in the 37-pin bundle using a hydraulic equivalent diameter in the bundle, the bundle average velocity and kinematic viscosity at average temperature along the heated length. The Re number in the 37-pin bundle was 650 in the flow conditions of 1.0 %.
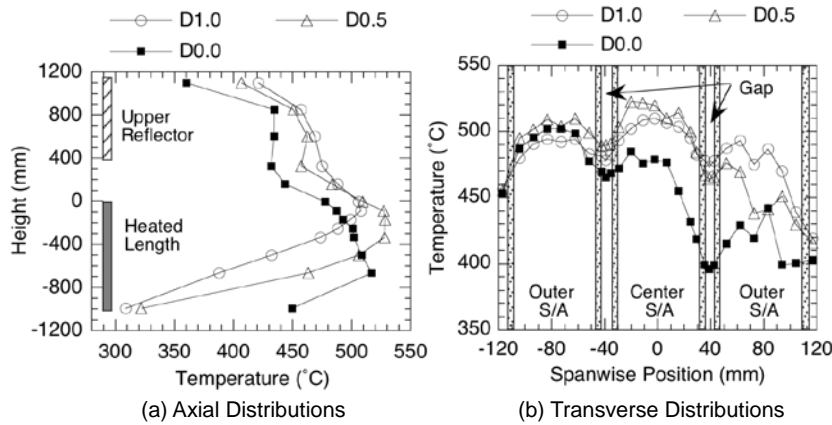

FIG. 4. Temperature Distributions in Core Model under Low Flow-rate Conditions.

The axial temperature distributions along the center subchannel in the center subassembly are shown in Fig. 4, (a). In Case D0.5, the upper 1/3 of the heated length showed a flat temperature profile due to heat removal by IWF. The temperature increase from the inlet was larger, by some 30˚C, in contrast to Case D1.0, as the flow rate in the subassembly was one-half that of Case D1.0 (heater power was identical). In Case D0.0, all feed lines into the subassemblies were closed by valves. The IWF could remove all heat generated in the subassemblies while maintaining the highest temperature below 600˚C. In the upper half of the heated length, the higher position exhibited a lower temperature than in the lower half. The highest temperature was registered at a position below the middle of the heated length where the power profile has a peak. A likely explanation for this heat sink trend is that the cold fluid in fact penetrates the gap regions from the upper plenum.

The transverse temperature distributions at the top of the heated length are shown in Fig. 4, (b). The temperature distributions showed decrease near the wrapper tube wall. This temperature gradient was larger in Case D0.5 than in Case 1.0 due to larger contribution of heat removal by IWF. In Case D0.0, a steep and asymmetric temperature distribution was seen in the center subassembly. This was caused by asymmetric flow in the inter-wrapper gap and also natural convection inside the subassembly.

The cooling effects of IWF were observed in the experiments. Figure 5 shows the influence of IWF on the highest temperature in the core in cases of the core power at 1.5%. The temperature increase at the peak point from the core inlet was normalized by the average temperature increase based on the flow rate and the heater power in the subassembly as follows,

$$T^* = \frac{T_{peak} - T_{in}}{\Delta T_{Q/F}}$$ (1).

Where Tpeak, Tin, and $\Delta T_{Q/F}$ are the peak temperature, inlet temperature and average temperature increase based on power and flow rate in the subassembly. In the cases without IWF (IHX is used to remove the core heat and there is no cold sodium in the upper plenum), the non-dimensional peak temperature tended to reach unity as the flow rate decreased because of flow redistribution in the subassembly, i.e., the flow rate in the hot subchannels increased due to buoyancy force. In the cases with IWF (using the DHX), the non-dimensional temperature decreased from unity as the flow rate decreased. The influence of IWF was significant when the flow rate in the subassembly was less than 1%. The IWF could maintain the temperature increase in the core at only one-half value, which was estimated under adiabatic conditions at the wrapper tube wall and 0.5% flow velocity. This indicates that IWF can remove 50% of the heater power in the center subassembly.
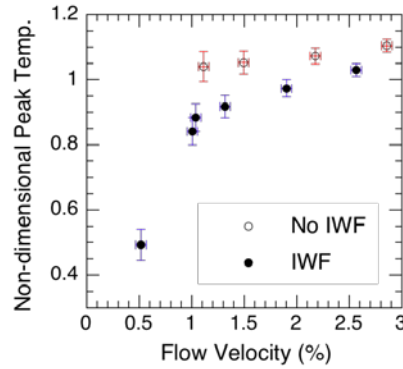

FIG. 5. Non-dimensional Peak Temperature in Core with and without Inter-Wrapper Flow.

4.2. Experiment on Start-up Transient in DHRS Loop

4.2.1. Concept of transient experiment

Transient characteristic in the primary system depends on those in the secondary system and also the decay heat removal system (DHRS). Heat transfer in the heat exchangers between these systems is significant for such interactions. Thus the sodium experiments are required to simulate the higher heat transfer, which can not be simulated in a water system, and also the transient behavior including the interaction between the heat transport systems.

In the experiments, start-up of the natural circulations in the primary loop and the DHRS including the natural draft in the air stack were investigated together with long-term behavior approaching to a cold condition at the air cooler outlet. The natural circulation flow course depends on the loop geometry and is not simulated precisely due to the limitations of geometry similarity. However, mechanism of the interactions is well examined by the sodium experiments.

4.2.2. Experimental conditions

The initial condition in the primary loop is 6% flow velocity in the center subassembly and 6% core power as compared with the full power condition of a core fuel pin heat flux. The Re number in the pin bundle is nearly 3,000 under forced convection. Transient curves of flows and power are shown in

Fig. 6. The heater power of the core was reduced quickly from 6% (500kW) to 1.8% (150kW) at t= 0 to 1s and kept at 1.8%, which simulated the decay heat level around 1000s from the reactor scram. The primary pump stopped at t=90s from the scram and then the natural circulation started. The secondary loop flow was also reduced and switched to natural circulation. The dampers of main air cooler in the secondary loop were closed at t=90s after the stop of air blower. However, the air leak flow continued through the dampers. The valve in the secondary loop was closed at 2030s in order to stop the natural circulation because of no heat sink in the secondary loop after the scram in JSFR.
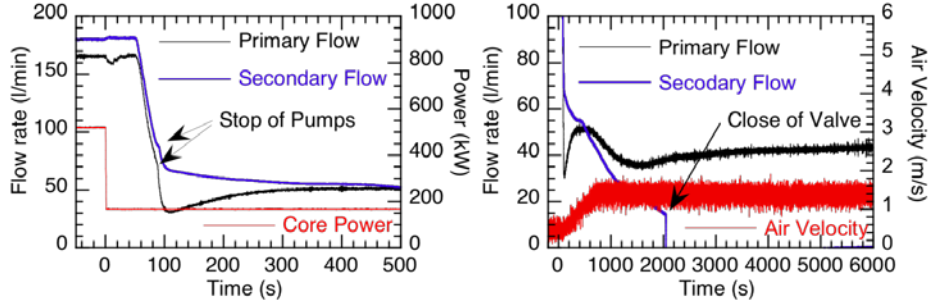

FIG. 6. Transients of Power and Flows from Forced to Natural Circulation.

The inlet damper of the DHRS air cooler was opened gradually during t=100 to 800s in order to mitigate thermal shock in the DHRS loop as shown in Fig. 7. The outlet damper was opened at t=100s. A blower of the air cooler and a sodium pump of the DHRS were not operated during the entire transient. The opening of the air dampers brought the natural draft through the air cooler and the stack and the air velocity in the stack increased up to t=800s.

(a) Sodium Flow rate and Air Velocity   (b) Temperatures around Air Cooler
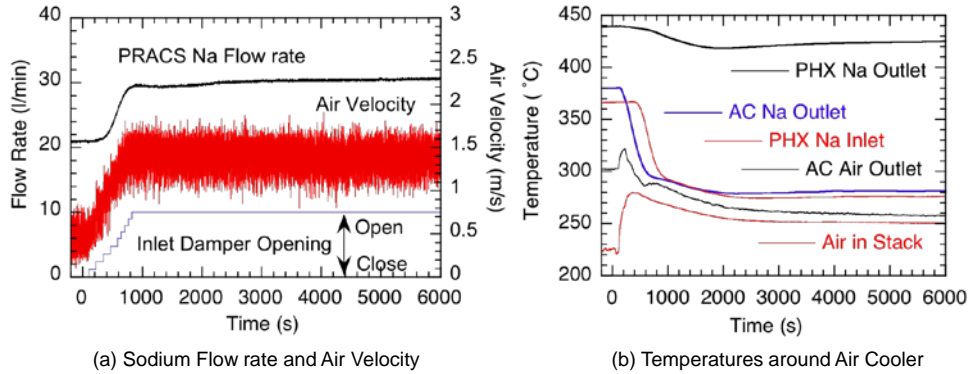
FIG. 7. Flow-rate and Temperature Trends in PRACS by Opening of Air Dampers.

4.2.3. Start-up transient of natural circulation

Air velocity in the air cooler duct and DHRS loop flow rate are shown in Fig. 7 together with the inlet damper opening. The air velocity increased immediately corresponding to the air damper opening. However, the sodium flow rate in the DHRS loop increased 100s behind from the change of the air velocity. The sodium velocity in the DHRS loop was slower than the air velocity. This caused longer transportation delay of the cold fluid in downward flow path of the DHRS loop and slower increase of the natural circulation head. Figure 7 also shows the air temperatures at just outlet of the air cooler and at the middle height of air stack and the sodium temperatures of the air cooler and the PHX. The delay of the sodium temperature drop at the PHX inlet (the end of downward flow path in the DHRS loop) was confirmed as compared with the air temperature responses.

The sodium temperature at the heated end of center subchannel in the central subassembly is shown in Fig. 8 as the highest temperature in the core model together with the subassembly inlet temperature in short and long terms. The highest temperature in the core showed the so-called second peak at t=220s after some delay from the pump stop due to fluid transportation along the heated length and heat capacity. After that, the temperature was decreased due to the increase of natural circulation flow rate as shown in Fig. 6. At t=1500s the third peak was registered. The temporal decrease of the primary loop flow rate due to reduction of natural circulation head via loss of heat sink in IHX resulted in the third peak of the core temperature. It was confirmed that smooth start-up of natural circulations in the whole systems from these figures.
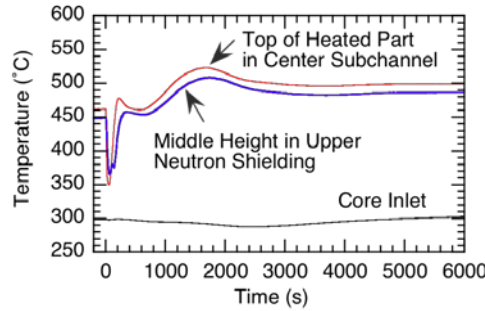

FIG. 8. Transient of Core Temperatures from Forced to Natural Circulation.

Long-term operation of decay heat removal will result in temperature decrease in the whole system. However, excess temperature decrease under natural circulation condition causes solidification of sodium and decrease of the flow rate. Thus, the vane and dampers of air cooler will be controlled to maintain the sodium temperature. Such low temperature conditions in the air cooler were also investigated. The primary loop was maintained at constant flow rate but the power in the core model was set zero. The PRACS were operated by natural circulation and natural draft for long term. Then air cooler outlet sodium temperature decreased gradually during several hours as shown in Fig. 9. Even if the sodium temperature at the air cooler outlet was below 190 ˚C, significant reductions of flow rate or temperature were not observed. However, increase of pressure loss coefficient in the PRACS loop was recognized under the temperature condition below 200 ˚C at the air cooler outlet depending the oxygen concentration in the sodium.
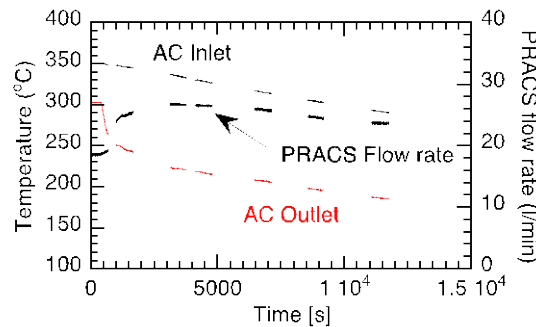

FIG. 9. Natural Circulation Flow Rate in PRACS under Low Temperature Condition.

5.   EXPERIMENTAL ANALYSES

5.1.   *Steady State of PHX Operation*

Steady state experiments were carried out to study influence of the bypass flow beside the PHX. The primary flow rate was a main experimental parameter. The natural circulation flow rate in a JSFR

primary loop is nearly 3% of full power flow rate. The average flow velocity in the IHX inlet annulus is 0.12 m/s. The parameter range of the primary flow rate in the experiment covered the average velocity of 0.12 m/s (at 300 l/min) and varied from 50 to 300 l/min. The PRACS flow rate was maintained at constant and the air flow rate was controlled to keep the air cooler outlet temperature at constant value by using the air blower. Thus, removed heat by PHX was nearly constant in each case.

Typical temperature distributions in a vertical cross section across the PHX tube bundle, which were calculated by the 3D simulation method are shown in Fig. 10. Increase of the primary flow rate resulted in temperature dip near the PHX tube bundle due to the bypass flow. This is consistent to the temperature distributions obtained by the experiments as shown in Fig. 11. The 3D simulation method can predict temperature profile around the PHX influenced by the bypass flow.
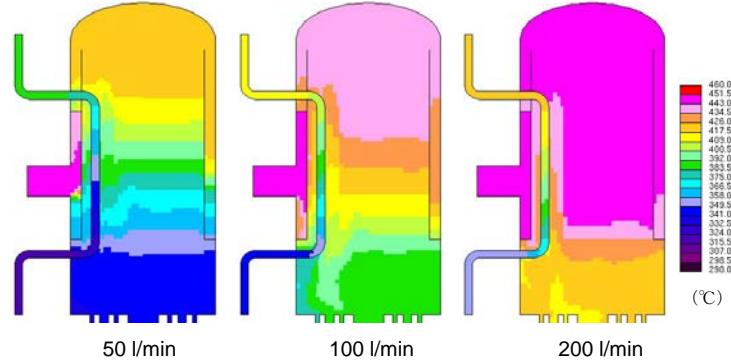
FIG. 10. Temperature Contour in IHX Inlet Plenum with PHX (Parameter of Primary Flow-rate).
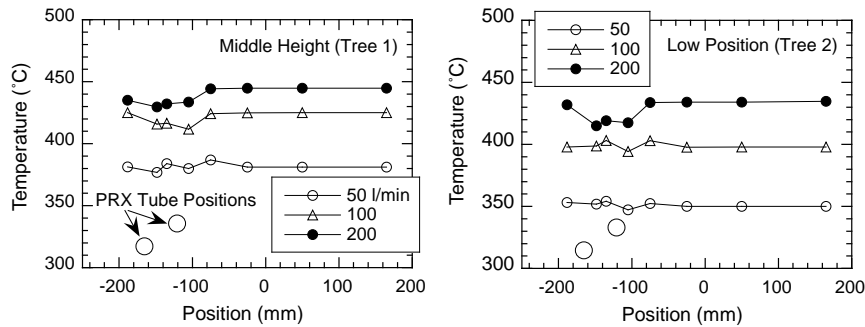
FIG. 11. Measured Transverse Temperature Distributions in IHX Inlet Plenum

5.2. Transient of PRACS Start-up

The 3D simulation method was applied to the transient experiment from forced to natural circulation. One of major 3D effects in the primary loop (except for the reactor vessel) is development of local natural circulation and thermal stratification in the IHX inlet plenum due to operation of PHX.

Figure 12 shows comparison of vertical temperature distributions in the IHX inlet plenum between the calculation and experiment and also temperature contour at t=1000s obtained by the 3D simulation. The calculated temperature profiles and time variations were in good agreement with the measured data. The 3D simulation method showed high applicability to simulate the development of thermal stratification in the IHX due to the PHX operation under the natural circulation condition.
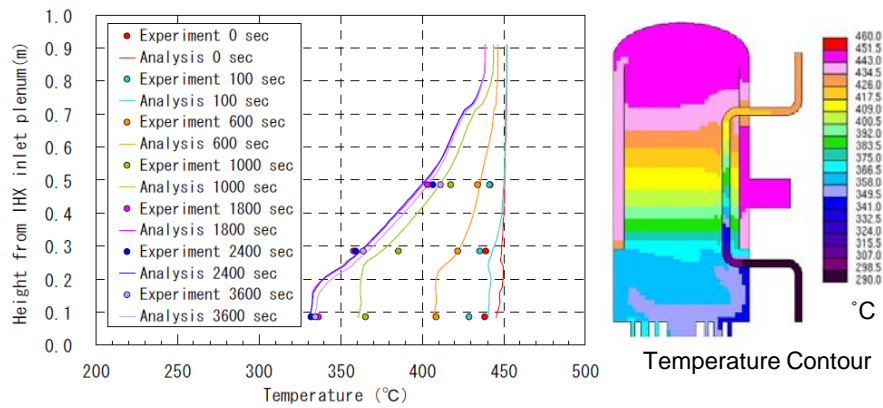
FIG. 12. Thermal Stratification in IHX Inlet Plenum in Transition of PRACS Start-up

6. CONCLUSIONS

Natural circulation is significant for decay heat removal function of a fast reactor. Sodium experiments were carried out to investigate start-up transient of natural circulation in the decay heat removal system including the natural draft. Low temperature condition in the air cooler was also examined. It was confirmed that smooth start-up of natural circulations in the whole systems. Heat removal capability of the inter-wrapper flow in the core was also confirmed. The 3D simulation method for the whole of the primary system was developed. High applicability of the 3D method to simulate bypass flow and thermal stratification in the IHX inlet plenum, where heat exchanger of PRACS was operated, was shown by the experimental analyses.

REFERENCES

[1] AOTO, K., UTO, N., SAKAMOTO, Y., et al., Design Study and R&D Progress on Japan Sodium-Cooled Fast Reactor, Journal of Nuclear Science and Technology, 48 (2011) 4, 463–471.

[2] STEHLE, H., DAMM, G., et al., Large scale experiments with a 5MW sodium/air heat exchanger for decay heat removal, Nuclear Engineering and Design, 146 (1994) 383-390.

[3] HENNIES, H.H., LEDUC, J., et al., "Development of Fast Reactors in Europe," Fast Reactors and Related Fuel Cycles (Proc. Conf., 1991), Vol.1, pp.1.2-1to11, Kyoto, Japan.

[4] KAMIDE, H., KOBAYSHI, J., et al., "Sodium Experiment on Fully Natural Circulation Systems for Decay Heat Removal in Japan Sodium-Cooled Fast Reactor," NURETH14 (Proc. Conf., 2011), NURETH14-179, Toronto, Canada.

[5] KAMIDE, H., NAGASAWA, K., KIMURA, N., et al., Evaluation Method for Core Thermohydraulics during Natural Circulation in Fast Reactors, JSME International Journal Series B, Fluids and Thermal Engineering, 45 (2002) 3, 577-585.

[6] WATANABE, O., SUEMORI, M., ENDOH, J., et al., "Development of Numerical Analysis Methods for Natural Circulation Decay Heat Removal System Applied to a Large

Scale JSFR," NURETH14 (Proc. Conf., 2011) NURETH14-258, Toronto, Canada.

[7]   WATANABE, O., KOTAKE, S., et al., "Study on Natural Circulation Evaluation Method for a Large FBR", NURETH-8 (Proc. Conf.,1997) Vol.2, 829-838, Kyoto Japan.

[8]   YAKHOT, V. and ORSZAG, Renormalization group analysis of turbulence – I: Basic theory, J. Scientific Computing, 1 (1986) 1-51.

[9]   YAKHOT, V., ORSZAG, THANGAM, S., et al., Development of turbulence models for shear flows by a double expansion technique, Phys. Fluids, A4(7) (1992) 1510-1520.

[10] STAR-CD, Methodology, Version 4.02, 2007. Computational Dynamics Limited.

[11] CHENG, S.K. and TODREAS, N.E., Hydrodynamic Models and Correlations for Bare and Wire-Wrapped Hexagonal Rod Bundles - Bundle Friction Factors, Subchannel Friction Factors and Mixing Parameters, Nuclear Engineering and Design, 92 (1986) 227-251.

Investigation of the Coupled Reactivity Effects of the Movable Reflector and Safety Control Rods in the GFR

B. Vrban[a], Š. Čerba[a], J. Lüley[a], J. Haščík[a], V. Nečas[a], S. Pelloni[b]

[a] Institute of Nuclear and Physical Engineering, Slovak University of Technology in Bratislava, Bratislava, Slovakia

[b] Laboratory for Reactor Physics and Systems Behaviour, Paul Scherrer Institute Villigen, Switzerland

Presented by Š. Čerba

Abstract. Since the transient behaviour of the reactor core depends also on the fraction of neutrons that leak out of the core, the core control and reactivity management may benefit from a system of partially moveable reflector incorporated in the design. In fast reactors a larger migration area leading to a significant leak of neutrons can be observed because especially the transport cross-sections are in general smaller as compared to light water reactors. The utilization of a moveable reflector system in conjunction with dedicated safety control rods can increase the ability of accident managing due to enhanced escaping neutrons which otherwise would be reflected back into the fuel zone. The paper demonstrates the possibility of better controlling the transient reactor by additionally moving selected reflector subassemblies with higher neutronics importance. The main purpose of the analysis of the Gas-cooled Fast Reactor (GFR) presented in the full paper are investigations of the kinetic parameters and of the control and reflector rod worths, as well as optimization of the parts used for partial reflector withdrawal. The results found in this study may serve for future design improvements.

1. Introduction

The Generation IV International Forum (GIF) is a cooperative international endeavour that is currently carrying out work to define and perform the research and development needed to establish the feasibility and performance capabilities of the next generation of nuclear energy systems [1]. The GIF Technology Roadmap [2] identified the Gas-cooled Fast Reactor as the technology that associates the advantages of fast spectrum systems for long term resources sustainability, in terms of using of uranium and waste minimization (through fuel multiple reprocessing and fission of long-lived actinides) with those of the high thermal cycle efficiency and industrial use of the generated heat. The GFR is a fast neutron spectrum system that must be seen as a complement and alternative to the SFR deployment, which benefits from a more mature technology [3]. Either fast or thermal reactor systems may benefit from the system of a partially moveable reflector incorporated in the design, since the significant adjustable leaks of neutrons may be used to control reactivity in the case of accident managing. In a fast neutron spectrum, due to the smaller transport cross-section, the migration area of neutrons is exceptionally large, and thus the possibility of reactivity control by the movable reflector appears to be a promising additional safety solution. In this paper we are presenting the results of a neutronic study of the GFR reactor core design developed by CEA (Commissariat à l'énergie atomique et aux énergies alternatives) and specified in GoFastR documents [4]. The worth of control rods at

several insertions coupled with the reflector positions were investigated. Parameters like k_{eff}, neutron flux distribution and local k_{eff} were studied and graphically interpreted. Apart from the mentioned ones, some additional parameters were investigated such as the mean free path, the average number of neutrons per fission event (nubar) and the effective fraction of delayed neutrons.

2. Material and methods

Due to the large computational complexity, a stochastic multigroup approach utilized by the SCALE6.1.1 system [5] was used partially with comparative calculations performed by MCNP5 v1.6 [6]. SCALE is a comprehensive modeling and simulation suite for nuclear safety analysis and design that is developed, maintained, tested and managed by the Reactor and Nuclear Systems Division (RNSD) of Oak Ridge National Laboratory (ORNL). SCALE provides a comprehensive, verified and validated tool set for criticality safety, reactor physics, radiation shielding, radioactive source term characterization, and sensitivity and uncertainty analysis. The KENO-VI module was chosen as a Monte Carlo criticality program used to calculate k_{eff} of three-dimensional systems and other quantities included lifetime, generation time, energy-dependent leakages, energy and region dependent absorptions, fissions, flux densities and fission densities. All the KENO-VI calculations were performed using the 238 group ENDF/B VII.0 data libraries. For cell data processing a cylindrical multiregion cell with an equivalent radius of helium area was used and a smeared region was created. A difference was observed in the values of excess reactivity between continuous (CE) and multigroup (MG) calculations, which may have been caused by the complicated multiregional cylindrical geometry of fuel pins in the triangular lattice. These computational complications are connected with the strong and different neutronic-physical properties represented by the absorption cross sections of liner materials. MCNP is a general-purpose Monte Carlo N–Particle code that can be used for neutron, photon, electron, or coupled neutron/photon/electron transport, including the capability to calculate eigenvalues for critical systems. The code treats an arbitrary three-dimensional configuration of materials in geometric cells. Pointwise cross-section data are used. Important standard features that make MCNP very versatile and easy to use include a powerful general source, criticality source, and surface source; both geometry and output tally plotters; a rich collection of variance reduction techniques a flexible tally structure and an extensive collection of cross-section data. For the MCNP5 calculations presented in this paper continuous energy ENDF/B VII.0 data libraries were prepared using the NJOY99 [7] code. Two Fortran utilities had been developed for SCALE results post-processing. The first one was designed for mesh flux processing and the second one for the local k_{eff} calculations. Both parameters are graphically illustrated. To determine the deviation between the different codes used in this study either continuous calculations have been performed for the basic geometry model. Concerning the excess reactivity the deviation between the two codes was 40.65 pcm for the CE case, which is at the uncertainty level of the Monte Carlo calculation. For the basic geometry model with the safety control rods above the core, the SCALE multiregion calculation caused the reactivity increase by 328.97 pcm, which is an acceptable value for such a design study. Taking into account that MCNP uses continues energy data libraries and KENO-VI uses MG method, the agreement between the two codes can be concluded as satisfactory. The figure of merit is the quantity used to characterize the performance of the system and method. The evaluation of this parameter helped us to choose the most appropriate calculation method for the analysis presented in this paper. The definition used for the Figure of Merit evaluation is shown in equation (1).

$$FOM = \frac{1}{T\sigma^2}$$
(1)

Table 1. Figures of Merit for the different calculation methods

Calculation method	Calculation time [min]**	Number of proccessors	σ^2	FOM	Relative FOM
MCNP	8550	12	0.00004	79099.42	1.00
SCALE CE	1136.5	1	0.000059	252770.6	3.20
SCALE MG	323.5	1	0.000059	888017.8	11.23

* Computer system configuration was not the same for different codes ** The calculation time for MCNP was obtained by multiplication of the calculation time for all processors by the number of processors

The Figures of Merit for different calculation methods are presented in the Table 1. The highest FOM value was achieved in the case of the SCALE multigroup approach, hence this method was selected for the further calculations.

Determination of local k_{eff} is based on the methodology described in the SCALE manual. Matrix k_{eff} calculations provide an alternative method of calculation the k_{eff} of the system. This method is based on calculating the fission production matrix by subroutine MATRIX in SCALE6.1. The fission production matrix is defined as the number of next-generation neutrons produced at position index J per neutron born at position index I. Collection and summation of these fission production matrices from all positions over the investigated source position represents the local k_{eff} of this source position [5].

3.   Geometry and material model description

The 3D hexagonal models of GFR-2400 MWth core were prepared in the SCALE and in MCNP5 on the basis of the carbide fuel pin type core design developed by CEA. The core model is composed of inner and outer heterogeneously modeled fuel regions with different Pu contents. The inner part consists of 264 and the outer one of 252 fuel assemblies. The control rod system is composed of 13 Diverse Safety Devices (DSD) and 18 Control and Safety Devices (CSD) with the same material composition of B_4C (90% of ^{10}B). The rod follower is made of a structural material (containing SiC) which was also implemented into this model. The initial or basic calculation core state refers to the state where all control rod assemblies are positioned at the top edge of the fuel part. The core fuel region is surrounded by six rings of Zr_3Si_2 reflector assemblies. The 3D cross-sectional view of the GFR core model from the SCALE system is shown in Fig.1a.
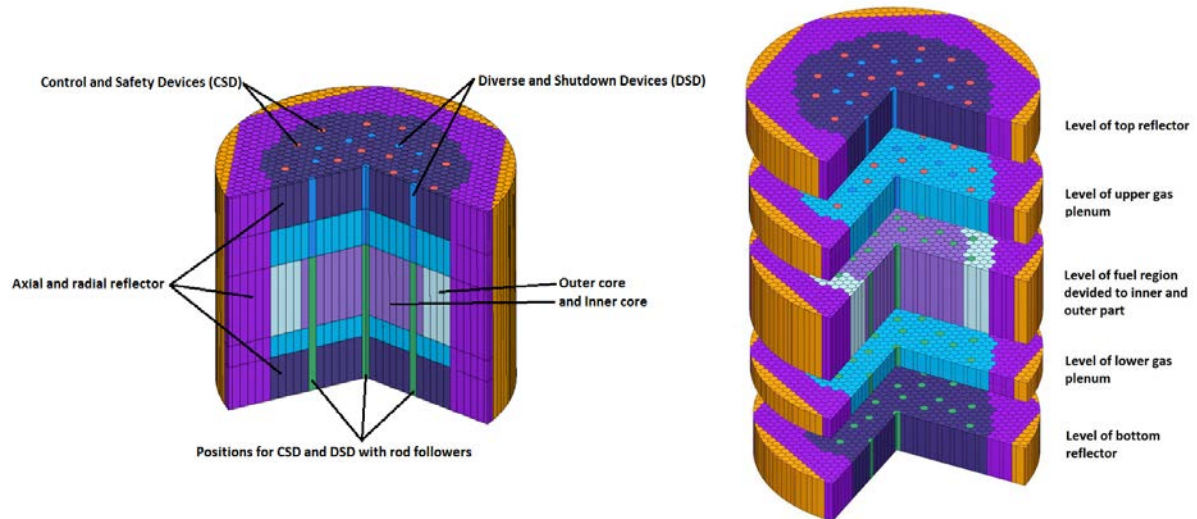
FIG. 1. a) 3D cross-sectional view of GFR reactor b) Axial configuration of the core

This reactor design is a helium-cooled system with a gas pressure of 70 bars operating with an average coolant temperature 913 K at nominal state. The fuel assemblies have hexagonal geometry definition, as it can be seen in Fig.1a. The reactor core consists of homogeneously modeled bottom and top axial reflector, lower and upper gas plenum and as mentioned above, a heterogeneously modeled fuel region. The axial configuration of the fuel assemblies and the core are presented in Fig.1b. The 165 cm long fuel region consists of an appropriate amount of fuel pins, silicon-carbide

wrapper and helium gap separating the bordering fuel assemblies. Fuel pins were defined as a fuel pellet made of UPuC with a temperature of 1263 K, the helium gap has 10 bar pressure and a temperature of 1263 K. The fuel cladding is composed of silicon-carbide. In this model also tungsten and tungsten-rhenium liners are used with a common temperature 913 K.

4. Definition of the calculation cases

The initial state of the reactor is in this paper defined as a reactor in nominal operation conditions, where all structural materials, fuel and coolant have nominal temperature and pressure as presented in Table. 2. The CSDs and DSDs are positioned in the upper edge of the fuel, marked as h=165cm (the so-called "all up"). For the initial state Doppler and void coefficient's calculations were performed, where in the Doppler case the fuel temperature was changed to $T_D = 2273$ K [8], which is a temperature exceeding the critical temperature of cladding failure. In the void case the nominal pressure of the coolant varied in a range from of $P_N = 70$ bar to $P_V = 1$ bar.

Table 2. Parameters for the Void and Doppler effects calculations

State	Fuel T (K)	Struc. Materials T (K)	Coolant P (bar)	CSD, DSD position h (cm)
Nominal	1263	913	70	165
Void	1263	913	1	165
Doppler	2273	913	70	165

The worths of CSDs and DSDs was investigated for the given groups configuration. Due to the one-sixth symmetry of the reactor core, only unique devices were investigated separately. The axial position of those devices and groups of devices was in the core geometry set up to the lower edge of the fuel (h=0 cm, the so called "down"). For the selected CSD also the integral characteristic (S-curve) was calculated. The applied numbering system for CSDs and DSDs is shown in Fig. 2. The reactivity worths of devices and groups of devices was calculated for CSD 2,3,10,11; DSD 0,4,5; CSD 1-6 group, CSD 7-18 group, CSD 1-18 group and DSD 0-12 group. Integral characteristics were calculated for CSD 2 and DSD 0.
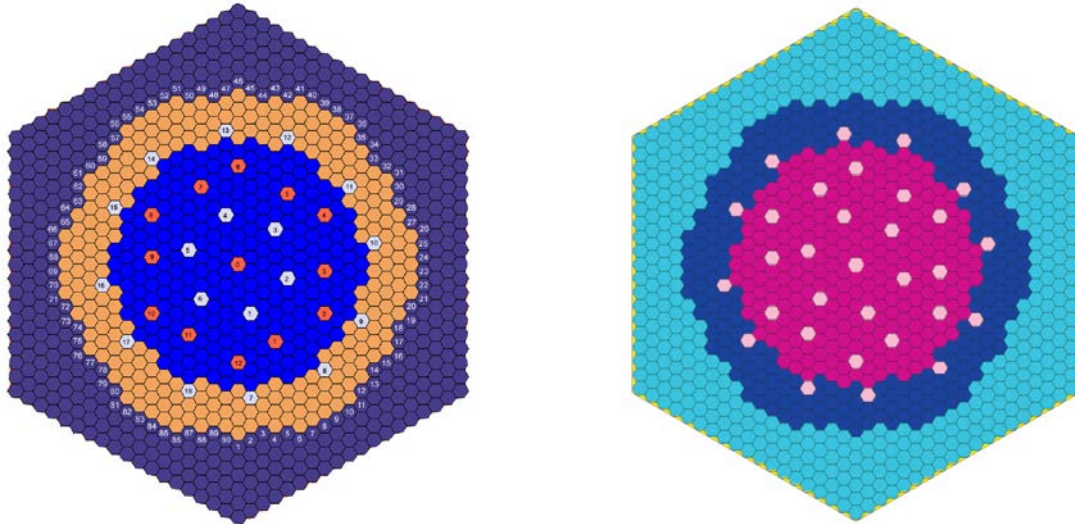
FIG. 2. a) Horizontal cross-sectional view of the GFR core model with blue inner fuel core, orange outer fuel core, red DSDs numbered from 0 to 12, white CSDs numbered from 1 to 18 and purple reflector b)The appropriate MCNP core model

The worth of reflector withdrawal was investigated for different reflector assembly configurations, but in this paper only the most promising solutions are presented. The removed assemblies were dropped to the lower edge of the fuel part. The configuration of the investigated

reflector groups was based on the results of the local k_{eff}, where at the beginning the integral worth characteristic of one reflector assembly was calculated. In this article two configurations are presented. The reactivity worth and the related parameters were investigated for the first ring of reflector assemblies around the core and for six groups per six assemblies symmetrically placed around the core (positions 4-9;19-24;34-39;49-54;64-69;79-84).

5. Results

The results of the Void and Doppler calculations are presented in Tab.3. The k_{eff} for each computational state is presented with its related standard deviation and the reactivity was calculated as a relative deviation of k_{eff} from one $\rho = \dfrac{k_{eff}-1}{k_{eff}}$. The Doppler constant (DC) was defined and computed using the following equation (2) $DC = \dfrac{\Delta\rho}{ln\left(T_2/T_1\right)}$.

$$DC = \frac{\Delta\rho}{ln\left(T_2/T_1\right)} \qquad (2)$$

Table 3. The results of the Void and Doppler calculations

Doppler calculation $P_{coolant}$= 70 bar					
T_{fuel} (K)	k_{eff}	σ_{std}	ρ (pcm)	$\Delta\rho$ (pcm)	DC
2273	1.012937	0.00006	1277.18	-638.99	1087.44

Void calculation T_{fuel} = 1263 K				
$P_{coolant}$ (bar)	k_{eff}	σ_{std}	ρ (pcm)	$\Delta\rho$ (pcm)
1	1.02294	0.000057	2242.56	326.39

The behavior of the defined system, which is caused by the change of basic parameters, corresponds to the theoretical assumptions. In the Doppler case, the decrease in k_{eff} represents the negative reactivity feedback, and in the void case, the increase in the k_{eff} corresponds to the positive reactivity change. The results of the excess reactivity and the calculations of the control rods worth are shown in Table 4. The obtained average mean free path of the system was in all cases in the range from 5.61 to 5.97 cm, where the minimum corresponds to the case, where all safety and control devices were fully inserted and the maximum to the case with the outer ring of CSDs inserted to the core. The average number of neutrons per fission event was calculated to 2.91 and this value did not change significantly from case to case. The effective fraction of delayed neutrons was calculated by MCNP5 using the adjoint-weighted point kinetics method [9]. The obtained value for the case with the CSDs and DSDs outside the core was 381 ± 7 pcm.

Table 4. Excess reactivity and control rod worth

Identifier	KENO-VI - CE/MG				MCNP5 - CE				ρ_{KENO} - ρ_{MCNP} [pcm]
	h [cm]	*k_{eff}	ρ [pcm]	**$\Delta\rho$ [pcm]	*k_{eff}	ρ [pcm]	**$\Delta\rho$ [pcm]		
All up -CE	165	1.019072	1871.5	0.00	1.01865	1830.85	0.00		40.65
All up - MG	165	1.021535	2108.10	0.00	-	-	-		328.97
All down	0	0.903204	-10716.95	-12825.1	0.90477	-10525.33	-12356.18		-191.63
CSD 2	0	1.018239	1791.23	-316.87	1.01557	1533.13	-297.73		258.10
CSD 3	0	1.018297	1796.82	-311.28	1.01561	1537.01	-293.85		259.82

CSD 10	0	1.018833	1848.49	-259.62	1.01601	1575.77	-255.08	272.72
CSD 11	0	1.018793	1844.63	-263.47	1.01597	1571.90	-258.96	272.74
CSD 1-6	0	1.005614	558.36	-1549.84	1.00362	360.69	-1470.16	197.57
CSD 7-18	0	0.9746	-2606.19	-4714.3	0.97275	-2801.34	4632.19	195.14
All CSD	0	0.941939	-6163.98	-8182.09	0.94176	-6184.17	8015.02	20.18
DSD 0	0	1.018153	1782.93	-325.168	1.01558	1534.10	296.76	248.84
DSD 4	0	1.018312	1798.27	-309.832	1.01563	1538.95	291.91	259.32
DSD 5	0	1.018220	1789.39	-318.705	1.01549	1525.37	305.48	264.03
DSD 1-12	0	0.977587	-2292.68	-4400.79	0.97685	-2369.86	4200.72	77.18
All DSD	0	0.976110	-2447.5	-4555.57	0.97529	-2533.61	-4364.46	86.14

* σ_k was 0.00006 for KENO VI and 0.00004 for MCNP5.   ** The range of $\sigma_{\Delta\rho}$ was 5 to 9 pcm

The largest deviation between MCNP5 and KENO VI was observed in the case where all devices were above the core ("All up") and it was 328.97 pcm. The deviations for cases where the whole group of CSDs or DSDs was inserted were 20.18 pcm and 86.15 pcm respectively. The total worth of all safety devices was calculated to 12825.1 (12356.18 pcm), the worth of the CSD devices 8182.09 (8015.02 pcm) and the worth of DSD devices 4555.57 pcm (4364.46 pcm). The determination of the integral characteristic of the control and diverse safety devices was performed separately in both codes. The obtained results may serve for verification of the theoretical assumptions and of the correctness of the created geometry model. The characteristics were calculated in 12 steps, where a steady state criticality calculation was performed in each step. Due to the very similar trends, only results for the central diverse safety device (DSD 0) are shown in Fig. 3. To fit the results a third degree polynomial was used for both curves.
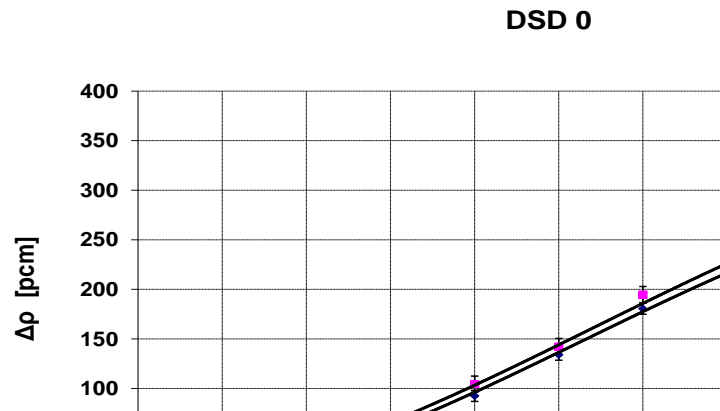
DSD 0

FIG. 3. The integral characteristic of the diverse safety device DSD 0

The local k_{eff} values defined above for the initial reactor state defined in chapter 4 ("All up") are graphically presented in the left side Fig. 4. The numerical values are also shown in the one-sixth of the reactor core. For comparison, the spatial distribution of the normalized neutron flux calculated approximately in the middle of the active height of the core is demonstrated. The figures are based on SCALE calculations.
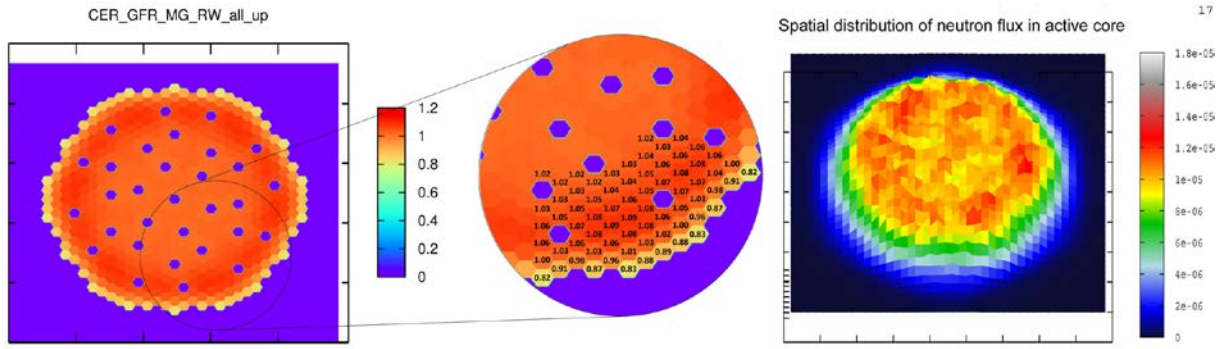
FIG. 4. Local k$_{eff}$ values and the spatial distribution of the neutron for "All up" case

In the following case, see Fig. 5, all control and safety rods are fully inserted in the active core ("All down"). Although the reactor is shut down, local areas were the local k$_{eff}$ values exceed number one (hot spots), can be distinctly seen, and they are represented by dark red colour in the local k$_{eff}$ figure. These areas also correlate with the places of the highest neutron flux represented by the red colour located in the right figure.
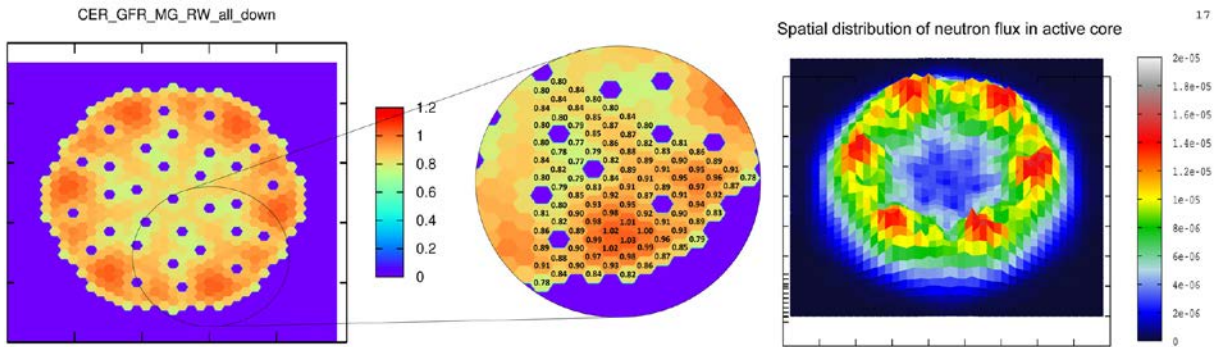
FIG. 5. Local k$_{eff}$ values and the neutron flux spatial distribution of the "All down" case

The results for the further investigations, where six groups of six assemblies symmetrically placed around the core were withdrawn are shown in Fig. 6. The reactivity decrease caused by the removal of the reflector configuration (36 assemblies) from the initial reactor state called "All up" was 466.5 pcm where the average reactivity worth of a single assembly was calculated to 12.96 pcm. The additional reactivity worth of this reflector configuration to the case called "All down" without reflector removal was calculated as 1345.31 pcm. The local k$_{eff}$ values are reduced in the left hot spot area by 0.01 on average. In this case the maximum of the normalized neutron flux in the area of interest is decreased as well.
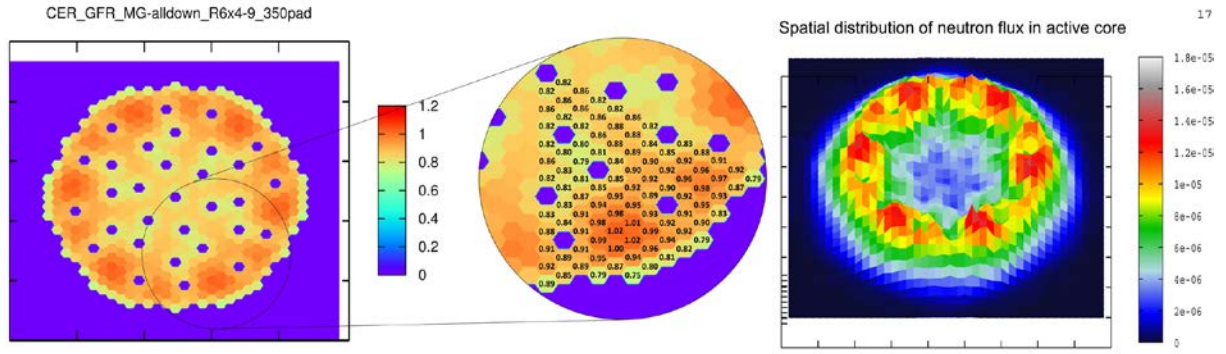
FIG. 6. Local k$_{eff}$ values and the spatial distribution of the neutron for "All down" case with six groups of six reflector assemblies withdrawn

The situation after withdrawal of the first ring of reflector assemblies (90 assemblies) in the case of control and safety rods inserted in the reactor core is graphically interpreted in Fig. 7. The reactivity worth coupled with reflector ring removal in the reactor state with withdrawn safety devices reached the value 1100.75 pcm. The average reactivity worth of a single assembly reaches the value 12.23 pcm. In the system with control rods inside the core ("All down") the influence of the reflector ring withdrawal was 2581.57 pcm. In this case, also the local k$_{eff}$ values were reduced forming a smaller hot spot. The flux figure shows that the neutron flux was significantly pushed from the outer part to the inner part of the reactor core.

FIG. 7. Local k$_{eff}$ values and the spatial distribution of the neutron flux for "All down" case with the first ring of reflector assemblies withdrawn

The Fig. 8 depicts the neutron flux mesh tally values obtained by MCNP calculations. The first figure from the left shows the horizontal spatial distribution of the core mid-height in the case of all control rods fully inserted in the core. The second figure corresponds to the case with six reflector groups withdrawn. The last figure presents the withdrawal of the first ring of reflector assemblies. The same hot spots areas were identified in both codes, so we can claim that these results of MCNP are in a good accordance with the results obtained by the SCALE system.
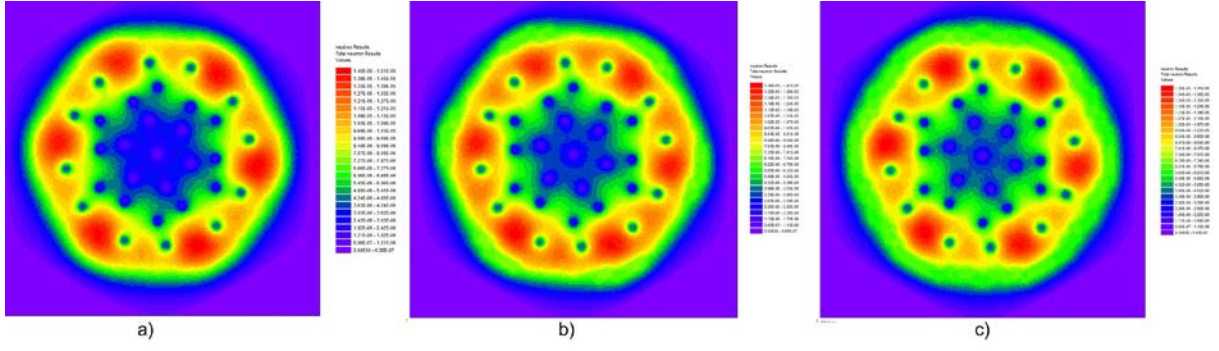
FIG. 8. MCNP Mesh Tally Plot - normalised value of neutron flux a) "All down" case b) "All down" case with the six reflector groups withdrawn c) "All down" case with whole ring of reflector assemblies withdrawn

In the last case, the control rods were replaced by black absorber and were fully inserted in the core. This configuration represents the theoretical maximum value of reactivity that can be inserted to the core. The results are shown in Fig. 9.
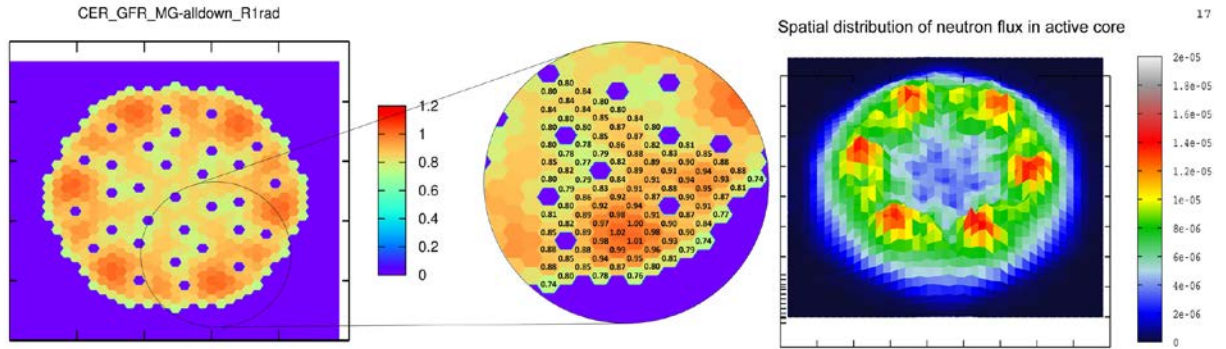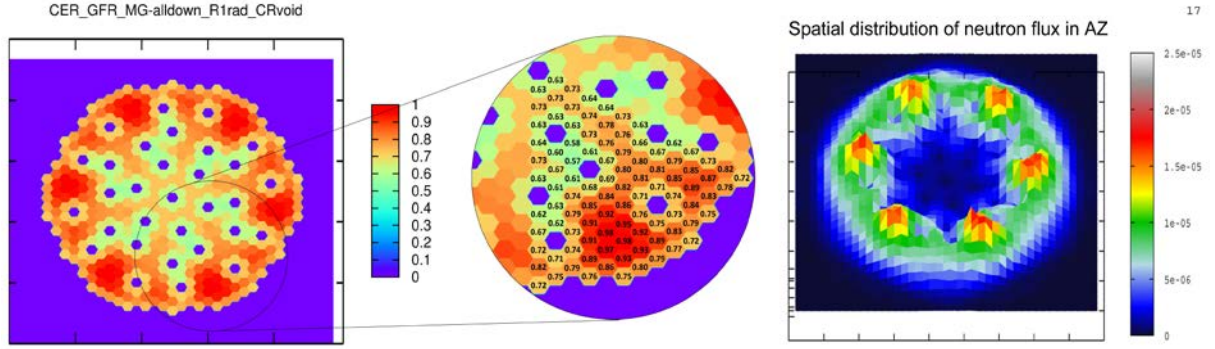

FIG. 9. Local k_{eff} values and the spatial distribution of the neutron flux for black absorber "All down" case with the first ring of reflector assemblies withdrawn

6.   Conclusion

Concerning the excess reactivity and the control rods worth the results show the large shadowing and anti-shadowing effects in the core. Moreover, either the CSD or the DSD devices are able to provide sufficient reactivity to shut down the reactor separately without requiring the other group of devices to be inserted to the core. An interesting finding is that if the central ring of CSD devices was stuck outside the core the outer ring would have sufficient negative reactivity to make the system sufficiently sub-critical. Due to the shape of the radial distribution of the neutron flux, which is mainly caused by a higher enrichment of the outer core, the worth of control rods in different radial positions do not differ significantly. The total worth of all control rods in this presented design reaches approximately the value of 32 *βeff* which is comparable with that in pressurized light water reactors. Based on the achieved integral characteristic of DSD 0, we can claim that the shapes of the curves are almost identical for both codes, however a slight shift can be observed which continued to grow for lower rod positions. This shift may be caused by statistical uncertainties but mainly by the differences between the CE and MG methods of MCNP and KENO. Finally, we can claim that the used computational methods are appropriate. For the system with the control rods above the core, the results were as we expected. The radial spatial distribution of the neutron flux was almost uniform, and the local k_{eff} values were lower only in the last ring of assemblies. In the next case, the control rods were fully inserted in the core. The graphic layouts of the results have highlighted several hot spots symmetrically distributed in the outer fuel zone. These results may indicate the existence of decoupled neutronic zones of the core, which may have originated from the higher Pu enrichment of the outer core and from the big distance between the control rods. In our case, the control rods were

modelled homogeneously and on the basis of the paper of Giradin [10] we expect a lower efficiency of the real heterogeneous control rod design. However, the possible existence of these zones would not be able to meet power flattening requirements associated to burnup and should be deeply investigated. The withdrawal of 6 reflector groups from the reactor in the initial state has demonstrated the possibility to insert additional negative reactivity to the active core (466.5 pcm), which is approximately equivalent to the worth of two control rods. In the situation when control rods were inserted in the core, the impact of the reflector withdrawal was demonstrated by changes of the local k_{eff} values in the left hot spot located opposite of the reflector group. This effect was observable to the level of five fuel rings; however, the influence was not sufficient. In the case of reflector ring withdrawal the reactivity worth achieved higher values (1100.75 pcm), which is equivalent to approximately four control rods. The presented efficiency of one control rod was better in the previous case, so we would conclude that six group's configuration might be a better solution for additional negative accidental reactivity insertion. From the local k_{eff} point of view, this configuration improved the situation in the right hot spot area, but no significant changes in the left hot spot were observed. The results of calculation with black absorbers show, that it is theoretically possible to reach local k_{eff} values smaller then one in hot spot areas. On the other hand, the real design may by limited by material and geometrical properties, which might be a topic of further investigations. The findings and results presented in this paper may serve as an auxiliary material for the future development of GFR and they may support the development of such an interesting design.

REFERENCES

[1] WALTAR E. ALAN., et al., "Fast Spectrum Reactors", Springer New York Dordrecht Heidelberg London, ISBN 978-1-4419-9571-1, DOI 10.1007/978-1-4419-9572-8, 2012

[2] UNITED STATES DEPARTMENT OF ENERGY, Energy Research Advisory Committee, Generation IV International Forum, "A Technology Roadmap for Generation IV Nuclear Energy Systems," 2002, Report GIF-002-00

[3] ANZIEU,P., STAINSBY, R., and MIKITIUK,K., "Gas-cooled Fast Reactor (GFR): Overview and perspectives", GIF Symposium - Paris (France) 9-10, 2009

[4] GOFASR, "GFR 2400 MWth pin core at start of GOFASTR", http://www.gofastr.org

[5] SCALE: "A Comprehensive Modeling and Simulation Suite for Nuclear Safety Analysis and Design",ORNL/TM-2005/39, Version 6.1, June 2011. Available from Radiation Safety InformationComputational Center at Oak Ridge National Laboratory as CCC-785.

[6] [MCNP] X-5 MONTE CARLO TEAM. "MCNP – A General N – Particle Transport Code, Version 5 – Volume I: Overview and Theory". Los Alamos, USA : Los Alamos National Laboratory, April 24, 2003 (Revised 10/3/05). LA-CP-03-0245.

[7] [NJOY] MACFARLANE. R.E., "Understanding NJOY", LANL USA, LNS015013 (2000)

[8] KATOH,Y., et al., "Assessment of Silicon Carbide Composites for Advanced Salt-Cooled Reactors", ORNL/TM-2007/168, September 2007, http://info.ornl.gov/sites/publications/files/Pub8156.pdf

[9] KIEDROWSKI,B.C.,BROWN,F.B.,WILSON,P.P.H., "Calculating Kinetics Parameters and Reactivity Changes with Continuous-Energy Monte Carlo" , 7/06, LA-UR- 10-2900

[10]   GIRARDIN,G., et al., "Development and characterization of the control assembly system for the large 2400 MWth Generation IV gas-cooled fast reactor", Annals of Nuclear Energy, Volume 35, Issue 12, December 2008, Pages 2206-2218

Safety design approach for JSFR toward the realization of GEN IV Sodium cooled fast reactor

S. Kubo[a], H. Yamano[a], Y. Chikazawa[a], Y. Shimakawa[b]

[a] Japan Atomic Energy Agency, O-arai, Japan

[b] Mitsubishi FBR Systems, Inc., Tokyo, Japan

Abstract. This paper describes the safety design approach for JSFR. To achieve safety goals for Generation IV reactor, design measures should be enhanced against design extension conditions including those for external events considering the lessons learned from the TEPCO's Fukushima Dai-ichi nuclear power plants accident. The current safety design approach for JSFR intends to meet the safety design criteria for Generation-IV SFR developed in the framework of the Generation-IV International Forum. Design extension conditions and related design measures are identified and selected with due consideration of the safety features of SFR. Design approach and measures for severe external events such as earthquake and tsunami, external missiles, failure to neutronic shutdown type events and failure to heat removal type events are shown. Several situations to be practically eliminated are proposed with possible design measures. Design approaches for sodium chemical reactions and fuel handling and storage systems are briefly described.

1. INTRODUCTION

The Generation IV International Forum [GIF] has been focusing on the development of a sustainable energy system for the next generation [1]. This paper describes the safety design approach for JSFR(Japan Sodium-cooled Fast Reactor) [2]. The JSFR, which is a conceptual SFR aiming at commercial use, covers power range of medium to large to satisfy its needs as sustainable base-load power supply. The safety approach was developed from the basis of that of Joyo and Monju and advanced features for prevention and mitigation of core damage are incorporated as built-in manner. The safety design for SFR has been implemented corresponding to the characteristics utilizing sodium as coolant and as fast neutron critical system. Moreover, taking lessons from the accident at the Fukushima Dai-ichi Nuclear Power Plant of Tokyo Electric Power Company [Fukushima Dai-ichi accident][3], safety improvement has been carried out to withstand severe conditions such as immense earthquake, tsunami, and long-term station blackout.

2. SAFETY DESIGN APPROACH

2.1 SAFETY DESIGN CRITERIA FOR GENERATION-IV SFR

The safety design criteria for Generation-IV SFR [GIF-SFR-SDC] developed in the framework of the GIF is used as basis of safety design of this study [4]. GIF-SFR-SDC refers to the structure of IAEA SSR 2/1 and is formulated as consistent with GIF's basic safety approach and with the aim of achieving the safety and reliability goals of GIF. Specific technical features of SFRs as well as the

latest knowledge such as R&D results for innovative technologies and lessons learned from the Fukushima Dai-ichi accident are incorporated. It should be noted that the following criteria, in which general characteristics of SFR are reflected, are introduced as design measures for design extension conditions [DECs] corresponding to the fourth level of defence in depth. It is important to establish design concepts to meet these criteria.

- Passive or inherent reactor shutdown capabilities
- Mitigation provision to avoid large mechanical energy release during a core degradation progression and means for decay heat removal of a degraded core
- Decay heat removal system with passive mechanism and diversity, which can be available even under extreme external hazards and their consequences such as long-term loss of all AC power supplies

2.2 LESSONS LEARNED FROM TEPCO'S FUKUSHIMA DAI-ICHI NPP'S ACCIDENT

The Fukushima Dai-ichi accident was caused by severe earthquake accompanied with severe tsunami in the Great East Japan Earthquake on 11 March 2011. Generation IV SFR shall be designed to avoid significant radioactive materials release to the environment even under such severe conditions. Any sort of severe external events beyond design basis selected as a result of siting evaluation, e.g., aircraft crash, volcano ash fall, strong wind, heavy snow fall, extreme temperature, external explosion and fire, flood as well as earthquake and tsunami shall be considered in design and accident management for reactor core, fuel handling and storage systems.

JSFR adopts seismic isolation technology to ensure integrity of the thin-walled structures of sodium contained components under severe earthquake condition [5]. Since the reactor building is installed on the seismic isolation devices, i.e., laminated rubber bearings, seismic loads on the sodium contained components, those of primary and secondary coolant systems, fuel handling and storage systems and sodium auxiliary systems, in the reactor building can be reduced. The safety systems for reactor shutdown, decay heat removal and containment are also seismically isolated. Therefore, it is considered the JSFR has comparable structural margin to the current LWRs in Japan.

Basic countermeasures against tsunami or flood are to have sufficient site elevation and to provide dike in order to prevent submersion of the reactor building. In addition waterproof measures will be applied for rooms for safety grade electricity facilities and for those components containing sodium such as dump tanks, which are on lower level of the building. Natural circulation heat removal by air cooling is effective under loss of electric power since it doesn't need driving power for motors and/or pumps and sea or ground water cooling systems, which shall be located on lower level. Main decay heat removal systems[DHRSs] for JSFR, one DRACS [Direct Reactor Auxiliary Cooling System] and two PRACSs [Primary Reactor Auxiliary Cooling Systems], are designed to maintain core cooling for long term even under long term loss of AC power condition after severe earthquake and tsunami.

Since the sodium-air heat exchangers of decay heat removal systems are directly connected to the surrounding environment of the plant, they might be affected by severe external events such as aircraft crash, volcano ash fall, strong wind, heavy snow fall, extreme temperature, external explosion and fire. Design measures, e.g., reinforcement of air stacks for strong wind, physical barriers and separation for external missiles, are required to protect the sodium-air heat exchangers against severe external events.

As mentioned above, taking the lesson-learned from the Fukushima Dai-ichi accident into account, it is required to prevent core damage and significant radioactive materials release even for severe external events. Reinforcement of decay heat removal measures is especially important to cope with them [6].

2.3 POSTULATED DESIGN EXTENSION CONDITIONS AND DESIGN MEASURES

For DECs, the design measures are those for "prevention of core damage" and for "mitigation to ensure containment function" [see Figure 1]. To determine the plant conditions postulated as a DEC, e.g., the core degraded state, the time margin to core damage and number of applicable measures need to be considered. Built-in design measures are to be incorporated for DEC, however, application of possible accident management measures is considered in the plant design in advance as a supplemental way.
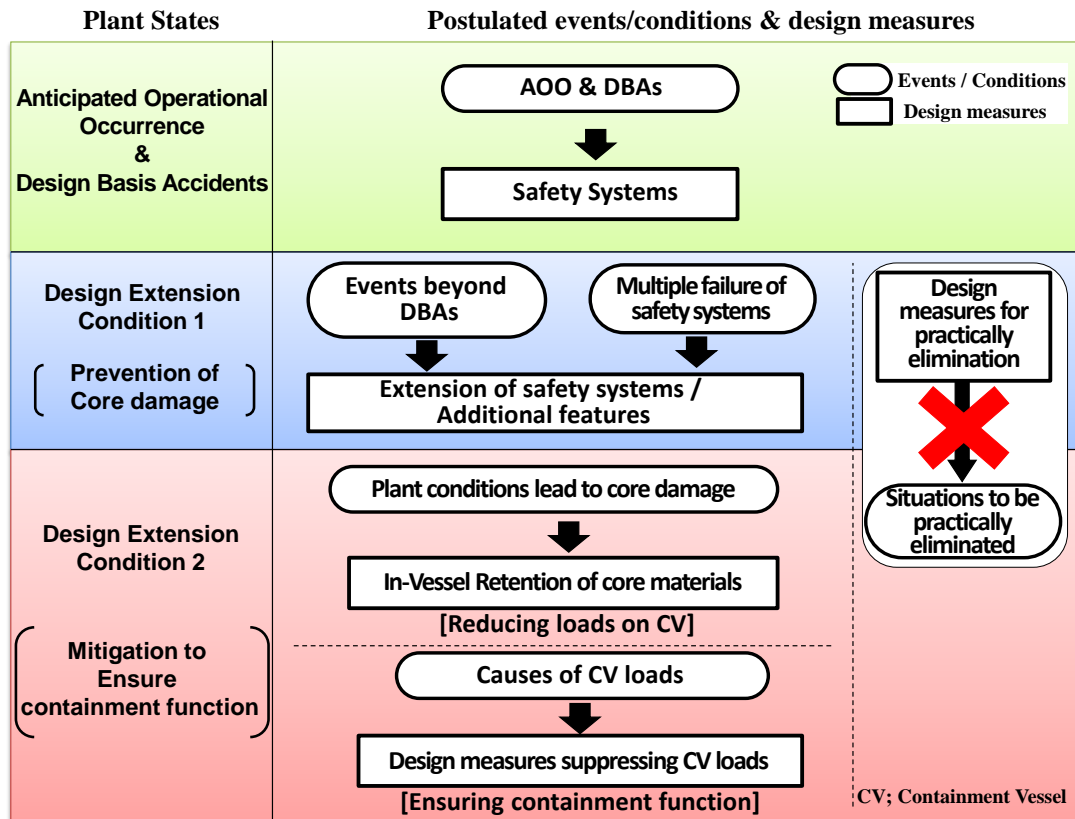
Figure 1 Plant states and design measures for JSFR

SFR DEC events can be grouped into the following two categories based on the characteristics of SFR and PSA studies [7][8].

1) failure to shutdown the reactor following an off-normal initiating event [ATWS type]

- · loss of flow with failure to scram,
- · overpower transient with failure to scram, and
- · loss of main heat removal with failure to scram.

2) failure to heat removal from the core following an initiating event with scram [LOHRS type]

- · loss of primary coolant flow (flow path becomes disrupted),
- · loss of primary coolant level (core becomes uncovered), and
- · loss of heat sink

As an SFR is operated under low pressure conditions, close to atmospheric pressure and temperatures far below the boiling point, coolant leakage or pipe break does not lead to the type of loss of coolant accident as in an LWR with depressurization, coolant boiling and the loss of cooling capability. Therefore, an emergency core cooling systems for coolant injection under high and low pressure

conditions, as used in the LWR, is not necessary in an SFR. The only requirements for SFR core cooling are the maintenance of the sodium coolant level above the reactor core in the reactor vessel along with sufficient heat removal capability. Primary coolant leakage doesn't cause pressure build up inside the containment vessel with adequate design for mitigation of leaked sodium combustion, i.e., holding leaked sodium by guard vessels and guard pipes with inertized atmosphere. In case of ATWS type events, degraded core materials can be retained inside the reactor vessel with adequate design, i.e., prevention of severe mechanical energy release and in-vessel core catcher. Thus, SFR can be designed to have less impact on the containment with measures for in-vessel retention of degraded core materials for ATWS type events, maintaining core cooling for LOHRS type events, and mitigation of sodium combustion (sodium-concrete reaction should be also prevented). In this case, main role of the containment is to prevent significant release of gaseous and volatile fission products. This is basic idea of the JSFR design measures for DECs [see Figure 2].

In ATWS type events, in-balance of power and cooling might causes core damage within a shorter time period. Passive shutdown mechanism such as SASS [Self Actuated Shutdown System] can prevent core damage even under such conditions. In addition mitigation of core damage is considered in design because of the shorter time period to core damage and of the potential mechanical energy release, which might appear in the core damage situations.

On the other hand, in the loss of heat sink type events of LOHRS, since the decay heat is at a few percent of the nominal power, the temperature of the reactor coolant system, including the core, coolant and reactor coolant boundary increasing slowly during a longer time period. Therefore there would be sufficient time margin to make recovery action for failed DHRSs and/or implementation of back up cooling measures. If no heat sink is available, the coolant boundary failure might occur due to creep damage anywhere in the primary and secondary coolant systems. A multiple failure might cause the containment bypass. Then the system temperature reaches sodium boiling point and sodium vapor is released into the containment. This might cause significant thermal loads not to be endured by the containment. Such situations shall be practically eliminated by design measures for enhancing core cooling capability. Concerning the loss of primary coolant flow type events of LOHRS (flow path becomes disrupted), total loss of flow paths to the heat sink has similar consequences as the loss of heat sink type events. Therefore, this shall be also practically eliminated by design measures.

In the loss of primary coolant level type events of LOHRS if the core becomes uncovered, it is impossible to avoid core melt and significant radioactive materials release into the containment atmosphere. The containment function under such situation would not be sufficient to mitigate the radioactive materials release to the environment below the level that emergency response is required for. Thus the design measures shall be such that core uncoverage is practically eliminated.
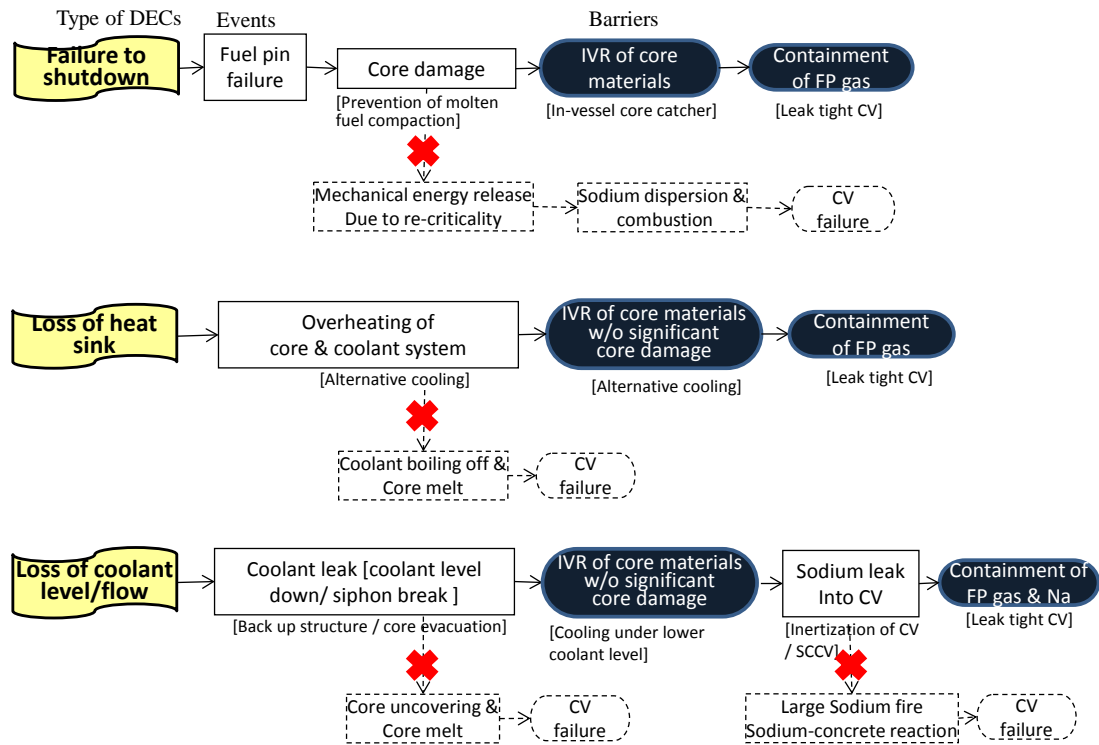
[ ]; Design measures, IVR; In-Vessel Retention, CV; Containment Vessel, FP; Fission Product, SCCV; Steel plate reinforced concrete CV

Figure 2 JSFR design approach for mitigation to ensure containment function

2.4 SITUATIONS TO BE PRACTICALLY ELIMINATED

Mitigation of the consequences of some accident situation should be excluded by design where feasible, because the implementation of additional mitigation devices, or the R&D necessary for demonstrating their effectiveness, may be prohibitively expensive or difficult to prove effective under DECs. However, for situations that are physically possible, the design process has to consider, within economic and physical constraints, all situations independent of their probability. Several situations to be practically eliminated, which are tentatively selected based on the design characteristics of SFR, are as follows. Design measures are investigated and provided in order to prevent occurrence of the following situations in JSFR design study.

· Abnormal reactivity insertion leading to prompt criticality (Large bubble ingress into the core, core configuration change due to beyond design basis earthquake, core displacement due to significant failure of the core support structure)

· Severe mechanical energy release due to coherent sodium boiling or molten fuel compaction, failure of decay heat removal from degraded core in ATWS type events

· Significant core damage in LOHRS type events

· Large scale sodium spray combustion inside the containment

· Hydrogen accumulation and deflagration/detonation due to sodium-concrete reaction inside the containment

· Containment bypass due to large scale rupture of steam generator tubes and subsequent failure of secondary coolant system boundary inside the containment

· Fuel melt in the fuel storage system

3. DESIGN MEASURES FOR INDIVIDUAL DEC

3.1 FAILURE TO SHUTDOWN AND ABNORMAL REACTIVITY INSERTION

The reactor core of JSFR, which has a homogeneous configuration aiming at achieving higher burn-up, longer cycle length and fuel cycle compatibility [9], is designed to have inherent reactivity feedback characteristics with negative power coefficient. The operation temperature range is set sufficiently below the coolant boiling temperature so as to avoid coolant boiling against anticipated operational occurrences and DBAs. If the plant state deviates from operational states, the safe reactor shutdown is achieved by automatic insertion of control rods. Two active reactor shutdown systems are provided. Failure of active reactor shutdown is assumed as DEC. The passive shutdown capability is provided by SASS, which is a passive de-touch mechanism of a control rod installed in the back-up reactor shutdown system. The followings are good points of SASS [10].

- Effective against all types of failure to shutdown events; loss of flow, loss of heat sink, over power
- Provide sufficient irreversible negative reactivity
- No interruption on normal operation
- Easy to reset after actuation
- Provide testability

Since mechanical control rod jamming might be major cause of scram failure, stiff core restraint and core support structures are equipped in order to ensure the control rod insertion even under severe earthquake.

As DEC, core disruptive accident is assumed. In order to prevent severe mechanical energy release which might cause containment function failure, sodium void worth is limited below 6 dollars and molten fuel discharge capability is utilized by FAIDUS. In-vessel core catcher is installed at the bottom of the reactor vessel in order to achieve In-Vessel Retention (IVR) [11].

The causes of rapid positive reactivity insertion shall be prevented by design. For instance, significant core configuration changes due to horizontal and/or vertical motions of fuel assemblies under beyond design basis earthquake are prevented by the stiff core restraint and support structures. Relative displacements between the control rods and the core are also limited by reinforcement of the upper internal structure, which supports the control rods.

3.2 FAILURE TO REMOVE HEAT FROM THE CORE

Adopting passive cooling feature utilizing natural circulation of sodium is crucial for SFR to remove decay heat after a reactor shutdown. JSFR design utilizes the characteristics of loop-type to realize natural circulation performance to the full extent. The DHRS does not depend on power sources. The only movable devices to be controlled are the dampers installed at the inlets and outlets of air coolers. The DHRS can cover entire range of the transient from just after the reactor shutdown to the cold shutdown state without particular operations such as switching to other systems or changing valve positions except controlling the damper opening. Moreover it enables, as an accident management, manually adjusting the damper opening to maintain the cooling performance even under DC power depletion for instrumentation and control as a consequence of a long-term loss of AC power. Furthermore, adopting diverse cooling facility as well as physical separation and protection of the DHRS is considered to cope with severe plant conditions such as external missiles (air craft crash, volcano ash fall etc.), strong winds, heavy load drop and fires on the roof of reactor vessel. The air coolers of DHRSs are physically separated and protected by the walls of reactor building against air craft crash so that at least one of these doesn't lose its functions. Protective walls are provided for DRACS against heavy load drop on the roof area of reactor vessel. In addition alternative cooling measures such as gas cooling of the water side of steam generators, additional cooling circuit to the sea water, are available [see Figure 3].
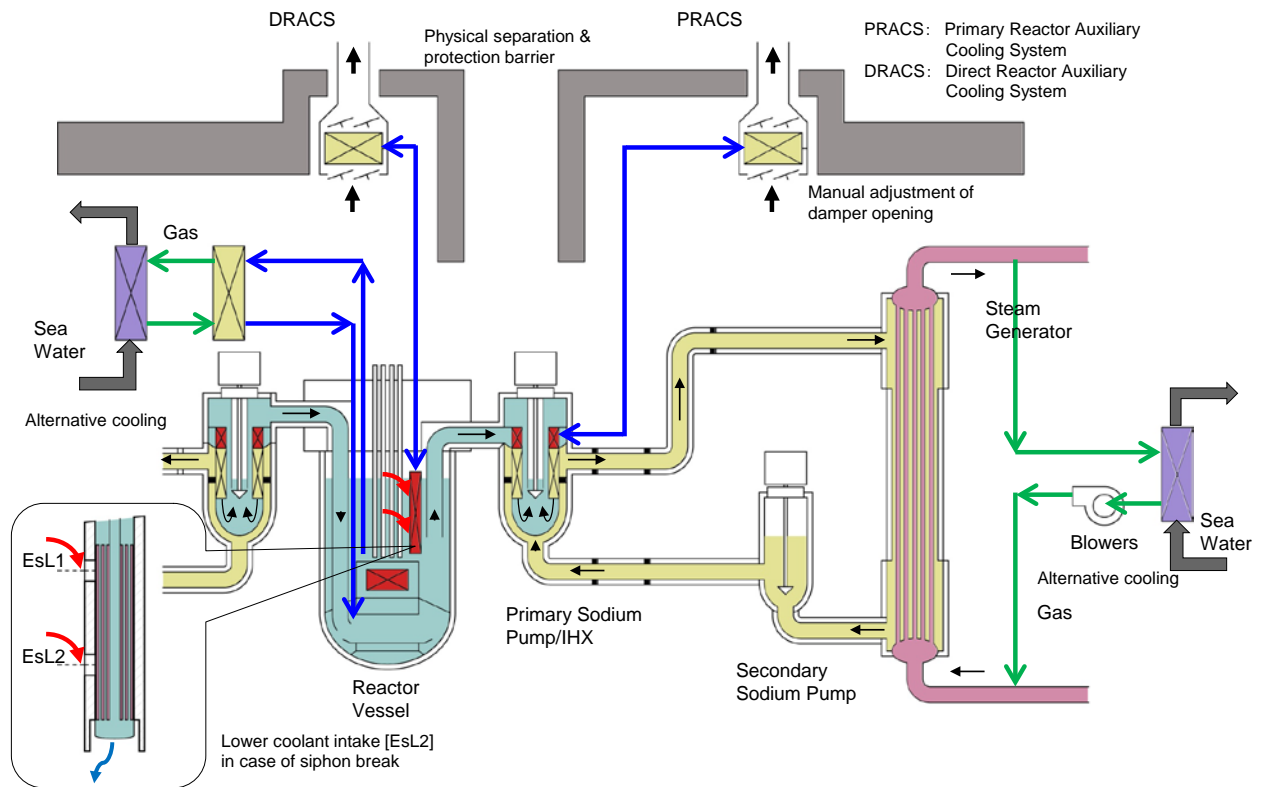
Figure 3 JSFR design measures for enhancing decay heat removal function

Double boundary concept [10] is introduced as a basic measure to prevent the loss of coolant level and the loss of coolant flow path. Although the reactor vessel and the guard vessel are to be designed, manufactured, installed and inspected in the highest design standards so that double leaks can be practically eliminated, whole core evacuation to the external vessel storage tank (EVST) is considered as an accident management. Since JSFR has two-loop reactor coolant system, the primary coolant flow path might be lost in the primary loop side, i.e., siphon break might happen in case of double leak in the primary loop side. As a measure to cope with such situation, additional sodium inlets are introduced at a lower level of the in-vessel heat exchanger of DRACS [see Figure 3].

3.3 CONTAINMENT

The JSFR reactor building is steel-plate reinforced concrete structure, and the section designated for primary coolant system is designed as containment vessel [13]. Major threats to the containment are large-scale sodium leakage and fire, deflagration/detonation of accumulated hydrogen induced by sodium-concrete reaction or fuel debris-concrete interaction, and mechanical energy release as a consequence of recriticality. These threats have to be practically eliminated by design measures. The mechanical energy release and the fuel debris-concrete interaction are prevented by avoiding severe recriticality and by achieving IVR. In order to prevent the large-scale sodium leak and fire and the deflagration/detonation of accumulated hydrogen, inertization of the containment atmosphere can be a measure in addition to the double boundary concept. Furthermore, the containment vessel is designed to withstand the load induced by the decay heat from the gaseous and volatile fission products dispersed in the containment vessel, and latent heat from leaked sodium.

3.4 SODIUM CHEMICAL REACTIONS

Major safety concerns about sodium as the coolant toward commercialization are considered as 1) To ensure reliability of the sodium components aiming at higher plant availability, and 2) To prevent sodium chemical activity from becoming causes of core damage even under design extension conditions. As for the latter issue, it is required to mitigate influences both of design basis accidents

and design extension conditions about sodium leaks and sodium-water reactions so as not to affect core cooling.

1) Sodium leaks from the coolant boundaries and fires

Design basis leaks are determined based on the evaluated break sizes by the leak-before-break methodology, while double ended break of main pipes are assumed as design extension conditions. The double boundary concept is applied. The outer pipes are designed to withstand the double ended break of the inner pipes in DEC.

The sodium components are designed to withstand against severe external events such as earthquake and tsunami, external missiles as mentioned in section 2.2.

2) Sodium-water reactions in steam generators

Double-walled heat transfer tubes are developed in order to improve reliability of steam generators for JSFR [14]. The inner and outer tubes are designed not to make penetration cracks at the same point by any possible causes such as fretting, flow-induced vibration, DNB: departure from nucleate boiling oscillation and creep damage. Therefore possible initial water-steam leak rate into the secondary sodium is limited by flow resistance of the gap between the inner and outer tubes even if the leak might happen. In addition design measures to prevent the secondary coolant boundary failure such as leak detection, pressure relief, treatment of reactision products, water/steam blow, isolation and inertization of water-steam side are provided.

In the domain of DEC, simultaneous double ended break of large numbers of tubes shall be practically eliminated. Because it might cause severe damage on the secondary coolant boundary to lead severe consequences such as containment bypass, large scale sodium leak and fire. Thus, the steam generators including their internals have to withstand severe external events such as earthquake and tsunami, external missiles. Maximum leak condition to be postulated by internal causes shall be considered based on mechanistic evaluation of the leak propagation. The mechanisms of leak propagation are known as "wastage" and "overheating rupture" [15]. Both of them might happen in case of the detection and/or the isolation failure in the smaller initial leak rate range less than one double ended break. The leak propagation doesn't occur in the initial leak rate larger than one double ended break due to activation of rupture disks for pressure relief.

3.5 DEC FOR FUEL HANDLING AND STORAGE SYSTEMS

The fuel handling and storage systems of JSFR consist of sodium cooling EVST, spent fuel water pool, fuel handling machine, fuel transport machine and so on. The safety measures equivalent to that for nuclear reactor as described in the section 3.2 is applied for EVST as the sodium leak countermeasure and heat removal. For the spent fuel water pool the design measures will be equivalent to that for LWRs.

4. CONCLUSION

To achieve safety goals for the Generation IV reactor, design measures should be enhanced for DECs including those for external events considering the lessons-learned from the Fukushima Dai-ichi accident. The current safety design approach for JSFR intends to meet the safety design criteria for Generation-IV SFR developed in the framework of the GIF.

DECs and related design measures are identified and selected with due consideration of the safety features of SFR. The thin-walled structures of sodium contained components are designed to be protected against severe earthquake with help of reactor building seismic isolation.

Taking the fact that SFR core is not in the most critical configuration into account, two active shutdown systems and one passive activation mechanisim (SASS) are installed. In addition mitigation

of core damage is considered in design because of the shorter time period to core damage and the potential mechanical energy release, which might appear in the core damage situations. The design measures are void worth limitation, molten fuel discharge(FAIDUS) and IVR.

Concernig the core cooling after reactor shutdown, essential requirements regardless of the core condition, intact or degraded, are to fill the core with sodium and to circulate coolant to the heat sink. As SFR is operated under low pressure conditions owing to physical properties of sodium, i.e., high boiling temperarue and high thermal conductivity, sodium level is maintaind with back up components such as guard vessel in case of sodium leaks. Natural circulation capability of sodium is ulilized for the decay heat tranport to the atmospheric air, which is hardly affected by tsunami and flooding. Furthermore, design measures, e.g., reinforcement of air stacks for strong wind, physical barriers and separation for external missiles, are considered to protect the sodium-air heat exchangers against severe external events. As an accident management, it enables manually adjusting the damper opening to maintain the cooling performance even under DC power depletion for instrumentation and control as a consequence of a long-term loss of AC power. In addition alternative cooling measures such as gas cooling of the water side of steam generators, additional cooling circuit to the sea water, are available. Since various measures can be used during the longer time period by the core melt, the design measures for LOHRS type events shall be such that significant core damage is practically eliminated.

Specific situations which can be threat to the containment and for which the containment failure is hard to be prevented shall be practically eliminated by design measures. Such situations are proposed as abnormal reactivity insertion lead to prompt criticality (large bubble ingress etc.), severe mechanical energy release due to recriticality, significant core damage in LOHRS type events, large scale sodium spray combustion inside the containment, hydrogen accumulation and deflagration/detonation due to sodium-concrete reaction inside the containment, containment bypass due to large scale rupture of steam generator tubes, fuel melt in the fuel storage system.

The leaktight containment is installed as the final barrier against radioactive materials release to the environment. Design measures to practically eliminate the above proposed events are considered. The containment vessel is designed to withstand the load induced by the decay heat from the gaseous and volatile fission products dispersed in the containment vessel, and latent heat from leaked sodium.

Design measures are provided so that the sodium chemical acitivity doesn't become causes of core damage even under DECs. The double boundary concept is reinforced to cope with boundary failure events severere than the design basis. Simultaneous double ended break of large numbers of heat transfer tubes in the steam generators shall be practically eliminated.

The safety measures equivalent to that for nuclear reactor is applied for EVST as the sodium leak countermeasure and heat removal. For the spent fuel water pool the design measures will be equivalent to that for future LWRs.

ACKNOWLEDGEMENTS

REFERENCES

[1] USDOE and GIF "A Technology Roadmap for Generation-IV Nuclear Energy Systems", GIF-002-00 (2002).
[2] K.Aoto, et al.," Reinforced JSFR Safety Design and Safety Criteria for Gen.IV Reactor", FR13, Paris, France (2013)
[3] Report of Japanese Government to the IAEA Ministerial Conference on Nuclear Safety, "The Accident at TEPCO's Fukushima Nuclear Power Stations" (2011)

[4]   R.Nakai, et al., "Development of Safety Design Criteria for the Generation-IV Sodium-cooled Fast Reactor ", NTHAS8, Beppu, Japan (2012)

[5]   S. Okamura, et al., "Seismic Isolation Design for JSFR", Proc. the Int. Conf. on Fast Reactors and Related Fuel Cycles (FR09), No. IAEA-CN-176-08-28P Kyoto, Japan, (2009)

[6]   H.Hayafune, et al., "Evaluation of severe external events on JSFR", FR13, Paris, France (2013)

[7]   S. Kondo, et al., "Integrated analysis of In-vessel and Ex-vessel severe-accident sequences", Proc. Int. Fast Reactor Safety Meeting, 1990, Snow bird, Utah, US

[8]   A. Bayer, K. Koberlein, "Risk-oriented analysis on the German Prototype Fast Breeder Reactor SNR-300", Nuclear Safety, Vol. 25, No.1, Jan.-Feb. 1984, pp19-32

[9]   T. Okubo, et al., "Conceptual Design for a Large-Scale Japan Sodium-Cooled Fast Reactor (3) Core Design in JSFR", Proc. ICAPP '11, No. 11345, Nice, France (2011)

[10] H.Yamano, et al., "Safety Design and Evaluation in a Large-Scale Japan Sodium-Cooled Fast Reactor" Science and Technology of Nuclear Installations, Vol. 2012, Article ID 614973, 14 pages

[11] Y.Tobita, et al., "Safety Strategy of JSFR establishing In-Vessel Retention of Core Disruptive Accident", FR13, Paris, France (2013)

[12] K. Ichikawa, et al., "Conceptual Design Study of JSFR (3)-Reactor Cooling System-", Proc. the Int. Conf. on Fast Reactors and Related Fuel Cycles FR09), No.IAEA-CN-176-08-12P Kyoto, Japan, (2009)

[13] H. Hara, et al., "Conceptual Design Study of JSFR (4)-Reactor Building Layout-", Proc. the Int. Conf. on Fast Reactors and Related Fuel Cycles FR09), No.IAEA-CN-176-08-13P Kyoto, Japan, (2009)

[14] Y. Chikazawa, et al., "Conceptual Design for a Large-Scale Japan Sodium-Cooled Fast Reactor (1) Feasibility of Key Technologies", Proc. ICAPP '11, No.11278, Nice, France (2011)

[15] T. Takata, A. Yamaguchi, A. Uchibori and H. Ohshima, "Computational Methodology of Sodium-Water Reaction Phenomenon in Steam Generator of Sodium-Cooled Fast Reactor," J. Nucl. Sci. Technol., 46, pp.613-623 (2009)

REACTIVITY EFFECT OF STEAM / WATER INGRESS IN GENERATION-IV GAS-COOLED FAST REACTOR CORE

Konstantin Mikityuk[a], Zoltán Perkó[b], Gaëtan Girardin[c]

[a] Paul Scherrer Institut, Switzerland

[b] Delft University of Technology, The Netherlands

[c] École Polytechnique Fédérale de Lausanne, Switzerland

Abstract. This paper presents a static neutronic calculational study of steam/water ingress into a Gas-cooled Fast Reactor (GFR Generation IV) core performed by using three Monte-Carlo codes, namely SERPENT version 1.1-16, KENO-VI module of the SCALE, MCNPX version 2.7.0, and different modern nuclear data libraries, i.e. JEFF-3.1, JEFF-3.1.1 and ENDF/B-VII. The analysis was performed for a wide range of water/steam densities $[0 – 1.0 \text{ g/cm}^3]$ within the core and the neutronic parameters were compared between the different codes and libraries. The obtained results demonstrate that this accidental event would result in a large negative reactivity insertion. The main reason of such core behaviour was found to be an increased neutron absorption rate in the cladding liner made of refractory metals (W and Re) due to the neutron spectrum thermalisation resulting from the steam/water ingress.

1. Introduction

The gas-cooled fast reactor (GFR) is one of the six Generation-IV systems currently being developed in the frame of the GIF-driven cooperation between France, EURATOM and Switzerland, in particular through FP7 EURATOM GoFastR project [1]. In the current reactor design of 2400 MWth the use of water as a working medium in the secondary side of the decay heat removal loop makes an accident scenario possible in which steam and/or liquid water could enter directly into the core. The neutronic response of the core to this event is analysed in this paper using three different Monte-Carlo codes, namely, the SERPENT version 1.1-16 code developed by VTT [2], the KENO-VI module of the SCALE code system developed by the Oak Ridge National Laboratory [3] as well as MCNPX version 2.7.0 developed by Los Alamos National Laboratory [4]. This study is an extension of the previous analysis [5] to the current pin-type European gas-cooled fast reactor design.

2. GFR core description and computer models

The GFR core is composed of hexagonal fuel assemblies containing fuel pins arranged in a triangular lattice. Each fuel pin constitutes of a column of (U-Pu)C pellets and a surrounding cylindrical cladding tube made of composite ceramic material SiC-SiC$_f$. The fragility of the ceramic cladding imposes a limitation on the fuel rod height. For this reason, each pin is made up of two half-pins to have the whole height of the fuel column equal to 165 cm. The lower and upper fuel rods have their own fission gas plenums below and above the fuel columns, and upper and lower reflectors are located above and below the fission gas plenums. The problem of a potential "transparency" of the composite cladding material to gaseous fission products [6] makes it necessary to use a liner applied on the inner surface of the cladding tubes. In the analysed design, a two-layer liner made of refractory metals (W-Re with 40 μm thickness and Re with 10 μm thickness) is considered to guarantee that fission gases remain inside the fuel pins. Finally, the assemblies are enclosed in hexagonal wrapper tubes made of SiC, hosting a bundle of 217 pins each.

For our neutronic study of the GFR behaviour under accidental steam/water ingress, fully heterogeneous three-dimensional (3D) models of the GFR fuel assembly were developed and used in the simulations with the above-mentioned Monte-Carlo codes. To represent an infinite array of assemblies reflective boundary conditions were used in radial direction and vacuum boundaries were assumed on the top surface of the upper reflector and on the bottom surface of the lower reflector. The upper and lower reflectors were supposed to be designed as a column of Zr_3Si_2 pellets inside the fuel rod cladding.

The GFR fuel assembly model (radial and axial view) is depicted in Fig. 1a, while a detailed view of a fuel pin is shown in Fig. 1b. For simplicity, no spacer grids and no control rods were simulated in the presented analysis. In order to break-down reactivity effects due to water ingress from other effects (Doppler, thermal expansion), all calculations were performed using nuclear data at room temperature (293 K). JEFF-3.1, JEFF-3.1.1 and ENDF/B-VII nuclear data libraries were used in this study. For steam/water, the thermal $S(\alpha,\beta)$ treatment was used for hydrogen combined to oxygen.

3. Methodology, results and discussion

The first two sets of calculations were done for nominal and depressurized conditions (helium coolant at 70 bar pressure and at atmospheric pressure respectively) to evaluate the void reactivity effect in case of loss of pressure in the primary circuit. The resulting difference in reactivity is the void effect and it equals to a positive effect of about 300 pcm (1 pcm = 10^{-5}). The details of these calculations are not presented in the paper, because the reactivity effect of any helium present in the core is negligible compared to the reactivity effect of steam/water.

The possible H_2O content in the core and the exact 3D distribution during water injection in the primary system depends on many factors: partial steam and helium pressures, temperature distribution in the core and primary system, etc. In the current parametric study, in order to cover the important range of steam and water densities, ten calculations were done with H_2O content varying from 0.1 g/cm^3 up to 1.0 g/cm^3 with a step of 0.1 g/cm^3. To simplify the analysis, it was assumed that only steam/water is present in the core and that the mixture is distributed uniformly over the whole subassembly model, i.e. over the fuel, plenum and reflector regions in place of the original helium coolant.

The calculated core effective multiplication factor, k_{eff}, versus smeared H_2O density in the core is shown in Fig. 2. It is interesting to note that the reactivity goes down to almost –8000 pcm at a steam density of 0.3 g/cm^3 and, then, starts to grow at higher values. The core reactivity reaches the value corresponding to the reference operating case (ρ_{H2O} = 0 g/cm^3, helium at atmospheric pressure) only at a relatively high smeared H_2O density. This water content (ρ_{H2O} = ~0.9 g/cm^3) approximately corresponds to the liquid water density at saturation line at a pressure slightly higher than 1 atm.

As shown in Fig. 2, the three codes qualitatively predict the same behaviour of the effective multiplication factor k_{eff} with the increase of the smeared H_2O density. However, for H_2O contents of 0.3 to 1.0 g/cm^3 there is a significant difference between KENO-VI predictions and the SERPENT/MCNPX results. It is observed that KENO increasingly underestimates the k_{eff} as the H_2O density rises. This discrepancy (up to ~1000 pcm) is due to a known issue in KENO-VI related to the $S(\alpha,\beta)$ treatment when using continuous energy cross sections, as in the current analysis. As reported in the SCALE Newsletter, Spring 2012 [7] there are "systematic biases for continuous-energy Monte Carlo calculations, especially for water-moderated mixed-oxide lattices", which are similar to the GFR lattice investigated in our study. Nevertheless, deviations up to 250 pcm between SERPENT and MCNPX results are also observed when compared with the same nuclear data library.

The code-to-code comparison also shows that the k_{eff} is sensitive to the nuclear data library. The reactivity difference is especially important at nominal coolant conditions (i.e. at 0.0 g/cm^3 water density), where results using ENDF and JEFF libraries deviate with 500 to 700 pcm. However, this library effect becomes less significant at higher water densities and typically remains below 150 pcm.

Upper reflector

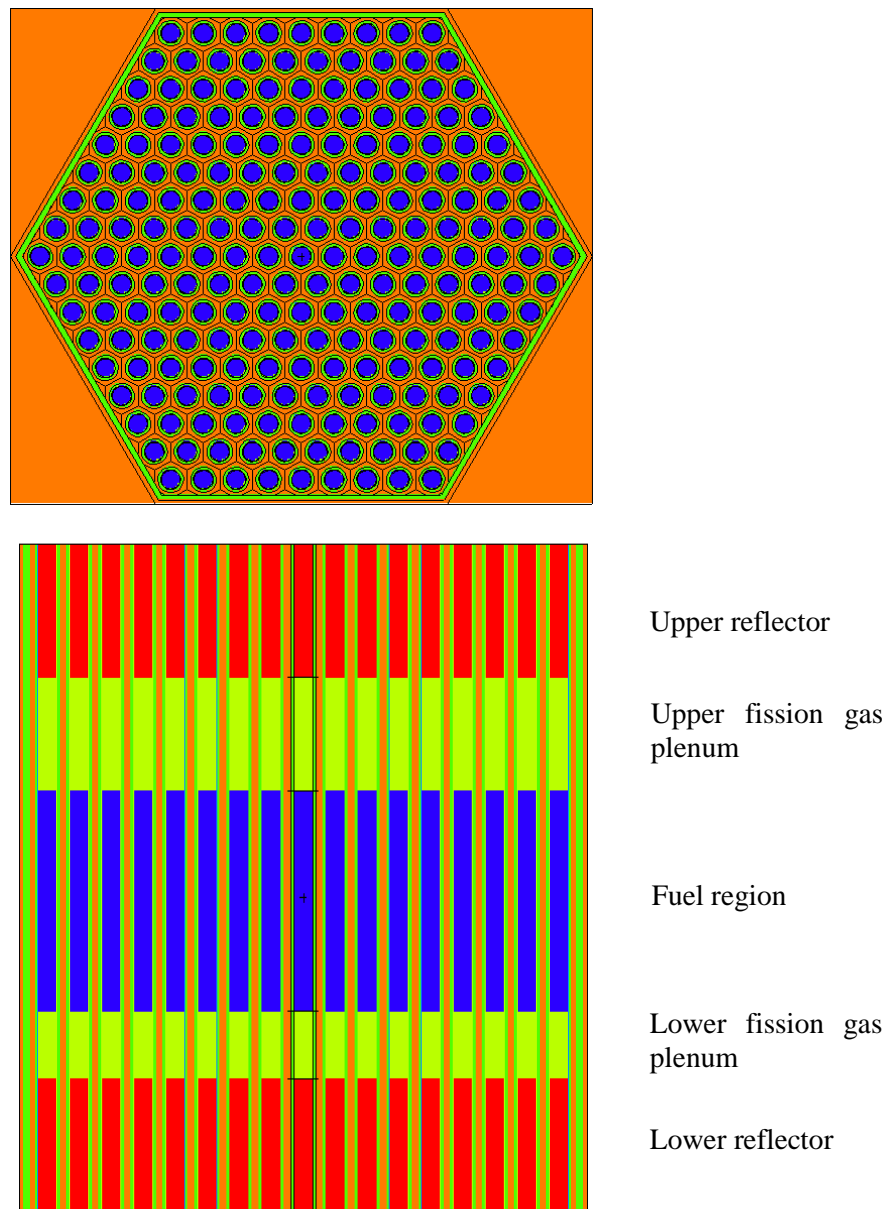Upper fission gas plenum

Fuel region

Lower fission gas plenum

Lower reflector

Fig. 1a. Top view and axial cross cut of the calculational model of the GFR fuel assembly

Fuel

W-Re/Re
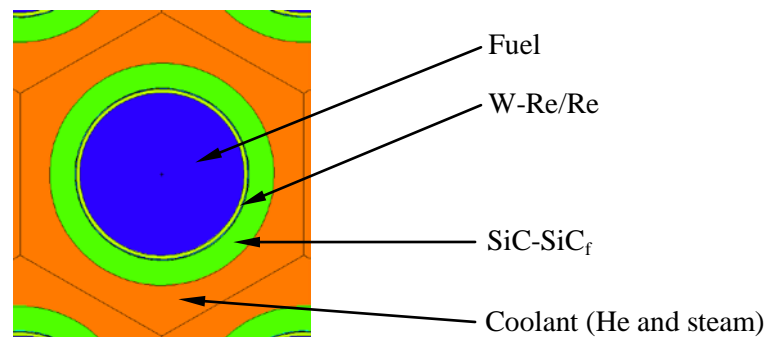
SiC-SiC$_f$

Coolant (He and steam)
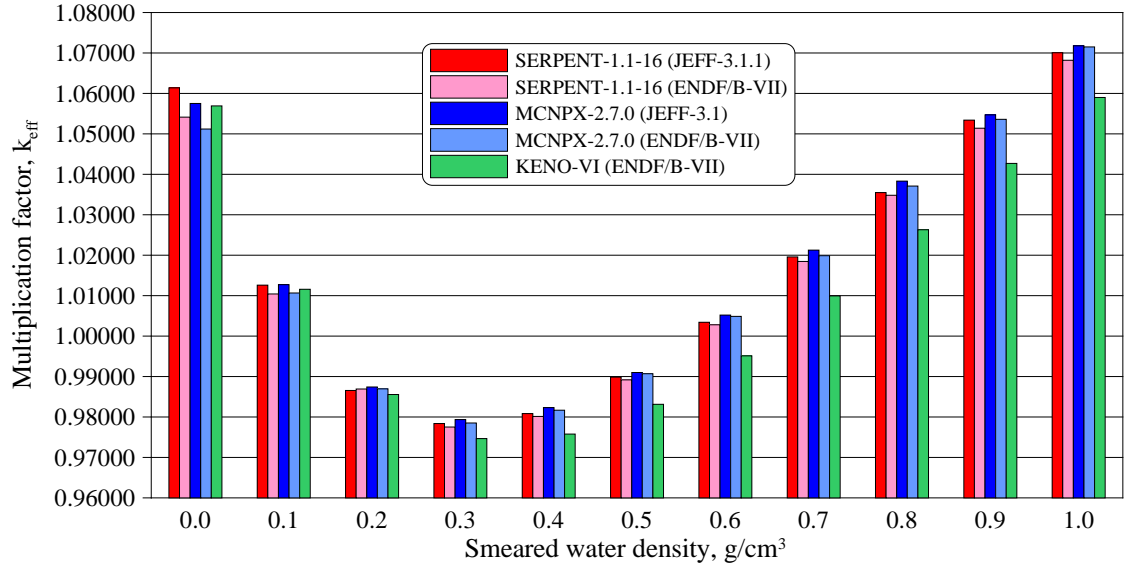
Fig. 1b Details of a fuel pin

Fig. 2. Multiplication factor k_{eff} versus smeared water density

This observation suggests differences in the neutron spectrum at high energies, coming from the different microscopic cross-sections of the isotopes used in the current GFR model.

Taking into account the high (n,γ) cross sections of tungsten and rhenium in the thermal and epithermal energy regions, the reactivity behaviour can be explained by the thermalisation of the spectrum with increasing H_2O content in the core. To visualise the thermalisation process, the neutron spectrum, integrated over the whole GFR sub-assembly is shown in Fig. 3 for the two extreme cases, i.e. water density of 0 g/cm^3 and water density of 1 g/cm^3. The neutron spectra were calculated with a fine energy structure with equal width in lethargy in case of MCNP and SERPENT and with the standard 238 group structure in case of KENO. A very good consistency is observed between all the codes and the neutron libraries. Some minor differences are slightly visible at high energies (~MeV) with KENO due to a different energy structure adopted for the simulations.

The thermalisation results in an increase of absorption rate due to W and Re, counterbalancing the positive reactivity effect due to the increasing neutron production rate. The fraction of neutrons absorbed in the liner is very high even in normal condition (~14%, whereas the volume fraction of the liner materials is only ~0.9% in the core) and it grows rapidly with the spectrum thermalisation (up to ~19%) until absorption in fuel becomes prevailing. The fractions of total neutrons absorbed in the liner (W-Re and Re) are depicted in Fig. 4 as a function of the smeared water density. For the sake of the code-to-code comparison the results obtained with KENO/ENDF/B-VII and SERPENT in conjunction with JEFF-3.1.1 and ENDF/B-VII are presented in Fig. 4.

The essential role of the metallic liners is further demonstrated when the same series of calculations is performed (i.e. water density gradually increased from 0.1 g/cm^3 to 1 g/cm^3) for the same infinite array of fuel assemblies, but with pins having no refractory metal liners. When these thin layers are substituted with SiC-SiC_f in the geometry and the cladding of the fuel rods is purely made up by the composite ceramics, the reactivity curve is substantially different (see Fig. 5).

The multiplication factor behaviour (Fig. 5) is a combined result of spectrum thermalisation, decreasing axial leakage, and a varying absorption in the ceramic cladding, the fuel and steam/water itself. At low steam/water density (at 0.1 g/cm^3 for instance), the decrease in neutron leakage (to practically 0) and the increase in neutron production causes an immediate increase in reactivity, which is counterbalanced by the increasing absorption in water at higher water contents (up to ~0.3 g/cm^3). After this point, the fraction of neutrons absorbed in water stays fairly constant, that in the fuel and the structural elements slowly increases and decreases respectively, while the spectrum becomes more and more thermal, causing the k_{eff} to gradually increase.
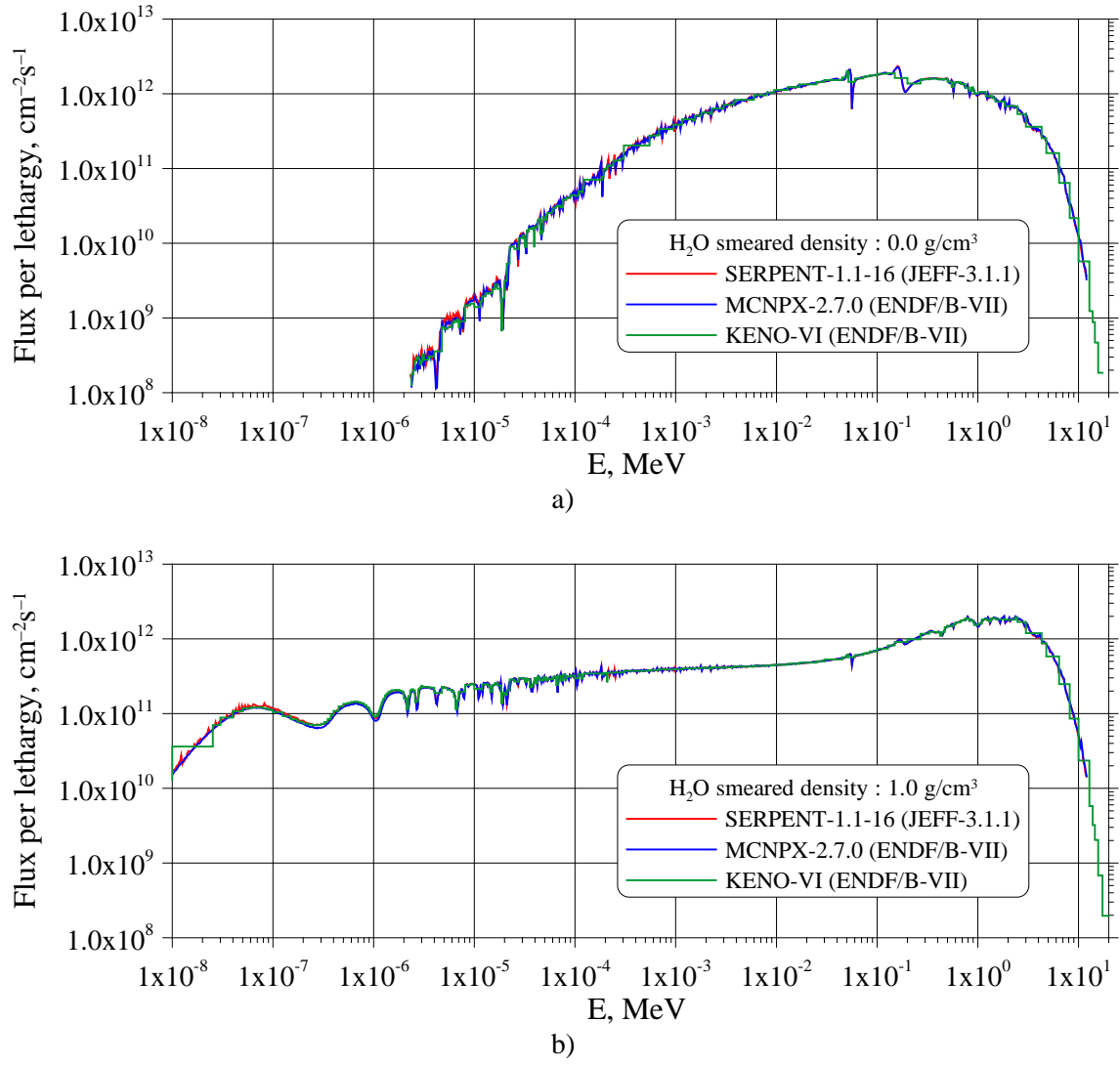
Fig. 3. Neutron spectra normalized to the same total flux for two different H_2O densities in the core: a) 0 g/cm^3 and b) 1 g/cm^3.
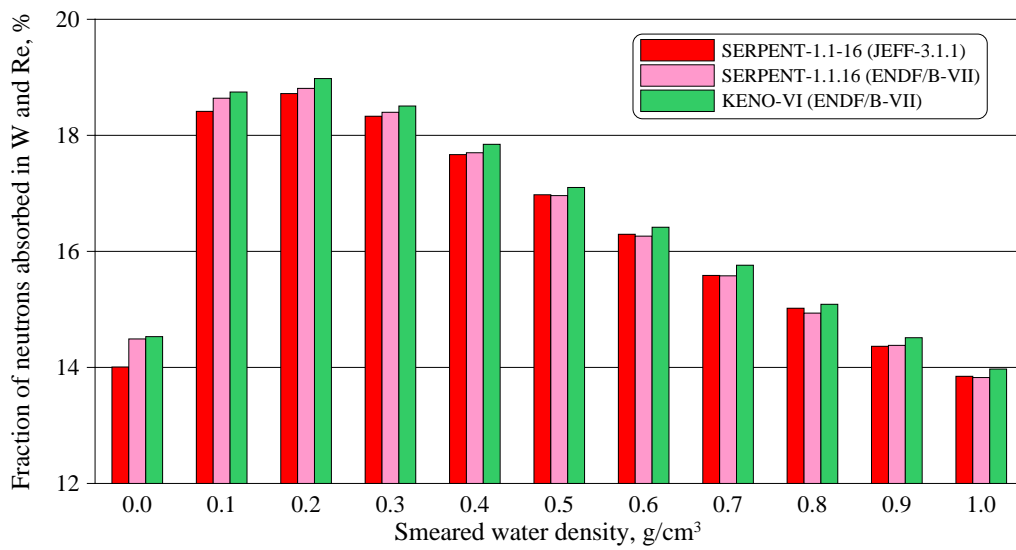

Fig. 4. Fraction of neutrons absorbed in W and Re as a function of smeared water density in the core

5
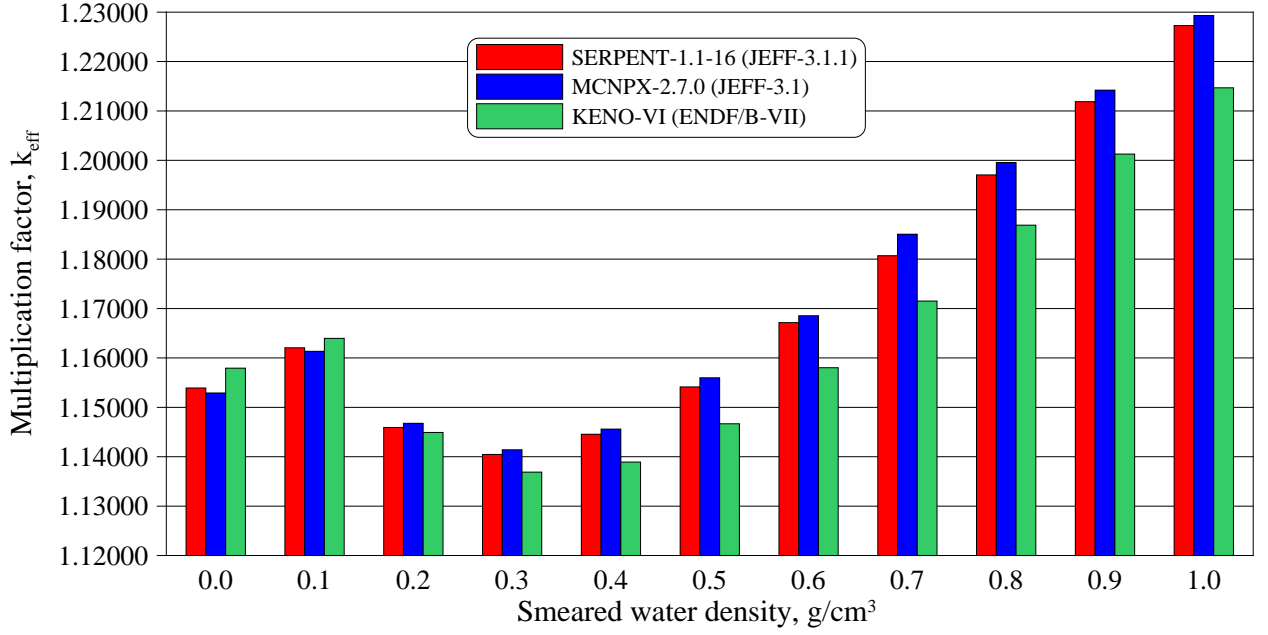
Fig. 5. Multiplication factor k_{eff} versus smeared water density in case of replacement of W and Re liners by SiC

Based on the above discussed results, there are two major differences to highlight between the cases with and without liners, which will impact the core safety. On the one hand, the immediate reactivity response of the reactor to the presence of water is positive without the liners (this negative safety-related aspect was already studied and obtained in the 70's with the development of GFRs), while the reactivity change of the core is strongly negative with liners of W-Re and Re. In addition to this observed difference, the core reactivity remains below its initial value up to a much higher water density (~0.9 g/cm^3) with the use of liners, than it does without it (~0.5 g/cm^3), confirming again the essential role played by this small amount of the liner materials in the core.

4. Conclusions

In the GFR design currently studied in frames of the FP7 EURATOM GoFastR project [1], refractory metals (W and Re) are used as materials for the cladding liners in order to improve the tightness of fuel cladding against the diffusion of fission gases into the coolant. This results in significant neutron penalty in normal operation due to the high absorption cross-sections of these metals. According to the conducted and presented analysis, however, these metals have a favourable effect in accidental situations in which spectrum thermalisation is to be expected. For example, in case of steam or water ingress within the core, in spite of the increasing neutron production rate due to spectrum thermalisation, the increasing absorption rate in W and Re will lead to a significant negative reactivity insertion of several thousands of pcm.

This observation suggests it is worthwhile to study the injection of borated water into the primary circuit as one of the possible and effective ways to remove decay heat in the most penalizing accidental scenarios for the GFR, i.e. depressurized conditions. Naturally, other aspects of the steam and water ingress, such as chemical interaction with core materials, dynamic response of the reactor and primary circuit, thermal-mechanical fuel behaviour, etc. will also have to be carefully evaluated and their interconnections should be well understood.

REFERENCES

[1]   Stainsby, R., Peers, K., Mitchell, C., Poette, C., Mikityuk, K., Somers, J. Gas cooled fast reactor research in Europe. Nuclear Engineering and Design 241 (2011) 3481– 3489.

[2]   Leppänen, J., 2010. "Serpent Monte Carlo Reactor Physics Code", In Proc. 20th AER Symposium on VVER Reactor Physics and Reactor Safety. Espoo, Finland, Sept. 20-24, 2010.

[3]   "SCALE, A Modular Code System for Performing Standardized Computer Analyses for Licensing Evaluations", Vols. I-III, Version 6, CCC-750; ORNL/TM-2005/39, Radiation Safety Information Computational Center, Oak Ridge National Laboratory (2009).

[4]   Waters, L.S. (Ed.), 2008. MCNPX User's Manual, Version 2.6.0, LA-CP-07-1473.

[5]   Girardin, G., Epiney, A., Mikityuk, K., Chawla, R. Neutronic analysis of water-steam injection accidents for Generation-IV gas-cooled fast reactors. Proceedings of PHYSOR 2010 – Advances in Reactor Physics to Power the Nuclear Renaissance, Pittsburgh, Pennsylvania, USA, May 9-14, 2010.

[6]   Zabiego, M., 2011. Nuclear Fuel Design and Associated Material Issues. GoFastR Workshop. Cadarache, France. June 29, 2011. http://gofastr.tnw.tudelft.nl/program.php.

[7]   SCALE Newsletter. Spring 2012. http://info.ornl.gov/sites/publications/Files/Pub35867.pdf

CFD Modeling of Sodium Fires

P. Sathiah and F. Roelofs

Nuclear Research and Consultancy Group, Petten, The Netherlands

Abstract. A sodium cooled fast reactor is one of the attractive concepts for the 4th generation nuclear reactors. For the safety of a sodium cooled fast reactor, sodium-air and sodium-water reactions must be avoided. A sodium-air reaction typically occurs in two dominant modes, namely the spray fire and the pool fire. To avoid sodium-air accidents and to deal with their consequences, it is essential to understand the physical phenomena. Numerical modeling is one of the methods, which can be used to understand all the physics involved. This paper will present new numerical methods to model sodium pool combustion based on advanced state-of-the-art Computational Fluid Dynamics techniques. The models have been developed, implemented and validated against available experimental data of Newman and Payne.

INTRODUCTION

Liquid sodium is used as a coolant for sodium cooled fast reactors because it has excellent thermophysical properties. In particular, it has high thermal conductivity, low absorption rate of fast neutrons and good fuel breeding performance. Moreover, it can be present in the liquid state in a wide range of temperatures. This enables liquid sodium to be used as a coolant.

However, liquid sodium has a serious shortcoming i.e. sodium when exposed to air or water reacts violently, which can be a potential fire hazard in a nuclear reactor. A sodium leak, which results from a pipe break up, releases sodium in the reactor in the form of a spray or a jet. A part of the released sodium collects on the floor and forms a sodium pool. The leaked sodium essentially burns in two different modes i.e. spray and pool modes. Figure 1a and b shows sodium pool and spray fire respectively. The spray mode of burning is generally more severe than the pool mode of burning since a spray burns at a higher rate as it burns in a highly divided state, i.e. in the form of droplets and it is not easy to extinguish. However, a pool combustion continues for a long time in comparison to spray combustion, but is easier to extinguish.

FIG. 1a) Sodium Pool Fire

FIG. 1b) Sodium Spray Fire (the pictures are taken from [26])

During a sodium spray or pool combustion, sodium reacts with air and water to form several sodium by-products, e.g. sodium oxide (Na_2O), sodium dioxide (Na_2O_2) and sodium hydroxide (NaOH),

which are released in the atmosphere in the form of aerosols. These aerosols are particles with a diameter ranging from 0.1 µm to 10 µm, which can cause structural damage to the equipment and to public health.

Several sodium leak and subsequent sodium fire accidents were reported in literature [1]. For example, a sodium fire accident occurred on 8th December 1995 in the Japanese Monju reactor in Tsuruga, Japan. Several mitigation systems have been proposed in literature. For example the Karlsruhe tray [2] and leak collection tray [3] to catch leaking sodium and avoid its contact with air or water. However, further work on optimization of the design of such mitigation systems is necessary before it can be used in a real sodium leak scenario in a sodium fast reactor.

To summarize, sodium leakage which leads to sodium reactions is dangerous for the safety of a sodium cooled reactor. Hence, sodium reactions must be avoided and therefore detailed experimental and numerical investigations of sodium reactions are important. In fact, understanding of sodium reactions with air and water is essential to develop computer codes, which can be used for the safety analysis of sodium fast reactors and to the design of mitigation systems.

In the past we have developed a method to simulate sodium spray combustion [25]. The focus of this paper is to propose a method to simulate sodium pool combustion based on Computational Fluid Dynamics (CFD). In particular, it presents the validation of a CFD based sodium pool combustion solver against well-defined experiments.

The paper is structured as follows: Firstly, governing equations, combustion model, pool evaporation model and radiation models are discussed in detail. In addition, the heat conduction modeling is presented in Section 2. Furthermore, it provides a short description of the model implementation and numerical scheme used. Secondly, Section 3 presents results and discussion. Finally, a summary and conclusion is presented in Section 4.

CFD MODEL

We have used a widely used commercial CFD code as the basis for development of a sodium spray and pool combustion solver. Within the code, the gaseous phase is simulated in an Eulerian phase. The unsteady Favre-averaged (density-averaged) Navier-Stokes equations are solved using the Low-Re k-ε turbulence model. The models and the governing equations are described below in the following subsections.

2.1 Eulerian Phase Governing Equations

Within the code, the following governing equations for the conservation of mass, momentum, energy and mixture fraction are solved.

Mass:

$$\frac{\partial \bar{\rho}}{\partial t} + \frac{\partial}{\partial x_j}(\bar{\rho}\tilde{u}_i) = S_m. \qquad [1]$$

Velocity:

$$\frac{\partial}{\partial t}(\bar{\rho}\tilde{u}_i) + \frac{\partial}{\partial x_j}(\bar{\rho}\tilde{u}_i\tilde{u}_j) = -\frac{\partial \bar{p}}{\partial x_j} + \frac{\partial}{\partial x_j}(\bar{\tau}_{ij} - \bar{\rho}\widetilde{u_i''u_j''}) + \bar{\rho}g_i + S_{mom}. \qquad [2]$$

Mixture fraction :

$$\frac{\partial}{\partial t}(\bar{\rho}\tilde{f}) + \frac{\partial}{\partial x_j}(\bar{\rho}\tilde{u}_i\tilde{f}) = \frac{\partial}{\partial x_j}\left(\rho D \frac{\partial \tilde{f}}{\partial x_j}\right) + \frac{\partial}{\partial x_j}\left(\frac{\mu_t}{\sigma_t}\frac{\partial \tilde{f}}{\partial x_j}\right) + S_m \qquad [3]$$

Variance of mixture fraction:

$$\frac{\partial}{\partial t}(\bar{\rho}\widetilde{f'^2}) + \frac{\partial}{\partial x_j}(\bar{\rho}\tilde{u}_j\widetilde{f'^2}) = \frac{\partial}{\partial x_i}\overline{\left(\rho D_f \frac{\partial f'^2}{\partial x_i}\right)} + \overline{2f'^2 \frac{\partial}{\partial x_i}\left(\rho D_f \frac{\partial \tilde{f}}{\partial x_i}\right)} + \frac{\partial}{\partial x_j}\left(\bar{\rho}\frac{\mu_t}{\sigma_t}\frac{\partial \widetilde{f'^2}}{\partial x_j}\right)$$
$$+ C_g\mu_t\left(\frac{\partial \tilde{f}}{\partial x_i}\right)^2 - C_d\bar{\rho}\frac{\epsilon}{k}\widetilde{f'^2}. \qquad [4]$$

Energy:

$$\frac{\partial}{\partial t}(\bar{\rho}\tilde{H}) + \frac{\partial}{\partial x_j}(\bar{\rho}\tilde{u}_i\tilde{H}) = \frac{\partial}{\partial x_j}\left(\frac{k_g}{C_p}\frac{\partial \tilde{H}}{\partial x_j}\right) + S_h. \qquad [5]$$

Here, $\bar{\cdot}$ and $\tilde{\cdot}$ are the Reynolds averaged and Favre-averaged quantities, respectively. $\tilde{u}_i$, $\tilde{f}$ and $\tilde{H}$ are the Favre-averaged velocity, the mixture fraction and the total enthalpy, D is the mixture fraction diffusivity, μ_t is the turbulent viscosity, σ_t is the turbulent Schmidt number, k_g is the thermal conductivity, S_m and S_{mom} are the mass and the momentum transfer to the gas phase from the liquid droplet or pool due to evaporation. S_h accounts for source term due to radiation heat transfer through wall boundaries, heat exchange with the liquid droplets or pool, t is the time, ρ is the density, p is the pressure, C_p is the specific heat capacity and g_i is the gravitational acceleration. In Eq. [3], the mixture fraction is defined as the ratio of mass of material having its origin in the fuel stream to the mass of the mixture and is given by Bilger et al. [24]

$$f = \frac{\gamma - \gamma_{ox,0}}{\gamma_{fu,0} - \gamma_{ox,0}} \qquad [6]$$

where γ is the oxidizer-fuel coupling function, $\gamma = Y_{fu} - Y_{ox}/S$ where, S is the stoichiometric oxygen to fuel mass ratio. If f=0, it means air mixture and while f=1 means fuel mixture. In Eq. [4] , $f'^2 = (f - \tilde{f})^2$ is the variance of mixture fraction. The default values of the constants σ_t, C_g and C_d are 0.85, 2.86, and 2.0, respectively. A detailed description of the combustion model is provided next.

2.2 Combustion Model

In the past, several model developers e.g. [4][5][6][7][8][9][10][11][[12] used the assumption of chemical equilibrium to simulate sodium-air reactions. This assumption means that the chemical reactions are faster than the fluid flow and species diffusion. In addition, they assumed that the chemical reaction reaches equilibrium as soon as sodium vapor comes in contact with air.

A mixture fraction based non-premixed combustion model is widely used to simulate a turbulent diffusion hydrocarbon flame. This model is well validated in different applications of hydrocarbon combustion, for example in piloted diffusion flame and in an hydrogen-air diffusion flame. In addition, it is also used to simulate fire and diesel engine applications. Because of its extensive validation, this model is also available in commercial codes for example in ANSYS FLUENT [13] and ANSYS CFX [14]. We used this model to simulate sodium combustion.

In this model, it is assumed that the reaction takes place on an infinitely thin flame sheet, where both the fuel and the oxygen species meet each other. In addition, it is assumed that the combustion is controlled by the mixing of fuel and oxygen. Due to this assumption, it is possible to represent all the

species relevant to the combustion process by one single parameter i.e. mixture fraction. Hence, the combustion modeling is reduced to a problem of mixing, which means finding a location of the flame surface (where fuel and air mixes together) by solving a mixture fraction equation. After that, the distribution of the species is calculated, which is obtained by assuming that the instantaneous thermochemical state (density, temperature and species mass fractions) of the fluid is related to the mixture fraction. For the latter purpose, the chemistry can be treated using a chemical equilibrium approach or a steady laminar flamelet approach [15]. In the chemical equilibrium approach, it is assumed that the chemical reactions are fast and reach equilibrium as soon as they meet each other. To consider the effects of finite rate chemistry, a steady laminar flamelet model can be used.

Here, to simulate sodium combustion we used the chemical equilibrium approach and to consider the effect of heat loss/addition to chemical equilibrium, non-adiabatic equilibrium tables were constructed. This means that chemistry i.e. the temperature, the density and the mass fraction of species are tabulated as a function of mixture fraction and enthalpy.

Once the value of the mixture fraction in a computational cell is known, the mean values of temperature and species mass fraction in a cell are then obtained by the following equation:

$$\tilde{T} = \int_0^1 \int_0^1 T(f, H) \mathrm{JPDF}(f, f', H) df\, dH \qquad [7]$$

and

$$\tilde{Y_k} = \int_0^1 \int_0^1 Y_k(f, H) \mathrm{JPDF}(f, f', H) df\, dH. \qquad [8]$$

Here, $T(f,H)$ and $Y_k(f,H)$ are the temperature and species mass fraction of kth species, which are obtained from the non-adiabatic equilibrium PDF table. JPDF(f,f',H) is the Joint Probability Distribution Function (JPDF) of the mixture fraction and enthalpy. It describes the joint probability that the flow field takes a certain value for the mixture fraction and enthalpy at a given point. A JPDF can be obtained as a product of PDF of mixture fraction PDF(f,f') and PDF of enthalpy PDF(H), if statistical independence of mixture fraction and enthalpy is assumed. In literature, the PDF of a mixture fraction is presumed to be β-PDF, since shape of the PDF can change continuously from single, double to Gaussian shape, while the PDF of enthalpy is assumed to be a single delta function, which means that the fluctuations in the total enthalpy are neglected. The β-PDF can be estimated from the first moment and the second moment of mixture fraction i.e. the mean mixture fraction and the variance of the mixture fraction as follows:

$$\mathrm{PDF}(f) = \frac{f^{\alpha-1}(1-f)^{\beta-1}}{\int f^{\alpha-1}(1-f)^{\beta-1}} \qquad [9]$$

where

$$\alpha = \tilde{f}\left[\frac{\tilde{f}(1-\tilde{f})}{\widetilde{f'^2}} - 1\right] \qquad [10]$$

and

$$\beta = (1 - \tilde{f})\left[\frac{\tilde{f}(1 - \tilde{f})}{\widetilde{f'^2}} - 1\right] \qquad [11]$$

are the β-PDF parameters.

Once the value of the PDF is known using Eq. [9], the mass fraction and the temperature are obtained by integrating the state function with the PDF over the complete physical range of the mixture fraction. Finally, the mean density can be calculated as follows

$$\frac{1}{\bar{\rho}} = \int_0^1 \frac{\text{PDF}(f, f', H)}{\rho(f, H)} df\, dH. \qquad [12]$$

where, $\rho(f,H)$ is obtained from the non-adiabatic chemical equilibrium table. To generate the non-adiabatic equilibrium PDF table, the equilibrium calculations were performed using ANSYS FLUENT and results were compared with the NASA CEA code.

To summarize, at every flow time step Eqs. [1]-[5] are solved to obtain the gas velocity, the pressure, the mixture fraction, the variance of the mixture fraction, the mass fraction of different species and the gas temperature. To calculate the gas phase source terms S_m, S_{mom} and S_h, we need an addition model for sodium pool evaporation, this is described next.

It is worth reminding that in this approach of sodium pool fire modeling, the liquid sodium is assumed to be stagnant and the spreading of sodium pool is negligible.

2.3 Pool Evaporation Model

The liquid sodium evaporates due to the heat which is released from the flame and the evaporated sodium comes in contact with the atmospheric oxygen and burns. Since the sodium vapor pressure is low (approximately 1-20 kPa), it burns very close to the sodium surface and a diffusion flame is established a few millimeters from the sodium surface i.e. in the boundary layer. In this layer, diffusion of heat and mass is dominant, while convection can be neglected.

The energy released due to sodium pool combustion is used to increase the gas temperature. A part of the heat is used to increase the liquid sodium temperature through heat conduction and a part of the heat is consumed in the form of enthalpy of vaporization. It is necessary to model accurately the evaporation and the heat conduction of liquid sodium, in order to compute the burning rate of the sodium pool accurately. Hence, we need an evaporation model. In this model, it is assumed that the net mass flux of sodium vapor from the surface is equal to the sum of the mass fluxes due to the convection and the diffusion (this is also known as Stefan's law [16]). The mass burning rate $\dot{m}$ ($kg/m^3 s$) of liquid sodium is then given by:

$$\dot{m} = \rho k \frac{1}{1 - Y_{f,s}} \left.\frac{\partial Y_f}{\partial y}\right|_s. \qquad [13]$$

Here, k is the mass transfer coefficient, $Y_{f,s}$ is the mass fraction of vapor sodium at the pool surface. The mass transfer coefficient k can be obtained as follows [17]:

$$\frac{h}{k} = \rho C_p Le^{(1-n)} \qquad [14]$$

where, h is the heat transfer rate, ρ is the gas density, C_p is the gas specific heat capacity, respectively. Here, Le is the Lewis number, which is defined as the ratio of the Schmidt number Sc to the Prandtl number Pr and n is the coefficient. The properties like the specific heat capacity, the thermal conductivity and the density are calculated at the pool temperature.

To obtain the mass fraction of liquid at the pool surface, it is assumed that the vapor and the liquid sodium are in equilibrium at the pool surface. It is further assumed that the vapor and liquid sodium reaches equilibrium faster than the other physical processes. Then, the mass fraction of the liquid sodium at the pool surface is given as:

$$Y_{f,s} = \frac{P_{f,s}M_f}{P_{f,s}M_f + (P - P_{f,s})M_g}. \qquad [15]$$

Here, M_f and M_g are the molecular weight of fuel and gas mixture and $P_{f,s}$ is the saturation vapor pressure obtained from the saturation vapor pressure correlation, which can be expressed as follows:

$$P_{f,s} = P_{f,s}(T_s). \qquad [16]$$

Here, T_s is the interface (between liquid sodium and vapor) liquid sodium temperature, which is obtained by solving the following equation

$$\lambda \frac{\partial T_s}{\partial z} = Q_f - \dot{m}' H_{fg}. \qquad [17]$$

at the interface. Here, $\dot{m}'$ is the mass flux per unit area, z is the distance normal to the fuel interface, Q_f is the total heat flux, which includes the convective and the radiative heat flux. The underlined term represents the heat loss due to the enthalpy of vaporization of the liquid sodium. The temperature in the liquid sodium is obtained by solving the enthalpy equation for the sodium pool and is described in the next subsection.

2.3.1 Modeling of Heat Conduction

In this approach, the liquid sodium is modeled as a thermally thick solid and to obtain the temperature across this layer, the following enthalpy equation:

$$\frac{\partial}{\partial t}(\rho_l h) + \frac{\partial}{\partial x_j}(\tilde{u}_i \rho_l h) = \frac{\partial}{\partial x_j}\left(\lambda \frac{\partial T}{\partial x_j}\right). \qquad [18]$$

is solved. Here, ρ_l is the density of the liquid sodium, h is the sensible enthalpy of liquid sodium and γ is the thermal conductivity of the liquid sodium. Since the thermal conductivity of liquid sodium is large, the temperature of the liquid sodium across the liquid pool is a constant.

2.4 Thermal Radiation Model

Thermal radiation is one of the dominant modes of heat transfer in a sodium pool fire [6]. In order to calculate the radiative heat transfer, the absorption coefficient of the gas phase must be known. This depends on the aerosol concentration and size distribution of the aerosols present in the gas phase. According to Newman and Payne [18], sodium oxide is the major oxide formed during the pool combustion, which is further oxidized to form sodium peroxide. The lighter sodium oxide gets settled on the sodium pool surface, while the heavier sodium peroxide is carried upwards by natural convection. Cherdron et al. [19] also experimentally observed that major oxide species in the pool are

sodium oxide, while aerosols are composed mainly of sodium peroxide. Hence, it can be concluded that sodium-air reaction mainly produces sodium oxide and peroxide aerosols.

In literature, many researchers have simulated aerosols and calculated the size distribution and concentration of aerosols using so called aerosol behavior models [6][7][8][9][10][11]. Although these models describe essential physics e.g. coagulation and deposition of aerosols, they are computationally expensive. Hence, we propose to use a computationally less expensive method. We estimate the aerosol concentration of sodium oxide and peroxide from equilibrium calculations described in Section 2.2. This type of model is used to calculate soot emissivity in hydrocarbon combustion [20].

Next to account for the radiation effects, the Discrete Ordinate (DO) radiation model is used here, which solves the following equation:

$$\frac{\partial (I(\vec{r},\vec{s}),\vec{s})}{\partial x_j} + (a + \sigma_s)I(\vec{r},\vec{s}) = an^2 \frac{\sigma T^4}{\pi} + \frac{\sigma_s}{4\pi} \int_0^{4\pi} I(\vec{r},\vec{s}')\phi(\vec{s}.\vec{s}')d\Omega' \qquad [19]$$

where, $I(\vec{r},\vec{s})$ is the radiation intensity vector, a is the absorption coefficient of the gas due to the presence of aerosol particles and σ_s is the scattering factor.

According to Yamaguchi and Tajima [6], the aerosols emissivity ε_i, depends on the local aerosol concentration and is evaluated as follows:

$$\epsilon_i = 1 - exp(-k_s L_i) \qquad [20]$$

where

$$k_s = 3.6 B_s T_g \frac{f_v}{c_2} \qquad f_v = Y_a \frac{\rho_g}{\rho_a} \qquad [21]$$

Here, B_s is a proportional constant, Y_a is the mass fraction of aerosols estimated from equilibrium calculations and ρ_g is the gas density.

The surface emissivity of the sodium pool is taken to be 0.65 based on Hasiguchi et al. [21], who reported that the pool surface emissivity increases to 0.65 when covered with sodium oxide particles and its value is 0.05 when it is not covered with these particles. Yamaguchi et al. [6][8][9] have suggested that the scattering phenomenon can be neglected for the aerosol particles, because of their small size.

To summarize, at every flow time step Eqs. [1]-[5], [7]-[9] and [19]-[21] are solved to obtain the gas velocity, the pressure, the mixture fraction, the variance of the mixture fraction, the mass fraction of different species and the gas temperature. Equations [13] and [14] are solved to obtain the evaporation rate of sodium, which is used to calculate the gas phase source terms S_m, S_{mom} and S_h.

2.5 Numerical Scheme and Grid Requirement

The simulations are performed using ANSYS FLUENT, which employs a finite volume method. The spatial and time discretization of the conservation equations are performed with second order upwind scheme and second-order implicit method, respectively. The pressure-velocity coupling is performed with the SIMPLE method and the discretized equations are solved using a segregated solver in an iterative manner.

Liquid sodium is solved as a "solid zone" while the gas (i.e. mixture of sodium vapor and air) is modeled as a "fluid zone". This means that only the heat conduction equation i.e. Eq. [18] is solved in the solid zone, while Eqs. [1]-[5] are solved in the gas phase. The mass evaporation rate depends on the mass transfer rate, which is estimated from the heat transfer rate close to the pool surface. Hence, the modeling of pool evaporation is sensitive to the grid close to the pool surface. The descriptions of the grid, initial conditions and boundary condition used are provided in Section 3.

2.6 Model Implementation

A mixture fraction based non-premixed combustion model is available in the code, which is well suited to solve problems related to hydrocarbon combustion. However, it is not straightforward to use this code for modeling sodium pool combustion. For example, sodium physical properties are not available in the code. User Defined Functions (UDF) in the code give the capability to implement new properties and models as an add-on to the existing models available in the code. Hence, a UDF was used in our implementation to implement additional properties and models. For example, the DEFINE-PROPERTY function was used to define the liquid sodium density, thermal conductivity, diffusivity, saturation pressure and enthalpy of vaporization in the code. The DEFINE-SOURCE function was used to define the source terms for mass, mixture fraction and energy (S_m, S_{mom} and S_h in Eqs. [1], [2], [3] and [5]). Sample calculations were performed to verify the implementation of these UDFs.

3 Results and Discussion

The model described above was validated against sodium pool experiments of Newman and Payne [22]. They conducted sodium pool (diameter of 0.1 m) combustion experiments in an ambient environment (temperature 300 K and pressure 1atm) with three different initial oxygen concentrations (4 %, 9.5 % and 21 % by vol). They measured the pool burning rate and the aerosol release fraction for different initial pool temperatures (532 K-1023 K).

To simulate this case, we performed 2D unsteady RANS (Reynolds Averaged Navier-Stokes) simulations. The steady state solutions were obtained by solving unsteady equations until steady state is reached. A no slip boundary condition for velocity and zero heat flux boundary condition are applied at the walls. At the outflow boundary, the normal gradients of the mixture fraction, the velocity, the temperature, the turbulent kinetic energy and the turbulent dissipation rate are assumed to be zero. At the interface between liquid sodium and air, a coupled boundary condition is applied. This means that Eq. [17] was solved. The flow is assumed to be quiescent initially. The initial values of turbulent kinetic energy 1e-04 m^2s^{-2} and turbulent dissipation rate 1e-08 m^2s^{-3} are used.

For each set of initial pool temperature and oxygen concentration, separate equilibrium calculations were performed to generate a non-adiabatic equilibrium table. This table was then used for each simulation. The grid adjacent to the pool surface must be fine enough to resolve the thermal and species boundary layer. Hence, the grid size is taken to be 0.025 mm. This resolution is also recommended by Yamaguchi and Tajima [7]. The burning rate varies over the length of sodium pool surface and hence the mean burning rate was calculated by averaging the burning rate over the length.
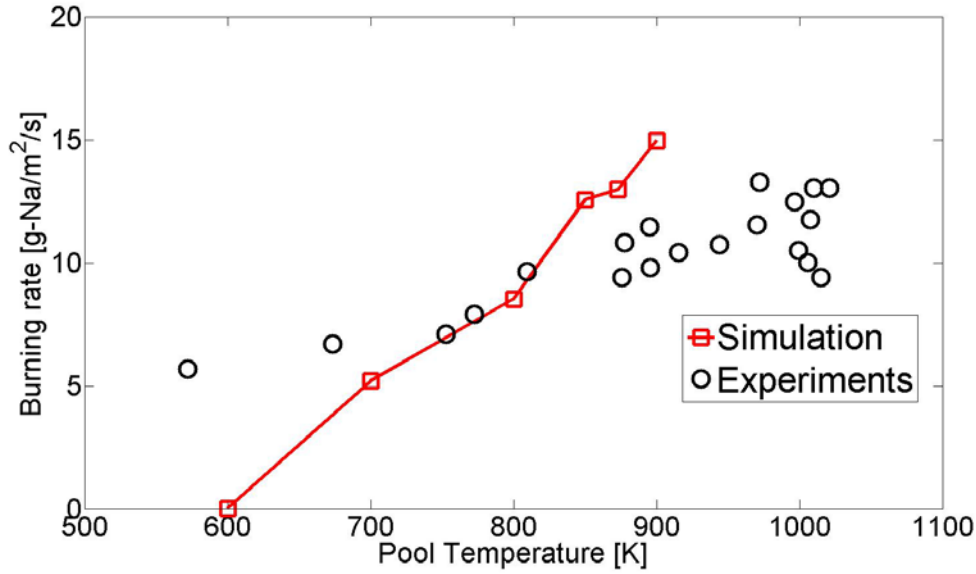
FIG. 1. The variation of the mean burning rate with initial pool temperature for an initial oxygen concentration of 21 % by volume.

Figure 1 shows the comparison of the mean burning rate of liquid sodium obtained using calculations and the experiments for an initial oxygen concentration of 21 (% vol). The results are shown here for various pool temperatures. The mean burning rate is predicted well for a temperature ranging between 750 K -900 K. However, the results obtained by simulations tend to overpredict at higher pool

temperatures. This is attributed to the use of our computationally less expensive than the detailed model usually applied model to determine the aerosol concentration. This model tends to underpredict the radiative heat loss. This leads to the overprediction of gas temperature, thereby leading to overprediction of the mean burning rate. This overprediction is more prominent in case of higher pool temperatures because radiation plays a dominant role in these cases as reported by Yamaguchi and Tajima [6].
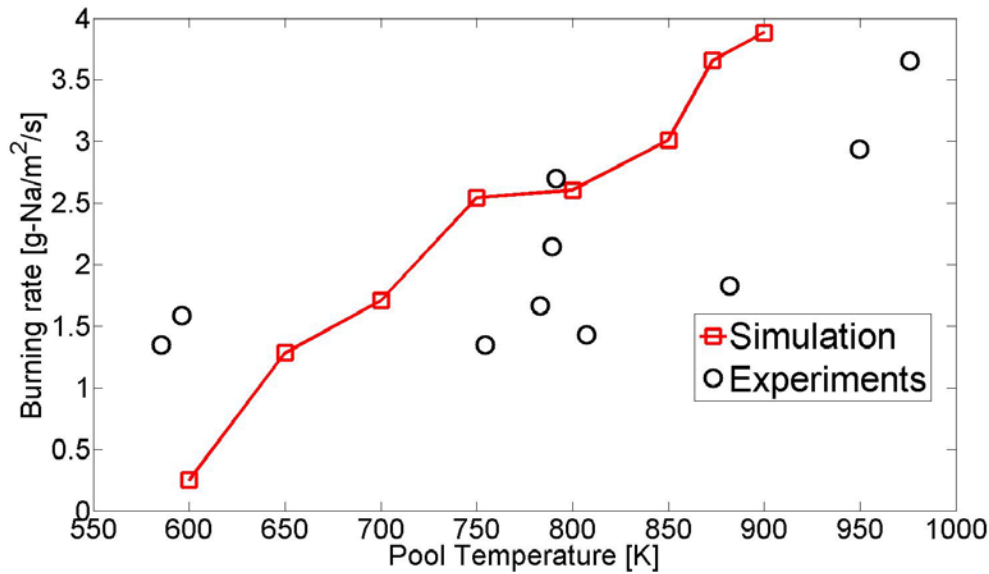

FIG. 2. The variation of the mean burning rate with initial pool temperature for an initial oxygen concentration of 4 % by volume .

Figure 2 plots the variation of the mean burning rate with initial pool temperature obtained using simulations (lines) and experiments (symbols). The results are shown here for an initial oxygen concentration of 4 (% vol). The overprediction of mean burning rate can also be seen in this case. The reason for this over-prediction is already explained above. The model tends to underpredict the mean burning rate at lower pool temperature. This is because at lower pool temperature, the vapor pressure is low and hence, a pool combustion phenomenon is governed by surface reaction instead of gas phase reaction. The model proposed by us simulates only the gas phase pool combustion phenomena and cannot describe surface reaction.

The overall trend of increase in the burning rate with initial pool temperature is captured well. In addition, the trends of decrease in the mean burning rate with decrease in oxygen concentration at a constant pool temperature are captured well.

4 Summary and Conclusion

The sodium fast reactor is one of the fourth generation nuclear reaction designs. It uses liquid sodium as coolant because of its excellent thermophysical properties. However, sodium reacts with air and water violently. Therefore, it is important to investigate sodium-air and sodium-water reactions in detail. A CFD based model is proposed here to simulate sodium pool combustion. The model solves Favre averaged Navier-Stokes equation with the Low-Re k-ε turbulence model. The mixture fraction based non-premixed combustion model is used for modeling.

The validation of the model is performed against sodium pool experiments of Newman and Payne [22]. The trends of increase in the mean burning rate with initial pool temperature and decrease in the mean burning rate with initial oxygen concentration are reproduced well.
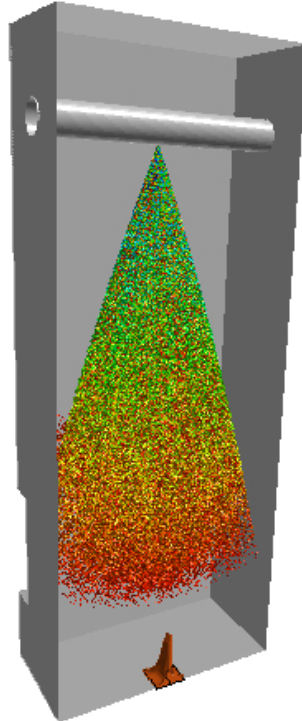

FIG. 3. Development of a spray from a pipe break. The color represents residence time of each droplet.

5 Future Work

In the past, we have presented our sodium spray combustion modeling and validation results in Sathiah et al. [25]. In this paper, we present our sodium pool combustion modeling approach and validation results. Our next step is to combine these approaches to model simultaneous sodium spray and pool combustion.

For this case, we considered a closed room containing a pipe (see Fig. 3). The room is assumed to be at ambient conditions, containing air, i.e. oxygen (21 % by vol.) and nitrogen (79 % by vol.). It is assumed that the pipe breaks and sodium is ejected in the form of spray. Furthermore, also sodium is collected on the floor forming a sodium pool. Preliminary computations are performed for a case in which both spray and pool are burning simultaneously. Figure 3 shows the spray development and its spreading with time. At the floor, the iso-surface of temperature is plotted to show the development of the pool fire.

This approach enables us to determine, the effects of spray and pool combustion on temperature distribution and pressure evolution. Therefore, such an approach, once well validated is considered a step forward in the safety analysis of sodium fast reactors.

6 Acknowledgments

References

[1]   T. Takata. *Multi-Disciplinary Phenomena of Chemical Reaction and Thermal Hydraulics in Sodium Cooled Fast Reactor*. PhD thesis, Osaka University, 2007.

[2]   F. Huber, P. Menzenhauer, and W. Peppler. Investigation of sodium area conflagrations and testing of a protective system. *Nuclear Engineering and Design*, 35(1):155–162, 1975.

[3]   S.V. Diwakar, P. Mangarjuna Rao, N. Kasinathan, Sarit K. Das and T. Sundararajan. Numerical prediction of fire extinguishment characteristics of sodium leak collection tray in a fast breeder reactor. *Nuclear Engineering and Design*, 241(12):5189–5202, 2011.

[4]   N. Doda, H. Ninokata, and H. Ohira. Prediction of release rate of sodium as aerosol. *Journal of Nuclear Science and Technology*, 38(1):30–35, 2001.

[5]   N. Doda, Y. Okano, and H. Ninokata. Numerical simulation of sodium pool fire. *Nuclear Technology*, 144(2):175–185, 2003.

[6]   A. Yamaguchi and Y. Tajima. Numerical investigation of mass and heat transfer in sodium pool combustion. *Numerical Heat Transfer Part A: Applications*, 41(6-7):697–709, 2002.

[7]   A. Yamaguchi and Y. Tajima. Numerical simulation of non-premixed diffusion flame and reaction product aerosol behavior in liquid metal pool combustion. *Journal of Nuclear Science and Technology*, 40(2):93–103, 2003.

[8]   A. Yamaguchi and Y. Tajima. Validation study of computer code SPHINCS for sodium fire safety evaluation of fast reactor. *Nuclear Engineering and Design*, 219(1):19–34, 2003.

[9]   A. Yamaguchi and Y. Tajima. Response surface modeling of aerosol release fraction in sodium pool combustion. *Journal of Nuclear Science and Technology*, 40(10): 862–870, 2003.

[10]   A. Yamaguchi and Y. Tajima. A numerical study of radiation heat transfer in sodium pool combustion and response surface modeling of luminous flame emissivity. *Nuclear Engineering and Design*, 236(11):1179–1191, 2006.

[11]   A. Yamaguchi and Y. Tajima. Sodium pool combustion phenomena under natural convection airflow. *Nuclear Engineering and Design*, 239(7):1331–1337, 2009.

[12]   A. Yamaguchi, T. Takata and Y. Okano. Numerical methodology to evaluate fast reactor sodium combustion. *Nuclear Technology*, 136(3):315–330, 2001.

[13]   ANSYS FLUENT. ANSYS-Fluent Inc., 2008 ANSYS-Fluent Inc., 2008. Fluent 12.0. Lebanon, N.H., 2008.

[14]   ANSYS CFX. *ANSYS, 2007 ANSYS Inc., 2007. ANSYS CFX-10.0 User Manual.*, 2007.

[15]   T. Poinsot and D. Veynante. *Theoretical and numerical combustion*. Edwards, 2005.

[16]   S. Turns. *An Introduction to Combustion Concepts and Applications*. McGraw-Hill Series in Mechanical Engineering, 2000.

[17]   Incropera and DeWitt. *Fundamentals of Heat and Mass Transfer, 3rd.*

[18]   R.N. Newman. Ignition and burning behavior of sodium metal in air. *Progress in Nuclear Energy*, 12:119–147, 1983.

[19]   R.K. Hilliard, J.D. McCormack and A.K. Postma. Aerosol behavior during sodium pool fires in a large vessel- CSTF tests AB1 and AB2. Technical report, HEDL-TME-79-28, 1979.

[20]   V. Novozhilov and H. Koseki. CFD prediction of pool fire burning rates and flame feedback, *Combustion Science and Technology*, 176:1283-1307, 2004

[21]   I. Hashiguchi, J. Hara, and H. Nei. *Proceedings of the Annual Meeting of Atomic Energy Society of Japan, (Paper A53)*, 1978.

[22]   R.N. Newman and J.F.B Payne. The burning rates of sodium pool fires. *Combustion and Flame*, 33:291–297,1978.

[23]   M.J. Pilat and D.S. Ensor. Plume opacity and particle mass concentration. *Atmospheric Environment*, 4:163–173, 1970.

[24]   R.W. Bilger, S.H. Starner and R.J. Kee, On reduced mechanisms for methane-air combustion in nonpremixed flames, *Combustion and Flame,* 80:135-149, 1980.

[25]   P. Sathiah, A. Siccama, F. Roelofs. CFD modeling of sodium spray combustion. *Proceeding of the 14th International Topical Meeting on Nuclear Reactor Thermal Hydraulics (NURETH-14)*, Toronto, Canada, September 25-30, 2011.

[26]   C. Casselman. Sodium Fires: Theory and Mitigation. ESFR SP5- Education and Training- Sodium Behavior and Safety, Cadarache, France 2009.

Licensing support experience of the BN-600 operation

N. Khrennikov, A. Sintsov[†]

Scientific and Engineering Center for Nuclear and Radiation Safety,
Moscow, Russian Federation

Abstract. The experience gained by the Russian regulatory body for licensing support of the operation of sodium-cooled fast reactor (Beloyarskaya nuclear power plant BN-600) from the standpoint of further evolution of the sodium-cooled fast reactors are described. For more than thirty summers period of the commercial operation of the BN-600 the regulatory body has fulfilled safety reviews of the wide range of justification report concerning of technical decision of the implemented modernizations which were carried out on the power unit to increase the technical and economic reactor indicators. Accident-free operation of the BN-600 reactor evidences both the quality of the development and level of mastery of this reactor technology, and performance of the appropriate supervision from the regulatory body.

On April 8, 2010 there was 30th anniversary from the start-up of the 3rd power unit of the Beloyarsk nuclear power plant with the reactor BN-600. It was achieved by the following operational characteristics [1]:

—— no depressurized pins;

—— negligible long-living gases and noble gases release;

—— last sodium leakage was in May, 1994;

—— no leaks in the steam generators in the last 19 years:

—— no failure of sodium equipments. In last years the refusals took place only in equipment of the third cycle and power supply systems;

—— no actuation of the emergency protections for the last 9 years (from 2001 to 2009) average operational factor is 74 % and it was generated about 112 billion kWh energy for 30 years.

These operational characteristics evidence both the quality of the development and level of mastery of this reactor technology and performance of the appropriate supervision from regulatory body. Moreover they were achieved due to research, scientific and technical programs continuously carried out in the unit for execution of the sodium technology [1]. For the last time it was tested, replaced and repaired main

---

[†] sintsov@secnrs.ru, tel +7 499 2640596, fax +7 499 2642859

equipments of the primary and secondary sodium systems, for example [1][3], main circulation pumps, steam generators, heat exchangers, rotating plugs. It was tested new construction of the fuel assemblies and control protection rods made from new structural materials. These examinations allowed to execute several modifications of the BN-600 core. Main design characteristics show in table 1 (the first and second column).

Table 1. Evolution of the BN-600 core characteristics

	Operation period /1, 2/			
	1980-86 year	from 2005 year	Planning characteristics	
Burn-up, % h.m.	7,2	11	11,7	15
Damage dose, dpa	44	82	87	110
Cycle length, EFPD	200÷300	560÷720	592	710÷770
Fuel construction materials Pin cladding Assembly cladding	EI-847 16Cr11Ni3Mo	EI-847 16Cr11Ni3Mo Ti	ShC-68 х.д. EP-450	? EP-450

The research, scientific and technical programs are still in progress. There are the main following programs: increase design burn-up, reliability of the in-core equipments operation, including fuel assemblies and control protection rods, experimental validation of the unreplaceable equipments working life. The operator planes to achive increase design burn-up at improvement of the pin cladding properties. Increase design burn-up is planed to achieve due to improvement material properties (for example forming, mechanical properties, corrosion resistance etc.) pin cladding steel. For last several years operator performed following investigations for improvement of BN-600 economical efficiency and increase its fuel burn-up [3][4][5]:

— pilot phase of the unit operation with increase cycle length;

— increase lifetime of the emergency protection rod;

— irradiation of the fuel assemblies with different steels samples;

— irradiation of the fuel assemblies with pins made from new steel;

— irradiation of the MOX-fuel assemblies.

The operator supposes, that perform of these investigations make it possible to carry out two updatings of the core (see table 1 the last two columns) and to achieve fuel burn-up of equal 15 % т.а.

All works, including fatigue tests of new types of fuel, are carried out at the unit 3 Beloyarsk nuclear power plants with the BN-600 reactor with the justification of the regulatory body. Justification procedure is standard for all power units and

independent from the reactor types. The procedure consists of review of the Safety analysis report (SAR) and revision of the license conditions. According to [9] the regulatory body and independent experts or technical support organizations, which can be involved in this work by the regulatory body, review SAR, operational manuals and other operator documents. The documents submitted to the regulatory body are reviewed on compliance with two criteria:

— safety requirements (i.e. Federal rules and codes). The project and design documents shall meet safety requirements;

— the technical and organizational measures for safety guarantee shall meet well-known results of the research investigations or shall be experimental validate.

It is very important and difficult to choose correct safety criteria used at safety review of the research, scientific and technical programs. The first of all it is concerned safety review of the in-core equipments (including fuel assemblies and control protection rods) lifetime tests. It is well known construction materials behaviour in the fast breeder reactors substantially depends on radiation damage and thermal loads, so limiting characteristics (long-term strength, structural strength, combined strength, fatigue strength, irradiation-induced swelling, deformation) of the safety important elements are not known before lifetime testing. Examination of construction materials after irradiation in the testing reactor more often does not give answer about limiting characteristics, because irradiation conditions (neutron spectrum and fluence, thermal load etc.) of the testing reactors do not correspond with conditions of BN-600.

As a rule, in this case safety criteria are defined by the operator and the regulatory body using following procedure. The operator makes special testing program for the in-core safety important elements and to describe and justify every test steps. The regulatory body fulfils safety review of this test program using update safety criteria, Federal standards and codes' requirements and independent expert experience. On the basis of results of the safety review the regulatory body makes decision on the program implementation.

The requirements for standard inspection program (procedure, rules) of the equipments and pipelines are defined in the PNAE G-7-008-89 [8]. The program is one of the obligatory documents. One of the main requirements for metal inspection is to use destructive and non- destructive methods. In this context destructive inspection of the metal and welds mechanical properties is implemented by testing of specimens installed in equipment or cut out (e.g. from the pipelines) according to requirements of the design documentation. The specimens are used for control of:

— change of mechanical properties (yield point, resistance to time, relative lengthening, relative narrowing);

— brittle fracture resistance properties (critical brittleness temperature, fracture toughness or critical opening of a rupture);

— properties of total and local corrosion (including pit corrosion, stress corrosion and intergranular corrosion).

The appropriate remote devices shall be provided for inspection of equipment in places where it can not be carried out by the standard devices due to radiation level or equipment layout.

In the BN-600 reference specimens testing were not placed therefore the operator carried out special experimental program. Within this program the operator irradiates special speciments into material assemlies. Speciments are irradiated on the periphery of the core.

In cases when reference specimens testing did not place, the operator shall carry out irradiation of the construction material specimens into such part of the core that irradiation conditions correspond to operational conditions in-core elements.

Non-destructive inspection of main elements and pipelines [8] shall be fulfilled periodically, and not later than 30000 hours of operation after the previous periodical inspection according to standard inspection program (procedure, rules). Inspection of the minor elements and pipelines important for safety – in each 45000 hours of operation after the previous periodical inspection.

The testing programs of the fuel assemblies and control protection rods are implemented step by step. Results received from previous steps are used to justify unit safety in next step. As a rule, the testing programe consists of the following steps: laboratory reseach of a new materials (in this steps special authorization are not needed), testing of a sampeles made by new steels (as a rule, this step consists of reactor irradiation and following distructive and non-destructive reseach), pins and FAs test, lifetime tests and determination of the operational and design limits. After that the operator shall make changes in the SAR and it is possible to carry out core modernization.

List of the steps are inderectly enumerated in the federal standarts and codes (OPB-88/97 [7] and NP-082-07 [5]). For example [7] requires that technical and administrative decisions made for ensuring NPP safety shall be well proven by the previous experience or tests, investigations, operating experience of prototypes and shall meet requirements of regulatory documents. Such approach shall be applied not only in development of equipment and design of the NPP but also in manufacture of equipment, construction and operation of the NPP, its backfitting and reconditioning of its systems (elements). In [5] this requirement is improved concerning (modernization of the reactor core, when new designs of fuel assemblies and new fuel compositions are applied, the improvement of control and protection system and other safety important systems, a required scope of bench and in-pile tests shall be carried out. And operator shall demonstrate that the sufficient number of studies has been conducted to prove that the required safety criteria were met. In additional operator shall determine and justify operational limits and conditions, safe operation limits and conditions and design limits established for design basis accidents. If operator uses

computer codes for justification of limits the using codes and methodologies shall be verified and certified in accordance with the established procedures.

In accordance with [5] operator shall demonstrate that the maximum design fuel damage limit established for design basis accidents with the severest consequences is not exceeded. The reactor RI designs shall establish design fuel damage limits for other design basis accidents; their values shall be less than the maximum design fuel damage limit. The maximum design fuel damage limit for BN type reactors are determined in [5]:

— fuel rod cladding temperature – 900°C;

— fuel temperature – 2300°C;

— volume swelling of FR cladding – 15%.

Moreover, operator shall justify that void effect in sodium coolant during normal operation and operational events, including design basis accidents is excluded. The core and its components' (including fuel rods and fuel assemblies) design and implementation during normal operation and operational events, including design basis accidents shall ensure fuel damage limits not exceed taken into account different factors to degrade mechanical properties of the core structural materials and integrity of the pin cladding.

When operator wants to use new construction materials for in-core elements including FAs and control protection rods he shall fulfille safety justification of use of these elements. The justification shall include analyses of the elments operability for the conditions of normal operation, abnormal operation, and accidents. The justification shall be fulfilled taking into account loads arisen due to design-basis failures of other systems.

When operator justifies implementation of materials used for in-core elements including FAs and control protection rods [6] substantiation shall be fulfilled for the conditions of normal operation, abnormal operation, and accidents and shall be took into account loads arisen due to design-basis failures of other systems is to be described, and characteristic of the measures to protect the system from being affected by these failures is to be presented. Main characteristics (mechanical, thermal-hydraulic neutronic, physicochemical, strength, etc.) and reliability features shall be presented for each mode of system operation including failures of other systems, as well as the main characteristics and reliability features are to be presented as ones being within permissible range predetermined.

In the conclusion it is necessary to note that accident-free operation of BN-600 confirms an approach to license support of the BN-600 operation used by the regulatory body now.

N. Khrennikov and A. Sintsov

ACKNOWLEDGEMENTS

REFERENCES

[1] N.N. Oshkanov, O.M. Saraev 30 Years of experience in operating the BN-600 sodium-cooled fast reactor - Atomic energy, vol. 108, issue 4, pp 234-239, August 2010.

[2] G.V. Babenko, A.V. Gavrilov Improvement of the Efficiency and the Economics of the Fuel Utilization at the Beloyarsk NPP BN600 Reactor – Transactions of Universities and Institutes (Izvestiya VUZov) (Известия ВУЗов). Nuclear Energy, pp 78-82 № 1, 2005 (in russian).

[3] V.V. Chuyev, V.F. Rosljakov, V.V. Maltsev Features of Constructional Materials' Behavior within Fast HighPower Reactor's Spectrum of Neutrons 3. – Transactions of Universities and Institutes (Izvestiya VUZov) (Известия ВУЗов). Nuclear Energy, pp 82-86 № 1, 2005 (in russian).

[4] A.I. Karpenko, E.A. Kozmanov, V.V. Maltsev, A.V. Zakharov, V.D. Risovany, A.A. Khudyakov Confirmation of the Design lifetime of the Test Safety Rods Manufactured of Refabricated Boron Carbide after Operation in the BN600 Reactor. – Transactions of Universities and Institutes (Izvestiya VUZov) (Известия ВУЗов). Nuclear Energy, pp 133-139 № 1, 2005 (in russian).

[5] NP-082-07 Nuclear safety rules for reactor installations of nuclear power plants. Moscow 2007.

[6] PNAE G-1-001-85Standard Content of Technical Safety Justification of Nuclear Power Plants (TS TOB AS-85). Moscow, 1985

[7] OPB-88/97 General regulations on ensuring safety of nuclear power plants (PNAE G-01-011-97). Moscow, 1997.

[8] PNAE G-7-008-89 Rules for arrangement and safe operation of equipment and piping of nuclear power installations. Moscow, 1989.

[9] Federal Law № 170-FZ от 21.11.1995 On the use of atomic energy.

SARGEN_IV: Proposal for harmonized European practices for the safety assessment of innovative fast neutrons spectrum reactors considered in Europe

D. Blanc[a], E. Wattelle[a], L. Ammirabile[b], K. Tucek[b], L. Burgazzi[c], F. Puente-Espel[d]

[a] Institut de radioprotection et de sûreté nucléaire, Fontenay-aux-Roses, France

[b] Joint Research Center, Netherlands, Petten

[c] Agenzia nationale per le nuove tecnologie, l'energia et lo sviluppo economico sostenibile, Bologna, Italy

[d] Gesellschaft für Anlagen und reactorsicherheit, Munchen, Germany

Abstract. In the aim of preparing the safety assessment of advanced reactor demonstrator and/or prototype with closed fuel cycle planned to be built in Europe (Fast reactors cooled by sodium, lead, lead/bismuth, or gas) the SARGEN_IV Project gathers 22 partners' safety experts from 12 Member States + European Commission (EC), including European Technical Safety Organizations, the EC's Joint Research Centre, designers, one utility, research institutes and universities in order to propose a European harmonized practices for the safety assessment. The paper is focused on the two first stages of the project:
1-review of the critical safety features of the concepts and their categorization to identify common phenomena, to highlight each concept specific topics; 2-review of the safety assessment practices adopted in European countries, used within FP7 projects, proposed by international organizations and presentation for a commonly agreed proposal for harmonized safety assessment practices for the above mentioned reactors.

1. Introduction: scope of the project

1.1. Technical context

The deployment of sustainable nuclear technology is likely to play a key role in the future energy policy considering the objectives set out by the European Union of transforming the current energy system based on fossil fuels into a more sustainable one based on a mix of low-carbon energy sources.

For sustainability purpose, the "European Sustainable Nuclear Industrial Initiative" (ESNII) was launched in November 2010 to anticipate the development of a fleet of fast reactors with closed cycle i.e. Sodium cooled Fast Reactors (SFR), Lead cooled Fast Reactors (LFR) and Gas cooled Fast Reactors (GFR). ESNII also includes some support infrastructures with in particular an irradiation fast spectrum test facility i.e the FAst Spectrum Transmutation Experimental Facility (FASTEF) able to test both the LFR technology and the Accelerator Driven System (ADS) technology.

1.2. Consortium as a whole

The SARGEN_IV Project represents an opportunity to prepare the safety assessment for the future innovative reactors. In this view, it becomes crucial to bring together European designers, Technical Safety Organizations (TSOs), research organizations and utilities already involved (or to be involved) in

innovative reactors and that constitute the best means in order to propose European harmonized safety assessment practices and to consolidate their work within the EURATOM contribution to the Generation IV International Forum (GIF).

All the requirements in terms of competences are fully satisfied by the group of the 22 partners from 12 Member States (+ the EC) consisting of Technical Safety organizations (the eight TSOs involved in the European Technical Support Organization Network - ETSON), national research organizations, designers, one utility, three universities and the EC's Joint Research Centre.

2. Organization

The SARGEN _IV Project has four main objectives:

— Identification and categorization of the critical safety features associated with the four concepts
— Review of the available safety methodologies followed by a proposal for harmonization of the safety assessment practices for innovative reactors
— Test application of the proposed European methodology
— Development of an European roadmap for the fast reactors safety R&D

SARGEN_IV Project started in January 2012 with two years duration. Only the main results of the two first objectives are presented hereafter.

3. Identification and categorization of the critical safety features associated with the four concepts

In a first step, relevant safety issues and corresponding initiating events have been identified for the four representative fast reactor systems selected in the ESNII Deployment Strategy.

Secondly, to further systematize the consideration of safety issues and characteristics for a consistent build-up of the safety architecture and development of adequate provisions, the SARGEN_IV Project aimed at categorizing the individual issues identified for the ESNII concepts to several common "families". The categorization was adopted according to:

— Common phenomena related to:
  - Materials (fuel, coolant, structure, absorber)
  - Aspects specific to fast reactors
  - Aspects specific to design solutions envisaged for ESNII concepts, and
— Possible impact on the fulfillment of fundamental safety functions related to
  - Control of reactivity
  - Removal of heat
  - Confinement of radioactive materials

The objective of the latter categorization was to assist in identifying measures to be implemented to accomplish the fundamental safety functions and consequently also to identify a representative set of initiating events and transients for the test application of harmonized safety assessment methodologies.

As an example, aspects specific to fast reactors were evaluated, incl. reactivity feedbacks (in particular void effect), risks for the core compaction and due to the handling operations and severe accidents. Resistance to external events is also evaluated. The analysis highlighted as well the erosion/corrosion issues and the high chemical activity with air and water as main risk factors as regards the use of specific coolant, respectively lead and sodium.

Behavior of the ESNII prototypes was also considered in the perspective of Fukushima-Daiichi TEPCO reactors events, incl. extreme earthquake, extreme flooding, total loss of electric power supply and/or the ultimate heat sink(s), and severe accident management.

Specific aspects related to design solutions envisaged for the ESNII concepts include steam generator tube ruptures for heavy liquid metal cooled concepts and beam window rupture for FASTEF.

The afore-mentioned categorization work also provides useful guidance for the identification and prioritization of R&D needs respective to the identified safety issues.

The document [1] makes the synthesis of the work performed in §3 and provides an identification and a ranking of safety issues for the four representative fast reactor systems selected in the ESNII Deployment Strategy.

4. Review of the safety methodologies scoping to propose a harmonization of the safety assessment practice for innovative reactors

4.1. Review of the existing safety methodologies

Various safety methodologies are already (or will be) available that could be applied to the ESNII prototypes, pilot plants and demonstrators, which need to be analyzed and disseminated inside the SARGEN_IV consortium such as:

⎯ Methodologies dedicated for innovative reactors and issued from the GIF Risk and Safety Working Group (RSWG) and from IAEA as the International Project on Innovative Nuclear Reactors and Fuel Cycles (INPRO) safety assessment methodology

⎯ National safety approaches (France, Germany, Spain Finland, Belgium) and the associated experience feedback in particular for the SFRs built in France and Germany and for the Finish European Pressurized Reactor (EPR^{TM})

⎯ Safety approaches adopted in European collaborative projects related to the four concepts (CP-ESFR for SFR, LEADER for LFRs, GoFastR for GFR, and CDT for FASTEF)

⎯ Documents coming from international organizations such as IAEA and the Western Europe Nuclear Regulators'Association (WENRA) and available for the safety assessment of innovative reactors including methodology used for the European nuclear power plant (NPP) "stress tests"

4.2. Proposal for a harmonization of the safety assessment practices for innovative reactors

Some differences exist in the approaches mentioned in § 4.1 and the objective is to provide harmonized safety assessment practices highlighting what is new and useful for innovative reactors.

Safety assessments should be performed for both reactor and fuel storage, in all plant states and conditions – including maintenance stages - over the lifetime of the installation, up to decommissioning. Waste management and workers radiological protection should also be taken into account. Moreover, human and organizational factors and man-induced situations are a part of the safety demonstration. Natural phenomena should be considered. Finally, security/safeguard aspect should be dealt in an integrated manner. Besides, chemical effects could be a challenging issue with regards of the current expected designs of ENSII reactors**.**

Ambitious safety objectives are aimed to be achieved even though safety goals of GIF are not particularly prescriptive, notably for the goal to eliminate the need for offsite emergency response. Nevertheless, the goal is to reduce potential consequences and impact on public, workers and environment as well as occurrence/frequency of incidental and accidental situations.

The work highlights the importance of safety principles in achievement of safety objectives:

- Defense-In-Depth (DiD) principle remains fundamental. An overall reinforcement of DiD is expected for ENSII prototypes, including a necessary enhancement of the effectiveness of the independence between all levels of DiD. A particularly important issue for ENSII prototypes reactor could be to clearly define level 4 for each plant design.
- Application of other principles as As Low As Reasonable Achievable (ALARA) principle and As Low As Reasonable Practicable (ALARP) principle should also be enhanced.
- Concerning fundamental safety functions, an inherent behavior of the plants should reinforce the fulfillment of fundamental safety functions e.g. the consequences for unprotected situations should be reduced and the grace periods should be extended. For that, the use of passive systems can be envisaged.
- Practical elimination is another important principle, but it requires in-depth analyses for ENSII prototypes.
- Lastly, the need of two complementary and integrated approaches, the deterministic and the probabilistic ones, is reiterated.

A safety assessment should be performed with regard to safety objectives in particular those proposed by WENRA and considering safety principles, SARGEN_IV project proposes to use some methodologies such as the Qualitative Safety Features Review (QSR), the Objective Provision Tree (OPT) and the Phenomena Identification and Ranking Table (PIRT) for the global safety assessment process to provide feedback.

Concerning the detailed safety assessment, there is no clear specificity for ENSII prototypes. Nevertheless, the comprehensive set of postulated initiating events could be quite different from ENSII prototypes. Moreover, they should be assessed with more stringent rules and acceptance criteria. Hazards assessment would be a tremendous aspect of next generation of NPP safety assessment and should be improved, which is confirmed by the first insights of Fukushima Daiichi TEPCO reactors accidents. These first insights, on the basis of the European Nuclear Safety Regulators Group (ENSREG) specifications and conclusions, should be extrapolated for new designs, that is another challenge for ENSII reactors.

For example the total loss of power sources, the total loss of the ultimate heat sink(s) and the combination of both have to be considered with also the management of a severe accident in this case. Provisions to cope with these events notably to improve the grace period before cliff-edge effects and thus to allow back-up measures to be implemented have to be defined and should be considered as hardened equipements.

The document [2] provides a synthesis of the work performed within § 4.2.

The next phase of the SARGEN_IV Project is comprised in the test application of the proposed harmonized European practices to the selected initiating events of the ENSII reactor prototypes. This will aimed to identify needs on R&D and provide feedback to the harmonized European practices in support for the EURATOM contribution to the preparation of GENERATION IV "white paper" on nuclear safety for European concepts.

5

REFERENCES

[1]: 7th Framework Programme - SARGEN_IV Project n°295446 - Deliverable D2.5: Identification and Ranking of Safety issues

[2]: 7th Framework Programme - SARGEN_IV Project n°295446 - Deliverable D3.5: Proposal for an harmonization of the safety assessment practices

ACKNOWLEDGEMENTS

Aspects of the core shielding assessment for the FASTEF-MYRRHA design

A. Ferrari[1,2], S. Di Maria[3], R. Fernandez[4], J. Konheiser[2], M. Ottolini[5], M. Sarotto[6], A. Stankovskiy[4]

[1]Institute of Radiation Physics, Nuclear Physics Division, Helmholtz-Zentrum Dresden-Rossendorf, PF 510119, 01314 Dresden, Germany

[2]Institute of Resource Ecology, Reactor Safety Division, Helmholtz-Zentrum Dresden-Rossendorf, PF 510119, 01314 Dresden, Germany

[3]Instituto Tecnológico e Nuclear, Estrada Nacional 10, 2686-953 Sacavém, Portugal

[4]SCK·CEN, Boeretang 200, 2400 Mol, Belgium

[5]Ansaldo Nucleare s.p.a., c.so Perrone 25, 16161 Genova, Italy

[6] ENEA, Via Martiri di Monte Sole 4, 40129 Bologna, Italy

Abstract. In the frame of the FP7 European project Central Design Team (CDT), an extensive simulation study has been done to assess the main shielding problems in view of the construction of the MYRRHA accelerator-driven system at SCK·CEN in Mol (Belgium). A method based on the combined use of the two Monte Carlo codes MCNPX and FLUKA has been developed, with the goal to characterize realistic neutron fields around the core barrel and build complex source terms, to be used in detailed analyses of the radiation fields due to the system in operation, and of the coupled residual radiation. The results evidenced a powerful way to analyze the shielding and activation problems, with direct and clear implications on the design solutions.

1. Introduction

Accelerator-driven systems (ADS) are one of the options studied for the transmutation of nuclear waste in the international community. With the goal to demonstrate efficient transmutation of high level waste and associated ADS technology, in the years 2009-2012 the FP7 European project Central Design Team (CDT) worked at the FAst Spectrum Transmutation Experimental Facility (FASTEF) design, on which the MYRRHA research facility [1] at SCK·CEN in Mol (Belgium) will be based. The heart of the system is a lead-bismuth eutectic (LBE) cooled reactor, working both in critical and in sub-critical operation modes. The neutrons needed to sustain fission in the sub-critical mode are produced via spallation processes by a 600 MeV, $\leq$ 4 mA proton beam, which is provided by a linear accelerator and hits a LBE spallation target located inside the reactor core (Figure 1). The combination with a nuclear reactor core operating in sub-critical mode with 94 MW power, or in critical mode with 100 MW power when not coupled with the proton beam, makes the shielding problem an issue, being the protection from the prompt[1] radiation and the spent beam handling the main points. In the

---

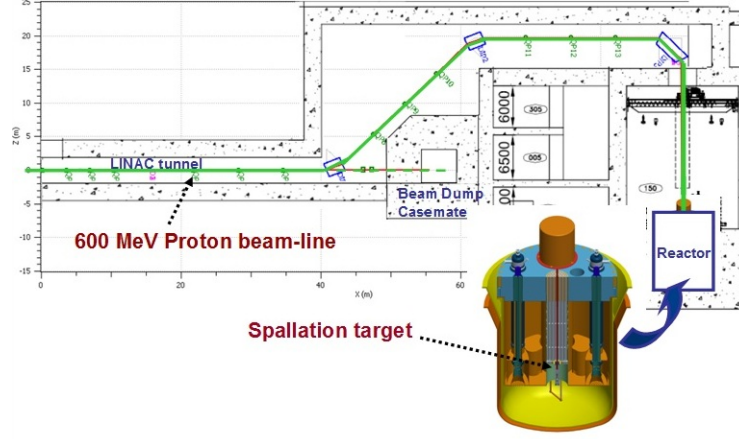[1] The adjective "prompt" is here referred to all the radiation due to the reactor in operation.

Figure 1: Final part of the FASTEF-MYRRHA proton beamline.

following it will be shown how the coupled use of the two Monte Carlo codes MCNPX [2] and FLUKA [3][4] can be the key of a powerful method to optimize the shielding design and to address the activation problems.

2. Shielding and activation analysis

The general problem of the radiation containment can be divided in two parts: the shielding of the accelerator tunnel and the shielding of the reactor building. The first problem has been addressed in [5] and [6], where a systematic study of the neutron production and the radioactivity induced by the MYRRHA proton beam in typical materials has been performed, to support the optimization of the elements devoted to the partial or the total beam absorption. The present work focuses on methodological aspects of the second problem. To assess the shielding of the reactor core, both critical and sub-critical operation modes have been studied [7]. Since in FASTEF the reactor is designed to operate at 100 MW core power in the critical mode and at 94 MW in the subcritical one, the critical mode exhibits the highest lateral neutron fluence at the fuel level, and can be reasonably considered the conservative case for the lateral radiation containment. At the contrary, because of the backscattered radiation from the spallation target and due to the presence of the beam pipe channel, the subcritical operation drives the vertical design [8].

An extensive simulation study has been done using two state-of-the-art Monte Carlo codes: MCNPX, version 2.6.0, and FLUKA, version 2011.2. MCNPX has been used in CDT to build the official core models in both the critical and the subcritical operation modes [7]. To simulate the high energy processes in the ADS mode, the Cascade-Exciton Model, CEM03 [9], has been used. FLUKA, which can simulate with high accuracy the interaction and transport of about 60 different particles from the very high energy range down to the thermal energies for the neutrons, has the unique possibility to evaluate, in the same simulation, not only the particle fluences and the ambient dose equivalent due to all the components of the prompt radiation field, but also the time evolution of the activation products and the transport of their emitted radiation. Given an irradiation pattern, the time evolution of the isotopic densities, N_i, in the irradiated material is evaluated runtime via the exact analytical solution of the Bateman equations, which for a particle fluence rate, $\varphi(E)$, constant during each considered time interval can be written as:

$$\frac{dN_i}{dt} = - \sum_{j \neq i} \left[\lambda^d_{ji} + \overline{\sigma}_{ji} \overline{\varphi} \right] N_i + \sum_{j \neq i} \left[\lambda^d_{ij} + \overline{\sigma}_{ij} \overline{\varphi} \right] N_j \qquad (1)$$

where λ^d_{ji} is the decay probability of the radionuclide i in the radionuclide j and σ_{ji} is the particle induced cross section for transmutation from the isotope i to the isotope j, and where the average spectrum, $\overline{\varphi}$, and the spectrum averaged, particle induced cross-section, $\overline{\sigma}_{ji}$, have been introduced:
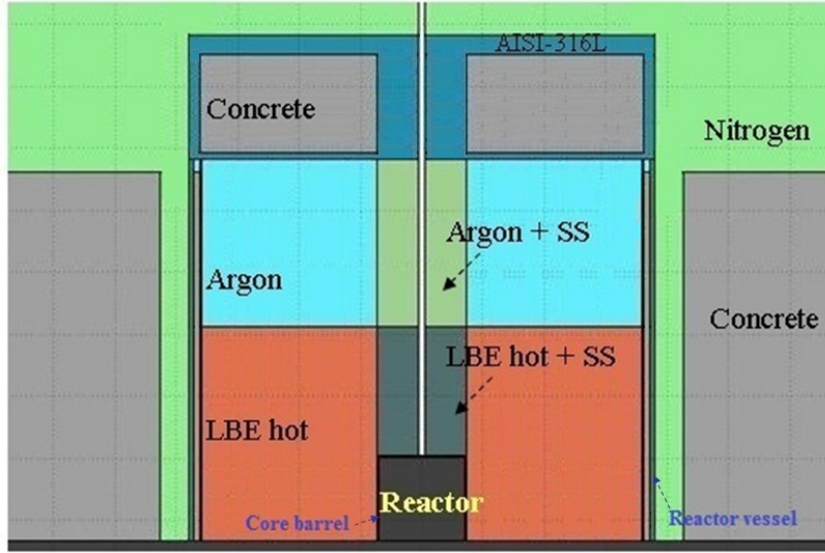
Figure 2: FLUKA model of the structure around the reactor core.

$$\bar{\varphi} = \int \varphi(E)dE \qquad\qquad \bar{\sigma}_{ji} = \frac{1}{\bar{\varphi}}\int \varphi(E)\sigma_{ji}(E)dE \qquad\qquad (2)$$

Besides the analytical calculation of the residual isotopic densities and their time evolution, at the same time FLUKA can perform the generation and transport of the emitted residual radiation (in the used version of the code extended to γ, β^+, β^-, X-rays and conversion electron emissions). In the same run we can obtain therefore the production of the residuals, their time evolution and the residual dose due to their decay.

Starting from the MCNPX critical and subcritical models of the structure in and around the core, which extend until the reactor vessel and where to be conservative the core compositions with fresh fuel have been considered, neutron radiation fields have been fully characterized on suitable surfaces on the core barrel and used to build complex source terms, input of a second row of FLUKA simulations. In the critical mode, to take properly into account the scattering effects of the neutrons in the coolant, the contribution of a vertical source term evaluated at the top of the fuel elements has been combined with the radial source terms, evaluated at the core barrel surface in three different regions around the fuel middle plane. In the subcritical mode, due to the strong angular dependence of the neutrons produced on the spallation target, the construction of a complex source term has been a more delicate issue. At the vertical level corresponding to the top of the fuel elements, a set of 10 different neutron spectra has been calculated in three radial regions inside the core barrel, corresponding to the boundaries of the fissile zone. The neutron spectra have been then computed as double-differential, in energy and in angular bins. The three angular bins: (0°, 30°), (30°, 60°), (60°, 90°) have been used for the external shells, while for the inner shell also a fine bin (0°, 1°) has bin evaluated.

A FLUKA model of the structural materials has been therefore built (see Figure 2), including at the reactor level the 'hot' (T = 350 °C) LBE coolant and all the containment structures until the walls in concrete. Above the hot LBE coolant a volume of argon has been described, followed by an initial, very preliminary design of the cover plate structure, in stainless steel and concrete. In the central column above the reactor, the presence of structural elements in stainless steel has been properly taken into account as material fraction in the argon and hot LBE coolant definition. In the subcritical analysis, the beam pipe in AISI-316L has been simulated at the center of the barrel column.
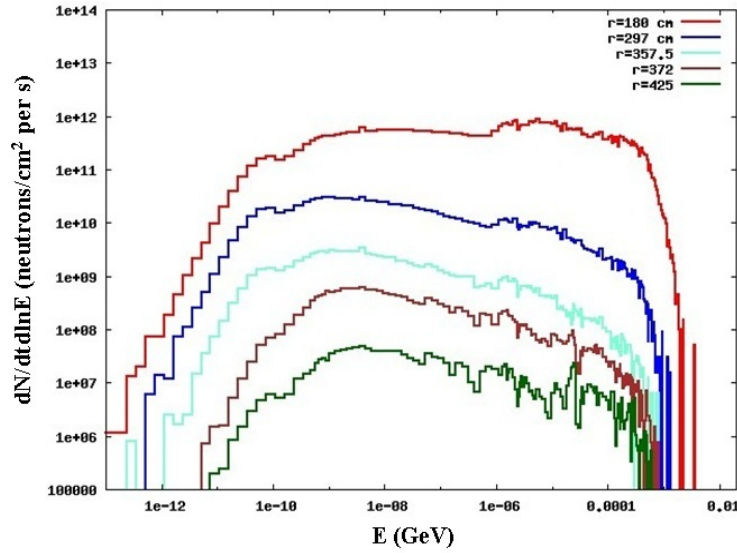
Figure 3: FLUKA neutron spectra at increasing radial distances in the hottest region across the fuel middle plane, in the critical operation mode.

The FLUKA/MCNPX comparison of the neutron fluence rates inside the reactor vessel at different radial and vertical distances from the core barrel shows a very good agreement, at the percent level in terms of total fluence rates, both in critical and in subcritical modes (in Figure 3 the FLUKA neutron radial spectra in the critical operation mode are shown). This agreement validates the FLUKA neutron source term description, on which the shielding and activation analysis is based. Dose distributions in terms of ambient dose equivalent rates, H*(10), have been then evaluated from the core barrel to the external containment and the shielding walls in the horizontal direction, and up to the last magnet of the proton beam-line and the final roof in the vertical one. It has to be stressed that to correctly evaluate the ambient dose equivalent in the structures around the core, until the external shielding walls, all the produced radiation must be taken into account. While the photons produced in the core give a negligible contribution to the total amount of radiation in the structures outside the reactor vessel (since they are absorbed in the coolant), the photons produced by neutron interactions with the materials outside the core - especially close to the reactor vessel - can play a role, as well as the ones produced directly in the shielding walls. In the present FLUKA evaluations of H*(10), these contributions are always taken into account. Figure 4 gives for example a 2D map of the photon fluence rate in the critical mode, evaluated in a narrow volume across the core middle vertical plane: a significant contribute in argon comes from the reaction $^{40}Ar(n_{th}, \gamma)^{41}Ar$, which exhibits a cross section of about 660 mb [10] at the 0.025 eV neutron energy. Such contribute is important also for his impact on the residual radiation at short cooling times. In Figure 5 and Figure 6 the H*(10) rates around the core, due to all the radiation components during the operation, are shown respectively for the critical and subcritical mode. These and similar results, which show already an optimal radial containment of the radiation, will drive the optimization of the cover design.

For the study of the residual radiation, three different irradiation patterns were considered for both the critical and subcritical mode: a medium-term (90 days sub-cycle), a long (5 years) and very long (15 years) irradiation period. To be conservative, the considered time intervals were assumed continuous, with three months stop per year (despite of the more limited availability of the system, due to the two different operation modes). Figure 7 shows the behaviour of the residual radiation in the structures around the core after 90 days of irradiation and 1 week of cooling in the ADS mode. The higher residual dose rates in the central column above the core are due to the activation of the stainless steel fraction assumed in the material composition, steel which is exposed to a harder neutron spectrum close to the spallation target. In the argon volume, the residual dose rates at this and longer cooling times are totally due to the ^{37}Ar isotope ($t_{1/2}$ = 35.04 d), which is produced from the natural argon via the $^{36}Ar(n_{th}, \gamma)^{37}Ar$ reaction, with a thermal cross section of about 5.2 b [10]. Besides the evaluation of the residual dose rates, the prediction of the isotope content in activated key materials has been
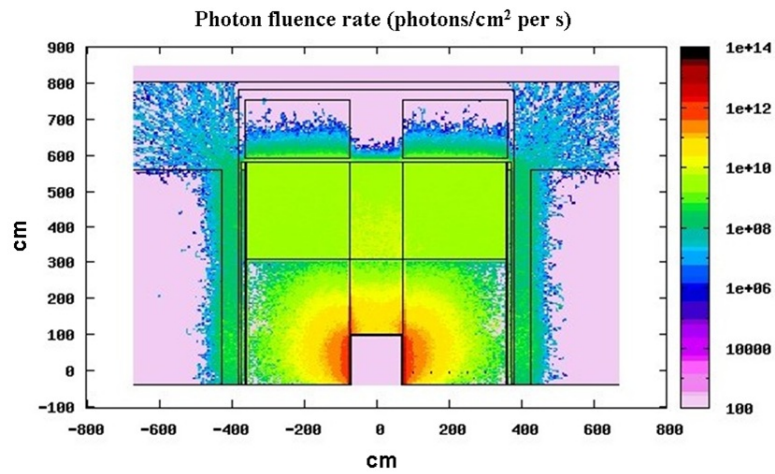
Figure 4: Photon fluence rate in the structures around the core during the critical operation mode.
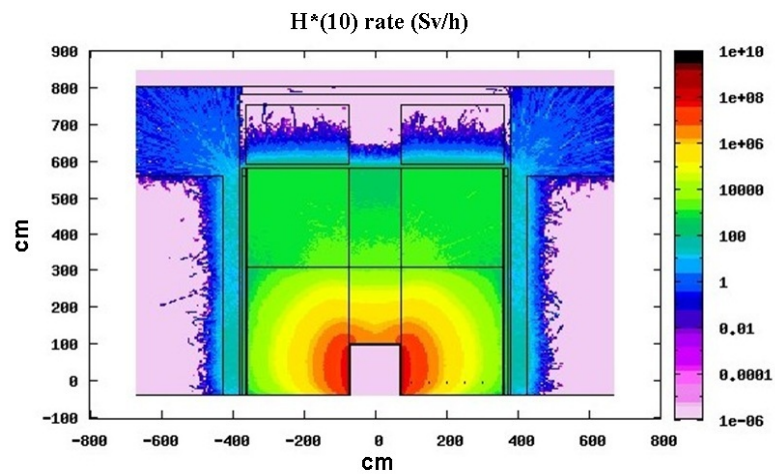

Figure 5: Ambient dose equivalent rate in the structures around the core in the critical operation mode.
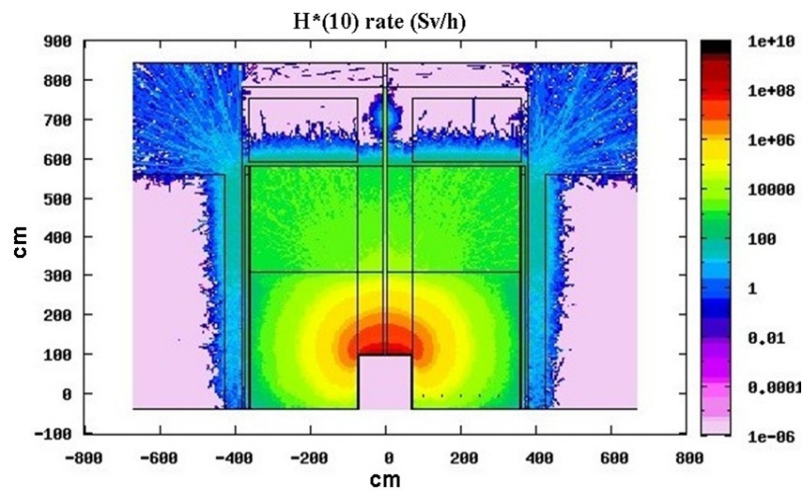

Figure 6: Ambient dose equivalent rate in the vertical structures above the core in the subcritical operation mode.
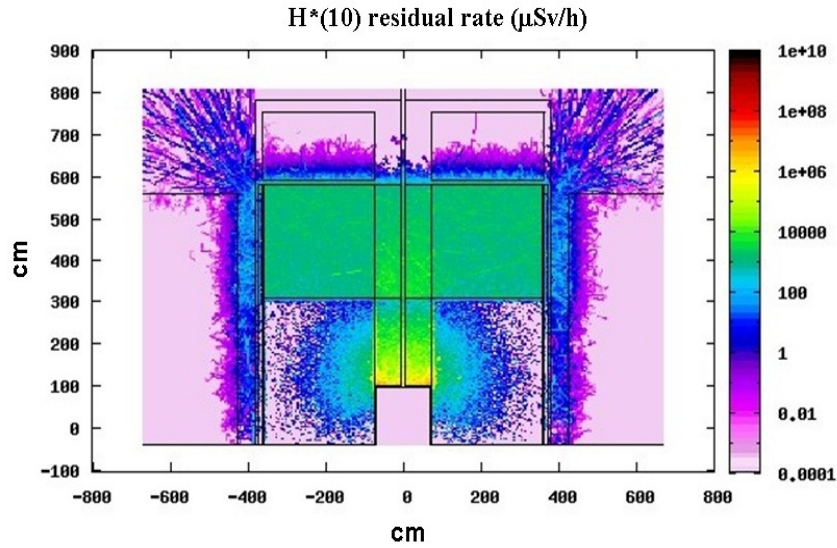
H*(10) residual rate (μSv/h)

Figure 7: Residual ambient dose equivalent rate in the structures around the core after 90 days of irradiation and 1 week cooling (subcritical operation mode).

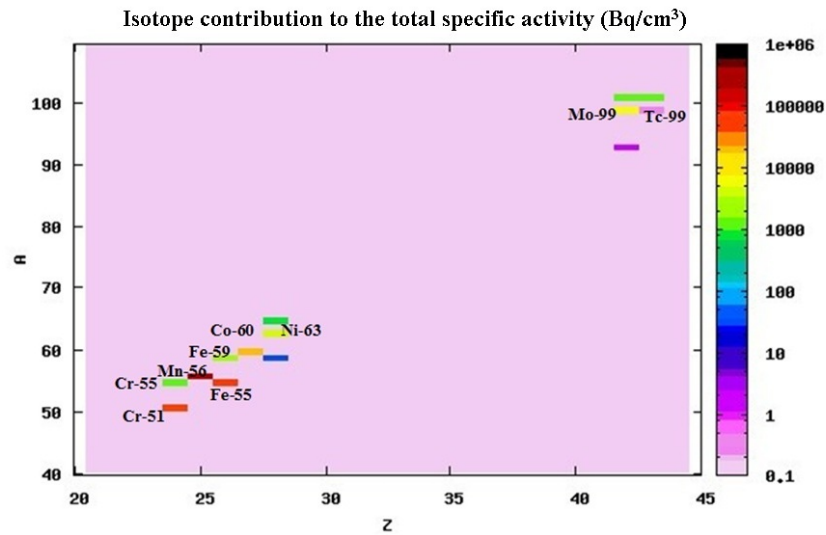**Isotope contribution to the total specific activity (Bq/cm³)**

Figure 8: Contribution of the main radionuclides to the total specific activity in a steel sample positioned in the LBE coolant in the hottest region close to the reactor vessel (end of 15 years irradiation).

performed. As example, Figure 8 shows the contribution of the main radionuclides to the total specific activity after a 15 years irradiation in a steel sample, positioned close to the reactor vessel at the fuel middle plane level.

3. Conclusions

A methodology based on the combined use of the two Monte Carlo codes MCNPX and FLUKA has been developed, with the aim to contribute with powerful tools to the shielding optimization of the MYRRHA facility in Mol (Belgium). The present simulation work addressed already the optimization of key elements, for example the cover plate design and (not showed here) the shielding structure above the last magnet for the operation in ADS mode. Besides the shielding, the present method will

allow a very accurate prediction of the activation levels of the structural materials, from the core barrel until the more external elements.

REFERENCES

[1]   D. De Bruyn, H. Aït Abderrahim, P. Baeten and R. Fernandez, "MYRRHA, the Multi-purpose hYbrid Research Reactor for High-tech Applications", *Proc. International Congress on Advances in NPPs (ICAPP '11)*, Nice, France, May 2-6, 2011, France Omnipress (2011), pp. 472-478.

[2]   MCNPX 2.6.0 Manual, LANL Report LA-CP-07-1473 (2008).

[3]   A. Ferrari, P. Sala, A. Fassò, J.Ranft, "FLUKA: A multi-particle transport code", CERN-2005-10   (2005), INFN/TC_05/11, SLAC-R-773.

[4]   G. Battistoni, S. Muraro, P.R. Sala, F. Cerutti, A. Ferrari, S. Rösler, A. Fassò, J. Ranft, "The FLUKA code: description and benchmarking", *Proc. Hadronic Shower Simulation Workshop 2006*, Fermilab 6-8 September 2006, AIP Conference Proceedings, 896, 31-49 (2007).

[5]   J.-L. Biarrotte, A. Ferrari, L. Perrot, H. Saugnac and D. Vandeplassche, "Accelerator design related issues", CDT Report D2.4 (2012), pp. 43-56.

[6]   A. Ferrari, J.-L. Biarrotte, L. Perrot, H. Saugnac and D. Vandeplassche, "Shielding and activation studies for the design of the MYRRHA proton beamline", *Proc. SATIF-11 Workshop*, Tsukuba, Japan (2012), OECD/NEA Publications, Paris (2013).

[7]   M. Sarotto, R. Fernandez, E. Malambu, A. Stankovskij, E. Bubelis, R. Dagan, W. Jäger, A. Travleev, M. Becker, F. Martin-Fuertes, M. Vásquez, F. Álvarez Velarde, A. Ferrari, S. Di Maria, L. Sabathe, M. Ottolini, "FASTEF design changes to operate in critical mode", CDT Report D2.4 (2012), pp.76-90 and pp. 137-150.

[8]   A. Ferrari, S. Di Maria, M. Sarotto, A. Stankovskiy, "Shielding and activation calculations for the MYRRHA ADS design in the sub-critical operation mode", *ICRS12 Conference*, Nara, Japan, 2-7 September 2012.

[9]   S.G. Mashnik, K.K. Gudima, R.E. Prael, A.J. Sierk, M.I. Baznat and N.V. Mokhov, "CEM03.03 and LAQGSM03.03 event generators for the MCNP6, MCNPX, and MARS15 transport codes", LANL Report LA-UR-08-2931 (2008).

[10]   S.F. Mughabghab, "Thermal neutron capture cross sections. Resonance integrals and G-Factors", INDC(NDS)-440, IAEA Report (2003).

Unprotected Overpower Transient Analysis of CEFR Core Using the SAS4A-SASSYS-1 Code

Yuanyu Wu[a], Lixia Ren[a], Wenjun Hu[a], Adrian Tentner[b], Tyler Sumner[b]

[a] China Institute of Atomic Energy, Beijing, China

[b] Argonne National Laboratory-ANL, Argonne, Illinois, USA

Abstract. In order to investigate China Experimental Fast Reactor (CEFR) core performance during unprotected transient overpower (UTOP) accidents, postulated control rod withdrawal accidents have been simulated and analyzed using the SAS4A/SASSYS-1 code. Researchers at China Institute for Atomic Energy (CIAE) performed the SAS4A safety analyses of CEFR in collaboration with Argonne National Laboratory (ANL) researchers. This collaboration is carried out within the framework of the Fast Reactor Technology Working Group of the U.S. – China Bilateral Civil Nuclear Energy Cooperation. Assumptions were made for the UTOP accidents that lead to relatively large reactivity insertions. The change of reactor reactivity and power as well as the fuel, cladding, and coolant temperatures during the transient process were analyzed in order to characterize the accident sequence. Accident consequences were studied with a focus on fuel and cladding melting and relocation behavior. The effects of different reactivity feedback mechanisms on the reactor power history during the transients were analyzed. The results showed that the negative reactivity feedback due to coolant temperature change and coolant voiding played an important role in counteracting the effects of the inserted positive reactivity. The simulation demonstrated the inherent safety characteristics of the CEFR core, which exhibits negative reactivity feedbacks during UTOP transients.

1. Introduction

The study of severe accidents is of high concern for sodium cooled fast reactors, especially after Fukushima Nuclear Accident. Unprotected overpower transients of sodium cooled fast reactors have been studied both theoretically and experimentally for a long time. With the insertion of a relatively large amount of positive reactivity and failure of reactor scram, the accident may possibly progress into a Hypothetical Core Disruptive Accident (HCDA) in which fuel melting and relocation will happen. In order to evaluate the core performance of China Experimental Fast Reactor under unprotected transient scenarios, postulated control rod withdrawal accidents have been simulated and analyzed using the SAS4A/SASSYS-1 code. The initiating phase of CEFR UTOP transient is studied until the melt of hexcan wall occurs.

The SAS4A/SASSYS-1 code [1][2] was developed at Argonne National Laboratory for analysis of severe accidents in liquid metal cooled reactors. The code was designed to analyze the initiating phase of core disruptive accidents resulting from under-cooling or overpower conditions. SAS4A is capable of simulating molten fuel relocation before fuel pin failure, fuel pin failure and disruption, mixture of molten fuel and fission gas ejection into coolant channel after fuel pin failure, etc.

2. CEFR Introduction and Model Description

CEFR is a sodium-cooled pool type fast reactor with 65MW thermal power and 25MW electric power. The core is composed of 81 fuel subassemblies, 3 safety rods, 2 regulating rods and 3 shim rods. The equivalent diameter of the core is 600 mm and the height is 450 mm.

There are 61 fuel pins in a CEFR fuel subassembly, which are fuelled by UO_2 with 64.4% U-235 content. The material for cladding and hexcan wall is 316 (Ti) stainless steel [3].

The SAS4A models of primary interest for the UTOP analyses presented in this paper are mainly the PLUTO2 and LEVITATE models, which are severe accident models developed at Argonne National Laboratory and validated by analyses of transient experiments carried out in Transient Reactor Test Facility (TREAT). PLUTO2 [4] can describe the initial stages of post-failure fuel motion and sodium voiding in subassemblies experiencing an overpower condition which leads to significant fuel melting, fuel-pin failures and fuel ejection into unvoided or partially voided coolant channels. LEVITATE [5] can treat fuel and cladding relocation, fuel-steel mixing, freezing, and solid blockage formation, as well as pin disintegration and the formation of solid fuel chunks. LEVITATE can be initiated directly after the fuel pin failure in voided coolant channels, or can be initiated in channels initially modeled by PLUTO2 when coolant voiding in these channels reaches a prescribed value.
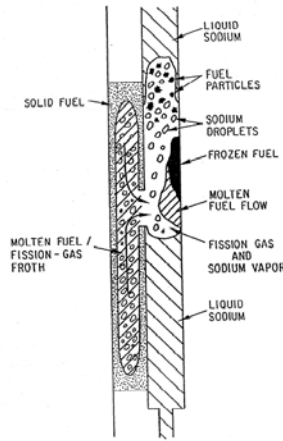

Fig.1. Typical PLUTO2 configuration [4]

3. A Postulated UTOP Transient Simulation and Analysis

A hypothetical UTOP transient simulation is carried out assuming the withdrawal of a CEFR shim rod without reactor scram. It's assumed that the reactor is operating at full power and fuel burnup is between 1.1 at% to 1.7 at% when the transient happens. The main parameters for defining steady state of CEFR operating are listed in Table 1. Positive reactivity is inserted linearly at a rate of 0.02 \$/s and reactivity insertion stops when it reaches 0.6 \$. It's noteworthy that there're protection systems in CEFR to limit the withdrawal of control rod and the possibility for this large amount of reactivity insertion is extremely low.

Table 1. Main Parameters for CEFR Steady-State Operation

Parameter	Value	Units
Total Reactor Power	65.5	*MW*
Total Fuel SAs Flow	264	*kg/s*
Inlet Temperature	633.15	*K*
Coolant Exit Pressure	233650	*Pa*

With the insertion of positive reactivity, the reactor power begins to increase as illustrated in Figure 2. The mismatch of reactor power and coolant flow causes the fuel temperature to increase continuously. At 17.75s, the maximum fuel temperature reaches the solidus temperature, which means fuel melting occurs, followed by the formation of molten cavity in the fuel pin. As the temperatures in the fuel pin continue to increase, the molten cavity which is filled with molten fuel and fission gas experiences growth in volume and increase in pressure. It is noted that the pre-failure in-pin fuel relocation model

was not activated in these preliminary analyses and therefore the fuel relocation begins only after the fuel pin failure. At 29.465s, the fuel pin failure criterion is satisfied and the pin failure occurs, leading to the onset of both in-pin and out-of-pin fuel relocation. At the time of pin failure the net reactivity is 0.256 \$ and the reactor power is 3.907 times nominal power. A mixture of molten fuel and fission gas is ejected into the coolant channel and the high temperature molten fuel rapidly heats the coolant sodium and initiates coolant boiling.
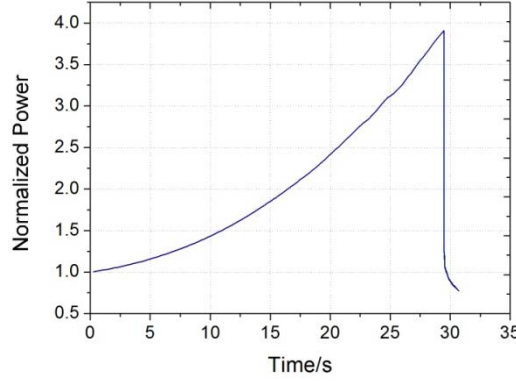

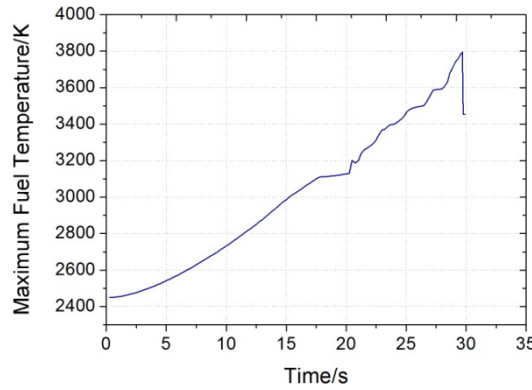*Fig.2. Normalized Power History during CEFR UTOP Transient*

Fig.3. Maximum Fuel Temperature during CEFR UTOP Transient

3.1. *Fuel Pin Failure and Post-failure Behavior*

When the molten fuel fraction reaches 50% in one axial segment, which happens at 29.465s, the fuel pin failure is assumed to occur. The cladding is no more capable of providing enough restraint for the fuel pin, and the mixture of molten fuel and fission gas is ejected into the coolant channel. This ejection is governed by a pressure equilibration model, assuming pressure equilibrium between the pin cavity and the coolant channel at the rupture location.

Although coolant temperature keeps increasing during the transient, coolant boiling is not initiated until the ejection of molten fuel and fission gas into coolant channel. After ejection of molten fuel and fission gas into coolant channel, the fuel-gas mixture begins to accumulate near the cladding rupture region, which causes direct contact of high temperature molten fuel with the coolant, cladding and structure material in coolant channel. Heating of the sodium coolant leads to sodium boiling, and subsequent sodium voiding and expulsion of the remaining liquid sodium slugs. The cladding and structure which get into contact with the fuel and gas mixture are heated and experiences a sharp temperature increase. Cladding begins to melt because of this temperature increase, which results in a larger rupture in the cladding and eventually to the total fuel pin disruption. This phenomenon is treated as fuel pin disruption in LEVITATE model, which is initiated at 29.490s, shortly after fuel pin

failure. The area previously occupied by pins becomes part of the coolant channel and only two fuel-pin stubs remain, as shown in Fig. 4.
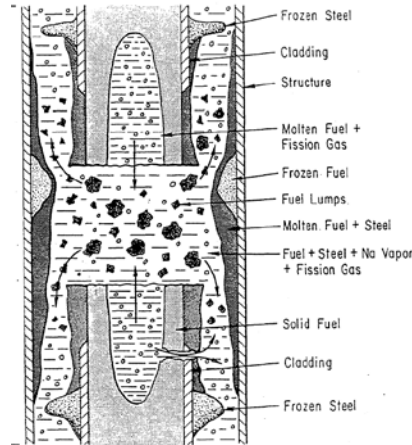

Fig.4. Fuel Pin and Coolant Channel Configurations after Fuel Pin Disruption[5]

Meanwhile, molten fuel contacting hexcan wall structure transfers heat to the relatively cold structure and causes the structure temperature to increase significantly. Molten fuel also freezes on the structure and cladding surface in a certain area, forming a frozen fuel crust. With enough heat transferred by the molten fuel to the hexcan wall and corresponding temperature increase the hexcan wall finally reach the solidus temperature at a certain axial point, thus leading to the failure of fuel subassembly, which happens at 30.744s. This signals the end of the initiating phase modeled by the LEVIATE model and the beginning of the transition phase. At this time the cladding has been disrupted in more than half of the driver fuel region axially.

3.2. *Discussion of Reactivity Feedbacks*

Driven by the inserted reactivity, the net reactivity keeps increasing steadily before fuel pin failure occurs as shown in Figure 5. During the pre-failure period, the coolant and axial expansion exhibit negative reactivity feedback and partially counteract the inserted positive reactivity. At 29.465s, which is when fuel pin failure happens, the net reactivity is 0.256$, the coolant reactivity feedback is -0.29$, while fuel Doppler and axial expansion reactivity feedbacks are -0.012$ and -0.008$ respectively.

The main reactivity feedback mechanisms which significantly reduce the net reactivity in post-failure period are coolant voiding and fuel relocation. After the onset of fuel pin failure, fuel dispersion in the coolant channel towards lower fuel worth regions introduces negative reactivity to the core.
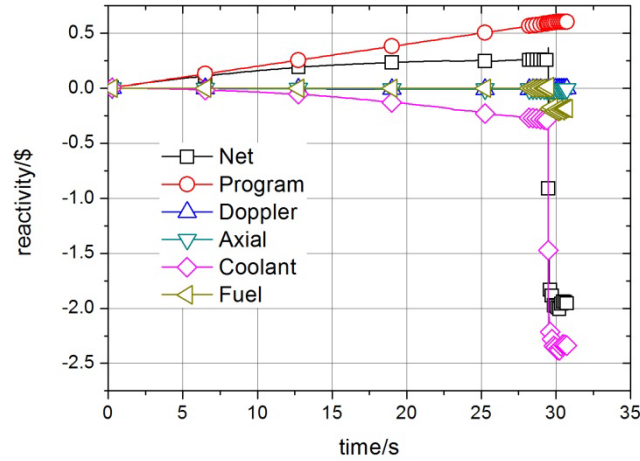
Fig.5. Net Reactivity and Reactivity Feedbacks during UTOP Transient

The effect of coolant reactivity feedback is also negative and more significant than the fuel reactivity feedback mechanism in this transient. Coolant void worth in the whole fuel region of CEFR is negative. From 0s to 29.4s, as coolant temperature increases, the coolant reactivity feedback exhibits a slowly increasing, in absolute value, negative reactivity feedback.

After the occurrence of fuel pin failure, sodium voiding is caused by the ejection of molten fuel and fission gas into coolant channel. Since sodium void worth is negative in CEFR fuel and blanket region, evacuation of sodium produces a significant negative reactivity feedback. The sodium in coolant channel is heated by the dispersed molten fuel and thus sodium boiling is initiated. In addition, the liquid sodium slugs are accelerated towards the axial core boundaries by the higher pressures in the pin-failure region, Sodium boiling and evacuation lead to a sharp decrease of total reactivity during post-failure period.

4. Conclusions

A detailed preliminary analysis of CEFR postulated unprotected overpower transient has been performed using the SAS4A Accident Analysis Code, from the initiation of transient until melting of hexcan wall occurs. Fuel pin failure and post-failure fuel relocation and associated phenomena are discussed with focus on cladding failure and fuel relocation. Coolant boiling is not initiated until the ejection of fuel and fission gas into coolant channel. Effects of reactivity feedbacks are discussed, and the results showed that the negative reactivity feedbacks due to coolant temperature change and coolant voiding played an important role in counteracting the effects of the inserted positive reactivity.

REFERENCES

[1] M.G. Stevenson, et al., Current Status and Experimental Basis of the SAS LMFBR Accident Analysis Code System, Proc. of the Fast Reactor Safety Meeting, 1974

[2] A.M. Tentner, et. al., The SAS4A LMFBR Whole Core Accident Analysis Code, Proc. of the International Meeting on Fast Reactor Safety Technology, 1985

[3] Final Safety Analysis Report of China Experimental Fast Reactor, China Institute of Atomic Energy, 2008

[4] H. U. Wider, PLUTO2: A Computer code for the Analysis of Overpower Accidents in

LMFBRs, Transactions of American Nuclear Society, Nov. 1977

[5]   A. M. Tentner, H. U. Wider, LEVITATE – A Mechanistic Model for the Analysis of Fuel and Cladding Dynamics under LOF Conditions, International Conference on Fast Reactor Safety Technology, 1979

Unprotected Loss-of-flow Accident Analysis of CEFR Core Using the SAS4A Code

Lixia Ren[a], Yuanyu Wu[a], Wenjun Hu[a], Adrian Tentner[b], Tyler Sumner[b]

[a] China Institute of Atomic Energy, Beijing, China

[b] Argonne National Laboratory-ANL, Argonne, Illinois, USA

Abstract. A severe unprotected loss of flow accident (ULOF) in an oxide-fueled sodium cooled fast reactor can lead to coolant boiling and associated core voiding. The outcome of the accident is largely dependent on the reactor size and design. In a large reactor the core voiding results in a positive reactivity insertion that can lead to a Core Disruptive Accident (CDA). For the China Experimental Fast Reactor (CEFR), a small reactor with a power of 65MWt, an ULOF accident will not lead to such severe conditions because the sodium voiding leads to a negative reactivity feedback. In order to investigate CEFR core performance, an ULOF accident with a flow halving time of approximately 10 seconds was simulated and analyzed using the SAS4A/SASSYS-1 code. Researchers at China Institute for Atomic Energy (CIAE) performed the SAS4A safety analyses of CEFR in collaboration with Argonne National Laboratory (ANL) researchers. This collaboration is carried out within the framework of the Fast Reactor Technology Working Group of the U.S. – China Bilateral Civil Nuclear Energy Cooperation, The accident scenario and consequences were studied, especially the detailed behavior of sodium boiling, fuel subassembly voiding, potential cladding melting and relocation, potential fuel melting and dispersal, and associated reactivity feedbacks during the transient. The analysis results showed that negative reactivity feedbacks in CEFR contribute to the mitigation of the ULOF accident. Cladding melting and fuel pin failure did not occur and the CEFR core demonstrated good inherent safety performance.

1. Introduction

The SAS4A code was developed at Argonne National Laboratory for the analysis of severe accidents in liquid metal cooled reactors [1][2]. SAS4A has extensive capabilities for the analysis of severe accidents, including both theoretical models describing the fuel, cladding and coolant performance and experimental knowledge obtained from experiments. The code was designed to analyze the initiating phase of core disruptive accidents resulting from under-cooling or overpower conditions. SAS4A contains detailed, mechanistic models of transient thermal, hydraulic, neutronic, and fuel-pin mechanical effects. It computes fuel/cladding/coolant heating, coolant boiling, cladding failure as well as fuel/cladding melting and relocation.

The main objective of this study is to evaluate CEFR core performance during unprotected loss-of-flow accidents, especially to investigate the coolant boiling behavior and evaluate the reactivity feedback mechanisms.

2. CEFR Core and ULOF Event Description

CEFR is a sodium-cooled pool type fast reactor with 65MW thermal power and 25MW electric power. The core is composed of 81 fuel subassemblies, 3 safety rods, 2 regulating rods and 3 shim rods. There are 61 fuel pins in a CEFR fuel subassembly, which are fuelled by UO_2 with 64.4% U-235 content [3]. The main parameters are listed in Table 1.

Table 1. Main Parameters for CEFR Steady-State Operation

Parameter	Value	Units
Total Reactor Power	65.5	*MW*
Total Fuel SAs Flow	264	*kg/s*
Inlet Temperature	633.15	*K*
Coolant Exit Pressure	233650	*Pa*

The reactivity feedback mechanisms considered in this paper include fuel Doppler, coolant voiding, core axial expansion and control rod driveline expansion (CRDL). The important reactivity feedback effects are listed in Table 2.

Table 2. Reactivity Feedback Effects of CEFR

Reactivity Effects	Values/$
Doppler reactivity (360℃-full power)	-0.0369
Axial expansion reactivity (360℃-full power)	-0.427
Sodium voiding reactivity (active core region)	-3.479

In the study, a severe unprotected loss of flow event (ULOF event) is assumed, which is initiated by a loss of electrical power to the primary coolant pumps without scram and emergency power unable to be supplied. Then the primary pumps coast down with a flow halving time of about 10s to a very small flow at about 80s after the event is initiated. The normalized coolant driving pressure in ULOF accident is listed in Table 3.

Table 3. Decrease of Coolant Driving Pressure in ULOF Accident

Normalized Coolant Driving Pressure	Time (s)
1.0	0.0
0.75	0.5
0.5	10.0
0.4	15.0
0.3	20.0
0.2	35.0
0.1	58.0
0.001	80.0
0.001	90.0

3. ULOF Accident Simulation and Analysis

3.1. Base case study

In the base case the control rod drive line expansion feedback and the radial feedback are ignored, and only the effects of Doppler reactivity, core axial expansion reactivity and coolant reactivity are taken into account.
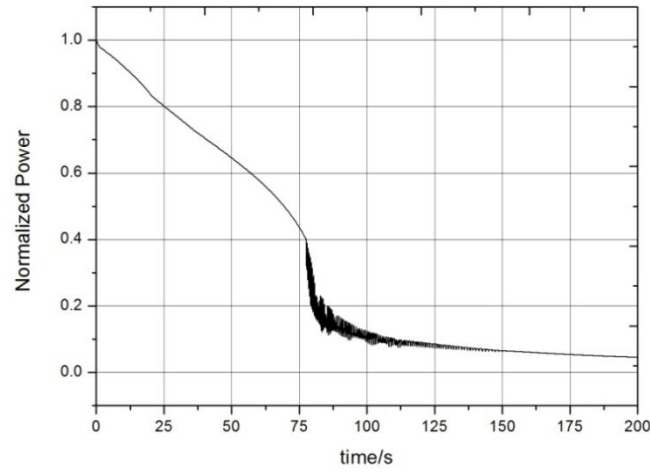
Fig. 1. Normalized power in ULOF base case

The reactor power decreases from 100% to 40% in 77 seconds from the initiation of the loss-of-flow, as illustrated in Fig. 1 which shows the normalized power as a function of time in ULOF base case. As this unprotected loss-of-flow accident is assumed to occur without the reactor scram, the reactor power decreases as a result of the reactivity feedback mechanism, avoiding the transient overpower plus loss-of-flow circumstances. At around 77 seconds, reactor power begins to fluctuate, indicating that there are high frequency fluctuations in net reactivity, typically associated with sodium boiling conditions. These fluctuations disappear at around 150 s, indicating that the sodium boiling has been suppressed. The reactor power decreases to a very low level (4.5%) at 200 s.
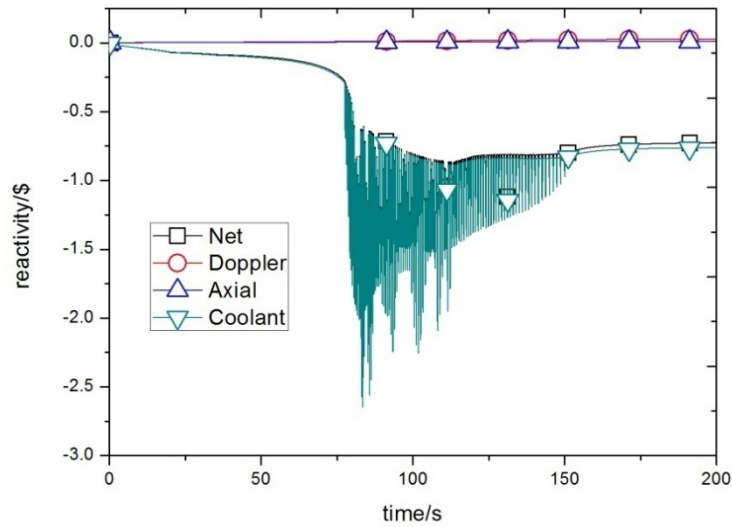

Fig. 2. Net reactivity and reactivity feedbacks in ULOF base case

The curves of net reactivity and reactivity feedback components during this ULOF transient are shown in Fig. 2. The net reactivity remains negative since the loss-of-flow accident initiation, and decreases with time. The negative net reactivity keeps the reactor power going down, which is in accordance with the reactor power curve. As a result of the negative net reactivity, the reactor can reach a safe condition even without the reactor scram. From around 77 seconds and until approximately 154 seconds the net reactivity begins to fluctuate rapidly, indicating the presence of coolant boiling.

Table 4. Reactivity at the onset of coolant boiling

Reactivity	Value @ 77.50s ($)
Net Reactivity	-0.275
Coolant Reactivity Feedback	-0.287
Doppler Feedback	0.008
Axial Expansion Feedback	0.004

The values of net reactivity and three reactivity feedback mechanisms are listed in Table 4. The time is chosen to be 77.50s, when the coolant begins to boil. Among the three main reactivity feedback mechanisms, coolant reactivity feedback makes the greatest contribution to net reactivity. Coolant reactivity begins to fluctuate after 77s, indicating the onset of coolant boiling. Doppler and axial expansion reactivities are mainly positive during the accident because fuel temperature is decreasing, but their contribution is quite small in absolute value when compared to the coolant reactivity feedback.
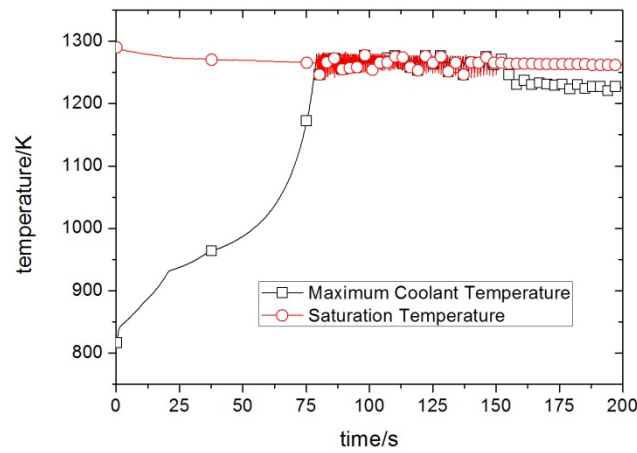

Fig. 3. Maximum coolant temperature and saturation temperature in ULOF base case

The maximum coolant temperature experiences a rapid increase after the initiation of loss-of-flow transient, and reaches saturation temperature at 77.50 s as illustrated in Fig. 3. Due to the effects of the negative coolant reactivity feedback, the maximum coolant temperature decreases below saturation temperature and coolant boiling is suppressed after 154.0 s, which demonstrates the inherent safety behavior of the CEFR core during the ULOF accident.

3.2. *Parametric case study*

In this parametric case the additional control rod driveline expansion feedback is accounted for. Inputs for steady state and transient simulation are the same as in the base case except for the inclusion of CRDL expansion feedback.
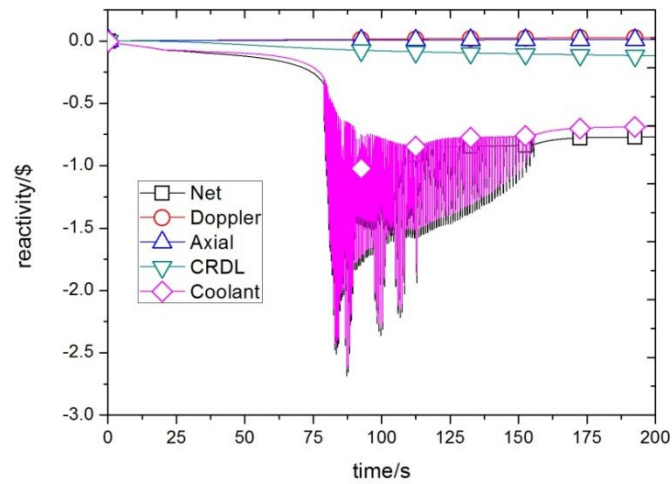
Fig. 4. Net reactivity and reactivity feedbacks in ULOF parametric case

CRDL expansion feedback is mainly negative during the accident, and is the second contributor to the total net reactivity. CRDL expansion feedback reaches -0.065$ at 78.90s, which accounts for 18.7% of the net reactivity.

Compared with the base case, including of control rod driveline expansion feedback does not cause significant changes to the ULOF scenario. It slightly delays the onset of coolant boiling.

3.3. Discussion

In the CEFR ULOF transient scenarios, the coolant reactivity feedback makes a major contribution in controlling the total reactivity, decreasing core power and mitigating possible severe consequences. The Control rod driveline expansion provides significant negative reactivity feedback during the transient, and is the second contributor to the total reactivity. The parametric case study indicated that control rod driveline expansion feedback does have an effect in decreasing the total reactivity, but does not change the ULOF scenario significantly.

4. Conclusions

Because the ULOF event is assumed severe and that the core flow is decreased to a very small flow near zero, the negative sodium coolant reactivity feedback is not sufficient to prevent the onset of coolant boiling. However, the large sodium voiding coolant negative reactivity feedback is instrumental in decreasing the reactor power and mitigating the event outcome. After about 80 seconds' of coolant boiling the boiling is suppressed leading the core to a safe steady state.

The analysis results showed that negative reactivity feedbacks in CEFR contribute to the mitigation of the ULOF accident. Cladding melting and fuel pin failure did not occur and the CEFR core demonstrated good inherent safety performance.

REFERENCES

[1] M.G. Stevenson, et al., Current Status and Experimental Basis of the SAS LMFBR Accident Analysis Code System, Proc. of the Fast Reactor Safety Meeting, 1974
[2] A.M. Tentner, et. al., The SAS4A LMFBR Whole Core Accident Analysis Code - Proc. of the International Meeting on Fast Reactor Safety Technology, Knoxville, Tennessee (Apr. 1985).
[3] Final Safety Analysis Report of China Experimental Fast Reactor, China Institute of Atomic Energy, 2008

Use of simplified PSA studies in support of the ASTRID design process

P. Gauthé[a], F. Curnier[a], F. Bertrand[a], N. Duflot[b], M. Balmain[c], V. Rychkov[c], Y. Banchieri[d]

[a] CEA, Saint Paul lez Durance, France

[b] AREVA-NP, Lyon, France

[c] EDF R&D, Clamart, France

[d] EDF SEPTEN, Villeurbanne, France

Abstract.

In the framework of the French Act of the 28th of June 2006 about nuclear materials and waste management, ASTRID (Advanced Sodium Technological Reactor for Industrial Demonstration), a GENIV and actinides incineration demonstration prototype, is to be commissioned in the 2020 decade to demonstrate the progress made in SFR technology on an industrial scale by qualifying innovative options, especially relative to safety and operability. More specifically, we aim for a level of safety at least equivalent to the EPR's one (third generation), with progress made in SFR-specific fields. So, the integration of safety issues in the early phase of the design of ASTRID is necessarily expected. For this purpose, CEA and its partners AREVA and EDF perform a level-1 Probabilistic Safety Assessment (PSA) to support the preliminary design of ASTRID.

This paper presents the PSA approach and current studies for the assessment of safety systems and the future work to be done for the 2013-2015 period. The preliminarily preparation of PSA studies is presented : objectives and scope of the early design phase PSA, definition of core damage states, selection and grouping of initiating events, assessment of safety functions and related systems. Work under progress is also presented: modelling of event trees, construction of fault trees of safety systems, transient calculations of accident sequences and reliability data assessment.

The main objectives of a level-1 PSA performed at the conceptual design stage are an early assessment of the safety architecture of the reactor and the most effective ways for improvement, but also the identification of dominant accident sequences and comparison with alternative designs. So, after the elaboration of a simplified level-1 PSA model for nominal state and main internal initiators, various alternative designs will be evaluated from the viewpoint of PSA in order to support the design choices for ASTRID.

1. Introduction

Sodium Fast Reactors (SFRs) are among the selected systems by the International Forum GenIV to address the sustainability issues with a coherent set of innovative requirements with significant improvements on safety, economy, environment, waste management and proliferation resistance as promising milestone towards a sustainable nuclear energy. In terms of safety, improved and robust safety demonstration with regard to former fast reactors is expected: enhanced prevention of whole core melting accidents, exclusion of credible way for energetic accident sequences, prevention and mitigation of risks due to sodium chemical reactivity, robustness to external hazards. The level of safety must be at least equivalent to Generation III reactors. Lessons learned from Fukushima accident will also be taken into account.

ASTRID (acronym for Advanced Sodium Technological Reactor for Industrial Demonstration) is a 1500MWth SFR pool type reactor of 600MWe whose features should be consistent with future high-powered industrial Sodium-cooled Fast Reactors [1][2]. The main objective of the ASTRID prototype is to demonstrate advances on an industrial scale by testing innovative options in dedicated areas (in particular safety, operability and in service inspection and repair). ASTRID will also be able to carry

out radioactive waste transmutation in order to demonstrate the industrial scale feasibility of this technique for reducing volume of end waste and lifetime of ultimate waste.

A first phase of the Preliminary Design Project is conducted from mid 2010 to the end of 2012. During this pre-conceptual design phase, the integration of safety issues is expected to support the design choices. To this purpose, performing a level-1 PSA is a good way to help the designers with an early assessment of the safety architecture of the reactor. Probabilistic insights are now increasingly employed for safety demonstration as a complement of traditional deterministic methods, at early design stages, the evolutionary feature of probabilistic models appearing as one major advantage. For some situations, like the failure of all Decay Heat Removal systems, PSA may help to convince that they are "practically eliminated", which is an issue in Generation IV roadmap. The level-1 PSA furnishes also valuable insights for Severe Accidents R&D prioritization. Furthermore, the slight effort in developing a level-1 PSA at pre-design phase should be appreciated with regard to the amount and deepness of insights gained, which are also accounting for all kind of dependencies (e.g. support systems, common materials or Common Cause Failures (CCFs)) that are inherent in a sophisticated system like a nuclear reactor.

Consequently to all these benefits, CEA and its partners AREVA and EDF have started PSA studies for ASTRID in 2011 to provide the first probabilistic insights on ASTRID design by the end of 2012 [3]. After that, PSA studies will be carried out matching the ASTRID design evolution until commissioning in the 2020 decade. This paper mainly presents the scope, objectives, preparation and first insights of the ASTRID level 1 PSA by the end of 2012.

2. The ASTRID reactor

First of all, the main features of the ASTRID design of 2012 are described. This design is used as a start point for the PSA studies to be performed.

The core design, named CFV, is investigated with the objective of reducing the probability of core meltdown and/or limiting the energy release during hypothetic accidents. The CFV core concept is based on a low sodium void effect [4]. This core concept involves in the inner part a heterogeneous axial fuel column made of $UPuO_2$ pellets with a thick fertile plate in the central zone and featured by an asymmetrical, crucible-shaped core with a sodium plenum above the fissile area. Sodium void worth is reduced to a negative value. At this point, the CFV core is considered as an attractive core with enhanced safety and is the reference.

The single conical redan is chosen for the inner vessel, similarly to the EFR (European Fast Reactor) project. The inner vessel separates the hot pool which contains the core subassemblies and the IHX inlets from the cold pool where are located the IHX outlets and the primary pumps inlets. Three mechanical primary pumps are located in the cold pool to feed the core with cold sodium. After flowing through the core, the sodium leaves the hot pool via the inlet windows of the four Intermediate Heat Exchangers (IHX) of 375MWth each. The secondary system transfers the heat from the IHX sodium/sodium to the Power Conversion System (PCS). This system comprises four 375MWth parallel and independent sodium loops, each connected to an IHX. Each loop includes one mechanical secondary pump, three modular sodium/PCS exchangers of 125MWth and one sodium dump vessel. The possibility to implement large flow electromagnetic pumps (EMP) is also evaluated. The motivation is driven by several gain and benefits in the design and maintenance : simplification of the design, easier natural convection establishment, absence of moving parts, absence of lubrication, reliability. Under normal conditions, power release is achieved using the secondary circuits and the PCS : classical steam/water plant (Rankine steam cycle) or innovative gas plant (Brayton gas cycle). Alternative gas PCS is studied together with sodium/gas heat exchanger design in order to eliminate sodium/water reaction risks. The gas PCS and its components have to be further studied from the safety and operation point of view; in particular, in case of gas leakage into sodium.

Concerning Decay Heat Removal (DHR) function, which is one of the main safety issues of a SFR, four Decay Heat eXchangers (DHX) are proposed: two in the hot plenum, and two in the cold plenum with a design different from the precedents. They are extracting the primary sodium heat with a sodium circuit and an air/sodium exchanger. Two circuits can operate only in natural convection on both sodium and air sides. The two others operate in forced convection with electro-magnetic pumps.

Investigations are carried out for the optimization of these DHR systems, especially regarding the passive operating possibilities of the two active circuits. The diversified design and operating modes of DHR system is designed to eliminate common cause failures. A DHR system through the reactor vault is also studied with the objective to complement the four DHX circuits. At the end of 2012, the whole DHR layout has still to be confirmed and assessed, especially using PSA studies.

The main characteristics of the ASTRID reactor are sufficiently known to start a level-1 PSA but there are still a lot of fundamental design choices to made, which could be helped by probabilistic insights.

3. Scope of the ASTRID PSA

3.1. Objectives

As a part of the design of a 4th generation reactor, the integration of safety considerations in the early phase of development of the concepts could be expected. To date, probabilistic insights are increasingly employed in the safety demonstration in combination with the deterministic and used, even at an early stage of design. The benefit of developing a probabilistic model to support the design of a GenIV reactor has been demonstrate by the CEA with the Gas-cooled Fast Reactor (GFR) [5].

It is generally proved that a level-1 PSA at an early stage of the conception of a reactor – in addition to the deterministic approach - enlightens the design choices in multiple way :

— to support the design of safety systems, especially for redundancy and diversification issues, with the treatment of common cause failures (CCF);

— to verify that the safety demonstration is well-balanced without accident preponderant in the contribution to the core damage frequency;

— to compare the global level of safety of a conceptual reactor with others reactors at the same stage of development or under operation;

— to contribute to the definition of operating conditions taking into account the combination of multiple failures in the accidental scenarios.

In our case, these studies, conducted in the pre-conceptual design phase of the ASTRID reactor in collaboration with CEA's industrial partners EDF and AREVA NP, consist in:

— performing reliability assessments of safety systems: shutdown systems and DHR systems ;

— developing a preliminary level 1 PSA to compare the design's choices of different systems from the safety point of view (impact on core damage frequency) and guide the design :
- architecture of DHR systems ;
- architecture of shutdown, including control and command systems ;
- use of secondary circuits to support the safety function of decay heat removal ;
- comparison of different PCS (water/steam or gas) ;
- impact of operator's actions.

The most important goal of the preliminarily level-1 PSA performing in 2012 is to compare design's choices. So, the main challenge to perform a PSA in the pre-conceptual design phase of a reactor is to be at a moment when :

— the data are representative of the future reactor enough to draw relevant analyses;

— the designers are still analyzing different options of design.

The more preliminary the design is, the less information we have to perform the level-1 PSA. The more advanced the design is, the less possible to modify the design with PSA insights is (*Fig. 1*).
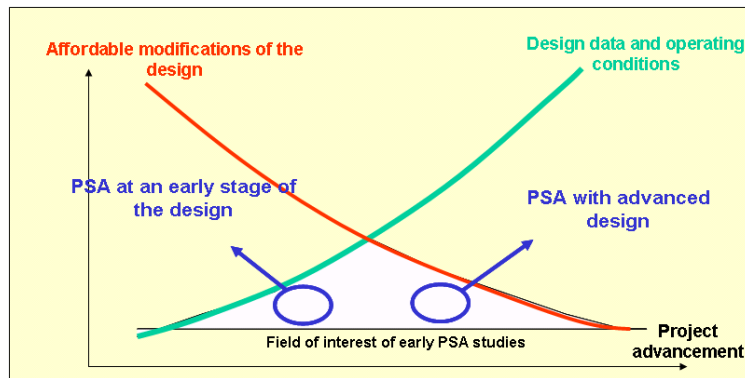
Fig. 1. Timing of early PSA studies

In 2011 and 2012, the thoughts were about :

— PSA specifications (decoupling criteria, safe state, mission times, initiating events);

— reliability data;

— methodologies to take into account :
  - the Human Factor from the first stage of the PSA : to balance automation and human supervision of the reactor;
  - the common cause failures;
  - the passive systems reliability;
  - seism as an initiator of a nuclear reactor accident.

First specific PSA results to support the design's choices of ASTRID are available at the end of 2012. The whole level-1 PSA model will be then available in 2013.

3.2. Core damage states

One of the first steps to perform level-1 PSA studies is to define the core damage states. It is currently assumed that the inacceptable consequences issued from the event trees of the PSA model are either the core meltdown or conservatively the fuel clad melt down. During the early stage of the ASTRID level-1 PSA in 2011-2012, the lack of design information prevents us from defining accurately the core meltdown states with physical criteria. For the moment, these physical decoupling criteria are taking into account :

— no fuel melting;

— hot sodium temperature below ebullition point;

— maximal clad temperature (to be defined);

— maximal sodium temperature in the cold pool of 650°C, to prevent thermal stresses on core support structures.

Further studies will allow us to choose the most accurate and pertinent values for all these criteria. Moreover, work is also in progress in the field of severe accidents for ASTRID, which could be also useful in the future for PSA, especially to define core damage states and accident sequences.

3.3. Initiating events

An important step to perform the PSA modeling is to select a preliminary list of initiating events to be taken into account during the early phase of the design. For now, only internal initiating events for nominal power state are considered. As soon as possible, initiating events for cold shutdown state will be included in the level-1 PSA. In fact, previous PSA studies for PWR or for SUPERPHENIX showed that cold shutdown state contribution to the core meltdown frequency is not negligible.

The selected initiators with their AOF (Annual Occurrence Frequency) for the very first stage of PSA studies are listed above in Table 1.

4

	AOF
Trip of one primary pump	1,40E-01
Trip of all primary pumps	7,00E-03
Control rod withdrawal	1,00E-02
Reactor trip	1
LOSSP < 2h	1,00E-02
LOSSP > 2h	1,00E-05
Loss of tertiary flow	1,07E-01
Trip of all secondary pumps	1,40E-02

Tab. 1. Preliminary list of initiating events

3.4. Reliability data

The problematic of the reliability data to be considered stands for an important part of the uncertainties associated to preliminary PSA studies. The available operating feedback of sodium fast reactors exists but is still very low in comparison with PWR. Nevertheless, we use different ways of gathering the reliability data needed for the PSA modeling [6]:

⎯ the database EGG-Na for sodium components, built on the experience of American and Japanese SFR ;

⎯ the database NUREG ;

⎯ the actual database used by EDF for the French PWR for all technology neutral components ;

⎯ the reliability data used for the PSA modeling of the SUPERPHENIX reactor in the 90's ;

⎯ expert judgement for components with innovative features or without sufficient feedback, based on the maturity level of the component technology.

The quantity and quality of reliability data will improve step by step with the project development when the new components tests and qualifications will begin. We also aim at introducing uncertainties studies about reliability data early in the project.

4. Current status of ASTRID PSA studies

4.1. Event trees

The preliminary event trees were built in a very simple way to start the PSA modeling. In fact, in the early phase of the design, operating conditions and piloting procedures are unknown what induces difficulties to match a specific event tree with each different initiating event. Furthermore, transient calculations are in progress to define the sequences to model, especially concerning DHR systems.

After the initiating event, the event tree is composed of function events related first to reactivity control, then to decay heat removal. We assume that each initiating event is protected by at least two trip signals which trigger scram. Then there are two independent shutdown systems. For DHR systems, their definition and integration are still in progress but we can assume that :

⎯ one secondary circuit with the PCS operating is sufficient to remove the decay heat. Nevertheless, these systems are not classified for safety purpose;

⎯ the first DHR system to operate is the active one then the passive one;

⎯ each of these systems can handle the decay heat after the scram;

⎯ a third system called RVACS (Reactor Vault Auxiliary Cooling System), through the main vessel, can remove the decay heat after some delay after the scram.

Dividing the event tree between two or more time periods concerning the DHR systems enables to take into account the specificities of DHR systems of a sodium fast reactor. The more the decay heat decreases, the less number of DHR systems are needed. Defining the safe state to be reached after each acceptable sequence of an event tree is crucial to define the mission time of DHR systems. The following criteria have been chosen for the moment to define the safe state :

⸺ decay heat lower than power removed by DHR systems ;

⸺ sodium temperature acceptable for long-term operating (<450°C for exemple)

⸺ the loss of all DHR systems at this moment is acceptable thanks to one of these reason :
  - the delay before reaching unacceptable sodium temperature (650°C) is sufficient to repair at least one DHR system able to remove the decay heat ;
  - the thermal losses of the reactor are sufficient to respect the limit of 650°C.

Work is in progress to assess this last criterion, which is not obvious to define accurately for the moment. An exemple of calculation performed in order to progress on this subject is presented in §4.3.

We aim at building a generic DHR event tree like *Fig.2*, where the entire mission time is divided into two periods T1 and T2 what enables us to valorize some DHR systems sufficient to remove the decay heat only after several hours, like the RVACS system (or the active DHR with passive capabilities).

Initiating Event	1/4 secondary loop + PCS during T1	1/2 active DHR loop during T1	1/2 passive DHR loop during T1	1/2 RVACS loop during T2	1/4 secondary loop + PCS during T2	1/2 active DHR loop during T2	1/2 passive DHR loop during T2	No.	Conseq.
IE	M1-T1	M2-T1	M3-T1	M4-T2	M1-T2	M2-T2	M3-T2		
								1	OK
								2	OK
								3	OK
								4	OK
								5	NOK
								6	OK
								7	OK
								8	OK
								9	OK
								10	NOK
								11	OK
								12	OK
								13	OK
								14	OK
								15	NOK
								16	NOK

Fig. 2 : Exemple of DHR event tree

That kind of event tree could be used as a report event tree to represent the decay heat removal sequence once the reactivity control function is achieved. These modeling options are still under investigation.

Early integration of human factors to support some design choices is a short term objective. The preliminary impact of human actions will be assessed in the event trees for two specific manual operating actions: manual scram and opening of the sodium/air exchangers dampers of the DHR circuits. Previous level-1 PSA for SUPERPHENIX showed that human failures in DHR systems operation are not negligible. For quantification of human faults, CEA has developed a methodology based on the complexity indicator of the safety systems [7]. This methodology will be applied for the early PSA model.

4.2. Fault trees

Fault tree modeling began in 2011 for some safety systems as DHR systems. The main fault trees which will be plugged to event trees in the preliminary level-1 PSA model correspond to :

⸺ passive DHR system in the primary circuit ;

⸺ active DHR system in the primary circuit ;

⸺ automatic shutdown of the reactor (including control rods faults and also I&C faults) ;

⸺ DHR system through the primary vault ;

⸺ Secondary circuits and associated Power Conversion System (PCS) with water/steam or gas.

These fault trees use some secondary fault trees concerning support systems as electrical supply, Instrumentation & Control, ventilation, lubrication, nitrogen and argon circuits. In fact, support systems may be a major part of the components failure modes so it becomes essential to take them into account early in the project. It will also be useful for the design of the electrical layout.

Moreover, reliability assessment of passive systems will be integrated very early in the project with a dedicated CEA methodology. This methodology has been applied to a DHR system, working in natural circulation, of the GFR [8]. The aforementioned method will be used in 2013 for introducing DHR passive system in the PSA of ASTRID, and if necessary for other passive systems (passive shutdown rods, innovative passive DHR system).

4.3. Transient calculations

An important part of level1 PSA modeling is to define the consequences for each combination of events with transient calculations. Building the event trees implies to know whether or not the sequences will lead to inacceptable consequences such as core meltdown. Using some decoupling criteria (cf. §3.2), transient calculations are performed with the thermal-hydraulic system code CATHARE2 [9].

A consequent effort has been made within AREVA and CEA in 2011-2012 to gather design data and build efficient CATHARE2 models of ASTRID which include the main design alternatives: homogeneous or heterogeneous core design, primary circuit geometries, DHR circuits, secondary circuits, water/steam PCS or gas PCS. Performing CATHARE2 calculations in parallel of the building of the level-1 PSA model is an efficient way to improve the global safety assessment of the reactor and to quantify the physical and probabilistic weight of design choices. An example is the integration in the CATHARE2 model of shutdown automatisms :

—— Definition and implementation of trip thresholds ;
—— Automatic decrease of secondary pumps speed after the scram ;
—— Potential decrease of primary pumps speed after the scram ;
—— Implementation of regulations of the PCS system.

It allows to calculate each transient first without scram then with the trip thresholds. We verify that each transient is well protected by several diversified trip thresholds. For example, in the LOF scenario (*Fig.3*), the scram occurred quickly with three different protections : core ΔT, power/flow rate ratio and core outlet temperature. Besides the trip thresholds studies, CATHARE2 calculations is also used for analyzing all DHR scenarios and defining the minimal number of control rods necessary for each transient. The last point is particularly important to put the emphasis on the new core designs with strong passive reactivity feedbacks. For exemple, in the LOF scenario, at least two control rods are needed to quickly decrease the power down to the decay heat (*Fig.4*).
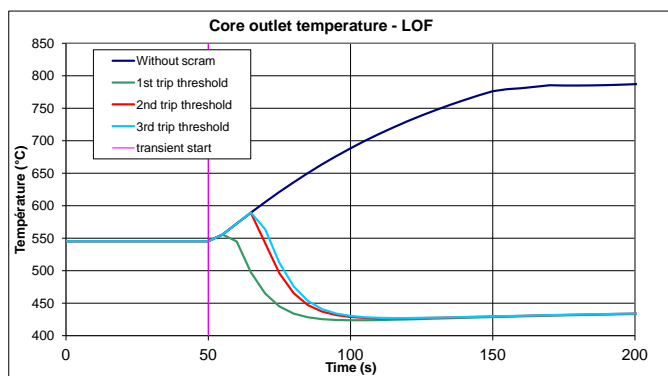

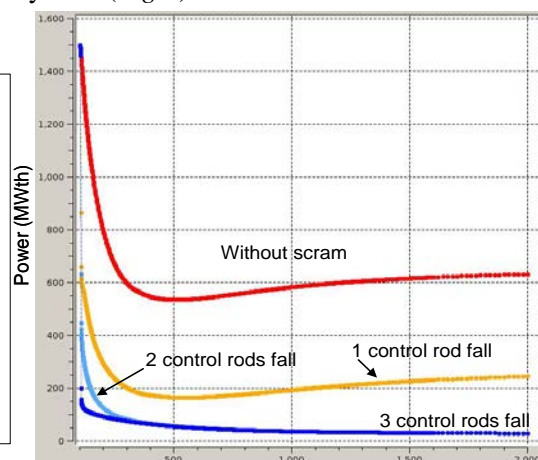*Fig. 3. Example of a LOF CATHARE2 calculation with trip threshold*

Fig. 4. Example of a LOF CATHARE2 calculation with 0,1,2 or 3 control rods fall

For long-term transients with DHR issues, a simple numerical tool has been created to quickly assess the sodium temperature reached depending on the number and type of available DHR systems. This tool is used to estimate which transients lead to go beyond the limit of 650°C. Work is also under progress in order to calculate the mission times of DHR systems, as aforementionned in §4.1. An exemple of these calculations is presented in *Fig.5* :
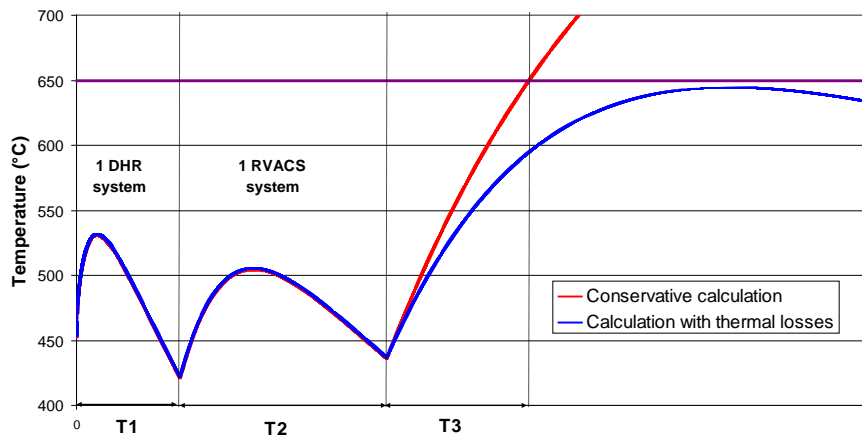

Fig. 5 : Long-term sodium temperature calculation

In this case, the global mission time is T1+T2, divided into two periods with 1 main DHR system during T1 and 1 RVACS system during T2. After T1+T2, the thermal losses are sufficient to maintain sodium temperature lower than 650°C. Moreover a conservative calculation without any thermal losses shows that there is a delay of grace T3 available to repair at least one DHR system. The real values of mission time are under still under evaluation because it depends on the ASTRID design and reparability of composants.

4.4. First results

4.4.1. DHR systems design

In order to have some early answers about the DHR systems layout, a static PSA study using only fault trees has been performed to assess the design options. This work intends also to identify the ways of imporvement of the DHR systems to practically eliminate the loss of all systems, which is a major stake of the ASTRID safety. The main design improvements, identified by PSA studies, that increase appreciably the DHR systems reliability are the draining valves diversification, the capability of local command of the Na/air exchangers dampers, the redundancy of active air blowers and the reinforcement of electrical supply. Other improvement tracks concerning passive capabilities of some systems are identified but not yet quantified. For the moment , the final result of this evaluation shows a very good reliability (~10-6). Nevertheless, further work is required to reach the practical elimination goal, for which we will also take into account the RVACS reliability assessment and the reparability of the DHR systems components.

4.4.2. Shutdown systems design

A PSA model has been performed for three shutdown system designs in order to look for discriminating elements in terms of reliability. These shutdown system designs can be classified into two categories :

(1)   standard design with functionnaly diversified rods : control rods and safety rods;
(2)   innovative design where all the rods participate in both control and safety functions. In this innovative design, the rods can be driven by a mechanism containing one or two electromagnets (one located in sodium, one in cover gas) depending on the design variation.

Given that I&C system is the major cause of shutdown system failure and the lack of reliability data for rods insertion failure, the results of the probabilistic analysis are for the moment not blatant. In order to progress on this subject, EDF R&D intends to develop a methodology for non insertion rods evaluation. This work may enlighten the design discrimination.

5. Future work

5.1. Complete PSA modelling

After 2012, PSA studies will continue in order to provide a full PSA model for the global safety assessment of the reactor. This work will include:

—— more initiating events and some internal and external hazards as seism;

—— cold shutdown states ;

—— transient calculations ;

—— uncertainties specific studies ;

—— human actions reliability ;

—— passive systems reliability assessment ;

—— sensitivity studies to evaluate the weight of components or initiating events in the global risk ;

—— fuel storage reliability.

5.2. Comparison of alternative designs

PSA will be used to compare relatively some design options. Work is under progress concerning :

—— DHR systems with capabilities of 2x2x100% or 2x3x50% or a mixed solution: the impact of this choice on the design and operating conditions is so important that these alternatives will be integrated as soon as possible in the model ;

—— Interest of active DHR systems with passive capabilities ;

—— Shutdown systems layout : number and type of control and safety rods ;

—— Interest of electromagnetic sodium pumps in the secondary circuit ;

—— Design of the PCS systems : classical water/steam PCS or innovative gas PCS ;

—— Use of secondary circuits in some cases for DHR safety function.

PSA could then enlighten future safety design choices which could appear in the project.

5.3. Safety assessment

The safety of French nuclear reactors is based essentially on a deterministic approach. However, a basic safety rule issued by the French regulator defines the scope of utilisation of PSA, presented as a method of investigation which supplements the conventional deterministic analyses. As such, they are of assistance in the definition and the prioritisation of the actions to be taken in order to attain or maintain a satisfactory safety level. In that purpose, probabilistic objectives could be used as orientation values but not as regulatory limits.

A target for the global frequency of core melt of less that 10^{-5} per plant operating per year, uncertainties and all types of failures and hazards is taken into account as an orientation value. In order to fulfill these objectives for ASTRID project, designers have proposed probabilistic safety objectives as orientation values but are not as strict limits (they do not correspond to a requirement of the regulator). Examples of these probabilistic objectives are :

—— a value of 10^{-6} per plant operating per year for the core meltdown frequency due to internal events, respectively for power states and for shutdown states ;

—— a value of 10^{-7} per plant operating per year for the scram system and for DHR systems failure.

PSA studies could also be used in the ASTRID project for : safety classification of components, support of the Safety Orientations Report, practical elimination demonstration of some situations as the loss of all DHR systems (for the reactor and the fuel storage), matching for regulatory requirements (ASN, WENRA) in terms of general probabilistic assessment.

6. Conclusion

In 2010, the CEA has decided to carry out PSA studies in support to the design of the prototype (named ASTRID) of French GEN IV Sodium Fast Reactors. A level-1 PSA performed at an early stage of the conception of a reactor – as a complement of the deterministic approach – enable to enlighten the design choices in a multiple way:

⸺ to support the design of safety systems and support the design choices;

⸺ to verify that the safety demonstration is well-balanced ;

⸺ to contribute to the definition of operating conditions ;

⸺ to match the probabilistic design targets.

PSA studies for ASTRID reactor in collaboration with CEA's industrial partners EDF and AREVA NP, consist in:

⸺ performing reliability assessments of safety systems: shutdown systems and DHR systems;

⸺ developing a preliminary level 1 PSA to compare the design's choices of different systems.

At the end of 2012, PSA main specifications have been defined (objectives, scope of work, initiating events, core damage states). First modeling options have been assessed and preliminary fault trees and event trees have been built, providing some preliminary results for DHR and shutdown systems.

The main objective now is to shape a representative and complete model to compare ASTRID main design choices and to assess ASTRID safety features. This model should evolve after that to take into account the design progression and the some valuable improvements (uncertainties, human actions, seism, common cause failures, support systems).

ACKNOWLEDGEMENTS

REFERENCES

[1] P. LE COZ et al.,"Sodium-cooled Fast Reactors: the ASTRID plant project"; Proceedings of ICAPP'11, Nice France; Paper 11151; 2011.

[2] M. SAEZ et al., "The pre-conceptual design of the nuclear island of ASTRID"; Proceedings of ICAPP'12, Chicago USA; Paper 12070; 2012.

[3] GAUTHÉ P. et al., "Use of simplified studies in support of the ASTRID design process" , proceedings of ICAPP'12, Chicago, USA, June 24-28, 2012.

[4] F. VARAINE et al.,"Pre-conceptual design of the ASTRID core"; Proceedings of ICAPP'12, Chicago USA; Paper 12173; 2012.

[5] BASSI C. et al. (2010), Level 1 probabilistic safety assessment to support the design of the CEA 2400MWth gas-cooled fast reactor, Nuclear Engineering and design, 240, pp 3758-3780.

[6] SAIGNES, P., "Reliability database for PSA in support to the design of the innovative CEA 2400MWth gas fast reactor, Proceedings of the international Probabilistic Safety Assessment and Management conference (PSAM 9) Hong-Kong, China, May 18–23.2008.

[7] PAPIN B., " Balancing human and technical reliability in the design of advanced nuclear reactors" Nuclear Engineering & Design , Volume 241, Issue 12, December 2011, Pages 5238-5244

[8] MARQUÈS M. et al., "Methodology for the reliability evaluation of a passive system and its integration in a Probabilistic Safety Assessment", Nuclear Engineering and Design, Volume 235, Issue 24, December 2005, Pages 2612-2631

[9] GEFFRAYE G. et al., "CATHARE2 V2.5 2 : A single version for various applications". Nuclear Engineering and Design, Volume 241, Issue 11, November 2011, Pages 4456-4463

Approach to the identification and evaluation of Sodium-Water-Air Reactions (SWAR) accidental scenarii in Steam Generator buildings

K. Daudin[a][1]**, F. Beauchamp**[a]**, C. Proust**[b]

[a] CEA (French Alternative Energies and Atomic Energy Commission),
Nuclear Energy Directorate,
Cadarache center, France
[b] INERIS (French National Institute of Industrial Environment and Risks)
Accidental Risk Department,
Verneuil-en-halatte, France

Abstract. One of the issues of Sodium-cooled Fast Reactor (SFR) is to deal with the high reactivity of liquid sodium with air and water. Many safety barriers exist to prevent and mitigate the potential events with regard to liquid sodium risks. To reinforce the robustness of safety demonstration, consequences of envelope accidents concerning Steam Generator buildings have to be quantified.

Regarding various accidents, it is possible to show that Sodium-Water-Air Reactions (SWAR) could be considered as envelope scenario that can occur in many different ways in the Steam Generator building. Thus it is necessary to analyze logical and temporal sequences of events. It will permit first to identify phenomena that may occur and also define the scenario for these reagents to come into contact. The effort is thus to improve understanding and present modeling approaches of sodium-water interactions in presence of air.

1. Introduction and context

The main principle of safety is to prevent accidents and limit their consequences. A clear and robust demonstration of the accident hazards management in future sodium-cooled fast reactors (SFR) is consequently required with regard to the presence of sodium liquid metal. The combustion of sodium in air and the fast and energetic reaction of sodium with water may occur since the presence of atmospheric oxygen and water. In SFRs, Steam Generator (SG) is the component where liquid sodium, coming from the reactor building, transfers its heat to water to produce vapor, going to the auxiliary nuclear building (see FIG. 1). This SG is located in a separate building than the reactor confinement, called the SG building.
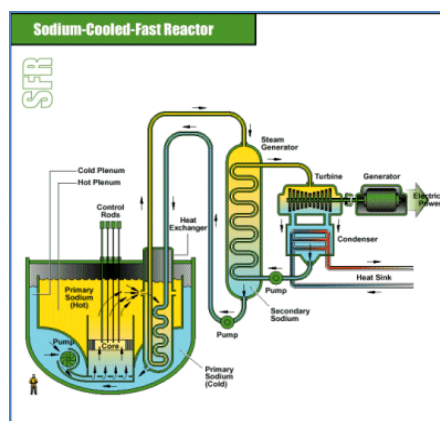

FIG. 1. Sodium Fast Reactor, GEN IV design

---

[1] Present address: CEA, DEN, Cadarache, DTN/STPA/LTRS, 13108 Saint-Paul-Lez-Durance Cedex, France

Envelope accidents concerning Steam Generator buildings could be considered as the consequences of multiple interactions of sodium with air and water. By extension, the result or the combination of those will be called Sodium-Water-Air Reactions (SWAR).

Accidents involving SWAR gather different concepts. First it can be perceived as a sequence of events leading to the contact of the three reactants, meaning that the chain effect has to be evaluated. For instance, a sodium fire may initiate the release of steam-water by domino effect [1]. This is what we will call the large SWAR. On the other hand SWAR also involves sodium-water interactions. The presence of air means that sodium combustion may occur. For example part of the sodium which has not reacted with water may induce sodium fire. Finally one of the main risk in presence of air is a large hydrogen explosion.

2. Identification of Sodium-Water-Air Reactions accidental scenarii

One of the major consequences of safety issues is to maintain risks under a given discretised envelope (called Farmer curve) so as to associate each situation with general objectives of safety. This curve is representative of the safety objective "a situation has to be as less plausible that its potential consequences are high".

SWAR accidents inside the SG building have a very low occurrence frequency and will only be studied as envelope scenario considered "practically eliminated" to contribute to the robustness of the safety demonstration (Fig. 2).
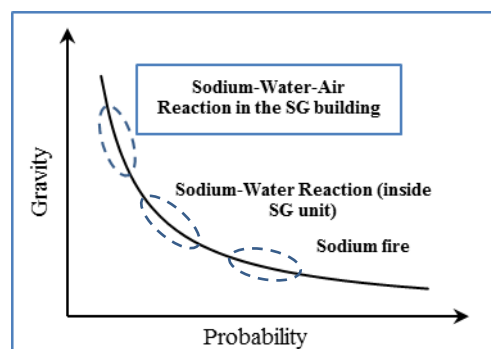

FIG. 2. Farmer curve related to sodium release risks

Identification of accidental sequences (logical and temporal) is necessary since these kinds of situations generally result in the combination of multiple failures and events.

2.1. Risks analysis : preliminaries

2.1.1. Past events

The analysis of past notified accidents does not highlight any major accident involving SWAR, and in particular any sodium water interaction in air occurred in the past. However, some leaks from exchange tubes inside SG units were observed in the world, five in the French reactor Phenix by which one of them partially damaged the SG bundle [2]. Therefore a loss of integrity of the SG might have occurred without the efficient and reliable leak detection systems that were available. A large leak involving Sodium-Water-Reaction inside the SG (SWR) occurred in PFR (UK) in which 40 SG tubes have been broken before the action of the passive protection system [2]. It can also be noted that an important number of leaks concerning sodium equipment took place in the past (32 leaks in Phenix [3]) by which some of them generated sodium fires, without any major damages on the structures [2].

2.1.2. System description

A scheme of Superphenix secondary sodium circuit is proposed in Fig. 3 and there are 4 circuits. To complete the general view of components present in the SG building, it must be added the sodium purification circuits and the steam-water circuit including pipes, tanks (starting up and decompression) and safety systems. An order of magnitude of the principal parameters concerning the SG unit is shown in the Table I below. It can be noted that total sodium inventory in secondary circuits is about 375 tons per circuit

Table I. Superphenix Steam Generator pipeworks characteristics (nominal power) [2]

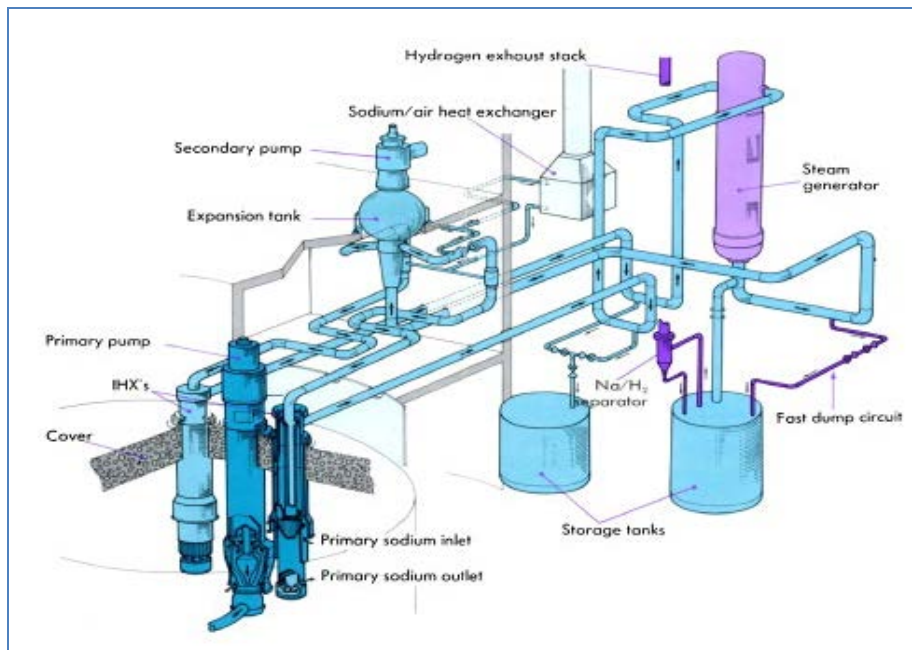| Component	Flow (kg/s)	SG input		SG output	
		Pressure (bar)	Temperature (K)	Pressure (bar)	Temperature (K)
Sodium	3270	~ 3	525	$\Delta P \sim 1$	345
Steam-water	340	219	237	184	490

FIG. 3. Superphenix secondary circuit

SWAR impacts and consequences have to be evaluated on sodium loops, primary circuits integrity, SG unit and SG building, reactor containment and sodium/air exchangers [4]. Safety functions to be ensured in case of a SWAR inside the SG building are so reactivity control, radiological confinement and decay heat removal.

2.1.3.   Main security barriers inside a SG building

Safety efforts concerning secondary loops were mainly in the past about R&D studies of sodium fires and SWR, improvement of detection systems, quality of fabrication of equipment and leak confinement of both sodium inside the SG building and steam-water inside the SG unit [5]. To limit sodium risks principal objectives are the control of chemical releases risk and the minimization of aggression risk on safety equipment and operators. The Table II presents the main technical barriers, separating those for sodium leak from steam-water leaks.

It is aimed to keep always two physical barriers between sodium and water, except inside the SG unit. Consequently SWR risks are higher inside this latter and so detection and mitigation barriers are placed to limit steam-water leaks (and hence propagation) into sodium. It can be also noticed that sodium fires are not only considered regarding their pressure and temperature effects, but also on the

chemical impacts induced by sodium aerosols release and potential toxicity [4]. Regarding the SWAR, the main orientations are to design the SG shell against any aggression (internal or external) and to design the building against aircraft impact [4].

Table II. Security barriers in the SG building regarding sodium fire and SWR

Category	Prevention and protection barriers
Sodium pipe leaks	Detection systems (leak detection and sodium fire detection)
	Draining systems
	Damper tank
	Ventilation systems and outlets
	Sodium premises partitioned
	Aerosols retention and relaxation volume
	Heat insulation and metal sheeting of concrete walls
Water-vapor leaks inside SG units	Detection systems (hydrogen detection, acoustic detection)
	Isolation and blow down of the steam-water side of the SG
	Bursting disks in sodium SG side for fast draining
	Cover gas in SG or surge tank argon volume
General	No common function shared between the secondary loops
	Modular SG design
	Physical sectoring between sodium and water-vapor areas

2.2. SWAR accidental scenarii : from Phenix to ASTRID

With regard to the previous section, the contact between sodium and water in air can only result from the combination of accidents occurred by domino and concomitance effect. This is the reason why the initiating events of SWAR are only results of uncontrolled accidents or incidents, so the list of events can be wide. A synthesis is proposed in Table III.

Moreover, constructive measures led to eliminate any fire with an electrical origin and the building flooding. This inventory gives also the evolution regarding safety approach of SWAR. Whereas safety analysis for Phenix and Superphenix was based upon SG shell supporting, some studies had been initiated within the framework of EFR project to assess the potential aircraft impact on a SG building (a probabilistic demonstration was necessary but not sufficient any more).

Concerning the future ASTRID prototype, SWAR events, in contrast with what was done in the past, are studied at the early design stage to demonstrate that they are physically impossible (constructive disposals) or to justify that they can be practically eliminated [4]. It is thus aimed to improve existing solutions and reinforce safety demonstration.

Table III. Review of SWAR initiating events and safety demonstration in the French SFR approach

Reactor	Accidental scenario	Safety demonstration
Phenix	A sodium leak generating a fire that could damage equipment(s) containing water-vapor	Constructive measures : risk excluded by conception (see Table II. : partitions, draining, …)
	Breaking of a steam-water-pipe inducing the breaking of an equipment containing liquid sodium	Constructive measures: risk excluded by conception (protection systems against pipes deviations and collection tank to eliminate flooding risk)
	Seism, aircraft fall or explosion linked to industrial environment causing the simultaneous breaking of sodium and water-vapor pipes	Constructive measures to handle seism risks (reinforcement of SG buildings, pipes designed to support seism, and protective systems on signal) and probabilistic analysis of other external aggressions to demonstrate that the induced risk is acceptable
	A SWR leading to the breaking of the SG shell	Constructive measures (see Table II.) and studies to demonstrate that even if the SG shell has a failure, the hydrogen formed and released from the SG reacts automatically with the oxygen of air so there is no hydrogen accumulation and explosive risk induced
Super-phenix	Some event from Phenix + Missile ejection from the primary pump + Missile ejection from the turbine or aircraft fall	Constructive measures on entrainment groups flywheel : risk excluded by design Probabilistic analysis to demonstrate that the risk induced is acceptable
EFR	Some event from Phenix and Superphenix + External risks like aircraft fall	A study had been initiated to evaluate the potential effects of a large sodium water interaction in an opened volume

2.3. Preliminary risks analysis

Qualitative risks analysis – first step of a complete risks evaluation – consists in identifying all dangers and quotes these events in order to prioritize them in a criticality matrix. The criticality is defined as the probability of occurrence of an accident by its gravity. Choosing accidental scenarii is an approach that should be logic, coherent and argued.

Among all methods, it has been employed the so-called "Process Hazard Analysis " (PHA) in which all possible dangerous situations are determined considering each dangerous identified element. Then accidents and their consequences are specified, and a list of security barriers is provided. The last step of this method consists in quoting the different accidental scenario. To be exhaustive, this method is performed thanks to experts in working groups. Nevertheless it should be noted that completeness is never achieved and the quoting step may not be easy at all. For the SWAR risk analysis in a SG building, PHA has been based upon family of dangerous equipment. Regarding system description, past safety reports and security barriers, the result of this analysis mainly shows that there are four classes of SWAR accidental scenarii inside a SG building:
  — Steam-water leaks from SG tubes inside the SG unit inducing a loss of confinement of the SG (drilling or breaking regarding the energy of the SWR) ;
  — Malfunction of any protection system inside the SG building, for example the failure of the isolation and decompression system may lead to the ingress of steam-water into the

sodium storage tank ;
— Important breach on sodium or water-vapor pipe combined with the loss of protective systems or inducing it, followed by either domino effect on pipes or equipment of the other class of reactant, or the presence of the other reactant because of another incident, accident, or phenomenon like condensation of vapor forming water liquid pool ;
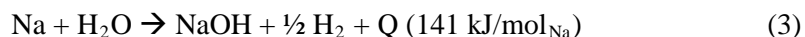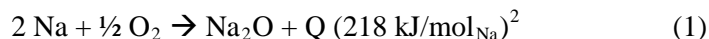— Ruin of SG unit or several equipment containing sodium and water-vapor due to an external aggression.

Description of these envelope situations will permit to identify the conditions of the contact between sodium and water, and thus give input data to assess the effects of sodium water interactions.

## 3. Evaluation of Sodium-Water-Air Reactions

Independently of the scenario, various phenomena are possible in a SG building. Their evaluation is necessary because SWAR are the result or the combination of accidental events. The later will only be considered with respect to sodium reactivity.

3.1. Basic knowledge of sodium related phenomena

The main issue concerning sodium is that it reacts vigorously with basic elements (water and air). The global reactions can be written as followed :

$$2\,Na + \tfrac{1}{2}\,O_2 \rightarrow Na_2O + Q\ (218\ kJ/mol_{Na})^2 \qquad (1)$$
$$2\,Na + O_2 \rightarrow Na_2O_2 + Q\ (260\ kJ/mol_{Na}) \qquad (2)$$
$$Na + H_2O \rightarrow NaOH + \tfrac{1}{2}\,H_2 + Q\ (141\ kJ/mol_{Na}) \qquad (3)$$

Hydrogen produced by reaction (2) is known to burn explosively with oxygen :

$$H_2 + \tfrac{1}{2}\,O_2 \rightarrow H_2O + Q\ (120\ kJ/mol_{Na}) \qquad (4)$$
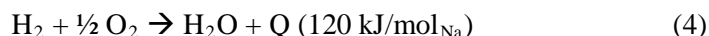
Because initial conditions can be very different from a scenario to another, it is essential to be able to calculate the effects of these reactions in various morphology, defining a specific dangerous phenomenon and its potential effects :
— Sodium spillage : pool fire, attack of concrete and release of water-vapor ;
— Sodium spray fire from a breach : jet formation, droplets rapid combustion and torch fire ;
— SWR : wastage, tube and shell breaking ;
— Sodium water interactions : penetration of sodium in water or conversely, studied until recently as a hydrogen explosion risk (see § 3.2.2).

The main parameters to be investigated are, for each of these phenomena, the kinetic of the energy release and its amplitude. It could be possible to eliminate some of them with these criteria, but keeping in mind all scenarii conceivable, each phenomenon may influence the global consequences.

3.2. Present understanding and modeling

3.2.1. Sodium combustion

One should note again that sodium fires are part of SWAR accidents since they may be considered as initiating events or contribute to the consequences of a sodium water interaction. On the other hand a sodium fire may compete with the sodium-water interaction and could minimize global consequences. There have been many studies about sodium fires in the past. It is thus not aimed to make a complete review but only to point out some keys features and the limits of their study regarding SWAR accidents.

---

[2] It should be noted that the values of heat release by these reactions are considered in normal temperature and pressure conditions.

3.2.1.1. Fundamental knowledge

Sodium combustion is the result of its surface oxidation, which, once ignition starts and the sodium vaporizes, is in competition with its vapor reaction with oxygen [7]. The point of ignition is the temperature at which oxidation becomes sufficiently rapid, on average of about 200°C but depending strongly on stirring condition (formation of an oxide layer broken in case of moving drops). This latter dependency resulted in the definition of two types of sodium fires related to the hydrodynamic behavior of sodium leakage (see Fig. 4). The flame temperature is generally considered about 1350°C, limit defined with regard to the decomposition of the most stable oxide [7].

FIG. 4. Sodium fire experiment pictures : pool fire on the left (CEA) and jet fire on the right (ANL)

The effects of a sodium fire are the release of energy and the formation of sodium oxide particles. The main parameters influencing sodium combustion consequences are sodium initial temperature, oxygen concentration and contact surface between reactants. Gas temperature elevation is confined in the vicinity of the flame, whereas the pressure elevation induced is quiet homogeneous in the volume concerned by the fire. Thus the general pressure peak occurs generally before the average gas temperature. Sodium aerosol particles make the volume opaque and may damage safety equipment.

3.2.1.2. Applicability limits

First it should be noticed that, depending on the source term of sodium/water interaction, sodium fire may or may not be taken into account. With regard to SWAR accidents, sodium releases are to be treated according to :
  — A sodium fire inducing, by domino effect, a sodium water interaction (without prejudging of the accidental sequence) will influence initial conditions of the latter ;
  — Large leak leading to sodium castings downward favouring pool fire or sodium-water reaction towards spray fire ;
  — Small sodium leakages at elevated temperature with a high jet fragmentation may have important damages on surroundings equipment (jet fire) by which some can contain steam-water.

Sodium fires are thus to be treated in a different way than usually [8-10] since main conservative approaches (overestimation of sodium combustion) may lead to underestimations of global consequences in a SWAR accidental scenario. It should be pointed out that it has not been talked so far about accident synergy, but considering the scenario of sodium leaking in a water pool, the more it burns in air the less is able to interact with water.

3.2.2. Sodium water interaction

As already said, contact between sodium and water may occur in different accidental configurations (inside a SG unit or in air) and this interaction is a normal operating condition for used the treatment of sodium residues on metal pieces (in particular the structures of the irradiated sub-assemblies). It will be only presented here the knowledge and modeling in opened volumes (in air or neutral atmosphere) because the high-pressure steam-water leaks into sodium (called Sodium-Water-Reaction) were in the focus of attention of many studies around the world.

3.2.2.1. Fundamental knowledge

The chemical reaction is known to be vigorous and that in some cases may involve high temperatures exceeding 1000 °C. Since hydrogen is normally produced, the general belief was that hydrogen-air explosions is the main "explosion" problem and the design of the equipment (such as the washing cells) is based on typical hydrogen explosion approaches [5].

Recent work [11] permitted to clarify the phenomenology of sodium water interaction based on open literature data, yet unreleased experimental data, and on some additional experiments. The main results are :

      (i)   The explosive character has clearly been demonstrated even without air ;

      (ii)   Product gases contain hydrogen and steam-water ;

      (iii) Under certain conditions, a fast expansion of gases due to the rapid transition phase may produce blast waves.

3.2.2.2. Modelling approaches

A first model was developed in the 80's to describe the pressure effects consecutive to liquid sodium falling into water pool. It was aimed to evaluate consequences of a postulated missile penetration inside the SG building generating this kind of accidental event within the framework of EFR safety assessment. The model was based on hydrogen combustion after an instantaneous contact between sodium and water. A bubble of hydrogen is formed and its expansion causes the development of a pressure wave. The main limit of this approach, beside the fact it considered only hydrogen production, was that results can't be easily extrapolated since it had been developed especially for experiments post-analysis. Moreover the hydrogen combustion was not well represented.

An alternative modeling approach has been proposed [11]. On the basis of the last results presented, an analytical method built on energy conservation to determine final pressure and temperature permits to calculate the mole number of steam-water formed, which then gives the part of initial energy available for the pressure generation from gases formation as a function of sodium fraction in the mixture (see FIG. 5). A maximum is obtained for a given sodium concentration, which corresponds to theoretical and experimental additional works showing that a fixed amount of chemical energy is generally transferred to the gaseous products in a short laps of time.
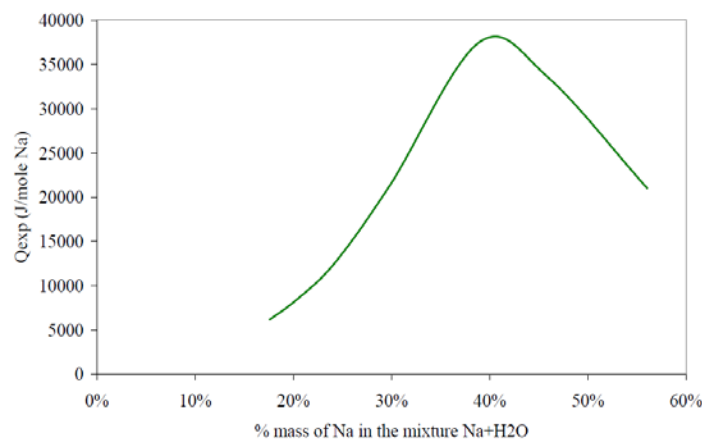

FIG. 5. Gas expansion energy as function of the intimate mixture ratio (excess water)

Moreover, it has been experimentally proven that half of the amount of gaseous products is generally steam-water (considering an excess of water). All in all, this methodology permits one to estimate equilibrium pressure due to the formation of hydrogen and steam-water (confined reaction with a slow mixing mode) and blast wave effects whenever the reaction takes place in open air or in an inert volume. For the latter, an estimation of the global reaction rate and the pressure wave induced led to the thinking that blast is generated by a rapid phase transition mechanism. An insight via modeling into the mechanism of vapor formation gave an estimate of the amount of steam-water explosively formed during the reaction. The final result for quantifying blast effects (energy released) is given in

terms of TNT equivalent in mass from 10% to 20%, permitting to evaluate the decrease in overpressure from a certain distance of the epicenter of the explosion. The results, first for the equilibrium pressure "peak" estimation and second considering the expansion energy only due to steam-water formation, are respectively less conservative than the previous engineering approach (described in [11]) and in good agreement with the few experiments available. The major limit of this methodology is that it hasn't been tested enough and it is only valid if water is in excess and the reactants well mixed. In those configurations hydrogen-air explosion should be mitigated by the large quantity of steam-water emanating from the reaction zone. Moreover the temperature in the reaction zone should be high enough to consider that hydrogen is partially burnt before its mixing with air.

It can be concluded that this last work concerning sodium water interactions in excess water offers better perspective of extrapolation to full scale installations but needs further developments because of the restrictions mentioned. However this "global" approach may not be adequate considering events inside a SG building where sodium should be in large excess. This is also of importance to evaluate the rapidity and the way sodium and water come into contact and to determine their influences on the global pressure effects.

4. Perspectives

The next step in the risks analysis consists in the construction of logical trees and the estimation of the very low probability of occurrence of large SWAR accidents inside the SG building. This work will permit to identify and quantify the different manners the reactants may come into contact and select the main parameters to be investigated with regard to sodium water interactions.

Regarding the evaluation of sodium water interactions, last work need to be developed concerning applicability limits of the methodology proposed and the suggestion of other global modelling approaches for other configurations. As it has been shown that pressure field depends on the dynamic of contact between reactants [11], this is of great importance to being able to determine the influence of parameters like the way and the rapidity of the contact, and the surface to volume ratio. Hydrogen resulting risk, whose effects are supposed to be delayed with regard to the fast blast effects of sodium water interactions, has also to be taken into account. Indeed there are different sources of hydrogen formation and parameters like rapidity of its release and probability of its inflammation have to be assessed. It also obviously depends on contact conditions.

Analytical and representative experiments have to in parallel to complete the current understanding and to study accidental scenario respectively. The two aspects, modelling improvement and experimental work, focus of the on-going PhD work, will permit to estimate the robustness of the safety demonstration.

REFERENCES

[1]   ABDOLHAMIDZADEH, B., ABBASI, T., RASHTCHIAN, D., ABBASI, S.A., Domino effect in process-industry accidents – An inventory of past events and identification of some patterns, Journal of Loss Prevention in the Process Industries 24 575-593, 2011

[2]   INTERNATIONAL ATOMIC ENERGY AGENCY, Liquid metal cooled reactors : experience in design and operation, IAEA-TECDOC-1569, Vienna, 2007

[3]   GUIDEZ, J., Phénix, Le retour d'expérience, Graphot, CEA, depot legal octobre 2012 (this book will be soon translated in English)

[4]   SAEZ, M., MENOU, S., BEAUCHAMP, F., BERTRAND, C., ALLOU, A., RODRIGUEZ, G., PRELE, G., Sodium-Water Reaction approach and mastering for ASTRID Steam Generator design, Proceedings of IAEA FR13 meeting, 2013.

[5]   GERBER, A., PIRUS, J.P., BEILS, S., CARLUEC, B., BEAUCHAMP, F., JEANNOT, J.PH., PRELE, G., Safety improvement research to design a sodium fast reactor steam generator with regard to sodium/water reaction risk – ICAPP-2010 San Diego, CA, USA, June 13-17, 2010

[7]   NEWMAN, R.N., The ignition and burning behaviour of sodium metal in air, Progress in Nuclear Energy, Vol 12, No 2 pp 119-147, 1983

[8]   TSAI, S.S., The NACOM code for analysis of postulated sodium spray fires in LMFBRs, BNL-NUREG/CR-1405, Brookhaven National Laboratory, Upton, NY, 1980

[9]   MIYAKE, O., MIYAHARA, S., OHNO, S., HIMENO, Y., Sodium pool combustion codes for evaluation of fast breeder reactor safety, Journal of Nuclear Science and Technology, 28 pp 107-121, 1991

[10]   INTERNATIONAL ATOMIC ENERGY AGENCY, Advanced nuclear reactor safety issues and research needs, Workshop Proceedings, Paris, 2002

[11]   CARNEVALI, S., Unsteady aspects of sodium-water reaction. Water cleaning of sodium containing equipments, PhD thesis realized at the CEA in collaboration with INERIS, 2012

Experimental programs and facilities for ASTRID development related to the Severe Accident Issue

C. JOURNEAU, C. SUTEAU, L. TROTIGNON, G. WILLERMOZ, G. DUCROS, J.J. COUROUAU*, J.M. RUGGIERI, F. SERRE

CEA, DEN, Cadarache
13108 St Paul lez Durance - FRANCE
christophe.journeau@cea.fr,
*CEA, DEN, Saclay
91191 Gif sur Yvette Cedex, France

Abstract

In support to the development and qualification of severe accident codes and mitigation devices for ASTRID, a comprehensive experimental programme has been designed. It encompasses in-pile experiments, prototypic corium experiments and simulant material tests. In particular, in-pile experiments are necessary to study the behaviour of large pins, of the ASTRID CFV heterogeneous subassemblies during severe accident transients and of in-core mitigation devices. Corium experiments are planned in the PLINIUS facility at small and medium scale and a new large scale facility, FOURNAISE, will be needed mainly for FCI, corium relocation and core catcher issues. This facility would be able to melt and study a few hundreds of kilograms of uranium-based prototypic corium. Prototypic tests will be complemented by new low temperature simulant material experiments e.g. for core catcher thermalhydraulics and jet ablation.

1. INTRODUCTION & CONTEXT

The ASTRID French Sodium Fast Reactor prototype developed by the CEA, with its industrial partners, will meet the requirements of the Generation IV reactor. Among the goals fixed to those reactors, one is to improve the safety and the reliability of such system (compared to previous built nuclear reactors), and to lower the likelihood and degree of reactor core damage. Therefore a significant severe accident R&D programme has been launched.

Although very thorough experimental researches had been conducted from the 60s to the 90s in support of SFR safety (see e.g. [1][2][3]) , it is necessary to obtain new experimental data for ASTRID [4], since present numerical tools require data that were not considered in former analyses and since new design options are being considered, as CFV heterogeneous core with pins having a significantly larger diameter than in previous reactors, Corium Discharge Channels and core catcher sacrificial materials [5], as well as the use of new cladding materials as ODS[6] or new fuel pin designs including minor actinides[4].

Severe accident sequences start with fuel melting (primary phase) due e.g.; to an Unprotected Loss of Flow, an Unprotected Transient OverPower or a subassembly blockage. Then during the transition and secondary phase, the molten materials may relocate in a critical configuration. Mitigation devices are under study to reduce this risks e.g. by providing corium discharge channels to extract fissile mass from the core area. In the so-called Post Accidental phase, the corium will finish its relocation and its decay heat must continuously be extracted to reach a safe state. Core catchers [5] are designed to hold and cool the corium either in debris or molten pool configurations.

A comprehensive severe accident experimental program is underway at CEA Cadarache. It includes experiments in reactor, with irradiated fuel, with prototypic (uranium-containing) melt and with simulant materials.

2. IN-PILE EXPERIMENTS

Some experiments cannot be performed outside the context of a nuclear reactor. This was the case of the CABRI and SCARABEE programmes in the past [1]. Currently, the EAGLE program at the IGR reactor in NNC IAE (Kurchatov, Kazakhstan) is devoted, under JAEA sponsorship, to the study of molten material relocation with the FAIDUS and CRGT discharge systems [7]. CEA has established collaboration with JAEA in order to benefit from the experimental results. Besides, discussions are underway to design specific IGR tests for the specific needs of ASTRID aimed at evaluating the influence of the internal fertile layer (FIG. 1) on the clad and fuel relocation:

- when clad is melting before fuel in a loss of flow test at nominal power (Instantaneous Total Blockage);

- during significant power increases leading to melting of fuel before clad (Transient OverPower).

In a second stage, it will certainly be necessary to test in pile the actual fuel rods (large diameter, ODS cladding[1]) that will be used in ASTRID, as well as pins including minor actinides. Besides, mitigation system introduced in the core region to improve the core behaviour in case of severe accidents will have to be tested, likely in reactor, except if they are close to the solutions already tested in the past.
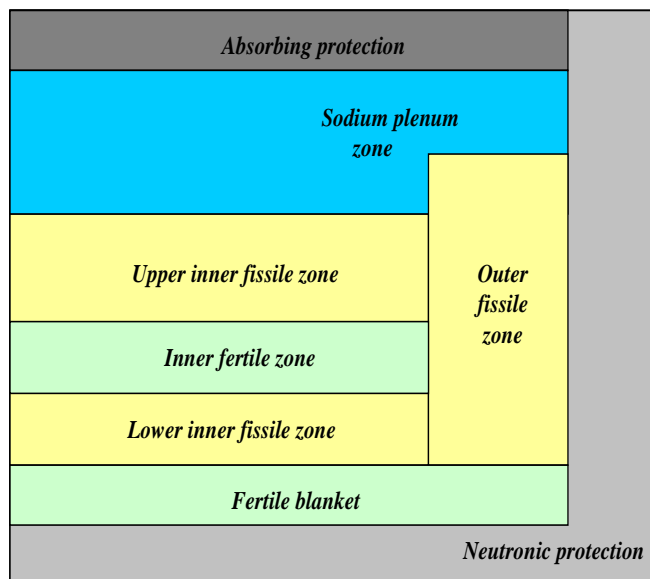

FIG. 1: Sketch of ASTRID CFV core

3 HOT CELL EXPERIMENTS

The final objective of severe accident studies is to minimize the risk of releasing radioactivity to the public and the environment. It is thus necessary to study in details the fission product release and transport during accidental sequences. Two tests had been performed in Japan on irradiated FBR MOX fuel pellets heated up to 2500 and 3000°C [8] showing a behaviour close to the LWR fuel for which a larger database exists. But these tests had been conducted in the absence of steel cladding, with a small burnup (65 GWd/t) and under neutral atmosphere of Ar, not so representative of the conditions that will be encountered for ASTRID.

It may therefore be necessary to conduct specific ASTRID related experiments in the MERARG [9] or [10] facilities at CEA Cadarache, in order to enlarge our validation database.

MERARG is an annealing facility made of an induction furnace capable to reach 2800°C in neutral atmosphere of argon, and 1400°C under air. The fission gas release kinetics is measured by gamma spectrometry (for radioactive gases) and gas-phase microchromatography (for the non radioactive isotopes).

The VERDON facility (FIG. 2) is more complex than MERARG as it can study not only the fission product release but also its transport and deposition under more various atmosphere, including mixtures of steam, hydrogen and/or air. Initially designed for PWR severe accident studies, the adaptation of this facility to simulate the behaviour of fission product under sodium vapours is under study.

---

[1] ODS cladding is not planned for the initial core and shall be progressively introduced at a later stage.
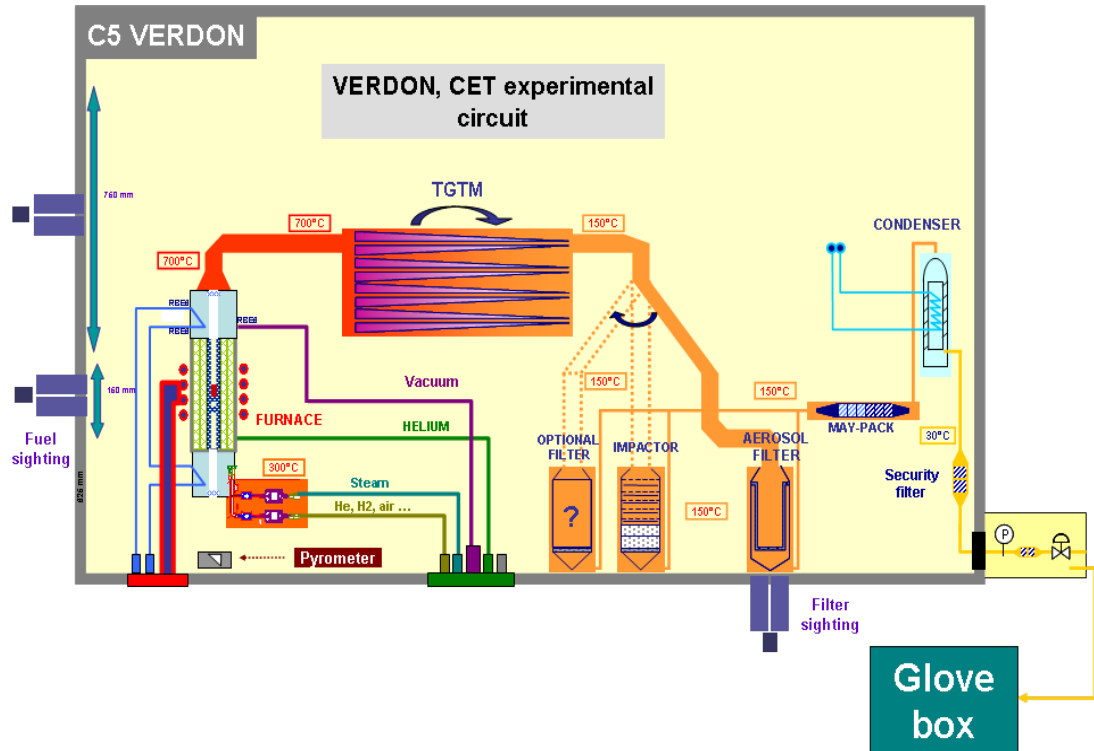
FIG. 2: Sketch of the VERDON facility

4 PROTOTYPIC CORIUM EXPERIMENTS

Corium is the molten material made of uranium oxides and other materials that is formed during a severe accident sequence. CEA Cadarache operates the PLINIUS prototypic corium platform [11] which had been initially designed for LWR severe accident studies but can be used for several fast reactor accident experimental research issues. A new facility, FOURNAISE [12], is under study to perform the needed experiments which are out of the scope of the PLINIUS platform either because they require larger masses of corium or the interaction of corium with sodium.

4.1 VITI FACILITY

VITI (FIG. 3) is a small scale facility in which a few grams of corium can be melted and studied. It can be used either in a crucible configuration for thermochemical studies [13] or in a gas-film levitation configuration for the measurement of thermophysical properties [14].

FIG. 3: VITI Facility

Left: general view   centre: induction coils and graphite furnace   right: crucible with UO_2- B_4C

In a first series of experiments, VITI has been used to study the phase diagrams between UO_2 and candidate sacrificial materials to be used in the core catcher [15]. The second configuration shall be used to estimate the density, viscosity and surface tension of mixtures of UO_2 and sacrificial materials.

4.2 SMHT HIGH TEMPERATURE MASS SPECTROMETER

To obtain more precise thermodynamic data on the mixtures of interest for the corium-sacrificial material phase diagram, experimental research has started on CEA Saclay High Temperature Mass Spectrometer [16]. Powders are heated in a Knudsen cell under secondary vacuum and the volatilized species are analyzed by the mass spectrometer. The first systems that have been studied include the U-Fe-O system to assess the solubility limit of Fe in UO_2 and the UO_2-B_4C system.

The results of these experimental measurements are to be capitalized in the FUELBASE thermodynamic database [17].

4.3 COLIMA AEROSOL RELEASE CONFIGURATION

In the COLIMA facility, several experiments have been conducted to study the release of aerosols from a corium pool [18][19]. Fission product prototypes are mixed with prototypic corium and other materials in a crucible which is heated above melting. The aerosols are collected – either thanks to inertial impactors which also provide size distribution or in a thermal gradient tube– and analyzed.

It will be necessary to test the selected candidate material to verify that no volatile species are created when corium is mixed to this material, since it would then increase the radioactive source term.

FIG. 4: Impactors for aerosol sieving and sampling [19]
Left: Impactor stacks and isokinetic pumps   Right: collector for the 0.4-0.7 μm bin

Therefore one or two COLIMA-type experiments are planned, either in the current COLIMA facility or in one of PLINIUS-platform corium furnaces.

4.4 VULCANO CORIUM MATERIAL INTERACTION TESTS

The VULCANO facility is dedicated to the study of larger masses (25-50 kg) of prototypic corium and of its interaction with various materials. In the LWR severe accident program, VULCANO has been used to study the interaction of corium with concrete[20] and with ceramic materials[21].
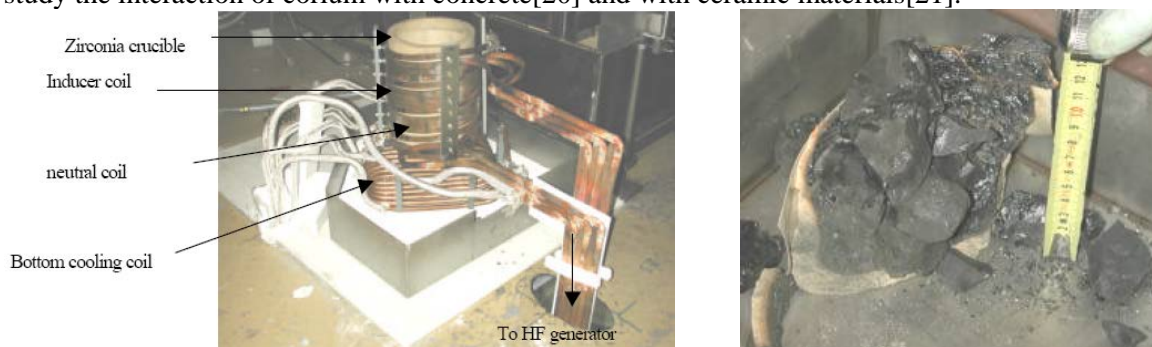
FIG. 5: VULCANO facility
Left: crucible + induction coils   Right: solidified corium and ablated ceramic crucible[21]

This facility is planned to be used to conduct experimental R&D on the sacrificial material melting and dissolution transient when it is in contact with corium. Since these tests will be dedicated to the corium-sacrificial material it will not be necessary to add sodium during the test.

The VULCANO facility will also be useful to study with prototypical materials the natural convection in presence of two immiscible liquid phases (oxide and metal) and in particular the effect of metal segregation on heat transfer.

4.5 SOFI FACILITY AT IGCAR

Currently the only operating corium-sodium interaction facility is the SOFI facility at IGCAR [22] in India. Its induction furnace is currently able to melt about one kilogram and release it in a sodium test section. Its capacities shall be increased to the 20-kg range.

There is currently an implementing agreement between CEA and IGCAR on corium melting experiments that could be used on the issue of Fuel Coolant Interaction experiments.

4.6 FOURNAISE: Large scale prototypic corium facility

It is necessary to perform prototypic experiments with larger masses both for Fuel Coolant Interaction (FARO experiments for Light Water reactors have indicated that a mass above 50 kg is needed to reach a steady state mixing of corium jet with coolant [23]) and for corium-material interaction where crust effects and convective cell size effects also require large volumes. CEA is considering a new facility, FOURNAISE [24] in which corium masses of several hundred kilograms can be molten and studied.

Two major experimental programs are planned on this facility and correspond to two different experimental configurations:

- Study of the Fuel Coolant Interaction in steady state (simulating large corium flows out of the core region) with a sodium-filled test section (FIG. 6). This encompasses the following research issues:
    - Risks linked to the core catcher ablation by a coherent melt jet ;
    - Debris bed formation in view of its coolability: During the 2 FARO tests with sodium, all the uranium oxide melt fragmented [25] while in the tests with water an unfragmented "cake" was found [23]; further experiments are needed to verify that a cake cannot be found in some sodium cases;
    - Sodium vapour explosion experimental data base shall be completed by a few tests with a low sodium subcooling (simulating a long-lasting melt flow to the lower plenum) and the effects of combined steel and uranium oxide jets.
    - Validation of relocation processes through engineered Corium Dispersion Channels.
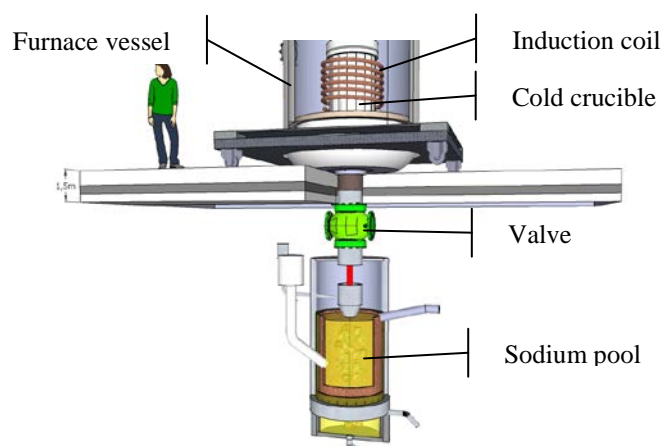- Longer term experiments to study the Post Accidental Heat Removal from debris bed and corium pools.

FIG. 6: Sketch of the FOURNAISE FCI test section and melting furnace

4.7 CORRONA corrosion testing

New materials will have to be installed in potential contact[1] with sodium, either inside or outside the main reactor vessel, their long-term corrosion behavior in liquid sodium in the conditions of the cold plenum is to be assessed, in order to assure that these safety related components would still be efficient when required. The CORRONA facility [24] is lab-scale test setup devoted to the studies of corrosion phenomena in liquid sodium and its modeling for the long term prediction, by performing static corrosion in controlled conditions [26][27](FIG. 7 left). Before and after the interaction with sodium, microscopic observations are performed to characterize the corrosion phenomena (FIG. 7 right) and to quantify corrosion kinetics versus exposure time when regular extractions of specimen is achieved. Experiments have been launched with aluminium and hafnium oxide ceramics, as well as with metallic hafnium. Preliminaries results for ceramics indicated that the actual composition, fabrication process parameters and the microstructure play a major role in the observed behavior in liquid sodium. For instance, high purity sintered alumina exhibited a corrosion behavior similar to the alumina monocrystal exposed in the same temperature of 550°C and oxygen conditions of around 10 wppm but for 2000h instead of 1000h: only a slight dissolution is observed over a depth restricted to a few hundredth of nm and no intergranular attack was observed (FIG 7). A sintered alumina of a slightly lower purity (99.5%) presented to the contrary an intergranular attack in the range of tenth of µm after sodium exposure at 500°C for 170h. Segregation of impurities such as silicon oxide at the grain boundaries is supposed to enhance the sodium attack through oxidation into a ternary oxide, $Na_2O.SiO_2$., which dramatically reversed the behavior of the ceramic. This effect is to be further confirmed, but suggests however that high purity sintered alumina could be present acceptable corrosion behavior in the conditions required.
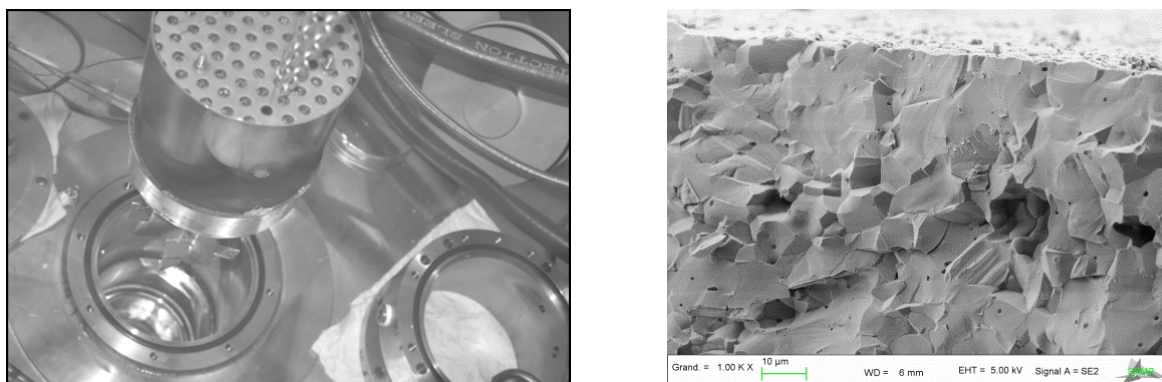

FIG. 7: CORRONA Facility :
Left: View of open sodium pot – Right: Micrograph of 99.7% alumina sample after 1000 h in sodium

5. SIMULANT MATERIAL TESTS

Due to the experimental difficulties linked with corium and/or sodium, it is sometimes useful to use simulant materials to perform well-instrumented separate effect tests, which, for instance, can lead to the elaboration of dedicated correlation, or to validation at a scale unachievable with prototypic materials.

5.1 Corium Pool Thermalhydraulics tests in CLARA facility.

New data are needed on the heat flux distribution in a biphasic (2 immiscible liquid phases: oxide and metal) pool submitted to an intense internal heat source. Different geometries must be studied to represent both in-core geometry and core-catcher geometry. These tests will also provide insight on the dynamic separation between the two phases and on segregation criteria.

---

[1] These core-catcher materials will likely be installed in some type of casing. But local ruptures cannot be excluded so compatibility with sodium is indeed an issue.

It is planned to adapt the CLARA facility [28] which has been built for LWR corium-concrete interaction pools. It is a versatile test section (2 m x 1.2 m x 0.25) made of 16 modules with 8 heat exchangers in the bottom and 8 on the side, in order to study the spatial distribution of heat fluxes due to convection (FIG. 8).

In a first step, scaling laws must be derived to select simulant materials for the ASTRID configurations (Currently CLARA uses aqueous solutions of hydroxyl-ethyl-cellulose to simulate LWR corium-concrete interaction).

A second issue is related to the transient dissolution of ceramic due to convection in a corium pool. In support to the prototypic corium tests in VULCANO and FOURNAISE, low-temperature simulant material tests will be needed to validate the dissolution models imbedded in the TOLBIAC SFR code. Whether these tests can be performed in an adapted CLARA facility or in a separate facility has not yet been decided.
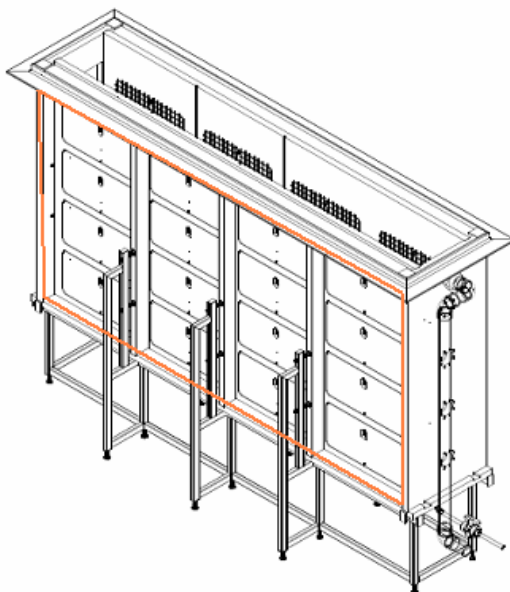

FIG. 8: Sketch of the CLARA facility

5.2 JET ABLATION EXPERIMENTAL PROGRAM

Corium jet could ablate the core catcher material when released from the core region. There are sufficient data for short jets, but more data is needed for long jets for which a molten pool can be created at the impact point that reduces the heat transfer at the jet-material interface. Furutani et al. [29] have performed some tests with paraffin and low-temperature metallic alloys. A scaling law analysis shall be performed to determine relevant simulant materials for ASTRID applications.

5.3 POST ACCIDENTAL CORE CATCHER COOLING EXPERIMENTS

A thermal hydraulic mock-up will be necessary to validation the natural convection heat transfer between the core catcher and the ultimate heat sinks. The PATH facility [29] has been designed at IGCAR to demonstrate heat removal capability for whole core melt down scenario with volumetric heated debris bed characteristics simulated from data generated from in-house Wood's metal–water, U–Na, UO_2–Na experiments. PATH is a 3.1 m diameter, 3.2 m high water mock-up. A sodium facility is also planned at IGCAR for subsequent experimental validation.

Presently, the design of the core catcher has not yet been selected [5] so it is not possible to currently design the required facility. If an in-vessel core catcher is selected for ASTRID, the core catcher cooling experiments will either be conducted in a facility resembling PATH or, through the French-Indian collaboration agreement, in a modified stage of PATH. If an ex-vessel or inter-vessel core catcher design is selected a specific thermalhydraulic facility shall be designed and constructed.

6. CONCLUSIONS

A comprehensive experimental program has been launched in order to gain new data in support of the severe accident studies related to the ASTRID demonstrator. The main new issues with respect to the historic experimental database are mainly related to new design options: heterogeneous core with thick pins, new materials, new severe accident mitigation systems such as corium discharge channels and core-catcher sacrificial materials. Some issues remain open as Fuel Coolant Interaction.

Experiments are needed both in-pile and out of pile. Depending on the objectives, the out of pile experiments can be conducted with simulant, with prototypic corium or with irradiated fuel. A new large scale corium facility, FOURNAISE, must be built to fulfill this program. Nevertheless, some tests have already started in existing facilities, such as VITI or CORRONA.

REFERENCES
[1] G. KEYSER, J. PAPIN, "The reactivity risk in fast reactors and the related international experimental programmes CABRI and SCARABEE, Progr. Nucl. Energ., 32 (1998) 631-638.
[2] P. ROYL, W. BREITUNG, E.A. FISCHER, G. SCHUMACHER, P.O. GAUNTT, S.A. WRIGHT, "Contributions from the ACRR in-pile experiments to the understanding of key phenomena influencing Unprotected Loss Of Flow accident simulations in LMFBRs", Nucl. Eng. Des., 100 (1987) 347-408.
[3] G. KAYSER, C, LE RIGOLEUR, "PAHR – Engineering problems and solutions", 5th Post Accident Heat Removal Information Exchange Mtg, Karlsruhe, Germany, 1982.
[4] F. GAUCHE, "Generation IV reactors and the ASTRID prototype: Lessons from the Fukushima accident, Cptes Rendus Phys.13 (2012) 365-371.
[5] F. SERRE, P. ALLEGRE, F. BERTRAND,. CHAMPIGNY, C. JOURNEAU, J.C. ROBIN, C. SUTEAU, C. VIALA, « R&D and design studies for the ASTRID core catcher », Int. Conf. Fast Reactors, FR13, Paris, 2013.
[6] P. DUBUISSON, Y. DE CARLAN, V. GARAT, M. BLAT, « ODS ferritic/martensitic alloys for sodium reactor fuel pin cladding, J. Nucl. Mater., 428 (2012) 6-12.
[7] Yu.S. VASSILIEV, A.D. VURIM, V.A. GAIDACHUK, A.A. KOLODESHNIKOV, V.A PAKHNITS, A.V. PAHNITS, A.S. MARININ, G.V. SHAPOVALOV, J.V. LOGACHEV, K. KONISHI, J.I. SATO, S. KUBO, S. KOTABE, K. KOYAMA, "Research on problems of safety of Nuclear Power Reactors in the IGR Reactor: the Results of Medium-Scale Experiments Realised under the EAGLE Project", 13th Int Conf on Radiation Physics and Chemistry of Inorganic Materials, Tomsk, 2006.
[8] I. SAITO, T. NAKARIGI, T. HIROSAWO, S. MIYAHARA, T. NAMEKAWA, "Fission product release and transport from irradiated FBR MOX fuel during transient conditions", J. Nucl. Sci. Technol. 40 (2003) 104-113.
[9] P. MENEGON, L. DESGRANGES, Y. PONTILLON, A. POULESQUEN, "Evidence of two gas release kinetics during the oxidation of an irradiated PWR UO_2 fuel", J. Nucl. Mater. 378 (2008)1-8.
[10] M.P. Ferroud-Plattet, J. Bonnin, A. Gallais-During, S. Bernard, J.P. Grandjean, G. Ducros, "CEA VERDON laboratory at Cadarache: new hot cell facilities devoted to studying irradiated fuel behaviour and fission product releases under simulated accident conditions", International HOTLAB conference, Prague, Czech Republic, 2009 September 21-23
[11] P. PILUSO, C. JOURNEAU, E. BOCCACCIO, J.-M. BONNET, P. FOUQUART, J.-F. HAQUET, C. JÉGOU, D. MAGALLON, "Corium Behaviour Research at CEA Cadarache: The PLINIUS prototypic corium experimental platform", International Conference Nuclear Energy for New Europe 2002, Kranjska Gora, Slovenia.
[12] C. JOURNEAU, J.M. RUGGIERI, P. PILUSO, "Plans for a new large scale facility at CEA Cadarache: the FOURNAISE project", European Review Meeting on Severe Accident Research (ERMSAR 2012), Cologne, Germany, 2012.
[13] K. PLEVACOVA, C. JOURNEAU, P. PILUSO, J. POIRIER, An experimental study of the effect of Boron carbide on the SFR corium composition, Proc. Int Young Nuclear Conf., IYNC 2010, Capetown (2010).
[14] D. GRISHCHENKO, P. PILUSO, « Recent progress in the gas-film levitation as a method for thermophysical property measurements : application to ZrO_2-Al_2O_3 system, High Temp. High Press. 40 (2011) 127-149.

[15] C. JOURNEAU, K. PLEVACOVA, G. RIMPAULT, S. POUMÉROULY, « Sacrificial materials for SFR Severe Accident Mitigation », ICAPP'10, San Diego, CA, 2010.

[16] M. BAÏCHI, C. CHATILLON, C. GUENEAU, S. CHATAIN,"Mass spectrometric study of UO_2-ZrO_2 pseudo-binary system", J. Nucl. Mater., 294 (2001)84-87.

[17] C. GUÉNEAU, S. CHATAIN, J.C. DUMAS, J. LECHELLE, C. RADO, F. DEFOORT, N. DUPIN, B. SUNDMAN, H. NOEL, R. KONINGS, "FUELBASE: a thermodynamic database for advanced nuclear fuels", HTR2006 : Third International Topical Meeting on High Temperature Reactor Technology, Johannesburg, South Africa, 2006.

[18] P. PILUSO, E. BOCCACCIO, J.-M. BONNET, C. JOURNEAU, P. FOUQUART, D. MAGALLON, I. IVANOV, I. MLADENOV, S. KALCHEV, P. GRUDEV, H. ALSMEYER, B. FLUHRER, M. LESKOVAR, "Severe Accident Experiments on PLINIUS Platform - Results of First Experiments on COLIMA Facility Related to VVER-440 - Presentation of Planned VULCANO and KROTOS Tests", International Conference Nuclear Energy for New Europe 2005, Bled, Slovenia, 2005

[19] S. MORANDI, F. PAROZZI, E. SALINA, C. JOURNEAU, P. PILUSO, Aerosol Retention in Containment Leak Paths: Indications for a Code Model in light of COLIMA Experimental Results, European Review Meeting on Severe Accident Research (ERMSAR 2012), Cologne, 2012.

[20] C. JOURNEAU, P. PILUSO, P. CORREGGIO, L. FERRY, G. FRITZ, J.F. HAQUET, J. MONERRIS, J.M. RUGGIERI, M. SANCHEZ-BRUSSET, C. PARGA, " Contributions of the VULCANO experimental Programme to the Understanding of MCCI Phenomena", Nucl. Eng. Technol., 44 (2012) 261-272.

[21] C. JOURNEAU, C. JÉGOU, J. MONERRIS, P. PILUSO, K. FROLOV, YU. B. PETROV, R. RYBKA, "Phase Macrosegregation during the slow solidification of prototypic corium", 10th International Topical Meeting on Nuclear Reactor Thermal Hydraulics (NURETH-10), Seoul, Korea, 2003.

[22] P. CHELLAPANDI, "Overview of Molten fuel coolant Interaction Studies towards SFR Development", OECD SERENA Project Seminar, Cadarache, 2012.

[23] D. MAGALLON, I. HUHTINIEMI, H. HOHMANN, "Lessons learnt from the FARO/TERMOS corium melt quenching experiments", Nucl. Eng. Des., 189 (1999) 223-238.

[24] G. RODRIGUEZ, L. AYRAULT, J. DUMESNIL, E. SANSEIGNE, F. DUJET, B. COLLARD, F. SERRE, C. JOURNEAU, "Development of experimental facility platform in support of the ASTRID program", Int. Conf. Fast Reactors, FR13, Paris, 2013.

[25] D. MAGALLON, H. HOHMANN, H. SCHINS, "Pouring of 100-kg-scale molten UO_2 into sodium", Nucl. Technol. 98 (1992) 79-90.

[26] F. BALBAUD-CÉLÉRIER, J.L. COUROUAU, L. MARTINELLI, "Corrosion of structural materials in liquid metals used as fast reactors coolants", Int. Conf. Fast Reactors, FR13, Paris, 2013.

[27] J.L. COUROUAU, V. LORENTZ, M. TABARANT, S. BOSONNET, F. BALBAUD-CÉLÉRIER, "Corrosion by oxidation and carburization in liquid sodium at 550°C of austenitic steels for sodium fast reactors", Int. Conf. Fast Reactors, FR13, Paris, 2013.

[28] M. AMIZIC, E. GUYEZ, J.M. SEILER, "Experimental Investigation on Heat Transfer for Two-Phase Flow under Natural Convection - First CLARA Test Results", ICONE20, Anaheim, 2012.

[29] A. FURUTANI, S. IMAHORI, K. SATO, M . SAITO, "Erosion behavior of a solid plate by a liquid jet – effect of molten layer", Nucl. Eng. Des., 121 (1990) 11-23.

[30] L. GNANADAS, A.K. SHARMA, B. MALARVIZHI, S.S. MURTHY, E. H. RAO, M. KUMARESAN, S.S. RAMESH, J. HARVEY, B.K. NASHINE, P. CHELLAPANDI, S.C. CHETAL, "PATH – An experimental facility for natural heat circulation heat transfer studies related to Post Accident Thermal Hydraulics", Nucl. Eng. Des., 241 (2011)3839-3850.

Control Rod Worth Measurement in Monju Restart Core

Yuko Kato, Yasushi Ohkawachi, Shin Usami

Japan Atomic Energy Agency, Tsuruga, Fukui, Japan

Abstract. The Japanese prototype fast breeder reactor (FBR) Monju resumed the system startup test (SST) in May 2010 after fourteen year and five month suspension since the sodium leakage of the secondary heat transport system in December 1995. Core confirmation test (CCT) is the first step of SST which consists of three steps, and finished in July 2010. Valuable basic data for FBR development was obtained in CCT, such as reactor physics data of the core which contained 1.5wt%/HM in average of Am-241 accumulated due to the Pu-241 decay during the long-term suspension. Control rod reactivity worth measurement was carried out to calibrate the reactivity worth of control rods and to confirm the core characteristics such as excess reactivity and reactivity shutdown margin to be satisfied with safety criteria. The high prediction accuracy of the core management code system was demonstrated based on the measured data. Furthermore, the examination was conducted to shorten the measurement period.

1. Introduction

Monju, a 280 MWe prototype FBR located at the Shiraki site on the Tsuruga Peninsula of Fukui Prefecture, restarted its system startup test (SST) and reached criticality on May 8, 2010. Fourteen years and five months have passed since the sodium leakage from the secondary heat transport system occurred at 40% rated power on December 8, 1995. The largest change between the restart core and the previous SST core in 1994 is in the contents of Pu-241 and Am-241. The content of Pu-241 has halved and that of Am-241 has more than doubled due to the Pu-241 decay during the suspension.

The SST is planned to be conducted in the three steps: Core Confirmation Test (CCT), 40%-power Confirmation Test and Power Rising Test. The present paper describes the evaluation of the control rod worth measured in the CCT.

2. Overview of SST

The SST consists of the three steps as shown in Fig.1. The CCT was completed to confirm core characteristics and functions of the primary and secondary sodium circuit. The test was conducted at a very low reactor power with heat removed by the air coolers. The turbine and generator in water/steam system was not in service in the CCT. After refueling succeeding to the CCT, 40%-power Confirmation Test will be conducted at the minimum electricity output of 40%. The soundness of the water/steam system and the turbine/generator system after long-term lay-down will be checked in the test. After another refueling, Power Rising Test will be carried out. Performances of whole plant will be checked in the output ranges to 100%. Integrated controllability of reactor output, primary sodium flow rate, secondary sodium flow rate and water/steam flow rate are evaluated. Automatic safety shut-down characteristics of the plant are also checked by simulating abnormal situations.

The CCT, which is the first step of SST, was carried out for 78 days and completed on July 22, 2010. The progress of the CCT is shown in Fig.2. The CCT consists of 20 test items in total, and they are divided into 2 groups. The 1st one is the tests to confirm the core characteristics to be satisfied with safety criteria, including the tests of "control rod worth measurement", "excess reactivity measurement", "reactivity shutdown margin measurement" and so on. The 2nd one is the tests to acquire the core characteristics data for R&D and to confirm the function & performance of the plant

system & equipment, including the tests of "Temperature coefficient evaluation", "Feed-back reactivity evaluation" and so on. Satisfactory operation was achieved with successful accomplishment of the CCT. By this achievement, the safety of the reactor core and the self-stabilization were confirmed. Furthermore, valuable basic data of FBR development was acquired, such as reactor physic data of the core which contained large amount of Am-241 accumulated during the long-term suspension. The control rod worth measurement was conducted on the first stage of the CCT.
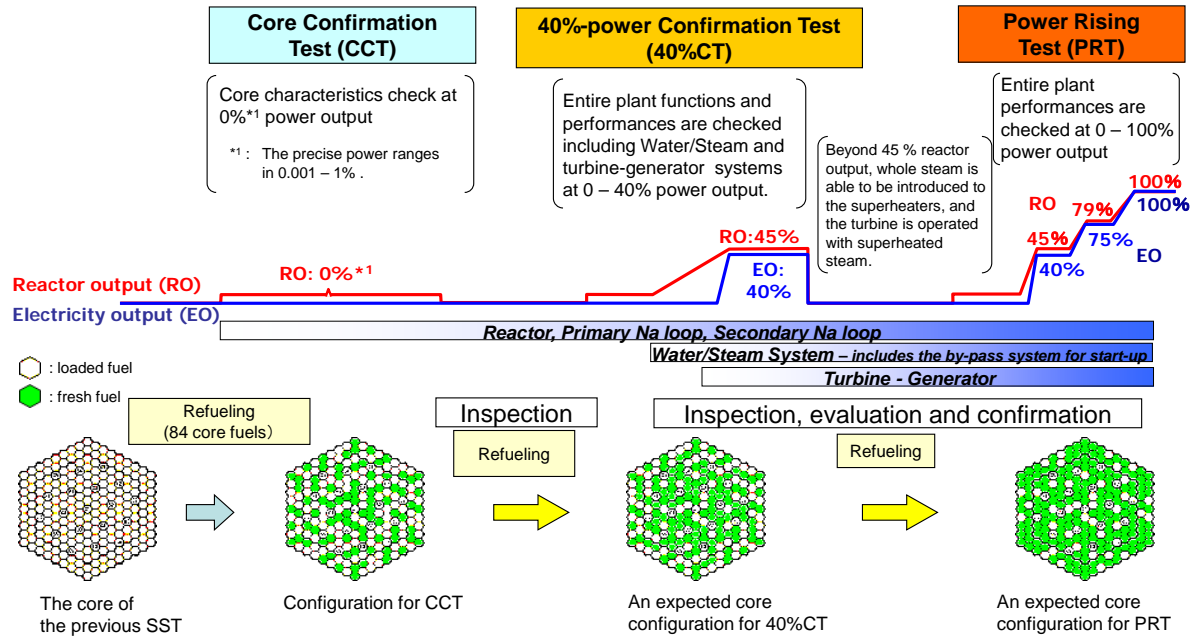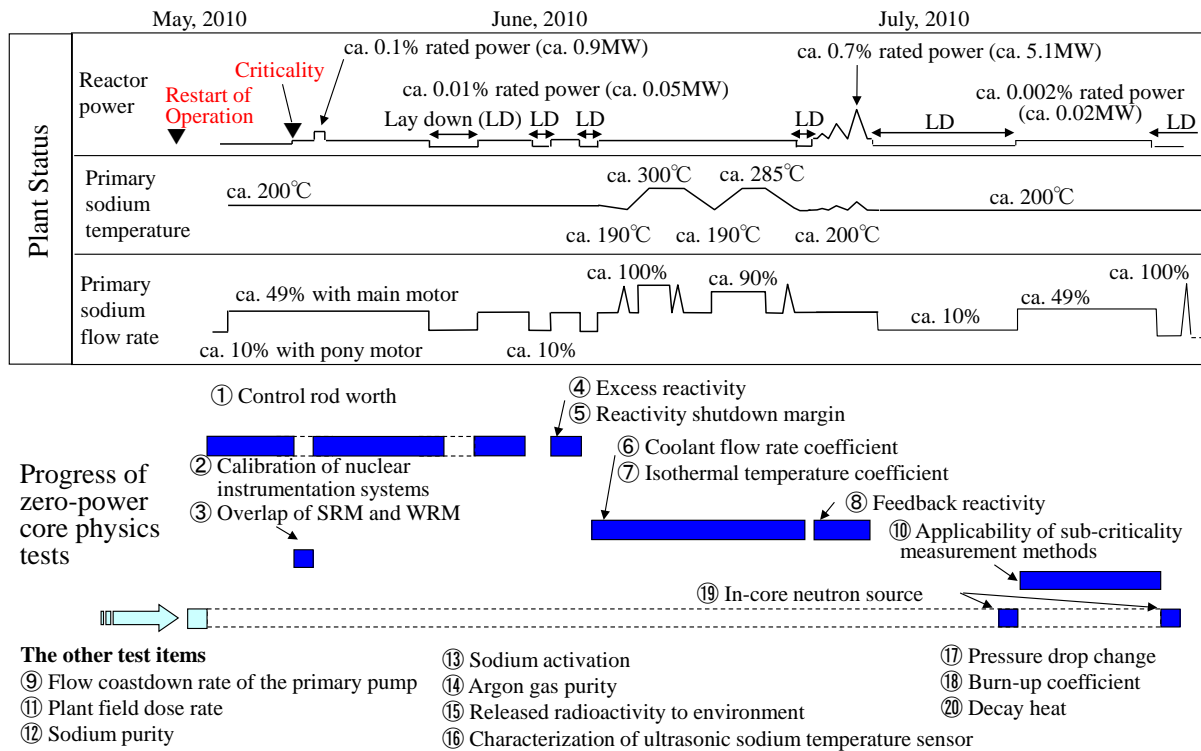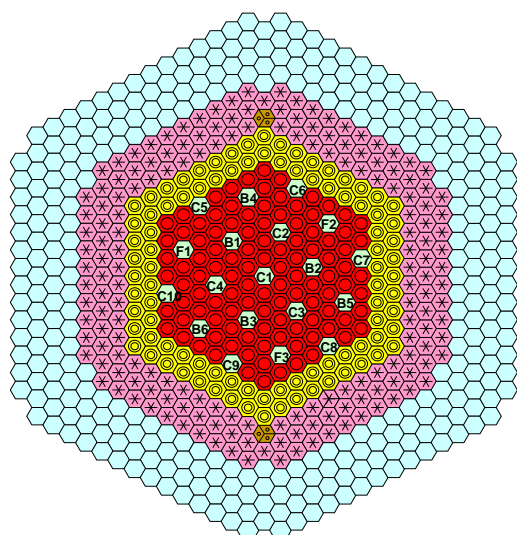

*Fig. 1 Overview of System Start-up Test (SST)*

Fig. 2 Core Confirmation Test (CCT) Progress

3. Reactor Core Description

Fig.3 shows the Monju core configuration. Monju is a sodium-cooled loop-type fast breeder reactor with an output of 280MWe (714MWt) fuelled with mixed oxides of plutonium and uranium. The number of driver fuel subassemblies is 198. The fueled region is divided into two Pu enrichment zones to flatten the power distribution. The inner zone Pu fissile enrichment is 15% to 16% and the outer zone Pu fissile enrichment is 20% to 21%. In the initial core at the present SST, 3-types of core fuels are used. Around them, there are the radial blanket region and the neutron shield region. Fine Control Rod (FCR) and Coarse Control Rod (CCR) are used for reactivity control and Backup Control Rod (BCR) is for emergency shutdown. The principal design and performance data of Monju is shown in Fig.3, too.
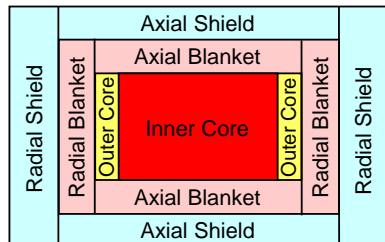
Core Zone	Inner Core		108
	Outer Core		90
Radial Blanket			172
Control Rod	Fine Control Rod (FCR)		3
	Coarse Control Rod (CCR)		10
	Backup Control Rod (BCR)		6
Neutron Source			2
Neutron Shield			324

Horizontal Cross Section

Vertical Cross Section

Principal Design and Performance Data of Monju

Reactor Type	Sodium-Cooled Loop-Type
Thermal Output	714 MW
Electrical Output	280 MW
Fuel Material	$PuO_2 - UO_2$
Core Dimension	
Equivalent Diameter / Height	1.8 / 0.93 m
Blanket Thickness	
Upper / Lower / Radial Equivalent	0.3 / 0.35 / 0.3 m
Plutonium Fissile Enrichment	(Inner Core / Outer Core)
Fuel of Initial Core Type 1	15 / 20 wt%
(SST core) Type 2	16 / 21 wt%
Type 3	16 / 21 wt%
Fuel of Equilibrium Core	16 / 21 wt%
Fuel Inventory	
Core (U+Pu+Am-241 metal)	5.9 ton
Blanket (U metal)	17.5 ton
Average Burnup	
Equilibrium Core	80,000 MWd/t
Cladding Material	SUS316
Cladding Outer (Diameter/Thickness)	6.5 / 0.47 mm

Fig. 3 Core configuration of Monju

Pu-241 with half-life of 14 years has spontaneously decayed and turned into Am-241 in the core fuel. A change in the contents of the two nuclides is shown in Fig.4[1]. The core average content of Am-241 in the restart core (hereinafter called "Core2010") is 1.5wt%, which is three times larger than that in the previous SST core in 1994 (hereinafter called "Core1994"). Since the Pu-241 decay caused a reactivity loss of 5%Δk/k as shown in Fig.5, 84 fuel subassemblies were replaced in 2009 to compensate for the reactivity loss before the restart.

The core region layouts before and after the refueling are shown in Fig.6 as Core1994 and Core2010, respectively. The newly loaded subassemblies are called "Type 2" and "Type 3", while the continuously used subassemblies are "Type 1". Type 1 is the already-existing burnt fuel subassembly which was used in the previous SST. Type 2 is the already-existing aged but fresh fuel subassembly, which was fabricated before the previous SST and stored outside the reactor core. Type 3 is the fresh fuel subassembly which was newly fabricated. Type 3 has the highest fissile Pu content, and the lowest Am-241 content, and six Type 3 fuel subassemblies were loaded around the core center in Core2010.
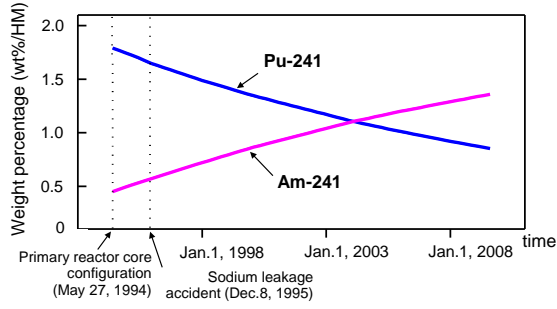
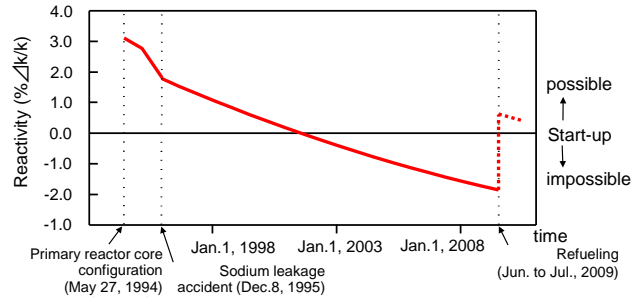Fig. 4 *Change in the core average contents of Pu-241and Am-241*

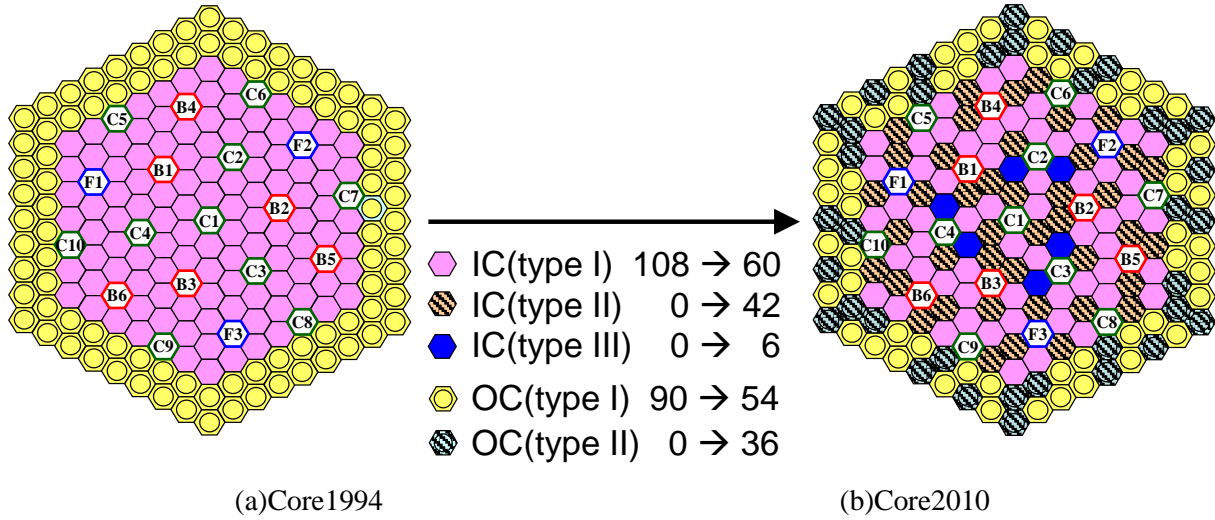Fig. 5 *Change in the core reactivity (at 180°C)*

IC(type I)	108 →	60
IC(type II)	0 →	42
IC(type III)	0 →	6
OC(type I)	90 →	54
OC(type II)	0 →	36

(a)Core1994 (b)Core2010

Fig. 6 *Core region layouts (a) before and (b) after the refueling.(IC=inner core; OC=outer core)*

4. Control Rod Worth Measurement

4.1. Measurement and Results

The control rod worth and the calibration curve of CCR1 (the central control rod) were measured step by step by the positive period method. In the positive period method, after inserting the reactivity by a certain length withdrawal of CCR1, the doubling time of neutron count rate was measured by a stop watch. The time gives the reactivity based on the following equation:

$$\rho = \frac{l}{T_d/\ln(2)} + \sum_{i=1}^{6}\left(\frac{\beta_{i,eff}}{1+\lambda_i \times T_d/\ln(2)}\right)$$

where, ρ : Reactivity

l Prompt neutron lifetime

T_d Doubling time

$\beta_{i,eff}$ Effective delayed neutron fraction for the i-th group

λ_i Decay constant for the i-th delayed neutron group

The control rod worth of CCR1 was approximately 1%Δk/k. Fig.7 shows the control rod worth calibration curve of CCR1. Due to the small excess reactivity of the core, the CCR1 was not fully inserted even with the other control rods at the upper position. The CCR1 worth over the measured

range was equivalent to the excess reactivity of the core. In the range outside of the measurement range, the reactivity was evaluated using the design calculation code (which was verified in the safety licensing examination).

The worth of each of the other control rods was measured by the rod swap method with the CCR1 worth as a reference. In the range outside of the measurement range, the reactivity was evaluated using the design calculation code. Fig.8 shows the control rod worth calibration curve of FCR1. In total, the control rod worth and its calibration curve of each of the 19 control rods were obtained. Based on the measured values, it was confirmed that the worth calibration curves of the control rods at the location of rotary symmetry in the core were coincident with each other within 0.4% of relative difference.
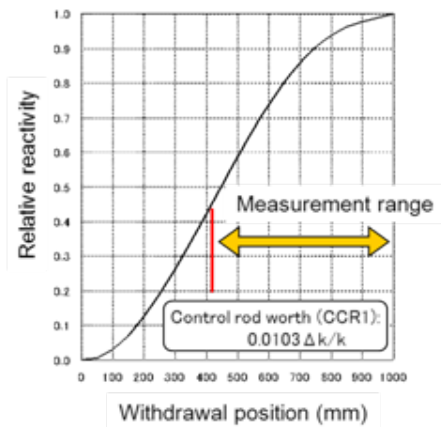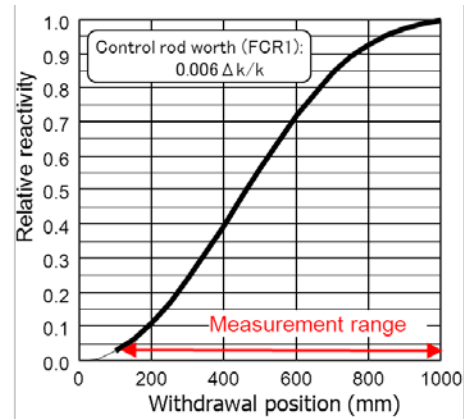

Fig. 7 *Control rod worth calibration curve of CCR1*

Fig. 8 *Control rod worth calibration curve of FCR1*

The results of the measured control rod worth in Core1994[2] and Core2010 are shown in Fig.9. The regulating control rods have the worth in the range of about 0.5%Δk/k to 1%Δk/k, depending on the loaded position in the reactor core. The backup control rods have the worth from about 0.9%Δk/k to 1.4%Δk/k. The components of the uncertainty in the measured worth consist of the criticality judgment, the control rod base position setting, the delayed neutron parameters, etc.[3]. For example, the relative uncertainty of CCR1 was in the range of -2 to +4 % as 2σ value of the experimental uncertainty.

The measured values of the control rod worth in Core2010 were larger than those in Core1994 in the central region of the core. That is due to the effects of the fresh fuel subassemblies loaded in the central region of the core.
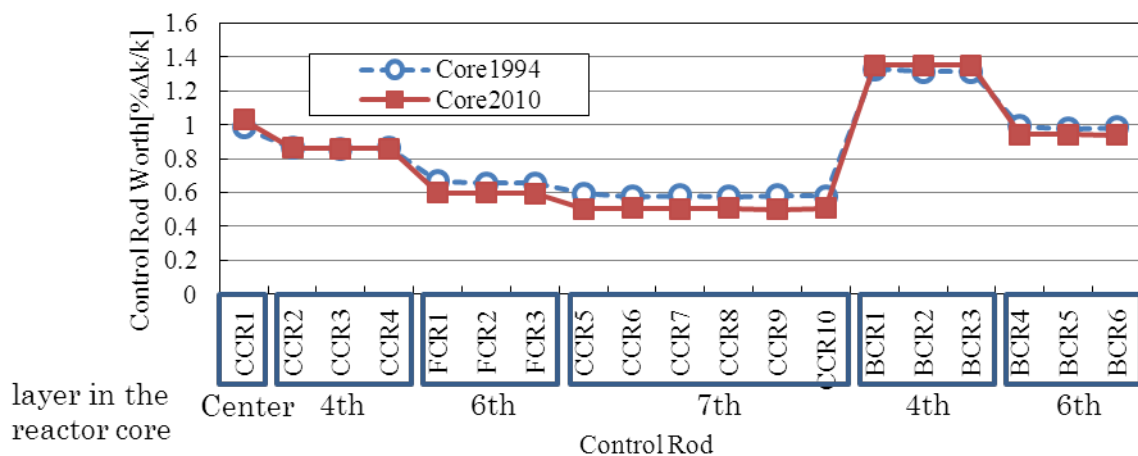

Fig. 9 *Results of Control Rod Worth Measurement*

The excess reactivity at 180 °C and the reactivity shutdown margin were evaluated from the control rod position at criticality and the control rod calibration curve. Reactivity insertion rate was also measured. As shown in Table 1, it was confirmed that the measured nuclear parameters such as excess reactivity, reactivity shutdown margin, reactivity insertion rate, etc. satisfied the safety criteria. It was also confirmed that the predicted value (0.4%Δk/k) and the measured value (0.6%Δk/k) of the excess reactivity were coincident with each other within the uncertainty of the predicted value ($\pm$0.3%Δk/k), demonstrating the high prediction accuracy for the core after 14 year and 5 month suspension. Hereupon, the components of the uncertainty of the predicted value consist of the systematic error related to the decay of Pu-241, the composition error, the measurement error in the previous SST, etc.

Table 1. Measurement of Reactivity etc. of Core2010

Item	Measurement	Safety Criteria
Excess reactivity (180°C)	0.006 Δk/k	$\leq$0.057Δk/k
Reactivity shutdown margin	0.067 Δk/k	$\geq$0.01Δk/k
Reactivity insertion rate	Max. 5.2×10^{-5} Δk/k/s (FCR1)	$\leq$8$\times10^{-5}$ Δk/k/s

4.2. Calculation

4.2.1. Core management Code System

The core management code system in Monju carries out the detailed calculation of the core characteristics with high reliability and high efficiency using the plant data and the fuel composition data stored in the database. This system is also capable of the core operation analysis (such as the refueling planning), the core structural confirmation analysis, the radiological analysis, and so on. The calculation data is stored in the database, too. Fig.10 shows the overview of the core management code system. The refueling and operation planning, the evaluation of fuel burnup and fuel inventory, the confirmation of core bowing behavior and so on are conducted using this system.
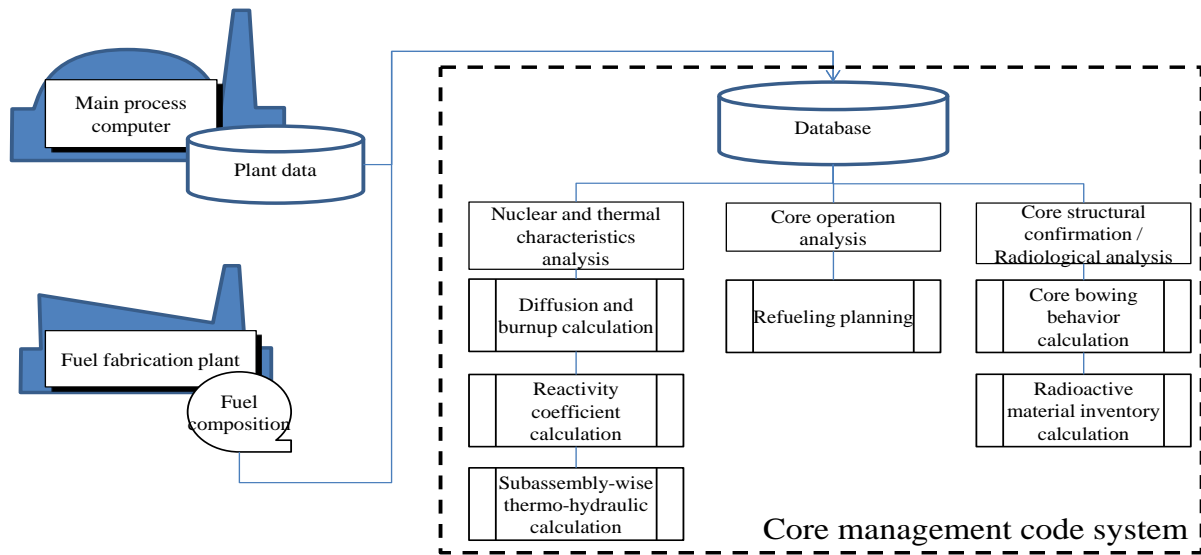
Fig. 10 Overview of the Core management code system

4.2.2. Calculation Method

Calculations are based on a deterministic method, which consists of a base calculation and correction, as shown in Fig.11. The base calculation results are obtained with the lattice cell calculation code SLAROM[4] and the diffusion core calculation code DIF3D[5]. The cell calculation is carried out to produce the effective cross-sections using the 70 energy-group constant set generated by the nuclear

data library JENDL-3.3[6]. The whole core calculation is carried out in the 6 energy-group structure and the triangle-Z geometry. The E-C or E/C bias factors are deduced from the previous SST data measured in 1994, and they are applied to the base calculation results as the corrections to minimize the calculation errors.
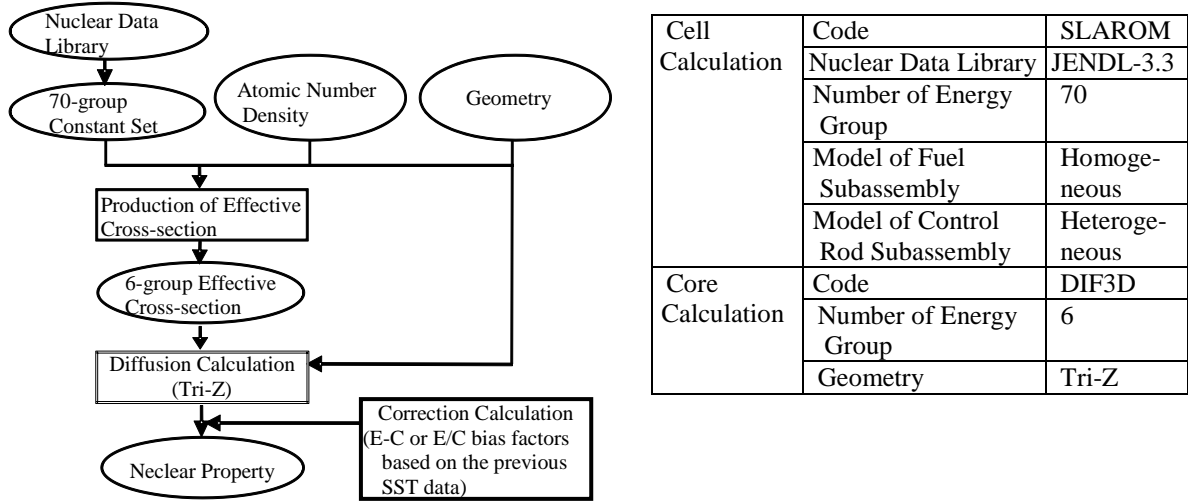

Cell Calculation	Code	SLAROM
	Nuclear Data Library	JENDL-3.3
	Number of Energy Group	70
	Model of Fuel Subassembly	Homogeneous
	Model of Control Rod Subassembly	Heterogeneous
Core Calculation	Code	DIF3D
	Number of Energy Group	6
	Geometry	Tri-Z

Fig. 11   Calculation Flow

4.2.3. *Calculation Results*

Fig.12 shows the comparison between the calculated and the measured values of the excess reactivity and the control rod worth in Core2010. The difference between the measured excess reactivity (E) and the calculated one (C) in Core2010, i.e. the E-C is 0.84%Δk/k without correction. However, when the E-C bias factor based on the previous SST data in Core1994 is taken into account as correction, the E-C of excess reactivity in Core2010 is improved to be 0.21% Δk/k. The ratios of the calculated control rod worth (C) to the measured one (E), i.e. the C/E values are in the range of 1.03 to 1.07 without correction. When the E/C bias factors based on the data in Core1994 are applied to them as correction, the C/E values of control rod worth in Core2010 are improved to be 1.01 to 1.05.

The values of the excess reactivity and the control rod worth in Core2010, calculated by the core management code system and corrected by the measured data in Core1994, are in good agreement with the measured values.
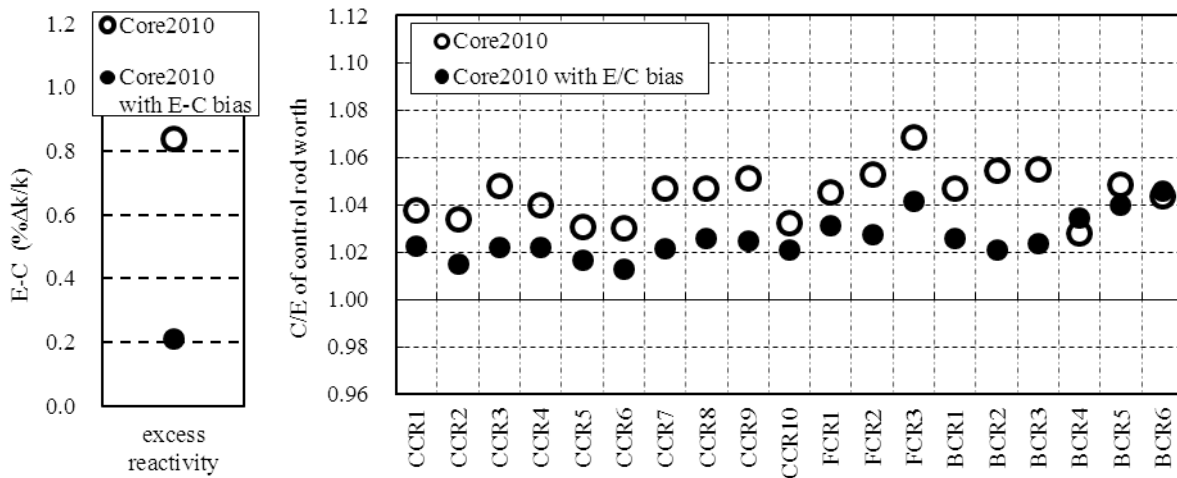

Fig. 12   E-C value for excess reactivity and C/E value for control rod worth

5. Rationalization of Control Rod Worth Measurement Method

In the control rod worth measurement in Core2010, the control rod worth and the reactivity insertion rate of each of all the control rods were measured cautiously using the positive period method and the swap method in the same way as in Core1994. The period required for both the control rod worth measurement and the legal inspection in Core2010 was 21 days. However, it is important for the improvement of economic competitiveness of FBR to improve the availability factor of the plant by shortening the reactor physics test period by the rationalization of the control rod measurement method. There are the other control rod worth measurement methods which have been used in the experimental fast reactor Joyo and were carried out experimentally in the previous SST in Monju. In order to shorten the period of the control rod worth measurement, the applicability of their methods to the next SST in Monju is evaluated as follows:

5.1. Multiplication Source Method (MSM)

The multiplication source method (MSM) enables subcritical reactivity levels to be derived from the measured subcritical counting rates corrected for spatial effects by the application of calculated correction factor called the MSM factor. To transfer the results from relative to absolute values, this method has to be complemented by the absolute calibration of at least one subcritical state. The measurement of control rod worth at Superphenix is mainly based on the MSM method. During the commissioning test of Superphenix, the measured worth of the main control rod system (SCP) in the full-power core was 8.294%Δk/k and the MSM correcting factor was 0.939 [7]. In Monju, the worths of CCR1 were measured by MSM method in Core1994. The experiment values agreed with the values obtained by the period method within approximately 10% and the MSM correcting factors were 1.1 to 2.2 for the subcriticality less than approximately 1%Δk/k. However, the control rod worth had the tendency to overestimate and the factors became larger, for the deeper subcriticality. If the calculation used for the production of MSM correction factors is improved, the measurement accuracy can be improved. However, because the factor become large and depend heavily on calculation, it is necessary to calculate the factor by high accuracy, thus the method is not suitable for the inspection.

5.2. Rod Drop Method

In the rod drop method, the reactivity is estimated based on the extrapolation method and the inverse kinetics method by measuring the time variation of the neutron flux with control rod drop. This method was applied to the control rod measurement in Core1994 and Core2010. The measurement values obtained by the inverse kinetics method agreed with the values obtained by the period method and the swap method within approximately 10%. It was confirmed that the method was also applicable to the prototype-size fast reactor.

When the rod drop method is applied to the control rod measurement in Monju, only one rod to be measured is dropped by turning off the magnet which connects the drive shaft of the control rod drive mechanism to the control rod. However, in order to reconnect them, the reactor must be shutowned that is, it is necessary to insert all of the control rods. From this point of view, it is difficult to apply the rod drop method to the reactivity inspection in Monju, because it takes a long time to repeat the measurement procedure for other control rods.

5.3. Rod-juggling Method

The rod-juggling method is the way to determine positive and negative reactivity from changing of the count rate by inserting and withdrawing each control rod, as shown in Fig.13. The doubling time or time during which count rate becomes half is measured in process of inserting and withdrawing each control rod. Doubling time is measured by stopwatch or by a neutron count rate data acquisition system of neutron count rate. The reactivity can be sequentially evaluated by the inverse kinetics method using the neutron count rate data. It is not necessary to keep critical state, and it is possible to measure multiple control rods because of the possibility to measure the negative reactivity. Thus, the method will lead to shortening of the measurement time.

This method was applied to the control rod measurement in Core1994 in Monju. It was confirmed that values obtained by the method agreed well with value obtained by the period method. Additionally, JOYO has experiences to carry out the reactivity inspection using the values obtained by the method[8].
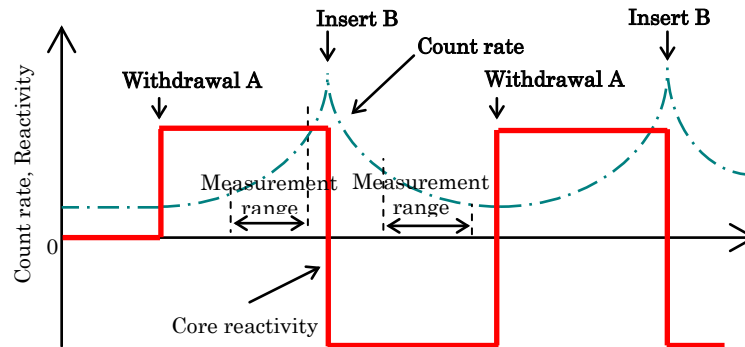

Fig. 13 Relationship diagram of the counting rate and reactivity of the rod-juggling method

Therefore, there is a plan to carry out the control rod worth measurement based on the four-rod-juggling method, using a neutron count rate data acquisition system in the next SST.

From the viewpoint of the rationalization of the control rod measurement method, it is effective to measure the control rod worth and the calibration curve for one control rod on each layer in the core (e.g. C1, C2, C5, F1) by using the rod-juggling method. The ratio of the experiment value (E) to the calculation value (C), i.e. the E/C value of the control rod worth and the calibration curve of one control rod on each layer in the core is evaluated. The other control rod worths are evaluated by multiplying the calculation values by the E/C value of the control rod on same layer in the core.

6. Conclusion

Monju restarted the system startup test (SST) in May 6, 2010 after 14 years and 5 month suspension, and the core confirmation test (CCT), which is the first step of SST, was accomplished successfully. The valuable basic data related to the control rod worth and the excess reactivity was obtained in the CCT core which contained 1.5wt%/HM in average of Am-241 accumulated due to the Pu-241 decay during the long-term suspension.

The control rod worth and the calibration curve of each of all the control rods were measured by the positive period method and the swap method. It was confirmed that the measured nuclear parameters such as excess reactivity, reactivity shutdown margin, reactivity insertion rate, etc. satisfied the safety criteria. It was also confirmed the values of the excess reactivity and the control rod worth in the CCT core, calculated by the core management code system and corrected by the measured data in the previous SST core in 1994, were in good agreement with the measured values.

In order to evaluate the rationalization of the control rod measurement method, there is a plan to measure the control rod worth and the calibration curve based on the four-rod-juggling method, using a neutron count rate data acquisition system in the next SST.

REFERENCES

[1] T. Deshimaru et al., "Restart and Progress of System Start-up Test in MONJU," Proceedings of GLOBAL 2011, Makuhari, Japan, Paper No. 391183

[2] S. Sawada et al., "Reactivity Characteristics Evaluations of the Initial Core of Monju," Proc. International Conference on the Physics of Reactors, Sept 16-20, 1996, Mito, Japan Vol.2, p.E-76.

[3] K. Takano et al., "Control Rod Worth Evaluation for the Monju Restart Core," Nuclear Technology Vol.179 Number2 pp.266-285

[4] M.NAKAGAWA and K.TSUCHIHASHI, "SLAROM: A Code for Cell Homogenization Calculation of Fast Reactor," JAERI 1294, Japan Atomic Energy Research Institute (1984).

[5] "DIF3D 7.0: Code System for Solving Finite Difference Diffusion Theory Problems," RSICC, CCC649(1997).

[6] K. Shibata et al., "Japanese Evaluated Nuclear Data Library Version 3 Revision-3: JENDL-3.3," J. Nucl. Sci. Technol., 39, No. 11, pp.1125-1136 (2002).

[7] J.C.Gauthier et al., "Measurement and Predictions of Control Rod Worth," Nuclear Science and Engineering: 106, 18-29(1990)

[8] T. Aoyama et al., "Core performance tests for the JOYO MK-III upgrade," Nuclear Engineering and Design 237(2007)353-368

Safety Strategy of JSFR to Establish the In-Vessel Retention of the Core Disruptive Accident

Yoshiharu TOBITA[a], **Ikken SATO**[a], **Kensuke KONISHI**[a], **Tohru SUZUKI**[a], **Kenji KAMIYAMA**[a], **Jun-ichi TOYOOKA**[a], **Ryodai NAKAI**[a], **Shigeru KUBO**[a], **Kazuya KOYAMA**[b]

[a] Japan Atomic Energy Agency, 4-49 Muramatsu, Tokai-mura, Ibaraki, 319-1184 Japan

[b] Mitsubishi FBR Systems, Inc., 2-34-17 Jingu-mae, Shibuya-ku, Tokyo, 150-0001 Japan

Abstract. In the JSFR (Japan Sodium Cooled Fast Reactor), design measure to eliminate severe power burst events and keep the cooling of core materials by sodium in the Core Disruptive Accident (CDA) is applied to achieve the retention of core materials within the reactor vessel. The design strategy is to control the potential of excessive void reactivity insertion in the early phase of the CDA by selecting appropriate design parameters such as maximum void reactivity, while fuel sub-assembly with inner duct is introduced to exclude core-wide molten-fuel-pool formation, which has been the main issue of CDA. The multi-layered debris tray is also applied in JSFR to realize the stable and permanent cooling of core materials after the relocation of core materials to lower plenum of reactor vessel. The effectiveness of these design measures is evaluated based on existing experimental knowledge and computer simulation with validated analytical tools. It is judged that the present JSFR design can exclude severe power burst events. Phenomenological consideration on general characteristics and preliminary evaluations for the long-term material relocation and cooling phases gave a perspective that in-vessel retention would be attained with appropriate design measures.

1. Introduction

Since the core of FBR is not designed in its maximum reactivity configuration, coolant boiling and core-material relocation have potential of reactivity insertion. Based on this characteristic of FBR core, potential impact of Core Disruptive Accident (CDA) caused by Anticipated Transient Without Scram (ATWS) has been addressed as an important safety issue from the early stage of the FBR development, although it is extremely unlikely.

In this study, based on the design characteristics of the JSFR (Japan Sodium Cooled Fast Reactor)[1], ULOF (Unprotected Loss of Flow) was selected as the representative initiating event of CDA. The potential of recriticality, which accompanies severe power burst and mechanical energy release, in the ULOF accident becomes eminent in two stages of the accident sequence. The first stage is the early stage of the accident where the boiling of sodium coolant occurs and the positive void reactivity drives the accident progression. This stage is called "initiating phase", for which certain amount of knowledge has been accumulated so that its consequences can be controlled by selecting appropriate design parameters. The second stage is the subsequent stage, in which the reactivity change due to the possible fuel relocation within the degraded core plays dominant role after the fuel disruption and the failure of the wrapper-tube of fuel sub-assembly. This second stage is the present main concern to be addressed.

In the JSFR approach, design measures are taken to achieve In-Vessel Retention of the accident (IVR). In order to achieve the IVR, both the mechanical boundary failure due to power excursion and the thermal boundary failure due to incomplete stable cooling should be prevented by adequate design measures In this paper, appropriateness of the design measure

to avoid mechanical boundary failure due to power excursion is discussed with available experimental data and the current evaluation on the stable cooling phase is briefly mentioned.

2. The Representative Initiating Event of ATWS in JSFR

Based on the existing studies, ULOF, UTOP (Unprotected Transient Overpower) and ULOHS (Unprotected Loss of Heat Sink) are regarded as important initiating events of ATWS leading to CDA. However, there is a certain difference in transient time scales among these ATWS events depending on the cause of the imbalance between heat generation and heat removal. In ULOF, where the pump trip is the cause of the imbalance, flow coasts down with a halving time of several seconds and the core disintegration takes place as early as 10-20 seconds after the initiation of the accident. In UTOP, where CR (Control Rod) withdrawal is the main cause, the time scale is regulated by the CR driving system. It is noted that the CR-drive system of JSFR is designed so that reactivity increase rate will be less than 0.5 cent/s. This means that the typical time scale of UTOP to reach core disintegration is several minutes. In case of ULOHS, where reduction of heat transfer either in IHX or steam generator is the main cause, thermal inertia of the primary loop serves as a dumper for the imbalance. Therefore, the typical time scale to reach core disintegration in ULOHS is also not less than several minutes.
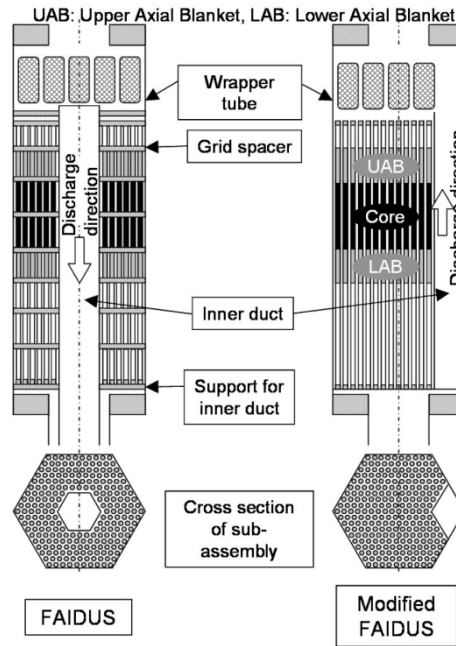

FIG. 1. JSFR fuel subassembly design options with the discharge duct.

In addition, JSFR adopts Self Actuated Shutdown System[2] (SASS) utilizing Curie-point magnet to sustain the backup control rods (primary control rods are sustained by the conventional latching mechanism). Although this SASS is designed to shutdown the reactor with certain margin for all of these ATWS events, its margin is dependent on the initiating events of the accident. The evaluated coolant temperature histories at the outlet of core for LOF, TOP and LOHS type ATWS events (SASS is functioning as protection means in these events) are presented in the literature[2]. The maximum coolant temperatures in TOP and LOHS-type ATWS events are much lower than the boiling point thus there are certain chances for these events to avoid CDA even well beyond the designed functioning condition of SASS. Considering the above characteristic of JSFR, probability of ULOF occurrence is much larger than that of UTOP and ULOHS. Furthermore, ULOF has certain potential of

neutronic power burst due to coherent and rapid core voiding caused by the flow coast down. Considering these factors, ULOF was selected as the representative ATWS category leading to CDA for JSFR.

3. JSFR Design Measures Related to CDA and Expected ULOF Scenario

Through the former studies, it had been known that the large molten-pool formation in the ULOF accident could cause severe recriticality events with coherent fuel motion. In order to eliminate this scenario, Inner Duct was adopted in the JSFR design as illustrated in FIG. 1.

With this innovative design, it is intended to realize early discharge of mobilized fuel from the core region and to prevent its coherent movement, which may cause severe recriticality by the insertion of reactivity, within the core. There are two possible options for the direction of discharge, upward and downward discharge. Upward discharge concept (modified FAIDUS) is adopted as the reference design in the present JSFR design since it has an advantage in limiting requirement for additional developmental efforts.

FIG. 2 illustrates the ULOF scenario aimed at by the JSFR design to achieve in-vessel retention of the ATWS. The first phase is "initiating phase" where core voiding takes place while material relocation is limited basically within each fuel sub-assembly. In the initiating phase, reactivity insertion due to core voiding drives accident progression. In JSFR, as is discussed later, appropriate design parameters are selected so that severe power burst in the initiating phase is avoided.
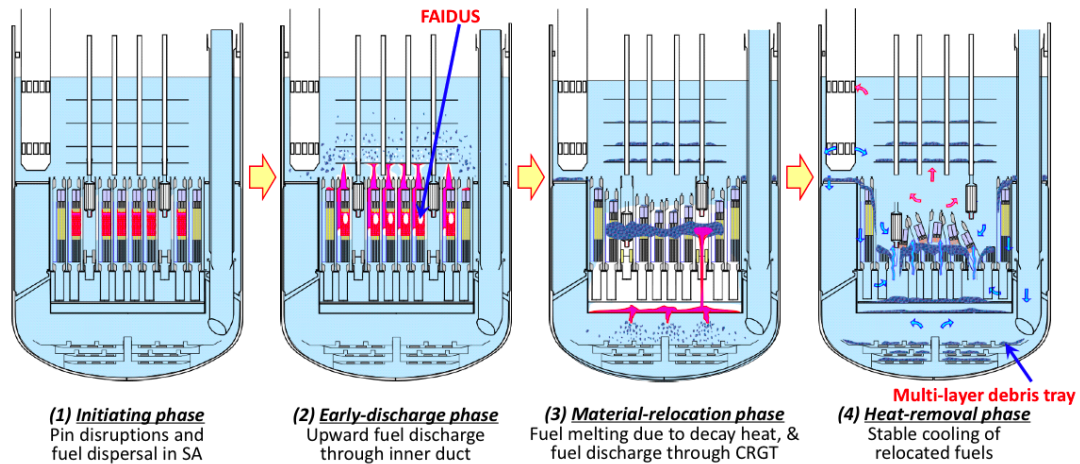

(1) Initiating phase
Pin disruptions and fuel dispersal in SA

(2) Early-discharge phase
Upward fuel discharge through inner duct

(3) Material-relocation phase
Fuel melting due to decay heat, & fuel discharge through CRGT

(4) Heat-removal phase
Stable cooling of relocated fuels

FIG. 2. Expected event progression of ULOF in JSFR.

In the mild progress of the initiating phase, the Inner Duct will fail by the high heat transfer to the surface of the duct from the molten core materials in fuel sub-assembly. Once duct fails, the molten core materials, which are pressurized by fission gas, will discharge through the duct as far as driving pressure is maintained. This phase is named "early fuel-discharge phase"[3]. After the discharge of mobile core materials from the core, only solid fuel will with low mobility remain in the core. The immobile fuel, in principle, does not cause rapid coherent fuel motion, which is a typical mechanism to drive severe recriticality. Thus, the potential of severe recriticality is eliminated by the early fuel discharge by FAIDUS.

Furthermore, during and after the power increase of the initiating phase and the upward discharge of molten core materials in the early fuel-discharge phase, hot coolant near boiling point and/or hotter materials such as disrupted core materials would reach the upper plenum of reactor vessel and heat the Curie-point magnet of SASS. In the light of the fact that the magnet loses completely its magnetic force at about 1100K, absorber elements would be surely released by this time point. Together with the negative reactivity brought by the early fuel discharge, this falling off of the absorber elements

would provide a large negative reactivity, which ensures the sub-critical state in the following event progression phases afterward.

After this phase, a longer-term "material-relocation phase" starts. It is unlikely that the decay heat of all the fuel remaining in the core is cooled down within the original core region. As a result, the fuel remained in the core will start to melt with the decay heat at the locations of high power density during the steady-state operation. Such molten fuel is likely to pour down into the lower sodium plenum.

In JSFR design of the structures below the core and the lower plenum, it is intended to realize effective quenching of the molten core materials and wide spread debris distribution into the multi-layer core catcher. Provided that a wide spread debris distribution is established, the long-term heat transfer to the final heat sink by natural circulation is possible in this "in-vessel cooling phase".

4. Evaluations of event progression to achieve IVR

4.1. Initiating Phase

The outline of the ULOF Initiating Phase scenario and several important elements involved are illustrated in FIG. 3. The main contributor of positive reactivity feedback is coolant void reactivity. On the other hand, fuel Doppler, fuel axial expansion and axial dispersion of disrupted fuel driven by fission gas would provide negative reactivities. Through the CABRI[4][5] and TREAT[6] experimental programs, an effective experimental database has been established for this phase. Based on this database, SAS4A code[7], which has mechanistic models corresponding to each of the important elements, has been effectively validated. With this established reliable evaluation method, the relationship between the core-design characteristics and severity of the ULOF initiating phase had been studied in the early phase of JSFR design. Through this early study, core-design parameters were selected for JSFR so that energetics in the initiating phase can be prevented[3].
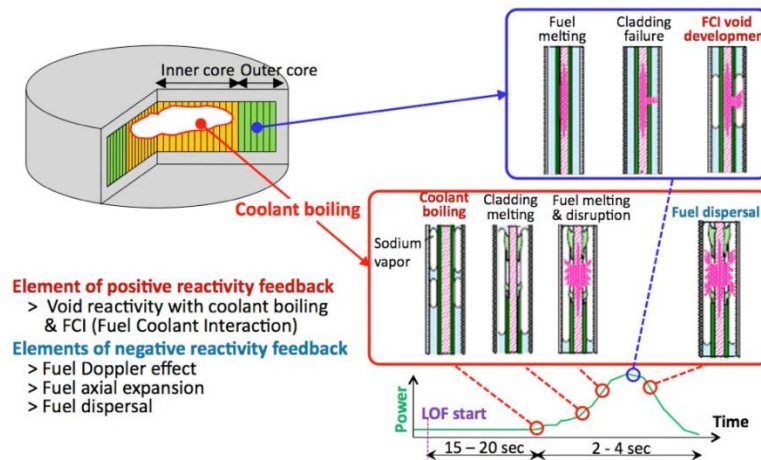

FIG. 3. Important phenomena in ULOF initiating phase

In the early stage of JSFR design, the competition process was evaluated with SAS4A and design parameters were selected so that energetic sequences could be avoided. Based on this preliminary evaluation, the core height of 1.0m was selected and maximum void reactivity was controlled below ~6$. Limiting the core height not larger than 1.0m contributed to keep the negative reactivity insertion by fuel dispersal at a certain level providing an effective fuel dispersal reactivity change. The fuel smear density of 82%TD (Theoretical Density) was selected from the viewpoint of fuel performance and it provided a high energy deposition threshold to fuel pin failure in single phase coolant, thus increasing the negative reactivity insertion by fuel dispersal before the insertion of positive void reactivity by FCI void development after the pin failure. The appropriateness of this strategy has been confirmed through the recent SAS4A code analysis[8] with consideration for uncertainty effects. An example of reactivity transient obtained by the parametric analyses is shown in FIG. 4. The

suppression of void worth less than about 6 $ as the design measure was obtained from these parametric analyses. In the parametric calculation with the maximum void worth above 6.5$, a power excursion before the significant fuel dispersal would take place.

4.2. *Early fuel-discharge phase*

In the former safety evaluation of ULOF accident, the propagation and connection of sub-assembly scale disruption region to form the whole-core molten-fuel pool after the initiating phase was assumed. The severe recriticality driven by coherent fuel motion within the pool was the main issue to be addressed. This has been the main concern of FBR as the "re-criticality issue". In the JSFR design, Inner Duct is adopted to eliminate possibility of this core-wide molten-fuel-pool formation itself. In order to demonstrate effectiveness of this design option in terms of excluding severe power burst, following three points must be confirmed.

(1)   Inner Duct in each fuel subassembly must fail before its wrapper tube fails.
(2)   Driving force for early fuel discharge must be available.
(3)   FCI and/or freezing during the discharge process must not hinder the discharge.

The first point (1) was confirmed by the EAGLE project[9][10] that the inner-duct failure would precede SA-can-wall failure, and the second point (2) was confirmed by CABRI[11] and TREAT[12][13] experiments that a sufficient driving force for upward discharge would be obtained. The third point (3) was also confirmed by EAGLE project[9][10], which showed smooth fuel discharge through the inner duct structure without plug formation. The excess pressure of the molten-fuel region was intentionally kept low (less than 0.12MPa) in this test. Even with this low pressure difference, the discharge was smooth. These test results support the scenario of no plug formation and smooth fuel discharge for JSFR
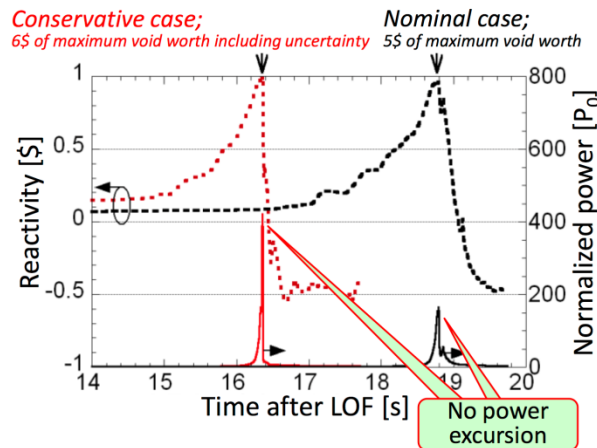

FIG. 4. Reactivity and power transients in the initiating phase evaluated by SAS4A code[8].

The evaluation of event progression by SIMMER-III code[14][15] based on the available knowledge for the early fuel discharge phase of JSFR was performed. The core region is represented by 5 groups of subassemblies for different power levels. Calculated history of fuel discharge amount in each region is plotted in FIG. 5. A smooth fuel discharge driven by sufficient fission gas pressure is predicted. The result shows ca. 20% of fuel discharge. The effect of FAIDUS on the reactivity transient is displayed in FIG. 6. In the case without FAIDUS, the reactivity and power was kept and the molten-core pool retained re-criticality potential. In the case with FAIDUS, on the other hand, molten-fuel was discharged through the inner duct before the formation of a molten-core pool and significant reduction of reactivity and power was achieved. At the end of the early fuel discharge, the fuel remaining in the core region is entirely solid and it does not have mobility. Therefore, coherent

fuel motion such as sloshing, which may result in a severe recriticality, cannot take place with this situation.

4.3. Core-material relocation phase

In the material-relocation phase, IVR failure is dominated by both mechanical and thermal boundary failures. The main factor of mechanical boundary failure is the power excursion due to re-criticality caused by core-remnant motion, where the mobility of fuel remaining in the core region would be significantly low in the early stage but would gradually increase due to the fuel melting by decay power in the late stage. The design measure to avoid the power excursion is the enhancement of molten-fuel discharge through control rod guide tubes (CRGTs). The main factor of thermal boundary failure, on the other hand, is the excess heating of the reactor vessel (RV) caused by the direct contact of discharged molten materials with RV. The design measure to avoid the excess heating of RV is the design optimization of the inlet/lower plenums with the aim of quenching discharged molten materials.
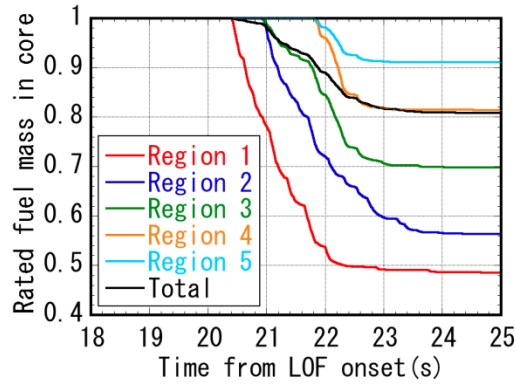

FIG. 5. Transients of fuel discharge behavior calculated by SIMMER-III code
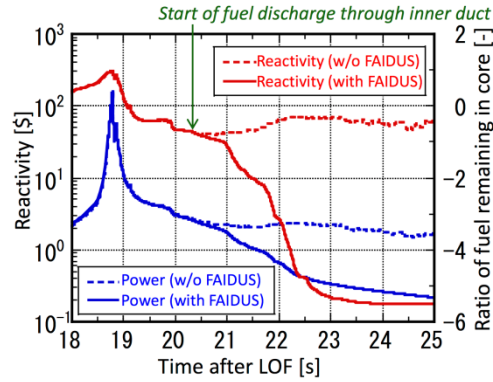

FIG. 6. Reactivity transient in the early-discharge phase evaluated by SIMMER-III code[8].

In the present study, the condition presented in Table 1 is adopted as the initial condition for the core-material relocation phase. As the reference condition, CRs (Control Rods) of the primary shutdown system which are held by the conventional latching mechanism are assumed to be held at the position before the accident, while CRs of the backup system held by the Curie-point magnet are assumed to have fallen down since no magnetic force to hold CRs is available at this time point.

Table 1.   Initial condition adopted in this study for the material relocation phase

Item	Adopted condition	Origin of the assumption
Amount of fuel discharged from the core region	20% of the initial fuel inventory	SIMMER-III evaluation
Status of primary control rods	Hanging at the position before the transient	Control rods of the primary shutdown system are held with the latching mechanism
Status of backup control rods	Having fallen down into the core region	The temperature of control-rod holding points is expected to exceed 1100K at which electromagnetic force becomes almost zero
Integrity of the CRGT (Control Rod Guide Tube)	Intact and liquid sodium is filling the internal space	Due to the early fuel discharge through Inner Duct, heat transfer from remaining solid fuel is limited (supposed by SIMMER-III evaluation)

After the early fuel discharge phase, certain amount of solid fuel remains in the core producing decay power. Based on a preliminary evaluation, remaining fuel in the core region is expected to start to melt by the decay heat at a few minutes after the early fuel-discharge. By this time, structures like cladding and can wall have already molten and molten fuel/steel mixture will be formed. Since the heat transfer from the molten-fuel/steel mixture to the surrounding structure is significant as shown in the EAGLE tests, this high temperature mixture has certain potential to move toward outside of the core region. The most likely path for such motion in the present scenario is the CRGT (Control Rod Guide Tube) space of the primary shutdown system. Although CRGTs of the backup shutdown system are expected to fail earlier than that of the primary system, presence of CR assembly inside the space and high thermal inertia of the structure at the bottom is likely to prevent creation of a path for downward movement. While for the CRGT of the primary shutdown system, thermal inertia of the structure at the bottom is intentionally kept small by design. Therefore, absence of CR assembly inside the CRGTs of the primary shutdown system and the small thermal inertia of the bottom structure is likely to allow a path for the hot mixture to move downward into the inlet sodium plenum. In the JSFR design, the core-inlet sodium plenum has holes at its bottom, which allow continuous transfer of molten core materials flowing from the core region down to the lower sodium plenum. Thus, hot core materials drained from the core region can be mixed with a large amount of liquid sodium, which is effective for quenching (rapid solidification). It is known that molten fuel is fragmented during quenching in liquid sodium.

The reactivity transient in this material-relocation phase was evaluated by a series of static neutronics calculations[16], taking into account the expected phenomena and design measures against the power excursion. As shown in FIG. 7, the significant reactivity insertion would be avoided by the enhancement of fuel discharge through primary CRGTs, and the sub-critical state would be ensured during the material–relocation phase including the uncertainty of phenomenological events such as the fuel compaction, diffusion of B/Fe (Borron/Steel) eutectic generated by backup-CRGT failure, and the amount of remaining core materials after the fuel discharge through primary CRGTs.

4.4. *In-vessel cooling phases*

The amount of draining core materials is important since higher amount of molten materials gives more loading for the core catcher. Considering the fact that the molten fuel/steel mixture has significant heat transfer capability, accumulating large amount of molten fuel without creating a

moving path is quite unlikely. In other words, creation of draining paths is likely in the early stage of fuel melting process. This aspect will serve as an important mechanism to limit the amount of fuel draining into the lower plenum for each draining event. Quenching characteristics of drained core materials are further being studied with experiments in the future so that effectiveness of the JSFR design will be confirmed.
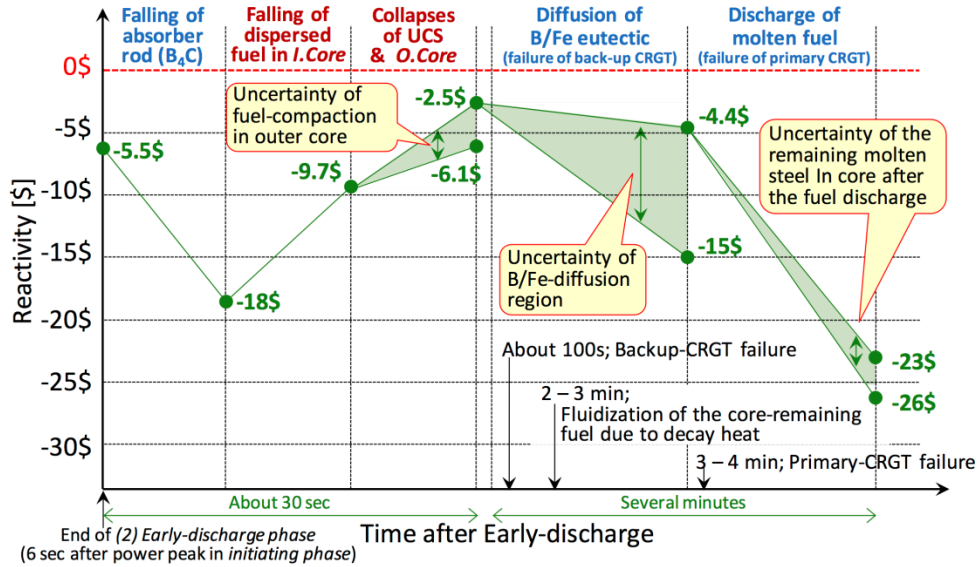

FIG. 7. Reactivity transient in the material-relocation phase evaluated by static neutronics calculation.

After the quenching, the sedimentation process of the fuel debris within the lower plenum would allow spreading of the debris on the multi-layer debris tray as shown in FIG. 8. The upper layer of the core catcher has some openings where the falling debris can go directly into the next layer of the core catcher. After the settle down of the sedimentation process, accumulated debris in each layer would have variation in the local debris depth. If the local depth is high enough sodium boiling will take place. However, the boiling process drives the debris in the upper part to the surrounding regions without boiling. Thus debris depth can be automatically be regulated down the boiling limit. This mechanism was identified in some tests[17][18] and was called "self leveling". In the JSFR design, taking the advantage of this mechanism, it is intended to transfer excess debris on the first layer down to the lower layer(s) so that a final distribution effective for cooled down can be obtained. In order to facilitate this layer-to-layer debris transfer, "debris guide tubes" are adopted. This structure consists of a hole surrounded by a vertical collar and allows pouring off of the excess debris above this collar. With the debris dispersion during the sedimentation process and the self-leveling mechanism after the accumulation on the debris trays, an effective settle down of the fuel debris into the multi-layered core catcher is aimed at. Precise design of this multi-layer core catcher so that effective debris settle down can be maintained is underway. Effectiveness of this design will be confirmed with future experiments and a validated evaluation method.
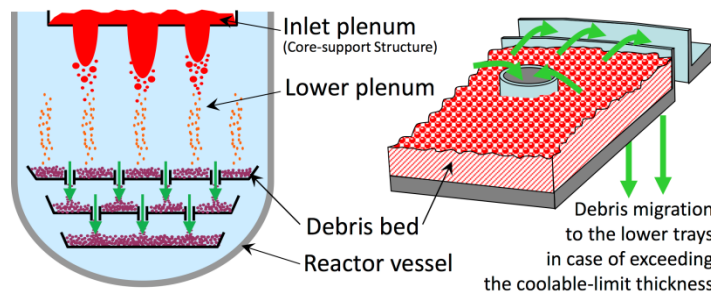

FIG. 8. Concept of multi-layer debris tray.

Permanent coolability of well-settled fuel debris was confirmed with a flow network code analysis[19]. FIG. 9 shows calculated results of coolant temperature at different positions. In this analysis, it was assumed that 100% fuel inventory relocated into the multi-layer core catcher as the bounding condition of the fuel melting and relocation scenario. The analysis showed that the decay heat from the 100% fuel inventory would be transported successfully to the heat sink by natural circulation.
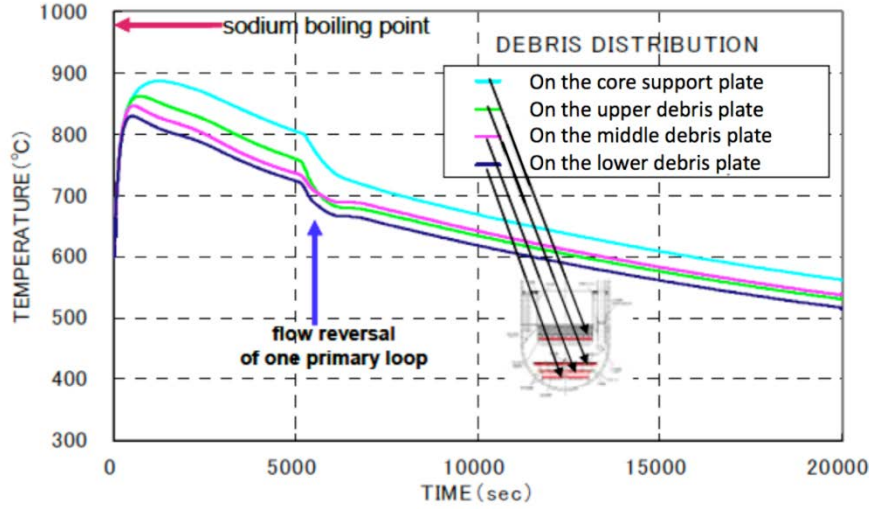

FIG. 9. Evaluated time history of the maximum coolant temperature in the debris bed.

5. Conclusion

The CDA scenario was evaluated against the ULOF for JSFR with full reflection of existing knowledge. With the present study, a perspective to eliminate severe power burst events and retain core materials in reactor vessel was obtained for these phases. Especially, it was shown that the risk of core-wide molten-fuel-pool formation would be clearly avoided with introduction of Inner Duct. This means that we found a solution for the "recriticality issue" of FBR. This conclusion is based mainly on the existing knowledge from the in-pile tests performed in CABRI and the fuel discharge tests performed in EAGLE project.

Once molten mobile fuel has been discharged from the core, the remaining fuel has no more sufficient mobility to cause rapid reactivity insertion with coherent fuel motion. Furthermore, reduction of fuel inventory and partial fall down of the control rod assembly into the intact CRGT would keep the subcriticality in the reference condition. Although uncertainty of this scenario should be investigated further considering the possible variation of the boundary conditions, a typical scenario for the later part of the transient until permanent cooling representing the JSFR design characteristics has been outlined.

REFERENCES

[1] M. Hishida, S. Kubo, M. Konomura, M. Toda, "Progress on the plant design concept of sodium-cooled fast reactor," *J. Nucl. Sci. and Tech.*, **4**[3], pp.303-308 (2007).

[2]   S. Nakanishi, et al., "Development of passive shutdown system for SFR," *Nuclear Technology,*, **170,** pp.181-188 (2010)

[3]   I. Sato, et al., "Safety Strategy of JSFR Eliminating Severe Recriticality Events and Establishing In-Vessel Retention in the Core Disruptive Accident," Journal of NUCLEAR SCIENCE and TECHNOLOGY, Vol. 48, No. 4, p. 556–566 (2011)

[4]   G. Kussmaul, et al., "The CABRI Project - Overall status and achievements," *Proc. of Science and Technology of Fast Reactor Safety*, Guernsey, Vol.I, p.103(1986).

[5]   M. Haessler, et al., "The CABRI-2 Programme - Overview on results," *Proc. of Int. Fast Reactor Safety Meeting,* Snowbird, Vol.II, p.209 (1990).

[6]   A.E. Wright, et al., "Fast reactor safety testing in TREAT in the 1980s," *Proc. of Int. Fast Reactor Safety Meeting,* Snowbird, Vol.II, p.233(1990).

[7]   A. M. Tentner, et al., "The SAS4A LMFBR whole core accident analysis code," *Proc. International Meeting on Fast Reactor Safety*, pp. 989-998, Knoxville, TN (1985).

[8]   I. Sato, et al., "Development of severe accident evaluation technology (Level 2 PSA) for sodium-cooled fast reactors – (2) Identification of dominant factors in initiating phase of unprotected events," *Proc. of 2009 International Congress on Advances in Nuclear Power Plants (ICAPP '09)*, Tokyo, Paper 9132 (2009).

[9]   Konishi, K., *et al.*, (2006). "The EAGLE Project to eliminate the Recriticality Issue of Fast Reactors –Progress and Results of In-Pile Tests," *Proc. NTHAS5*, F001, Jeju, Korea, November 26-29.

[10]   Konishi, K., et al., (2007). "The Results of a Wall Failure In-Pile Experiment under the EAGLE Project," Nuclear Engineering and Design, 237, pp. 2165-2174.

[11]   Nonaka, N., et al., (1992). "Improvement of Evaluation Method for Initiating-Phase Energetics Based on CABRI-1 In-Pile Experiments," Nucl. Tech., 98, pp. 54-69.

[12]   Rothman, A. B., *et al.*, (1979). "TREAT Experiments with Irradiated Fuel Simulating Hypothetical Loss-of-Flow Accidents in Large LMFBRs," *Proc. Int. Mtg. Fast Reactor Safety Technology*, p.924, Seattle, USA, August 19-23.

[13]   Bauer, T. H., et al., (1986). "Post-Failure Material Movement in the PFR/TREAT Experiments," Proc. Int. Mtg. on Fast Reactor Safety and Related Physics, p.1647, Guernsey, UK, May 12-16.

[14]   Kondo, Sa., *et al.*, (1992). "SIMMER-III: An Advanced Computer Program for LMFBR Severe Accident Analysis," *Proc. ANP'92*, **IV**, p. 40.5-1, Tokyo, Japan, October 25-29.

[15]   Kondo, Sa., et al., (1992). "SIMMER-III: An Advanced Computer Program for LMFBR Severe Accident Analysis," Proc. ANP'92, IV, p. 40.5-1, Tokyo, Japan, October 25-29.

[16]   T. Suzuki, et al., "Evaluation of Core Disruptive Accident for Sodium-Cooled Fast Reactors to Achieve In-Vessel Retention," Proc. NTHAS 8, paper No. N8P1063, Beppu, Japan, December 9-12, 2012.

[17]   J. Gabor et al., "Studies and experiments on heat removal from fuel debris in sodium," Proc. ANS Fast Reactor Safety Meeting, Beverly Hills, p.823 (1974).

[18]   Bin Zhang, et al."Self-leveling onset criteria in debris beds," *J. Nucl. Science and Tech.*, **47** (4), pp.384-395 (2010).

[19]   K. Koyama, et al., "Development of severe accident evaluation technology (Level 2 PSA) for sodium-cooled fast reactors – (4) Identification of dominant factors in core material relocation and heat removal phases," *Proc. of 2009 International Congress on Advances in Nuclear Power Plants (ICAPP '09)*, Tokyo, Paper 9126 (2009).

Development of diverse methods for drop time measurement of PFBR shut down mechanisms

V. Prakash, B.K. Nashine, G. Padmakumar, R. Vijayashree, Prashant Sharma, Sudheer Patri, S. Chandramouli, K.K. Rajan

Indira Gandhi Centre for Atomic Research,
Kalpakkam, India

Abstract. *Prototype Fast Breeder Reactor (PFBR) is equipped with two shutdown systems namely, Control and Safety Rod Drive Mechanism (CSRDM) and Diverse Safety Rod Drive Mechanism (DSRDM). DSRDM is used for the safe shut down of the reactor. During a SCRAM, DSR is released from its electromagnet and falls into the reactor core under gravity. It is a safety requirement to measure the fall time of DSR during each SCRAM. As no sensor can be attached to the moving part of DSR, non-contact type measurement techniques namely acoustic and eddy current methods are envisaged for the measurement of DSR fall time in PFBR. Acoustic technique uses accelerometer mounted on upper part of DSRDM for the detection of acoustic events during the movement of DSR in the DSR subassembly. Measurements were carried out in various water/sodium facilities and an On-line measurement system for PFBR has been developed. The developed system was tested for its performance and results were compared with ultrasonic method to establish its measurement sensitivity. Eddy current position sensor uses the property of change in inductance due to the entry of DSR piston into the DSR dashpot region. DSR piston, which is made up of modified 9Cr-1Mo steel, replaces the liquid sodium in the dashpot, which results in a change in inductance in the sensor coil embedded in DSR subassembly sheath near the entry of dashpot. A sensor with two pick-up coils was successfully developed and tested in sodium at various temperatures for various test conditions. The developed eddy current system was installed in prototype DSRDM, tested for its performance and the results are compared with acoustic technique. This paper discusses the details of the developmental activities of both the techniques and their experimental verification using prototype DSRDM.*

1. INTRODUCTION

Prototype Fast Breeder Reactor (PFBR), which is under construction at Kalpakkam, is a 500 MWe, Sodium cooled pool type reactor. As a diverse safety mechanism, three Diverse Safety Rods (DSR) are provided in PFBR core for its safe shutdown during a SCRAM. DSR Drive Mechanisms are housed and supported at top of the control plug, which is situated right above the core. During a SCRAM, DSR will be released from the electromagnet and it will fall into their respective subassemblies. Fig. 1 shows the position of DSR subassemblies in the PFBR core. A sodium dash pot is provided inside the DSR subassembly for decelerating the DSR and to bring it into its rest position. Fig. 2 shows the DSR and its subassembly. The total fall height of the DSR is 1075 mm and the designed fall time of DSR is less than one second.

As a safety requirement, it is required to measure the total fall time of DSRs, to ensure their proper insertion into the core. As no sensor can be attached to the DSR, non-contact type measurement techniques namely acoustic and eddy current methods are envisaged for the measurement of DSR fall time in PFBR. Acoustic technique uses accelerometer mounted on upper part of DSRDM for the detection of acoustic events during the movement of DSR in the DSR subassembly. Eddy current position sensor uses the property of change in inductance due to the entry of DSR piston into the DSR dashpot region. DSR piston, which is made up of modified 9Cr-1Mo steel, replaces the liquid sodium in the dashpot, which results in a change in inductance of the sensor coil embedded in DSR

subassembly sheath near the entry of dashpot. This paper discusses the details of the techniques, instrumentation and the test results and conclusion.
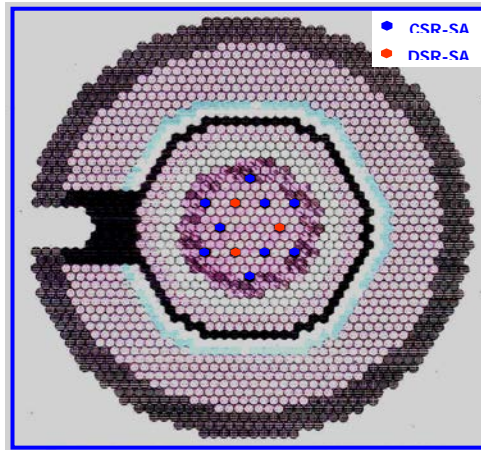

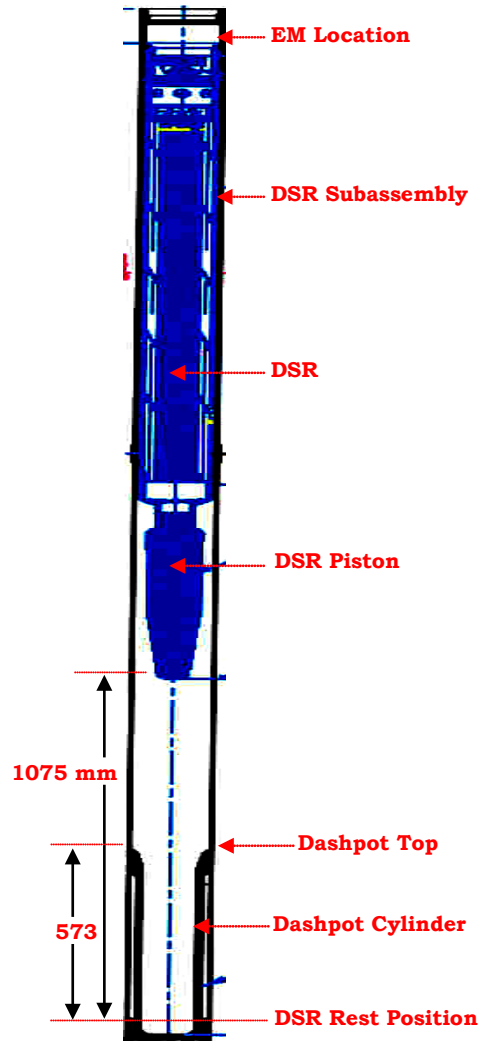*FIG. 1. DSR location in PFBR core.*

FIG. 2. DSR and its assembly.

2. ACOUSTIC TECHNIQUE

Acoustic technique is based on the detection of shock signals produced at the end of free fall and during deceleration of DSR in the dashpot [1]. Once the DSR is released from EM, at the end of free fall, DSR hits at the entry of the dashpot and will generate a shock signal. Similarly at the end of braking (deceleration) time another shock pulse is generated. By measuring the time delays between the step transition of electromagnet signal and the above shock signals, free fall and braking times can be estimated. Piezoelectric accelerometer is used as the primary sensing element for this technique.

The output of the accelerometer is amplified and fed to a digital high speed data acquisition system for analysis and measurement of free fall time. The free fall time is defined as time elapsed between the instant at which the EM holding the DSR gets de-energizes and the instant at which the dashpot action is initiated. At the end of free fall, deceleration of DSR will take place in the dashpot region. The time taken for completion of deceleration of DSR is called braking time. The summation of free fall time and braking time will give the total drop time of DSR.

2.1. *Development of acoustic technique*

Extensive experiments were carried out in different phases in various test facilities to develop and establish acoustic technology. The first phase of experiments started with preliminary studies to check the feasibility of acoustic technique for the detection of DSR drop time. The result indicated that the acoustic sensors gave very good response to the impact noises of DSR during its entry and its decceleration in dashpot. Followed by the feasibility studies, measurements were carried out in different test setups and signals were recorded and analyzed. During these measurements sampling frequency and other signal acquisition parameters were optimised to obtain a clear distinction between the impact signal and other background noises. Tests were carried out in sodium as well as in water. Measurements were also carried out to study the characteristics of the signal at the source by mounting sensors directly on the dashpot location.

Fig. 3 shows a typical time signal obtained during the DSR dropping with acoustic sensors mounted on top end of upper tube sheath (Fig. 4) of DSR Drive Mechanism (DSRDM). The free fall time was measured to be 552 ms and the total drop time of DSR was found to be 751 ms in sodium at 500^0C.
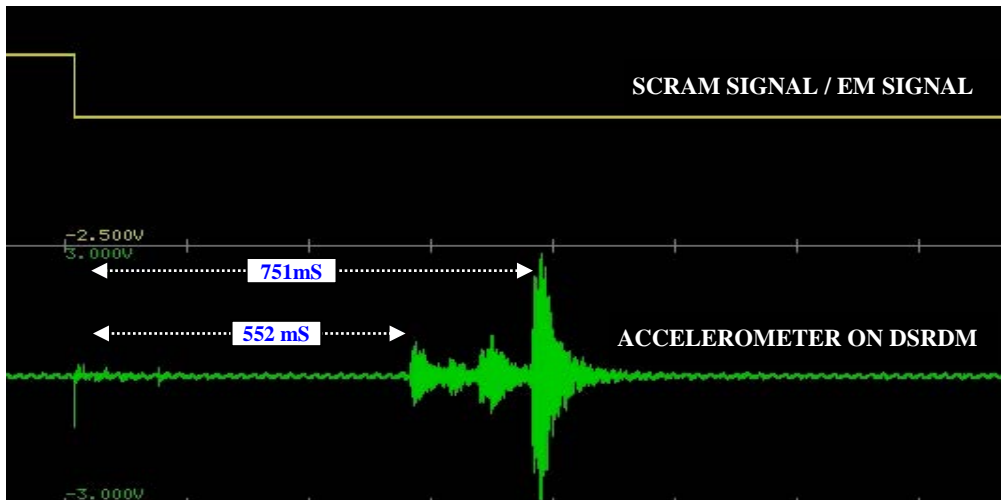

FIG. 3. Time signal for drop height 1075mm at 500^0C.

FIG. 4. Acoustic sensor location.

During the next phase of experiments, validation of acoustic technique was carried out using ultrasonic method in sodium at 200ºC [2]. Fig. 5 shows a typical time signal plot recorded during the test for a DSR drop height of 1075mm in sodium. The variation in total travel time between the acoustic and ultrasonic method was found to be less than 10 mS. Apart from this, measurements were carried out during the endurance testing of DSR and drop time of DSR was recorded during the entire testing. Measurements were also carried out in Fast Breeder Test Reactor (FBTR), which is under operation at Kalpakkam, to characterize the reactor background noise and the signal generated during the dropping of FBTR control rods.

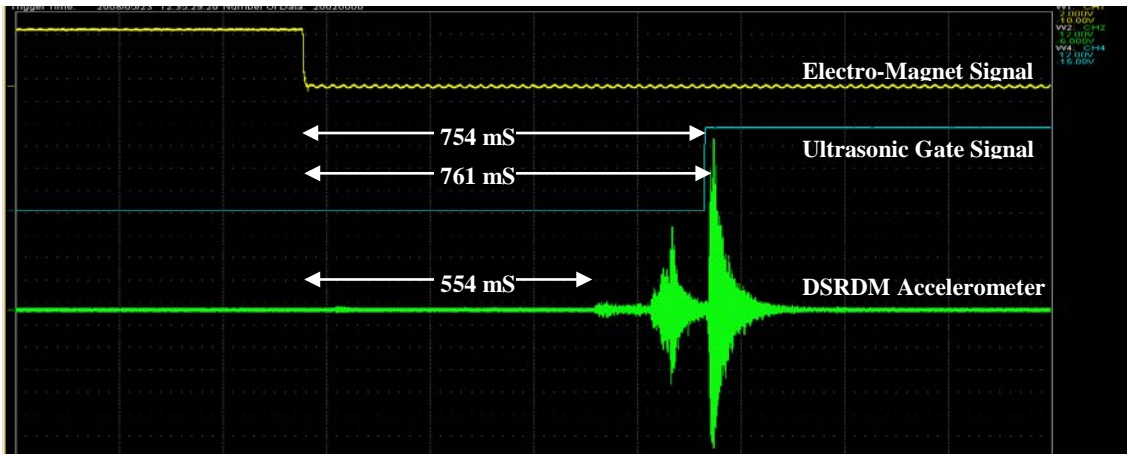*FIG. 5. Time signal during DSR dropping (1075mm).*

Based on the experimental results obtained during the measurements, the configuration of a dedicated system for on-line drop time measurement has been arrived at. This was fine tuned and finally a prototype system in LabVIEW platform was developed. Schematic of the system architecture is as shown in Fig. 6.
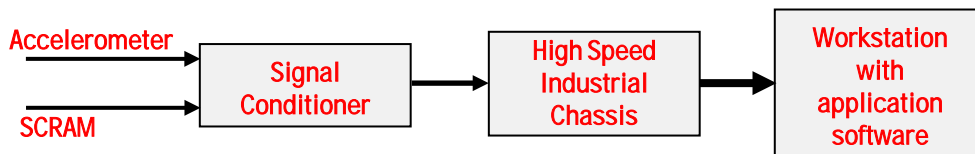

FIG. 6. Schematic of prototype system architecture.

The architecture of the system includes sensor inputs from the field, accelerometers on the top end of the upper tube sheath of DSRDM and Electro-magnet relay output signal indicating the initiation of SCRAM. Accelerometer and SCRAM signals are amplified using signal conditioners and the amplified signals are streamed to the work station PC using industrial high speed chassis.

Application software in LabVIEW running in the PC is used for the real time acquisition and analysis of the data. The digital input signal from the electromagnet acts as the trigger during any SCRAM event to start the signal logging and DSR drop time calculation. Once the SCRAM is activated the accelerometer signal as well as the SCRAM signal will be recorded and DSR drop time will be displayed on the screen and stored in the system memory.

The performance of the online system was checked during the endurance testing of PFBR DSRDMs. Accelerometers were mounted to the mechanism and signals are acquired using the system. The developed system was also tested in FBTR. Fig. 7 shows the signal recorded using the developed system in FBTR during the dropping of one of the control rods from a height of 400mm. The measured fall time using the prototype system was found to be 350ms.
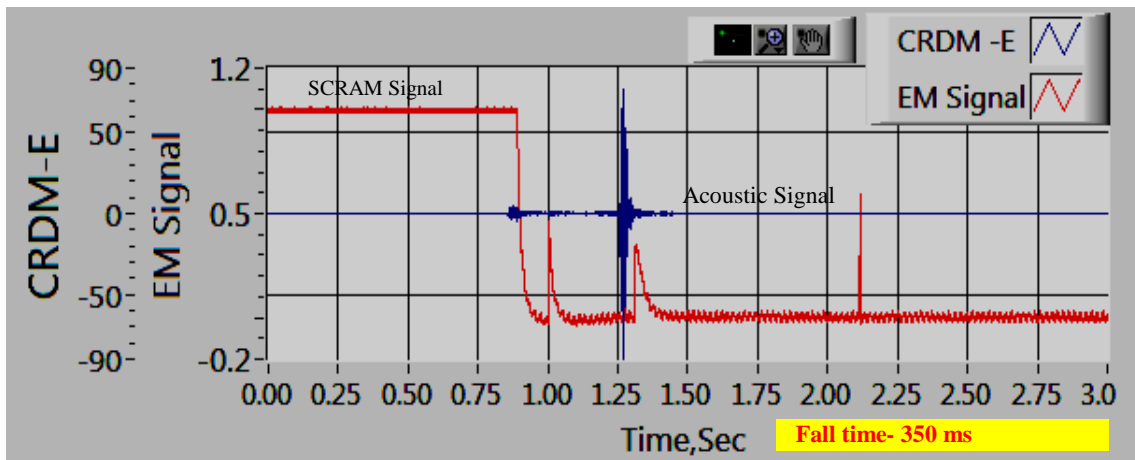

FIG. 7. Time signal (Control rod drop height 400 mm).

3. EDDY CURRENT TECHNIQUE

Eddy current position sensor (ECPS) is used in this technique for measurement of fall time of DSR. The ECPS [3,4,5] consists of primary coil, bottom and top pickup coils, secondary coil and sensor coil (Fig. 8). The schematic representation of these coils are shown in Fig. 9. The bottom and top pickup coils and primary coil are housed near the electromagnet assembly of DSRDM. The secondary coil is embedded in the DSR subassembly sheath concentric with the primary and the pickup coils (Fig. 8). Sensor coil is embedded in the DSR subassembly sheath near the entry of sodium dashpot. The secondary and sensor coils form a closed circuit. The DSR piston is made up of Modified 9Cr-1Mo steel, which is a ferromagnetic material.

The working principle of the ECPS is that, when the DSR piston enters the dashpot, it replaces the conducting and non-magnetic sodium with less conducting and ferromagnetic material. This change of material in the dashpot changes the inductance of the sensor coil. Axial misalignment of up to 45mm can take place between the primary and the secondary side coils due to thermal and radiation induced dimensional changes. Hence two pickup coils are provided to give a measurable output voltage under various misalignment conditions occuring during reactor operation.

All the coils of ECPS should be capable of continuous operation in sodium environment upto 600ºC as well as should withstand radiation exposure in the reactor core. The coils are made of mineral insulated (MI) high temperature cable. The number of turns and the dimensions of the coils were finalized based on FEM modelling of the coil configuration and the dimensional constraints of the system.
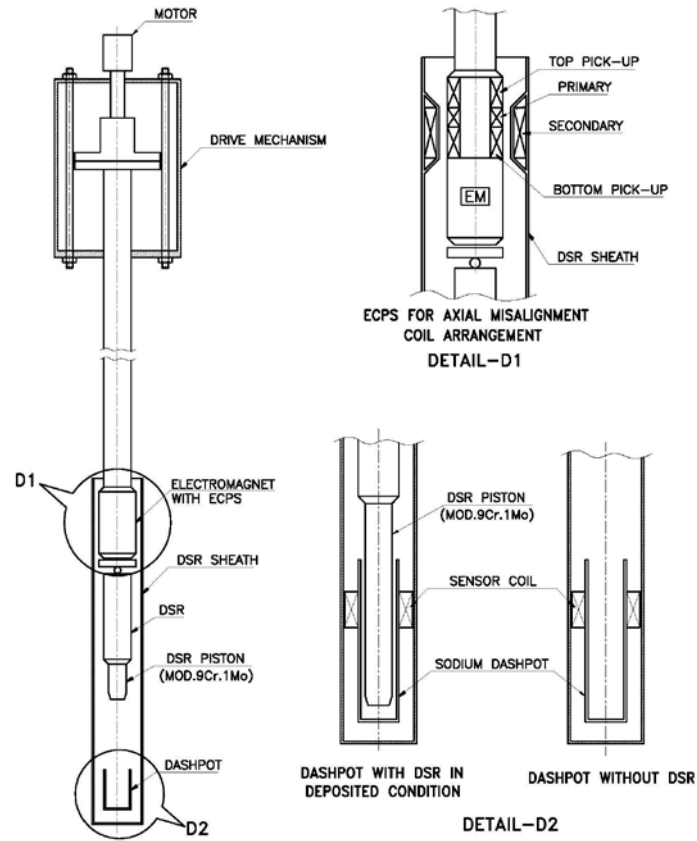
FIG. 8. Location of ECPS coils in mechanism.
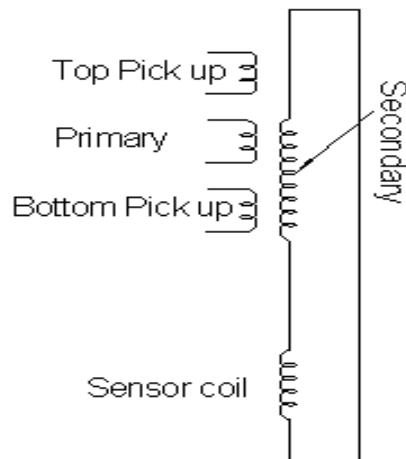
FIG. 9. Schematic of Eddy Current Position System.

The primary coil is excited by a constant current sinusoidal source. The flux generated from the primary winding crosses the gap (which is filled with non-magnetic stainless steel and sodium) and generates voltage in the secondary coil and thus a current flows in the secondary circuit. This current inturn produces a flux which links with pickup coils and induces sinusoidal voltages in them. When DSR falls in the dashpot, the inductance of the sensor coil increases which leads to a reduction in current of secondary coil and increase in flux linking with the pick-up coils, which will cause increase in voltage induced in pick up coils. By monitoring the output of the pickup coils entry of DSR into the

6

dashpot can be detected and drop time can be deduced from SCRAM signal and output of pickup coils.

The frequency of the primary current plays an important role in the working of ECPS because of skin effect in conducting sodium which affects the flux linking between various coils. As sodium temperature increases, the conductivity of sodium decreases and this also affects the flux linkages. Thus for getting higher change in output voltage of pick-up coils with insertion of DSR, optimum frequency selection is also very important.

3.1. Development of eddy current technique

In order to check the effectiveness of the selected configuration in high temperature sodium environment, a 1:1 model of ECPS was fabricated. In this model, the free fall of DSR was not simulated but the effect of insertion of DSR piston into the sodium dashpot was checked to ascertain feasibility of detecting the entry/position of piston in the dash pot. The sodium testing was carried out at temperatures upto 550ºC at aligned condition and also with axial misalignment (between primary and secondary coils) of 15mm, 30mm and 45mm. The performance of the sensor is evaluated in terms of sensitivity which is defined as,

$$\text{Sensitivity} = \frac{100 \times (\text{ Pick-up Voltage with DSR Piston - Pick-up Voltage without DSR Piston })}{\text{Pick-up Voltage without DSR Piston}}$$

The sensitivity of bottom pick-up coil is shown in Fig. 10 and the sensitivity of top pick-up is shown in Fig. 11. It can be observed from the experimental results (Fig. 10 & 11) that the sensor is able to provide a minimum sensitivity of 4-5% for various conditions of axial misalignments.
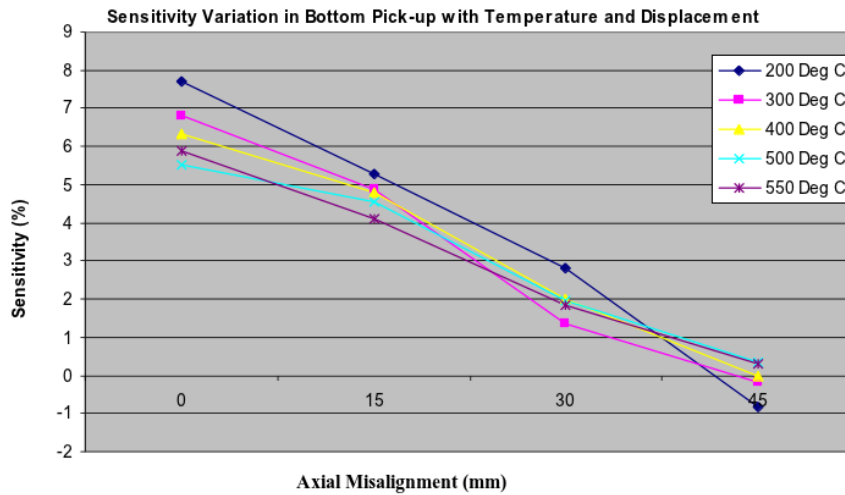

FIG. 10. Experimentally obtained sensitivity of Bottom Pick-up in sodium.

In order to test ECPS along with the DSR Drive Mechanism (DSRDM), it was integrated with DSRDM and tested in Air/Water with an axial misalignment up to 50mm. The axial misalignment was created by placing the electromagnet at different positions with respect to the DSR sheath.
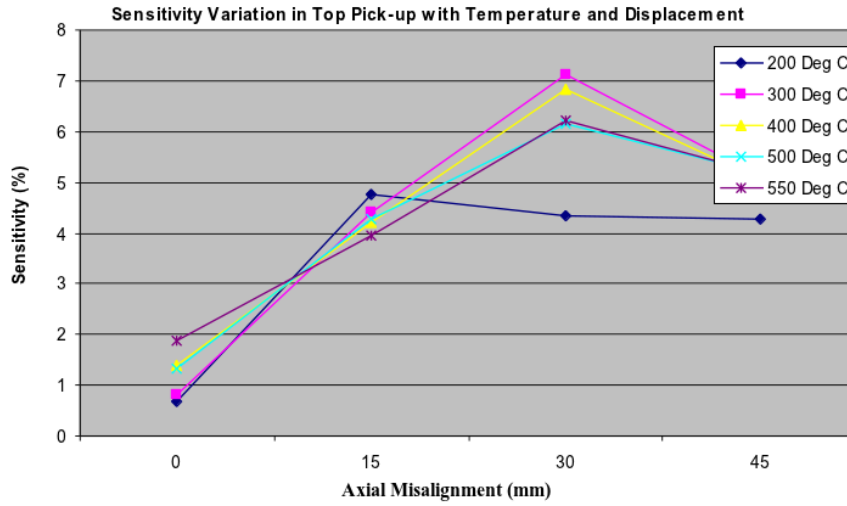
FIG. 11. Experimentally obtained sensitivity of Top Pick-up in sodium.

ECPS primary winding was energised at a constant current of 200mA at 200Hz and voltages of both the pick-ups were recorded for DSR deposited and not deposited conditions. From the plot of the pick-up voltages, the free fall time of DSR was calculated. The typical variation of pick-up voltage with insertion of DSR in the dashpot is shown in Fig. 12a. From the envelope the free fall time (i.e. the time the DSR takes to reach the sensor coil location after the SCRAM command) is measured (Fig. 12b). During testing, acoustic sensors were also used for measurement of drop time. The combined curves for both the ECPS and acoustic signal for DSR drop height of 940mm are shown in Fig. 13. It can be observed that both the sensors yield almost identical values of DSR free fall time.
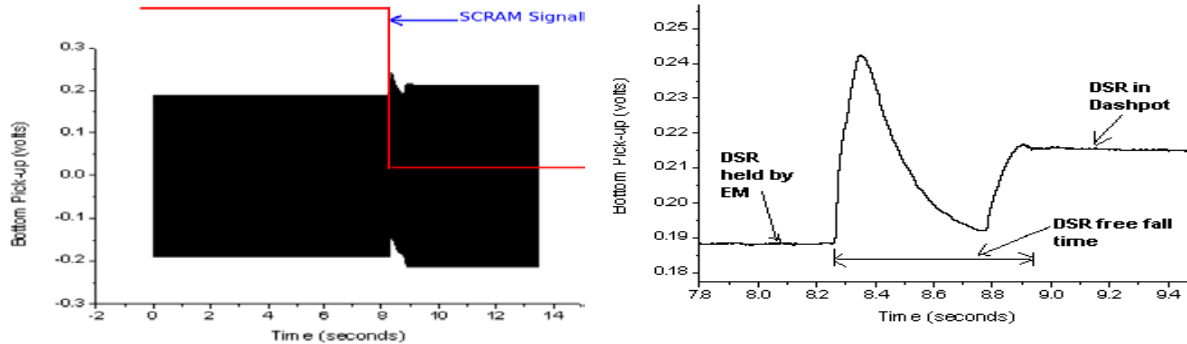
FIG. 12. a) Variation of pick-up voltage.   *12. b) Free fall time measurement.*

4. CONCLUSION

Two diverse methods, acoustic and eddy current method for drop time measurement of PFBR Diverse Safety Rods were developed in IGCAR. Acoustic technique uses accelerometer mounted on upper part of DSRDM for the detection of acoustic events during the movement of DSR in the DSR subassembly. Measurements were carried out in various water/sodium facilities and an on-line measurement system for PFBR was developed. The developed system was tested for its performance. Eddy current position sensor uses the property of change in inductance due to the entry of DSR piston into the DSR dashpot. DSR piston, which is made up of modified 9Cr-1Mo steel, replaces the liquid sodium in the dashpot, which results in a change in inductance in the sensor coil embedded in the dashpot. ECPS was designed to meet various dimensional and functional constraints. The developed

system was installed in prototype DSRDM, tested for its performance and the test results are comparable with acoustic technique.
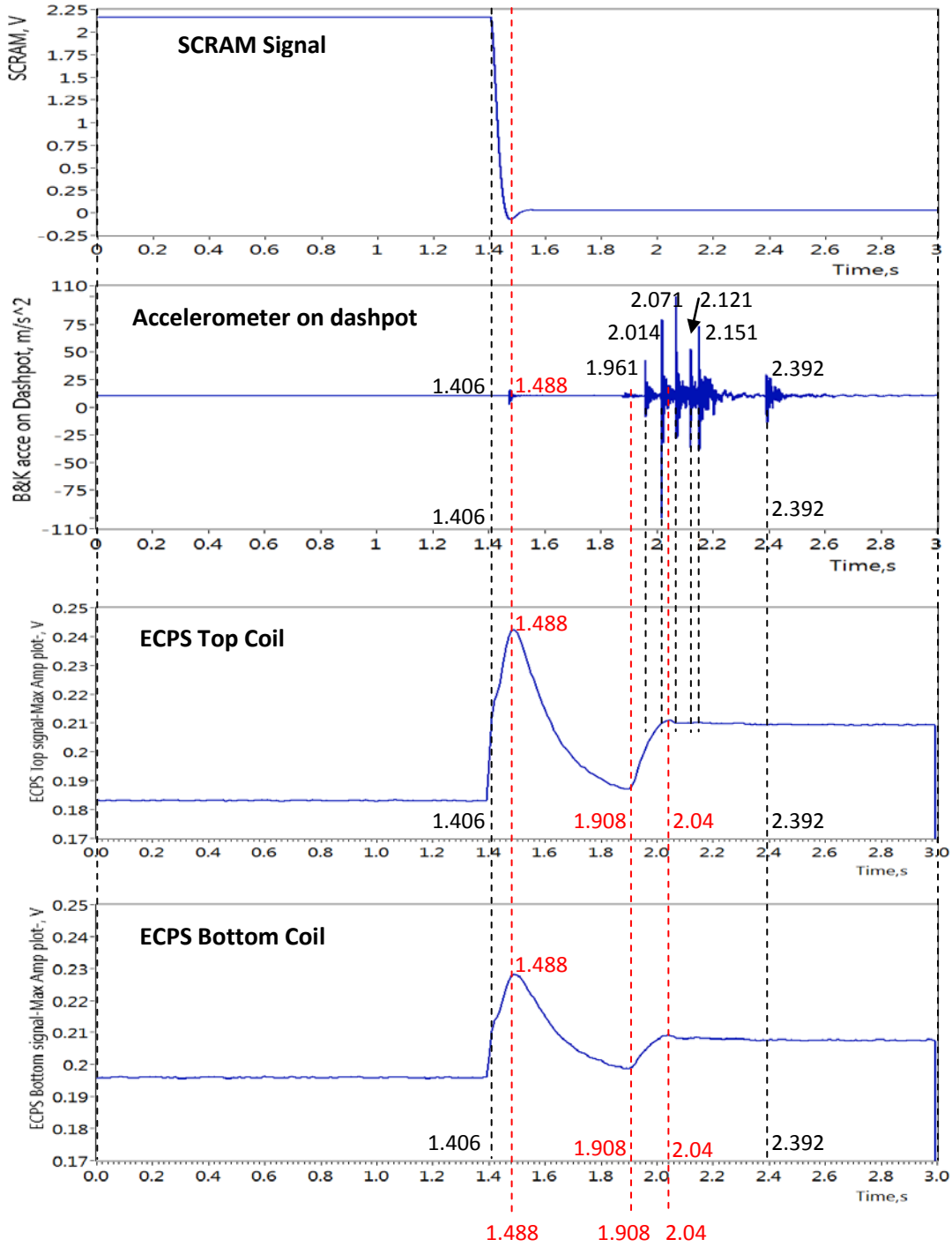
FIG. 13. Comparison of acoustic technique and ECPS technique.

5. ACKNOWLEDGEMENTS

6. REFERENCES

[1] PRAKASH, V., et al., Application of Acoustic Technique for Surveillance and Anomaly Detection in LMFBRs, INTERNATIONAL CONFERENCE ON NUCLEAR ENGINEERING- ICONE 16, Paper No: 48252, Orlando, Florida, USA (2008).

[2] ASOKANE, C., et al., Validation of Acoustic Technique using Ultrasonic Technique for PFBR Safety Rod Drop Time Measurement, NATIONAL SEMINAR ON NON-DESTRUCTIVE EVALUATION- NDE-2008, Lonavala, India (2008).

[3] BABU RAO, C., et al., Eddy current position sensing system for diverse safety rod of PFBR, FIRST INTERNATIONAL CONFERENCE ON ADVANCEMENTS IN NUCLEAR INSTRUMENTATION, MEASUREMENT METHODS AND THEIR APPLICATIONS- ANIMMA, FRANCE (2009).

[4] VIJAYASHREE, R., et al., Development of engineering model for eddy current position sensing of diverse safety rod of FBR, ANIMMA INTERNATIONAL CONFERENCE, GHENT, BELGIUM (2011).

[5] PRASHANT SHARMA., et al., Sensor development for position detection of diverse safety rod of fast reactor, JOURNAL OF ANNALS OF NUCLEAR ENERGY, vol. 46, pp. 189-196 (2012).

Experimental and Numerical Simulation of Sodium Safety in SFR

D. Ponraju, Hemanth Rao, Sanjay Kumar Das, G Punitha , B.K. Nashine, P. Chellapandi

Reactor Design Group, Indira Gandhi Center for Atomic Research, Kalpakkam, India

Abstract. Basic research and engineering studies are carried out to understand the safety aspects of sodium fire. Many innovative experimental facilities such as MINA (Mini Sodium fire facility), SOCA (SOdium-CAble fire facility) and SFEF (Sodium Fire Experimental Facility) have been developed to study small, medium and large scale sodium fires. Experiments on sodium spray fire through single nozzle and multiple nozzles simulating the condition of sodium ejection into the reactor containment building through annular gaps of top shield platform during Core Disruptive Accident (CDA) and testing of integrity of components like DHX piping and measurement of temperature and pressure rise in reactor containment building during combined sodium fire and cable fire were conducted. Containment code was developed by integrating the results obtained from modeling of single droplet burning and its energy release. Sodium spray fire scenario during sodium leak in steam generator building was studied. Studies on qualification of indigenously developed carbon microsphere based sodium fire extinguisher, mitigation of sodium fire by injection of nitrogen gas and qualification of full scale Leak Collection Tray system (LCT), performance evaluation of wet scrubber system for removal of sodium fire aerosol were carried out. Apart from this, studies on plugging and unplugging characteristics of small sodium leak in terms of temperature and pressure were carried out. This paper describes the salient features of experimental facilities, benchmark experiments and results towards SFR safety.

1. Introduction

Liquid sodium is used as coolant in Proto type Fast Breeder Reactor (PFBR) and will be continued to be used as coolant for future Fast Reactors in India. However, due to its high chemical reactivity, some outstanding safety issues are to be addressed. In case of sodium leak, sodium undergoes spontaneous combustion with oxygen in air due to its high chemical reactivity [1-3]. The aerosols produced in the sodium fire cause a potential hazard to the plant and operating personal thereby making it difficult to access the event spot for "fire fighting" [4]. Sodium leak and the resultant sodium fire is an important safety issue with reference to the structural integrity of Reactor Components and Reactor Containment Building (RCB). Sodium ejected under postulated core disruptive accident reacts readily with oxygen and the resultant sodium fire can cause secondary fire from the large number of electrical and instrumentation cables laid in top shield platform. It is essential to study the effect of combined sodium-cable fire on (i) integrity of important components like DHX piping, (ii) damage to the cable insulation resulting in loss of power and control supply to the equipments and (iii) temperature and pressure rise in RCB.

Leakage of sodium cannot be completely ruled out despite of leak proof design and adequate safety measures like quick sensing and mitigation. Though Dry Chemical Powder (DCP) is being used as sodium fire extinguisher, the quantity required is very high and it will be very difficult to remove and dispose after applying over burning sodium. Hence, there is a need for development of a novel sodium fire extinguisher without such drawbacks. Flooding of nitrogen in case of sodium spray fire is considered as active method for sodium fire mitigation. For handling large scale sodium fire a passive leak collection tray (LCT) system is used in FBRs. It is mandatory to qualify them for large sodium leak. Performance evaluation of the total system involves melting of fusible plug system and subsequent draining of sodium into dump tank.

Interaction of leaked sodium and its fire with concrete results in severe cracking and dehydration of concrete [5] with production of hydrogen as well as other gases. It is important to study the thermo-hygro-chemo-mechanical phenomenon on degradation of mechanical strength of concrete [6].

Understanding and development of suitable codes for understanding the sodium fire scenarios and estimation of pressure buildup in RCB would give important feedback for future designs. Though sodium spray fire scenario was modeled by several researchers and codes such as CONTAIN code, SOFIRE II code, NACOM code and NAFCON code [7-11] are available, experimental data are to be generated for validating these codes.

Thus in depth understanding of all the sodium fire associated phenomena is inevitable for the safe design and operation of a sodium cooled Fast Breeder Reactors. This paper describes our strategy on experimental and numerical simulation studies on sodium safety. Sodium safety issues such as fundamental understanding of sodium fire scenario, sodium aerosol generation and their removal, mitigation of sodium fire by nitrogen injection, qualification of leak collection tray system, development of sodium fire extinguisher and development and validation of containment code are addressed. Facilities constructed for the above studies along with their salient features, instrumentation and availability for future studies are described in this paper. Both experimental and numerical simulation studies on sodium safety and the benchmark results obtained in various safety experiments are discussed in this paper.

2. Fundamental studies on Sodium Spray Fires

Small scale sodium spray fire studies were carried out in MINA facilities (fig.1 &2). It is a very unique facility designed and constructed for understanding spray fire scenario, evaluation of sodium burning rates and validation of containment code developed for determining pressure buildup and temperature rise in containment building under Core Disruptive Accident (CDA). Fundamental experiments on small and medium scale sodium spray fire with sodium inventories few grams (2-5 g) to few Kg (2-5 Kg) have been carried out in this facility with main objectives of studying sodium droplet size distribution, aerosol characterization, modeling of spray fire combustion mechanism and generating scientific data.

Fig.1 MINA (1) Facility   Fig.2 MINA (2) Facility

MINA (2) Sodium Fire Facility has an experimental hall of 139 m^3 volume (5.6 m $\times$ 5.4 m $\times$ 4.6 m) and its design pressure is 4 bar at 500°C. The inner surface of the experimental hall is lined with 1.6 mm thick SS 304L sheets and provided with a leak tight door of 2.0 m $\times$ 1.5 m, sodium loop with necessary tanks, valves, heaters, argon cover gas system and sophisticated instrumentation.

Small scale sodium spray fire scenario studied in MINA (1) facility is shown in fig. 3. The particle size of sodium droplets ejected through a nozzle of 1.6 mm was measured using laser scattering technique and shown in fig. 4. The variation in flame diameter of burning droplets (fig. 5) with time was measured by using high speed camera. The life time of single burning droplet was measured by processing the image captured during combustion (fig. 6). About 80% of sodium was observed to be burnt during the spray fire. Sodium combustion aerosol was characterized using lazer scattering technique and their size distribution is shown in fig. 7.
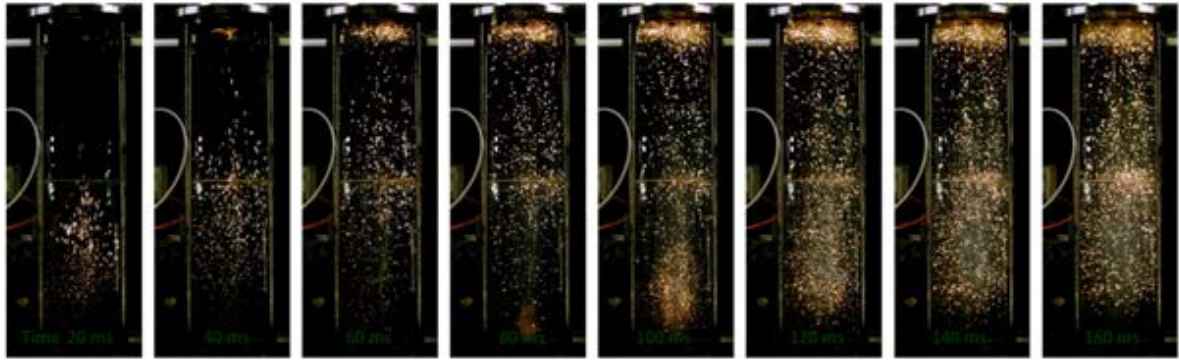
Fig.3. Small scale sodium spray fire scenario
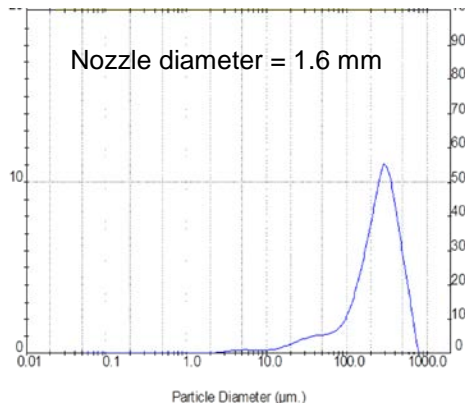
Fig.4. Sodium droplet size distribution
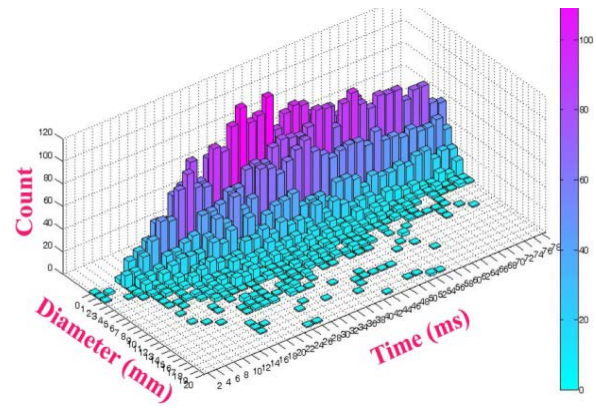
Fig.5. Variation of burning sodium flame diameter
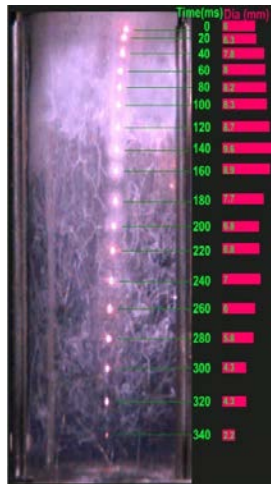
Fig.6. Burning of single sodium droplet
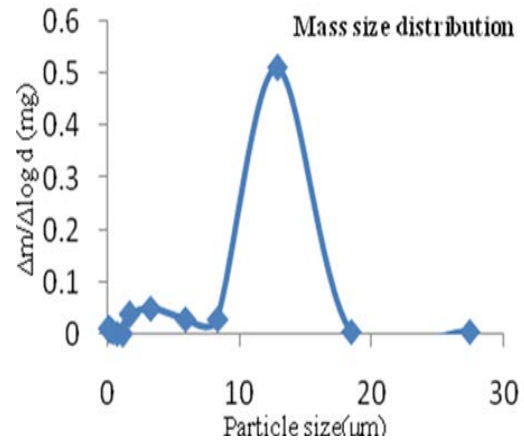
Fig.7. Sodium oxide aerosol size distribution

Theoretical calculations were carried out along with experiments to study the ignitability of sodium droplets as a function of sodium temperature, sodium droplet size and oxygen mass fraction. The heat absorbed by the shrinking droplets as a result of the exothermic combustion of outer layers has been used in analyzing the temperature rise of the droplet. Ignition delay time of droplets and limit of ignitability of sodium droplets were determined by numerical method. Ignition of sodium as a function of sodium temperature and oxygen concentration was studied in Mini MINA fire facility and it was observed that ignition of sodium at $500^{o}C$ occurs above the oxygen concentration of 4-5% (fig 8).
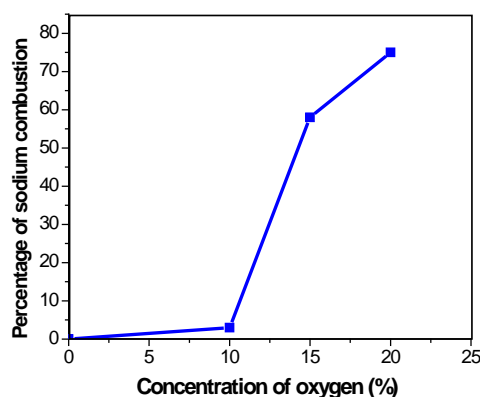
Fig.8. Role of oxygen on ignition of sodium

3. Sodium fire Scenario in Top Shield Platform during CDA

Simulation studies on sodium ejection from the annular gap of RS-LRP during CDA were carried out in SOCA facility (fig. 9). It consists of a test chamber designed to withstand instantaneous burning of 10 kg sodium spray fire i.e. 10 bar pressure and 773 K temperature. It is provided with sodium loop with necessary tanks, valves, heaters, argon cover gas system and sophisticated instrumentation. The jets of sodium are created by means of a ring header which contains equally distributed nozzles (69 nos. of 1.5 mm dia.) along the circumference. The sodium release system is a unique design to eject sodium through multiple nozzles at desired rate. The combined effect of sodium and secondary cable fire on the integrity of important components like DHX piping was studied. The spray fire scenario and average temperature rise in air during sodium spray fire experiment in SOCA facility is shown in fig.10 and 11 respectively. It was observed that the sodium spray fire was highly aggressive and random. It was observed that sodium fire penetrated aluminum cladding wrapped over the heaters of ring header and interacted with the insulating material.

Fig. 9. SOCA   Fig.10. Sodium spray fire scenario   Fig. 11. Temperature rise
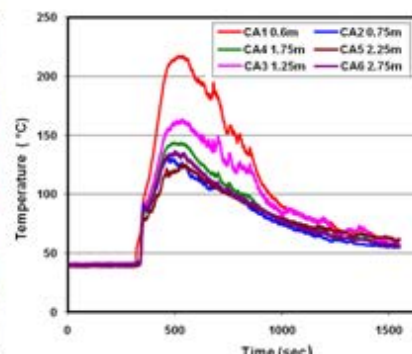
These experimental data are being used for validation of containment code developed for calculating the impact of sodium fire on reactor containment building. The rise in gas temperature and pressure during combustion of 5.5 Kg of sodium in SOCA facility was calculated using NACOM and NAFCON codes and results are shown in fig. 12 and 13. These calculations do not agree with the observed values of SOCA experiment. It was observed that the calculated amount of heat was not liberated in the combustion reaction. It could be due to the reasons such as (i) incomplete combustion of sodium (ii) absorption of liberated heat by the container walls or dissipated further into the atmosphere and (iii) absorption of portion of liberated heat by the unburned sodium.
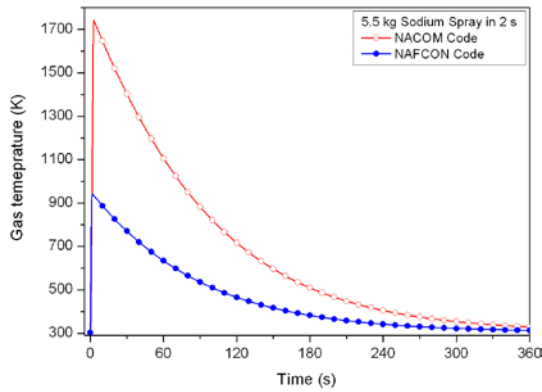
Fig.12. Variation of air temperature with time
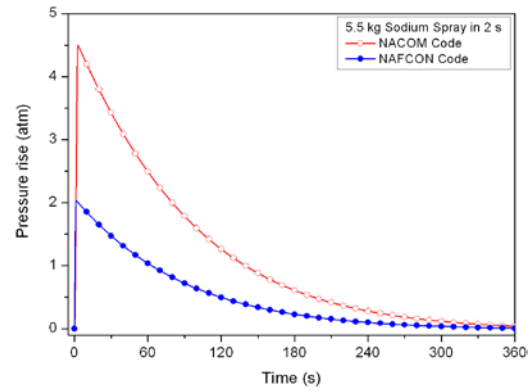
Fig.13. Variation of pressure during combustion

The effect of sodium fire on electrical and instrumentation cables and resultant secondary fire consequences were studied using Poly vinyl chloride (PVC) and Flame Retardant Low Smoke (FRLS) cables. The fire scenario recording using high speed camera is shown in fig.14. A photograph of PVC cable before and after exposure to sodium fire is shown in fig.15. Sodium spray fire event was observed only for 500 ms where as the ignited cable fire was prolonged for 18 sec. Gas analysis showed that no toxic gases were produced during the secondary fire. The variation in electrical resistance measured before and after sodium fire experiment is shown in fig.16. It was observed that in case of PVC cables, the electrical resistance values decreased from $1.1x10^{10}$ ohms to $2x10^{9}$ ohms whereas in case of FRLS cables, the decrease was from $5.62x10^{10}$ to $2.24x10^{10}$ ohms. This indicates that FRLS cables are more sodium fire resistant that ordinary PVC cables.

Studies on combined effect of sodium and secondary cable fire on the integrity of important components like DHX piping is in progress.
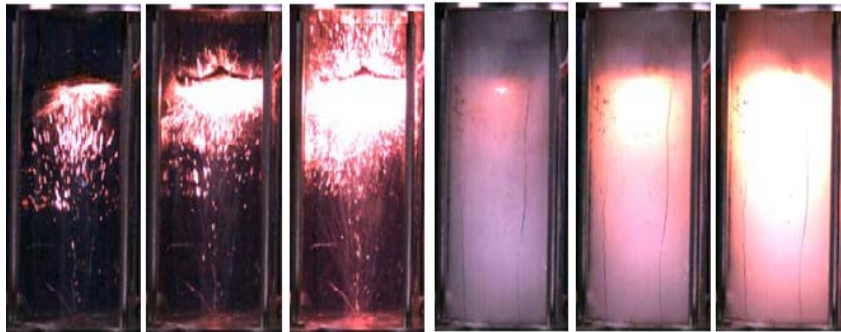
Fig.14. Sodium fire-Cable fire scenario

Fig.15. PVC Cable before and after exposing to sodium fire   Fig.16. Variation in insulation
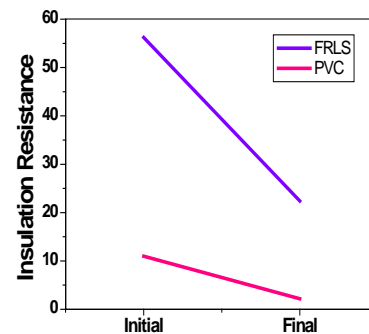
4. Sodium fire Scenario in Steam Generating Building

Simulation studies on sodium leaks in Steam Generating (SG) building were carried out in the range of few grams to 100 kilograms in various fire facilities.

Studies on plugging and unplugging characteristics of small sodium leak are being carried out using a dedicated innovative experimental setup (fig.17). It consists of a SS chamber with 0.3 dia hole, argon line, heaters and instrumentation including on-line mass measuring device for evaluation of sodium leak rate.

	LEGEND
1	Electonic Precision Balance
2	Leak collector
3	Stainless Steel Enclosure
4	Sodium Hold Up Vessel
5	Heater Furnace
6	Pressure Guage (PG-1)
7	Needle Value (V1)
8	Pressure Guage (PG-2)
9	Rotameter
10	Needle Value (V2)
11	Argon Cyclinders
12	Needle Vaule (V3)

Fig. 17. Sodium small leak experimental setup

The results show that the leak rate is a function of temperature, pressure and sodium purity. Leak rates are found to be random and the average leak rates are in good aggreement with the theoretically calculated values. It was observed that plugging plays an important role in small sodium leaks. The measured leak rates and plugging of sodium at various pressure are shown in fig. 18.   Conditions for unplugging have been established in terms of temperature and pressure. The condition for no plugging of sodium under argon atmosphere was above $290^{\circ}C$ and 4 bar pressure.
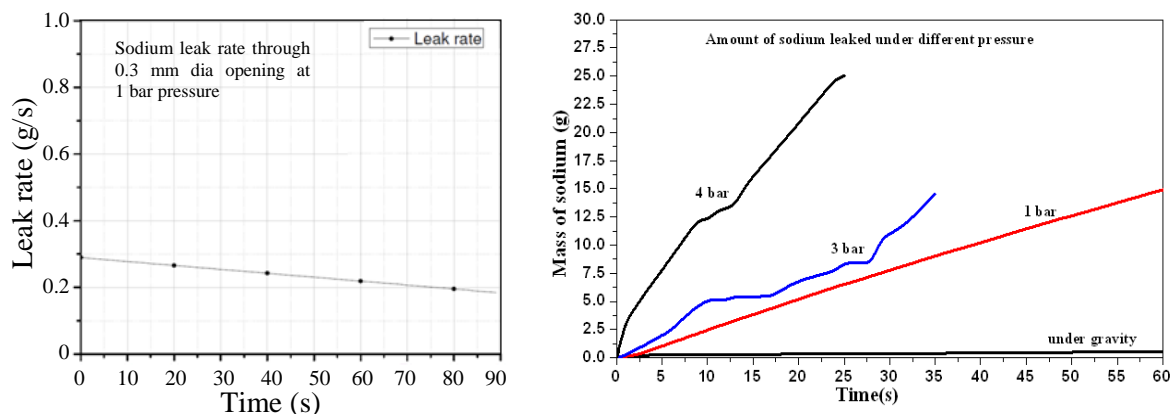
Fig.18. Sodium leak at various pressures through 0.3 mm dia opening

In case of sodium fire at SG building due to sodium leak, the resultant sodium fire shall be extinguished by both active method and passive method. Applying fire extinguishing powder over burning sodium and injection of nitrogen are the active mitigation methods. An innovative carbon microsphere based sodium fire extinguisher has been developed and qualified in various sodium fire facilities.   The indigenously developed carbon microsphere extinguishes sodium fire by covering the sodium metal surface and thus separating the metal from an oxygen source (fig. 19).   The excellent flow characteristics, high thermal conductivity, chemical inertness and non-smoking properties of these microspheres highly promise as an efficient extinguisher for sodium fire. The sodium metal could be

easily recovered once the fire is extinguished. The scanning electron microscope image of carbon microspheres is shown in fig. 20.
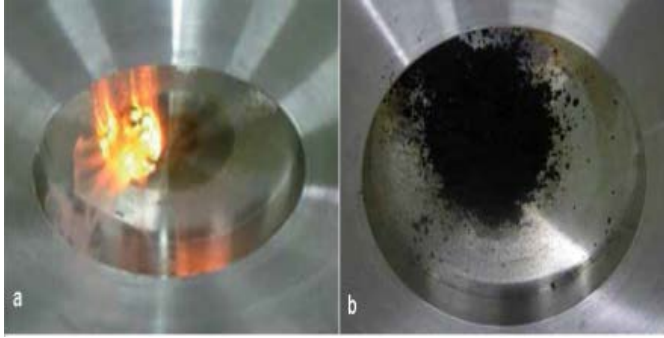
Fig.19. Sodium fire and its extinguishment using CMS
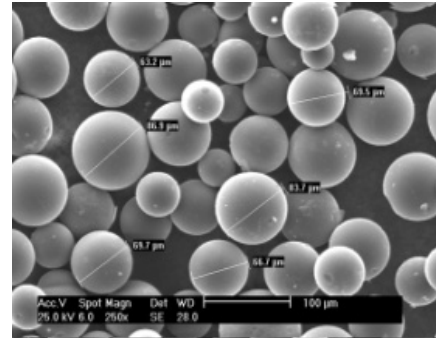
Fig.20. SEM image of CMS

Nitrogen flooding into the area of sodium fire shall reduce the oxygen percentage below the limit where sodium-oxygen reaction will not be sustained. Also nitrogen injection into the area at sufficiently high rate prevents inflow of air. Mitigation of sodium fire as a function of oxygen concentration and effect of nitrogen injection rate on mitigation rate were studied in SOCA facility. Preliminary experiments were conducted in Mini MINA facility at various oxygen concentrations (1% to 22%) in the nitrogen atmosphere and it was observed that a minimum of 6% oxygen is required for ignition of sodium droplets (100-200 µm) sprayed at 400°C and 4% oxygen in case of sodium droplets sprayed at 500°C. Theoretical calculation on nitrogen injection rate to reduce the oxygen percentage below 4% was made using the following analytical equation,

$$y = A1 exp\left(-\frac{x}{t1}\right) + A2 \exp\left(-\frac{x}{t2}\right) + y0$$

Curves were plotted for different injection rates of nitrogen and different suction rates of air, keeping one parameter constant at a time (fig. 21).
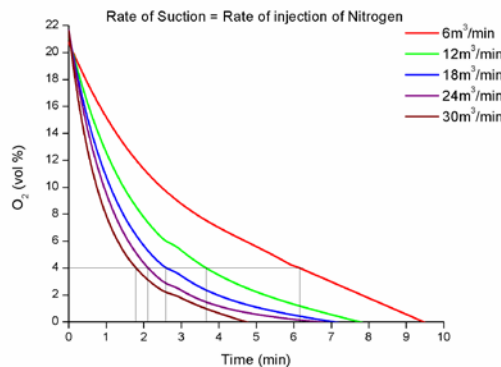
Fig.21. Reduction in oxygen concentration by nitrogen injection

Leak collection trays (passive method) provided below the sodium pipelines and tanks in PFBR were qualified in SFEF facility. LCT collects the leaked sodium in a hold up vessel, suppress the sodium fire by oxygen starvation and guide the sodium to inert sodium transfer tank. Towards this, a network of carbon steel pipelines is laid out connecting all the LCT to sodium transfer tank, with each pipe having a fusible plug. The plug separates air environment in LCT and argon environment in transfer tank. Woods metal with low melting point is the preliminary choice for the plug. Leaked sodium by virtue of its high temperature melts the plug and drains into transfer tank. A schematic of complete LCT system is shown in fig.22.
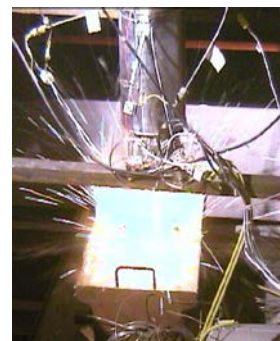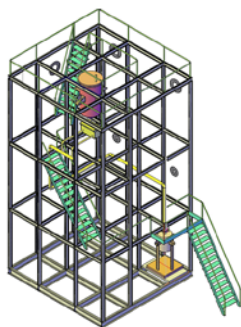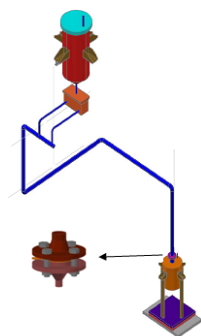
Fig. 22 Schematic of complete LCT system

Fig.23. Sodium collection in LCT

Experiment was conducted by pouring 100 Kg of sodium at 400°C into the leak collection tray. The fire scenairo is shown in fig. 23. It was observed that only about 20% of sodium was burnt during sodium collection. The aerosol generated during sodium fire spead all over the room and settled down on the floor. It was observed that for complete settling of sodium oxide aerosol occurred within a time period of 3 days (fig. 24). Entry into the experimental hall was permitted only after the reduction of aerosol concentration below 2 mg/m^{3}. It was also observed that all the sodium oxides got converted into sodium carbonate by forced circulation of air into the experimental hall.
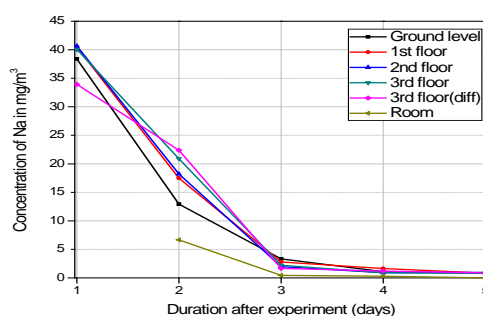
Fig.24. settling behavior of sodium aerosol

Sodium fire due to leaked sodium produces white dense smoke which is corrosive in nature. The concentration of sodium aerosol in the area has to be reduced below 2 mg/m^{3} before venting it into the atmosphere. An exhaust gas treatment system has been designed, fabricated and installed at SOCA facility to remove the harmful sodium aerosols and other toxic gaseous products from the exhaust gas. This system consists of a venturi scrubber followed by two countercurrent packed bed columns connected in series. The schematic of the system is shown in fig. 25. The performance evaluation of the scrubber unit was carried out during the sodium spray fire experiment conducted with 2 Kg of sodium. It was observed that removal of sodium aerosol was successful and the sodium aerosol concentration in the exit gas was less than 2 mg/m^{3}.
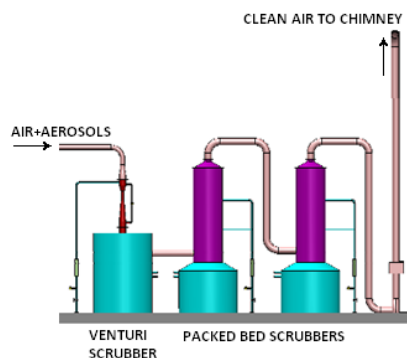
Fig. 25 Schematic of Scrubber system installed in SOCA facility

When burning sodium interacts with concrete, a multitude of exothermic chemical reactions occur resulting degradation of mechanical strength due to severe cracking, dehydration and release of hydrogen and other gases. The effect of flowing and stagnated hot sodium on concrete is being studied. The concrete sample and the sodium injection line are shown in fig. 26. Experiments will be conducted in MINA facility by pouring about 2 Kg of hot sodium and release of hydrogen, loss of water, length of sodium penetration and change in mechanical properties will be measured.

Fig.26. Limestone concrete along with sodium injection line

5. Conclusion

Sodium can be handled safely and it will be continued to be the universal coolant for Fast Reactors. Dedicated innovative facilities (MINA, SOCA and SFEF) were established for investigation of safety issues related to sodium fire. Studies on single sodium droplet combustion have provided more fundamental data for modeling of combustion mechanism. Investigation on small sodium leak through small openings showed that the sodium leak rate is a random phenomenon and varies with sodium temperature and argon pressure. Sodium plugging occurs at lower temperature and pressure and unplgging was achieved at high temperature and high pressure. The condition for no plugging of sodium under argon atmosphere was above 290°C and 4 bar pressure. Studies on sodium fire-cable fire interactions with PVC and FRLS cables reveal that short time exposure of sodium fire cause secondary fire and FRLS cables are possessing greater sodium fire resistance than ordinary PVC cables. Complete leak collection tray system (passive method) was successfully qualified and a novel carbon microsphere based sodium fire extinguisher (active method) has been developed and tested on small scale sodium fire. Experimental and theoretical studies on mitigation of sodium fire by nitrogen injection revealed that sodium fire is getting extinguished when the oxygen concentration is reduced below 4%. Hence, nitrogen can be used in secondary sodium systems to mitigate the sodium fire. The experimental results were used for validation of codes such as NACOM, NAFCON, SAFIRE and CFD calculations. These codes over estimates the pressure buildup and temperature rise in the containment building. Construction of experimental facilities for future sodium safety studies such as sodium-water reaction, sodium-steam interaction, sodium-cover gas interaction, sodium-insulation material interaction, impact of sodium jet on adjacent pipe, Large scale sodium pool and spray fire scenario and leak before break concept etc. are in progress.

6. Acknowledgements

7. References

[1] H.A. Morewitz, Sodium Spray Fires, *Nuclear Engineering and Design*, Vol. 55, 1979, pp 275-281.

[2] Acosta, Robert , Study of Sodium Spray Fires for Sandia National Laboratories, 2008.

[3] Makino, Atsushi , Ignition Delay and Limit of Ignitability for Sodium Pool, JSME International Journal , Series B, Vol. 49, No.1, 2006, pp 92–101.

[4] R. Baskaran,V. Subramanian, B. Venkatraman and P. Chellapandi, Sodium Aerosol Studies for Fast Reactor Safety, Energy Procedia, Vol. 7, 2011, pp 660–665.

[5] Parida F.C et al., Degradation Behaviour of Limestone Concrete Exposed to Liquid Sodium, 1st National Conference on Nuclear Reactor Safety, Mumbai, Nov. 2002. (NRT-1044).

[6] Sanjay Kumar Das et al., Experimental study on thermo-chemical phenomena during interaction of limestone concrete with liquid sodium under inert atmosphere, Construction and Building Materials Vol.23 (2009) 3375–3381.

[7] Zeldovich, Ya. B. et al, The Mathematical Theory of Combustion and Explosions, Consultants Bureau, New York, 1985, pp 59-65.

[8] Okano, Yasushi. et al, Numerical simulation of a free – falling liquid sodium droplet combustion, Annals of Nuclear Energy, Vol. 30,2003, pp 1863–1878.

[9] M.Heisler, H.A. Morewitz, An Investigation of Containment Pressurization by Sodium Spray Fires, Nuclear Engineering and Design, Vol. 55, 1979, pp 219-224.

[10] Koshizuka, Seiichi et. al, Numerical Analysis of Droplet Breakup Behavior using Particle Method, Journal of Nuclear Science and Technology, Vol. 38 (12), 2001, pp 1057-1064.

[11] P. Mangarjuna Rao et.,al, Modeling of quasi-static sodium droplet combustion in convective environment, International Journal of Heat and Mass Transfer, Vol. 55, 2012, pp 734-743.

Safety Analysis Results of Representative DEC Accidental Transients for the ALFRED Reactor

G. Bandini[a]**, E. Bubelis**[b]**, M. Schikorr**[b]**, M.H. Stempniewicz**[c]**, A. Lázaro**[d]**, K. Tucek**[d]**, P. Kudinov**[e]**, K. Kööp**[e]**, M. Jeltsov**[e]**, L. Mansani**[f]

[a] ENEA, Bologna, Italy

[b] Karlsruhe Institute of Technology, Eggenstein-Leopoldshafen, Germany

[c] NRG, Petten, The Netherlands

[d] JRC-IET, Petten, The Netherlands

[e] KTH, Stockholm, Sweden

[f] Ansaldo Nucleare, Genova, Italy

Abstract. The conceptual design of the Advanced Lead Fast Reactor European Demonstrator (ALFRED) is under development within the LEADER project to meet the safety objectives of Gen-IV nuclear energy systems. This paper presents the main results of the safety analysis for beyond design basis conditions, namely design extension conditions (DEC), which include the failure of prevention and mitigation systems, like the reactor scram in the so-called unprotected transients. The main objective of this analysis is to evaluate the impact of the core and plant design features on the intrinsic safety behaviour of the ALFRED reactor. Several computer codes: SIM-LFR, RELAP5, CATHARE, SPECTRA and TRACE are applied to evaluate the consequences of representative unprotected accident scenarios such as Loss-of-Flow, Loss-of-Heat-Sink and Reactivity initiated accidents. Additionally, the consequences of steam generator tube rupture and partial sub-assembly flow blockage events are assessed by means of appropriate fluid-dynamic codes.

1. INTRODUCTION

Among the promising reactor technologies, the Lead Fast Reactor (LFR) has been identified as a technology with great potential to meet the safety goals of Gen-IV nuclear energy systems. The LFR system features a fast-neutron spectrum and a closed fuel cycle for efficient conversion of fertile uranium and management of actinides.

The LEADER project of EU 7th Framework Program (FP) deals with the development of such a technology and is mainly based on the previous achievements obtained during the 6th FP in the ELSY project. Further advances are proposed and the conceptual design of a scaled down facility for the European LFR, namely ALFRED (Advanced Lead Fast Reactor European Demonstrator), is the main topic of LEADER.

One of the objectives of the project is the evaluation of safety aspects and a preliminary safety analysis of ALFRED. On the basis of the design solutions envisaged for ALFRED, a simplified line-of-defence strategy was applied for the identification of accident initiators. The identified event initiators were categorized and the most representative for each category were selected for the safety analysis.

Both Design Basis Conditions (DBC) and Design Extensions Conditions (DEC) have been considered in the safety analysis of ALFRED. The DEC accident scenarios are very low probability events, which include the failure of prevention or mitigating systems. The main objective of DEC transient analysis is to evaluate the impact of the core and plant design features on the intrinsic safety behaviour of the plant. In this paper the results of analyses of representative DEC events for ALFRED, performed with various system codes, are presented and discussed.

2. ALFRED CONFIGURATION

The LEADER project, which started in April 2010, carries out an important set of activities having two main goals: the advancement of the conceptual design of the industrial size plant to the present European LFR (ELFR) configuration rated at 600 MWe, and the development of the design of the LFR demonstrator ALFRED [1].

The ALFRED configuration is illustrated in Fig. 1.
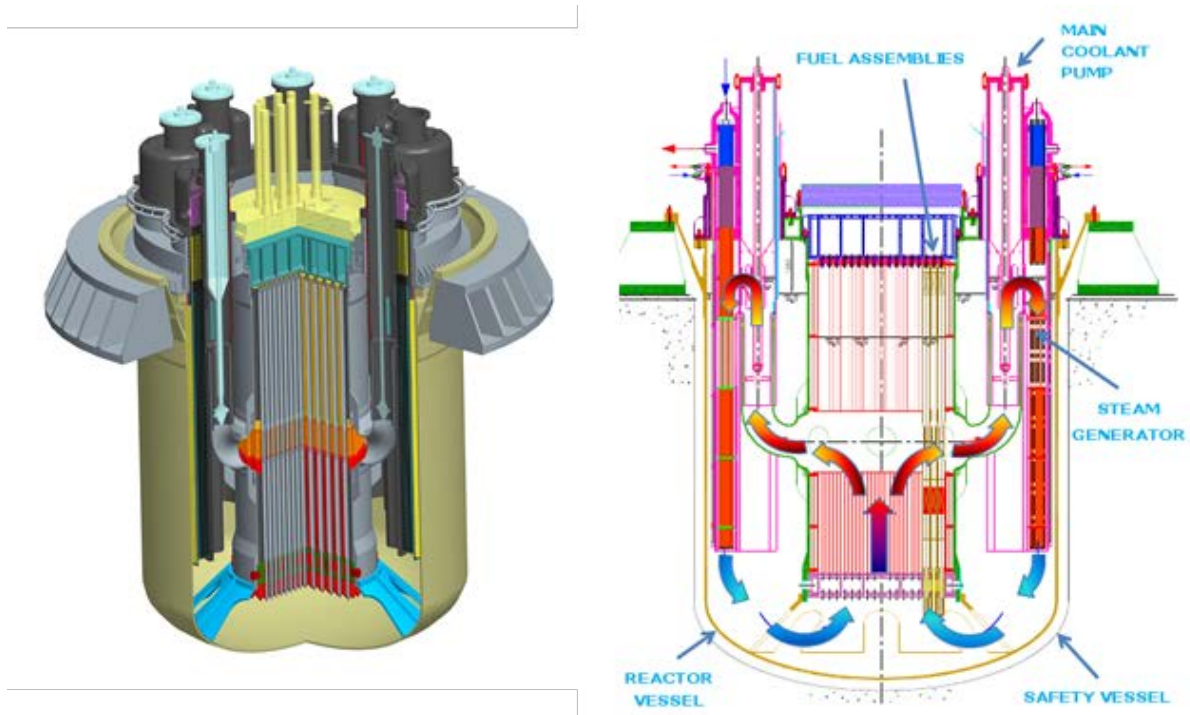
FIG. 1. ALFRED configuration (3D view on the left and 2D vertical section on the right)

Main features of the ALFRED design are:

- Pool type configuration characterized by a reactor vessel and the cavity liner safety vessel,

- Hexagonal wrapped fuel assemblies (FA) extended to cover gas to simplify fuel handling (FAs weighted down by tungsten ballast for refueling and kept in position by upper grid springs during operation),

- Mechanical pumps located in the hot collector,

- Double-walled straight steam generator (SG) tubes with continuous monitoring of tube leakages.

The thermal cycle is completely consistent with the ELFR thermal cycle: primary lead temperature being between 400-480°C, secondary side pressure 180 bars, and once through SGs with water/steam temperature ranging from 335 to 450°C in superheated conditions. The overall efficiency has been

evaluated being higher than 42%. ALFRED will also allow testing the connection to the electrical grid, with a generated electrical power of about 120 MWe.

Safety of ALFRED is extensively based on the use of the defense in depth principles, enhanced by the use of passive safety systems (actively actuated through locally and always available stored energy source, and fully passively operated). Safety features of the LFR system have been designed since the beginning of the design activities to face challenging conditions and events, thanks to the very forgiving and benign characteristics of the coolant. As an example, there is no need for off-site or emergency AC electrical power supply to manage the design basis accident conditions; the only action needed is the addition of water to maintain the level in the decay heat removal (DHR) pools, which are already sized to guarantee at least three days of unassisted fully passive operation and can be easily re-filled in the following days.

3. SUMMARY OF DEC TRANSIENT ANALYSES

The DEC events that are representative for the safety analysis of ALFRED have been identified by means of common safety approach adopted for liquid metal fast reactors and on the basis of engineering judgment, taking into account the specific features of the ALFRED design. These events of very low frequency are characterized either by the failure of reactor scram (so called unprotected accidents) involving:

- Unprotected reactivity insertion transient (UTOP),
- Unprotected loss of flow transient (ULOF),
- Unprotected loss of heat sink transient (ULOHS),
- Unprotected loss of flow and heat sink transient (ULOF+ULOHS),
- Unprotected partial FA blockage,

or by the simultaneous occurrence of multiple failures in some protected transients:

- Loss of all secondary circuits with total unavailability of DHR system,
- Loss of all primary pumps with reduction of feedwater temperature (loss of one preheater),
- Loss of all primary pumps with increase of feedwater flowrate by 20%.

The last two protected transients are mainly investigated to assess an important aspect for LFR systems related to the risk of lead freezing in the primary cooling circuit. This specifically concerns situations after reactor shutdown and activation of the DHR system, since, in the medium term, heat removed by the DHR system (which is almost constant in time) is expected to exceed the decreasing decay heat. The preliminary safety analysis has demonstrated that in this case the lead freezing might become an issue only after several hours, thanks to the large thermal inertia of the primary system and thus there is more than enough time for the operator to undertake appropriate corrective actions. Furthermore, the analysis of the extremely unlikely event characterized by the failure of all secondary circuits with total unavailability of any DHR system, leading to a progressive increase of the primary temperatures, has highlighted the large grace time left to the operator before reaching limiting temperatures for the core and the vessel structures.

The unprotected transients are mainly investigated to obtain insights on the intrinsic safety behaviour of ALFRED and thus verify the adequacy of the solutions adopted for the core and the plant design. In following subsections, results of the preliminary analysis performed for the above mentioned unprotected transients are presented. All the unprotected transients are considered to start at full power (300 MWth) from end of cycle (EOC) conditions. Transient analyses performed for the beginning of cycle (BOC) conditions with the SIM-LFR code confirm that the general situation does not differ significantly from EOC conditions, thus similar conclusions apply in both cases.

3.1. *Unprotected reactivity insertion transient (UTOP)*

This transient is initiated by a reactivity insertion of 250 pcm in 10 s without reactor scram, and with the secondary circuits remaining operational in forced circulation. This amount of reactivity might be inserted into the core due to core compaction or voiding of part of the active core region. The core voiding should envelop the transient following a steam generator tube rupture or leakage [2] with steam bubbles being possibly entrained in coolant and eventually transported to the core inlet. The reactivity ramp taken as a reference in this transient should be confirmed by detailed 3D CFD analysis of steam bubble transport in the primary circuit and 3D neutronic calculations for the evaluation of reactivity effects.

The results of the analysis performed with the TRACE code are presented below. The TRACE code has been adapted by JRC/IET to deal with lead coolant in the primary cooling system, by replacing the lead-bismuth coolant properties embedded in the code source with more accurate lead thermo-physical properties obtained from the available experimental and literature data.

The reactivity insertion leads to a core power excursion up to ~610 MW power in 11 s as shown in Fig. 2. The positive reactivity inserted is mainly counterbalanced by the negative fuel expansion and Doppler effects and then by negative core radial and coolant thermal expansion feedback effects resulting from the progressive core structures temperature rise (Fig. 3). The primary coolant and core temperature increase is limited also due to the increase of power removed through the SGs. The maximum clad temperature at t = 200 s is below 600 °C, but is still slowly increasing (Fig. 3). The maximum fuel temperature calculated in the center of the fuel pellet of the hottest FA (T = 2745 °C after 15 s) exceeds the melting point of fuel (MOX) by about 80 °C, so that local fuel melting cannot be excluded in the hottest FAs of the core.
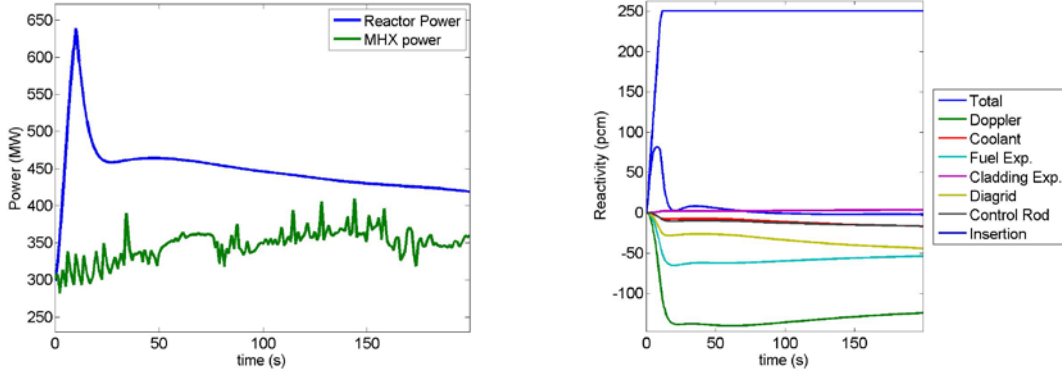
FIG. 2. Reactor and SG (MHX) powers (left) and reactivity feedbacks (right) as calculated by TRACE
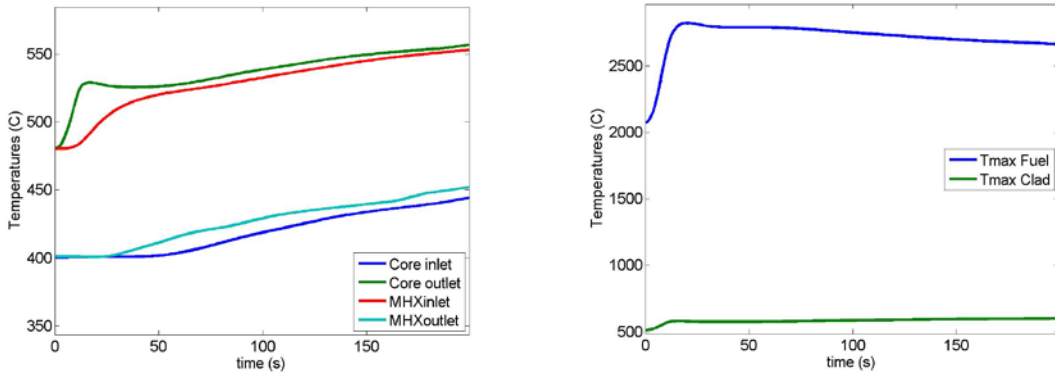
FIG. 3. Primary lead temperatures (left) and maximum fuel and clad temperatures (right)
as calculated by TRACE

The trend of TRACE results for this unprotected overpower transient is confirmed by the analyses performed with SIM-LFR and RELAP5 codes. A slightly higher power excursion up to 660-680 MW is calculated with these codes due to reduced axial fuel expansion feedback (clad-linked effect after fuel rod gap closure with increasing fuel temperature at EOC). As a consequence the maximum fuel temperatures approaches 3000 °C in the hottest FAs, but only local fuel melting is being confirmed. The peak clad temperature remains relatively low (< 700 °C), thus clad failures are not predicted.

3.2. *Unprotected loss of flow transient (ULOF)*

This transient is initiated by the loss of all primary pumps at t = 0 s without reactor scram. The secondary circuits remain operational in forced circulation providing a nominal feedwater flowrate at the SG inlet and a constant steam pressure at the SG outlet.

The simultaneous coastdown of all primary pumps leads to the transition from forced to natural circulation in the primary circuit. The choice by design of low pressure loss through the core and the whole primary circuit (1.0 bar and 1.5 bar in normal operation, respectively), connected with the differential height between the mid-planes of the core and SGs, favours the establishment of natural convection in the primary circuit, and thus limits the core temperatures rise during the ULOF transient.

As calculated by the RELAP5 code, after a small initial core flowrate undershoot related to the equalization of the lead free levels inside the reactor vessel, the natural circulation flowrate through the core stabilizes at ~5800 kg/s (~23% of nominal value) as it is shown in Fig. 4. The resulting core temperature rise and corresponding negative reactivity feedback effects (due to the expansion of FA spacer pads, coolant and control rod drivelines) leads to a progressive reduction in the core power, which stabilizes at ~200 MW after t = 300 s (Fig. 4) and later tends to come into equilibrium with the power removed by the secondary circuits.
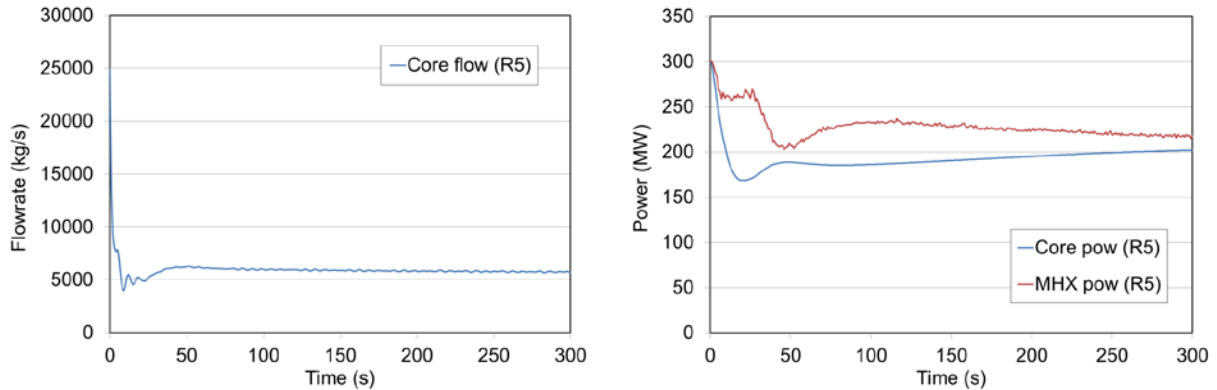
FIG. 4. Active core mass flowrate (left) and core and SG (MHX) powers (right) as calculated by RELAP5

Because of the initial core flow rate undershoot, the clad temperature of the hottest pin increases from 508 °C up to 764 °C at t = 10 s, and then decreases down until stabilizing below 650 °C (Fig. 5). Due to the very low amplitude of the initial clad temperature peak, clad failures are not expected during the ULOF transient. The peak fuel temperature reduces during the transient, according to the core power decrease, from the initial value of ~2000 °C down to ~1550 °C (Fig. 5).
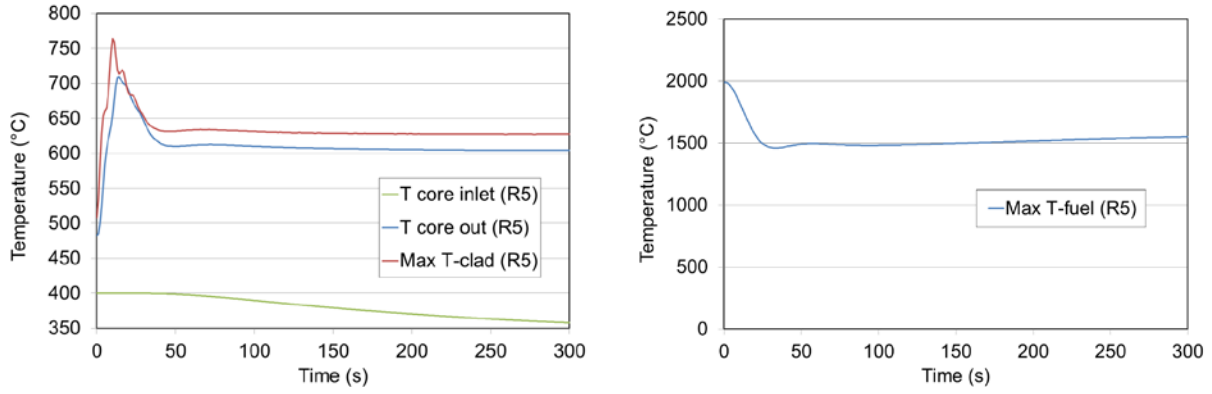
FIG. 5. Core and peak clad temperatures (left) and peak fuel temperature (right) as calculated by RELAP5

Similar ULOF transient results have been obtained using other codes: SIM-LFR, CATHARE and TRACE. All the analyses show that the initial clad temperature peak is limited below the RELAP5 calculated value and the clad temperature of the hottest pin stabilizes below 700 °C. Furthermore, the thermo-mechanical model of SIM-LFR code confirms that there is a very large margin to clad failure, that is primarily due to the relatively high lead natural convection core mass flow rate of about 24% nominal and the relatively low fission gas pressure in the peak power pin at EOC (~20 bar during the ULOF transient).

Of particular importance are the calculated fuel and cladding temperatures during the ULOF transient, since the ALFRED primary system was specifically designed with the intention of being able to accommodate the ULOF transient without significant pin failures.

3.3. Unprotected loss of heat sink transient (ULOHS)

For this calculation the primary heat transport path through the steam generators was assumed to fail at time t = 0 s. Additionally, despite of the various signals for reactor shutdown, it was assumed that all reactor shutdown systems are inoperable. In order to get even more conservative analysis results, a simultaneous failure of one DHR-1 subsystem (Isolation Condenser, IC) was postulated. It means that from that point onwards, only three out of four DHR-1 subsystems are responsible for removing heat (total of ~5 MW) from the primary cooling circuit. The primary pumps are assumed operational thereby assuring an efficient heat distribution throughout the primary cooling system providing the nominal coolant flow rate.

As calculated by the SIM-LFR code, the unprotected loss of heat sink event leads to all core and vessel temperatures to fairly uniform heatup at a rate of ~3.1 °C/min, based on the masses of coolant (~3570 tons) and structural materials inside the primary cooling circuit, as shown in Fig. 6. The power level in the core reduces down to about 2.5% of nominal value (7.5 MWth) at 3600 s (1 hour) into the transient due to negative temperature reactivity feedbacks effects related to thermal expansion of fuel, diagrid, spacer pads, lead and control rod drivelines.

FIG. 6. Peak fuel, clad, coolant and vessel wall temperatures (left) and relative core thermal power and flow rate (right) as calculated by SIM-LFR

At the end of the simulation (1 hour into the transient), the average vessel wall temperature approaches 662 °C, thus questioning the possibility to maintain the long term structural integrity of the vessel under these elevated temperature conditions, unless corrective actions are taken. At t = 3600 s into the transient the peak pin clad temperatures will reach about 700 °C, but due to the rather low fission gas pressure of ~28 bar, the clad of the peak power pin will stay intact, showing clad failure time of about 4.9E+6 s (see Fig. 7). If the operator will not react to terminate this transient, all these temperatures will still continue to slowly increase, until the core power reduces down to the DHR removal power level of 5 MW.
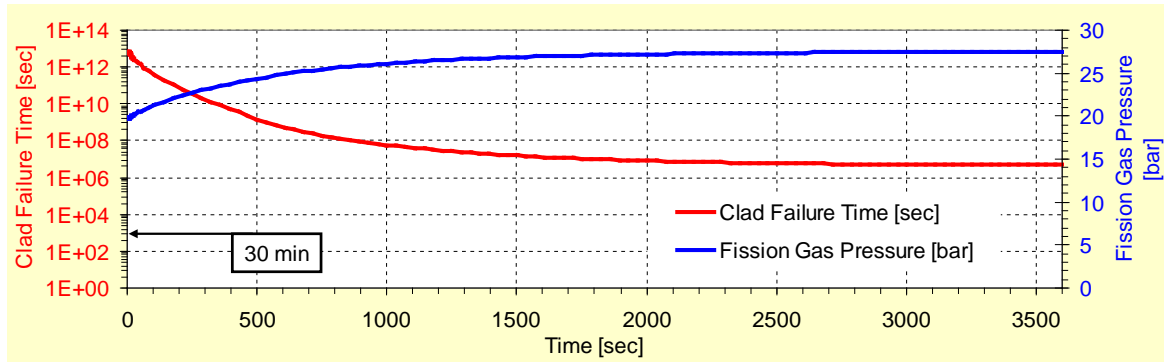
FIG. 7. Peak pin fission gas pressure and clad failure time as calculated by SIM-LFR

The SIM-LFR results for the ULOHS transient are confirmed by the analysis performed with other system codes. The RELAP5 and CATHARE codes predict very similar trend for core power and both peak clad and average vessel wall temperatures. The maximum clad and vessel wall temperatures calculated by these codes into 1 hour transient are just 10 to 20 °C above the temperature values calculated by the SIM-LFR code.

The favourable response to this DEC transient is due to a rather large cumulative negative reactivity feedback effect consequent to the thermal expansion of fuel, diagrid, spacer pads, lead and control rod drivelines. Sufficient grace time (>> 30 min) is available for the operator intervention to terminate this transient by manually initiating the shutdown of the reactor and cool down of the primary cooling circuit.

3.4. Unprotected loss of flow and heat sink transient (ULOF+ULOHS)

In case of the loss-of-offsite power (LOOP) event, all primary pumps and the primary heat transport path through the steam generators are assumed to fail simultaneously at time t = 0 s. Additionally, despite of the various signals for reactor shutdown, it was assumed that all reactor shutdown systems fail, so that the LOOP (LOF+LOHS) transient is simulated as an unprotected transient. In order to get

even more conservative analysis results, a simultaneous failure of one DHR-1 subsystem (IC) was postulated. It means that from that point onwards, only three out of four DHR-1 subsystems are responsible for removing heat (total of ~5 MW) from the primary cooling circuit. Stopping of the primary pumps at the beginning of the transient means that primary coolant circulation is only by natural convection, which does not result in a well-mixed, uniform temperature distribution throughout the primary system, as in the case when the primary pumps are operating normally.

As calculated by the SIM-LFR code, the unprotected loss of flow leads first to a sudden core outlet temperature increase, up to about 700 °C, due to transition from forced to natural circulation in the primary circuit, as shown in Fig. 8. Successively, the loss heat sink leads to all core and vessel temperatures to fairly uniform heatup at a rate of ~2.5 °C/min (due to faster reduction of the reactor power level in comparison with the previous ULOHS case). The power level in the core reduces down to ~2.9% at 3600 s (1 hour) into the transient due to negative temperature reactivity feedback effects.
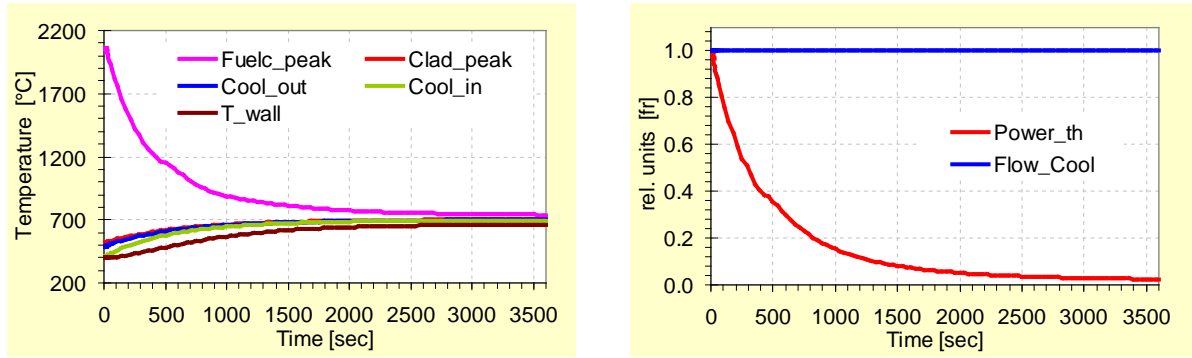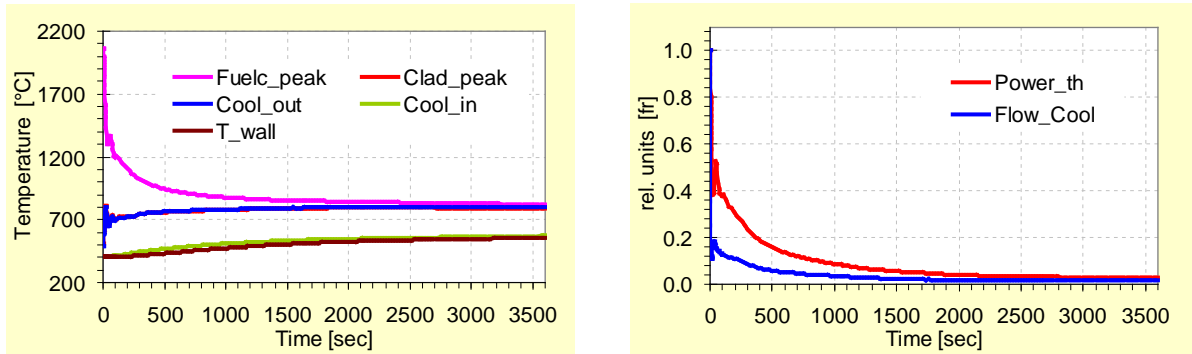

FIG. 8. Peak fuel, clad, coolant and vessel wall temperatures (left) and relative core thermal power and flow rate (right) as calculated by SIM-LFR

At the end of the simulation (1 hour into the transient), the average vessel wall temperature approaches ~555 °C, thus the long term structural integrity of the vessel is guaranteed. At t = 3600 s into the transient peak pin clad temperatures will reach ~790 °C, but due to the rather low fission gas pressure, the clad of the peak power pin will stay intact, having a failure time of about 2.2E+4 s (~6 hours), as shown in Fig. 9.
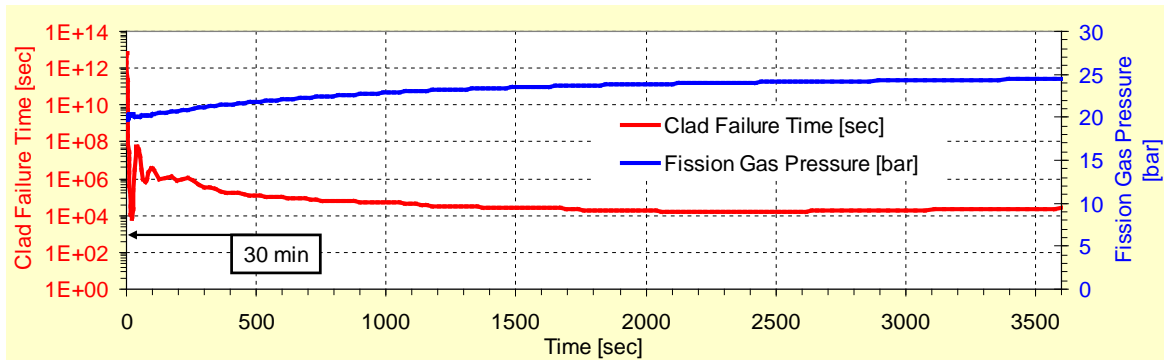
FIG. 9. Peak pin fission gas pressure and clad failure time as calculated by SIM-LFR

The SIM-LFR results for the ULOF+ULOHS transient are confirmed by the analysis performed with RELAP5 and CATHARE codes. The maximum clad temperature calculated by these codes 1 hour into the transient is slightly higher (by about 30 °C) than the one predicted by SIM-LFR, while the maximum vessel wall temperature reduces below 510 °C, consequent to a much more pronounced decrease of natural circulation flowrate in the primary cooling system as predicted by RELAP5 and CATHARE codes.

The favourable response of ALFRED to this DEC transient can be ascribed to a rather large cumulative negative reactivity feedback effect due to thermal expansion of fuel, diagrid, spacer pads, lead and control rod drivelines. Also here, sufficient grace time (>> 30 min) is available for the operator intervention to terminate this transient by manually initiating the shutdown of the reactor and cool down of the primary cooling circuit.

3.5. Unprotected partial FA blockage

The unprotected partial FA blockage transient has been investigated using both SIM-LFR and RELAP5 codes. Hereafter the main results from the RELAP5 analysis are reported. The progressive reduction of FA inlet flow area in the hottest FA has been assumed in the RELAP5 calculations up to a maximum of 97.5% of blocked inlet flow area. The local pressure loss at the FA inlet has been evaluated to about 22% of the entire FA pressure loss that is equal to 1 bar. For a conservative analysis the heat exchange with surrounding FAs through the inter-wrapper gap is neglected.

As a result of the reducing inlet flow area, the mass flow rate in the hottest FA decreases as shown in Fig. 10. A 75% blockage at the FA inlet leads to about 50% mass flow rate reduction inside the FA. The corresponding maximum FA temperature increase for the coolant, the clad and the fuel is represented in Fig. 10. The maximum clad temperature reaches the temperature limit of 700 °C after an inlet area blockage of about 85%. Clad melting (Tmelt ~1500 °C) is not expected for blockages below 95%. The fuel melting temperature (Tmelt ~2670 °C) in the center of the peak power fuel pellets is exceeded only if the area blockage is close to 97.5%.

The partial FA blockage has been simulated under unprotected conditions, that is without reactor scram. However, temperature measurements are provided by thermocouples positioned at the outlet of each FA, in order to detect an eventual flow area blockage in a FA. From the above results it appears that a 50% blockage at the FA inlet would lead to a temperature increase at the FA outlet sufficient to overcome the reactor scram threshold set-point value (ΔT through the FA greater than 1.2 nominal value), thus limiting and terminating the FA temperature increase well within the safety limits.
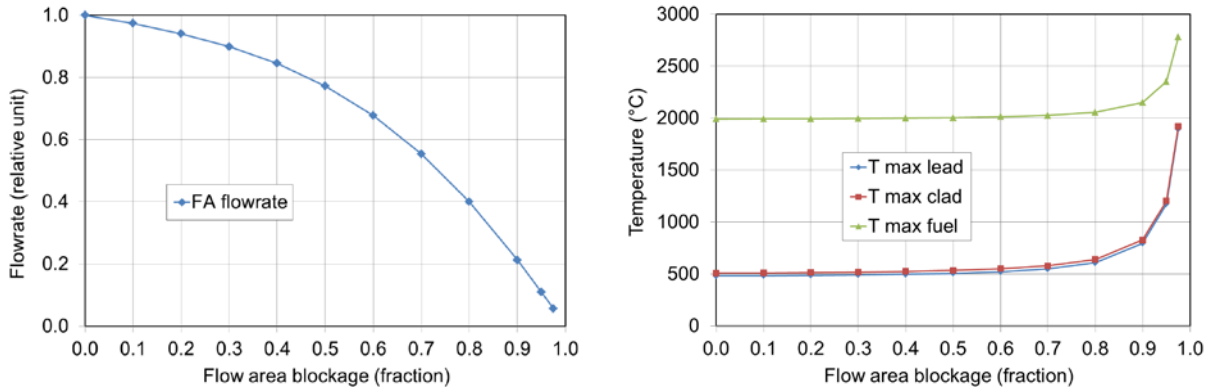
FIG. 10. Hottest FA mass flowrate (left) and maximum temperatures (right) versus inlet FA flow area blockage as calculated by RELAP5

4. CONCLUSIONS

The analysis of the representative DEC transients for ALFRED has highlighted very good intrinsic safety features of the reactor design. In particular, the results of the unprotected transients presented in this paper underline that the reactor can be maintained in a safe and controlled state even under the unlikely accident conditions, that include the failure of the reactor scram, thanks to:

- The establishment of enhanced and stable natural convection in the primary cooling circuit following the loss of the primary pumps,

- The dominant negative reactivity feedback effects obtained by optimizing the neutronic core design,

- The large thermal inertia of the primary cooling system,

- The passive and efficient operation of the DHR system for decay heat removal.

In all simulated unprotected transients the core temperatures are maintained well below the safety limits to be considered for DEC accidental transients. In particular:

- In all simulated transients there is a very large margin to coolant boiling, since the coolant temperature is always at least 900 °C below the lead boiling point (1740 °C);

- No clad failure is predicted in any of the simulated transients, unless in case of an undetected FA blockage greater than ~85%, which might be excluded by design (there are many orifices for coolant ingress at the FA inlet), and in case of the very unlikely ULOF+ULOHS event, when the time-to-failure reduces down to a few hours, but still leaving enough grace time for corrective operator actions;

- Fuel melting is excluded in all simulated transients except for local fuel melting (in the fuel pellet center) in the hottest FAs in case of reactivity insertion involving core compaction or core voiding due to passage of steam bubbles transported at the core inlet following the steam generator tube rupture event;

- The vessel integrity is guaranteed in the long term in all simulated transients except for the ULOHS transient, but even in this case there is enough grace time for corrective operator actions.

As a general conclusion, no relevant safety issues have been identified for ALFRED in case of representative DEC events. In particular, the ULOF transient can be accomodated without the need of corrective operator actions. Finally, the analysis of DEC transients for the lead-cooled ALFRED design has demonstrated the extremely forgiving nature of this plant when compared to other similar plant designs.

ACKNOWLEDGEMENTS

REFERENCES

[1]   ALEMBERTI, A., et al., "The Lead fast reactor - Demonstrator (ALFRED) and ELFR design", International Conference on Fast Reactors and Related Fuel Cycles: Safe Technologies and Sustainable Scenarios (FR13), Paris, France (2013).

[2]   JELTSOV, M., KUDINOV, P., "Simulation of steam bubble transport in primary system of pool type lead cooled fast reactors", 14th International Topical Meeting on Nuclear Reactor Thermalhydraulics (NURETH-14), Toronto, Ontario, Canada, September 25-29, 2011.

Safety orientations during ASTRID conceptual design phase

Pierre LO PINTO[1], Raphaëlle DOUSSON[1], Jean-Charles ROBIN[1],
Bernard CARLUEC[2], Sophie EHSTER-VIGNOUD[2], Stéphane BEILS[2],
Patrick MARITEAU[3], Florence GIFFON[3]

[1]: *''Commissariat à l'énergie atomique et aux énergies alternatives (CEA)''*
DEN/DER/CPA, 13108 Saint-Paul lez Durance Cedex, France
[2]: *AREVA NP, 10 rue Juliette Récamier 69456 Lyon Cedex 06, France*
[3]: *EDF SEPTEN, 12-14 avenue Dutrievoz, F-69628 Villeurbanne Cedex, France*
Contact author: Pierre LO PINTO, +33442254328, pierre.lo-pinto@cea.fr

Abstract. In France, Safety Options Report is the first document issued in the frame of the licensing of any new nuclear facility. It is usually issued at the end of the conceptual design phase. For the ASTRID project, a Safety Orientations Document was first prepared during the pre-conceptual design phase. This document, transmitted to the French Safety Authority, aims at supporting the conceptual design studies, the associated R&D program and then, selecting the basic design safety options.

ASTRID safety orientations are based on the previous Sodium-cooled Fast Reactors feedback, safety standards evolution, and other feedbacks such as the lessons issued from Fukushima accident. Safety goals set for ASTRID, considered as a demonstrator of future SFR, are ambitious, anticipating potential evolution of safety regulation.

Among the safety orientations of ASTRID, the following items are developed in this paper:

- Distinction between design domains which are: severe accident prevention, severe accident mitigation and practically eliminated situations,
- Safety classification of equipment,
- Identification of elements to be included into the "hard core" list,
- Approach for severe accident,
- Concept of "lines of mitigation",
- Demonstration of practical elimination of unacceptable situations.

1. Introduction

The current project of demonstrator of advanced sodium cooled fast reactor, ASTRID project [1], is at the pre-conceptual design phase, devoted to the choice of the most structuring design options [2]. In order to integer earlier the safety concerns in the design project, a first safety document was issued with a double purpose:

- To set the safety orientations to be used during the conceptual design phase for selecting the design options from safety viewpoint,
- To define the safety approach to develop in the safety assessment studies,
- To interact with the licensing authority earlier in the project process before the selection of the most structuring design options.

This Safety Orientations Document (DOrS) was delivered to the French Safety Authority, mid 2012. The Technical Safety Organisation in support of the French Safety Authority is evaluating the DOrS content. Then, safety recommendations should be issued, mid-2013.

The DOrS will be followed by the safety options report (DOS) by end of the conceptual design phase (2015) which will present and justify the choice of the safety design options which will be used for the detailed studies. This choice will take into account the safety recommendations resulting from the DOrS assessment by the licensing authority.

This paper presents the main safety orientations specific to the ASTRID project, which are developed in the Safety Orientations Document.

2. Global safety objectives

The global safety objectives for ASTRID can be considered as a step towards the future safety objectives of the 4th generation power plant. Assuming that the current probabilistic targets related to severe accident and unacceptable radiological releases are already very low, the safety improvements are mainly focused on the robustness of the safety demonstrations and on the consequences in the environment of a severe accident. This objective for ASTRID, consistent with the WENRA objectives [3], is defined as follows: "In case of the most severe accident considered, radiological releases must be postponed and limited in time and in area, and compatible with efficient off-site countermeasures."
Then, the proposed global objective for the 4th generation could be further: "No technical justification of off-site countermeasures". Nevertheless, despite this stringent objective associated to the level 4 of the Defence-in-Depth principle that concerns the plant designer, the following level 5 of D-in-D that concerns the Public Authority, could be kept complying with the independence of the D-in-D levels.
All the various items of the safety approach are then defined and applied in order to reach the global safety objectives.
Degraded plant situations that could lead to early or important radioactive releases in the environment, with therefore, a possible "cliff edge" effect on the consequences, and which are not reasonably manageable by design, must be "practically eliminated" that means a design allowing a safety demonstration with a high level of confidence so as to justify sufficient prevention provisions against any events capable to lead to the considered eliminated situation.

3. Safety principles at the pre-conceptual design phase

At the pre-conceptual design phase of ASTRID, a significant part of the design basis safety principles are relating to the manner of implementing the basic D-in-D principle. This evolution is presented below through two main items of the safety approach: "risk diagram" and "safety classification", the former concerns the analysis of the power plant operating conditions and situations whereas the latter concerns the SSC assuring safety functions.

3.1. Specific risk diagram of ASTRID

The risk diagram of ASTRID (figure 1) has two main areas with appropriate approaches:
- First area where, complying with the safety design criteria, the corresponding events have no significant safety consequences. The purpose is then to reduce the events frequencies by safety design provisions. The plant operating conditions are classified into four categories, as usually defined in the past 'design basis' (DB) domain.
- Second area where the probabilities of the degraded plant situations are very low, so the effort is preferably devoted to the reduction of potential consequences, either in terms of severe accident prevention or in terms of radioactive release.
This second area, which was called in the past 'beyond design basis' (BDB) domain, is split for ASTRID in three domains, as follows:
- Domain of severe accident prevention (SP): The purpose is to extend, as far as physically possible, the prevention area beyond the previous DB domain. Thus, the conceptual design of ASTRID is oriented so as major part of hypothetical plant situations (including postulated serious events, multiple-failures accidental sequences and transients combined with the postulated failures of safety systems, e.g., anticipated transients without scram) cannot lead to a severe accident. In particular, the reactor is designed for favoring its natural behavior so as there is no escalation into

a severe accident despite the hypothesis that the safety systems are not operating (e.g. no reactor shutdown, no electrical backup …).

- Domain of severe accident mitigation (SM): Despite a high level of prevention reached through the implementation of the SP domain, ASTRID approach intends to take account of the potential consequences of several types of severe accidents (level 4 of D-in-D) arising from various initiating events families (LOF, TOP, SAF) with the aim to implement appropriate safety design provisions for severe accident mitigation.
- Domain of practically eliminated situations (SPE): Despite the design orientations for allowing high capabilities to mitigate severe accident, the consequences of some hypothetical situations cannot reasonably be limited at a low level. These situations must be identified and reliable dedicated prevention measures must be implemented so as to compensate lack of design provisions to mitigate efficiently their consequences. After their identification based on the fundamental characteristics of the concept, the purpose is to minimize through the design the number of situations practically eliminated. These situations must be strongly prevented by design and a robust and confident safety demonstration has to be drawn up. For this purpose, the design orientation consists to implement at least three lines of defense (see section 4.1) not influenced by common causes faults (CCF). The design rules applied to the materials and provisions ensuring the prevention are those applied in the DB domain.

For each domain, specific safety analysis rules are settled.
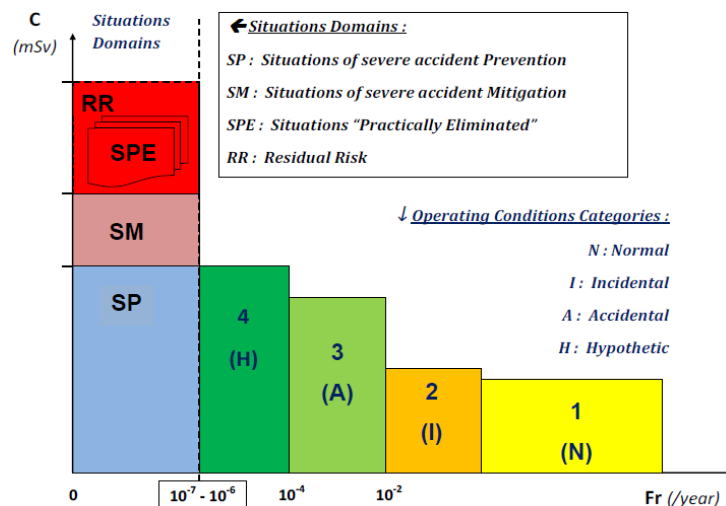
FIG.1. Risk diagram of ASTRID safety approach

3.2. Definition of safety classes

The orientation takes profit of the safety analyses after which the various safety functions are identified and the necessary lines of defense and lines of mitigation are defined. The method used for the classification of the SSC allows considering not only the significance of the safety functions ensured by the SSC but also other relevant indicators, notably:

- Level of consequences in case of failure of the considered equipment expected to act individually or associated with other materials acting for the same function, considering also the expected reliability of the safety SSC implemented for attenuation of consequences just after failure of the considered equipment,
- Grace delay and other time notions when the material is loaded or expected to act.

The significance of the equipment role as a part of a line of defense (LoD) or line of mitigation (LoM) is a major guide (see section 4.1) for the ranking of equipment in the safety classes. This approach pays particularly attention on materials involved in safety demonstrations of SPE, or ranked as a component of the "hard core" (see section 5.5) against extreme natural hazards.

A similar approach is being developed as regards the need of in-service inspection.

4. Conceptual design methodology

4.1. *Implementation of well-tried safety analysis methods*

The fundamental safety principles (e.g. D-in-D) are top-level notions that require to be translated in practical analysis tools, in order to allow an adequate implementation of these fundamental principles into the conceptual design. The methodology is basically deterministic just like the safety principles with possible probabilistic insights so as to be consistent with the probabilistic safety objectives and for verifying an homogeneous safety level.

The methods chosen for orienting the ASTRID conceptual design are:

- The "lines of defence" method (LoD) defined and well-tried in the frame of previous SFR projects (ex. RNR-1500, EFR), mainly applied for the prevention of severe accident; for example this method is used either to prevent the loss of a safety function, to give a first estimate of the expected reliability of a safety system, or to classify events and to assess the classification of an accidental sequence.
- The "lines of mitigation" method (LoM) defined in the current frame of ASTRID project as an analysis tool for implementing appropriate mitigation design provisions.

Features of these two complementary methods are shown in Table 1.

	S.A. Prevention:	S.A. Mitigation:
Method:	Lines of defense (LoD)	Lines of mitigation (LoM)
Approach type:	"Bottom-up"	"Top-down"
Objective:	Probabilistic targets	Consequences reduction
Validation criteria of application:	Number of LoD, reliable, independent, risk of CCF	Equipment ensuring all functions of one LoM. Each LoM homogeneous: approach "weak link of chain"
Demonstration:	Equivalent to "2 strong + 1 medium" lines (2a+b)	Radiological release minimization with "decoupling" approach
Application domain:	Prevention including "SPE"	Complementary to 'analysis by barrier' method
Safety classification of SSC:	Complementary to the 'analysis by function'	Complementary to the 'analysis by function'
« Hard Core » content:	One LoD per SPE	All equipment involved in a same LoM

TAB.1. Conceptual design analysis methods

The junction between the bottom-up approach by LoD and the top-down approach by LoM is made within the implementation of the D-in-D level 4 (figure 2). The process relating to this peculiar meeting point is presented in section 4.2.
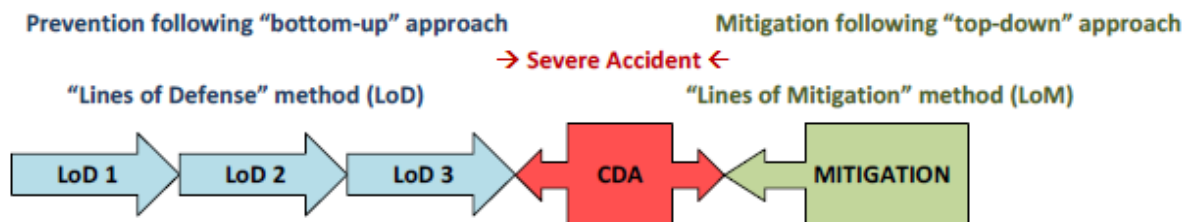
FIG.2. Simplified illustration of the bottom-up and top-down approaches

4.2. *Decoupling between core disruptive accident studies and accident of confinement design*

Sufficient independence between the levels of the D-in-D implementation is required by the European Safety Authorities bodies [3]. In addition to this safety measure, ASTRID approach plans to introduce, inside the D-in-D level 4, a separation between the results of core severe accident studies (CDA) and the accidental conditions both for the containment and the confinement designs. These disconnected approaches comply with the notion of defense in depth within the same D-in-D level 4, in particular palliate the limited full-scale experimental evidence on phenomena occurring during severe accident, and make compatible two safety objectives with safety margins:

- To minimize by conceptual design the potential consequences of a core severe accident (CDA), in particular to aim at a low mechanical energy release,
- To maximize, as far as reasonably practicable, the containment resistance and confinement efficiency, thus that means design input conditions not based on the results from the studies associated to the former objective.

In practice, several safety measures are implemented, in particular:

- Conceptual design is oriented so as that core severe accident is prevented even if the safety systems fail. Conceptual design is also oriented so as that a hypothetical core disruptive accident cannot lead to a significant mechanical energy release. Despite this target, materials ensuring mitigation of a hypothetical CDA are designed to withstand, as far as reasonably practicable, to a significant mechanical energy release.
- Conceptual design is oriented so as to limit the radioactive source term mobilized during an accident, concerning either the core or other source terms localized somewhere in the plant site. Even if study results confirm that the mobilized source terms are not significant, structures and equipment ensuring the confinement function, are designed to be efficient for retention and to postpone a possible off-site radiological release.
- Conceptual design is oriented for minimizing the amount of sodium and fission products ejected out of the primary circuit. Despite that, the containment structures around the primary circuit are designed assuming high amount of ejected sodium and radioactive materials, e.g., regarding the pressure loading and the hydrogen risk associated to sodium ejection.
- A core catcher is implemented with capability to retain in safe conditions a large amount of molten core.

5. Essential notions introduced in the safety demonstrations

5.1. Safety demonstration robustness

The robustness notion intends sufficient appropriate measures for getting high level of confidence on the safety demonstrations. This objective involves several measures like for example:

- Justified rules of conservatism for the safety analyses (pessimistic hypotheses, aggravating combination …),
- Validated rules for the treatment of uncertainties,
- Several safety notions like some ones presented below (progressiveness, common mode fault minimization …),
- Demonstration methods translating the safety principles.
- Extended application of D-in-D principle.

It is planned to build safety demonstrations that are convincing through evidences understandable by everybody, for example understandable calculation modeling in particular as regards severe accident scenarios modeling.

5.2. Safety approach progressiveness

Each events family (LOF, LOHS, TOP, SAF) is analyzed by a serial of events with a progressive severity, from anticipated frequent events to postulated hypothetical situations that could lead to a severe accident to be mitigated, and then, if needed, to practically eliminated situations. This progressiveness allows:

- Preventive design provisions to be exhaustive (e.g. appropriate detection-protection devices) as well as for mitigation design provisions,
- To prevent that a too short accidental sequence could lead to a severe accident, that means such a sequence must involve multiple failures not due to a common mode risk.
- To avoid to consider practically eliminated situations which should not be associated to similar but less severe situations mitigated by adequate design provisions.

The benefit of this notion can be illustrated, for example, by progressiveness introduced before a practically eliminated situation (i.e. similar situations classified in other domains before a SPE). For example, when some eliminated situations such as "core-support structure failure" or "radial core compaction" are considered, in fact only few extreme cases are in the SPE domain, most of these cases are covered by postulated situations ranked in SP and SM domains.

5.3. Separation of risks

There exist conventional hazards (e.g. heavy load drop) and specific hazards (e.g. sodium fire) during the operation of the reactor plant. These hazards could have two types of impacts: as an attack of the nuclear island or as a direct risk for human or environmental concerns. The conceptual design is oriented so as to separate, as far as reasonably practicable, the nuclear risk from the other risks, aiming at:

- Risk minimization of possible nuclear plant damage induced by a conventional or chemical accident, in particular this latter must not be an initiator of a severe nuclear accident,
- Prevention of worsening of consequences of a postulated nuclear accident, due to its possible impact on some plant zones containing chemical or conventional risks.

5.4. Common mode risk minimization

When a high level of reliability is already got for a function, in particular thanks to redundancy of safety systems, remaining way to minimize more again the risk of loss of one safety function is to face any common mode risk of multiple failures.

The different sources of common mode failures and equipment that could fail simultaneously are investigated in order to take into account this kind of risk when the conceptual design options are chosen. Among the design provisions against such a risk, some diversification is introduced between systems or components ensuring a same safety function. Different ways to diversify are foreseen depending on the type of failures mode: material diversification, operating conditions (e.g. active or passive modes), spatial segregation, support systems …

5.5. Integration of lessons from the Fukushima accident

One of the major lessons learned from the Fukushima accident is to consider that situations beyond the design basis can occur and that such situation could result from natural hazards, whatever the characteristics of the natural hazards considered for the design. This reinforce the ASTRID approach which considers that despite the high level of prevention, situations with failure of safety systems,(in the SP domain) and additionally severe accidents (SM domain) have to be considered in the conceptual design process. One of the lessons of Fukushima accident is that the more severe situations considered for the design could result from the occurrence of an extreme natural hazards (i.e. natural hazards higher than the ones considered for the design). The first conclusions from that accident, considered for the conceptual process are:

- To identify the hazards which could lead to the cliff edge effect corresponding to high radiological releases in the environment and to check that these hazards are well-beyond the realistic ones considered for the design and defined by the regulation. Additionally, the possible weak points of the concept may be reinforced by design in order to obtain a homogeneous behavior of the plant in case of natural hazard(s), single or combined, higher than the ones considered for the design.

- To assess the time between failure which can potentially lead to the cliff edge effect, and the high radiological release. This time is available for implementing emergency procedures. If relevant, the design could be improved in order to maximize this time (e.g. in case of postulated loss of safety systems).
- To check whether the lists of plant situations already classified in domains SP, SM and SPE, are exhaustively identified (i.e. including hypothetical situations resulting from extreme hazards).
- To define a group gathering a limited number of equipment and other safety provisions, called "hard core", necessary to avoid important radiological releases, in particular equipment needed for mitigation of a severe accident. The "hard core" equipment is designed against natural hazards with significant margins in comparison with the design hazards considered for the plant design (e.g. margins equivalent to one decade lower in terms of hazard probability could be pointed out, for information). Following this approach, the "hard core" equipment has to be protected against any potential consequences of the extreme hazards, e.g. failure of other equipment that could endanger this latter.

In addition, other lessons from the Fukushima accident are relevant:

- Autonomous behavior of the systems, autonomy duration, passiveness and grace delay have to be promoted by conceptual design, in order to limit any need of supply sources (power, water, inert gas …), of automatic control actions, and to give time for backup operator actions.
- A severe accident could be a consequence of single or combined extreme hazard(s), and thus, among events families considered as initiating transients towards a severe accident, initiating conditions of a severe accident representative of an extreme hazard loading have also to be taken into account in the frame of severe accident studies (SM domain). In particular, some equipment involved in the lines of mitigation (LoM) is included in the "hard core".
- A natural hazard exceeding the reference design case must not be originally the cause of a "cliff edge" effect on the consequences. Following this approach, among the materials involved in the safety demonstration of a situation "practically eliminated", some of them equivalent to one line of defense (LoD) are ranked in the "hard core".

6. Design approach implementation based on cross-analyses

In order to get an exhaustive safety design approach, "cross-analyses" are implemented early at the conceptual design phase:
- Analysis by safety functions all over the power plant (e.g. design analysis of SSC),
- Analysis by operating conditions and plant situations (e.g. analyses by events or by plant states).

6.1. Approach by safety functions

6.1.1. Neutron reactivity mastery
First step of the conceptual design is rather conventional:
- To prevent any initiating fault resulting in either slow or fast reactivity insertion,
- To implement two main shutdown systems designed following stringent negative reactivity criteria and diversification criteria.

In addition, other safety design provisions, relating to the reactivity mastery, are taken into account in ASTRID, either as prevention or as mitigation measures:
- To prevent by natural reactor behavior, in particular by core feedbacks, any entrance in a severe accident scenario in case of transients without scram. Once this risk is overcome, a comeback to a safe state (i.e. zero fission power at low temperature) is achieved at long term thanks to a complementary safety device (CSD) if needed.
- In case of hypothetical entrance in a severe accident, to prevent any escalation into a high power excursion (i.e. prompt criticality) so as to exclude a significant energetic CDA scenario.
- During the different degradation phases of severe core accident, the risk of re-criticality is managed either by natural behavior or by additional design provisions, so as to limit cumulative

energy production. As an objective, design devices (CSD) allowing an early transition towards a degraded core phase driven only by decay heat, is sought through R&D efforts.

Definitively subcritical degraded configurations should be reached in the core region as well as in the core debris tray, in a final phase.

6.1.2. Heat removal mastery

As an objective, total and definitive loss of "heat removal" function has to be practically eliminated (SPE). In order to build the related safety demonstration, an equivalent of three lines of defense (LoD) has to be implemented. As a general rule, a system achieving a strong LoD has to be reliable and therefore is designed with stringent rules, so each corresponding DHR system has to be designed consistently with the "single failure" criterion (CDU). The reliability of these three LoD can be favorably combined only if the risk of common mode failures is minimized. For this aim, a total diversification is thought between the DHR systems, through the conceptual design of ASTRID, that means diversified materials, diversified operating conditions (e.g. passive versus active) and also diversification relating to:

- Inherent sodium risk (e.g. freezing): alternative cooling fluids (NaK and/or oil) and heat sink sources (water versus air) are investigated,
- Geographic location: an auxiliary cooling system located in the reactor vault is investigated, as a totally different DHR means in comparison with the circuits of the main DHR systems, running through the reactor roof.

After a hypothetical core severe accident, a "heat removal" safety function is also required to achieve the containment function, in particular to cool the core debris tray and then the containment structures. A hypothetical CDA could alter the primary sodium convection and also could impact the heat exchangers implemented in the primary circuit (i.e. risk of DHR circuits leakage). Thus, the post-severe accident heat removal means must be protected against the mechanical effects of a hypothetical energetic CDA (see section 4.2). So, a thermal-hydraulic backup loop connecting the heat transfer from the corium to be cooled towards the post-accident DHR system (e.g. reactor vault auxiliary cooling system) and then with the ultimate heat sink, is anticipated by conceptual design.

The post-severe accident heat removal function is a very long term function requiring: reliability of heat sink, autonomy duration of DHR circuits, grace delay and passiveness features. All these concerns are taken into account in the conceptual design phase.

The ultimate DHR means acting for the DHR function in one side (included in SPE demonstration) and for the post-severe core accident function in the other side (same or different means for these two different functions), are designed according to the ''hard core'' requirements.

6.1.3. Containment and Confinement mastery

In order to cope with all potential risks there exist in the power plant site, a generic approach by barriers is applied for the nuclear sources as well as for conventional or chemical risk. This latter is considered both as aggression of the nuclear areas and as possible source of toxic releases. Physical and dynamical separations are implemented, if needed with detection-protection devices, so as to prevent abnormal plant situations worsened by common mode failures or by aggravating events.

In the frame of this approach, the risk of sodium interactions is either made physically impossible by the design options choice (e.g. sodium-gas heat exchanger instead of steam generator concerning the risk of sodium-water interaction) or reduced by design provisions (e.g. room with limited air volume and large air-exit outlet concerning the risk of sodium fire). The risk of off-site aerosols release from a sodium fire is minimized by the conceptual design, complying at least with the existing regulation applicable for any facility classified for environmental protection (ICPE).

As concerns the application of the D-in-D level 4 and the risk of radiological consequences in general, a specific design approach, called« Top-Down » approach, is applied through the « Lines of Mitigation » method (LoM). This approach is illustrated above in sections 4.1 and 4.2.

6.2. Approach by events or plant states

6.2.1. Approach by events family

Six types of initiating events are considered and defined with a progressive escalation starting from the DB category 2 and for each category or domain, up to the SPE:

- Slow or fast loss of flow (LOF),
- Slow or fast transient of overpower (TOP),
- Local subassembly fault involving sodium boiling or fuel melting phenomenon (SAF).

The approach consists in reducing the probability of each considered event but also, concerning the plant situations, in making acceptable their consequences in such way that most of the situations are ranked in SP domain. One of the objectives is thus to reject in the SM domain a limited number of situations resulting from input data quite nonrealistic (e.g. pessimistic inserted reactivity law in comparison with possible natural phenomena) and when their consequences are not reasonably manageable by mitigation means, to eliminate these ultimate cases (SPE) through appropriate safety demonstrations.

A new approach is in particular envisaged as regards the SAF family for ASTRID. The benefit, in terms of safety, of the progressiveness considering various events from a "partial fuel subassembly blockage" without melting towards the risk of "global core meltdown" propagation, is as follows:

- Exhaustive sensitivity studies on efficient detection-protection devices for different local fault sizes and types,
- Knowledge and understanding of the physical evolution of different cases of fuel subassembly fault (e.g. interaction phenomena, propagation delay),
- Tacking account of a global core meltdown induced by a SAF with the aim, among other objectives, to demonstrate that this scenario of CDA is not energetic.

In the previous SFR approach, only one case of fuel subassembly melting was postulated: the "total and instantaneous blockage" (TIB).

6.2.2. *Core disruptive accident studies*

The assessment of the potential consequences of a severe accident is based on studies considering all the initiating events families that could influence the consequences. In comparison with the previous SFR approach, the choice of only one accident scenario as the reference sequence cannot be postulated, but would be the result of the studies if one of the different scenarios is enveloping all the others.

The typical safety demonstration, based on theoretical and experimental knowledge of the phenomena, takes also account of some validation limits concerning the calculation modeling in such a domain where full scale tests, including "system effect", are not feasible. Thus, the safety demonstration robustness will depend on the methods used to be free from the validation and qualification limits of the modeling. In this kind of approach, identification of the main key parameters leading on to the significant consequences, as well as verification of no risk of "cliff edge effect" by sensitivity study, are essential elements of the demonstration.

7. Concluding remarks on ASTRID safety orientations

The conceptual design phase in progress of ASTRID project is supported by the Safety Orientations Document (DOrS) which influences the definition of the design studies, the choice of the basic design options, and also allows exchanging earlier with the Safety Authority and the associated technical support bodies, with a view to initiating the licensing process. In France, the last licensing process dates from the RNR-1500 project in the early 80's. Thus, the ASTRID project intends to include worthwhile safety experiences gathered since this period, by means of safety orientations which translate this feedback in well-defined safety analysis methods and recommendations for the conceptual design.

In comparison with the previous SFR, new safety features are formulated in the DOrS in particular on:

- Safety improvements concerning the local faults (e.g. ICRW),
- More in depth prevention of severe accident, favoring in particular the natural behavior of the reactor (i.e. unprotected transients),

- New approach devoted to the severe accident, considering all the initiating events families and with alternative approaches (i.e. not only mechanistic and best estimate) compensating for unavoidable limited validation field,
- Integration of Fukushima lessons, involving a new analysis of the BDB domain and the definition of a "hard core",
- Safety demonstrations justifying the "practical elimination" of some extreme situations,
- Rational classification of the SSC not only based on the significance of the safety functions ensured,
- Implementation of specific analyses methods translating, at the conceptual design phase, all the major safety principles that must be applied.

The aim of this paper has been to introduce and comment some specific safety orientations extracted from the ASTRID Safety Orientations Document.

NOMENCLATURE

BDB	Beyond Design Basis domain
CCF	Common Cause Faults
CDA	Core Disruptive Accident
CDU	"Critère de Défaillance Unique"
CSD	Complementary Safety Devices
DB	Design Basis domain
DHR	Decay Heat Removal
D-in-D	Defence-in-Depth principle
DOrS	Safety Orientations Document
DOS	Safety Options Report
EFR	European Fast Reactor project
ICPE	"Installation Classée pour la Protection de l'Environnement"
ICRW	inadvertent Control Road Withdrawal
LOF	Loss Of Flow
LOHS	Loss Of Heat Sink
RNR-1500	French SFR project following Superphenix (also called SPX-2)
TIB	Total and Instantaneous fuel assembly Blockage
TOP	Transient of Over-Power
S.A.	Severe Accident
SAF	Sub-Assembly Fault
SM	"Situations of Mitigation" domain
SP	"Situations of Prevention" domain
SPE	"Situations Practically Eliminated" domain
SSC	Structures, Systems and Components

REFERENCES

[1]   F. Gauché; The French Prototype of 4th Generation Reactor: ASTRID; Annual meeting on nuclear technology, Berlin, May 17&18th; 2011.

[2]   P. Le Coz *et al.*; Sodium-cooled Fast Reactors: the ASTRID plant project; Proceedings of ICAPP'11, Nice France, May 2-5, 2011; Paper 11249.

[3]   Western European Nuclear Regulator's Association; Safety objectives for new power reactors, studied by WENRA Reactor Harmonization Working Group, December 2009.

LFR safety approach and main ELFR safety analysis results

E. Bubelis[a], M. Schikorr[a], M. Frogheri[b], L. Mansani[b], G. Bandini[c], L. Burgazzi[c], K. Mikityuk[d], Y. Zhang[d], R. Lo Frano[e], N. Forgione[e]

[a] Karlsruhe Institute of Technology, Eggenstein-Leopoldshafen, Germany

[b] Ansaldo Nucleare, Genova, Italy

[c] ENEA, Bologna, Italy

[d] Paul Scherrer Institute, Villigen PSI, Switzerland

[e] CIRTEN - University of Pisa, Pisa, Italy

Abstract. This paper summarizes the approach to safety for the LFR systems, developed on the basis of the recommendations of the Generation IV International Forum (GIF) Risk and Safety Working Group (RSWG) and taking into account the fundamental safety objectives and the Defence-in-Depth approach, as described by IAEA Safety Guides, as well as the Safety quantitative objectives reported in the European Utilities Requirements (EUR). LEADER project activities are focused on the resolution of the key issues as they emerged from the 6th FP ELSY project attempting to reach a new industrial size European Lead-cooled Fast Reactor (ELFR) configuration. Apart from the safety approach, the main results of the ELFR safety transient analysis, where the most important design basis condition (DBC) and design extension condition (DEC) transient initiators were re-analyzed using the system codes RELAP5 (ENEA), TRACE-FRED (PSI), SIM-LFR (KIT) and SIMMER (CIRTEN), are summarized.

1. INTRODUCTION

The LEADER (Lead-cooled European Advanced DEmonstration Reactor) project, funded by the European Commission in the frame of 7th framework program, aims to the development to a conceptual level of a Lead Fast Reactor Industrial size plant and of a scaled demonstrator of the LFR technology - ALFRED.

The project started from the results achieved in the previous ELSY (European Lead-cooled SYstem) project (6th FP), during which a pre-conceptual design of an industrial plant (600 MWe) was developed. Safety analysis of the re-designed ELFR was performed addressing all the "weak" points in the LFR design that were determined during the previous ELSY project. All the most important design basis condition (DBC) and design extension condition (DEC) transients were repeatedly reanalyzed for the re-designed ELFR configuration and conclusions from this activity are presented in this paper.

2. SAFETY APPROACH FOR LFR PLANT

As one of the six currently developed and analyzed Generation IV reactor systems – LFR, follows the general guidelines of the Generation IV safety concept recommendations. Among the goals for future nuclear energy systems, improved safety and higher reliability are recognized as an essential priority

in the development and operation of nuclear power plants. A global safety approach for the LFR reference plant has been assessed and the safety analyses methodology has been developed [1].

The fundamental safety objectives and the Defence-in-Depth (DiD) approach, as described by IAEA Safety Guides, have been preserved. The ideal outcome will be a design that optimizes both capital costs and safety by applying defence in depth where it will have the desired effect, but not to "over-design" in a way that adds cost but provides little additional value in safety.

The recommendation of the Risk and Safety Working Group (RSWG[1]) has been taken into account, in particular:

- safety is to be **"built-in"** to the fundamental design rather than **"added on"**;

- full implementation of the Defence-in-Depth principles in a manner that is demonstrably exhaustive, progressive, tolerant, forgiving and well-balanced (e.g. rejection of "cliff edge effects" and availability of a sufficient grace period and the possibility of repair during accidental situations);

- "risk-informed" approach - deterministic approach complemented with a probabilistic one;

- adoption of an integrated methodology that can be used to evaluate and document the safety of Gen IV nuclear systems - Integrated Safety Assessment Methodology (ISAM). In particular the Objective Provision Tree (OPT) tool is the fundamental methodology used throughout the design process. The OPT is a top-down method which, for each level of DiD and for each safety objective/function, identifies the possible challenges to the safety functions, their related mechanisms, and the provisions needed to prevent, control or mitigate their consequences.

3. ELFR PLANT REFERENCE CONFIGURATION

The configuration of the ELFR primary system (Fig. 1) is pool-type [2]. This concept permits to contain all the primary coolant within the Reactor Vessel, thus eliminating all problems related to out-of vessel circulation of the primary coolant.

The Reactor Vessel (RV) is cylindrical with a torospherical bottom head. It is anchored to the reactor cavity from the top, by means of a vessel support. A steel layer covering the reactor cavity, constitutes the Safety Vessel (SV). The primary coolant always covers the SG inlet so to indefinitely maintain the lead flow path. The volume between the primary coolant free levels and the reactor roof is filled with an inert gas.

The core is made of 427 hexagonal and wrapped fuel assemblies (FAs) and 24 control/safety assemblies. Each FA is about 10 m long and consists of 169 fuel pins, fixed to the bottom of the wrapper and restrained sideways by grids. To maintain each fuel element in its position, a tungsten deadweight (Ballast) counterbalances the lead buoyancy during refueling.

The Inner Vessel (IV) the first structure around the core, has two main functions: 1) Fuel Assemblies support, and 2) Hot and cold plenum separation.

The LFR plant is equipped with two diverse, redundant and separate shutdown systems: 1) gravity driven system (only shutdown) passively inserted by a pneumatic system (by depressurization) from the top of the core. In case of failure of the pneumatic system, the safety rods are equipped with tungsten ballast that forces the absorber down by gravity with a lower velocity; 2) control/shutdown system inserted from below the active core zone using the strong lead buoyancy.

---

[1] The RSWG was formed in the frame of Generation IV International Forum (GIF) to promote a homogeneous and effective approach to assure the safety of Generation IV nuclear energy systems

The eight steam generators and primary pump are integrated into separate vertical units. The primary pump is placed in the centre of the flat-spiral type steam generator, having its mechanical suction in the hot pool inside the inner vessel. The primary coolant moves upward through the pump impeller to the vertical shaft and then transversally (radially) through SG tubes on the shell side out of the steam generator to the downcomer through perforated double-wall casing.
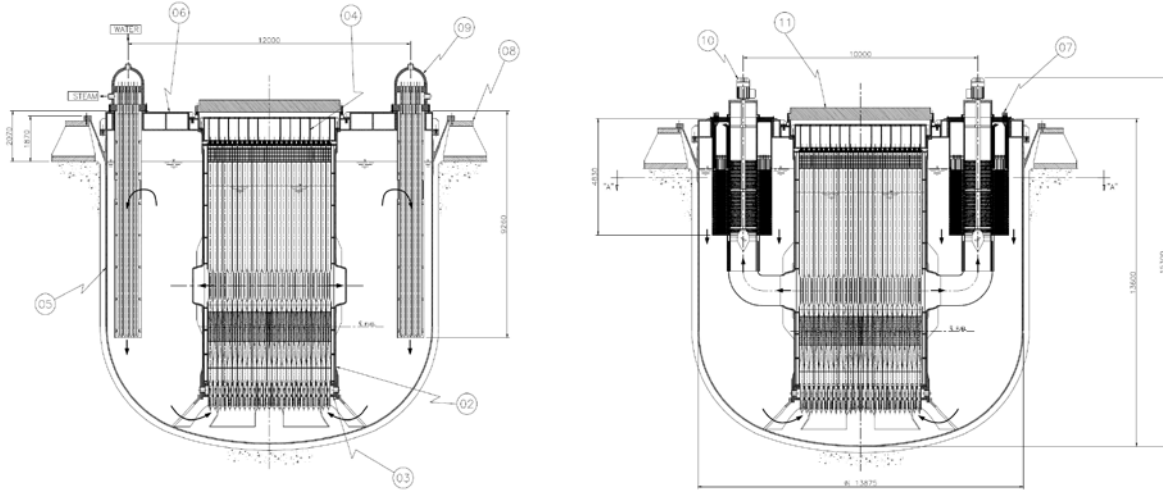
FIG. 1. Reactor block vertical sections: 01) Fuel assembly ;02) Inner vessel; 03) Core lower grid; 04) Core upper grid; 05) Reactor vessel ; 06) Reactor cover; 07) Steam Generator; 08) Vessel support; 09) DHR dip cooler; 10) Primary pump; 11) Reactor FAs cover)

The Decay Heat Removal system consist of two independent, redundant and diverse systems: 1) The Isolation Condenser System (IC) connected to the Steam Generator (i.e. four units provided on four out of eight plant steam generators); 2) DHR-2 System, constituted of four independent loops, equipped with eight dip coolers operating with water, immersed in the reactor pool. Both systems are completely passive, with an active actuation (valves). The IC system is the first line of defence whereas the DHR-2 comes into operation only in case of failure of the first one.

Each component inside the Reactor Vessel is removable and the fuel assemblies upper end extends beyond the lead free surface in the cover gas for refueling, without the need of in-vessel machines. This design solution is viable because the refuelling could be performed by opening the reactor cover (a flat steel plate with penetrations for the Steam Generator/Primary Pump units and Dip coolers) and accessing the fuel assemblies directly from the containment.

4. SUMMARY OF THE ELFR SAFETY ANALYSIS

As it was already mentioned before, safety analysis of the ELFR was performed testing all the "weak" points in the LFR design that were determined during the previous ELSY project. The most important design basis condition (DBC) and design extension condition (DEC) transients were repeatedly reanalyzed for the re-designed ELFR configuration.

The full list of the analyzed transients for ELFR is as follows:

- Protected loss of flow transient (PLOF),
- Unprotected loss of flow transients (ULOF),
- Unprotected loss of heat sink transient (ULOHS),
- Unprotected reactivity insertion transient (UTOP),
- Unprotected loos of flow and loss of heat sink transient (ULOF+ULOHS),

- Protected overcooling transient (OVC),
- Protected steam line break transient (SLB),
- Unprotected sub-assembly (SA) blockage transient, and
- Steam generator tube rupture (SGTR) accident.

The main results of all the analyzed unprotected transients are briefly presented in the following sub-sections of this paper.

4.1. *Unprotected loss of flow transient (ULOF)*

The Unprotected Loss of Flow (ULOF) accident is initiated by the drop of primary pump head with a halving time of the pump of 0.56 seconds. During the entire ULOF transient, the reactor protection system failed to operate, but the steam generator (SG) could work normally.

As the primary coolant flow starts to decrease (Fig. 2), the core power shortly increases to around 1600 MW, which is due to the positive reactivity feedback incurred by the coolant temperature increase. After the coolant temperature increase moves from core active region to core diagrids and pads, significant negative reactivity feedbacks will be generated due to the radial expansion of diagrids and pads. This negative reactivity feedback, together with other negative reactivity feedbacks induced by fuel axial expansion and the Doppler effect, can take over the positive reactivity feedback caused by coolant density decrease. Hence, core power will begin to decrease and eventually stabilize at approximate 1200 MWth (Fig. 2). Besides, the maximum temperatures of fuel and clad will also decrease and reach ~ 1400 ^{o}C and ~ 700 ^{o}C after 300 seconds into the ULOF transient (Fig. 3).
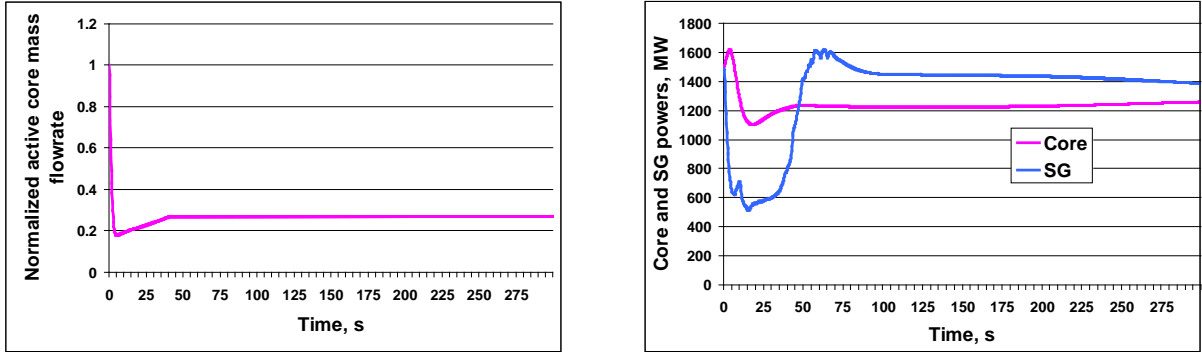
FIG. 2. Evolutions of primary coolant flowrate (left) and core/SG power (right) with time for End-of-Cycle (EOC) as calculated by TRACE/FRED (PSI)
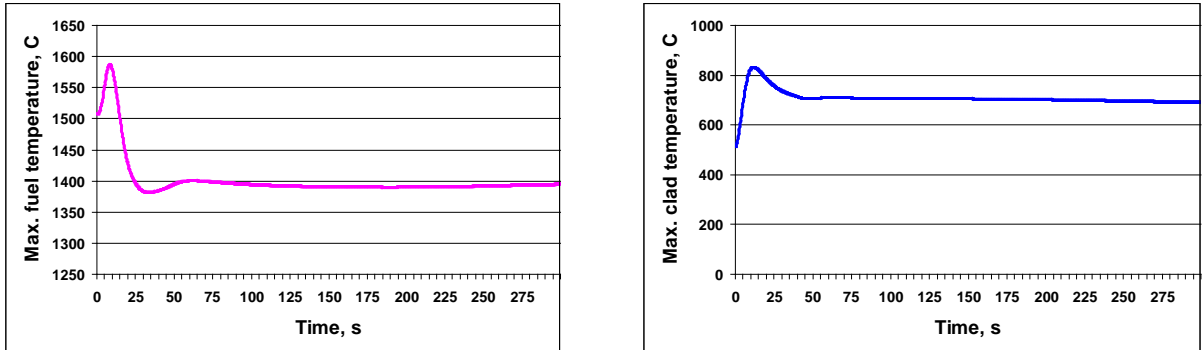
FIG. 3. Evolutions of the peak fuel (left) and clad (right) temperatures with time for End-of-Cycle (EOC) as calculated by TRACE/FRED (PSI)

Since SG power will be higher than core power after 50 seconds into the transient (Fig. 2), the maximum temperature of clad will continuously decrease. The highest temperatures that can be attained by fuel and clad of the peak fuel pin during ULOF are 1586 ^{o}C and 828 ^{o}C respectively, lower than their corresponding failure limits as minimum clad failure times of 10^{+5} seconds under the minimum coolant flow conditions (flow undershoot conditions) are calculated.

Based on the above observations one can state that the ELFR plant as designed can accomodate a ULOF transient.

4.2. *Unprotected loss of heat sink transient (ULOHS)*

The unprotected ULOHS transient is initiated by the loss of feedwater to all steam generators without reactor scram. The secondary circuits are automatically isolated and the DHR-1 system is activated (3 out of 4 IC loops are supposed to be in service).

The primary system remains in forced circulation, so the core mass flow rate does not significantly decrease during the transient (Fig. 4). The core power progressively reduces (Fig. 4) towards the decay level due to negative reactivity feedbacks introduced by the core temperature increase. The steam generator power (Fig. 4) in excess to DHR-1 power in the first 1000 s of the transient is caused by water vaporization and steam release to the atmosphere through the relief valves, because of the over pressurization of the secondary circuits in the initial phase, after their isolation and DHR-1 start up.
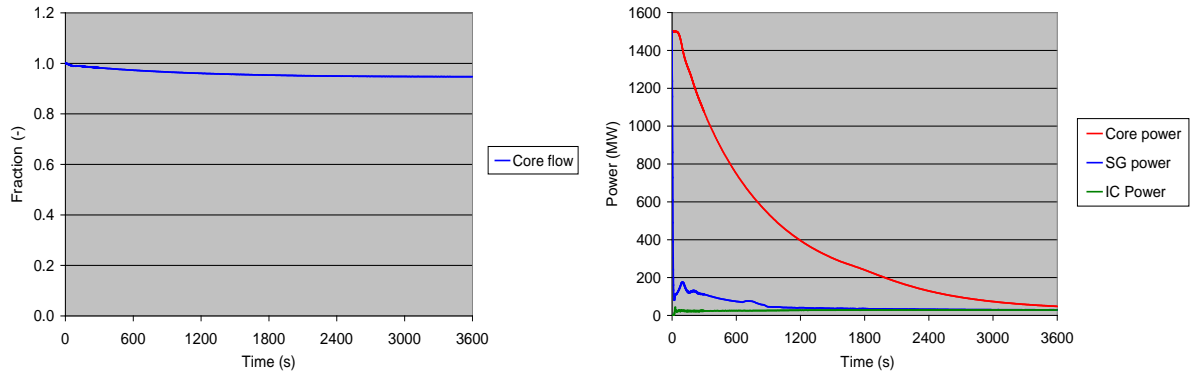
FIG. 4. Evolutions of core mass flowrate (left) and core/SG/IC powers (right) with time for EOC as calculated by RELAP5 (ENEA)
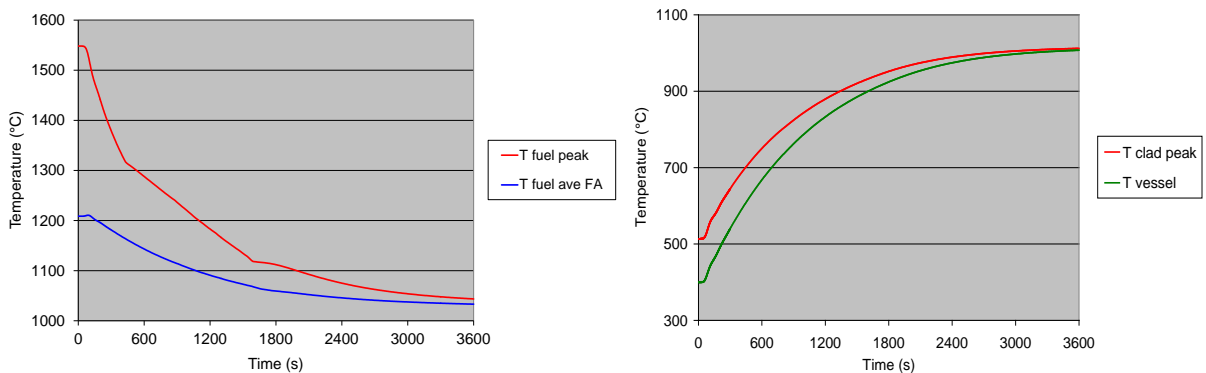
FIG. 5. Evolutions of peak fuel (left) and clad/vessel wall (right) temperatures with time for EOC as calculated by RELAP5 (ENEA)

The primary temperature progressively increases because of the strong mismatch between core power and heat removed by the secondary side of SG. At the same time, the ΔT through the core reduces according to the power decrease, leading to a practically uniform temperature distribution in the whole primary system. Also the vessel wall temperature reaches the equilibrium with the lead temperature in the medium term. As the power level decreases, the maximum fuel temperatures decrease close to clad temperatures (Fig. 5). After one hour, the level of temperature reached in the primary system is about 1000 °C, so that the integrity of the fuel rod clad cannot be assured from this point onward. However, the most challenging situation involves the vessel structure. Because of the very high temperature increase, the structural integrity of the vessel cannot be guaranteed in the long term.

4.3. Unprotected loos of flow and loss of heat sink transient (ULOF+ULOHS)

The unprotected ULOF+ULOHS transient is initiated by the simultaneous loss of primary pumps and of feedwater to all steam generators without reactor scram. The secondary circuits are automatically isolated and the DHR-1 system is activated (3 out of 4 IC loops are supposed to be in service). The results of these calculations are very similar to those of the ULOHS case as sufficient natural circulation (> 10% nominal) in the ELFR assures sufficient mixing of the coolant throughout the primary system. Again, high vessel temperatures cannot guarantee the long term structural integrity of the vessel.

4.4. Unprotected reactivity insertion transient (UTOP)

ELFR overpower transient at Hot Full Power (HFP) and EOC conditions is reported in this section, namely: 260 pcm reactivity insertion within 10 sec time interval.

As can be observed in Fig. 6, an insertion of 260 pcm in 10 sec time interval at EOC conditions leads to a power jump of ~ 2.42 nominal. The maximum fuel and clad temperatures under EOC conditions increase from 1539°C and 513°C to 2677 °C (fuel in the fuel pellet center will start melting, but fuel melting will not progress to the fuel pellet surface) and 719 °C respectively (Fig. 6).
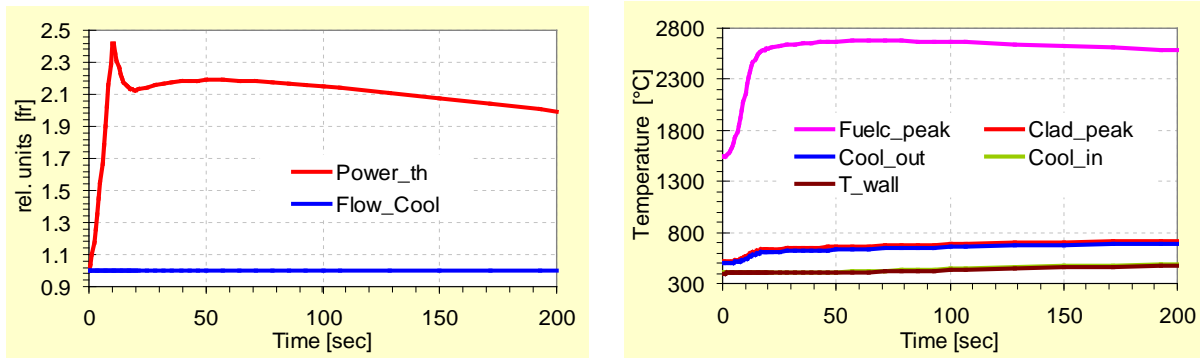
FIG. 6. Evolutions of core power and flowrate (left) and peak fuel/clad/coolant/vessel wall temperatures (right) with time for EOC as calculated by SIM-LFR (KIT)

From the performed analysis one can see, that ELFR reactor peak fuel pin cladding survives this transient, however local fuel melting should be expected in the center of the peak fuel pins (pellets).

4.5. Unprotected sub-assembly (SA) blockage transient

Two types of calculations were performed (for both cases nominal power at HFP, no reactor trip and no radial heat transfer are assumed) when analysing unprotected SA blockage transient:

Case 1: The flow area through the hottest SA is blocked 97.5% instantly at 1 sec transient time. Thus a flow area of only 2.5% remains open for the flow of coolant. Of interest here is time to clad failure after blockage initiation.

Case 2: The maximum clad temperatures of the peak pin as a function of the blockage area are determined.

The simulations were performed using SIM-LFR code. However it should be noted here that in both cases it was assumed that coolant flow in the blocked SA is linearly proportional to the SA blocked flow area.

For the 97.5% SA blockage transient at EOC, the peak pin will fail ~93 sec into the transient (transient initiation at 1 sec transient time) as the cladding temperature will reach 1015 °C (Fig. 7), with a peak pin fission gas pressure of ~41 bar.

As a result of the SA blockage, the flow rate will initially decrease to ~ 14 % nominal, gradually recovering to about 24% flow rate at ~50 sec into the transient due to changing SA pressure conditions. The power remains at 100% nominal throughout the transient (Fig. 7).
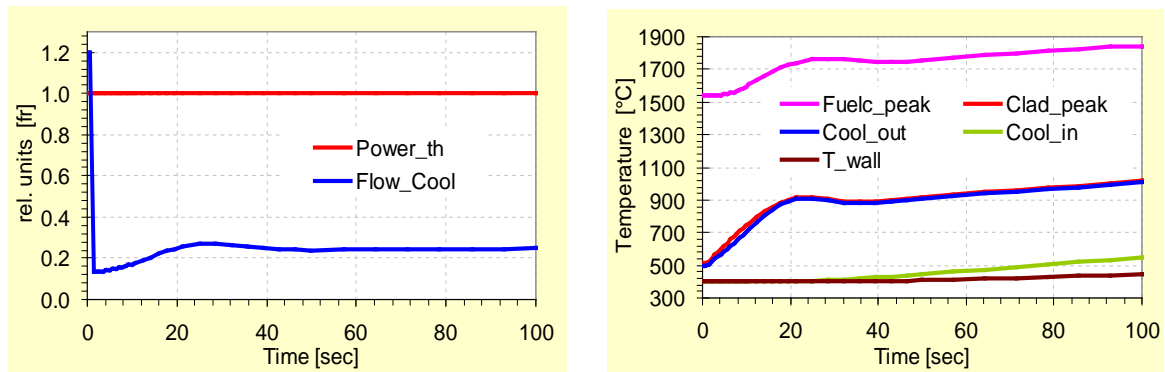
FIG. 7. Evolutions of core power and flowrate (left) and peak fuel/clad/coolant/vessel wall temperatures (right) with time for EOC as calculated by SIM-LFR (KIT); Case 1 (97.5% flow area blockage)

When determining the maximum clad temperatures of the peak pin as a function of blockage area – analyzing Case 2, several different cases were run at EOC conditions, varying the blockage area ranging from 20% to 97.5% (20, 40, 60, 65, 70, 75, 80, 90, 95 and 97.5%). Simulation results are presented in Fig. 8.

Following the performed analysis, it can be stated that:

(1)   The ELFR will not experience any fuel pin failure for blockage areas less than 75%, even under unprotected conditions;

(2)   For blockages above 75%, clad failures must be expected (Fig. 8);

(3)   Fuel melting is not an issue for the ELFR. Fuel melting temperatures are not reached even in 97.5% SA blockage case.
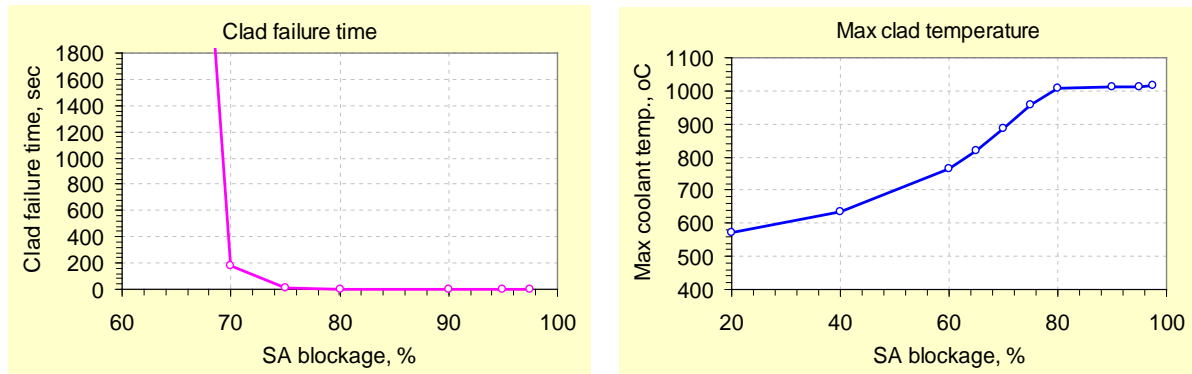
FIG. 8. Evolutions of clad failure time (left) and peak clad temperature (right) with time for EOC as calculated by SIM-LFR (KIT); Case 2

4.6. *Steam generator tube rupture (SGTR) accident*

The SGTR accident initiates with the postulated sudden rupture (induced by a variety of degradation processes, such as cracking, wall thinning, etc.) of one or more SG tubes. As a result, a water flow rate is injected into the hot lead (lead-water interaction - LWI) determining the resultant pressure peak due to water vaporization. The induced consequences of the SGTR tube rupture failure (e.g. production of high pressure steam bubbles, pressure wave propagation in the SG itself and/or in the whole primary system) are strictly dependent on the injected water flow rate and total inventory interacting with hot lead.

Two types of calculations have been performed with SIMMER III code: sub-series A and B, simulating respectively the single and double-ended guillotine rupture. In the latter case check valve failure was also assumed. Moreover water flow rate limiting mechanisms, such as the adoption of a Venturi nozzle, was placed inside each spiral tube to limit the amount of water injected (A3 simulation).

Basically, without any engineering safeguards, the initial interaction of the two fluids results in an instantaneous vaporization of injected water, responsible for the pressurization of the inner SG region. This is a very conservative hypothesis that needs experimental verification. In some reported experiments at higher pressures [3] only a small fraction of the injected water vaporized as most of the water (77.2% of the injected water mass) was transported in liquid form inside the steam bubbles to the cover gas region to be then separated into small droplets above the free lead surface.

The pressure peak (the duration of which is in the order of 10^{-4} s and thus not relevant from a mechanical point of view), close to the rupture location, reached ~140 bar in all the B sub-series and ~120 bar in all the A sub-series (Fig. 9) simulations, while the mean pressure in both cases is below 20 bar.

The pressure peak induced a lead displacement upwards in the SG pressurizing and compressing the cover gas, a second pressure peak (of about 35 bar in the A sub-series simulations) appears close to the upper SG plate.

The adoption of a Venturi nozzle allows limitation of the water mass flow rate injected into the lead and, in turn, the peak pressure due to LWI is greatly reduced. The maximum pressure close to the upper SG plate was less than 10 bar (Fig. 9), and the calculated mean value was about 3 bar.
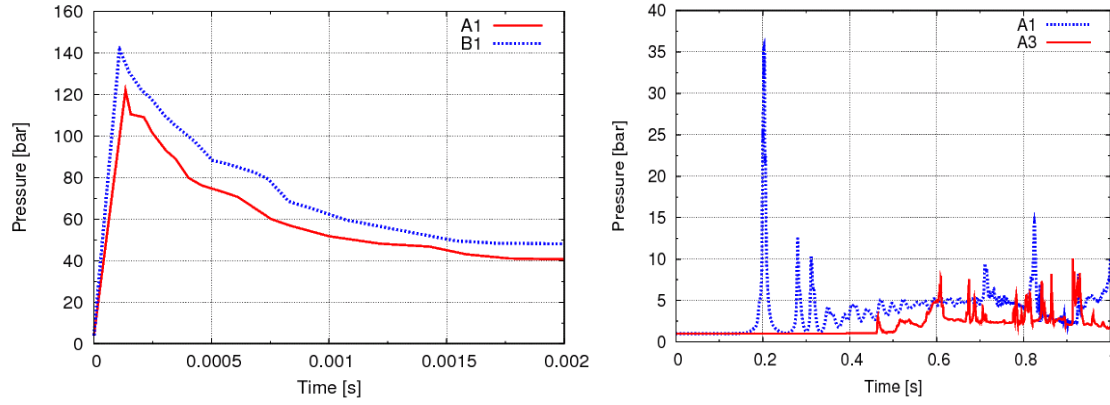
FIG. 9. First pressure peak inside the lead region close to the rupture (left) and pressure impulse on the upper plate (right), as calculated by SIMMER (CIRTEN)

Following this preliminary analyses, it can be stated that:

(1)   without any engineering safeguards or limiting mechanisms (e.g. Venturi nozzle, safety valves on the upper side of the vessel, etc.), the LWI induced pressures, in case of instanteneous vaporization, could be severe enough to lead to structural risks for the SG itself (e.g. collapse of adjacent tubes), while it poses no likely threat for the integrity of the in-vessel structures;

(2)   the vapour bubbles, generated during the LWI, have difficulty in reaching the core inlet section, as confirmed by the KALLA experimental data, under the action of the drag force produced by the liquid metal flowing downward in the downcomer region of the reactor (see also [3]).

5. CONCLUSIONS

In the framework of the LEADER project, the safety approach for a European Lead-cooled Fast Reactor (ELFR) has been defined and, in particular, all the possible challenges to the main safety functions and their mechanisms have been specified, in order to better define the needed provisions.

Safety analysis of the ELFR was performed testing all the "weak" points in the LFR design that were determined during the previous projects. The most important design basis condition (DBC) and design extension condition (DEC) transients were repeatedly analyzed for the re-designed ELFR configuration. The results of the safety analyses can be summarized as follows:

- Protected transients (PLOF, OVC and SLB): the automatic reactor shutdown activated by different scram signals is able to rapidly bring the ELFR plant to safe plant conditions. The consequent isolation of the secondary circuits and start up of decay heat removal system is able to maintain the plant in safe conditions in the medium and long term. In all transients, the potential of lead freezing in the coldest points of the primary system is reached after several hours into the transient, assuring sufficient grace time for manual, corrective operator action.

- Unprotected transients (ULOF; ULOHS and ULOF + ULOHS): due to the enhanced natural convection capability in the primary circuit, in case of ULOF the maximum temperatures reached in the primary system are low enough to assure the integrity of the clad and the vessel in the short term, providing sufficient grace time for corrective operator action.

  The main potential safety issue is the maximum reactor vessel wall temperature that might exceed 700 °C within ~12 min. The integrity of the clad and the vessel seems not guaranteed in the medium/long term, because of the high temperatures reached in the primary system. An optimization of the neutronic core design, in order to reduce the positive coolant expansion reactivity feedback could provide additional grace time.

- Reactivity insertion: for reactivity insertion of 200 pcm in 10 sec time interval at EOC conditions, peak fuel pin cladding survives and fuel melting is not observed, even in the center of the peak fuel pins (pellets). For reactivity insertion of 260 pcm in 10 sec time interval at EOC conditions, peak fuel pin cladding survives, however fuel melting should be expected in the center of the peak fuel pins (pellets). These transients envelope positive reactivity insertions of the Design Basis events such as fuel handling errors, control rods withdrawal or seismic core compaction.

- FA flow blockage: for blockages less than 75% blockage area, it is not expected any pin failures nor fuel melting, even under unprotected conditions. For blockage above 75%, peak power pins clad failure shall be expected, but fuel melting is not expected even for blockage over 97.5%. However there is time (several hundreds seconds) to detect the flow blockage occurrence, by means of temperature measuring devices installed at each FA outlet.

- SGTR accident: several limiting mechanisms and potentially important effects have been analyzed and suggest that: (i) the initial pressure shock wave poses no likely threat to in-vessel structures, except very few adjacent heat-exchange tubes; (ii) the sloshing-related fluid motion is well bounded in a domain beyond the heat exchanger; and yet (iii) the steam/water entrainment is expected to be comparatively limited due to the very large difference of density between steam and lead. The potential gradual pressurization of the vessel after SGTR due to inflow of the steam is limited by rupture disks to relief the resulting over-pressure. Moreover, a Venturi nozzle placed inside each spiral tube, mitigate the severity of SGTR interaction and reduce the potential effects on the entire reactor system. Anyway, a dedicated scaled facility should be foreseen to analyze in depth the SGTR phenomena further as part of the future R&D activities.

In order to assure prevention of freezing of the lead coolant at the coldest location of the primary loop, a tight and continuous operational control of the secondary coolant conditions is needed. Under certain adverse transient conditions it is conceivable that the primary lead HX outlet temperature (nominally 400°C, well above the freezing point of lead (327°C)) decreases to the feedwater inlet temperature 335°C, (only 8 °C margins to freezing). In addition, any malfuction in the FW temperature control could progressively bring the coolant to its freezing point.

In general, the safety analysis performed for the lead-cooled ELFR design demonstrated the extremely robust nature of this plant design when compared to other similar plant designs, ascribable to the inherently, large thermal inertia of the lead-cooled primary system and optimization of safety relevant control, safety systems and components.

Acknowledgements

References

[1]   ALEMBERTI, A., et al., "The European lead fast reactor: design, safety approach and safety characteristics", IAEA Technical Meeting on Impact of Fukushima event on current and future FR designs, Dresden, Germany (2012).

[2]   ALEMBERTI, A., et al., "The Lead fast reactor - Demonstrator (ALFRED) and ELFR design", International Conference on Fast Reactors and Related Fuel Cycles: Safe Technologies and Sustainable Scenarios (FR13), Paris, France (2013).

[3]   BEZNOSOV, A.V., et al., "Experimental studies of the characteristics of contact heat exchange between lead coolant and the working body", Atomic Energy, Vol. 98, No. 3, 2005.

Safety analysis results of the DBC transients performed for the ALFRED reactor

E. Bubelis[a], M. Schikorr[a], L. Mansani[b], G. Bandini[c], K. Mikityuk[d], Y. Zhang[d], G. Geffraye[e]

[a] Karlsruhe Institute of Technology, Eggenstein-Leopoldshafen, Germany

[b] Ansaldo Nucleare, Genova, Italy

[c] ENEA, Bologna, Italy

[d] Paul Scherrer Institute, Villigen PSI, Switzerland

[e] CEA, Lyon, France

Abstract. The LEADER project aims at the development to a conceptual level of a Lead Fast Reactor Industrial size plant and at a scaled demonstrator of the LFR technology - ALFRED. This paper presents the main safety analysis results of the selected set of DBC (Design Basis Condition) transients for the ALFRED reactor. Apart from the traditional set of protected transients (PLOF, PTOP, PLOOP), safety analysis was carried out for a number of carefully selected plant specific DBC transients, thus covering a wide spectrum of design basis conditions.

1. INTRODUCTION

The LEADER (Lead-cooled European Advanced DEmonstration Reactor) project, funded by the European Commission in the frame of 7th framework program, aims at the development of a conceptual level of a Lead Fast Reactor Industrial size plant and of a scaled demonstrator of the LFR technology - ALFRED.

Safety analysis of the ALFRED reactor was performed within the LEADER project, analyzing in detail a wide spectrum of possible DBC (Design Basis Condition) and DEC (Design Extension Condition) transient intiators. This paper presents the main safety analysis results of the selected set of DBC transients for the ALFRED reactor. All DBC transient initiators identified were analyzed and conclusions from this activity are presented in this paper.

2. ALFRED PLANT REFERENCE CONFIGURATION

The LEADER project, started on April 2010, carried out an important set of activities with two main goals: the advancement of the conceptual design of the industrial size plant to the present European LFR (ELFR) configuration rated at 600 MWe, and the development of the design of the LFR demonstrator ALFRED [1].

The ALFRED configuration is illustrated in Fig. 1.
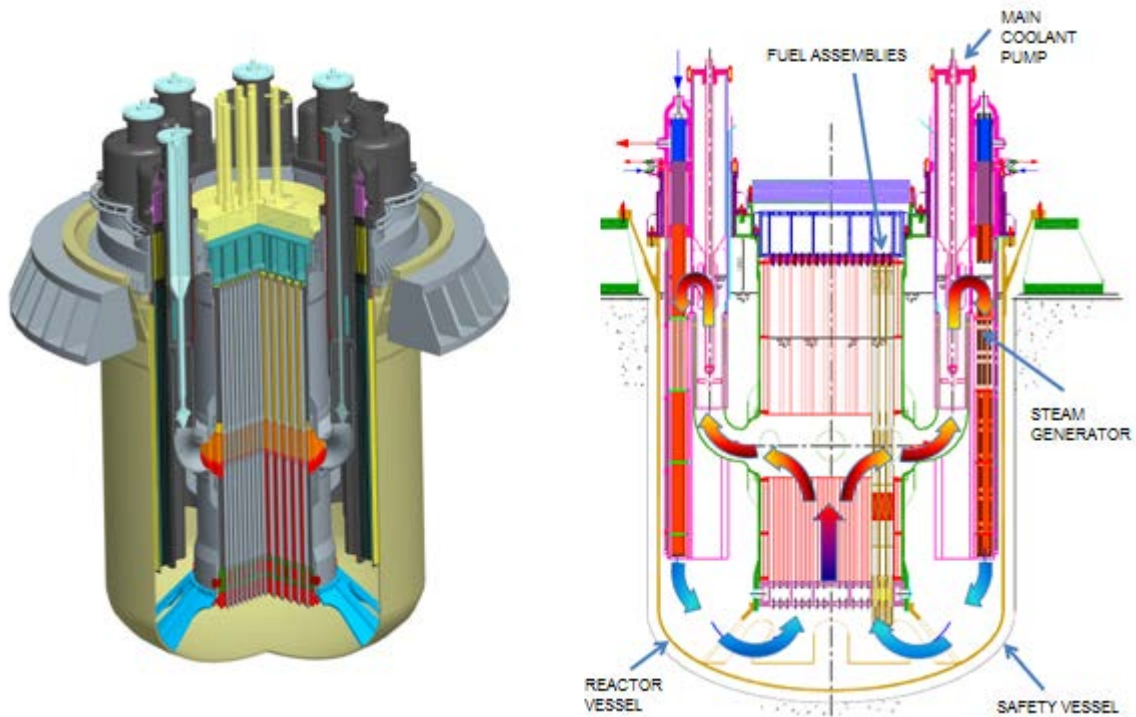
FIG. 1. ALFRED configuration schematics

Main features of the ALFRED design are:

- Pool type configuration characterized by a reactor vessel and the cavity liner safety vessel,
- Hexagonal wrapped fuel assemblies extended up into the cover gas region to simplify fuel handling (FAs weighted down by tungsten ballast for refueling and kept in position by upper grid springs during operation),
- Mechanical pumps located in the hot collector,
- Double-walled straight SG tubes with continuous monitoring of tube leakages.

The thermal cycle is completely consistent with the ELFR thermal cycle: primary lead temperature being between 400-480°C, secondary side pressure 180 bars, once through SGs with water/steam temperature ranging from 335 to 450°C in superheated conditions. The overall efficiency has been evaluated higher than 42%. ALFRED will also allow for testing the connection to the electrical grid, with a generated power of about 120 MWe.

Safety of ALFRED is extensively based on the use of the defense in depth criteria, enhanced by the use of passive safety systems (actively actuated by means of a local stored energy source - that is always considered available, and thereafter fully passively operated). Safety features of the LFR system have been designed since the beginning of LFR related activities to face challenging plant conditions and events, taking into account the forgiving and advantageous physical characteristics of the coolant. As an example, there is no need for off-site or emergency AC electrical power supply to manage design basis accident conditions, as the only manual action needed is the supply of additional water to maintain the water level in the decay heat removal (DHR) pools that are sized to guarantee at least three days of unassisted, fully passive operation. These pools can be easily re-supplied with water in the subsequent days.

3. SUMMARY OF THE DBC TRANSIENT ANALYSIS FOR ALFRED

Within the LEADER project all of the most important DBC transient initiators were analyzed for the ALFRED reactor. The full list of the analyzed DBC transients for ALFRED is as follows:

- Spurious withdrawal of the most reactive control rod (PTOP),
- Reactivity (100 pcm) insertion due to fuel loading error,
- Spurious reactor trip,
- Turbine trip,
- Loss of AC power (PLOOP),
- Loss of one primary pump (AC power available),
- Loss of all primary pumps (PLOF),
- Protected partial flow blockage in the hottest fuel assembly,
- Reduction of FW (feed water) temperature from 335 $^{\circ}$C to 300 $^{\circ}$C,
- Increase of FW flowrate by 20 %, and
- Steam system piping break.

However, due to the limited scope of the paper, only the results of a selected set of the analyzed DBC transients are briefly presented in the following sub-sections.

3.1. Spurious withdrawal of the most reactive control rod (PTOP)

For this simulation it was assumed that: 1) at t = 0 sec, the event of spurious withdrawal of the most reactive control rod (CR worth: 250 pcm) starts; 2) CR withdrawal velocity by mechanical means is limited to 0.1 mm/s, or 0.15 pcm/s; 3) as all CRs at EOC (End-Of-Cycle) condition are withdrawn from the active core region, the BOC (Beginning-Of-Cycle) condition is used for this simulation as all CRs are inserted into the active core region by 16 cm, 4) spurious withdrawal of the most reactive CR proceeds, and at t = 524 sec, a reactor scram signal is being generated based on high neutron flux > 120 % nominal, but this signal is being neglected; 5) at t = 548 sec, the second reactor scram signal is generated based on peak power FA temperature difference being > 1.2; 6) based on this reactor scram signal, the reactor is being shutdown at t = 549 sec into the transient; 7) main steam lines and main feedwater lines are then closed in ~2 sec time interval, while condensate isolation valves of four Isolation Condensers (ICs) of the DHR-1 system fully open in ~ 20 sec, removing maximal 7 MW of heat from the primary cooling circuit.
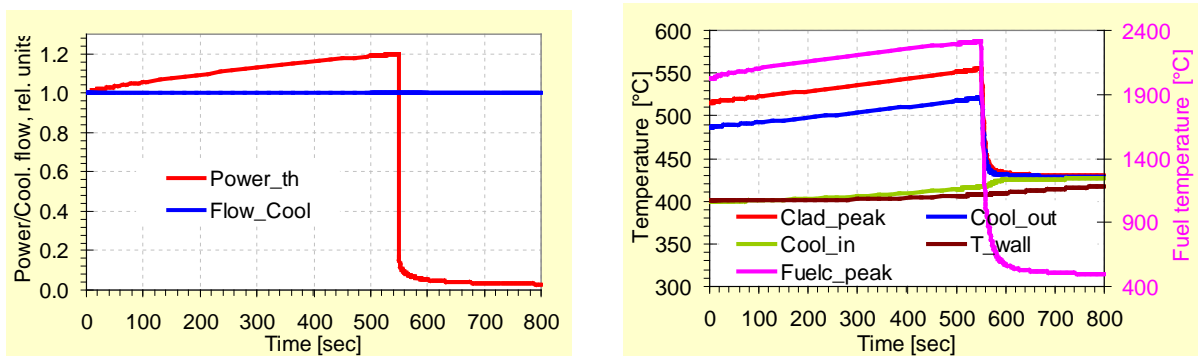
FIG. 2. Evolutions of reactor power and primary coolant flowrate (left), and peak fuel, clad, coolant and vessel wall temperatures (right) with time for BOC as calculated by SIM-LFR (KIT)

As can be observed in Fig. 2, CR withdrawal out of the active core region continues for 549 sec until the reactor trips. During this time interval a total positive reactivity of ~83 pcm is being inserted into the core. Insertion of ~83 pcm in 549 sec time interval at BOC conditions leads to an increase in reactor power ~ 1.2 nominal. The maximum fuel and clad temperatures increase from 2028°C and 516°C to 2313 °C and 555 °C respectively. Minimum clad failure time of the peak pin during the transient always remains above 1E+11 sec and thus no fuel pin failure (creep rupture) is expected.

As related to the above study, one can observe that for reactivity insertion of ~83 pcm in 549 sec time interval of the most reactive control rod (250 pcm total worth at BOC, HFP: Hot Full Power conditions), the ALFRED peak fuel pin cladding accomodates this transient; in addition no fuel melting is expected.

3.2. *Loss of AC power (PLOOP)*

This transient is initiated by assuming the total loss of offsite power supply (station blackout). As a consequence, the forced circulation in the primary system is lost (pump coastdown) with simultaneous turbine trip, feedwater pump shutdown on the secondary side and reactor scram. The secondary system is isolated by the main steam and feedwater isolation valves closure, and the decay heat removal by the DHR-1 system (four IC loops are supposed in service) is promptly activated through the opening of the triggering valve positioned below the isolation condenser.

Despite of the very low primary pump inertia (speed halving time < 1 s), there is a smooth core flow rate reduction in the initial phase of the transient (see Fig. 3) due to lead free levels equalization in the primary system. As a result, the initial clad peak temperature increase is not significant (max T-clad = 564 °C) from the safety point of view.

The core decay power is first removed by water evaporation inside the main heat exchanger (MHX) and then by steam condensation inside the isolation condenser immersed in the boiling water pool, with final decay power release to the atmosphere. The whole system functions passively in natural circulation; the pool water storage is guaranteed for at least three days of DHR-1 operation. Additional water can be easily supplied manually, thereby assuring practically unlimited operation.
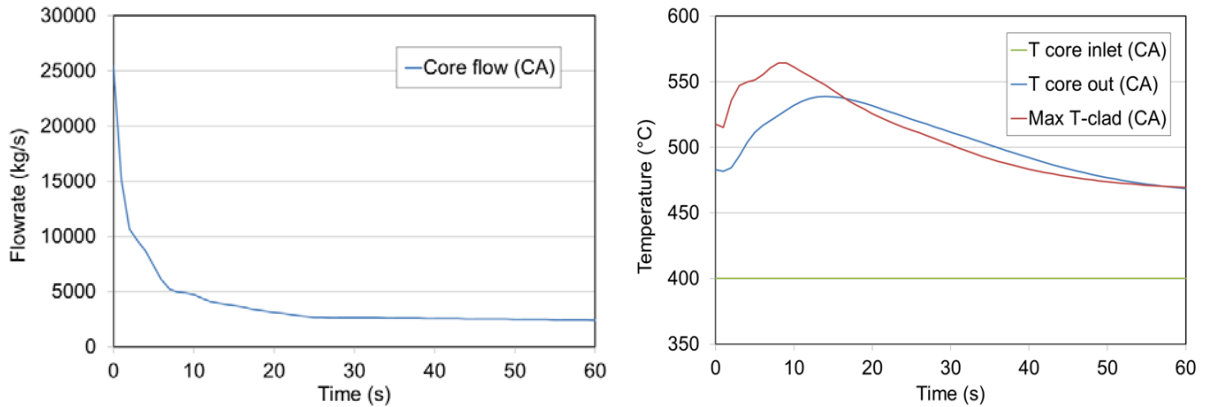
FIG. 3. Evolution of active core mass flowrate (left) and core temperature (right) as calculated by CATHARE (CEA) in the short term
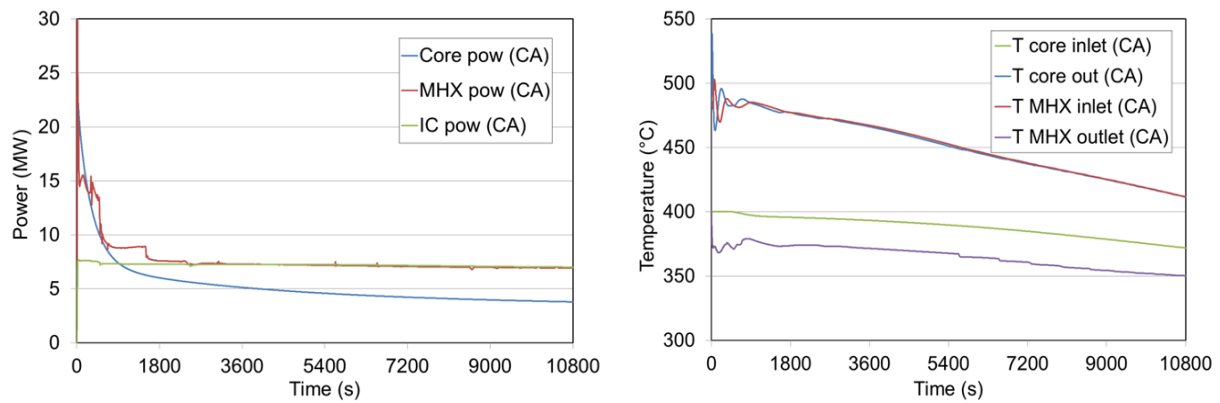
FIG. 4. Evolution of core decay heat, MHX and DHR-1 (IC) powers (left) and primary lead temperatures (right) as calculated by CATHARE (CEA) in the medium term

The Fig. 4 shows that the core decay power is efficiently removed by the DHR-1 during the whole transient phase. The MHX power in excess to IC power in the initial phase is removed by steam release through the safety relief valves of the over-pressurized secondary circuits. After about 15 minutes, the DHR-1 power removed (about 7 MW for 4 IC loops) surpasses the core decay heat and the lead temperatures in the primary circuit start to decrease (see Fig. 4). After 3 hours the minimum lead temperature is reached at the MHX outlet (350 °C), still sufficiently distanced from the lead solidification point (327 °C). Manual control of the IC unit operation is needed in the long term to avoid potential lead freezing. Passive control of the operation of the IC units is under investigation in order to avoid the need for manual operator intervention.

Based on the above results it is concluded that, in case of total loss of offsite power supply, the core decay heat is removed safely indefinitely in a passive manner without the need of active energy sources.

3.3. *Protected partial flow blockage in the hottest fuel assembly*

Transient analysis of the unprotected partial flow blockage of the hottest FA w/o credit to radial heat transfer between adjacent FAs of ALFRED are summarized as follows:

(1)   ALFRED will not experience any fuel pin failure for flow reductions due to blockages less than 75%, even under unprotected conditions;

(2)   For flow reductions above 75%, clad failures (creep rupture) should be expected;

(3)   Fuel melting is not expected to be a safety issue for the ALFRED as fuel melting temperatures are not reached, even in 97.5% FA flow reduction conditions.

Using these results, the influence of delaying reactor trip by 1, 2, 3, 5 and 10 sec assuming a 70% FA flow reduction was analysed. Blockage was assumed activated at t = 1 sec transient time, followed by reactor trip (signal based on the peak FA temperature difference value exceeding 1.2 nominal) assuming different time delays in order to evaluate the impact of the trip signal delay on the maximum fuel and clad temperatures. Reactor trip thus postulated to occur at time t = 4, 5, 6, 8 and 13 sec into the transient. Main steam lines and main feedwater lines are being closed in 2 sec time period, at the same time the condensate isolation valves of the four ICs of the DHR-1 system are opened, removing maximal 7 MW of heat from the primary cooling circuit.

Simulations showed that the maximum clad and coolant temperatures are achieved when the reactor trip is being delayed for 10 sec. The maximum increase of the peak clad temperature in this case is 172 °C for BOC (from initially 516 °C) conditions, and 185 °C for EOC (from initially 514 °C)

conditions. The maximum increase of the peak coolant core outlet temperature is 184 ^{o}C for BOC conditions (from the initial value of 487 ^{o}C) and 195 ^{o}C for EOC conditions (from initially 487 ^{o}C). Later, following reactor trip, all core and primary cooling circuit temperatures decrease.

The 70% FA flow reduction case for 10 sec reactor trip delay at EOC is shown below in Fig. 5.
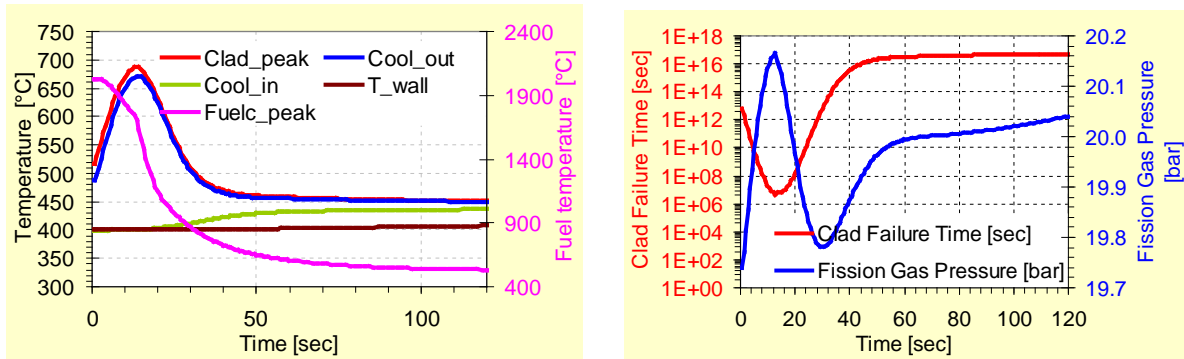
FIG. 5. Evolutions of peak fuel/clad/coolant/vessel wall temperatures (left) and peak pin fission gas pressure and clad failure time (right) with time for EOC as calculated by SIM-LFR (KIT); Case (70% flow reduction and reactor trip delayed by 10 sec)

The maximum clad temperature of the peak pin increases from 514 ^{o}C up to 699 ^{o}C (Fig. 5) at transient time t ~ 14 sec. At the same time point minimum clad failure time of the peak pin drops down to 5E+6 sec (Fig. 5), later recovering to 5E+16 sec, indicating that the clad material is not challanged. The fuel temperature of the peak pin is the highest at the beginning of the transient (2064 ^{o}C), decreases after reactor trip. All other temperatures around the primary cooling circuit also decrease following reactor trip.

The performed analysis demonstrated that the clad of the peak pins of the ALFRED reactor has a very large margin to clad failure (rupture) during the simulated peak power FA for the 70% flow reduction transient. Reactor safety is ensured by the reactor protection system, shutting down the reactor, in conjunction with the DHRs, efficiently removing the decay heat from the reactor primary cooling circuit. Even a 10s delay in reactor trip does not challenge the integrity of cladding material in ALFRED.

3.4. *Reduction of FW (feed water) temperature from 335 ^{o}C to 300 ^{o}C*

The over-cooling (OVC) transient was initiated by the hypothetical reduction of feedwater temperature from 335 °C to 300 °C within 1 second. When feedwater temperature was lower than 327 °C, the SCRAM signal was triggered to shutdown the reactor with 1 second delay. Later, main steam lines and main feedwater lines in SG system were closed in 2 seconds. At the same time, condensate isolation valves are fully opened, leading to the functioning of DHR systems, that are able to provide 7 MW heat removal capability. The opening process of condensate isolation valves takes 20 seconds. During the whole transient, safety valves maintain the pressure in isolation condensers under 195 bar and temperature of liquid water leaving isolation condensers is kept at 300 °C.

Simulation results of the OVC transient are presented in both short-term and long-term time scales.

When condensate isolation valves start to open, liquid water stored in isolation condensers will flow into steam generators and evaporate, leading to a significant increase of MHX power up to 140% nominal. Thereafter, MHX power will continuously decrease with the core power, but it is still sufficient to reduce the temperature difference between the core outlet and core inlet, until only negligible temperature difference between core inlet and outlet remains, as it is shown in Fig. 6.
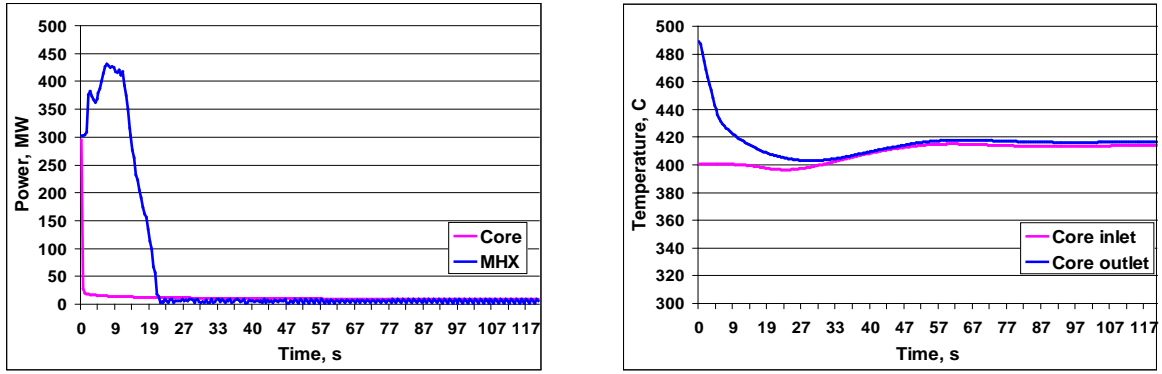
FIG. 6. Evolutions of core/SG powers (left) and core inlet/outlet temperatures (right) with time in short-term time scale as calculated by TRACE (PSI)
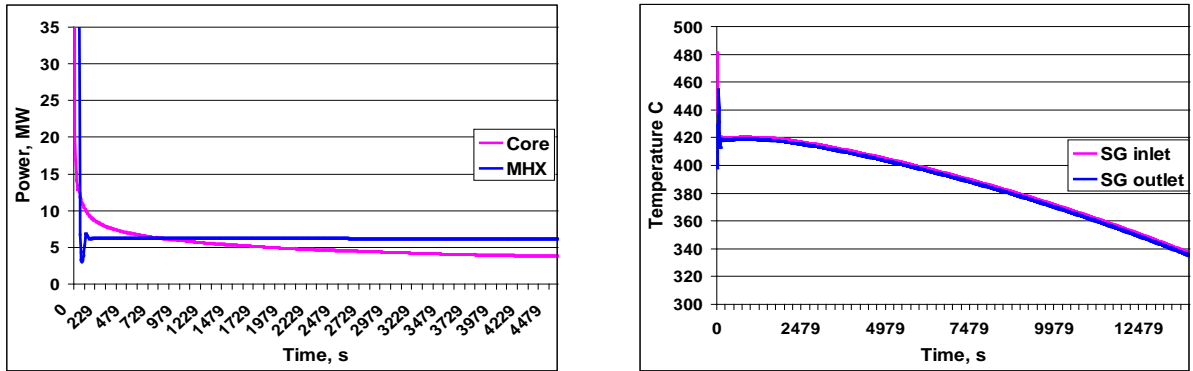
FIG. 7. Evolutions of core/SG powers (left) and core inlet/outlet temperatures (right) with time in long-term time scale as calculated by TRACE (PSI)

As a design basis, the rated power of one DHR system is 7 MW, which will be higher than core power after 900 seconds decay. Hence, primary coolant temperature will decrease slowly as it is shown in Fig. 7. After 14000 seconds, the lowest coolant temperature in the primary circuit (at the MHX outlet) will be lower than the freezing point of lead (~ 327 °C), lead at that location will freeze, unless manual intervention will reduce the DHRs heat removal capability by shutting down appropriate sub-systems of the DHRs.

3.5. *Increase of FW flowrate by 20 %*

This transient is initiated by a control malfunction on the secondary side leading to a an increase of the feedwater flowrate (+20% in 25 s) at the inlet of all MHXs.

As a consequence of the feedwater flowrate variation, the power removal through the MHX increases with corresponding reduction of the lead temperature on the primary side at the MHX outlet as shown in Fig. 8. The maximum MHX power increase is about 10% nominal. The temperature perturbation from the MHX outlet propagates through the core and then back to the MHX inlet in approximately one minute, starting the decrease of the MHX removed power. The core temperature decrease leads to a total positive reactivity insertion (see Fig. 9), mainly driven by positive reactivity contributions due to radial core, coolant and control rod drivelines contraction, with consequent progressive core power increase that comes to equilibrium with the MHX power in about 5 minutes. After this time new steady-state conditions are reached in both primary and secondary systems, without exceeding any reactor trip set-points. The maximum temperature decrease calculated at the core inlet is of 13 °C,

while the core power and the core ΔT increase is below 6%. Furthermore, the fuel peak temperature increase is not very significant (~70 °C, see Fig. 9).

The performed analysis demonstrates that this transient has no safety implications for the ALFRED reactor.
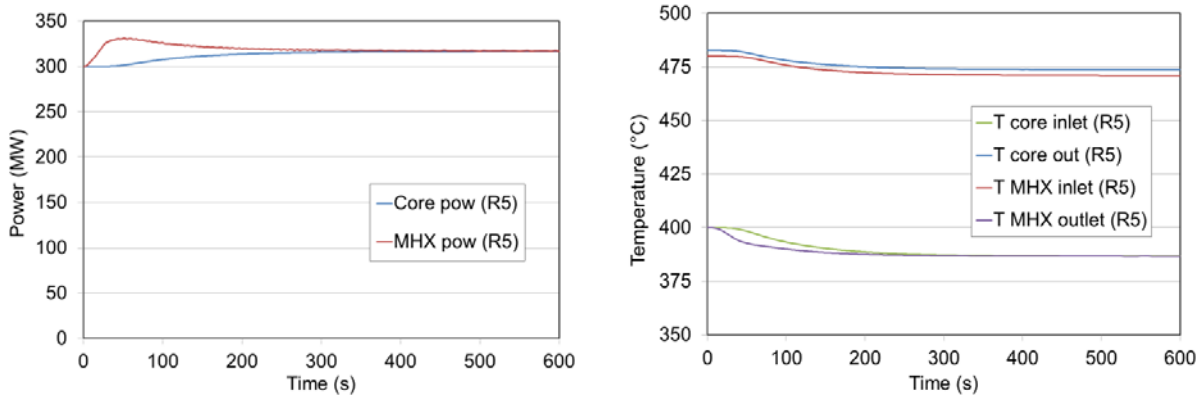
FIG. 8. Evolution of core and MHX powers (left) and primary lead temperatures (right) as calculated by RELAP5 (ENEA)
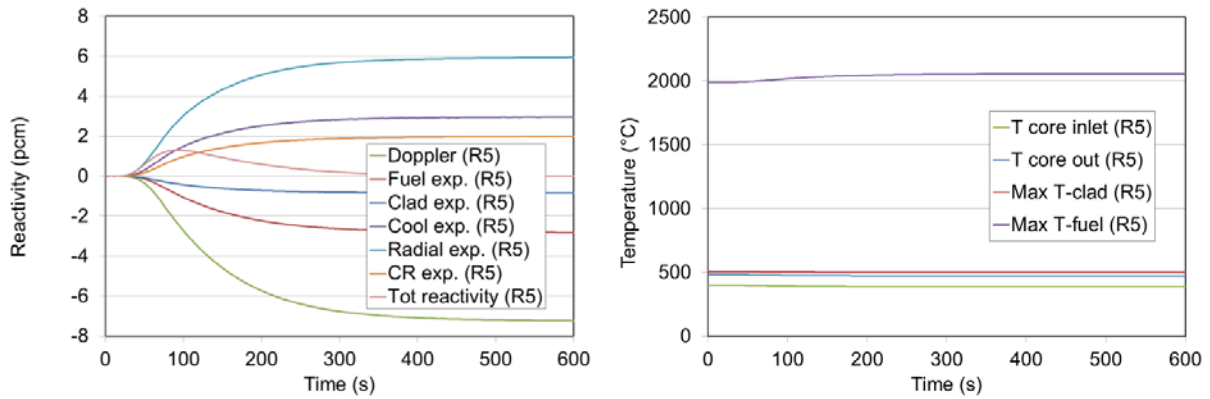
FIG. 9. Evolution of total reactivity and feedbacks (left) and core temperatures (right) as calculated by RELAP5 (ENEA)

3.6. Loss of all primary pumps (PLOF)

This transient is initiated by the loss of all primary pumps (with subsequent coastdown) at t = 0 s. The reactor scram on low primary pump speed signal should be effective just after 1 s, because of the low pump speed halving time (< 1 s), but for conservative analysis this first scram signal is neglected. Therefore, the automatic reactor shutdown is actuated at t = 3 s, with one 1 s delay after the second scram signal, based on the ΔT increase through each individual FA (ΔT > 1.2 nominal value), is detected (t = 2 s). Following the reactor scram the secondary system are promptly isolated (main steam and feedwater isolation valves closure) and the DHR-1 system is actuated to remove the core decay power. For conservative analysis against maximum core temperature reached, only three out of four IC units of the DHR-1 system are supposed to be in service.

After the loss of primary pumps, the transition from forced to natural circulation in the primary circuit is similar to the one already observed in sub-section above for the loss of AC power transient. However, since in this case the reactor scram is delayed, the peak clad temperature increases reaching

a maximum at t = 4 s slightly below 650 °C (see Fig. 10). After reactor scram the lead and clad temperatures at the core outlet progressively reduces, according to the residual core flowrate and the core decay power level.

Despite the reduced availability of the DHR-1 system (3 IC unit), which is now able to remove a total of about 5 MW power during the transient, the DHR-1 heat removal surpasses the core decay heat after about one hour, and then the primary temperature tends to reduce (see Fig. 10). The core temperature increase at the core outlet after the initial transient phase is not significant from the safety point of view. In fact, the maximum core temperature rises up to about 475 °C, that is below the normal operating value.

The risk of lead freezing at the MHX outlet after DHR-1 start-up is excluded, since the minimum lead temperature (350 °C) is far enough from the freezing point of 327 °C. After 3 hours the lead temperature at the MHX outlet is still above the lead solidification point. As in case of loss of AC power, manual control of the IC unit operation is needed in the long term to avoid potential lead freezing.

In spite of the conservative assumptions regarding the failure of the first scram signal and of one IC unit of the DHR-1 system, the analysis demonstrate that, also in case of total loss of forced circulation in the primary circuit, the protection and safety systems are able to bring and maintain the plant in safe conditions in the short and long term.
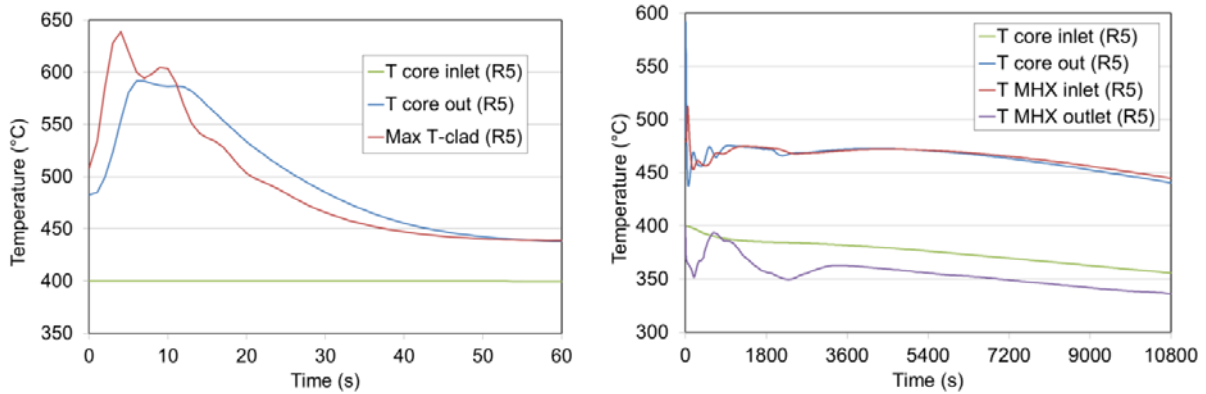
FIG. 10. Evolution of core temperatures in the short term (left) and primary lead temperatures in the long term (right) as calculated by RELAP5 (ENEA)

4. CONCLUSIONS

The presented results show, that ALFRED meet the DBC acceptance criteria. Calculated peak pin temperatures are not exceeding 700 °C, thus no clad failures (creep rupture) are expected, even during the loss of AC power (PLOOP) and loss of all primary pumps (PLOF) transients. This is mainly due to the large thermal inertia of the Pb-cooled primary system and the relatively high Pb natural convection core mass flow rate observed at the initial stage of the transient. In the long-term, in case of PLOOP or PLOF transients, following reactor trip, core decay heat can be passively and safely removed indefinitely by the DHR-1 system without the need of any AC power.

Large margin to clad failure (rupture) for the clad of the peak pins of the ALFRED reactor was confirmed also during the simulated peak power FA 70% flow reduction transient. Reactor safety in this case is ensured by the reactor protection system, shutting down the reactor, as well as by DHRS, efficiently removing the decay heat from the reactor primary cooling circuit. Reactor trip delay even by 10 sec does not lead to clad failure for the ALFRED reactor.

During the protected feedwater temperature decrease to 300 $^{\circ}$C transient, apart from an issue of Pb-freezing several hours into the transient at the outlet of the MHX for the ALFRED reactor, no safety related issues are observed. During this time period the operator has sufficient time to deactivate sub-systems of the DHR-1 system, in order to prevent Pb-coolant freezing at the outlet of the MHX.

As a general conclusion, no relevant, immediate safety issues have been identified during the performance of the simulated transients aside of potential Pb-freezing several hours into the transient in case of all protected DBC transients. Reactor safety is assured by the reactor protection system, shutting down the reactor, in conjunction with a heat removal system (DHRS), removing tightly controlled amounts of decay heat from the reactor primary cooling circuit to assure prevention of freezing of the Pb-coolant at any location of the primary cooling circuit. However design modifications to the DHRs are under study in order to avoid the need of operator intervention to prevent freezing, thus warranting an infinite grace time (DHRs with indefenitely passive operation).

As related to the DBC transients, all selected transients examined proved that the ALFRED plant can accomodate a rather wide range of accidental events. The ALFRED plant has proved to be able to enter a safe shutdown phase after every DBC accident analyzed.

The analysis indicated, that ALFRED is a very forgiving plant design, and there is an extended time margin (grace time) of several hours for possible manual operator intervention even under worst accidental conditions (potential of Pb-freezing in the long term, in case of uncontrolled decay heat removal by the DHRs).

Acknowledgements

Reference

[1]   ALEMBERTI, A., et al., "The Lead fast reactor - Demonstrator (ALFRED) and ELFR design", International Conference on Fast Reactors and Related Fuel Cycles: Safe Technologies and Sustainable Scenarios (FR13), Paris, France (2013).

Aspects of Safety Analysis for Sodium Cooled Fast Reactor Design and Licensing

Bao Truong[*], Jesse Cheatham, Nicholas Touran, Robert Petroski

TerraPower LLC, Bellevue, WA, U.S.A

Presented by Bao Truong

Abstract. This paper discusses aspects of safety analysis of a sodium cooled fast reactor (SFR) that are necessary for nuclear plant design and licensing. In the last two decades, SFR safety analysis has focused mostly on anticipated transients without scram (or unprotected transients). These include unprotected loss of flow, unprotected transient over power and unprotected loss of heat sink. While these transients provide a bounding safety assessment, other more probable transients need to be assessed to support SFR design and licensing efforts. Using a representative traveling wave reactor (TWR) reactor core, different aspects of safety analysis are discussed with example results from SASSYS-1/SAS4A calculations and their implications on SFR design. First, transient event classification is presented. Then, the effects of protected transients (where the reactor scrams) on various design parameters (scram set-points, delay time, peak cladding temperature limit etc.) are demonstrated. Third, the effects of uncertainties of various parameters are demonstrated. Finally, sensitivity analyses and their implications on the reactor design and safety profiles are discussed.

1. Introduction

Safety has always played a crucial part in current and conceptual reactors. Following the Fukushima accident, more emphasis has been placed on reactor safety around the world. This applies for both current light water reactors (LWRs) as well as future Gen-IV reactors. The sodium-cooled fast reactor (SFR) has been shown to have some advantageous safety features. One of the attractive safety features of SFR is the ability to shut down in anticipated transients without scram (ATWS). This was demonstrated experimentally for the EBR-II reactor [1]. The term "inherently safe reactor" is often used for reactors having this capability of achieving shutdown from net negative reactivity feedback mechanisms, which are inherent to the reactor system. Therefore, for many conceptual SFR designs, a lot of focus has been placed on achieving inherent safety [Refs 2, 3, 4, 5, 6, 7 and 8]. However, the term "inherently safe reactor" is not consistent with the IAEA definition, where inherent safety is characterized by the elimination or exclusion of inherent hazards by means of fundamental design choices, because the presence of radioactive sources or decay heat in the core after reactor shutdown does not eliminate the hazard of this radioactive source. For this reason, use of the term "inherent safety" for the entire plant is questionable, but the plant can have inherent safety features. Therefore, we will use term "inherent safety features".

While it is desirable to achieve this inherent safety feature for a SFR, ATWS analyses are not the only event analyses necessary to develop a licensable and economical reactor design. Therefore, analysis of transients within the design basis envelope rather than of the ATWS events is of primary interest. In this paper, a representative TWR core configuration is used with the SASSYS-1/SAS4A safety code [Refs 9, 10] to demonstrate different aspects of safety analysis for SFR for selected design basis events. The beyond design basis ATWS are also addressed. These aspects include effects of uncertainties, sensitivity on scram delay time and different set-points for the reactor protective system. How these affect different design parameters is also discussed.

---

[*] Corresponding author: btruong@terrapower.com

Bao Truong*, Jesse Cheatham, Nick Touran, Robert Petroski

2. Reactor Core Description

The reactor core used for this study is a one of the representative TWR cores, which was created using the TerraPower Advance Reactor Modeling Interface (ARMI) computing platform [11]. This is a 1200 MWt reactor design using 70% smear density metallic fuel. The core map (1/3 symmetry) is shown in FIG. 1. The core contains 12 control rods and 3 diverse safety rods, which have B_4C as poison. There are two rings of reflector and 1 ring of shield assemblies. A Materials Open Test Assembly (MOTA) is at the center of the core. The feed fuel assemblies (FAs) are located in the inner rings and the outer rings while the driver FAs reside in the central rings (approximately between ring 4 and ring 8). The reference hex assembly design is summarized in TAB. 1.
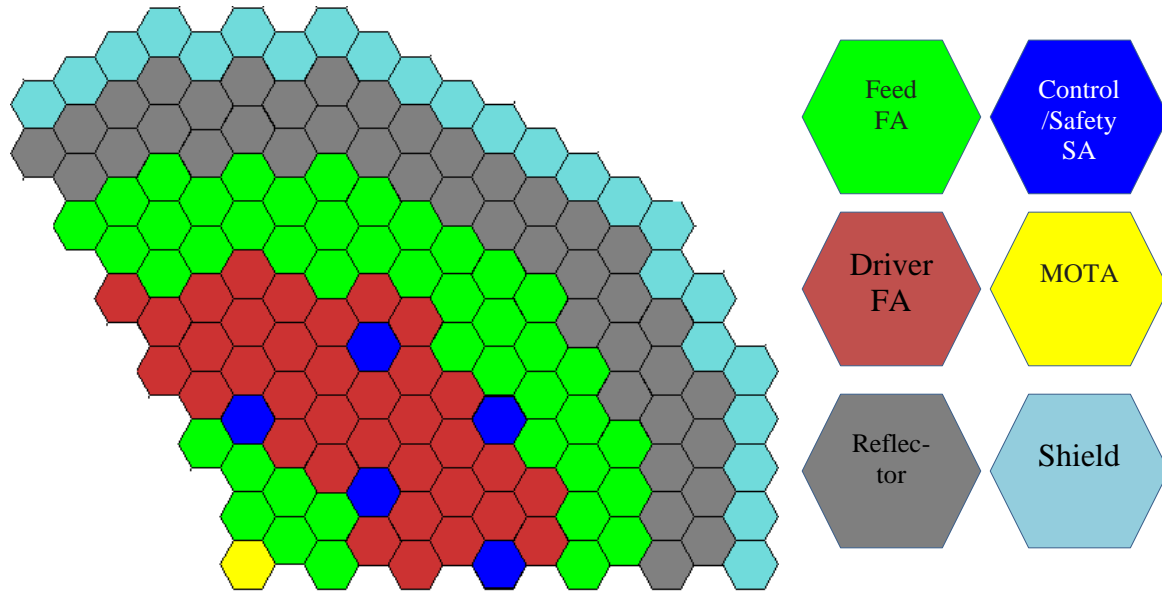
FIG. 1. Reactor Core Map (1/3 Symmetry)

TAB. 1 Reference Core Parameters

Power	1200 MWt
Smear density	70%
Clad OD	8.4 mm
Clad thickness	0.56 mm
Pins/assembly	271
Fuel form	U-10Zr w/ Na bond
Driver U-235 enrichment (BOL)	8 wt % - 16 wt %
Feed U-235 content	0.3 wt %
Structural material	HT-9
Duct Inner flat-to-flat	160.0 mm
Wire wrap OD	1.2 mm
Fueled height	180 cm
Number of assemblies	237
Core inlet temperature	360°C
Core average outlet temperature	505°C

A layout/cut-away view of the TWR reactor plant is shown in FIG. 2. The TWR is a pool-type reactor with two primary loops, each with an associated primary pump and piping. The sodium flows downward from the cold pool, up through the core and into the hot pool. The heat is removed from pool by the four intermediate heat exchangers (IHX). The intermediate heat transport loop (IHTS), not shown in the picture, takes sodium from the IHX to the steam generator. In a normal shutdown

Bao Truong*, Jesse Cheatham, Nick Touran, Robert Petroski

condition, the decay heat is removed via the steam generators. The TWR also has 4 passive Direct Reactor Auxiliary Cooling Systems (DRACS), which can be used to remove decay heat. Only one out of four DRACS is required to keep peak cladding temperature below 715℃ and maintain ASME limits for the reactor vessel.
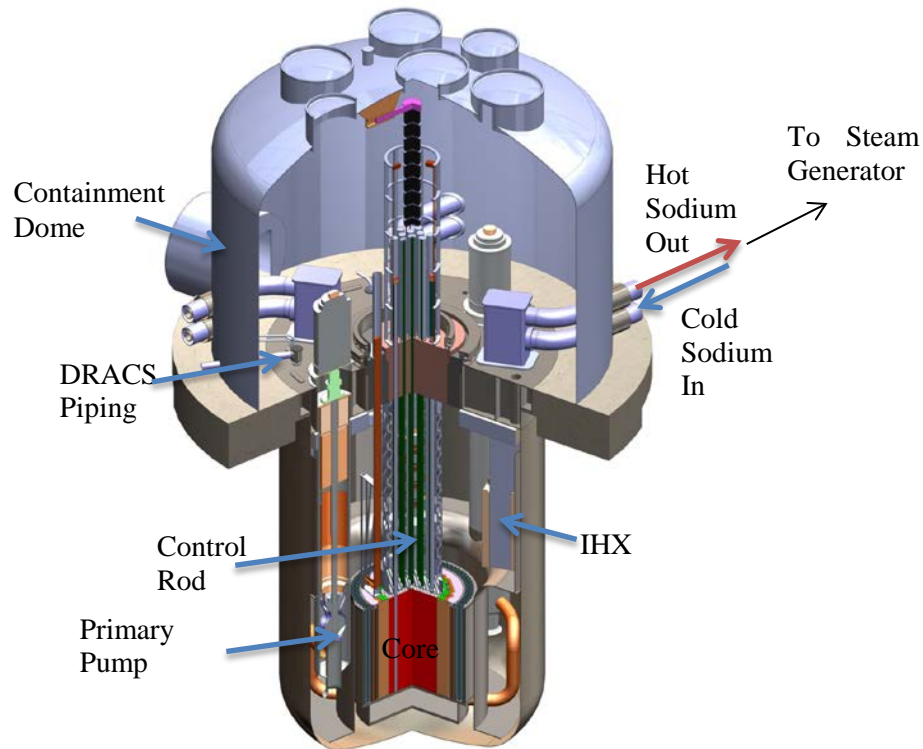
FIG. 2. Layout of TWR Reactor

3. Safety Analysis Methodology

3.1. *Overview of the Approach to Safety*

For a safe reactor design, the most important goal is to prevent radiological release to the public, and the TWR design follows this philosophy. In addition, a safe reactor design helps to protect valuable nuclear equipment (fuel, pump, heat exchanger, etc…) from damage during transients. In order for the verification, update, and implementation of the design as it progresses, a systematic and quantitative approach is used in TWR development. A Probabilistic Risk Assessment (PRA) is used in TWR design to provide risk-informed guidance for design and safety analyses from conceptual to final design. To assure safety, conservative acceptance criteria are used and uncertainties are included for safety calculations.

For the TWR reactor, safety assurance can be accomplished at different levels. At the first level, normal operation and accident prevention are necessary. This can be achieved via high quality design, construction, maintenance, and quality assurance. However, it is expected that abnormal events happen from time to time. Therefore, in the second level of safety, the focus is on the prevention of propagation of these abnormal events. This is achieved with the plant protection system (PPS) and the shutdown heat removal system. The high reliability and high quality of these systems are crucial in limiting the propagation of these events. The next level of safety focuses on events that are not expected to occur throughout the lifetime of the plan. While these events are extremely unlikely, their analyses are required to ensure that key reactor components do not sustain damage that would lead to radioactivity release. The final level of safety focuses on beyond design basis events, which includes ATWS.

Bao Truong*, Jesse Cheatham, Nick Touran, Robert Petroski

3.2. Events Selection and Criteria

For the TWR, three different levels of events are classified. These include Anticipated Operational Occurrences (AOOs), Design Basis Accidents (DBAs) and Beyond Design Basis Accidents (BDBAs). The AOOs are expected to occur over the lifetime of the reactor with probability/reactor-year larger than 10^{-2}. AOO will not cause any fuel damage. DBAs are expected to happen less frequently ($10^{-6} < P < 10^{-2}$). The criterion for TWR DBAs is that there is no unacceptable radiological or chemical hazard impact. The BDBAs are the typical unprotected transients (ATWS). Currently, the limit for ATWS is set at no sodium boiling, which is a good indication for no major energetic reactivity insertion. The acceptance criteria for these three levels of events are shown in TAB. 2. The classification of events and acceptance criteria are preliminary and can change as more data become available. The peak cladding temperature (PCT) here is driven by fuel performance limit such as clad strain, creep, and fuel clad chemical interaction.

TAB. 2. Sample Event Categories and Acceptance Criteria

Event Classification	Probability (per reactor year)	Sample Event	Peak Cladding Temperature (°C)
Anticipated Operational Occurrences (AOO)	$10^{-2} < P < 1.0$	Protected Loss of Flow (PLOF) Protected Transient Over Power (PTOP)	650[*]
Design Basis Events (DBA)	$10^{-6} < P < 10^{-2}$	Seizure of One Primary Pump (SOPP)	725[**]
Beyond Design Basis Events (BDBA)	$P < 10^{-6}$	Unprotected Loss of Flow (ULOF) Unprotected Loss of Heat Sink (ULOHS) Unprotected Transient Over Power (UTOP)	No boiling of sodium

[*] Calculation for cladding temperature for comparison with these limits should take into account the uncertainty margin with at least 2σ confidence level. ; [**]Based on the fuel-cladding chemical interaction limit for U-10Zr/HT9 per [Ref 12].

A requirement for the AOOs and DBAs is to take into account the hot channel factors, which include both uncertainties and peaking factors when calculating the peak cladding temperature (PCT). However, uncertainties are not required for BDBAs.

4. Reference Transient Results

The SASSYS-1/SAS4A code was used to perform the aforementioned transients. The core was divided into 8 channels, each having its own hot channel to represent the highest power to flow ratio fuel assembly. The primary system has two primary loops, each containing a primary pump, two IHXs, and associated piping. SASSYS models the reactor up to the intermediate sodium side of the steam generators. The focus here will be on the results for protected transients.

4.1. Protected Loss of Flow Transient (AOO)

This transient starts with a loss of power to one primary pump at 4 seconds, causing it to coast down normally. The reactor will scram due high "flux^2/pump pressure" ratio trip. Subsequently, the power to the second primary pump is isolated and this pump also starts its coast-down. The results for this transient are shown in Fig. 3. The PCT of channel 2 gets close to 650°C but never exceeds the limit. The steady state PCT is limited to less than 625°C for this design in order to prevent PCT exceeding 650°C in a transient.

Bao Truong*, Jesse Cheatham, Nick Touran, Robert Petroski
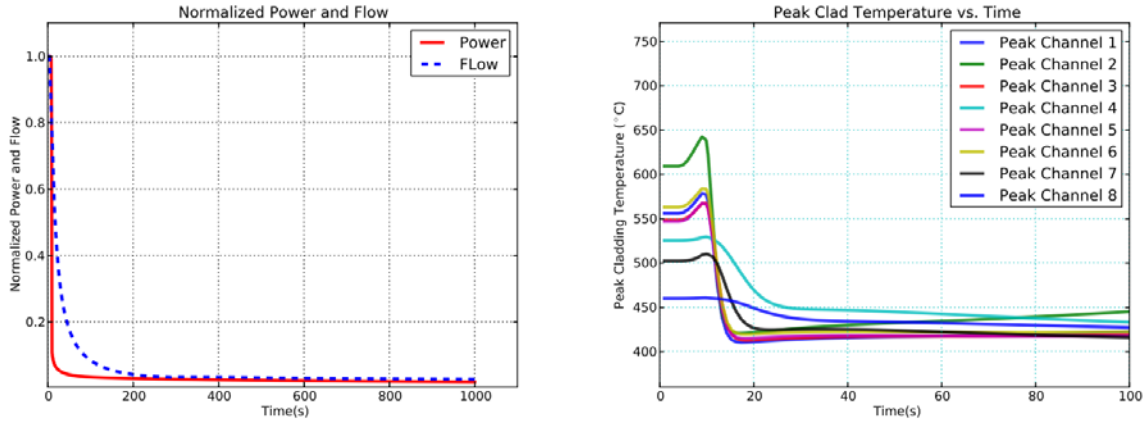
FIG. 3. Protected Loss of Flow Transient Results

4.2. Protected Transient Over Power (AOO)

This transient is initiated by insertion of positive reactivity in the core, which can be due to uncontrolled withdrawal of one control rod. The power of the reactor will increase until high power trip signal comes in, causing the reactor to scram. The pumps will then start coasting down. This transient causes power and temperature to rise until the reactor scrams.

The inserted reactivity (0.008$/s) is shown by the green curve (labeled "Program") in the reactivity plot on the left in FIG. 4. The occurrence of a reactor scram is indicated by the sharp drop in the net reactivity curve (blue). Again, the PCT gets very close to 650°C but never exceeds this limit. This is another confirmation that the steady state PCT of the final design would need to be about the same as this core.
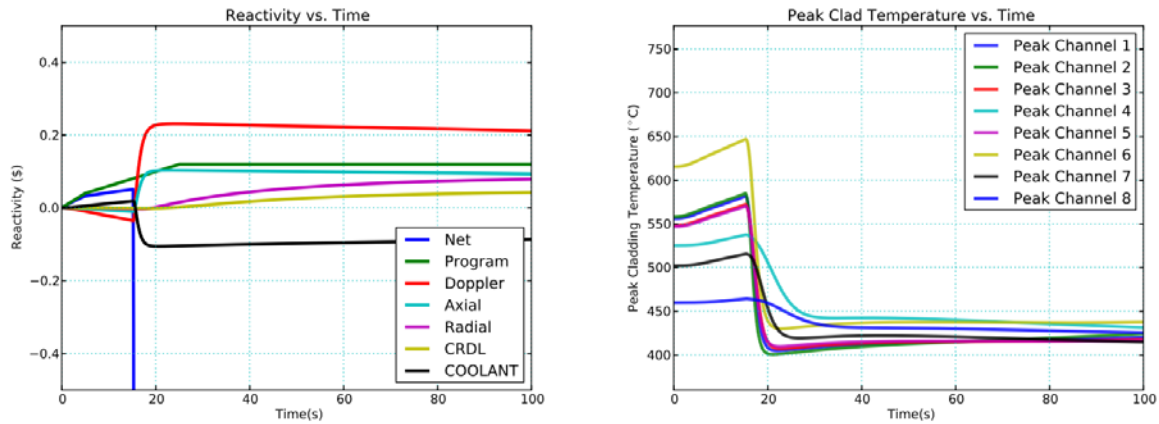
FIG. 4. Protected Transient Over Power Results

4.3. Seizure of One Primary Pump (DBA)

In this transient, one of the primary pumps seizes due to a locked rotor. The reactor will scram due to high "flux^2/pump pressure" trip. Subsequently, the power to the other primary pump is isolated and this pump starts its normal coast-down. This is one of the most limiting transients because a locked rotor causes a sudden drop in core flow rate while the reactor is still at full power. This will cause a spike in temperature that can exceed the peak cladding temperature (PCT) limit. Also, a seized rotor could mean that a severe damage, such as a broken shaft, has happened to the pump.

The results of this transient presented shown in FIG. 5, where the power, temperature, and pump flow rates vs. time are shown. The power increases momentarily due to reactivity feedback of the coolant but the plant protection system (PPS) shuts it down (indicated by a sharp drop in reactor power) once the

set-point is met. The PCT reaches 675°C in the hottest channel, which is still below the PCT acceptance criterion of 725°C. In terms of flow, one can see that due to the locked rotor in pump 1, the pressure drops and there is actually backflow through the locked pump, indicated by the negative normalized flow. Following the reactor scram, power to pump 2 is cut and it coasts down normally.
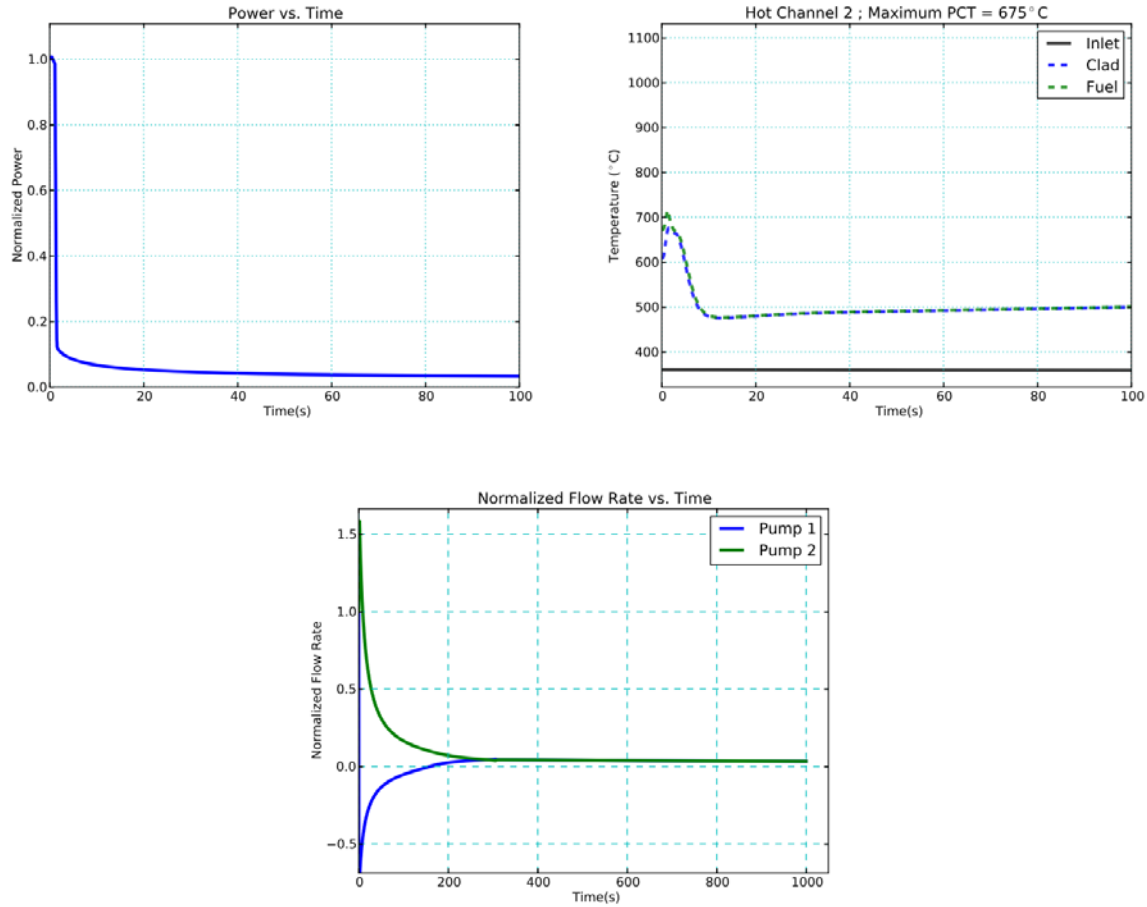
FIG. 5. Locked Rotor Transient Results

5.   Reactivity Uncertainty and Design Parameters for Protected Transient Results

5.1.   *Effect of Reactivity Uncertainty*

For the results shown in section 4, the nominal values for reactivity coefficients were used. For the AOOs and DBAs analyses to be conservative, the reactivity feedback uncertainties need to be considered. The reactivity feedback coefficients themselves need to be biased in conservative directions dependent on the transient type. Also, the control rod drive line (CRDL) expansion feedback is not credited because CRDL is assumed to be very weak. A value of 20% is used for 2σ uncertainties based on a study by the NEA Nuclear Science Committee [13]. TAB.3 below lists how the reactivity coefficients should be biased. Heat-up here means core temperature increases while cool-down means core temperature decreases.

TAB.3. Reactivity Uncertainties and Biases

Parameter	Heat-up Phase	Cool-down Phase
Coolant Void Worth	+20%	-20%
Doppler Coefficient	-20%	+20%
Clad Axial Expansion	-20%	+20%
Fuel Axial Expansion	-20%	+20%
Radial Expansion	-20%	+20%

Bao Truong*, Jesse Cheatham, Nick Touran, Robert Petroski

For each AOO and DBA, there can be heat-up at the beginning and then cool-down later on, or cool-down first and then heat-up later. Therefore, a case with heat-up phase reactivity coefficients and a case with cool-down phase reactivity coefficients should be run to establish the bounded conditions.

The effect of applying conservative reactivity coefficients on the above transients are shown in TAB. 4. Overall, there are small changes in PCT between the difference cases. The PCT varies with less than 3°C from the reference cases.

TAB. 4. Effect of Reactivity Uncertainties and Biases on PCT

Transient	Reference PCT	Heat-up Case PCT	Cool-down Case PCT
Locked Rotor	675°C	677°C	673°C
Protected Loss of Flow	644°C	643°C	645°C
Protected Transient Over Power	646°C	646°C	647°C

The results above are counterintuitive for the protected loss of flow transient. One would expect that the cool-down case, which has the best reactivity feedback coefficients, should have lower PCT than the reference or heat-up case. Instead, the cool-down case has the highest PCT. This is due to the fact that the transient was simulated realistically using the plant protection system to initiate a scram. For the protected loss of flow transient, the scram set point was set at $flux^2/Pressure_{pump} = 1.2$. The rods unlatch with a time delay of 1 second. For all three PLOF cases, the set point and the delay time were identical.

The reactivity insertion curves for all three PLOF cases are shown in FIG. 6. The heat-up case scrams the earliest (identified by a large negative reactivity insertion) while the cool-down case scrams the latest. Looking at the integrated power-to-flow ratio over time for all three PLOF cases in FIG. 6, the heat-up case has the smallest value while cool-down case has the largest value. The value of the integral of power-to-flow ratio curve up to the scram point (indicated by the sharp change in slope of the curve) dictates the PCT. Therefore, the cool-down case has the highest PCT, then the reference case and finally the heat-up case. This agrees with results in TAB. 4.

The results show that it's important to simulate protected transients realistically. If one had simulated this protected loss of flow transient by inserting negative reactivity at some predetermined time, the effect above could have been missed.
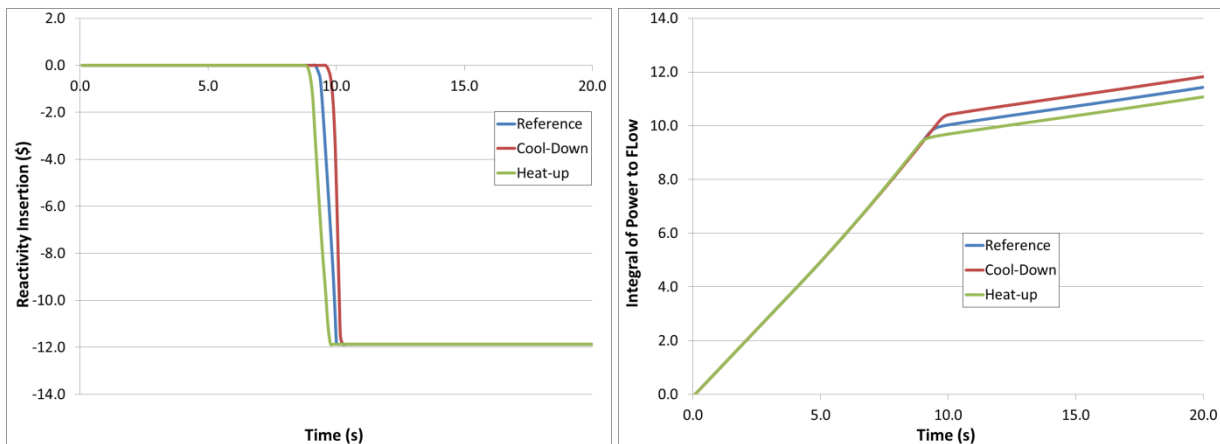
FIG. 6. Reactivity Insertion and Integrated Power to Flow Ratio as Function of Time for Protected Loss of Flow

5.2. *Effect of Scram Setpoints and Scram Delay Times*

In this section, the effect of scram set-points and scram delay times for protected transients are examined. The focus here is on the protected loss of flow transient since similar results would be expected for other transients. In the reference case, the scram set-point was "flux²/pressure" exceeding

1.2 with the delay time of 1 second for the control rod to unlatch and insert negative reactivity. For this study, the scram set-point was varied from 1.10 to 1.25 and the delay time was varied from 0.5 seconds to 2.0 seconds.

The effect of different scram delay and set-point are shown in TAB. 5. As the scram set-point for power-to-flow ratio increases, the PCT temperature increases. Similarly, the longer the delay time for the control rods to unlatch and insert negative reactivity, the higher the PCT is.

TAB. 5. Effect of Scram Set Point and Delay Time on PCT in PLOF Transient

Case	Scram Set Point	Scram Delayed Time (s)	PCT (°C)
Effect of Scram Set Point			
SP 1	1.10	1.0	632.9
SP 2	1.15	1.0	637.9
Reference	1.20	1.0	644.0
SP 3	1.25	1.0	648.2
Scram Delay Time			
DT 1	1.20	0.5	638.3
Reference	1.20	1.0	644.0
DT 2	1.20	1.5	646.6
DT 3	1.20	2.0	650.5

The results in TAB. 5 are useful for both design and operation limit purposes. For example, in our reference case, the PCT goes from 616°C at steady state to a maximum of 644°C during the transient. This is a 27°C increase but it still meets the AOO limit. However, one can see that changing the set-point or the delay time can have an impact on PCT. The results here provide the instrumentation and control (I&C) engineer an idea of how fast the system must be able to transmit a scram signal. However, there is always a limit on the response time, which is limited by technology and cost. On the other hand, setting the scram set point too low could cause spurious scrams, which is undesirable. The core designer will desire the highest possible limit on the steady state PCT. Therefore, the scram set-point and delay time must be determined iteratively between I&C, operation, core design and safety teams.

The results presented are an example of how a non-limiting transient affects both the operation and the design of the reactor. As more of these transients are analyzed, more insights will be available for other aspects of reactor design and operation strategy.

6. Effect of Reactivity Uncertainty on Unprotected Loss of Flow Transient

Up to now, the focus has been on protected transients. For an SFR, as previously mentioned, one of the attractive features is that it can achieve inherent shutdown in an ATWS. This section will demonstrate how sensitivity analysis can be done for these unprotected transients. The focus will be on the effect of reactivity feedback coefficient variations on the unprotected loss of flow (ULOF) transient, one of the most severe accidents for an SFR.

First, each reactivity feedback coefficient has uncertainties that are assumed to follow some statistical distribution. To perform the sensitivity study, the reactivity variations for each reactivity coefficient are chosen randomly from a statistical distribution for each case, as shown in the left of FIG. 7. In this case, the variation is assumed to have a normal distribution with mean of zero and standard deviation of 0.1 ($N(\mu = 0.0, \sigma = 0.1)$), as shown in the right image in FIG. 7. The curves here are plots of the random data on the left image to verify that they do follow a normal distribution. These are then added into SASSYS input decks appropriately. One thousands of these cases are then run in parallel for this sensitivity study.

Bao Truong*, Jesse Cheatham, Nick Touran, Robert Petroski
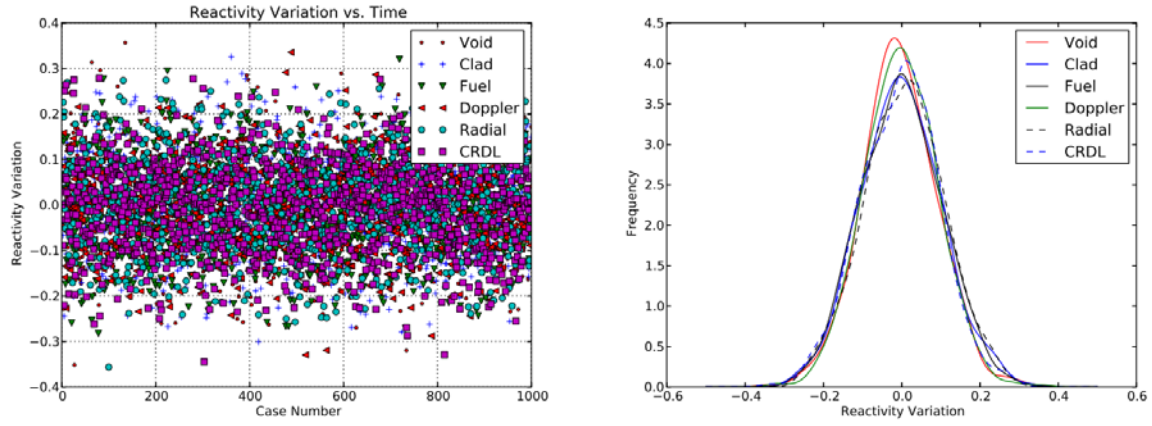
FIG. 7. Random Selection and Normal Distribution Verification of Reactivity Feedback Coefficient Variation

The results of 1000 cases are summarized in FIG. 8. The histogram shows the distribution of the PCT for all cases. The PCT distribution here does not look normal and this could be due to different time constants of the different reactivity feedbacks. Also, the fraction of cases that did not cause sodium boiling is calculated. The result shows that the current core can nominally survive ULOF (no sodium boiling with more than 50°C margin to boiling). However, with the reactivity feedback coefficient varying in the worst direction, sodium boiling could occur at about a 2% rate. This information is useful for PRA analysis. This TWR core has similar nominal ULOF behavior compared to that of the KALIMER-600 reactor [4].
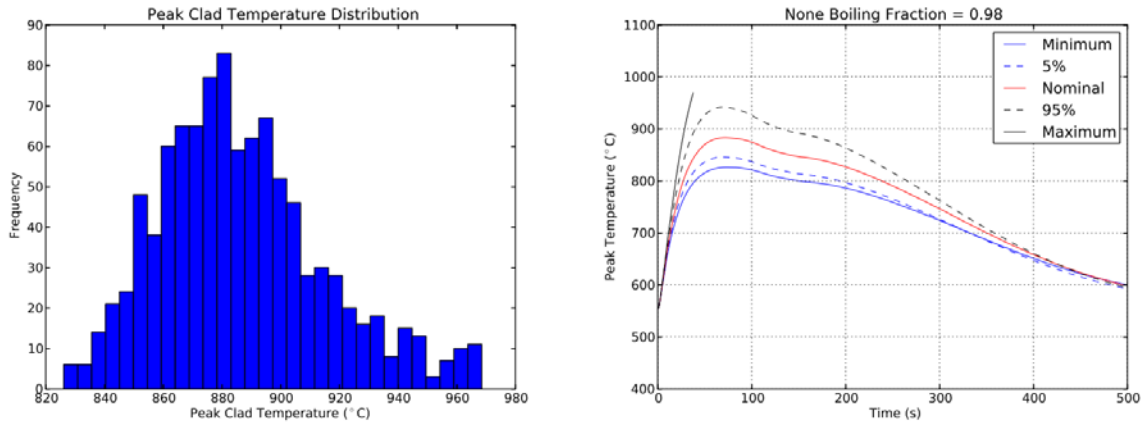
FIG. 8. Example Output for Sensitivity Analysis for Reactivity Uncertainty on ULOF

The sensitivity analysis capability described above has been built into TerraPower ARMI computing platform. This allows quick calculations for sensitivity analysis. Also, expansion of this sensitivity analysis beyond reactivity coefficients' variation to other input parameters in the SASSYS model can be easily implemented for unprotected as well as protected transients. Other statistical distributions for uncertainties can be used and how they affect the PCT distribution can be investigated in more details. However, before this can be done, the set of important parameters must be determined and that is work in progress.

7. Conclusions

This paper discusses the importance of safety analysis of events beyond the more frequently discussed anticipated transient without scram (ATWS) for sodium fast reactors. While more severe than other accidents in an SFR, consideration of ATWS alone is not adequate for reactor licensing and design of a SFR. An examination of less severe protected transients shows that many design parameters, such as scram set-point, and scram delay time can have a substantial impact on the peak cladding temperature during a transient. Also, it is important to model these protected transients as realistically as possible to capture the right behaviors, as shown in the case of protected loss of flow. Finally, the capability to

Bao Truong*, Jesse Cheatham, Nick Touran, Robert Petroski

perform sensitivity analysis on different input parameters for a transient case was demonstrated. This capability provides important data for PRA as well as the ability to estimate the effect of uncertainty in individual or collection of parameters on one or more transients. This capability is valuable for many subsequent licensing analyses.

REFERENCES

[1] PLANCHON, H.P., SINGER, R.M., MOHR, D., FELDMAN, E.E. CHANG, L.K., BETTEN, P.R., The Experimental Breeder Reactor II Inherent Shutdown and Heat Removal Tests – Results and Analysis, Nuclear Engineering and Design **91** (1986) 287.

[2] KWANT, W., BOARDMAN, C.E, PRISM-liquid metal cooled reactor plant design and performance, Nuclear Engineering and Design **36** (1992) 111.

[3] SATHIYASHEELA, T., RIYAS, A., MOHANAKRISHNAN, P., CHETAL, S.C., BALDEV RAJ, "Comparative study of unprotected loss of flow accident analysis of 1000 MWe and 500 MWe Fast Breeder Reactor Metal (FBR-M) cores and their inherent safety", Annals of Nuclear Energy, **38** (2011) 1065.

[4] CHANG, W. P., KWON, Y. M., JEONG, H. Y., SUK, S. D., LEE, Y. B., "Inherent Safety Analysis Of The Kalimer Under LOFA With A Reduced Primary Pump Halving Time", Nuclear engineering and technology : an international journal of the Korean Nuclear Society **43** (2011) 63.

[5] SINGH, O. P., HARISH, R., PONPANDI, S., RAO, P.B., SINGH, R. S., Analysis Of Passive Shutdown Capability For A Loss Of Flow Accident In A M E D I U M Sized Liquid Metal Fast Breeder Reactor, Ann. Nucl. Energy **21-3** (1994) 165.

[6] MERK, B., FRIDMAN, E., WEIß, F.-P., On the use of a moderation layer to improve the safety behavior in sodium cooled fast reactors, Annals of Nuclear Energy **38** (2011) 921.

[7] MORRIS, E.E., NUTT, W.M., Uncertainty Analysis for Unprotected Loss-of-Heat-Sink, Loss-of-Flow, and Transient-Overpower Events in Sodium-Cooled Fast, IAEA FR 09, (2009), Kyoto, Japan.

[8] HIDEAKI, K., SAWADA, T., NINOKATA, H., ENDO, H., Inherent and Passive Safety Sodium-Cooled Fast Reactor Core Design with Minor Actinide and Fission Product Incineration, Nuclear Science and Engineering **38** (2001) 205.

[9] CAHALAN, J. E., SASSYS Manual, ANL-FRA-1996-3, Vol. 1, August 1996.

[10] CAHALAN, J. E., TENTER A. M., MORRIS E. E., Advanced LMR Safety Analysis Capability in the SASSYS-1 and SAS4A Computer Codes, Prod. International Topical Meeting on Advanced Reactors Safety, ANS, Pittsburgh, PA, April 17-21, 1994.

[11] TOURAN, N., CHEATHAM, J., PETROSKI, R., Model Biases in High-Burnup Fast Reactor Simulations, Advances in Reactor Physics – Linking Research Industry and Education, PHYSOR 2012, Knoxville, Tennessee, USA, 2012.

[12] CHANG, Y. I., Technical Rational for Metal Fuel in Fast Reactors, Nuclear Engineering and Technology, **39-3** (2007) 161.

[13] SALVATORES, M., Uncertainty and Target Accuracy Assessment for Innovative Systems using Recent Covariance Data Evaluations, Nuclear Science, NEA, PWEC-26, 2006, ISBN 978-92-64-99053-1.

Comparison of Results of SAS-SFR Calculations of the CP-ESFR Working Horse and Optimized Core Designs during the Initial Phase of an ULOF Accident

R. Krüssmann, A. Ponomarev, W. Pfrang, M. Schikorr, D. Struwe

Institute for Neutron Physics and Reactor Technology, Karlsruhe Institute of Technology, Karlsruhe, Germany

Abstract. Simulations using the code SAS-SFR were performed to assess the behaviour of two core designs investigated within the European Collaborative Project CP-ESFR. The results for an unprotected loss of flow (ULOF) accident in the initiation phase are presented and analysed for the Working Horse and Optimized Oxide core designs under Beginning-Of-Life (BOL) conditions.

The core geometry has to be represented according to simulation capabilities of the SAS-SFR code. The values for the spatial distributions of material worth (sodium, fuel, and steel) and Doppler coefficient were calculated with the modular code system KANEXT using the JEFF 3.1.1 cross section data library.

The cores are compared regarding the design optimization related to the consequences of severe accidents. For the optimized core design, the grace time rises considerably and the power excursion is milder. It is a step in the right direction, but not yet sufficient to prevent core destruction.

1. Introduction

In the framework of the European Collaborative Project CP-ESFR, two reactor designs were developed: The Working Horse (WH) and the Optimized Core (OC) design. Simulations with the code SAS-SFR Ref2011 were performed to assess the behavior of these two cores in the initiation phase of an unprotected loss of flow (ULOF) accident with a pump halving time of 10 s and at the Beginning-Of-Life (BOL) core state.

In the following, the main design parameters will be summarized and results for both cores will be given. The effect of the design optimization on accident consequences will be discussed.

2. Comparison of Working Horse and Optimized Core design

The design characteristics of the WH core were provided by the CP-ESFR project [1]. The OC design was elaborated within the project. The same reactor power of 3600 MW(th) is considered for both options, core arrangement given in Fig. 1 is identical as well.

Sub-assemblies of inner core (225 SAs)	Control rods (24 CSDs)
Sub-assemblies of outer core (228 SAs)	Shutdown rods (9 DSDs)
Radial steel reflector sub-assemblies and central dummy channel	
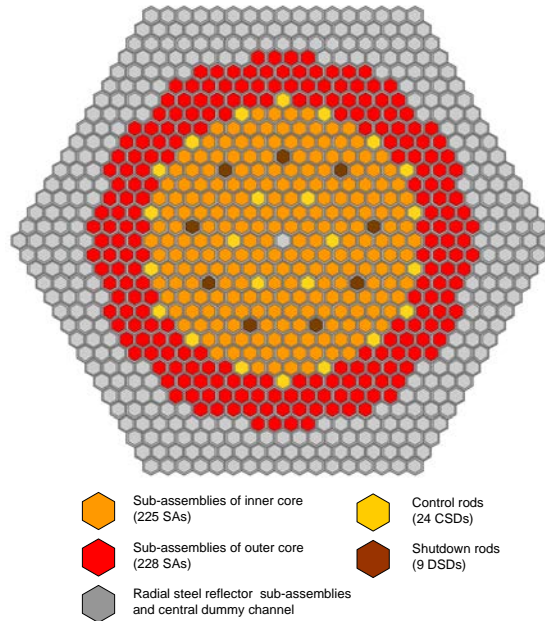
FIG. 1. Cross section of both core designs

Both cores consist of 225 inner fuel subassemblies (SA) with a Pu mass fraction of 14.05% (WH) or 14.76% (OC), and 228 outer SAs with 16.35% Pu (WH) or 17.15% Pu (OC), respectively. The central assembly is a dummy; its design is identical to the radial reflector assemblies. The SA consists of a hexagonal wrapper tube with triangular arrangement of 271 fuel pins with helical wire wrap spacers. The control rod system is composed of 9 DSDs (Diverse Shutdown Device) and 24 CSDs (Control and Shutdown Device).

The OC design is based on the WH core design. Several changes were made to the axial lay-out aimed mainly on the sodium void reactivity reduction. In particular, an absorber layer and a large sodium plenum above the core were introduced in order to increase neutron leakage and introduce additional negative reactivity during a boiling event. In addition, the lower axial steel reflector was replaced by a uranium blanket and Pu content in core was slightly increased [2]. Fig. 2 shows the axial structure of SAs for both cores. Table 1 shows the effect of the enlarged sodium plenum on the void worth of the cores.
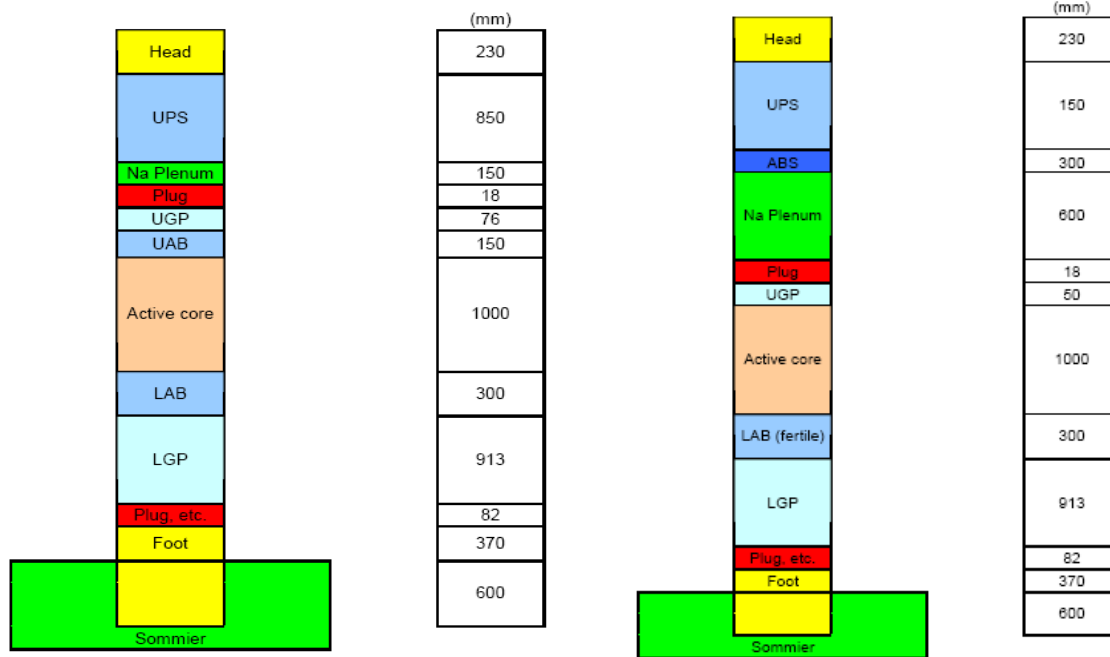
Fig. 2 a: Axial structure of the WH design.   **Fig. 2 b : Axial structure for the OC design.**

Sommier = SA diagrid, insert, thimble; LGP = Lower gas plenum; LAB = Lower axial blanket (reflector); UAB = Upper axial blanket; UGP = Upper gas plenum; ABS = Absorber layer; UPS = Upper reflector. Dimensions are given for the cold ("as fabricated") geometry.

FIG. 2. Axial structure

Table 1. Reactivity effects for WH and OC.

Parameter	WH	OC
Doppler constant, pcm	-1094	-990
Sodium void effect in active core, pcm	+1784	+1683
Sodium void effect in plenum, pcm	-112	-760
Sodium void effect in active core and plenum, pcm	+1656	+813

3.   Grouping of subassemblies into representative SAS channels

Subassemblies having similar characteristics in thermal, hydraulic, neutron physics and fuel pin mechanics behaviour are grouped together into one representative SAS channel. Fig. 3 shows the allocation of the SAs to the 10 channels (marked by colours) with ratio of given SA power to average SA power of the channel. Some important characteristics of the different channels can be found in Table 2. The mass flow rates were adjusted to obtain a flat temperature outlet profile and a balanced power-to-flow ratio.
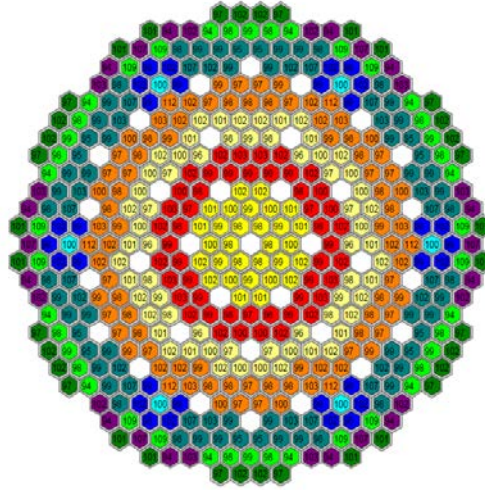
FIG. 3. Allocation of the SAs to the 10 SAS channels (WH).

Table 2. SAS-SFR channel grouping for WH and OC design.

Channel group No.	SA number / sub-core type	Average SA power in group, MW	Average SA mass flow, kg/s	Group power-to-flow ratio MW/(kg/s)
1 (yellow)	30 / inner	6.64 / 5.36	34.23 / 28.17	**0.1941 / 0.1904**
2 (red)	48 / inner	7.04 / 6.05	36.30 / 31.79	**0.1941 / 0.1904**
3 (light yellow)	63 / inner	7.56 / 7.08	38.95 / 37.19	**0.1940 / 0.1903**
4 (orange)	84 / inner	8.02 / 8.31	41.35 / 43.69	**0.1939 / 0.1903**
5 (light blue)	6 / outer	11.00 / 11.34	53.40 / 56.48	**0.2061 / 0.2007**
6 (dark blue)	30 / outer	10.34 / 10.75	53.40 / 56.48	**0.1937 / 0.1903**
7 (sea green)	84 / outer	9.33 / 9.93	48.12 / 52.21	**0.1938 / 0.1903**
8 (light green)	42 / outer	7.90 / 8.23	40.83 / 43.24	**0.1935 / 0.1903**
9 (lila)	30 / outer	6.79 / 6.96	35.07 / 36.55	**0.1937 / 0.1903**
10 (dark green)	36 / outer	5.38 / 5.56	27.74 / 29.20	**0.1939 / 0.1903**

4. Geometry representation of the subassemblies respecting SAS-SFR simulation capabilities

The main thermal-hydraulics input data of a SAS-SFR coolant channel is built from the coolant flow area and the hydraulic diameter dependent on axial height. Only the heat transfer within the assemblies

is considered. It is assumed that the temperature of the inter-wrapper coolant has the same axial distribution as the coolant inside the subassemblies. The mass of the wire wraps is added to the hexcan structure along fuel pin height, to consider its thermal inertia during transients approximately correct without violating the clad thickness important for the appropriate calculation of the cladding stress – strain behaviour. The upper shielding pin section is simulated as a reflector having a wetted perimeter and a thickness representing the structure material appropriately.

5. Calculation of the material worth distributions

The values for the spatial distributions of material worth (sodium, fuel, and steel) and Doppler coefficient were calculated with the modular code system KANEXT [3] on basis of the JEFF 3.1.1 cross section data library. For the chosen 10 channel group allocation there are 8 different reactivity feedback sets considered in accord with the ring wise approach. Spatial distributions are constructed based on direct reactivity difference after the perturbation is inserted locally in the considered region in accord with axial and radial discretization scheme of the model. Regions involved in the analysis are the lower axial blanket, fissile core, upper axial blanket, upper gas expansion plenum and sodium plenum.

As an example, Fig. 4 shows the axial and radial distributions of sodium material worth for the WH and OC designs. The individual values are defined depending on the SAS channel position within the core and on the axial location, leading to a quasi three-dimensional distribution. During the transient, SAS-SFR calculates the cumulated reactivity feedback effects on basis of these data and then uses the result within the point kinetics solution algorithm.
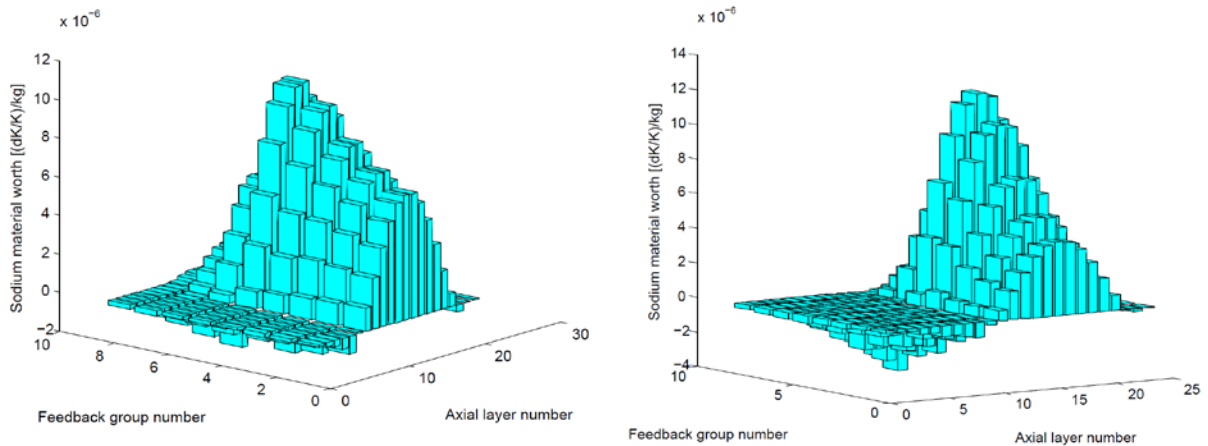
FIG. 4. Sodium material worth distribution for WH and OC designs.

6. Thermal-hydraulic boundary conditions

The primary cycle of the plant is simulated by the PRIMAR-4 model of SAS-SFR. It calculates coolant and gas pressures, coolant flow rates and component temperatures in the primary and intermediate circuits. As boundary condition for the heat sink during transient calculations, a simplified model of the Intermediate Heat Exchanger (IHX) was chosen. It uses the temperature drop between inlet and outlet of the primary side obtained with the SIM-SFR simulation code [4].

The initial steady state coolant inlet temperature, the outlet plenum pressure and the flow rates are specified as initial conditions leading to a coolant heat-up of 150 K. The total coolant flow rate

through the core is about 18400 kg/s. The calculated pressure drop along core height is 4.8 bar including contributions from SA inlet throttling and the grid plate.

The ULOF transient was specified by the project: Starting from nominal operating conditions at BOL the pumps coast down with a flow halving time of 10 seconds.

The reactivity feedback effects of the control rod drive lines expansion was taken into account, but the models for these effects built-in SAS-SFR are not experimentally validated. All transients are calculated until a critical situation, exceeding the applicability limits of SAS-SFR, or until a stabilized state is reached. In SAS-SFR, calculations end when 5 hexcan axial nodes are molten provoking radial spread of the mobile core material which is not modelled in SAS-SFR.

7. Results of the calculations

Table 3. Boiling phase

	Working horse	Optimized core
Boiling onset (time into the transient, s)	31.63	43.16
Boiling time until first fuel pin failure, s	8.48	23.49
Power at first fuel pin failure, -	28.79	4.90
Net reactivity at first fuel pin failure, $	0.89	0.75
Total energy released up to first fuel pin failure, fps	43.78	54.50

Table 3 compares the results for the boiling phase up to the first fuel pin failure. In the OC design, boiling starts more than 11 s later into the transient and the boiling time until the first fuel pin failure occurs is enhanced by 15 s.

Table 4. Comparison of results for the power excursion

	Working horse	Optimized core
Max. normalized power, -	84.29	18.10
Max. net reactivity, $	0.95	0.88

Both core designs enter into a void-driven power excursion after the first fuel pin failure. Table 4 shows the maximum values for net reactivity and power for both designs. Due to the efficient transient core materials relocation after failure, the net reactivity decreases and the further progression of the accident is mild. Both cores never exceed prompt-criticality. The failures are all of the break-up type, i.e. when reaching a fuel melt fraction larger than 20 % and when the fuel melt cavity pressure exceeds the coolant channel pressure the fuel pellet looses its integrity and core materials become available for relocation in the coolant channel. Break-up occurs at a failure position above fissile core mid plane (between 50 and 60 cm from bottom of fissile column) at reasonably high fuel enthalpy levels and at clad temperatures which indicate the clad material has already been molten or is close to the melting temperature. Pressures in the fuel melt cavity are small, below 1.5 MPa. Fig. 5 and Fig. 6 show the development of the accident.
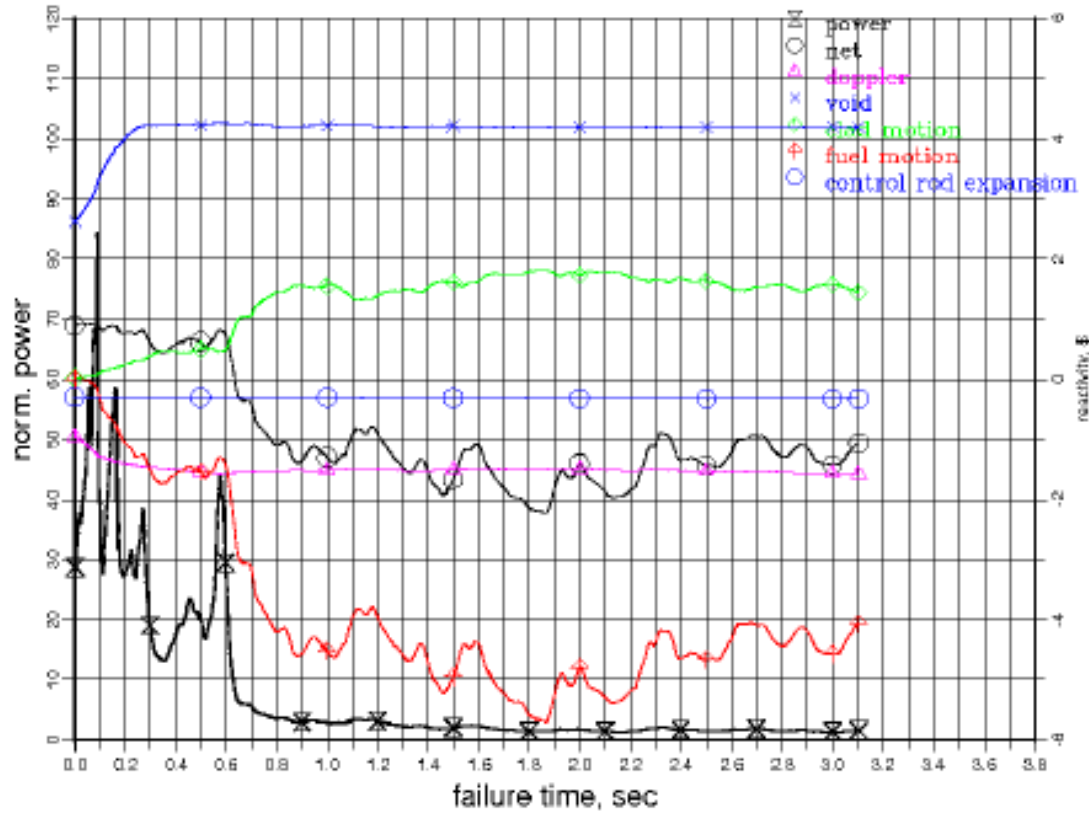
FIG. 5. Transient variation of the normalised power and reactivity contributions during the post failure phase of the accident, WH design.
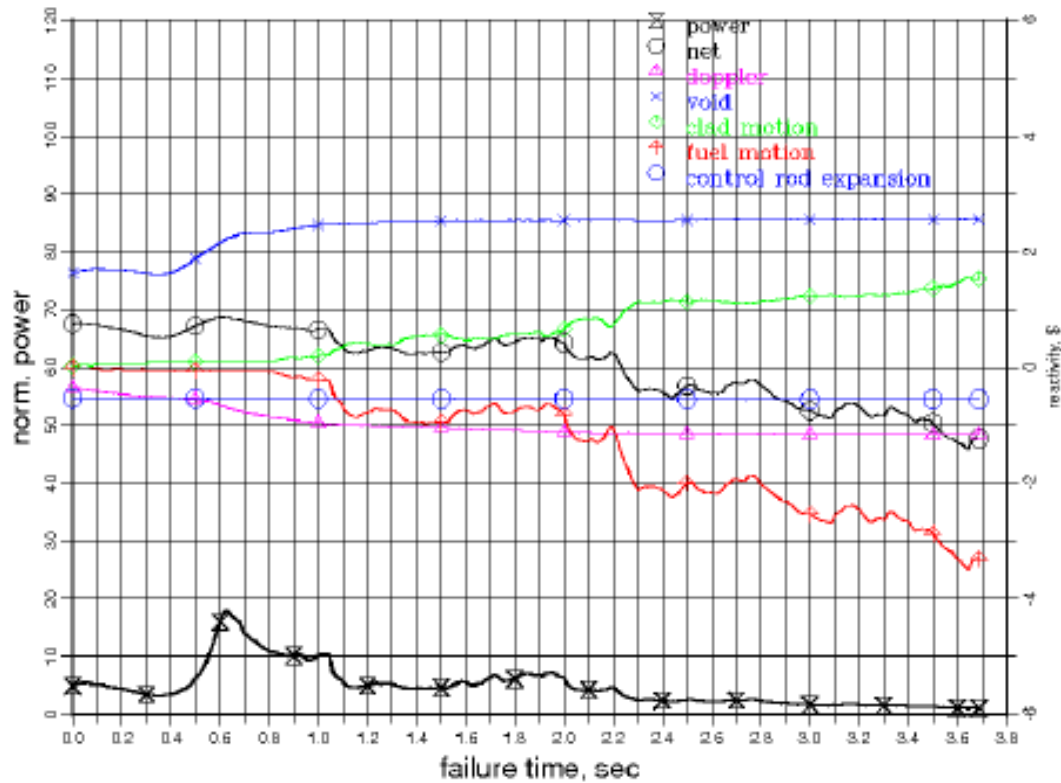
FIG. 6. Transient variation of the normalised power and reactivity contributions during the post failure phase of the accident, OC design.

After pin break-up, the fuel melt fractions reached in the peak power positions lead to a fuel mobility high enough so that the reactivity feedback due to fuel relocation over-compensates the increase of the sodium void reactivity. Thus the net reactivity decreases and the normalised power decreases, but this does not lead to a complete shut-down of the reactor.

Table 5. Status at the end of calculations

	Working horse	**Optimized core**
Calculation ends after boiling time, s	11.58	27.18
Normalized power, -	1.62	1.11
Net reactivity, $	-1.07	-1.23
Total energy released, fps	67.69	72.28

Calculations stop when 5 axial hexcan nodes are molten and the accident enters the transition phase where the movement of the fuel becomes three-dimensional. The status at this point in time is shown in Table 5. The amount of fuel relocation is not sufficiently large to assume permanent reactor shut-down and it becomes necessary to investigate consequences of subsequent accident phases. Both cores are almost voided, but while all channels of the WH design have failed, 5 channels of the OC design are still intact.

8. Summary and Conclusion

This paper describes simulations using the SAS-SFR severe accident code for the initial phase of an unprotected loss of flow (ULOF) transient in two core designs, the WH and OC design of the CP-ESFR project. The reduced void reactivity effect of the OC-design increases the grace time up to boiling onset and leads to a prolonged boiling period. After first fuel pin failure, the development of the accident is similar in both cores, but develops for the OC on an expanded time scale. For the OC core, the maximum values for power and net reactivity are less, but the accumulation of energy in terms of full power seconds (fps) during the accident is a little bit higher. The optimised design is a step in the direction of less severe accident consequences, but not yet sufficient to prevent a power excursion and core destruction as consequence of an ULOF accident initiator.

REFERENCES

[1] A. Vasile, G. L. Fiorini, Ph. Dufour, J. M. Bonnerot, Ch. Latgé, B. Riou, R. Stainsby, M. Rini, D. Verwaerde, D. Struwe, R. Stieglitz, F. Badea, The Collaborative Project for a European Fast Reactor CP ESFR. ICAPP 2011, Nice, France, May 2-5, 2011, Paper 11297.

[2] K. Sun, J. Krepel, K. Mikityuk, R. Chawla, An Optimization Study for the Safety and Performance Parameters of a 3600 MWth Sodium-cooled Fast Reactor. ICAPP 2011, Nice, France, May 2-5, 2011, Paper 11304.

[3] KANEXT / KANEXT description: http://inrwww.fzk.de/kapros.html

[4] E. Bubelis and M. Schikorr, personal communication.

Post-Fukushima lessons and safety orientations for ASTRID

B. Carluec[a], S. Beils[a], J.F. Sauvage[c], P. Mariteau[c], P. Lo Pinto[b]

[a] AREVA, 10 rue Juliette Récamier F-69456 Lyon Cedex 06, France

[b] CEA Cadarache, DEN/DER/CPA, F-13108 Saint-Paul lez Durance Cedex, France

[c] EDF SEPTEN, 12-14 avenue Dutrievoz, F-69628 Villeurbanne Cedex, France

Presented by B. Carluec

Abstract. The Fukushima accident occurred quite simultaneously with the launching of ASTRID preconceptual design phase (March 2011). Thus the workprogram has been able to take into account the main lessons from the Fukushima accident at the very early stages of ASTRID project. The paper presents the main lessons retained from the Fukushima accident, and the safety orientations deduced for ASTRID design. The major items are identified with a focus on the consideration of natural hazards, and the post-accidental management. On each item, safety orientations defined for ASTRID are presented. One of the most important orientation concerns the consideration of extreme natural hazards with the objective to increase safety margin before cliff-edge effect in terms of radiological releases into the environment. Principles for identifying among the safety provisions a "hardened safety core" of features resistant to extreme natural hazards are described. In this context, favorable intrinsic behavior of the concept is underlined.

1. Introduction

The earthquake and the tsunami that occurred in Japan on March 11th, 2011 have led to the accident of Fukushima Daiichi nuclear plants. This accident occurred while the preconceptual design phase of the project of demonstrator of advanced sodium-cooled fast reactor, ASTRID project [1] was being to be launched in France. The safety orientations which were used for the preconceptual design phase of ASTRID have been immediately reassessed in order to take into account the lessons from the accident.

The main safety orientations issued from the assessment of the Fukushima accident are presented. The process of integration of the lessons issued from the Fukushima accident is continuous and is a fundamental item for the selection of the technical options.

The lessons from the Fukushima accident take also into account the results of the French stress test analyses performed on the existing facilities.

2. Overview of the ASTRID safety approach

The first safety orientations for ASTRID defined before the accident occurred, even then were ambitious, in particular concerning severe accident. These orientations may be summarized as follow (more details are presented in [2]):

— A high level of prevention was required, based on the implementation of multiple lines of defense. At least, one of them shall be based on a favorable natural behavior of the reactor.

— Despite the prevention, severe accident situations shall be mitigated by adequate design provisions.

— The situations which cannot be reasonably mitigated shall be identified and the reactor design shall allow to practically eliminate them.

3. Main safety issues resulting from the Fukushima accident analysis and considered for the ASTRID conceptual phase

The analysis performed for the ASTRID project is not limited to the events that occurred at Fukushima. Its ambition is to be more generic.

3.1. Consideration of natural external hazards

Firstly, the natural external hazards to consider in the design have to be adequately defined. Additionally, the combination of hazards has also to be assessed (e.g., combination of earthquake and flooding).

Then, the occurrence of more severe natural external hazards has to be assessed.

Secondly, the implementation of the defense-in-depth principle regarding hazards has to be re-assessed. Indeed, up to now, external hazards were mainly considered as loadings taken into account for the design of safety equipment. This evolution reinforces the ASTRID design approach which postulated some combinations of earthquake with the failure of some seismically designed equipment (*e.g.*, combination of earthquake and failure of sodium pipe).

Thirdly, the Fukushima accident shown that because of the occurrence of external hazard with a magnitude beyond the one considered in the design basis, multiple failures may occur inside a given plant, or simultaneously in different plants located in the nuclear site, or inside the nuclear site and outside the nuclear site. Generally, the situations considered for designing a plant were not assumed to occur simultaneously. Nevertheless for the ASTRID design, it was considered the combination of off-site electrical supply failure with any design basis condition.

3.2. Considerations of situations resulting from external hazards with magnitudes more severe than the ones considered for the design basis

A first generalization of the Fukushima accident is to consider that situations beyond the design basis may occur. This established fact was already taken into account as safety orientation for ASTRID. Indeed, the classical list of design basis operating conditions was completed by hypothetical situations (named Prevention Situations – SP) defined independently from their expected very low occurrence frequency, and for which the design objective is to prevent severe accident. Such situations included combinations of events with the failure of engineering systems, and postulated situations representative of the inherent risk of the concept (*e.g.*, local core melting). The Fukushima accident confirms and reinforces the need of such considerations. This is also completed by situations resulting from severe accident occurrence, defined for designing the equipment needed for mitigation of their consequences (named Mitigation Situations – SM). It is a lesson from the Fukushima accident that mitigation of severe accident situations, except if physically impossible, has to be considered for the plant design.

The lessons from the accident are that a common cause could lead to multiple failures, and also, that a severe accident could result from an external hazard. Additionally, multiple severe accidents related to several plants or to several parts of a same plant (*e.g.*, core damage in the reactor and spent fuel damage in the storage pool) could also result from an external hazard.

Generally, the nuclear plants were designed with a high level of segregation of safety systems and segregation of the high-risk areas. This should allow to limit the consequences of simultaneous

occurrence of situations, compared to their single analysis. Nevertheless, this has to be verified and included in the conceptual process.

On the other hand, the Fukushima accident has shown that the post-accident management of SP and SM situations is strongly affected by simultaneous occurrence of several situations.

In the ASTRID project, situations which must be practically eliminated because their consequences cannot be reasonably mitigated (named Practically Eliminated Situations – SPE), have been identified and the plant is designed for achieving this objective. The lesson from the Fukushima accident is that the demonstration of their practical elimination has to be reinforced by consideration and improvement, if needed, of margins provided by the design basis assessment, in particular with regards to the loadings due to extreme external hazards.

3.3. *Post-accident management*

The post-accident management at Fukushima has been difficult and its duration has been very long. The main reasons are:

— Combination of several simultaneous accident situations.
— Occurrence of situations not expected and therefore not assessed.
— Failure of some on-site accident management devices and difficulty for accessing to some area.
— Failure of off-site infrastructures leading to difficulty for accessing to the damaged plants.

The potential for extreme natural hazards need to be addressed in emergency planning.

4. Complementary safety assessments of the existing plants

In the frame of the ASTRID project, the results of the stress tests (named complementary safety assessments) performed by the French utilities and examined by the French safety authority (ASN) have been analyzed [3]. This has been done for confirming the new safety orientations defined for ASTRID. Only the main points relevant for the design of ASTRID are presented.

4.1. *"Any accident cannot be excluded"*

This means that a situation which is not physically impossible has to be considered and that the design shall implement mitigation devices for limiting its consequences.

Nevertheless, for some situations implementation of mitigation devices is not reasonably possible. Such situations shall have an exceptional nature. They shall be identified and the design shall allow to justify their practical elimination. The lesson from Fukushima is that some of the devices implemented for practically eliminating such situations have to be designed considering that loadings higher than the design basis loadings could occur.

Also, for the severe accident situations for which mitigation devices are implemented, it has to be postulated that these situations could result from loadings beyond the loadings considered as design basis.

4.2. *"The assessment allows also to take into account some situations resulting from malevolent actions"*

Consideration of malevolent actions is also a fundamental orientation for the design of ASTRID.

4.3. *"Verification by the safety margins, of the robustness of the plant regarding extreme situations"*

This point specific to existing plant reminds that the design based on application of stringent rules, such as the ones defined in the relevant codes and standards, provides margins. Now, it is necessary to assess and quantify these margins in order to demonstrate they are sufficient and to improve the plant, if possible.

The plant resistance regarding extreme situations is firstly based on the consideration in the design basis of the hypothetical situations SP, SM and SPE.

This leads to the following orientations for the ASTRID design:

—— To favor the natural behavior of the plant for limiting the consequences of the SP situations.

—— To maximize the time before limitation devices are required to prevent severe accident occurrence in case of SP situations.

—— To maximize the time before mitigation devices are required for avoiding important radiological releases in case of SM situations.

—— To minimize the need of support functions, in particular the need of AC power, I&C, human actions for the management of SP and SM situations.

Therefore, among the equipment sufficient for achieving the associated objectives (*i.e.*, prevention of severe accident for SP, mitigation of consequences for SM and practical elimination for SPE), at least one of them shall provide margins. For ASTRID, the approach is not limited to the quantification of the margins. The orientation is to improve the design by reinforcement of potential weak points in order to achieve a homogeneous plant behavior regarding extreme situations. This approach was initially used for the ASTRID design. The lesson from Fukushima is to consider also in particular, the loadings due to extreme external hazards.

4.4. *"Implementation of a "hardened safety core" of material and organizational devices allowing to achieve the fundamental safety functions in extreme situations; deployment of the Nuclear Fast Action Force (FARN) in less than 24 hours; reinforced devices for decreasing the risk of fuel draining in the spent fuel pools"*

Each fundamental safety function is achieved by a set of systems, structures and components eventually completed by human actions. Generally, the failure of a safety function requires multiple failures of equipment. As indicated above, the first design orientation for ASTRID is to improve the natural behavior, to maximize the time before significant consequences occur and to minimize the need of support functions. Nevertheless, some devices remain necessary for achieving these goals. These devices are in the hardened safety core.

Taking into account the expected high level of prevention and mitigation of severe accident, the method allowing to identify these devices is focused on the risk of important radiological releases in the environment. Then, important radiological releases in the environment could result from the failure of:

—— Devices necessary for limiting the consequences of severe accident.

—— All the devices allowing to practically eliminate a SPE situation (*i.e.*, a situation which cannot be reasonably managed). At least one of these devices shall be selected as belonging to the hardened safety core.

Concerning the improvement of accident management by external emergency teams, the design orientation is to maximize the allowable times (time before severe accident in case of SP situations

and time before important releases in case of SM situations) if failures of on-site equipment are postulated, and to favor the capability for corrective actions and connection of emergency devices.

The facilities for storage of fresh and spent fuel shall be designed and analyzed with the same safety level than the reactor.

4.5. *"The experience feedback from the Fukushima accident will lead to reinforce the safety references, in particular concerning the earthquake, flooding and risks associated to the industrial environment"*

The regulatory methods defining the hazard characteristics and magnitudes to consider for the design basis of the plant have not been modified currently. Nevertheless some evolutions of the regulation are expected. The design of ASTRID shall anticipate possible evolution, firstly by the minimization of the impact on the design of reasonably possible evolutions.

5. Main conclusions issued from the analysis of the Fukushima accident and the complementary safety assessment of the existing plants

The main lessons relevant for the design of a new reactor are deduced from the accident analysis and the complementary assessment of the existing plant:

— It cannot be excluded, except if physically impossible, that those situations beyond the design basis could really occur. Therefore, the plant design should facilitate the management of such situations. For this purpose:
  - The reactor design should be done for obtaining long time before safety systems are required to operate for avoiding the occurrence of a severe accident situation.
  - The prevention of the severe accident should include capabilities offered by natural behavior and the reactor design should minimize the need of support functions, in particular electrical supply.
  - The mitigation of severe accident shall be considered in the reactor design. The design should be done for obtaining long time before mitigation systems are required to operate for avoiding the occurrence of important radiological releases in the environment.

— The devices absolutely necessary for avoiding important radiological releases in degraded situations shall be identified and integrated in the hardened safety core. The design of these devices should include:
  - The combination of loadings due to natural phenomena having an exceptional magnitude, beyond the magnitude consider for the whole design of the plant.
  - The combination of an extended failure of AC power supplies and failure of the main heat sinks.
  - The accident situations occurring in several areas inside the plant and inside the nuclear site.
  - The difficulty to access to the site and to certain plant areas in accident conditions.

— The situations which cannot be reasonably mitigated in term of radiological releases in the environment, shall be identified and the subject of a specific demonstration of practical elimination. This demonstration should include the possible occurrence of beyond design basis loadings, in particular loadings due to extreme natural hazards.

6. First orientations for the ASTRID design issued from the analysis of the Fukushima accident

Some of the following orientations were considered in the design of ASTRID. The occurrence of the Fukushima has reinforced the necessity to consider them. The main orientations considered at the current conceptual phase of the project are:

— To reinforce the combinations to consider for the design, in particular, the combination of hazard and failure of equipment, even if the equipment is designed considering the hazard. This concerns mainly the earthquake for which combination with failure of some sodium pipe and vessel is taken into account despite the seismically design of the pipes and vessels.

— To reinforce the design for limiting the consequences of the failure of any AC power supply and loss of the main heat sink. This leads to improve the capability of primary circuit and some decay heat removal systems to operate in natural circulation, at least during a long period of time. Also, this reinforces the need to develop the design for avoiding occurrence of a severe accident in case of loss of cooling of the main safety structures (*e.g.*, roof, reactor pit).

— To reinforce the capability of the emergency heat sinks to resist to hazards. This reinforces the need to diversify the related equipment. Their diversity is assessed considering also the occurrence of extreme hazards.

— To maximize the grace time available before initiating corrective actions in accident conditions, including the severe accident situations.

— To improve the application of the defense-in-depth principle as regards hazards (*e.g.*, in case of external flooding, the orientation is not only to provide a sufficient ground level for the plant or to implement a dyke, but also to postulate flooding inside the site.

— To evaluate the possible advantages provided by specific devices implemented for reducing the loadings due to the hazards, especially with regards to earthquake (*e.g.*, earthquake-resistant devices).

Concerning the safety demonstration, the main orientations due to the Fukushima accident are:

— To re-assess the SP and SM situations considered for the design in order to identify the ones which could result from hazards, and to verify if additional situations resulting from hazards should be considered.

— For the situations which could result from hazard, to verify that the devices needed for limiting their consequences at an acceptable level are not damaged by the hazard and their design provides significant margins..

— To assess the combination of the loss of AC power and more generally the failure of active systems and operator action with any design basis condition. The orientation is to verify that unacceptable consequences cannot occur at short term.

7. First considerations concerning the ASTRID hardened safety core

7.1. Identification of the hardened safety core devices

For the conceptual phase of ASTRID, the identification of the hardened safety core concerns the equipment and not the organization aspects. The principles considered for identifying the devices requiring being in the hardened safety core are:

— The hardened safety core devices are absolutely necessary for avoiding unacceptable consequences. Taking into account that severe accident situations are considered for the design and that mitigation devices are implemented for avoiding important radiological

releases in the environment, the relevant devices are therefore the ones absolutely necessary for avoiding important radiological releases in case of severe accident situations.

— The consequences of a practically eliminated situation, if it would occur, should be unacceptable. Therefore, among the devices implemented for achieving the objective to practically eliminate the situation, at least one of them shall be included in the hardened safety core.

— Additionally, the devices necessary for performing emergency actions and emergency planning should also be included in the hardened safety core.

In order to reduce the sensitivity of the reactor to the earthquake and also the inherent uncertainties related to the characterization of the seismically-induced loadings, the implementation of seismic isolation devices below the basemat is envisaged for ASTRID. Such devices shall be designed in order to be efficient even in case of earthquake having magnitude more severe than the one considered in the design basis.

7.2. *Design of the hardened safety core devices*

The hardened safety core devices are designed for achieving their absolutely necessary functions even if hazards with magnitudes more severe than the ones considered in the design basis would occur.

For this purpose the following design orientations are considered:

— To intrinsically reduce the sensitivity of the device to hazards, including combination with events which could be associated to the hazards.

— To minimize the need of support systems for operation of the devices. In particular the need of AC power supply, I&C and human action, at short term, shall be minimized.

The devices are first designed considering the loadings due to hazards with the conventional conservative rules. Then, the margins provided by the conventional rules shall be quantified and the weakest part of the devices is identified and if necessary reinforced in order to obtain about homogeneous behavior of the device. If it is reasonably feasible, the whole behavior of the device with regards to hazards might be improved.

8. Conclusion

The first analysis of the Fukushima accident and the impact of the lessons learned for the conceptual phase of ASTRID are mainly:

— The Fukushima accident does not throw the ASTRID concept back in question. The intrinsic characteristics of liquid metal reactors allow to reduce the needs to AC power and fast emergency actions for the prevention of severe accident.

— These intrinsic characteristics shall be reinforced in order to maximize the capabilities to consider the natural behavior and the grace time before actions of safety systems.

— The need to mitigate the severe accident situations is reinforced with a particular attention of their combination with hazards.

— The identification of situations needing to be practically eliminated is reinforced and the consideration of hazards as potential initiators of these situations shall be also reinforced.

The hardened safety core devices absolutely necessary for avoiding unacceptable consequences (i.e., important radiological releases in the environment) shall be identified and their design shall be reinforced with regards to hazards.

The implementation of the lessons learned by the analysis of the Fukushima accident allows to improve the safety more generally than only consideration of external natural hazards. In particular, the consideration of situations resulting from hazards with magnitudes higher than the ones considered for the design, should also improve the resistance of the plant with regards to malevolent actions.

The results of the analyses of the Fukushima accident itself as well as the lessons learned for the other plants in operation or under development, will be assessed during all the design phases of ASTRID.

REFERENCES

[1] P. Le Coz *et al.*; Sodium-cooled Fast Reactors: the ASTRID plant project; Proceeding of ICAPP'11, Nice France, May 2-5, 2011; Paper 11249

[2] P. Lo Pinto *et al.*; Safety orientations during ASTRID conceptual phase; International Conference on Fast Reactors and Related Fuel Cycles: Safe Technologies and Sustainable Scenarios (FR13); Paris France, March 4-7, 2013; Paper IAEA-CN-199-267

[3] Avis n° 2012-AV-0139 de l'ASN du 3 janvier 2012 sur les évaluations complémentaires de la sûreté des installations nucléaires prioritaires au regard de l'accident survenu à la centrale nucléaire de Fukushima Daiichi

ESFR Severe Accident Analyses with SIMMER-III

M. Flad[a], **D. Zhang**[a], **C. Matzerath Boccaccini**[a], **F. Gabrielli**[a], **B. Vezzoni**[a],
W. Maschek[a], **G. Brillant**[b], **H. Bonneville**[b]

[a] Karlsruhe Institut of Technology (KIT)
Eggenstein-Leopoldshafen, Germany

[b] Institut de Radioprotection et de Sûreté Nucléaire (IRSN)
Saint-Paul-Lez-Durance, France

Abstract. The Collaborative Project on European Sodium Fast Reactor, CP-ESFR, combines European efforts advancing fast reactor technology towards economics, safety and nuclear waste reduction. A key issue of development is the promise of a higher and improved safety level. Both on the prevention and mitigation side significant efforts are invested to fulfill the high safety goals. Research in severe accident phenomenology and safety analyses help to develop means for better prevention and mitigation. Within this framework accident initiators are investigated leading to an unprotected loss-of-flow (ULOF) and a total instantaneous blockage (TIB) scenario. Simulations focusing on the energetics behavior apply SIMMER-III, an advanced accident code coupled with space- and energy-dependent neutronics. For the ULOF especially the transition phase with its recriticality potential has been of interest, while for the TIB the issue of melt propagation has been a key focus. In addition it has been investigated whether the available core material removal paths are sufficiently effective to prevent recriticality scenarios. The ULOF conditions for SIMMER have been provided by a SAS-SFR simulation of the ULOF initiation phase. For the TIB the SIMMER simulations started from steady state core conditions.

1. Introduction

Fast Reactors possess the unique capability as sustainable energy source. A closed fuel cycle allows a significant improvement of the usage of natural resources and allows the reduction of radiotoxicity, volume and heat load of high-level waste. Among the fast reactor systems, the sodium-cooled fast reactor has the most comprehensive technological basis, due to past and on-going operation of experimental, prototype and commercial size reactors [1].

The Collaborative Project on European Sodium Fast Reactor (CP-ESFR) merges contributions of 25 European partners for further development of the sodium fast reactor. As described in [2]: The CP-ESFR has the ambition to contribute establishing a "*sound scientific and technical basis* for the European Sodium Fast Reactor in *order to accelerate practical developments for the safe management of long-lived radioactive waste, to enhance the safety performance, resource efficiency and cost-effectiveness of nuclear energy and to ensure a robust and socially acceptable system of protection of man and the environment against the effects of ionising radiation.*"

One key focus point in the CP-ESFR project is safety. The sub-project SP3 is especially in charge to demonstrate adequate safety measures. Working horse (WH) cores and plant designs are provided by other sub-projects. For the analyses the MOX core has been chosen. Using the working horse core, the SP3 aimed at investigating safety issues in a well balanced level of detail. The work package WP3.3 investigated representative transients and accident scenarios for design basis and beyond design basis

events. Task 3.3.2 concentrated on the consequence analyses of design extension conditions (DEC), especially the potential of core disruption and evaluation of the severe accidents phenomenology. A key focus was on potentially new effects introduced by the design features of the ESFR core.

In the current paper the safety analyses [3] based on the SIMMER-III code system [4, 5] are described, investigating at first a 'global' transient, the Unprotected Loss of Flow (ULOF) and secondly a 'local' initiator, the Total Instantaneous Blockage (TIB). For the ULOF especially the transition phase with its recriticality potential has been of interest, while for the TIB the issue of melt propagation has been a key focus. In addition it has been investigated whether the available core material removal paths are sufficiently effective to prevent recriticality scenarios. The ULOF conditions for SIMMER have been provided by a SAS-SFR simulation of the ULOF initiation phase[3, 6]. For the TIB the SIMMER simulations started from steady state core conditions. For the ULOF it was decided to analyze the ESFR End of Equilibrium Cycle EOEC core and for the TIB analyses the Beginning of Life BOL core has been chosen.

The SAS-SFR simulations of the initiation phase of the ULOF show a rather benign accident development with peak temperatures of the hexcans just reaching the melting temperature locally at the end of the calculation. The core is almost completely voided and almost all pins in the subassembly groups have failed. As most of the fuel is still allocated within the core region the further accident scenario simulated with SIMMER-III is characterized by multiple recriticalities and secondary power excursions in the transition phase. Fuel coolant interactions with sodium in the control and absorber rods and in the radial reflector region strongly influence the accident development. The fuel removal via the special elements in the core were not sufficient for preventing recriticalities. Optimization of the design could increase the fuel relocation potential. An important reactivity effect reflecting the transition from a heterogeneous pin arrangement to fully broken-up pin has been identified which has to be included in future initiation phase analyses.

The TIB simulations with SIMMER-III were performed in two steps, investigating the blockage impact of a single subassembly and its surrounding 6 neighbours and finally analyzing the impact of a blocked subassembly embedded in the whole CP-ESFR core including full core neutronic feedback. According to the current simulations a propagation of the damage beyond the seven subassemblies and a whole core involvement have to be expected.

2. SIMMER-III Steady State Preparation for the DEC Analyses of the Working Horse Core

The CP-ESFR "Working Horse" core configuration is described in detail in [7]. The thermal power is 3600 MW, core inlet and outlet temperatures are 674 K and 818 K respectively and the average fuel temperature is around 1500 K. The CP-ESFR WH core consists of two core zones, the BOL Pu content being 14.43 at% and 16.78 at% in the 225 inner and 228 outer core SAs (Fig. 1).
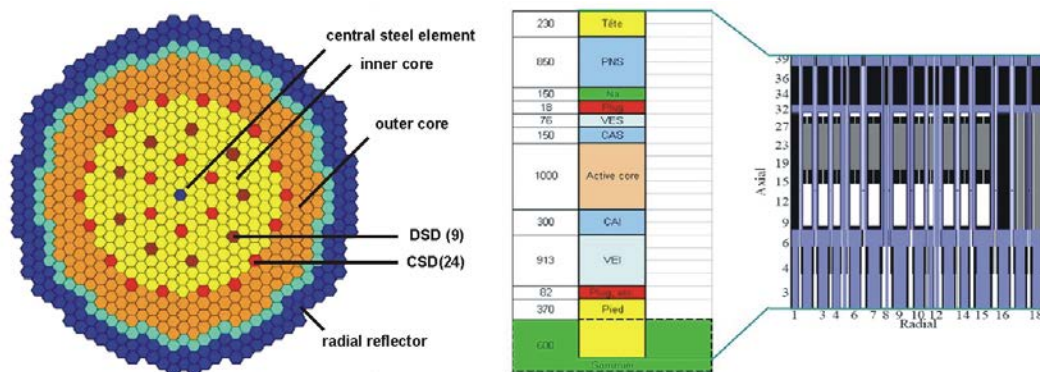

FIG. 1. CP-ESFR WH radial and axial core layout and SIMMER core set-up

 The fuel residence time at EOL is assumed to be equal to 2050 Equivalent Full Power Days (EFPDs), with a reloading strategy of about 1/5 of the core every 410 EFPDs. The average and maximum core burn-up values are 100 GWd/tHM and 145 GWd/tHM, respectively, for the average power density of 206 W/cm^3. The control system includes 9 DSDs (Diverse Shutdown Devices) and 24 CSDs (Control and Shutdown Devices). The CSD rods contain natural boron carbide (B$_4$C with ~19.9% of ^{10}B) whereas the DSD rods contain enriched boron carbide (B$_4$C with ~90% of ^{10}B). The radial reflector containing EM10 steel surrounds the core and includes three rings of SAs.

The steady state calculations of the CP-ESFR WH core were carried out with SIMMER-III at the Beginning of Life (BOL) and End of Equilibrium Cycle (EOEC) conditions, respectively. The BOL one is prepared for the TIB simulation, while the EOEC one is for the ULOF simulation. Different cooling schemes were adopted for the BOL and EOEC simulations. In Fig. 2 the normalized power distribution of the BOL and EOEC core are displayed showing the large radial shift of the power between the BOL and EOEC core. For the EOEC core a special cooling strategy has been chosen for the initiation phase analyses of the ULOF with SAS-SFR. However these cooling strategy leads to too high clad temperatures in the BOL core. For the TIB calculations, performed for BOL, therefore a different cooling strategy has been chosen to respect the safety limits of the clad. In Tab. 1 safety relevant data as the void worth or the Doppler value for the EOEC core are displayed.
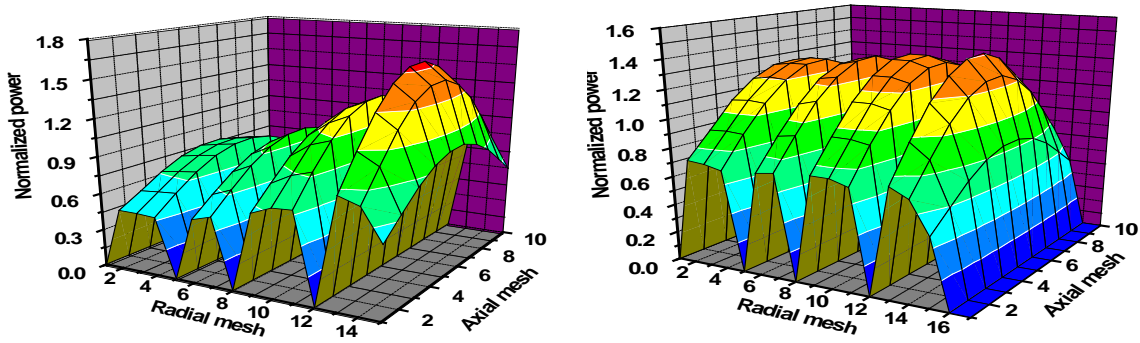
FIG. 2. Normalized power of the BOL core (left) and EOEC core (right)

Table 1. Neutronic parameters at steady state: Reference [7] and SIMMER-III calculations

Parameter	Unit	Reference [7]	SIMMER-III (EOEC)
K-effective	[-]	1.01662/1.01803	1.00778
Beta-effective	[pcm]	–	343
Total core void worth	[pcm]	+2216/+2206	+2108
Doppler constant KD	[pcm]	-809/808	-843 (1500 K-2100 K)
Total power peaking factor	[-]	1.581	1.411

3. Investigations on the Heterogeneity Effect for the ESFR WH Core

In the wake of the SIMMER analyses of the CP-ESFR WH core and related to former developments in SIMMER to treat heterogeneity effects [8] an important reactivity effect has been identified in cores with fat pins. The effect plays an essential role especially in cores with low void worth with a delicate reactivity balance. The identified effect must be included under such conditions in all initiation phase analyses with phenomena as break-up of pin structures and going from heterogeneous configurations to more homogeneous configurations with fuel and steel mixed. The effect takes place at a sensitive accident phase, near prompt critical when fuel breaks up. The so-called 'double heterogeneity' effect [9], [10] in fast reactor lattices was largely investigated in both critical experiments and power reactor

lattices (Superphénix). The double heterogeneity effect is related to the fact that actual fast reactor lattices are made up of a lattice of fuel pellets, clad, liquid sodium and the hexcan wall. Currently a cell-wise resolution of the heterogeneity effect is possible with SIMMER up to pin break-up. A further model covering the impact on local reactivity after pin break-up is under consideration. Present results show that the effect of the double heterogeneity on the k_{eff} eigenvalue is about -640 pcm. The Doppler constant K_D is not affected by the heterogeneity.

4. SIMMER-III ULOF Calculations for the CP-ESFR "Working Horse" Core Starting from SAS-SFR Initiation Phase Conditions

As described before, the SIMMER transition phase simulation of the ULOF starts after a SAS-SFR simulation of the initiation phase at a certain cross-over point. The data transformation from SAS to SIMMER is a complex procedure and SAS-SFR and SIMMER models are quite different (partly Lagrangian versus Eulerian description; multiple 1D versus 2D/3D, different approaches with respect to material properties, velocity fields, neutronic data and methods etc.). The special interface code, SAME, for connection between SAS and SIMMER was developed at JAEA. As a basic assumption taken in the coupling procedure, the reactivity and power trace should be continued and be monotonous to conserve the phenomenology. Currently this path is taken for pragmatic reasons, but one should be aware of the modeling and data differences.

In Fig. 3 the material distribution at the SAS-SFR coupling point and the power history are shown. All fissile subassemblies from the core region are voided with still intact pin structures in Channel 29 and 30. In SIMMER-III the geometrical position of the subassembly is of importance. The geometrical set-up is performed via a ring structure in 2D. One ring should consist of elements with similar neutronic (fuel) and thermal-hydraulic conditions. In the current ESFR case a complex channel distribution is envisaged. For the SIMMER set-up therefore some compromises had to be made for casting the SAS into the SIMMER geometrical framework. In Fig. 4 the basic SIMMER set up is displayed.
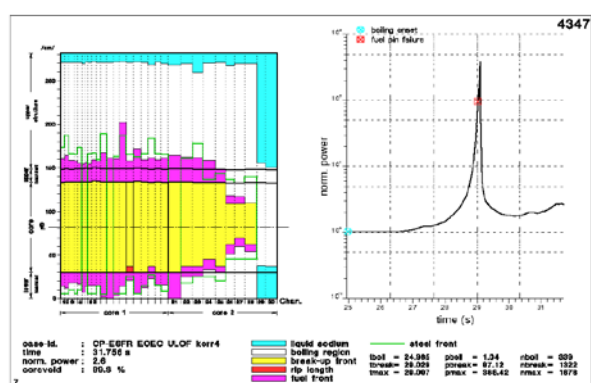
FIG. 3. SAS-SFR material conditions at the coupling point and power transient.
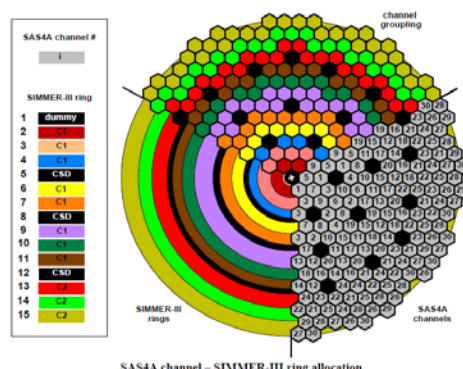
FIG. 4. SAS channel – SIMMER ring allocation for the CP-ESFR design

In the following some transient calculations for the transition phase of the ESFR with the SIMMER-III code are described. The calculations should cover a range of scenarios and important boundary conditions. Especially the status of the control rod structures and their influence on the transition phase scenario were studied. The control rod rings are modeled as consisting of a hexcan structure at similar temperature or different temperature level as the neighboring hexcans and not voided. For the reference case L-1 the special elements are filled with sodium at 900 K.

In Fig. 5 the power and reactivity history is displayed for reference case L-1. The power trace shows the typical accident development during a transition phase with excursions caused by recriticalities until sufficient fuel is discharged to lead to subcritical conditions. Reactivities are given in $. Prompt criticality is reached a couple of times and the maximum excursion goes up to 1.54E+14 W.
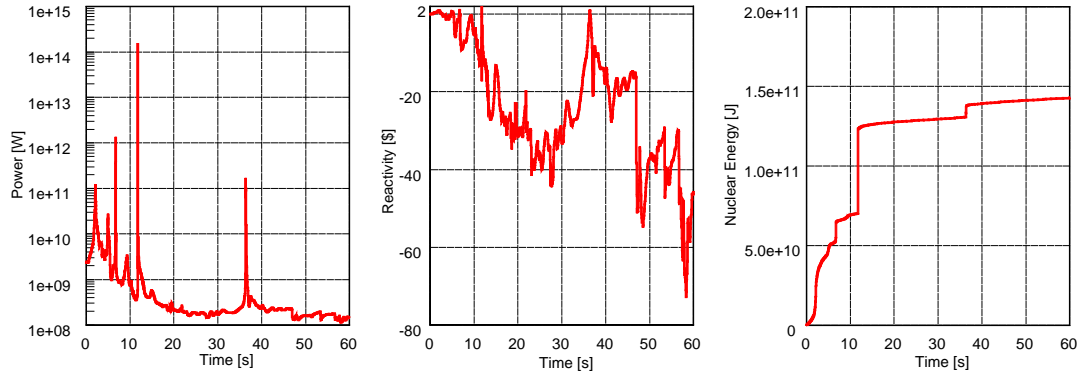
FIG. 5. Power and reactivity trace and thermal energy accumulation of the Case L-1

As a general tendency it can be seen that the first accident phase (up to ~ 15 s) is neutronically highly active. The high fuel inventory allows the easy achievement of recriticalities and the failure of the control rod and absorber rod structures at 0.6 s, 0.7 s and 3.6 s triggers sloshing processes caused by fuel-coolant interactions (FCI) and fuel compaction/expansion cycles.
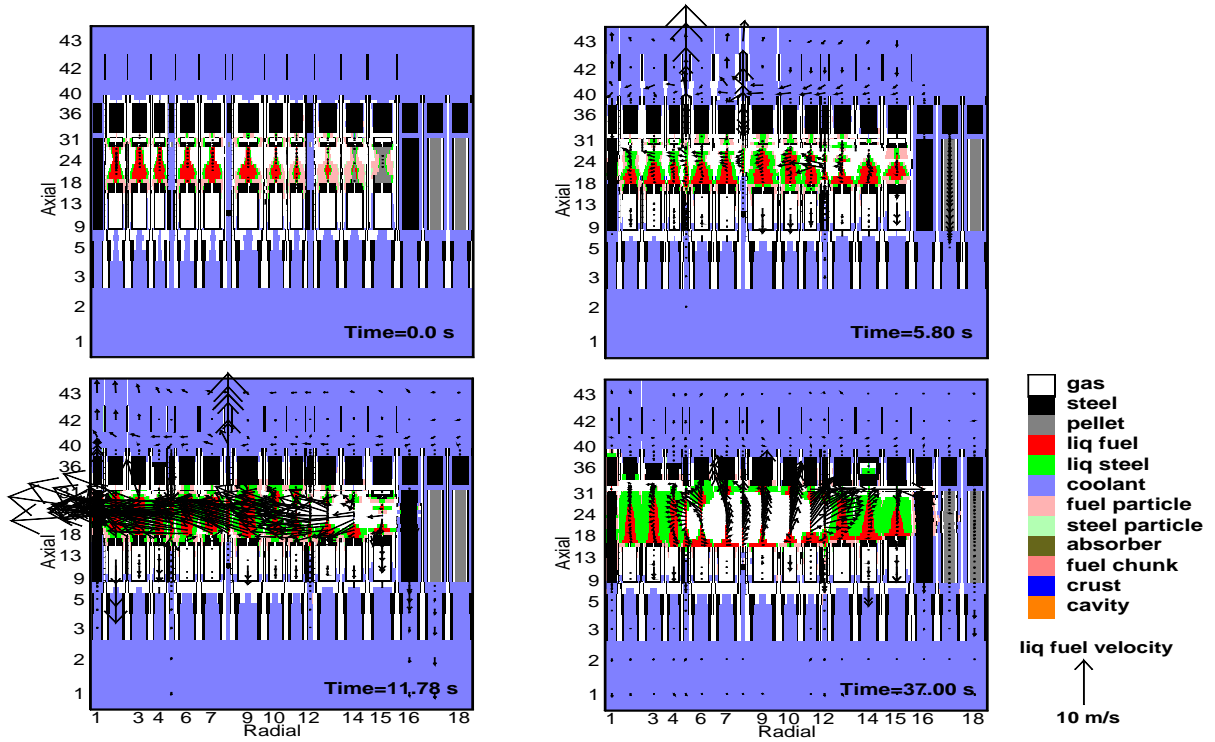
FIG. 6. Material configurations and sloshing motion patterns leading to recriticalities and excursions

In Fig. 6 the material configuration is displayed for some important branching points of the accident evolution of Case L-1. The early failure of the control- and absorber rod structures allows full radial material movement and sloshing [11]. The failure sequence and failure position of the CDS and DSD structures is also of importance influencing the fuel sloshing motion. As can be observed, the accident evolution is significantly driven by FCI processes. After this first period roughly 20 % of the fissile fuel inventory has been relocated and a more quiet accident phase is entered.

A noteworthy point is the observed fuel release via these reflector and shield structures. This effect will be even more pronounced in cores with optimized sodium plena for void reduction. The fuel relocated upwards into this open plenum could be diverted radially to the outer reflector areas. It is also observed that downward fuel relocation via these structures takes place defining a relocation path into the below core structures and a potential core catcher area.

5

The results of the transition phase could be significantly influenced by the stability of the upper structures. In the simulation the upper shield stays in place even if the below structures have vanished. The original SIMMER modeling philosophy was influenced by the MONJU and CRBR core designs [4], where the upper structures where held together tightly and stayed in place under the condition of a molten pool below. The stability of the upper structure is complex to assess as it is affected by design and irradiation conditions (pad forces, irradiation and temperature effects, force bridges etc.) but also depends on fuel and steel freezing procedures during the accident. For the ESFR, the conditions of the upper structure behavior were not fully defined. There are reasons to assume that for the ESFR the upper structures will enter the core after hexcan melting and the cycle of recriticalities could be interrupted. An important point is the aforementioned fuel relocation upwards into the axial reflector and shield structures and their damage further increasing the potential for an upper structure collapse. A SIMMER development for movement of larger upper structures is therefore of high importance.

In another case, Case L-4, it has been investigated if the absorber and control rod structures could be 'optimized' to increase the fuel relocation potential and if this could lead to a relief of the recriticality concern. Therefore the below core structures of the special elements were simplified and the free streaming paths were increased by removing the dashpot necking.
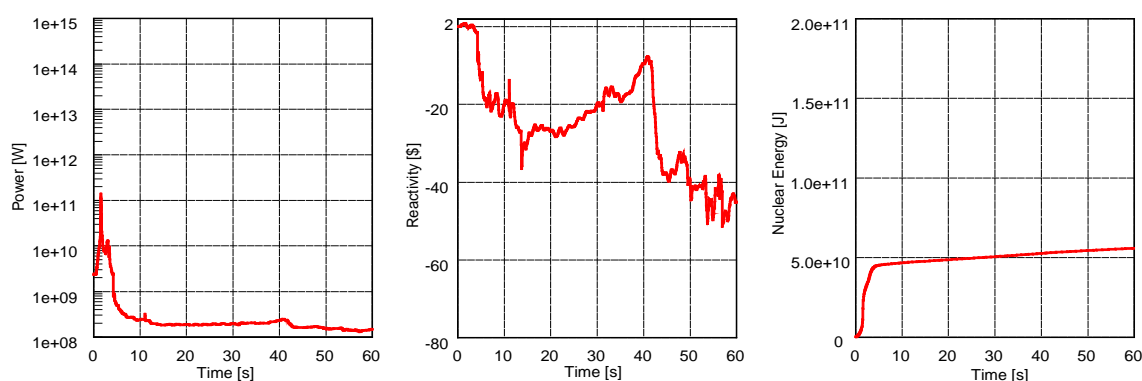
FIG. 7. and reactivity trace and thermal energy accumulation of the Case L-4

From the power development in Fig. 7 it can be observed that no severe recriticality takes place. The overall scenario resembles that of the Cases L-1, as can be seen in the reactivity plot. Again at 10 s reactivity increases and also later at 40 s reactivity is rising due to fuel/steel separation in the pool. But the early loss of fuel during the first 10 s shifts the reactivity and reactivity swings to a lower level. The idea to enhance early fuel relocation by optimizing release paths and/or installing special devices can be regarded as a potential measure for breaking the recriticality cycle.

5. SIMMER-III TIB Calculations for the CP-ESFR "Working Horse" Core

Besides the global initiator of a ULOF a local initiator, the Total Instantaneous Blockage Accident (TIB) has been investigated. The TIB starts from a local perturbation (e.g. one subassembly) with the rest of the core still under full coolant flow and undisturbed.

The key questions following from these conditions are:

- Does a local severe single subassembly perturbation as a TIB lead to a propagation scenario with involvement of surrounding subassemblies?
- Is there sufficient grace time for detection and reactor trip?
- Does propagation include escalation with decreasing time scales?
- What does propagation mean for the whole core involvement taking into account the neutronic feedback effects of the core?

The TIB is a very specific accident as it is assumed that the whole flow is instantaneously lost in one subassembly. The total instantaneous blockage (TIB) accident has been considered in the past e.g. for the RNR 1500 as a beyond design reference accident in the frame of licensing procedures [12], [13]. The interest in this transient is also grounded in the extensive SCARABEE-N experimental program [14]. The conclusion of the SCARABEE-N assessment was that e.g. for SPX1 conditions [13] the perturbation from the blocked assembly will propagate within ~15 sec into the 6 surrounding subassemblies and in another 15 sec the next 12 assemblies could be involved. Within the time-frame of 15 sec the propagation should be detected by Delayed Neutron Detectors (DND) and stopped by a reactor scram. Further extension of the damage will be prevented. Additional insight into the evolution of the TIB accident can be gained in the paper on a TIB in a Phénix subassembly [14]. As a conclusion, experimental results seem to confirm propagation but also confirm the possibility to detect the transient in due time and initiate a reactor scram. Concerning the detection of the TIB, the thermocouples with a delay time less than 5-10 seconds, delayed neutron detectors (DND) with response times of 15-35 seconds, depending on the reactor design and reactimeters with a time scale of less than a second (100-200 ms) [12], [13], [14] would be available.

The choice of a total blockage seems to be grounded in past near blockage (SPX) or actual blockage events (Fermi reactor, BN-600, PFR). Blockage formation itself and blockage extension is difficult to predict and still beyond a mechanistic modeling by codes. The investigations of the SCARABEE team laid the ground for the assessment of the blockage accident both for the SPX and the EFR. In these reactor designs the subassemblies have an average power of ~ 10 MW/sub. In addition both the SPX and the EFR are high void cores equipped with axial blankets. The SCARABEE experiments and conclusions drawn reflect these conditions. There is only one SCARABEE-N experiment BE+3bis with no upper blanket structures. The experiments also have been done for BOL conditions [13].

The ESFR core shows marked differences. First, the central subassemblies in the inner core at BOL have only half the power of a SPX or EFR subassembly. In addition the ESFR is already a core with lower void and it also has no axial fuel blankets but steel reflector structures. The early studies mostly concentrated on thermal-hydraulic investigations. A geometry of 7 subassemblies was investigated with the central subassembly blocked. The impact of the local perturbation on the whole core and the feedback of the whole core on the propagation has been firstly assessed in [15] for a specific core which takes parts of the ESFR design but has high power central subassemblies, high void worth and axial blankets. The idea in these preliminary calculations was to assess the SIMMER-III [4], [5] code for its capability to investigate the TIB close to the SCARABEE assessment conditions. The conclusion from these simulations were, that a propagation process after blockage formation takes place in a very similar way as is described and visualized in [13] where the SCARABEE-N findings are extrapolated to the reactor case. Fuel release via the Control Rod Guide Tube (CRGT) rings seems to be insufficient to counter the reactivity increase during the accident evolution and damage propagation. The initial propagation time scales are in accordance with the estimates made within the SCARABEE-N program. From a certain point in time the power increases steadily and the whole core is finally subjected to an overpower transient. The power excursion is caused by the radial and axial void growth and by fuel compaction within the already destroyed core regions. The reactivity and power increase in the first seconds of the transient, sufficiently long before the final excursion, would trigger a scram signal besides the DND and would lead to a shut-down of the reactor.

The simulation of a TIB is more complex than a ULOF due to limits in the simulation capability. In the case one simulates a seven subassembly geometry, the pin, hexcan and gap structures can be modeled in detail but the neutronic feedback from the whole core is not taken into account. If the whole core is modeled with e.g. a central subassembly perturbed, the subassemblies are represented as a rather homogeneous entity with e.g. no temperature profile or flow profile in the individual subassemblies. For the whole core simulation experience from simulations of the small size EFIT and XT-ADS heavy metal cooled subcritical reactors were available.

The modeling details have an important impact on the simulations. Based on the findings of the preliminary simulations and the findings of SCARABEE-N it was decided to perform two types of SIMMER simulations to obtain a valid assessment of the propagation potential.

- The TIB is investigated concentrating on a seven-subassembly geometry with imposed power profiles, simulating the small scale pin and subassembly geometry.
- The TIB is studied simulating the whole core and its neutronic feedback effects on the propagation potential caused by a local perturbation.

In the first part of the transient analysis, in the seven subassembly approach cases have been investigated with either inter wrapper gaps filled by sodium or gaps already been closed. It has been observed in the SCARABEE experiments that the internal wrapper bow due to thermal and pressure constraints, get close to the neighboring wrapper, and consequently stop the sodium flow in the inter wrapper gap. In addition the influence of various power profiles and sodium conditions have been investigated. The adjacent hexcans have been modeled either individually with the gap in between, or the hexcans have combined at one side of a mesh cell. Full heat transfer between the hexcans and the gap is then modeled in the SIMMER framework. In the default SIMMER modeling the gap between two adjacent hexcans is assumed as a now-flow area and no heat transfer is assumed via the gap.

The simulations of the 7 subassembly approach was performed on basis of a SIMMER fluid-dynamic code version with imposed power (flat, cosine and asymetrical profiles). All cases considered featured a propagation from the centrally blocked subassembly to the 6 surrounding ones.

For the whole core simulation including neutronics, first the SIMMER default model has been chosen. For large cores this significantly increases the mesh number and calculational time. Analyses showed, that for the low power central subassemblies near propagation conditions were reached but finally no propagation took place. To increase modeling details, a gap has been introduced in the second set of calculations. In addition the model with the re-setting of the hexcans has been chosen. With this refined modeling potential fuel/coolant interactions with the gap sodium could be modeled. Note that failure of the hexcan might not only happen by fuel crust break-up and hexcan melting, but also by steel jets impinging on the hexcan without fuel crust.

In the following the results of Case T-4 [3] with combined hexcans, allowing heat transfer via the gap are presented. The accident was triggered by blocking the top cells of the subassembly foot section at a problem time of 65 s. The damage propagation can be identified by the failure of the hexcans and finally involves the whole core also with an increase of reactivity and power. The propagation finally leads to shortened failure time intervals and the involvement of the whole core (Fig. 8).
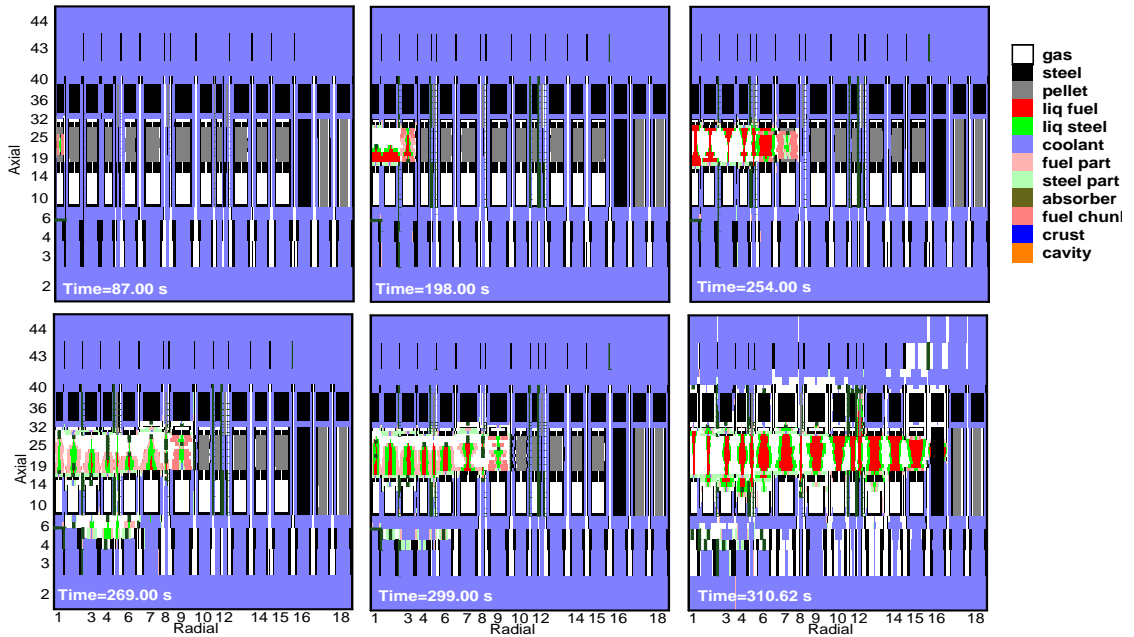

FIG. 8. Failure and material distribution for case T-3 (Blockage at t = 65 s)

Both the consumption of the core void and fuel compaction processes drive the propagation and finally the escalation of the transient. Due to missing driving pressures from fuel/coolant interactions and the large chunk fuel and particle fraction at the start of the transient also no massive fuel discharge takes place which could stop the failure propagation and escalation of the transient. The investigations with SIMMER revealed a sensitive interplay of the reactivity time-step and the heat transfer phenomena, which are taking place on the same time level. Care must be taken in defining the time-step criteria for the individual cases by monitoring the reactivity calculation.

Concluding from the analyses the posed questions can be answered as follows:

- The TIB has a high probability to lead to a propagation scenario
- The TIB has a high chance to be detected and the reactor can be tripped in time
- The damage propagation includes escalation with decreasing time scales
- Without scram a whole core involvement has to be expected with a power transient

6.   Conclusions

Safety analyses for the CP-ESFR are described based on the SIMMER-III code, investigating both a 'global' transient, the Unprotected Loss of Flow (ULOF) and secondly a 'local' initiator, the Total Instantaneous Blockage (TIB). For the ULOF especially the transition phase with its recriticality potential has been of interest and for the TIB the melt propagation. In addition it has been investigated whether available core removal paths are sufficient to prevent recriticality scenarios. The ULOF conditions for SIMMER have been provided by a SAS-SFR simulation of the ULOF initiation phase. For the TIB the SIMMER simulations started from steady state core conditions. For the ULOF it was decided to analyze the ESFR EOEC core and for the TIB analyses the BOL core has been chosen.

The coupled SAS-SIMMER analyses for the ULOF revealed an energetic transition phase if not sufficient fuel is discharged from the core. Fuel coolant interactions following from failure of the control and absorber rod structures strongly influence the transition phase scenario. Especially the failure of the radial reflector elements triggers a severe recriticality. Fuel discharge via the radial reflector region into the upper plenum and below core structures can be observed in the ESFR transition phase. Fuel and especially molten steel from the core can massively damage the surrounding structures of the core. Upper structure collapse could severely influence the transition phase scenario but currently can not be mechanistically modeled in SIMMER. This point will be an important future model development for SIMMER. In the current ESFR design the fuel relocation via control and absorber rods is not sufficient to prevent recriticalities. Optimization of the special elements like control and absorber rods or diluents for an increased and early fuel discharge could influence the transition phase scenario and break the recriticality cycles. An important reactivity effect reflecting the transition from a heterogeneous pin arrangement to a fully broken-up pin with a homogenized mixture of fuel and steel exists in the initiation phase when fuel disruption starts during the primary excursion.

The results of the TIB simulations for the whole core including all neutronic feedback effects showed that the simulation needs a good resolution of the local structures including the heat transfer paths. The simulation with the standard SIMMER option of a non-flow gap region between the individual subassemblies is not sufficient. This is especially important for low power and low void worth subassemblies. The results of the simulations showed that, (1) local perturbation (TIB) leads to a propagation scenario, (2) the TIB can be detected and the reactor can be tripped in time with proper means, (3) the propagation includes escalation with decreasing time scales and (4) without scram a whole core involvement has to be expected with a power transient.

The investigations provided valuable insights into options for preventive and mitigative measures for recriticalities giving useful hints for further investigations.

REFERENCES

[1] GIF IV Technology Roadmap; November 2002 (www.gen-4.org)

[2] Fiorini, G.L., 2009. The Collaborative Project on European Sodium Fast Reactor (CP ESFR), FISA 2009, 22-24 June, Prague, Czech Republic

[3] Deliverable SP3.3-D2: Results of transient analyses for representative accidents within the beyond design basis domain including sequences leading to core destruction and core material relocation down to the ultimate retention device, CP ESFR Collaborative Project for a European Sodium Fast Reactor, 7th FP EURATOM, Contract Number: 232658 (2012)

[4] Kondo S., Morita, K., Tobita, Y., Shirakawa, N., 1992. SIMMER-III: An Advanced Computer Program for LMFBR Severe Accident Analysis, ANP'92, Tokyo, Japan, Oct. 25-29, No. 40-5

[5] Kondo, Sa., Yamano, H., Tobita, Y., Fujita, S., Kamiyama, K., Maschek, W., Coste, P., Pigny, S., Louvet, J., 2000. Phase 2 code assessment of SIMMER-III, a computer program for LMFR core disruptive accident analysis. JNC Report. Japan Nuclear Cycle Development Institute, JNC TN9400 2000-105

[6] W. Pfrang, D. Struwe: SAS-SFR Ref 2008 Rel 1.0 Input Data Documentation (August 2008)

[7] L. Buiron, "CP ESFR Working Horses Core concept definition". CP-ESFR D SP2.1.2.0 D1, June 2009

[8] F. Gabrielli, Models for Transient Analyses in Advanced Test Reactors, Ph. D. thesis, IKE of Stuttgart University, 22. February 2011, Stuttgart, Germany

[9] T. Takeda, H. Unesaki, T. Yamamoto, K. Kinjo, T. Sandia, Evaluation of Neutron Streaming in Fast Breeder Reactor Fuel Subassembly by Double Heterogeneous Modeling, Nucl. Sci. Eng., 101, 179-184 (1989)

[10] M. Nakagawa, H. Inoue, Double Heterogeneity Effect of Fuel Pin and Subassembly in a Fast Power Reactor, *Nucl. Sci. Eng.*, 83, 214-228 (1983)

[11] Maschek, W., C. D. Munz, L. Meyer, Investigation of Sloshing Motions in Pools Related to Recriticalities in Liquid-Metal Fast Breeder Reactor Core Meltdown Accidents, Nucl. Techn. 98, 27, (1992)

[12] Papin, J., Sesny, R., Soussan, P., Mac Dougall, J., Stansfield, R., 1990. The SCARABEE Total Blockage Test Series: Synthesis of the Interpretation, The 1990 Int. Conf. on FR Safety, Snowbird, Utah, USA, August 12 -16

[13] Kayser, G., Charpenel, J., Jamond, C., Berthoud, G., Schleisiek, K., 1994. Main SCARABEE lessons and most likely issue of the sub-assembly blockage accident, Int. Top. Mtg. Sodium Cooled FR Safety, Obninsk, Russia

[14] Cadiou, T., Louvet, J., 2006, Evaluation of the Accident Scenario Initiated by a Total Instantaneous Blockage in a Phénix Subassembly, Nuc. Techn., Vol. 153, pp 256- 263

[15] W. Maschek, M. Flad, C. Matzerath Boccaccini, S. Wang, F. Gabrielli, V. Kriventsev, X.-N. Chen, D. Zhang, K. Morita, Prevention and Mitigation of Severe Accident Developments and Recriticalities in Advanced Fast Reactor Systems, Progress in Nuclear Energy, Sept. 2011, Vol. 53, No. 7, pp. 835-841

Major Remaining Uncertainties Associated with Source-Term Evaluation for SFR Severe Accidents

M.P. Kissane[a], M. García-Martin[b], L.E. Herranz-Puebla[b,1]

[a] Institut de Radioprotection et de Sûreté Nucléaire (IRSN), PSN-RES/SAG, BP 3, 13115 St-Paul-lez-Durance, France

[b] Centro de Investigaciones Energéticas, Medioambientales y Tecnológicas (CIEMAT), Avda. Complutense, 40, 28040 Madrid, Spain

[1] corresponding author

Abstract. SFR accidents involving severe core damage could entail highly-energetic in-vessel phenomena provoking ejection into the containment of sodium and disrupted-core components. The present work results from completion of a Phenomena Identification and Ranking Table (PIRT) exercise applied to radiocontaminant-transfer aspects of a severe accident (undertaken for the FP7 Collaborative Project for a European Sodium Fast Reactor, CP-ESFR). The PIRT exercise covered phenomenology from initial fuel-pin disruption to aerosol evolution in the containment. The main expected phenomena were identified and ranked from a safety point of view with, broadly, the idea of an oxide-core pool-type reactor affected by ULOF in mind; the associated current knowledge status and modelling capabilities were evaluated. Finally, a list of the most important uncertainties is proposed, i.e., those that potentially have high influence on contaminant transfer, e.g., rate of radionuclide leaching from core debris by liquid sodium or formation of volatile organic iodides in the containment.

1. Introduction

During hypothetical sodium-cooled fast-neutron reactor (SFR) accidents leading to severe core damage, highly-energetic phenomena in the reactor vessel can be envisaged that lead to ejection from the primary system into the containment of sodium along with much of the reactor-vessel cover gas and some components of the disrupted core; these components would include fuel-pin filler gas, varying fractions of the fission products and probably some fuel and steel as particulate suspended in the gas phase or in the ejected liquid sodium.

The present work has been carried out with the aim of evaluating source-term modelling capabilities with respect to severe-accident scenarios. This paper constitutes a summary of the work performed where the current format obviates presentation of full details. The approach adopted was to develop, in as generic a manner as possible, phenomena identification and ranking tables (PIRTs) for source-term phenomena in relation to a beyond design-basis accident (BDBA). Nevertheless, some restrictions were applied since many potential design options exist for SFRs and taking account of all of them here would have required far more effort than that available; the choice was made to reflect more-or-less the situation in Europe where ideas focus on a pool-type power reactor using (at least in the first instance) mixed-oxide fuel without minor actinides. Moreover, some options that have been little studied in realistic accident conditions would have required rather speculative assessments (e.g., the disruption of minor-actinide fuel pins).

The major steps in this approach were as follows:

- adopt a widely-studied severe-accident scenario;

- conduct a thorough literature survey;

- identify the phenomena involved affecting radionuclide transfer and associated transfer pathways;

- evaluate the importance of the phenomena on the evolution and consequences of the accident, notably with respect to exacerbation of the source term;

- review the available models and analysis tools for the identified phenomena;

- identify major gaps in knowledge and analytical capability;

- propose priority research topics.

On the first step, it was decided to base the approach on the unprotected loss-of-flow (ULOF) scenario leading to a so-called core-disruptive accident (CDA) – more of which below in §2.1. In fact, it turns out that this choice has little influence on the major results of the PIRT exercise.

Lastly, it should be clarified that the literature that was collated and reviewed in support of the present PIRT was vast (hundreds of documents): this literature cannot be cited here. Instead, only a selection of some of the more relevant references is provided.

2. Source term

2.1. Primary system

A SFR severe accident implies the disruption of the core by supercriticality involving more-or-less violent rupture of fuel pins and destruction of a certain number of fuel assemblies [19, 27, 28, 50]. Subsequently the interaction between hot fuel and liquid sodium can lead to a vapour explosion which could create a breach in the primary system [43, 47]. Some primary sodium would thus be ejected into the containment building where this sodium would oxidize and catch fire (see §2.2 below). This sodium would be both contaminated with components from disrupted fuel as well as activated (notably ^{24}Na, a β^- and γ emitter with a 15-hour half-life).

During a severe accident, the phenomenology in the primary system is at every stage very complex. The initial event is absence of (or reduced) liquid-sodium cooling in some zone on the core. Such a situation may arise due to a number of combined events where a classic scenario is long-term absence of forced circulation (due to pump inoperability or absence of power) with failure of reactor shut-down systems: this is the ULOF scenario. This will lead to heat up and, ultimately, boiling of the primary-system sodium. From this point, the accident evolves rapidly starting with very fast neutronic overheating of the fuel in the dried-out zone which is supercritical; fuel-pin centre-line temperatures can potentially exceeding 4000 K where the violence of their subsequent rupture mainly depends on the rate of temperature increase and the fuel burn-up, i.e., primarily the gaseous and volatile fission-product inventory. Disruption of the supercritical zone occurs while the extra thermal and neutronic energy of this zone is able to propagate to neighbouring fuel assemblies causing a rapid cascading dry-out and disruption event that can potentially affect the whole core: this is the CDA. This stage is governed by tightly-coupled mechanisms including neutronics, melting and vaporization, pressure- and temperature-induced cladding failures and propulsion of debris from degraded fuel pins into surrounding vaporized and liquid sodium. The hot debris from the core has the potential to create a vapour explosion where this is most likely when the debris are small and the liquid sodium in and around the core is already close to its boiling point: this is the case for the ULOF scenario where the core would heat the primary sodium for a long period before core disruption occurs (accident scenarios exist where the sodium is subcooled except for a small fraction in the core). This fuel-coolant interaction (FCI) is termed energetic if it causes a vapour explosion.

Assuming occurrence of energetic FCI, a foaming and expanding mixture of liquid and vaporized sodium, core debris, vaporized fuel components and gases (fuel-pin filler gas and fission gases) forms. This then transforms by liquid-sodium decanting and vaporization into a large debris-containing expanding bubble which mechanically uplifts the overlying sodium. The resulting impact of the liquid sodium on the reactor vessel head can breach either the rotating plug seal or the cover-gas purification circuit (for example). The large expanding bubble is unstable and breaks up where cooling of smaller bubbles will lead to a number of mechanisms entraining radioactive components suspended in the bubbles into the liquid sodium, e.g., condensation of sodium vapour, condensation of all but the most volatile fission products and sedimentation and impaction of debris and particles on the interface with the liquid-sodium. This pool-scrubbing phase, characterized by the bubbles rising and ultimately bursting at the sodium surface, leads to the so-called instantaneous source term comprising the initial transfer of radiocontaminants into the containment. A longer-term source arises from evaporation and resuspension of radionuclides from the surface of the sodium that remains in the reactor vessel and continued degradation (by leaching) of core debris settled onto the core catcher. The main character of the different radionuclides once in contact with the primary sodium is provided below in Table 1.

Accident scenarios exist where the primary sodium may boil for some time and this would

Element	Caracteristics in Na(l)	State	Main location(s)
Noble gases Xe, Kr	Inert, almost-zero solubility	element	gas phase
Halogens I, Br	Very volatile but react with Na $\rightarrow$ low volatility	NaI, NaBr	mainly Na (liq.)
			some phase gaz
Alkali metals Cs, Rb	Soluble, high volatility	Cs, Rb	some Na(l)
			mainly gas phase
Alkali-earth metals Sr, Ba	Low volatility either as metals or oxides	SrO, BaO in suspension; Sr, Ba soluble in Na(l)	Na(l)
Noble metals Ru, Pd, Rh, Ag	Very-low solublity (except Ag), very-low volatility	metallic, in suspension	Na(l)
Other metals Mo, Tc	Very-low volatility	metallique &/or oxide, in suspension	Na(l)
Actinides, U, Pu	Very-low volatility	MetalO$_2$ in suspension	Na(l)
Others Te	React with Na creating telluride of low volatility	Na$_2$Te, solid in suspension	Na(l)

considerable enhance transfer of contamination into the containment.

Table 1: principal characteristics of fission products and actinides in liquid sodium

2.2. *In-containment source term*

During CDAs, one can envisage the ejection of material in the form of liquid sodium mixed with fuel and fission products from the primary circuit into the containment. A consequence assessment of these low-probability scenarios requires knowledge of the major aerosol properties and evolution under the anticipated conditions within the containment.

In any accident, the vapour phase and the aerosols in the containment constitute the two main vectors for radioactive releases by their potential to transport contamination into the environment.

Under accidental conditions, aerosols form essentially by three processes:

- vaporization of core materials and subsequent re-condensation where this would happen mainly in the primary-system sodium and such particles would be largely retained in the primary sodium;

- coolant vaporization and subsequent re-condensation (Na-aerosols) where this would happen mainly in the primary system and such particles would be partly retained in the primary system and the leak path to the containment; and

- ejection of sodium into air where burning occurs producing sodium-oxide aerosols that continue to react with the humidity and carbon dioxide of the air (so-called aerosol ageing) creating, in general, aerosols of mixed composition, i.e., Na_2O_2-NaOH-Na_2CO_3-NaHCO$_3$.

The largest source of aerosols in the containment arises from burning of ejected sodium and condensation of the combustion products (i.e., homogeneous nucleation). Hence, one of the key accident variables is the total amount of sodium entering the containment. The importance of the sodium aerosols in the containment arises from three features of their nature: they include activated isotopes (most notably ^{24}Na, as already mentioned); their potential to act as a carrier of radioactive contaminants; and their potential to harm people and equipment due to their chemical speciation given that the oxides and the hydroxide are very corrosive compounds.

In the general case, sodium combustion produces aerosols initially composed of both sodium oxide and sodium peroxide. Very high aerosol concentrations can arise in the containment due to combustion, as much as >10 g.m^{-3}. The subsequent evolving, mixed speciation of these aerosols depends on the kinetics of the ejection event given that aerosols that form early in the accident will have more opportunity to react with the air and reach the bicarbonate form; for later aerosols, reacting gases (i.e., H_2O and CO_2) may become depleted or vanish and little or no change to these later aerosols would occur. Nevertheless, with such high aerosol concentrations, agglomeration will be significant tending over time to render the overall composition of individual aerosols more uniform.

3. The PIRT process on accident scenarios and the approach to evaluation of modelling capabilities

In addition to the summary of the different steps comprising the current exercise given in the introduction, here we expand two of the steps:

- the evaluation of the importance of the phenomena (viz. High, Medium, Low) with regard to the evolution and consequences of the accident; a description of the issues and the associated rationale for ranking must be provided;

- the evaluation of the status of knowledge based on the review of available results of the respective R&D work (main outcomes, pending questions); the status of knowledge is graded relative to full knowledge where we rank this as K = known with a knowledge level of 100%-75%, PK = partially known with a knowledge level of 75%-25%, or UK = unknown with a knowledge level of 25%-0%.

The knowledge-evaluation step draws on the knowledge of the authors of this report and on thorough compilation of relevant literature (journal papers, conference proceedings, records of expert meetings and workshops and technical reports). Of course, identification of interesting conferences, meetings and reports does not always mean that the relevant document can still be found since much good work was done as much as 50 years ago. Nevertheless, it has been possible to compile an extensive document database on which to base the work for this PIRT. As already said, not all of this documentation can be cited here but an extensive bibliography is provided.

As a second step, for the identified and ranked phenomena of a scenario, the evaluation of the modelling capability is based on the following considerations:

- availability of physical modelling;

- type and accuracy of the modelling (theoretical, semi-empirical, empirical/correlation based);

- available database for model qualification (support tests for precise quantification, global tests);

- validation domain and limits of the modelling and extrapolation capacity to other conditions;

- conclusion on the modelling adequacy, qualification level and needs of additional R&D work for improved physical understanding and reduction of source-term uncertainty.

4.   Principal concerns and associated actions already engaged

From the PIRT process, the large tables of which are not presented here, the main outcome is identification of phenomena that are poorly known but that are thought to play an important role in governing contaminant transfer. These phenomena can then be targeted in terms of research efforts. We are able, therefore, to draw attention to the issues listed below in terms of prioritizing research (the order is not a priority order but an order based on evolution of the accident).

1. Radionuclide release from fuel at high-temperature during a CDA (i.e., partitioning).

2. Energetic FCI and the associated impact on partitioning of radionuclides between fuel, liquid sodium and the vapour phase.

3. Retention of solid/liquid particles (core debris, nucleated vapours) suspended in rising bubbles.

4. Rates of leaching of radionuclides from core debris by liquid sodium, i.e., contaminant mobilization contributing to the longer-term source term.

5. Enrichment of the sodium-pool surface by dissolved and/or suspended contaminants with the potential to enhance contaminant transfer by evaporation and/or sparging.

6. In-containment aerosol formation including Na vaporization, chemical reaction with oxygen and steam, combustion-product nucleation and primary-particle agglomeration.

7. FP partitioning in the containment between liquid sodium, aerosol and vapour phases, e.g., Ru transfer during sodium combustion, thermal decomposition of NaI, chemical affinities with respect to oxide, hydroxide and carbonate aerosols, etc.

8. Reactions of iodine species in the containment to form volatile organic iodides.

9. FP release during contaminated-sodium/concrete interaction (if this risk is not designed out).

It was possible to anticipate some of the above key priorities before the present PIRT exercise was completed. This allowed work to be already engaged or proposed in order to begin responding to some of the above gaps in our evaluation capability. Hence, wishing to report on this PIRT-stimulated research in the context of the current renewal of SFR-related activities, below we highlight the actions already taken.

- IRSN has started PhD research (with partial financial support from AREVA NP) on modelling sodium-aerosol chemical transformations and their influence on transfer of key FPs. This will include experimental work of the transformation kinetics in containment conditions (with partial financial support from the 7th Framework Programme project JASMIN).

- CIEMAT has started PhD research on modelling combustion-vapour nucleation and turbulence effects on in-containment aerosol behaviour. This research is co-supervised by IRSN with two periods of the PhD researcher at IRSN/Cadarache (with mobility support from the 7th Framework Programme project CP-ESFR).

SELECTED BIBLIOGRAPHY

[1] Adams R.E., Kress T.S., Han J.T., Parsly Jr. L. F., 1979. Behavior of sodium-oxide and uranium oxide aerosols in a large vessel. Proceedings of the International Meeting on Fast Reactor Safety Technology, Seattle, Washington, CONF-790816-18.

[2] Adams R.E., Han J.T., Kress T.S., Silberberg M., 1980. Behavior of sodium oxide, uranium oxide and mixed sodium oxide-uranium oxide aerosols in a large vessel. Proceedings of CSNI specialist meeting on nuclear aerosols in reactor safety, Gatlinburg, TN, USA, CONF-800434-3.

[3] Allelein, H-J., Auvinen, A., Ball, J., Güntay, S., Herranz, L.E., Hidaka, A., Jones, A.V., Kissane, M.P., Powers, D., Weber, G., 2009. State-of-the-art report on nuclear aerosols in reactor safety. OECD report NEA/CSNI/R(2009)5.

[4] Barbe-le-Borgne, M., Boulaud, D., Madelaine, G., Renoux, A., 1986. Experimental determination of the dynamic shape factor of the primary sodium peroxide aerosol. J. Aerosol Sci. 17(1), pp. 79-86.

[5] Berlin, M., et al., 1982. Evaluation of the sodium retention factors for fission products and fuel. Int. Conf. on Liquid Metal Fast Reactors, Lyon, 19-23 July 1982.

[6] Brockmeier U., Koch M., Unger H., Schütz W., 1994. Volatile fission product and sodium release from liquids. Nuclear Engineering and Design, Vol. 148, pp. 499-507.

[7] Cahalan, J.E., *et al*., 1994. Advanced LMR Safety Analysis Capabilities in the SASSYS-1 and SAS4A Computer Codes. Proc. of the International Topical Meeting on Advanced Reactors Safety, Pittsburgh, 17-21 April 1994, American Nuclear Society.

[8] Castleman A.W., Jr, 1973. A review of the current status of research on the chemical and physical aspects of Liquid-Metal-Cooled-Fast Breeder reactors safety. I. Fission product behavior in sodium. BNL-14278.

[9] Cherdron W., Jordan S., 1980. Determination of sodium fire aerosol process coefficients from FAUNA-experiments. Proceedings of the CSNI Specialists Meeting on Nuclear Aerosols in Reactor Safety, NUREG/CR-1724, ORNL/NUREG/TM-404, CSNI-45, pp. 129-138.

[10] Cherdron W., Bunz H., Jordan S., 1985. Properties of sodium fire aerosols and recalculation of their behaviour in closed containments. Proc. CSNI Specialist Meeting on Nuclear Aerosols in Reactor Safety, Karlsruhe, CSNI-95, pp. 395-405.

[11] Clough W.S., 1971. The behaviour of barium and strontium fission products in liquid sodium. Journal of Nuclear Energy, Vol. 25, pp. 437 to 443.

[12] Clough W.S., Garland J.A., 1971. The behaviour in the atmosphere of the aerosol from a sodium fire. Journal of Nuclear Energy, Vol. 25, pp. 425-435.

[13] Clough W.S., Fraser A., 1973. Tellurium, Caesium, Iodine and Methyl Iodide in fast reactors. Journal of Nuclear Energy, Vol. 27, pp. 1-14.

[14] Clough W.S., Wade S.W., 1971. Caesium behaviour in liquid sodium – the effect of carbon. Journal of Nuclear Energy 25, pp. 445-456.

[15] Cooper, D.W., 1980. Prediction of the rates of chemical transformation of sodium fire aerosols. Proceedings of the CSNI Specialists Meeting on Nuclear Aerosols in Reactor Safety, NUREG/CR-1724, ORNL/NUREG/TM-404, CSNI-45, pp. 221-235.

[16] Cosandey, J.O., von Rohr, P.R., 2001. Entrainment of soluble and non soluble tracers from a boiling water surface. Nuclear Engineering and Design 208, pp. 87–97.

[17] Dehbi, A., Suckow, D., Guentay, S., 2001. Aerosol retention in low-subcooling pools under realistic accident conditions. Nucl. Eng. Des. 203, pp. 229-241.

[18] Dunbar, I.H., Fermandjian, J., 1984. Comparison of sodium aerosol codes. CEC report EUR 9172.

[19] Fischer, E.A., Wright, S.A., 1984. Analysis of the SANDIA fuel disruption experiments FD2/4. Nucl. Sci. Technol. Vol. 5, No. 6, pp. 1493-1514.

[20] Güntay, S., 1990. Experiment POSEIDON: Pool scrubbing effect on iodine decontamination. ENC'90, ENS/ANS-Foratom Conference Transactions, Verlag TÜV Rheinland, pp. 937-941.

[21] Hashimoto, K. Soda, K., Uno, S., 1991. High pressure pool scrubbing experiment for a PWR severe accident. ANS International Topical Meeting on Safety of Thermal Reactors, Portland, Oregon, 21-25 July 1991.

[22] IAEA, 1993. Fission and corrosion product behaviour in liquid metal fast breeder reactors (LMFBRs). IAEA-TECDOC-687, ISSN 1011-4289, Vienna.

[23] Jordan, S., 1976. Release of fission products from contaminated sodium fires. Proc. Int. Meeting on Fast Reactor Safety & Related Physics, 5-8 Oct. 1976, Chicago.

[24] Jordan, S., Cherdron, W., Malet, J.C., Rzekiecki, R., Himeno, Y., 1988. Sodium Aerosol Behaviour in Liquid- Metal Fast Breeder Reactor Containments. Nuclear technology, Vol. 81, pp. 183-192.

[25] Jordan, S., Ozawa, Y., 1976. Fuel particle and fission product release from LMFBR core catcher. Proc. Int'l Meeting on Fast Reactor Safety and Related Physics, Chicago, November 1976, ANS.

[26] Kawahara S., *et al*. 1976. Release of sodium and radioisotopes into air associated with sodium combustion. Journal of Nuclear Science and Technology, Vol. 13, pp. 382-388.

[27] Kayser, G., Papin, J., 1998. The reactivity risk in fast reactors and the related international experimental programmes CABRI and SCARABEE. Progress in Nuclear Energy, Vol 32(3–4), pp 631–638.

[28] Klickman, A.E., *et al*. 1982. Review of Recent ANL safety experiments in SLSF and TREAT. Int'l Topical Meeting on LMFBR Safety, Lyon,18 July 1982.

[29] Koch, M., *et al*., 2000. Radionuclide re-entrainment at bubbling water pool surfaces. J. Aerosol Sci. Vol. 31(9), pp. 1015-1028.

[30] Koch, M., Brockmeier U., Schütz W., Unger H., 1991. A code for the prediction of sodium and volatile fission product release from a liquid pool into an inert gas

atmosphere. Journal of Aerosol Science, Vol. 22, pp. S709-S712.

[31] Koch M., Brockmeier U., Schütz W., Unger H., 1992. The code RENONS for the prediction of non-volatile species release from liquid surfaces into a gas. Journal of Aerosol Science, Vol. 23, pp. S835-S838.

[32] Herranz L.E., García M., 2011. SOAR and PIRT Tables on in-containment transport and behavior of fission products and aerosols in sodium fast reactors. CIEMAT report DFN/SN-03/OP-11

[33] Herranz, L.E., Garcia, M., Kissane, M.P., 2012. In-containment source term in accident conditions in sodium-cooled fast reactors: data needs and modelling capabilities. Prog. Nucl. Ener. 54(1), 136-149.

[34] Lhiaubet, G., Bunz, H., Kissane, M.P., Seino, H., Miyake, O., Himeno, Y., Casselman, C., Such, J.M., Rzekiecki, R., 1990. Comparison of aerosol behaviour codes with experimental results from a sodium fire in a containment. International Fast Reactor Safety Meeting (American Nuclear Society), Snowbird, Utah, Aug. 1990. (& EUR 12374, 1991).

[35] Marcos-Crespo, M.J., *et al.*, 1994. LACE-España experimental programme on the retention of aerosols in water pools. CEC report EUR 15455 EN.

[36] Marimuthu K., Mitragotri D.S. and Sundararajan A.R., 1984. Sodium fires and aerosols. Journal of Nuclear Science and Technology, Vol. 21, pp. 686-693.

[37] Minges J., Sauter, H., Schütz, W., 1992. Retention factors for fission products from sodium tests to simulate a severe LMFBR accident. Nuclear Engineering and Design 137, pp. 133-138.

[38] Miyagi, K., S. Miyahara, S., 1996. Development of In-Vessel Source Term Analysis Code, TRACER. Technical Committee Meeting on Evaluation of Radioactive Materials Release and Sodium Fires in Fast Reactor, IWGFR/92, O-arai, Japan.

[39] Nishio G., Kitani S. and Takada J., 1975. Evaluation of plutonium oxide aerosol release from an LMFBR in a hypothetical accident. Nucl. Eng. Desi. 34, pp. 417-428.

[40] Nishio G., Kitani S. and Takada J., 1977. Behavior of sodium oxide aerosol in closed chamber under thermal convection flow. Journal of Nuclear Science and Technology 14, pp. 12-21.

[41] Owczarski, P.C., Burk, K.W., 1991. SPARC-90, a code for calculating fission product capture in suppression pools. NUREG/CR-5765.

[42] Postma A.K., Owen R.K., 1980. Comparison of aerosol behavior during sodium fires in CSTF with the HAA-3B code", HEDL-SA-1982-FP. Proceedings of CSNI specialist meeting on nuclear aerosols in reactor safety, Gatlinburg, TN, USA, CONF-800434-7, pp. 517-530.

[43] Powers, D., Clément, B., Denning, R., Ohno, S., Zeyen, R., 2010. Advanced sodium fast reactor accident source terms: research needs. SNL report SAND2010-5506.

[44] Ramsdale, S.A., Guentay, S., Friederichs, H.G., 1994. Bubble Scrubbing Algorithm BUSCA, Analysis of radionuclides scrubbing in water pools, model description and user manual for BUSCA June-91 version. Report SRD/N1496 - PSI Bericht Nr. 95-05 -

GRS mbH Koeln Nr. 116.

[45] Sauter, H., Schütz, W., 1983. Aerosol and activity releases from a contaminated sodium pool into an inert gas atmosphere. Kernforschungszentrum Karlsruhe, report KfK 3504.

[46] Sundarajan A.R., Mitragotri D.S. and Mukunda Rao S.R., 1982. Effect of relative humidity on growth of sodium oxide aerosols. Journal of Nuclear Science and Technology, Vol. 19, pp. 151-157.

[47] Tobita, Y., Kondo, S, Yamano, H., Morita, K., Maschek, W., Coste, P., Cadiou, T., 2006. The development of SIMMER-III, an advanced computer program for LMFR safety analysis, and its application to sodium experiments. Nucl. Technol. 153(3), pp. 245-255.

[48] Van de Vate J.F., Plomp A., Jong C. and Smit H.C.D., 1976. Deposition of aerosols formed by HCDA due to decay heat transfer on LMFBR inner containment atmosphere. Proceedings of International Meeting on Fast Reactor Safety and Related Research, Chicago, Illinois, CONF 76 1001, pp. 1915-1923.

[49] Wassel, A.T., Farr, J.L., Hoseyni, M.S.,1985. SUPRA: a code for simulating removal of radionuclides by water pools under severe accident conditions. EPRI NP 3886-CCMP.

[50] Wright, S.A., *et al.*, 1985. In-pile observations of fuel and clad relocation during LMFBR core disruptive accidents in the STAR experiments. Nucl. Technol. 71, p. 187.

Introduction of reliability, safety and risk monitoring technology in BN-600 power unit

L.V. Abramov, A.M. Bakhmetyev, I.A. Bylov, Yu.L. Kamanin, E.A. Zvyagin[a], Yu.A. Makhaev, E.L. Rozenbaum, V.A. Shamansky[b]

[a] JSC "Afrikantov OKBM", Nizhny Novgorod, Russia

[b] "Beloyarsk Nuclear Power Plant", Branch of JSC "Rosenergoatom Concern", Zarechny, Sverdlovsk Region, Russia

Abstract. Rosenergoatom Concern OJSC Operating Entity set the task to introduce risk monitoring technology for continuous estimate and control of nuclear units quantitative safety measures change. JSC "Afrikantov OKBM" and "Beloyarsk NPP" developed risk monitor system "RIM" which is introducing now at Beloyarsk NPP BN-600 unit 3. To estimate quantitative safety measures Level 1 PSA for internal initiating events for full power operating conditions model of Beloyarsk NPP BN-600 unit 3 is used. PSA model was developed using national certified PSA software CRISS.

To ensure NPP reliability and safety, implementation of comprehensive systematic study (monitoring) of NPP operating experience is of fundamental value. To solve this problem, JSC "Afrikantov OKBM" and "Beloyarsk NPP" developed and introduced the system for analytical reliability and safety monitoring of BN-600 power unit based on information retrieval system (IRS) "Istochnik-BN".

The paper describes system objectives, main characteristics and results of reliability, safety and risk monitoring technology introducing at Beloyarsk NPP BN-600 unit 3.

1. Introduction

Modern requirements for safety analysis and safety assessment of nuclear plants involve usage of deterministic and probabilistic methods as an essential condition for completeness of nuclear plant safety study at all stages of the lifecycle. In accordance with IAEA recommendations [1] the results of the safety assessment have to be used to make decisions in an integrated, risk informed approach based on the above mentioned methods.

One of the fundamental element of integrated, risk informed approach is implementation of the current safety level monitoring process, as well as systematic comprehensive study of nuclear plant operation experience, causes and prerequisites for abnormal operation of equipment and plants and adjustment of predictions and working out of measures to prevent undesirable events [2].

To solve the problem of power unit safety-level estimation during operation using probabilistic methods, JSC "Afrikantov OKBM" and "Beloyarsk NPP" (branch of JSC "Rosenergoatom Concern") developed the integrated reliability, safety and risk monitoring system being currently introduced at the Beloyarsk NPP unit 3.

This paper describes the developed system, as well as some results of its implementation.

L. Abramov, A. Bakhmetyev, Yu. Kamanin, E. Zvyagin and Yu. Makhaev, E. Rozenbaum, V. Shamansky

2. Risk monitoring system "RIM"

The risk monitoring system is being introduced in order to:

— Increase power unit safety through targeted informing of personnel on most adverse conditions and events related to safety;

— Reduce maintenance and repair costs of equipment for safety-important systems;

— Increase the power factor through re-sharing safety-important system maintenance activities performed when the reactor is at power and when the reactor is shut down;

— Increase the NPP personnel qualification related to safety.

To perform risk monitoring for the Beloyarsk NPP BN-600 unit 3, JSC "Afrikantov OKBM" developed the risk monitoring system "RIM". The "RIM" makes it possible to:

— Estimate core damage frequency for various configurations of power unit systems and different initiating events;

— Calculate the allowed outage time for certain configurations of power unit systems produced by removing equipment from operation for repair or maintenance;

— Assess the integral safety level of the power unit over an assigned time period;

— Check that safe operation conditions are fulfilled for different configurations of power unit systems;

— Develop equipment maintenance and repair schedules based on information about the power-unit safety level;

— Grade power unit equipment according to importance for safety;

— Make prediction estimates of the power-unit safety level for cases when equipment fails and normal operation is violated;

— Obtain information on the current condition of the power unit equipment from the power plant maintenance and repair planning system and return the value of the current safety level to the system;

— Obtain information on equipment reliability from the information retrieval system "Istochnik-BN" to update the PSA model;

— Collect operational documentation on power unit systems and equipment in the database to be used promptly;

— Work out reporting documentation that contains information on the power-unit safety level during operation.

The risk monitoring system "RIM" was developed based on the "client-server" architecture using the common administered database where user rights to make changes are differentiated. As the database management system the Oracle Database 10g Express Edition is used.

The general flow-chart of the risk monitoring system "RIM" is given in Fig. 1.

During activities to extend the power unit service life the full scope of probabilistic safety analysis was fulfilled for the Beloyarsk NPP unit 3, i. e. fulfilled was probabilistic safety analysis for internal initiating events, for low power and shutdown modes, internal hazards (fires and floods) and external hazards. PSA model of the power unit was developed out using the software package CRISS 5.1, which was developed by JSC "Afrikantov OKBM" and certified by Rostechnadzor.

The risk monitoring technology was introduced at the Beloyarsk NPP unit 3 in 2011 starting with pilot operation of the risk monitoring system. Based on the results of pilot operation, requirements for the program were specified, and users' comments were resolved.
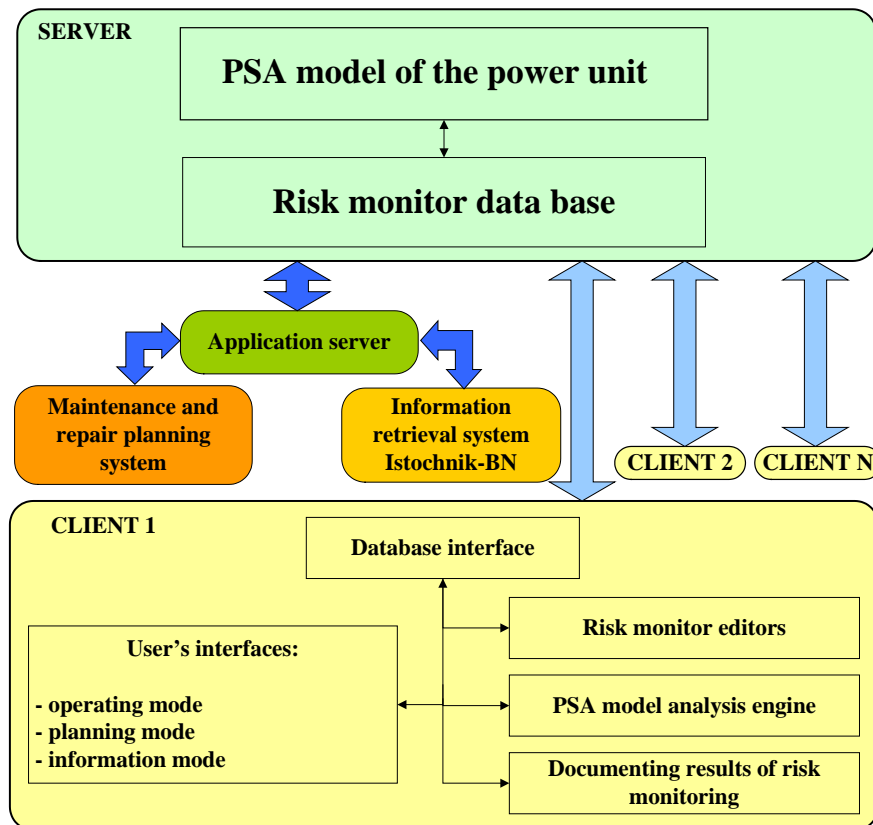
L. Abramov, A. Bakhmetyev, Yu. Kamanin, E. Zvyagin and Yu. Makhaev, E. Rozenbaum, V. Shamansky

FIG. 1. General flow-chart of the risk monitoring system "RIM".

One main problem solved before implementation of the specified technology is a revision of probabilistic safety analysis models used to implement risk monitoring procedures, as well as enlarging a list of equipment, operation conditions and initiating events accounted for. Basic directions of revision are as follows:

— A database of equipment in the power unit is developed; a relation between PSA basic events and equipment is established; equipment design description and actual description of equipment are coordinated.

— Simplifications are excluded in the model that relate to grouping of initiating events and equipment within systems.

— Fault trees are adjusted to provide full account of equipment within systems.

— Basic events are excluded, which were introduced to take account for removing of equipment for repair.

To monitor the risk at the Beloyarsk NPP unit PSA models of the power unit for internal initiating events for full power and for low power and shutdown.modes have been revised. Revised models were verified by comparing results of qualitative and quantitative analysis against the base model. Results of verification showed that the results were identical, and changes introduced were appropriate.

Interrelation between the risk monitoring system "RIM" and the maintenance and repair planning system, as well as with the analytical reliability monitoring system "Istochnik-BN" available at the Beloyarsk NPP unit 3 was ensured. The "RIM" system is connected with the specified systems using a special program, namely an application server. Information is exchanged between the programs via the transition control protocol; data transmission formats are regulated. A connection with the maintenance and repair planning system supplies the risk monitoring system with actual information on the equipment current condition and planned maintenance and repair.

L. Abramov, A. Bakhmetyev, Yu. Kamanin, E. Zvyagin and Yu. Makhaev, E. Rozenbaum, V. Shamansky

The information retrieval system "Istochnik-BN" gathers information on reliability of elements within systems, which are important for safety, and on the frequencies of initiating events making it possible to update the relevant database of the risk monitoring system.

3. Analytical reliability and safety monitoring system "Istochnik" for nuclear plants

The analytical monitoring system is a continuous-operation man-machine system, which ensures the following:

— Collection of information formatted as specified;

— Creation of the computer database within the information retrieval system;

— Analysis of the data obtained with estimation of reliability indices and safety indicators, as well as their trends;

— Working out of recommendations based on the results of analysis, analysis of effectiveness of measures implemented;

— Support for utilities in generalizing information and automated preparation of regular reports (operational reports).

The analytical reliability and safety monitoring system for the BN-600 unit was developed and implemented by OKBM and "Beloyarsk NPP" based on the information retrieval system "Istochnik-BN" [3], [4], [5].

The information retrieval system "Istochnik-BN" was developed based on the database management system Oracle; it has the "client-server" architecture and supports large number of users. The information retrieval system uses the universal data format to collect information concerning equipment operation experience. The program ensures information storage in the form of a certain structure, data systematization and processing; it has the developed data search and exchange system.

The system "Istochnik-BN" makes it possible to:

— Automatically calculate reliability indices and safety indicators for nuclear plants by operation years (power factor, operation factor, availability factor, portion of unplanned outages, portion of planned outages and number of unplanned emergency shutdowns per 7000 h of operation);

— Automatically plot distribution diagrams of nuclear plant malfunctions (power reduction and unplanned outages), release amount, ejection of radioactive products to environment from the nuclear plant, personnel exposure doses at the nuclear plant by operation years;

— Accumulate data for the operation model of certain equipment or group of equipment providing a possibility of comparing operation modes against the design model to monitor the residual lifetime of equipment;

— Automatically calculate reliability indices for critical equipment by type of equipment based on operation experience (total time, failure number and rate, average operating time to failure, possibility of failure to fulfill the requirement);

— Automatically plot distribution diagrams for number of failures for single-type equipment by operation years, as well as dependences of the failure rate and possibility of failure-free operation of single-type equipment on operating time;

— Promptly search for information by the certain set of criteria;

— Automatically make reports on operational experience of critical equipment within the BN-600 unit.

The information retrieval system "Istochnik-BN" is integrated with the maintenance and repair planning system of the Beloyarsk NPP concerning provision of information interaction between systems. "Istochnik-BN" system apart from OKBM is also installed at the Beloyarsk NPP; data are electronically exchanged between these two enterprises.

L. Abramov, A. Bakhmetyev, Yu. Kamanin, E. Zvyagin and Yu. Makhaev, E. Rozenbaum, V. Shamansky

Since operation of the power unit in 1980 up to now, the information retrieval system "Istochnik-BN" has created the database on BN-600 equipment reliability, availability and malfunctions, including information on unplanned loop shutdowns and scrams. Data accumulated are updated at regular intervals, and they are used to prepare annual reports on field supervision of BN-600 operation.

The distribution diagram for annual average values of the power factor for the BN-600 is given in Fig. 2. The average power factor for the 30-year BN-600 operation period (1982 – 2011) is 74.1 %. Over the last 11 operation years (2001 – 2011), the power factor for the BN-600 is 77.9%.

The distribution diagram for emergency shutdowns of the BN-600 reactor by operation years of 1980 – 2011 is shown in Fig. 3. The BN-600 reactor was emergently shut down 29 times over the specified period that is 0.92 accounting for 7000 h of reactor operation. At that, 69% of these were automatic actuation; and 31 % of them were initiated by personnel. There were no emergency reactor shutdowns over the last 12 years.
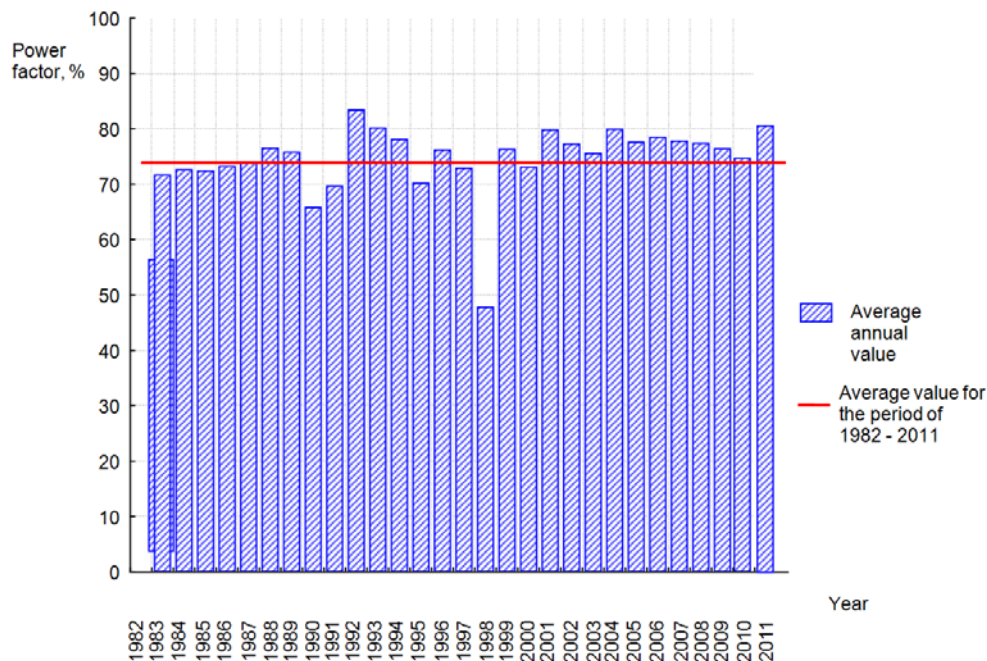

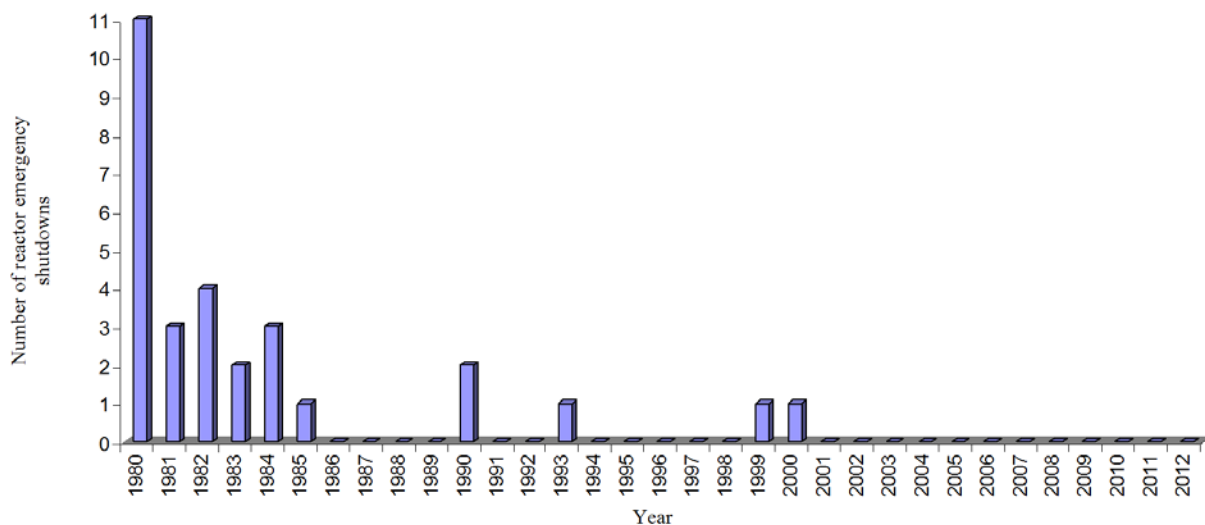*FIG. 2. Power factor for the BN-600 over the period of 1982 – 2011.*

FIG. 3. Distribution of number of emergency shutdowns for the BN-600 reactor.

L. Abramov, A. Bakhmetyev, Yu. Kamanin, E. Zvyagin and Yu. Makhaev, E. Rozenbaum, V. Shamansky

4. Conclusion

(1) To estimate the current safety level of the Beloyarsk NPP unit 3 during operation using the risk-informed technologies, JSC "Afrikantov OKBM" and "Beloyarsk NPP" (branch of JSC "Rosenergoatom Concern") developed and implement the reliability, safety and risk monitoring system for the power unit.

(2) Pilot operation of the risk monitoring system "RIM" was carried out in 2011 – 2012 at the Beloyarsk NPP unit 3. Based on the results of pilot operation, requirements for the program were specified, and users' comments were resolved. Level - 1 PSA models are being revised; the list of equipment, operation conditions and initiating events accounted for is being enlarged.

(3) Since operation of the power unit up to now using the analytical reliability and safety monitoring system (based on the information retrieval system "Istochnik-BN") for the power unit, the database has been created on BN-600 equipment reliability, availability and malfunctions, including information on unplanned disconnections of circuits and actuation of emergency protection. Data accumulated are updated at regular intervals, and they are used to prepare annual reports on field supervision of BN-600 operation.

(4) The risk monitoring system "RIM" and the information retrieval system "Istochnik-BN" are integrated with the maintenance and repair planning system of the Beloyarsk NPP concerning provision of information interaction between systems thus ensuring updated information being processed.

REFERENCES

[1] INTERNATIONAL ATOMIC ENERGY AGENCY, Safety Assessment for Plants and Activities, General Safety Requirements, Part 4, IAEA Safety Series, No. GSR, Part 4, IAEA, Vienna (2009).

[2] INTERNATIONAL ATOMIC ENERGY AGENCY Framework for an Integrated Risk Informed Decision Making Process, INSAG-25, Report by the International Nuclear Safety Group, IAEA, Vienna (2011).

[3] Bakhmetev, A.M., Kamanin, Yu.L., Makeev, Yu.A., Popov, L.A., "About the reliability and safety monitoring system for the BN-600 plant", University News – Nuclear Power, No. 1, 2006.

[4] Bakhmetev, A.M., Bylov, I.A., Karpenko, A.I., Makhaev, Yu.A., Zabegaev, V.P., Rozenbaum, E.L., "Program-methodical support of reliability and safety analysis for nuclear plants during development and operation", ISTC – 2010, Moscow.

[5] Bakhmetev, A.M., Bylov, I.A., Makeev, Yu.A., Popov, V.M., Smirnov, A.S., Analytical Reliability and Safety Monitoring System for NPP pump equipment, Report at the Scientific Session of NRNU MEPhI – 2010, Obninsk, Jan. 25 – 31, 2010.

Analytical and experimental study for validation of the device to confine BN reactor melted fuel

S.A. Rogozhkin, S.L. Osipov, V.A. Sobolev, S.F. Shepelev[a], A.A. Kozhaev, M.S. Mavrin, A.A. Ryabov[b]

[a] JSC "OKBM Afrikantov", Nizhny Novgorod, Russia

[b] JSC "SENC", Sarov, Nizhniy Novgorod Region, Russia

Abstract. The paper presents the set of analytical and experimental studies performed to validate the design of special supporting device (tray) for protection of BN reactor vessel in case of severe beyond-design accident with core melting, namely:

— description of test facility "Poddon" developed and fabricated at OKBM;

— analysis of experimental investigations carried out at the test facility;

— technical approach developed for numerical simulation;

— results of physical experiment and numerical simulation comparison using CFD code;

— results of numerical simulation as applied to the reactor for two ultimate accident scenarios.

Based on the analysis of the results, the efficiency of special supporting device design is shown, and its operability is validated.

1. Introduction

To validate the design and confirm the design characteristics of the special retaining device (core catcher) used for protection of BN reactor vessel in the case of a severe beyond-design basis accident with core melting, a calculational and experimental studies was carried out. The Tray test facility that uses water as coolant was developed and fabricated by OKBM; experimental studies were performed. To verify the methodical approach used for the calculational study, experimental results obtained in the Tray test facility were compared with numerical simulation results obtained by the STAR-CCM+ CFD code.

2. BN reactor core catcher

Core melting is postulated for the BN-800 and BN-1200 reactors despite the extremely low probability of such event (residual risk accident). Fragments of the wrecked core are supposed to move down, melt through the lower breeding blanket, headers, discharge chamber and enter the lower sodium cavity above the vessel bottom.

To prevent the reactor pressure vessel and safety vessel from melting, a core catcher intended to confine the molten core (corium) is installed under the discharge chamber.

The device for collection and confinement of BN reactor molten fuel (Fig. 1) is a core catcher consisting of a bottom, cone barrel welded to the bottom periphery, support structure and seven vertical draft tubes. The internal surface of the core catcher is lined with the high-temperature melting point molybdenum alloy.
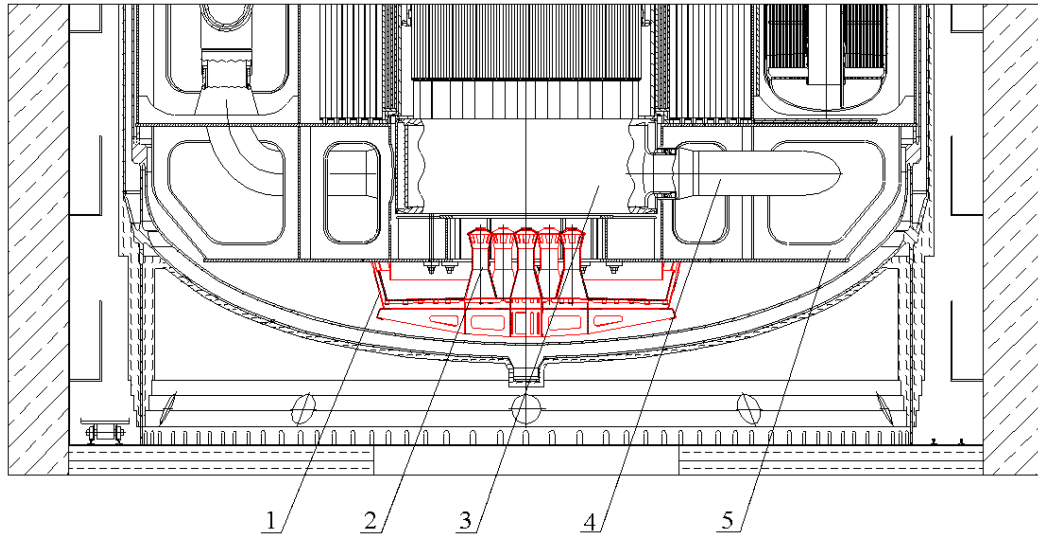
FIG. 1. Design of the Tray test facility model:

1 – cone barrel; 2 – draft tubes; 3 – discharge chamber; 4 – tube from the pump; 5 – support structure.

3.   Experimental studies in the Tray test facility

To simulate thermal-hydraulic processes in the lower part of the reactor vessel near the core catcher, the Tray test facility was created. Its design has geometric similarity to the reactor with the scale of 1:10. The test facility utilizes water as coolant. The heat release of the molten core fuel in the core catcher is simulated by two plate-type spiral electrical heaters with the total power of 50 kW. Six intermediate heat exchangers (IHX) are replaced by one annular distillate-delivery water heat exchanger. Melting of the discharge chamber plates postulated in the beyond-design basis accident is simulated by the perforation ratio in the upper and lower plates of the discharge chamber model. The design schematic and general view of the Tray test facility are given in Fig 2.
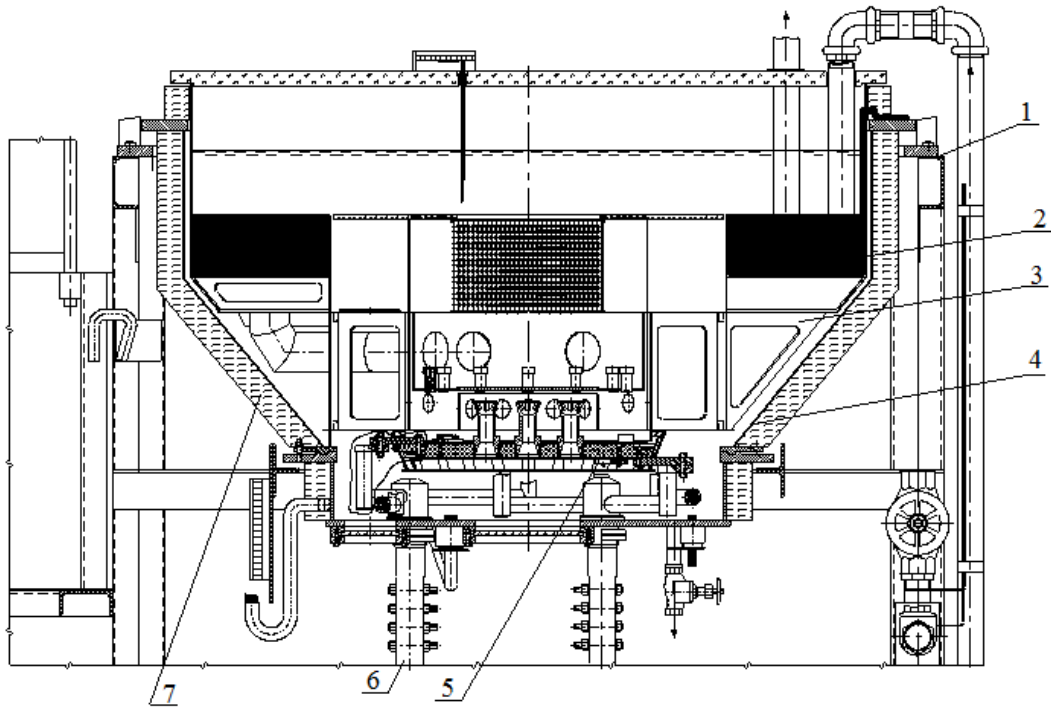
FIG. 2. Design of the Tray test facility model:

1 – pedestal; 2 – heat exchanger; 3 – support belt; 4 – vessel; 5 – core catcher with heaters; 6 – current distributor; 7 – thermal insulation.

The test facility is equipped with parameter monitoring and measuring instrumentation, which is a part of the information-measurement system. Sight glasses are also installed in the facility to visualisation monitor development of natural circulation.

The aim of the experimental studies in the test facility was to obtain information [1] about the circulation circuits taking place in the model and about their stability, as well as about distribution of water temperatures in the circuits. This information was required to verify CFD codes.

4.   Numerical simulation of thermal-hydraulic processes in the Tray facility

To verify the STAR-CCM+ CFD code that is used to solve the reactor problem of validating the core catcher, thermal-hydraulic processes in the Tray facility were numerically simulated. Numerical simulations were done for various combinations of perforation ratios in the upper and lower plates. In so doing, the most effective methodical approach to solving the problem and the level of simplifications required for the computer model were determined [2].

While solving the problems, the convergence analysis was made based upon the following parameters: achieving 10^{-3} by normalized discrepancies (normalization is made for absolute values); achieving the power balance between the heater and heat exchanger; achieving steady-state values of thermodynamic magnitudes in checkpoints.

The developed computer models were verified through comparing the experimental results with numerically simulated results (Fig. 3) for the set temperatures in twenty points.
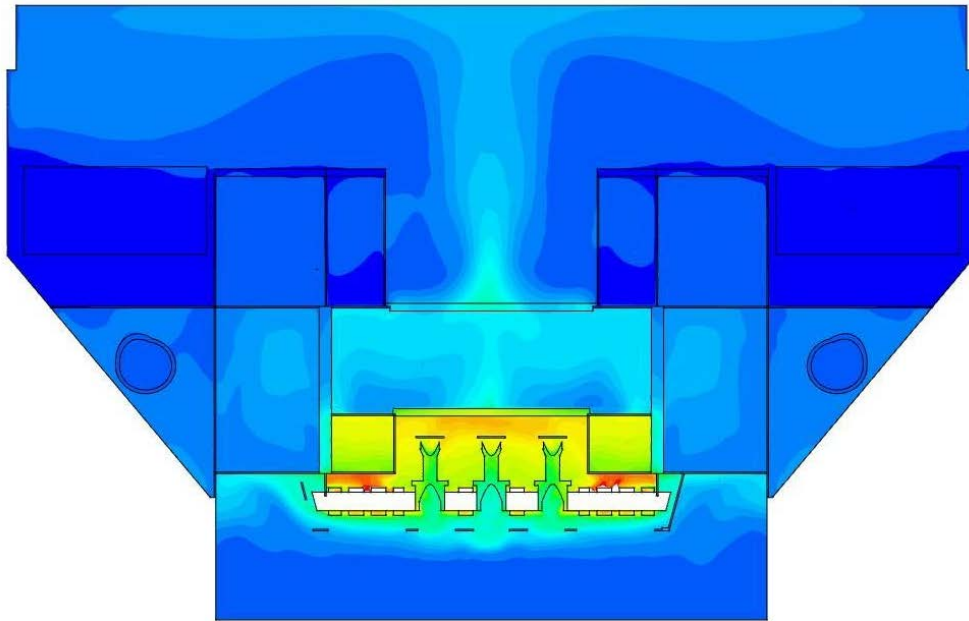
FIG. 3. Results of numerical simulation. Temperature distribution in the model.

The comparative analysis showed that calculated and experimental temperatures are quite close in all options under consideration. The average deviation is 5%, and the maximum deviation does not exceed 8% while normalizing for the difference between the maximum and minimum temperatures in the test facility [2].

Calculational and experimental studies of thermal-hydraulic processes in the Tray test facility proved that the developed methodical approach is applicable to solving the class of problems under consideration.

5. Numerical simulation of thermal-hydraulic processes of cooling core fragments in the core catcher

Thermal-hydraulic processes occurring when core fragments are being cooled in the core catcher were numerically simulated based upon the verified STAR-CCM+ methodology for two ultimate options of developing of coolant natural circulation that are possible in the accident:

— The failure of the discharge chamber does not prevent development of coolant natural circulation through the wrecked core (Fig. 4).

— The failure of the discharge chamber results in that flow passages are completely blocked with molten FA steel in the lower plate of the discharge chamber (Fig. 5).

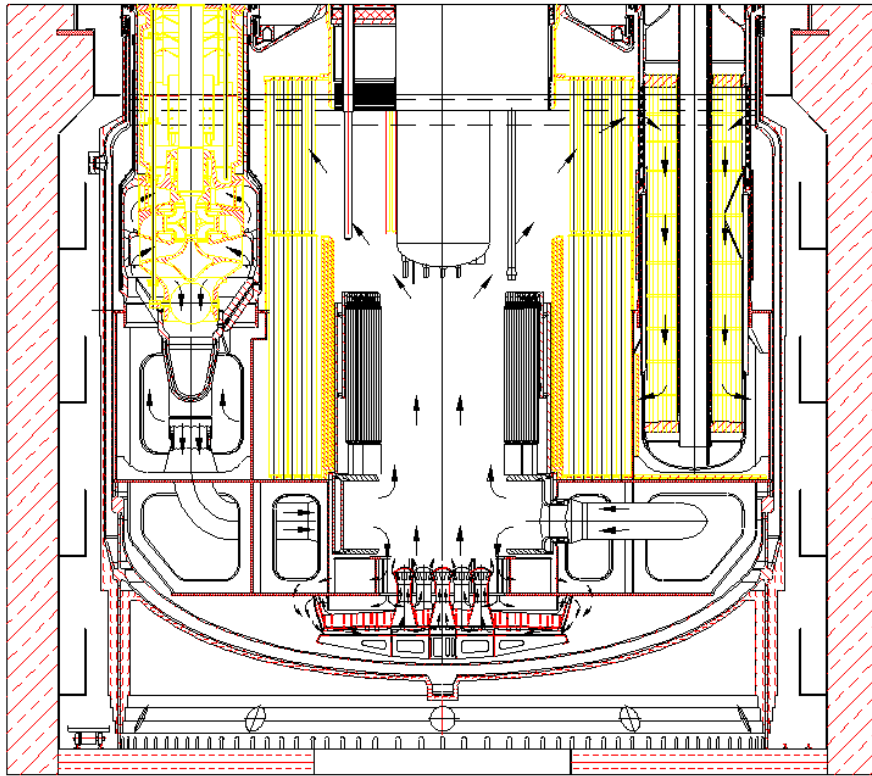*FIG. 4. Coolant circulation diagram in case the discharge chamber is burned-through.*
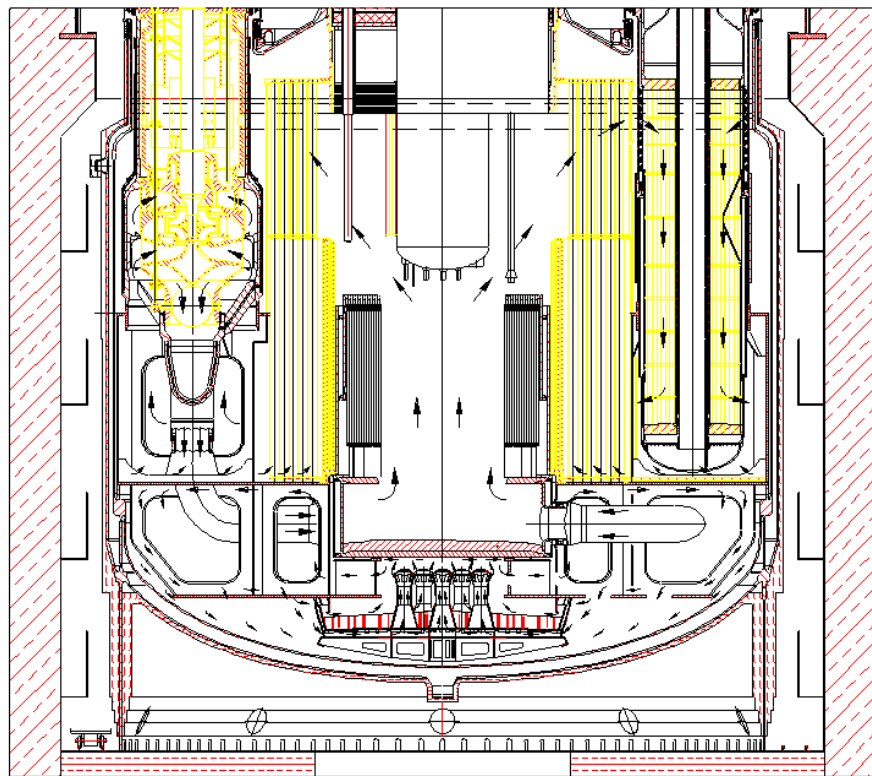

FIG. 5. Coolant circulation diagram in case the lower plate of the discharge chamber is blocked with molten FA steel.

The simulation used difference schemes of the second order of accuracy that had been obtained by the finite volume method. For the calculations, a volumetric mesh adjusted at the fluid-solid interface was

generated based on multifaceted cells. At the solid-liquid media interface, near-wall prismatic layers were built required for a high-precision description of the flow in the near-wall area.

The calculations were carried out under the following conditions:

—— coupled solver – because this model is the most suitable one for solving this class of problems;

—— realizable k-Epsilon Two-Layer, All y+ Wall Treatment turbulence model;

—— polynomial density for coolant.

The CAD reactor model used to solve the problem is given in Fig. 6. Due to complexities in reactor design geometry and in simulated physical processes, the problem was solved by methods that made it possible to avoid direct simulation of equipment. The solution that employs direct simulation of reactor equipment significantly complicates the problem, results in higher demand for system resources and consequently extends the problem solving time.

In this respect, heat exchangers and pumps were indirectly simulated by the method with substituting them with solid porous medium having equivalent hydraulic resistance. At the same time, the heat removal in the heat exchanger was simulated using a negative power source the value of which at each point in the heat exchanger depends upon parameters of the coolant passing through it.
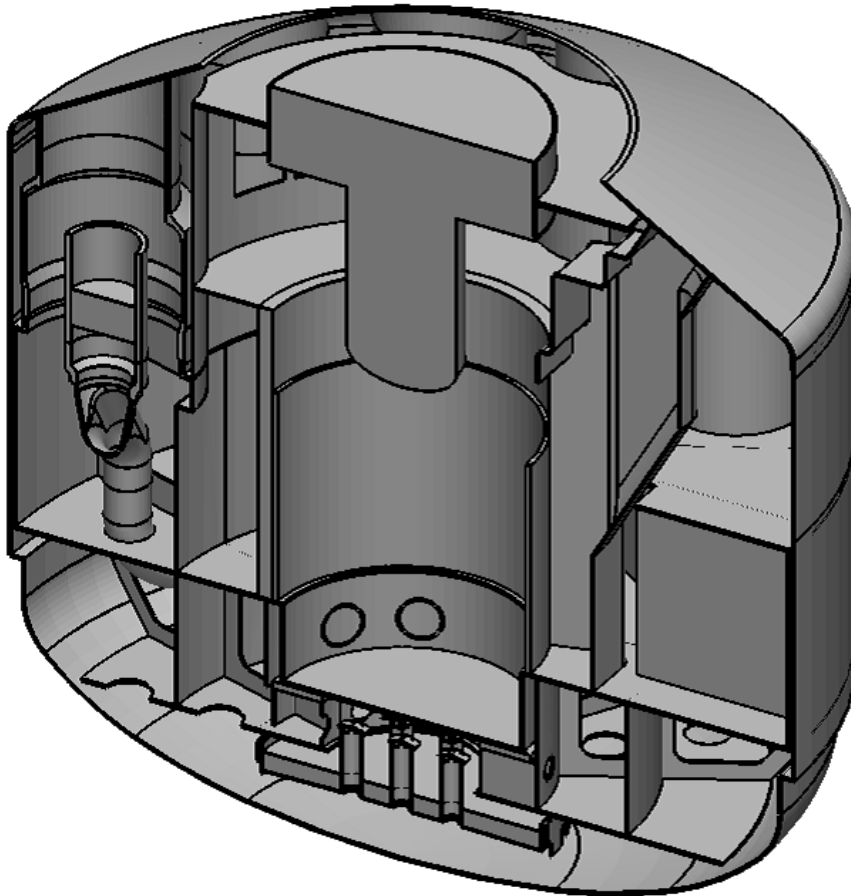
FIG. 6. CAD model of BN-800 reactor.

While carrying out this activity, several options of computational mesh were generated for the two cases under consideration (accident scenario options) with the dimensionality of the order of 20×10^6 cells. Based on the results of a number of calculation startups for each case, options were selected that provided the best solution convergence. Convergence of the numerical solution was estimated by

normalized discrepancy graphs; by monitoring the integral temperatures and velocities in the model; and by monitoring temperatures and velocities in checkpoints.

Calculational studies of steady-state thermal-hydraulic processes in the BN-800 reactor showed following:

— Proposed core catcher design makes it possible to remove heat form the corium to the secondary coolant by natural circulation of primary coolant.

— At 13 MW assumed as the maximum estimated power in the established sodium circulation mode, maximum coolant temperatures take place in the corium area and reach 355 °C, if the discharge chamber is not blocked; and 525°C, if the discharge chamber is completely blocked (Fig. 7).

The calculational and experimental works show that has been implemented confirmed the efficiency of the developed core catcher design and validated its operability.
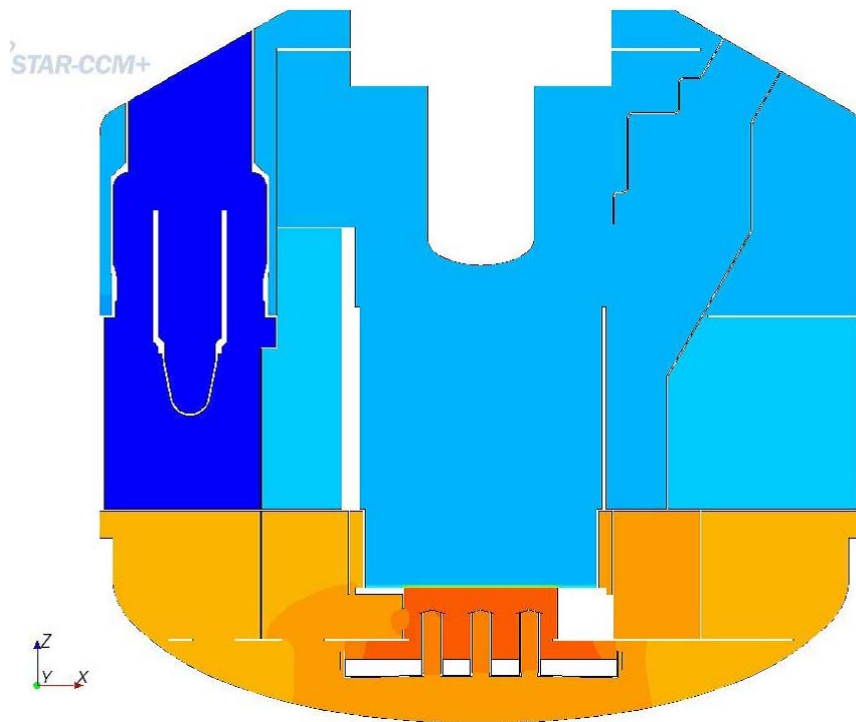
FIG. 7. Results of numerical simulation. Temperature distribution in the reactor for the option with the lower plate blocked with molten FA steel in the discharge chamber.

REFERENCES

[1] OSIPOV, S.L., ROGOZHKIN, S.A., SOBOLEV, V.A., SHEPELEV, S.F., Experimental studies to validate the BN-800 core catcher. – Issues of nuclear science and engineering. Nuclear reactor physics series. 2008, Issue 3. p. 65–70.

[2] OSIPOV, S.L., ROGOZHKIN, S.A., SHEPELEV, S.F. et al., Calculational and experimental studies of thermal hydraulic processes in the Tray test facility. – Bulletin of Lobachevsky NNSU, 2009, No. 4, p. 101–109.

SFRs and GEN IV: ASN actions

Author : Autorité de sûreté nucléaire (ASN) - France

ASN carries out several actions regarding the 4th generation of reactors (GEN IV) and the sodium fast reactors (SFRs).

First of all, ASN considers that GEN IV reactors have to be safer than the EPR reactor currently under construction in France (at Flamanville).

Regarding GEN IV in general, the "generation IV international Forum" (GIF) has identified six technologies of reactors for which the possibility of an industrial development could be considered (SFR, GFR, HTR/VHTR, LFR, MSR, SCWR) ; these six technologies include fast reactors. Based on documents sent by French nuclear operators at its request, ASN will organize a technical expertise, with the technical safety organization IRSN and ASN Advisory Committees, in order to have an overview, in terms of safety, R&D needs and possibility of transmutation of these six technologies. The conclusions of the technical expertise are expected by the end of 2013.

Concerning SFR in particular, the French operator CEA submitted to ASN in June 2012 a file presenting the general safety orientations of the prototype reactor ASTRID (Advanced Sodium Technological Reactor for Industrial Demonstration). ASN has organized, with IRSN and ASN Advisory Committees, a technical expertise to analyse this file. The conclusions of this technical expertise are expected by mid-2013.

Besides, a specific analysis is going on about the transmutation. The conclusions of the analysis could be known in 2013, subject to the transmission of documents by the end of 2012.

***

Introduction

Since 2000, French nuclear operators have started to consider the 4th generation of reactors (GEN IV), in particular within the "Generation IV International Forum" (GIF). The objective of the GIF is to regroup and carry out research and development (R&D) actions and give the choice of industrial development possibilities among the six reactor technologies (i.e. SFR, GFR, HTR/VHTR, MSR and SCWR) selected by the GIF.

The industrial development of the 4th generation of reactors (GEN IV) is currently foreseen in France in the middle of this century (a national debate on "energy transition" will take place in the first half of 2013 and may result or not in changes in French energy policy with regard to nuclear energy). As an intermediate step, it requires the development of a prototype, which is due in 2020, according to the June 28th 2006 French act regarding the sustainable management of radioactive materials and wastes.

In 2010, the French nuclear operator CEA began the studies of a SFR prototype: the ASTRID[1] project. For the CEA, ASTRID is a necessary step to develop a SFR of 4th generation. Although ASTRID power will be lower than the one of reactors of this 4th generation, its power will be sufficient, according to the CEA, to validate the options of the 4th generation reactors and will allow to test options and continue with the experiments on the transmutation of minor actinides.

Comparison of the six reactor technologies identified

The GIF identified six nuclear reactor systems for which the possibility of an industrial development could be considered:
- sodium fast reactor (SFR);
- gas fast reactor (GFR);
- molten salt reactor (MSR);
- very-high-temperature reactor (HTR/VHTR);
- lead fast reactor (LFR);
- supercritical water reactor (SCWR).

ASN considers important to have the elements to justify the "choice", in terms of nuclear and radiation safety, as well as protection of the environment, of one technology of reactor among the others technologies identified by the GIF. In particular, the technology which will be selected for the 4th generation has to present a safety level (in the meaning of the French environmental Code) higher than the 3rd generation of reactors, which corresponds in France to the EPR reactor currently under construction (at Flamanville).

ASN requested the French nuclear operators to provide documents concerning the advantages and drawbacks of the six technologies of reactor and the SFR operating feedback (in particular from operating Phénix and Superphénix).
At the end of 2012, ASN will request its technical support organization (IRSN) and ASN Advisory Committee in charge of reactors to analyse these documents in order to have an

---

[1] ASTRID : Advanced Sodium Technological Reactor for Industrial Demonstration

opinion on the characteristics of these six technologies, in terms of nuclear safety and radiation protection. Members of the Advisory Committee in charge of laboratories and plants and of the Advisory Committee in charge of waste will be associated. This opinion will provide ASN with elements to define its position, in terms of safety, regarding the choice of one technology for the 4th generation of reactors. It will likely also point out R&D needs, possibility of transmutation of long-lived radioactive elements and constraints related to the fuel cycle.

The conclusions of this expertise are expected by the end of 2013.

ASTRID

Concerning SFR in particular, in June 2012 the French operator CEA submitted a file presenting the general safety orientations of the prototype reactor ASTRID to ASN. This kind of document precedes the safety options review defined at the 6th article of the November 2th 2007 decree concerning the regulation of civil nuclear installations. The safety options review is a voluntary step which precedes the licensing procedure.

In September 2012, ASN has initiated a technical expertise in order to analyse the safety orientation file of ASTRID prototype. This technical expertise will be performed by ASN's technical support organization (IRSN) and by ASN Advisory Committee in charge of reactors, with members of Advisory Committees in charge of laboratories, plants and waste.

This expertise will focus on:
- the orientations chosen by the CEA with regard to the main objectives of the SFR prototype design ;
- how the SFR operational experience was considered in the definition of the safety orientations of ASTRID prototype (feedback[2] from French SFR (Rapsodie, Phénix and Superphénix) and from others SFR worldwide) ;
- the main safety principles and the safety approach chosen by CEA, in particular:
  o the implementation of the defence in depth principle;
  o the principles of the practical elimination ;
  o the principles of the situation and equipment categorization/classification ;
  o the approach for taking into account internal events, internal or external aggressions, severe accidents, etc.
- the relevance of the safety requirements used at the preliminary design stage (codes…);
- the preliminary list of initiating events.

Lessons learned from the TEPCO Fukushima Daiichi nuclear accident and the R&D needs regarding SFRs will also be analysed.

Taking into account when ASTRID may be build, ASN considers that the safety level of ASTRID has to be at least the same as the 3rd generation reactor (e.g. EPR reactor).

The conclusions of the technical expertise on the ASTRID safety orientation file are expected around the middle of 2013.

---

[2] The feedback from SFR concerns for example the incidents occurred, the learning from final tests carried out on Phénix reactor in 2009, the dismantling operations, etc.

Transmutation

A specific analysis is going on about the transmutation. The conclusions of the analysis could be known in 2013, subject to the transmission of documents by the end of 2012.

Conclusion

As a conclusion, ASN, with IRSN and ASN Advisory Committees, are carrying out two analyses:

-   the first one on the safety benefits and drawbacks of the six technologies of reactor identified by the GIF for the 4th generation of reactor. Impact on fuel cycle facilities will also be considered;
-   the second one on the safety orientation file of the ASTRID prototype.

The conclusions of both analyses are currently expected by the end of 2013.

Analysis of Unprotected Blockage Accidents in FASTEF Subcritical Core with SIMMER-IV

V. Kriventsev, X.-N. Chen, D. Zhang, A. Rineiski, W. Maschek

Karlsruhe Institute of Technology (KIT), Germany

Abstract. The FAst Spectrum Transmutation Experimental Facility (FASTEF) core proposed for the MYRRHA reactor in Belgium is cooled by Lead-Bismuth Eutectic and can operate in both critical and subcritical modes (as an accelerator-driven system, ADS). FASTEF development is sponsored by EURATOM. In the paper subcritical 94 MWth ADS FASTEF is considered at the end of cycle conditions. To achieve a complete view on the safety behaviour, several severe accident scenarios are investigated including Unprotected Blockage Accidents (UBA) without switch-off of the ADS neutron source. The UBA transients have been simulated in 3D with the SIMMER-IV code. To provide a basis for transient analyses, the core has been first analyzed under nominal conditions. Then several hypothetical blockage events in a single fuel subassembly (SA), starting from 50 % of the nominal coolant flowrate to the total instantaneous blockage (TIB) have been simulated. Using of SIMMER-IV instead of two-dimensional SIMMER-III allows simulation of the blockage event in the non-central fuel SA, while some approximations, such as ignoring coolant flow in gaps between the SAs and restricting the computation domain spatially are made to avoid a strong increase in the computation time. Thanks to the low power density and small variations in the power, no pin failure occurs if the flowrate is reduced by 70 to 75 % from the nominal level. The 85 to100 % blockages lead to cladding failures in 6 to7 seconds. After 15 to 20 seconds, SA walls also fail resulting in coolant redistribution between the blocked SA and neighboring channels thus increasing the flowrate and recovering the cooling in the affected SA. The SIMMER calculations show that effects of the single SA blockage are limited in subcritical FASTEF by single and neighboring SA failures. The results are in line with SIMMER-III calculations obtained in the past for UBAs in other ADS designs.

1. Introduction

MYRRHA (Multi-purpose hYbrid Research Reactor for High-tech Applications) is a flexible experimental Accelerator-Driven System (ADS) currently under development at SCK-CEN [1-4]. MYRRHA is designed to help fuel developments for innovative reactor systems, radioisotope production for medical and industrial applications, and other experimental and demonstration purposes. Since 2009, MYRRHA development is conducted under the FP7 EC Project CDT where the reactor is designed as FASTEF [2]. FAst Spectrum Transmutation Experimental Facility (FASTEF) is an innovative accelerator-driven system cooled with Lead-Bismuth Eutectic (LBE) developed to achieve high safety-by-design levels. To reach these goals, an essential part of the project effort is devoted to safety analysis of transient behaviour of the core under severe accident conditions. For the safety assessment of the FASTEF reactor, a number of design basis and design extension conditions are analyzed. One of such scenarios includes an Unprotected Blockage Accident (UBA) [5] that is the main object of analysis in the present work. Analysis of unprotected transients allows establishing of the upper safety limits and plays and important role in the overall safety assessment as the most conservative approach. Under UBA conditions, it is assumed that a single fuel assembly is partly or fully blocked thus lowering the flowrate. This finally results in fuel and clad overheating. To simulate the UBA transient we use a computational code, SIMMER, that was originally developed for the safety analysis of critical sodium-cooled fast reactors. The modern code version allows using additional fuel, steel and coolant materials, including LBE and has a capability for three-dimensional

simulations [6]. Both critical and subcritical systems can be analyzed. SIMMER-IV is a 3D, multi-velocity, multi-phase, multi-component fluid dynamic and thermal hydraulic code including a structure model for fuel pins, hexcans and other structures and coupled with a space-, time-, and energy-dependent transport neutron dynamic model. In addition, an analytical equation-of-state (EOS) model is used for closure of fluid-dynamic momentum and energy conservation equations.

2. FASTEF Subcritical Core Design and SIMMER Model

The FASTEF core with 72 fuel assemblies of 94 MW power is shown in Fig. 1. In addition to the fuel assemblies (FA) the core contains a row of dummy subassemblies filled with the LBE coolant and an external row of reflector S/As, as well as six irradiation IPSs (in-pile sections) and six empty channels for absorber rods which are inserted during the core loading and maintenance. The central subassembly is reserved for the spallation target channel.
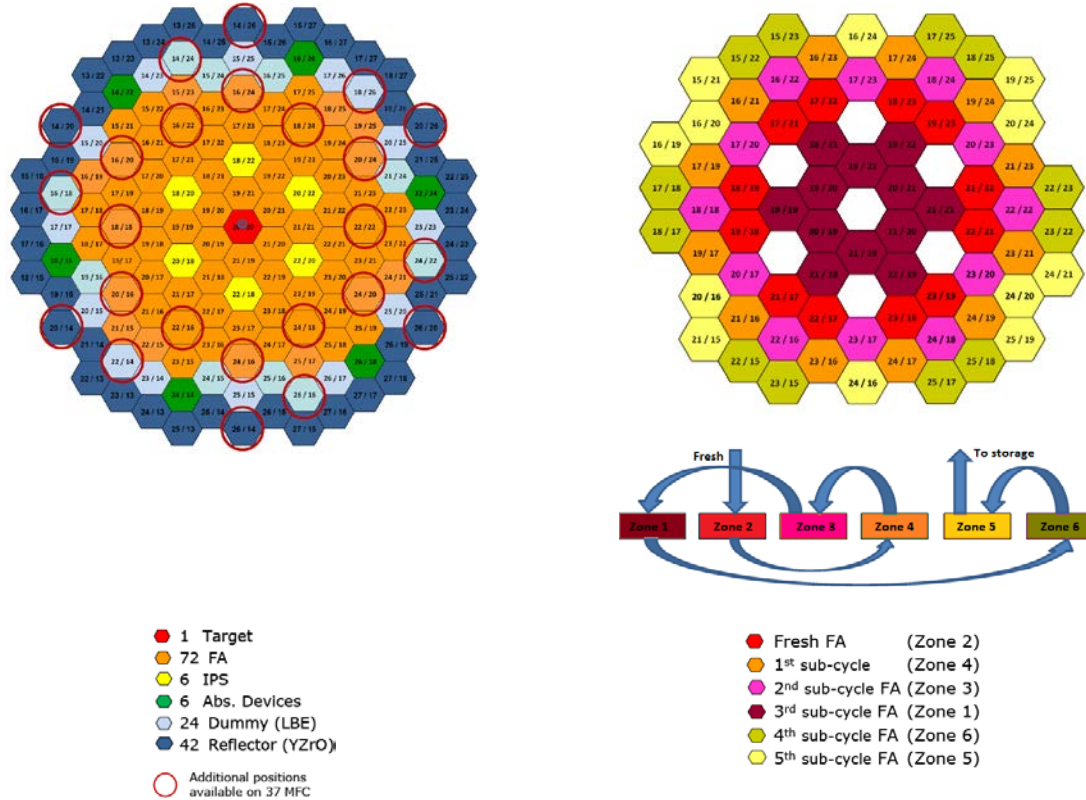

FIG 1. FA-94 MW Sub-Critical Equilibrium Core Design and Shuffling Scheme

The FASTEF fuel assembly is similar to that of the Phenix reactor and includes 126 fuel pins and an empty central pin. Unlike power generation reactors, the power density and neutron flux distributions in the FASTEF irradiation facility are shaped to maximize the neutron flux inside the IPS channels and, at the same time, to minimize the total core power. Figure. 1 also shows the shuffling scheme chosen to reach the desired flux distribution.

A three-dimensional SIMMER-IV model is prepared to simulate the 94 MW sub-critical equilibrium core with 72 fuel assemblies at end-of-cycle (EOC) conditions [2-4]. The core axial layout and SIMMER meshing system are shown in Fig. 2 (a). In SIMMER-IV, every hexagonal subassembly is modelled by two rectangular cells with the same cross area as shown in Fig. 2 (b). The calculation regions adopted in the SIMMER model are explained in Table 2.1.
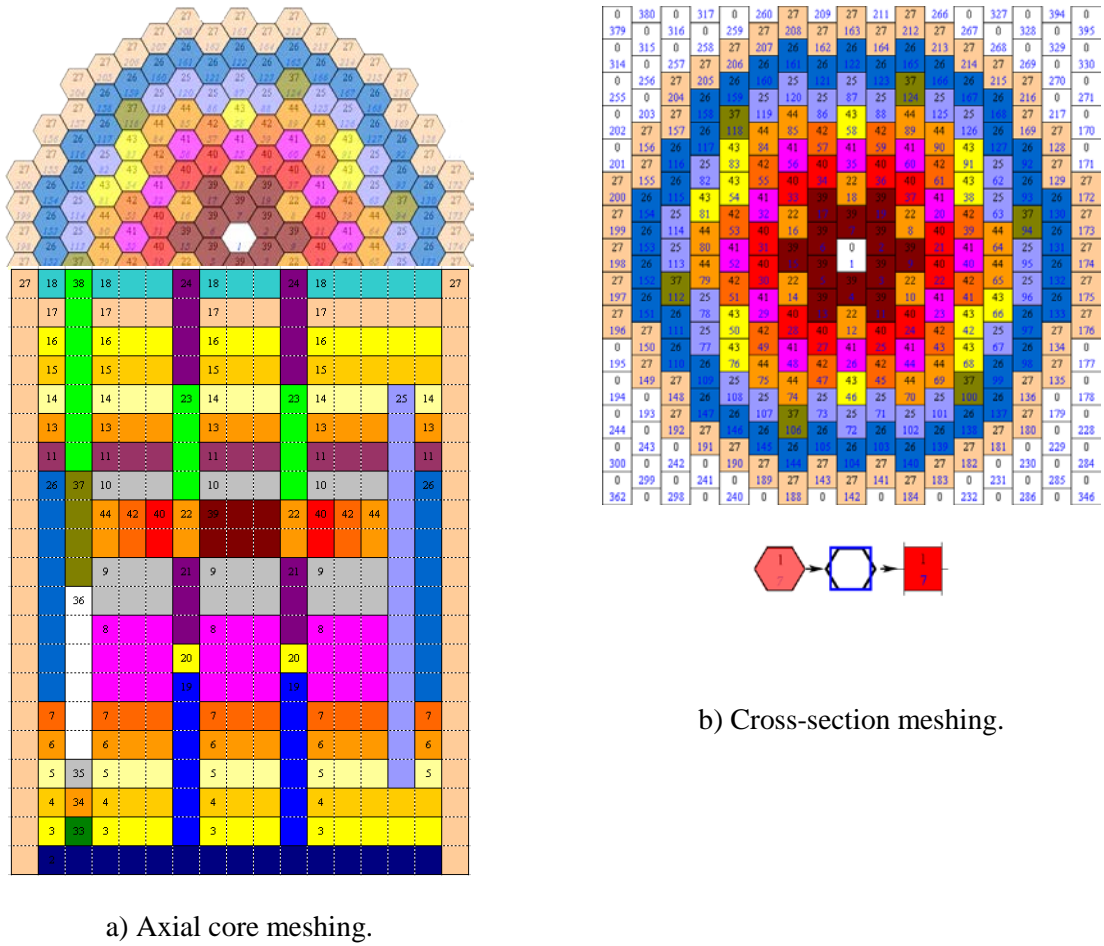
a) Axial core meshing.

b) Cross-section meshing.

FIG. 2. SIMMER-IV Model of 72 FA-94 MW Sub-Critical Equilibrium Core

Table 2.1. SIMMER calculation regions.

1	Fuel	16	Nozzle Out 2	31	YZrO SR
2	LBE Inlet	17	Nozzle Topplate	32	B4C SR
3	Nozzle In 1	18	LBE Outlet	33	Roller CR
4	Nozzle In 2	19	LBE In IPS	34	Grid CR
5	Grid In Wrap	20	He IPS	35	YZrO CR In
6	Grid In	21	YZR IPS Low	36	B4C CR
7	Pin In	22	Sample IPS	37	YZrO CR Out
8	Gas Plenum	23	Plenum IPS	38	Plenum CR
9	Insulator In	24	YZR IPS Up	39	Fuel Zone 1
10	Insulator Out	25	LBE Dummy	40	Fuel Zone2
11	Spring	26	YZR_INSU Outer Dummy	41	Fuel Zone 3
12	Pin Out	27	Barrel	42	Fuel Zone 4
13	Grid Out	28	Grid In SR	43	Fuel Zone 5
14	Grid Out Wrap	29	Tube SR	44	Fuel Zone 6
15	Nozzle Out 1	30	Roller and Grid SR		

Six fuel zones with different isotopic compositions are modelled in SIMMER-IV as a mix of two "fertile" and "fissile" isotopic vectors by applying an "enrichment" for every zone. The vectors and zone enrichments are obtained from the solution of the error minimization in isotope inventories for the burnup zone 2 (fresh FA after the first cycle) and the total core mass. SIMMER enrichments for every burnup zone are given in Table 2 while the resulting mass errors due to the approximation method are shown in Table 3. As one can see, the maximal error for the fissile isotopes never exceeds few grams, while for U238 the maximal error is about 0.2 kg (0.7 %) in the core outermost burnup zone.

Table 2. Burnup zone enrichment

	Group 1	Group 2	Group 3	Group 4	Group 5	Group 6	Total
enrichment	0.316	**0.250**	0.290	0.268	0.344	0.332	**0.300**

Table 3. Mass error within six burnup zones (gram)

Isotope	Zone 1	Zone 2	Zone 3	Zone 4	Zone 5	Zone 6	Total
U235	-0.2	0.0	0.0	0.2	0.1	-0.2	0.0
U238	-78.8	0.0	37.3	150.0	89.4	-198.1	-3.3
PU238	1.1	0.0	0.5	0.2	-1.6	-0.2	0.0
PU239	15.7	0.0	0.4	-2.1	-12.7	-1.4	-0.8
PU240	9.0	0.0	-1.4	-4.7	-7.6	4.6	-0.4
PU241	1.2	0.0	-1.6	-5.9	3.6	2.8	-0.1
PU242	1.4	0.0	-0.6	-0.8	-0.8	0.8	-0.1
AM241	1.3	0.0	2.1	5.7	-6.6	-2.4	0.0
AM243	0.5	0.0	-0.2	-0.5	-0.2	0.4	0.0
CM242	-0.7	0.0	-0.4	-0.4	1.1	0.3	0.0

The main steady-state calculation results are shown in Table 4. k_{eff} is about 0.95 which is in good agreement with SCK•CEN calculations [4].

Table 4. FASTEF 72 FA-94 MW Sub-Critical Core Power and Peaking Factors at Steady-State

	SIMMER-IV 3D
k_{eff}	0.95166
K_r (radial peaking factor)	1.502
K_z (axial peaking factor in max power S/A)	1.261
K_r (peaking factor within max power S/A)	1.109
Maximal S/A Power	1.948 MW
Average S/A Power	1.294 MW
Minimal S/A Power	0.825 MW
Neutron Flux in IPS	$3.62 \times 10^{15}/cm^{-1}/s^{-2}$

In the SIMMER-IV model, the pressure boundary conditions are defined at the core inlet and outlet, i.e. at the bottom and top of the calculation model shown in Fig. 2 (a). The outlet pressure is assigned as a constant value of 2 bar, while the inlet pressure is adjusted to fit the input design value of 71.39 kg/s for fuel S/A. In other regions, such as Inner and Outer dummy S/A, the orifice coefficients have been tuned to match full and half of the fuel S/A flowrate correspondingly. Note, that flowrates in different core zones are not exactly the same but distributed according to the power and coolant heat-up.

The calculated relative S/A power distribution is shown in Fig. 3. The radial power peaking factor K_r is 1.50, the highest power being in the first row of fuel S/As, SIMMER-IV calculations also show a sharp power variation in plane near the target region. The peaking factor within the hottest fuel S/As reaches 1.11 as calculated by SIMMER-IV two-cells – one S/A model. The intra-subassembly power and coolant flow distribution is approximate in the employed SIMMER-IV model.
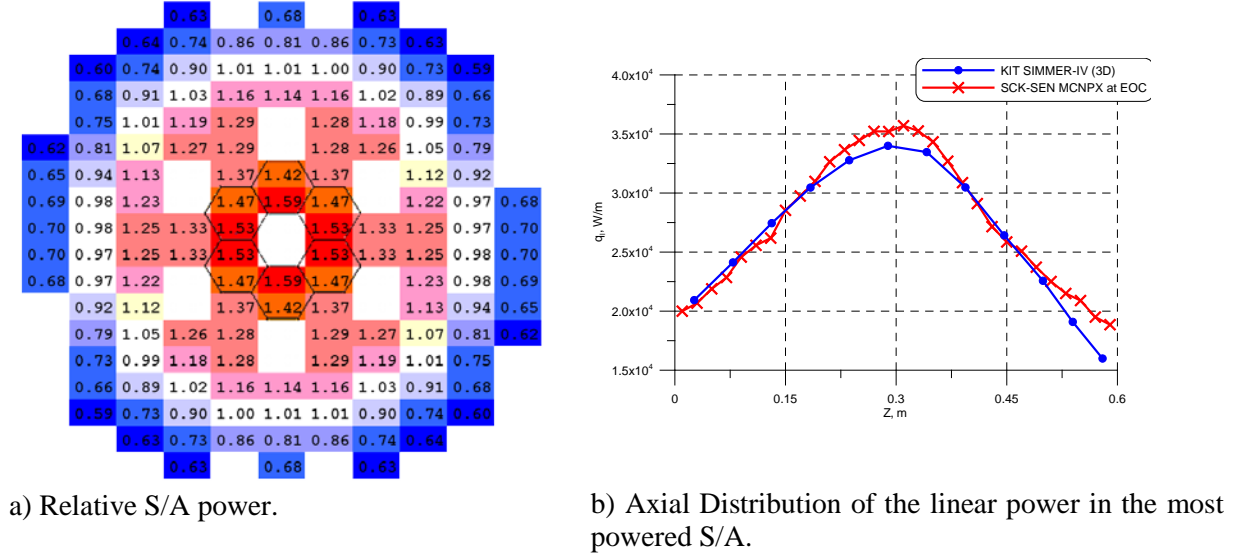
a) Relative S/A power.

b) Axial Distribution of the linear power in the most powered S/A.

FIG. 3. Radial and axial power distribution.

3. Unprotected Blockage Accident Analysis

The unprotected blockage accident (UBA) represents a potential path to core damage. UBA analysis played a significant role in the safety assessment and licensing for sodium cooled fast reactors. The key question is, if and how far damage propagation from a single blocked subassembly is possible. For the heavy-metal cooled reactor conditions with missing operational experience and the potential of corrosion and oxidation product formation the blockage accidents are of special interest.

Two-dimensional SIMMER-III code was applied to simulations of the blockage accident in the experimental PDS-XADS LBE-cooled system [8], a predecessor of FASTEF. It was shown that no cladding failure might be expected thanks to the intensive radial heat transfer and the coolant flow in the hexcan gaps. However, simulations with artificially suppressed radial heat transfer showed the occurrence of the pin failure in the blocked fuel assembly but subsequent fuel sweep-out into the upper plenum region brings a reactivity reduction and no power excursion. Another study was performed with SIMMER-III with transient analysis of the lead-cooled EFIT ADS core [9, 10]. The UBA transient simulations predicted that if pin failure happens in the core center, the failure propagation is possible while the core finally arrives at the lower power conditions due to sweeping out of the fuel from the active core. Again, the results were obtained under conditions of the significant interwrapper flow removing enough heat from the blocked fuel assembly. However, the quantitative value of the interwrapper flow and heat transfer is difficult to estimate due to uncertain geometrical and boundary flow conditions. Thus, neglecting the interwrapper flow eliminating the radial heat exchange can be considered as a most conservative case in the UBA simulations in present study. Note that in sodium cooled reactors the TIB accident phenomena are essentially different due to the possibility of sodium boiling and fuel crust formation on the hexcan walls after pin melting. For the current study, an ultimate goal is to determine the maximum FA blockage that does not immediately lead to the severe core damage under the conservative condution mentioned above. Since only one non-central fuel subassembly is assumed to be blocked, the radial symmetry is not possible; therefore the 3D SIMMER-IV model is applied. We assume that an instantaneous blockage occurs in a single fuel subassembly located in the first row from the core center with maximal FA power as shown in Fig. 4. We also assume that fuel assembly is blocked close to the inlet area and in the SIMMER model such blockage is simulated as a local hydraulic resistance that lowers the coolant flowrate through the affected subassembly.
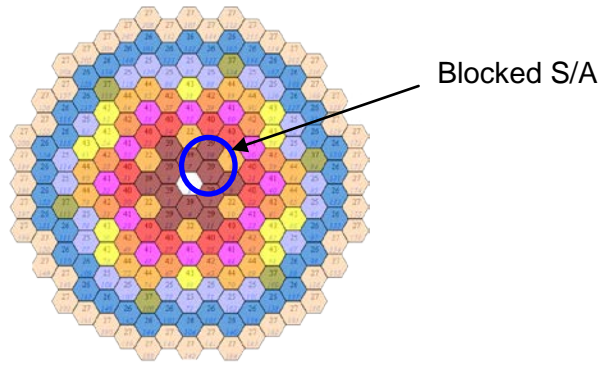
FIG. 4. Location of blocked fuel assembly.

3.1. Maximal Acceptable Blockage

Steady-state calculations show that the S/A radial peaking factor can reach 1.5, so the maximal S/A power is about 1.95 MW. In case of the LBE-cooled core the maximal acceptable blockage is determined by maximal tolerated cladding temperature, which, in turn, must be significantly lower thanshow taht steel melting temperature (~1370C). The maximal tolerated temperature depends on current and past operating conditions. In this study, we assume that cladding failure temperature is about 1100 C. At steady-state, the maximal cladding temperature is reached at the core outlet, being slightly higher (10 to 20 C) than the coolant outlet temperature.

A simple analytical balance model can easily yet accurately predict the blocked S/A outlet temperature at steady-state. The maximal outlet temperatures in the blocked subassembly are shown in Fig. 5. Both analytical solution and SIMMER-IV simulations show that the cladding creep failure limit (~1100 C) is reached when the flow is reduced by about 75%, while the cladding temperature does not exceed the steel melting point up to the blockage of about 80%.
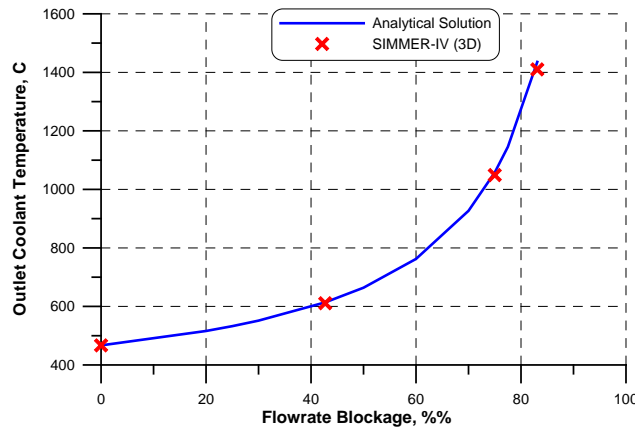

FIG. 5. Steady-state coolant outlet temperature in partly blocked S/A (Analytical solution and SIMMER-IV simulations).

3.2. SIMMER-IV Simulations for Core Destructive Blockages

Several SIMMER-IV simulations have been performed for flowrates below 20 % of the nominal one in the blocked fuel assembly. The flowrate and cladding temperature histories are shown in Fig. 6 for

the 80, 90, and 95 % blockage cases. One can see that in the UBA case of 80% the cladding survives, while the its temperature approaches 1100 °C. In other cases (90 and 95 % blockages) the cladding temperature quickly, in 7 to 8 seconds, reaches the steel melting point, then the cladding fails. In the two latter cases, the flowrate is recovered in about twenty seconds after failure of the wrapper of the neighbouring subassemblies, from which the flow finds its way to the blocked S/A thus partly restoring cooling of the remaining fuel.
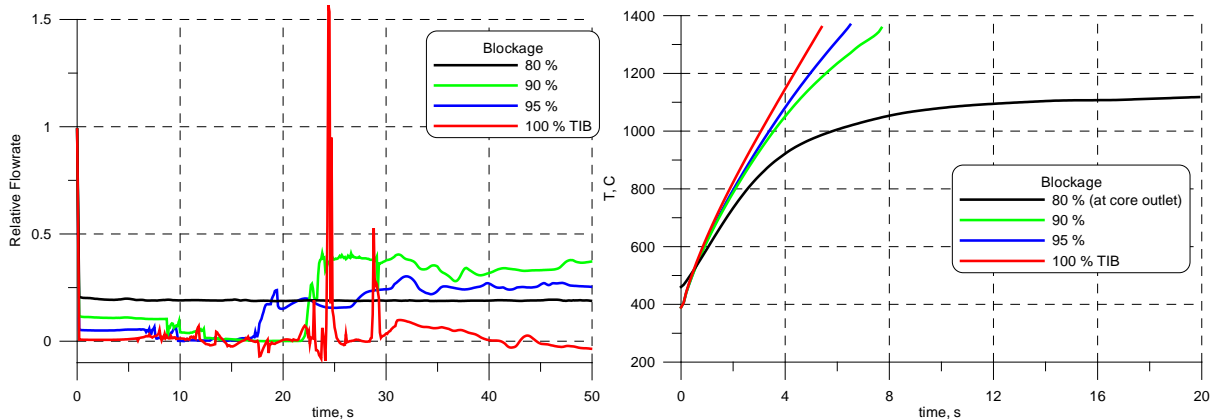

FIG. 6. Flowrate and cladding temperature history in partly blocked fuel assembly.

In the following section two blockage simulations of 95 % UBA and Total Instantaneous Blockage (TIB) are given and discussed.

3.3. *Simulation of Severe Blockages (95% UBA and TIB)*

This analysis is performed mainly in order to understand the overall phenomenology and identify the key safety parameters which influence the simulation of the blockage beyond the safe limits discussed in the previous section. The general phenomenology is as following. After blockage formation the coolant is quickly heated up so the cladding temperature quickly reaches the creep failure limit (~1100 C). Clad failures lead to a blow-out of the fission gas from the plena after local clad failures. The coolant and clad temperatures are increasing until the clad looses its strength and the fuel pellets become mobile and the molten steel floats upwards. Depending on the fuel behaviour and other parameters either the fuel can leave the core driven mainly by buoyancy or - if the fuel pellets get stuck – the damage propagates until larger open areas are created for the fuel escape.

To give an insight into these scenarios, two severe blockages cases, 95 % UBA and 100 % Total Instantaneous Blockage (TIB) are presented and discussed in the following in more details. Figure 7 shows the history of the coolant, cladding and fuel temperatures, including liquid steel and fuel pellet chunks. After about seven seconds of the transient the cladding temperature reaches the melting point and cladding fails making possible direct contact between coolant and fuel pellets. At this moment, the maximal fuel temperature at the pellet center is about 2500 °C, i.e. higher than LBE boiling point but the temperature on the fuel surface is 1630 °C, i.e. lower than LBE boiling point temperature which is about 1800 °C at the FASTEF core pressure levels. Thus, according to the used SIMMER models, fuel pellets are broken in chunks and coolant does not boil. However, due to uncertainties in pellet break-down models and several additional effects, such as possible pressure fluctuations, the local LBE boiling cannot be completely excluded, and this issue should be studied in more details. In the 95 % UBA case, at 17 seconds after the beginning of the transient, SIMMER simulations predict failure of the wrapper tubes of the blocked S/A and three neighbouring S/As, as well as walls of the IPS and spallation target channels as shown in Fig. 8. As a result, the flowrate in the blocked S/A is partly recovered and becomes high enough to cool the remaining fuel.
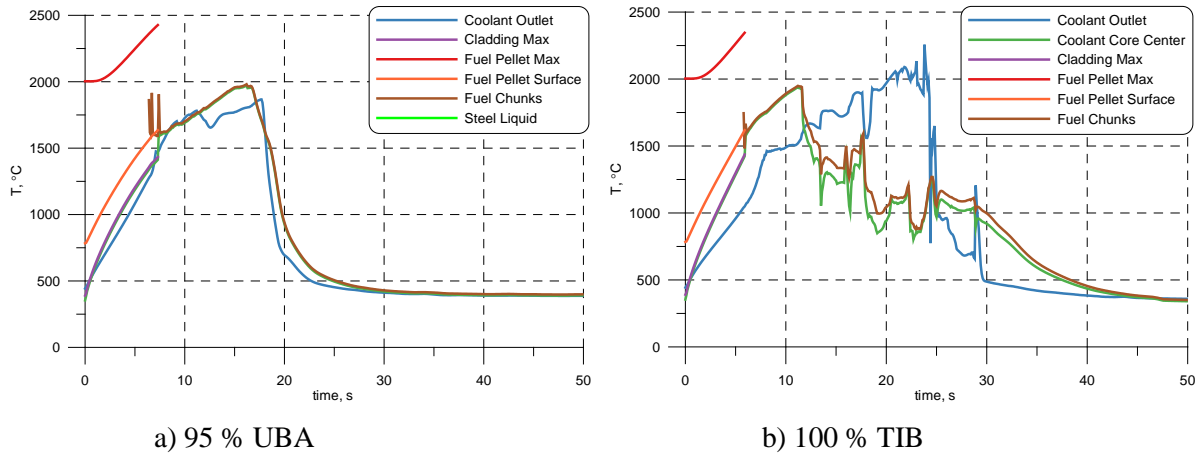
a) 95 % UBA   b) 100 % TIB

FIG. 7. Coolant, cladding, and fuel temperature history. (LESS DETAILS!!)

The flowrates in the neighbouring subassemblies shown in Fig. 9 (a) remain sufficient for the cooling too. At these flowrates (higher than 60 % of nominal) other fuel S/As are kept at relatively safe conditions. A similar behaviour is observed in the TIB case, while the final flowrate redistributions is reached later, after 25-30 s of the TIB transient. In both cases no propagation is predicted, the core damage is limited to the blocked S/A and its closest neighbours.
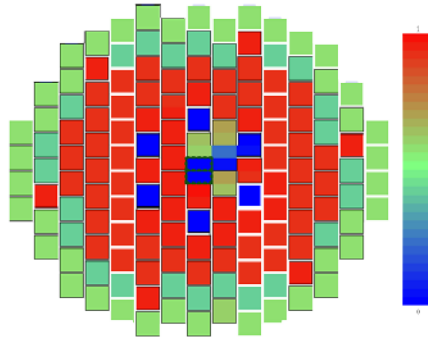
FIG. 8. Core flowrate distribution at 19.5 sec. of UBA 95 % transient.

a) 95 % UBA   b) Total Instantaneous Blockage (TIB)
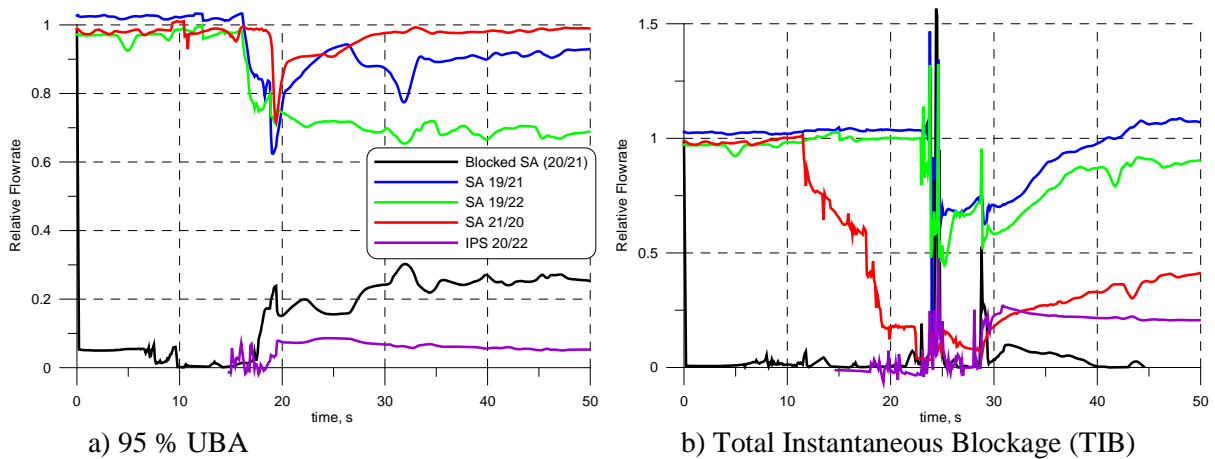
FIG. 9. Flowrate history in blocked and neighbouring fuel assemblies.

Destruction of the spallation target channel definitely shuts down the reactor, however in the safety analysis we assume the neutron source is independent and therefore not affected. The transient is continued and stabilized at a slightly lower power level (~ 77-79 MW) as shown in Fig. 10.
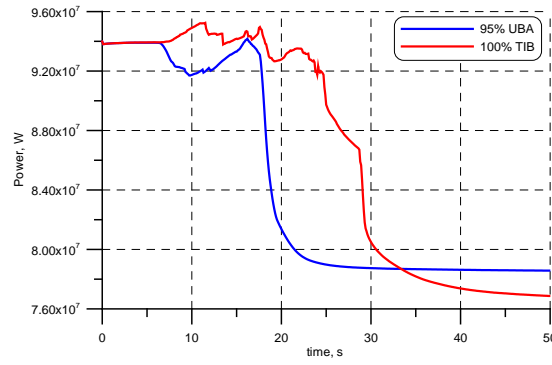
FIG. 10. Core power history

Several snapshots of the axial plane material distribution in the 95 % blocked S/A , two neighbouring ones and IPS channels are given in Fig. 11.
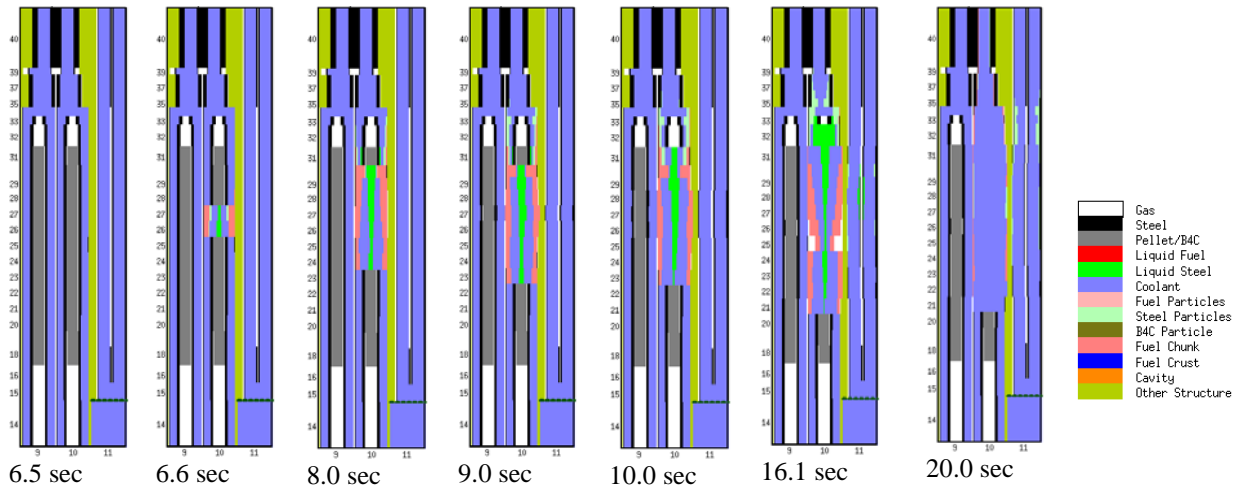

FIG. 11. Material distribution in blocked S/A (95 % UBA).

The fuel pins fail at 6.6 seconds, the cladding melts while the fuel pellets breaks into chunks. Wrapper tube walls fail after 15 seconds making possible mass exchange, when the hot coolant, liquid steel and fuel chunks move to the IPS channel, and the cold LBE inflow from the IPS channel makes possible to restore (partly) flow in the blocked S/A. A low-scale local boiling is observed at 16.1 sec. Later neighbouring S/A wall also fail, and the process stabilizes after about twenty seconds. At this new steady-state, the LBE flowrate is enough to provide an appropriate cooling.

4.   Concluding Remarks

The unprotected blockage accident scenarios in the FASTEF subcritical core have been analysed. Both analytical and SIMMER-IV 3D calculations show that for the FASTEF 94 MW sub-critical equilibrium core with 94 MW power at EOC conditions, the blockage in the single fuel assembly becomes severe at the level of 75 %, i.e. when the flowrate in blocked S/A becomes lower then 25 % of the nominal value. At the 75 % blockage, the bulk coolant temperature reaches 1000 C in ten seconds. However, the local coolant and cladding temperatures can be even higher due to variations in the neutron flux and power-to-flowrate ratio in central and peripheral sub-channels. Therefore, the "safe" limit should not exceed 70 % of the flowrate blockage. At the 80% blockage in the single innermost ring S/A, cladding temperature already reaches the steel melting point. Note that these evaluations are made under conservative assumption of no-flow in gaps between S/As.

Several severe UBA simulations have been analysed. Details of two UBA transient with the 95 % blockage and the 100 % total instantaneous blockage (TIB) have been discussed. The 3D SIMMER simulations show that fuel pins in blocked fuel assembly fail after six-seven seconds from the

beginning of transient. Fuel pellets broke in chunks contacting the LBE coolant bringing a potential possibility of the local boiling. After fifteen to twenty seconds, assembly hexcan walls also fail resulting in the intensive mass exchange between the blocked fuel S/A and neighbouring ones, affecting the central spallation target channel and irradiation channels. Note, the coolant modelling for the target region is approximate, heat production in the target due to spallation reactions being not considered. Due to mass and energy exchange, few seconds later (about twenty-thirty seconds after the beginning of UBA), the LBE coolant flow is partly restored in the blocked fuel assembly. The total flow remains enough to cool all affected subassemblies, thus preventing further propagation of the core disruption. The core power is stabilized at about 80 % of the nominal value and no power excursion observed in the SIMMER simulations. As a very conservative condition of non-interwrapper flow has been assumed in this analysis, a more accurate modelling of the interwrapper flow would probably show more favourable accident development.

The SIMMER-IV simulations confirm that LBE-cooled subcritical core of the FASTEF/MYRRHA reactor shows remarkable resistance against severe accidents related to the subassembly blockages. Thanks to the low power-to-flow ratio, the FASTEF core can survive short-time accidents when the flowrate in the blocked fuel assembly remains higher than 25 % of the nominal value. For large blockages, up to 100 % TIB, the fuel pin failure area is limited by the affected subassembly and its closest neighbouring channels.

REFERENCES

[1]   H.A. Abderrahim, P. Baeten, D.D. Bruyn, R.Fernandez, MYRRHA – A multi-purpose fast spectrum research reactor, Energy Conversion and Management, Vol. 64, pp.4-10, (2012)

[2]   D.D. Bruyn, P. Baeten, S. Larmignat, H.A.Woaye, L. Mansani. The FP7 Central Design Team project: towards a fast-spectrum transmutation experimental facility. In: International congress on advances in nuclear power plants (ICAPP'10). San Diego (California, USA), paper 10114; p. 470–476, (2010)

[3]   R.Fernandez, et al., Definition of MYRRHA-FASTEF specifications, design choices and detailed work programme. Deliverable D1.4 of the EURATOM FP7 CDT project, ANS-PSD/RF/rf.3933.ARTD00CDT-01.827/10-27.

[4]   SCK.CEN. MYRRHA sub-critical core configuration, http://myrrha.sckcen.be/en/Engineering/Sub-critical_core, 01.10.2012

[5]   G. Kaiser, J. Charpenel, C. Jamond, C. Berthoud, K. Schleisiek, "Main SCARABEE lessons and most likely issue of the sub-assembly blockage accident," Int. Top. Mtg. on Sodium Cooled Fast Reactor Safety, Oct 3-7, 1994, Obninsk, Russia (1994).

[6]   H. Yamano, S. Fujita, Y. Tobita, I. Sato, H. Niwa, Development of a three-dimensional CDA analysis code: SIMMER-IV, and its first application to reactor case. Nucl. Eng. Des. 238, 66–73, (2008)

[7]   W. Maschek, A. Rineiski, T. Suzuki, S. Wang, Mg. Mori, E. Wiegner, D. Wilhelm, F. Kretzschmar, Y. Tobita, H. Yamano, S. Fujita, P. Coste, S. Pigny, A. Henriques, T. Cadiou, K. Morita, G. Bandini, SIMMER-III and SIMMER-IV Safety Code Development for Reactors with Transmutation Capability, M&C 2005, Avignon, France (September 12-15, 2005)

[8]   T. Suzuki, X-N. Chen, A. Rineiski, W. Maschek, Transient analyses for accelerator driven system PDS-XADS, using the extended SIMMER-III code, Nuclear Engineering and Design, vol.235, pp.2594–2611, (2005)

[9]   P. Liu, X.-N. Chen, A. Rineiski, W. Maschek, Transient Analyses of the 400 MWth-Class EFIT Accelerator Driven Transmuter with the Multi-Physics Code: SIMMER-III, Nuclear Engineering and Design, Vol. 240, pp. 3481-3494, (2010)

[10]   W. Maschek, X.-N. Chen, P. Liu, A. Rineiski, M.Flad, G. Rimpault, Safety and Design Concepts of the 400 MWth-Class EFIT Accelerator Driven Transmuter and Considerations for Further Developments, Energy Conversion and Management 51, p. 1764-1773 (2010)

Principles of Inherent Self-Protection
Realized in the Project of Small Size Modular Reactor SVBR-100

G.I. Toshinsky[a], **V.V. Petrochenko**[a],

O.G. Komlev[b], **I.V. Tormyshev**[b],

A.V. Dedul[c]

[a] JSC "AKME-Engineering", Moscow, Russia

[b] State Scientific Center Institute for Physics and Power Engineering (SSC IPPE), Obninsk, Russia

[c] JSC Experimental Design Bureau "Gidropress" (JSC EDO "Gidropress"), Podolsk, Russia

Abstract. In the presented report the advantages and drawbacks of different coolants are analyzed, factors of hazard peculiar to reactor facilities are considered, a provision concerning the determinative effect of potential energy stored in coolant on safety is validated. The high level of inherent self-protection and passive safety of reactor SVBR-100 is demonstrated.

1. INTRODUCTION

During a historically short period of nuclear power (NP) development, a number of low probability accidents of various extent of severity occurred in different countries. The accidents resulted in strong exhausts of radioactivity into the environment and/or considerable economical losses are as follows:

—   Three Mile Island Unit 2 (TMI-2) accident in 1979 (USA). The accident in PWR type reactor at nuclear power plant (NPP) resulted in core meltdown due to loss of primary circuit coolant;

—   Chernobyl disaster occurred on 26 April 1986. An explosion in the Unit 4 reactor caused by prompt neutrons runaway resulted in catastrophic release of large quantities of radioactivity into the atmosphere;

—   In 1995 fire occurred at fast sodium reactor "Monju" (Japan). It happened as a result of non-radioactive sodium leak in the intermediate circuit pipeline;

—   In 2011 the disaster happened at NPP Fukushima 1 (Japan) because of the earthquake and long total blackout caused by subsequent tsunami.

The initial events for these accidents are very unlike. These are such as personnel's errors, technical failures, design defects, extremal external impacts. However, there is a common cause of the severe consequences of all considered accidents. They are the result of release of various types of potential energy accumulated in different materials, first of all, in the reactor facility (RF) coolant:

—   Compression energy of water coolant;

—   Chemical energy resulted from interaction of water steam with zirconium;

—   Chemical energy resulted from interaction of hydrogen produced by steam-zirconium reaction with air oxygen;

—   Chemical energy resulted from interaction of sodium with air oxygen.

Because of those accidents, in many countries the population trust in the NPP safety was lost. Therefore, in order to win the population confidence, it is necessary to make corrections in the strategy of NP development.

Touching on a subject of Russia response to the disaster happened at NPP Fukushima 1, Sergey Kirienko, Director General of the State Atomic Energy Corporation ROSATOM, in his speech at the Special Plenum Session of 2011 International Congress on Advances in Nuclear Power Plants (ICAPP 2011, Nice, France, May 2-5) clearly justified three stages of the response actions [1]:

The first near-urgent stage is performing stress-tests for all operating NPPs in Russia, equipping these NPPs by transportable means of emergency electricity and water supply and associated training of the operating personnel. By now that task has been finished successfully.

The second middle-urgent stage is making corrections in constructing and developing NPPs for the purpose to enhance more their safety in conditions similar to those at NPP Fukushima 1.

The third long-urgent stage is changeover to construction of NPPs with natural safety reactors [2], in which severe accidents with grave consequences have been eliminated deterministically by laws of nature.

The necessity to develop reactors with such level of safety was first highlighted in paper [3] in 1985 prior to occurrence of Chernobyl disaster. In paper [3] those class reactors were called inherently safe reactors. The arguments in support of the necessity to develop such reactors and general principles of their design were presented in paper [4] in 1990 after Chernobyl events. In that paper it was highlighted that from the standpoint of population, the opportunity of catastrophic consequences caused by nuclear accident was much more important than very low possibility of its realization. Though, in compliance with the reliable statistical data, the man-caused risks from operation of industrial enterprises and their fuel-energy infrastructure are many orders greater than the corresponding risks from NP.

From the standpoint of nuclear community and educated people that interpretation of NP is irrational. Nevertheless, this is a real factor that we should take into consideration and high safety of the NPP should be validated by clear arguments without use of probabilistic analysis methods.

Reactor facility SVBR-100 [5] (lead-bismuth fast reactor with equivalent electric power of 100 MWe) is a facility, in which there are no materials capable to accumulate the kinds of potential energy specified above.

In the report the major advantages and drawbacks of different coolants are discussed, basic factors of the hazard associated with the RF and caused by potential energy stored in coolant are considered, characteristics of inherent self-protection and passive safety of RF SVBR-100 are presented.

2. EXAMINATION OF ADVANTAGES AND DRAWBACKS OF DIFFERENT COOLANTS

The RF coolant much determines the RF design as well as safety and economic characteristics of the NPP power-unit. Each of coolants used or proposed for usage possesses its own advantages and drawbacks, their significance is determined by the reactor purpose and external conditions. During a long process of mastering the different coolants, their drawbacks were compensated by technical means and organizing measures, in case it was possible and expedient, which differently affected their technical and economical characteristics.

The value of potential energy stored in a volumetric unit of coolant is the most important coolant characteristic. It is the parameter that determines the safety level of the RF and NPP power-unit (see section 3 and section 4).

The major advantages and drawbacks of different coolants conditioned by their natural properties are considered below.

Water coolant.

Owing to the fact that water has been mastered in traditional power, in the NP water coolant is dominating. Heat can be well removed by water, water is available and cheap. Drawbacks of water coolant are as follows: high pressure in the primary circuit is required; being exposed to radiation and chemical interaction in emergency conditions with zirconium, water is decomposing with release of hydrogen.

<u>Sodium coolant.</u>

Thermal and physical properties of sodium are very high and, therefore, sodium can provide high power density of the core and short doubling time of plutonium. The advantage of sodium and other liquid metals is that there is no necessity to maintain high pressure in the primary circuit. There are no limits on raw material resources. Drawbacks of sodium coolant are as follows: high chemical activity while reacting with air and water that is possible in events of accidents, high induced gamma-activity that hampers the access to the equipment to perform maintenance and repair works during a long time (2-3 weeks).

<u>Lead-bismuth coolant (LBC).</u>

Advantages of LBC are as follows: chemical inertness to water and air, lack of the necessity to maintain high pressure in the primary circuit, high nuclear-physical characteristics. LBC was mastered in conditions of operating the nuclear submarines' (NS) reactors [5]. However, for civilian NPPs this experience needs to be verified by operating the experimental-industrial reactor. The drawback of LBC is that alpha-active polonium-210 is accumulated during the operation. Bismuth resources are limited but sufficient enough for real scale development of LBC cooled reactors.

<u>Lead coolant.</u>

Lead coolant possesses the same advantages as LBC and a lower level (by 4 orders of magnitude) of induced polonium activity. It is cheaper than LBC and its raw material resources are more available. The drawback of lead coolant is high melting point (327 ºC), that is by 200 ºC higher than that of LBC (123,5 ºC). That drawback of lead will hamper RF operating.

<u>Coolants' technology.</u>

All coolants need quality control in order to eliminate accumulation of solid deposits and assure corrosion resistance of selected structural materials during a given service life within the required temperature range. These tasks have been solved or can be solved.

For water it is necessary to maintain approximately 10 quality parameters within the required interval. For sodium it is necessary to maintain dissolved oxygen concentration to be lower than the specified level. For coolants containing lead it is necessary to maintain concentration of dissolved oxygen within the indicated range that is wider for LBC and narrower for lead.

3. MAJOR HAZARD FACTORS ASSOCIATED WITH THE RF

The hazard associated with the RF is determined by two factors:

(1)   Radiation potential accumulated, i.e., total radioactivity (more exactly, radiotoxicity) contained in the RF,

(2)   Amount of radioactivity release into the environment for different initial events.

The first factor does not depend strongly on the RF type, because total radioactivity contained in the RF is determined mainly by the amount of fission products and associated primarily with thermal power of the reactor and total duration of its operation at this power level, i.e., by energy production.

The second factor depends strongly on the RF type and is determined by reactivity margin, feedbacks, design features, and potential energy accumulated in the RF materials (nuclear energy, internal thermal energy, coolant compression energy, chemical energy), which in an event of its release can cause exhaust of radioactivity into the environment. Therefore, the hazard associated with the RF (for identical power levels and operation time) will be determined by the second factor.

The nuclear fission energy which can be released under conditions of reactivity accidents, must be minimized as early as at the reactor design phase. That factor of hazard and efficient methods for its neutralization will be considered below. Otherwise, potential (non-nuclear) energy stored in the RF coolant is an inherent property of coolant material and cannot be changed by engineering solutions.

Upgrade of safety for the NPP with traditional type RFs requires build up of the number of safety systems and defense-in-depth barriers, which diminish the probability of severe accidents (but do not

eliminate deterministically their reasons) and weight of their consequences. While assessing this probability, failures of the basic equipment, safety systems, protection barriers, and personnel's errors are considered as random events.

However, there are many uncertainties in the results of safety substantiation by probabilistic safety analysis (PSA) methods as applicable to severe accidents, their probability being very low (~ 10^{-6} per reactor-year and less). Therefore, a credibility value of these results is not within the required range. Moreover, PSA methods make no sense in case we consider the pre-planned initial events, in which all active safety systems (or passive ones with some movable parts), which are in a standby mode, and protection barriers can be disabled on purpose (for example, over-normative external impacts in nature or man-caused impacts, ill-intended people's actions), and a value of radioactivity exhaust can achieve a disastrous level.

The values of the specific (per a volume unit) stored potential energy for different coolants E_{pot}, which could be released in events of severe accidents, are summarized in Table 1 (the reference data were used in computations).

Table 1. The values of stored potential energy for different coolants

Coolant	Water	Sodium	Lead, LBC
Parameter	P = 16 MPa, T = 300 ºC	P = 0,1 MPa, T = 500 ºC	P = 0,1 MPa, T = 500 ºC
Total potential energy, GJ/m³, including:	~ 21.9	~ 10	~ 1.09
Thermal energy	~ 0.90	~ 0.6	~ 1.09
Including potential compression energy	~ 0.15	None	None
Potential chemical energy of interaction	With zirconium ~ 11.4	With water ~ 5.1 With air ~ 9.3	None
Potential chemical energy of interaction of released hydrogen with air	~ 9.6	~ 4.3	None
Potential compression energy and chemical energy	~ 21	~ 9.4	None

Release of such components of total potential energy as potential compression energy and chemical energy stored in coolant (their values for different coolants are cited in the last line in Table 1) can cause loss of coolant and termination of coolant removal from the reactor core, damage of safety systems and protection barriers, and exhaust of radioactivity into the environment.

The issues of accounting for potential (non-nuclear) energy, which can be released in events of over-normative external impacts, were studied earlier [6, 7] in the analysis of nuclear installations safety. The importance of the analysis of such scenarios is verified by the fact that they also have been addressed by IAEA [8]. This is owing to the fact that RFs, in which the potential energy is accumulated in coolant in great amounts and can be released in an event of tightness failure in the primary circuit, could be used by terrorists as an instrument of political blackmail.

When analyzing the consequences of potential energy release, we should keep in mind the following:

(1) For water coolant, some quantity of stored thermal energy can be converted into kinetic energy of steam expansion (assessment in Table 1 is performed for adiabatic process) that can cause mechanical destruction in the equipment, and water evaporation can cause loss of core cooling. Moreover, in an event of the severe accident while steam is chemically interacting with zirconium, thermal energy and hydrogen are released additionally in large quantities. Hydrogen, in turn, is a high-rating source of hazard;

4

(2)   For sodium coolant while contacting with air, the release of stored chemical potential energy can cause fire and, in an event of the unfavourable scenario, also loss of core cooling; while contacting with water, thermal energy and hydrogen will be released in large quantities;

(3)   For heavy liquid metal coolants (lead-bismuth alloy, lead), the stored thermal potential energy cannot be converted into kinetic energy. There is no essential release of energy in an event of coolant chemical contacting with air, water, and structural materials. There is no loss of core cooling in an event of tightness failure in the gas system.

As an illustration of the above postulates, Fig. 1 presents a hazard/safety diagram [9] showing the quality dependence of the probability of radioactivity release on its values for reactor facilities with identical radiation potentials, which differ by values of potential energy stored in coolant.
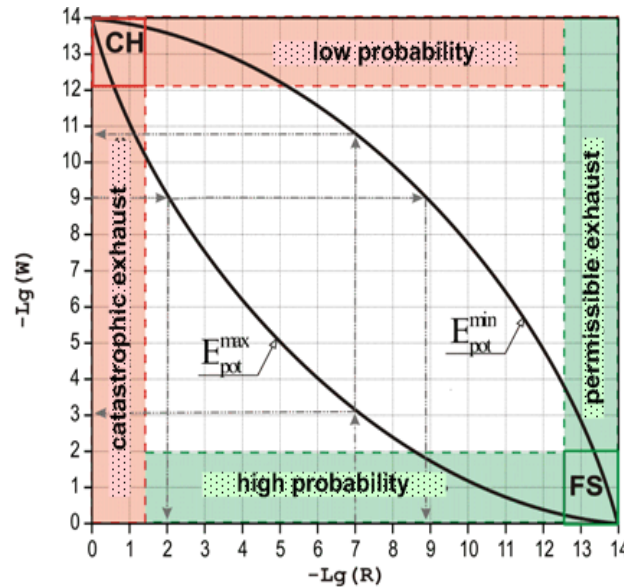

FIG. 1 RF hazard/safety diagram

On a vertical axis of the diagram a negative value of logarithm of probability of radioactivity release **W** is shown. Conditionally it is accepted that value **W=10⁻¹⁴** is corresponding to the release of total radioactivity accumulated in the RF. On the horizontal axis a negative value of logarithm of radioactivity release in relative units **R** is shown (**R=1** means that the whole amount of radioactivity accumulated in the RF is released into the environment; **R=10⁻¹⁴** means that radioactivity release is corresponding to a background level). The value of stored potential energy is designated E_{pot} for the corresponding curves.

In the part of the diagram designated **FS** (full safety), in which the value of radioactivity release is below the permissible level (normal operating conditions), reactors of each type are virtually safe. The probability of such operating conditions is high.

In the part of the diagram designated **CH** (catastrophic hazard), reactors of each type are catastrophically hazardous, because almost the whole amount of radioactivity stored in the RF can be released into the environment as a result of extremal initial events, their probability being very low.

The general tendency of decreasing the probability of radioactivity release while increasing its value is evident. Nevertheless, within these extreme situations there is a wide range of real accidents of different severity levels, on the hazard/safety diagram it is limited by corresponding curves on top and bottom. These curves define the reactors with high and low values of stored potential energy. For the identical probability of radioactivity release, its value may differ much that depends on the value of stored potential energy, or at the same value of radioactivity release the probability of its realization may differ much.

Of course, the diagram proposed for the safety analysis of RFs with different coolants does not take into account a number of other factors, which also determine the value of radioactivity release. For example, capability of fuel to retain fission products at accidental temperatures, not to enter into

exothermal chemical reactions similar to fuel designed for high-temperature gas reactors, chemical compatibility of fuel with coolant, capability of coolant to retain radioactivity under conditions of severe accidents development, and so on.

The value of radioactivity release also depends very strongly on the scenario of accident evolution determined by the RF and power-unit design, behavior and scale of the initial events. Therefore, the hazard/safety diagram reflects the real situation correctly in terms of quality only while all other conditions being equal (except for the potential energy stored in coolant).

In view of the aforesaid the conclusion that RFs with coolants, in which potential energy is stored in large quantities (water, sodium), are less safe a priori than RFs with heavy liquid-metal coolants (lead-bismuth, lead) isn't right. The required safety level is also achieved by equipping the NPP with the necessary number and power of defense-in-depth barriers and safety systems. However, that in different ways affects their economical characteristics.

Along with this, "transparency" of safety proofs for RFs with a low value of potential energy stored in coolant is much higher than for RFs, in which a high safety level has been validated by PSA methods. That will result in different social acceptability of NPPs with such RFs.

Now we are going to consider a factor of hazard associated with an opportunity to insert in the reactor a positive reactivity exceeding the effective delayed neutrons fraction 1 \$ and prompt neutron runaway. Catastrophic consequences of such accident caused by damage of protection barriers and radioactivity exhaust into the environment will be only observed provided growth in coolant temperature caused by power increase results in inadmissibly high increase of pressure. Otherwise, possible melting of the core that is a severe accident itself will not result in catastrophic exhaust of radioactivity into the environment. For the coolants considered above, which boiling point under the atmospheric pressure is 100 ℃, ~ 900 ℃ and ~ 1700 ℃ (water, sodium and HLMC correspondingly), growth in pressure will be the least for coolants with the highest temperature of boiling.

Insertion of positive reactivity exceeding 1 \$ can occur either in case of unauthorized influence on reactivity controls, or as a result of feedback effect. For the whole period of NP development no reactivity accidents caused by operator's extraction of absorbing rods from the core or failures in the reactivity control system ("self-extraction" of rods) have happened at the NPP reactors (as a rule, their reactivity margin exceeded 10 \$). Elimination of reactivity accidents due to these reasons is ensured first of all by technical means provided in the CPS: limited rate of rods extraction, multi-channel (not less than three channels) non-switching emergency protection (EP) that actuates at signals of decreasing of the period of reactor runaway and/or increase of power. Efficiency of EP rods must exceed with necessary margin the power reactivity effect from nominal power to the "cold" state of the reactor. The opportunity to extract the absorbing rods must be technically eliminated prior to EP extraction.

Moreover, in new reactor designs in addition to the highlighted measures the additional direct acting EP system that actuates in case of temperature increasing or coolant flow rate decreasing is provided.

Another way that theoretically excludes an opportunity of reactivity accidents is associated with designing the reactors, which reactivity margin does not exceed 1\$ during the entire lifetime. As computations have revealed that opportunity can be realized in fast neutron reactors which core breeding ratio (CBR) is near 1. However, practical realization of that opportunity is hampered due to the following reasons:

— For assured elimination of the opportunity of reactivity accidents, it is required that at any moment of lifetime effective multiplication coefficient (K_{eff}) does not exceed (1+1 \$) with some margin. On the other hand, it is also necessary that at any moment of lifetime K_{eff} exceeds 1 with some margin in order to provide criticality of the reactor. For uranium-plutonium fuel of equilibrium composition, which provides CBR to be near 1, 1 \$ equals to ~ 0.004. In case the mentioned margins are adopted to be of about 0.0015 (this value is very optimistic), during the whole lifetime K_{eff} should be within the extremely narrow interval: $1.0015 \le K_{eff} \le 1.0025$.

— The error of calculated K_{eff} and its change during the lifetime that is caused by uncertainties in nuclear-physical constants is not less than 0.005; the technological error in the value of K_{eff}

determined by incorrect knowing of the core material content is not less than 0.005 as well. Moreover, it is necessary to take into account neptunium reactivity effect that will increase K_{eff} by ~ 0.0010 – 0.0015 each time after reactor shutdown. It is also necessary to take into account difference in plutonium isotope vectors in fresh fuel caused by unavoidable difference in times of cooling after chemical reprocessing of spent nuclear fuel (SNF) that is resulting in different content of fissile ^{241}Pu, which half-life period is ~ 14 years. It is also necessary to take into account that in several first lifetimes K_{eff} is influenced by deviation of fuel content from equilibrium, opportunity to use plutonium extracted from SNF of thermal reactors, which isotope content is various and depends on the depth of burnup and time of cooling prior to reprocessing.

— While operating the reactor at lowered power level and particularly while putting in operation, reactivity margin will surely exceed $ because of power reactivity effect that must be negative.

The analysis of listed reasons shows that the considered way of elimination of prompt neutron reactor runaway can result in an event of non-achieving the stated goal. Along with this, it is possible to assure elimination of prompt neutron reactor runaway by coupling the technical means provided in the CPS with negative feedbacks.

Reactor SVBR-100 meets these requirements, though while using the nitride uranium fuel, the calculated reactivity margin is less than 1 $ during the whole lifetime [10].

The potential energy stored in coolant is not affecting only safety characteristics but NPP economic parameters as well. For the NPP with traditional type reactors (with a high value of potential energy stored in the RF coolant), safety and economic requirements are in contradiction. The highlighted conflict appears as follows: while heightening the safety requirements, the NPP economical parameters are deteriorating that is caused by necessary increase of the number and efficiency of safety systems and defense-in-depth barriers.

Therefore, the most expedient way to upgrade the NPP safety that simultaneously improves the economic characteristics is use of RFs, in which the value of stored potential energy is the lowest and in which the inherent self-protection and passive safety properties can be realized to the maximal extent. For example, those are the RFs based on modular fast reactors SVBR-100 with heavy liquid metal coolant – eutectic lead-bismuth alloy [11]. In an event of the situation occurred at NPP Fukushima, there will be no radioactivity exhaust beyond the NPP fence.

Those RFs cannot amplify the external impacts, therefore, the scale of damages will be only determined by energy of the external impact, the radioactivity exhaust being localized. Such type RFs will possess the robustness properties, which will ensure their enhanced stability not only in events of single failures of the equipment and personnel's errors, but also in events of malevolent actions when all special safety systems operating in a standby mode could be disabled intentionally. That is especially viable when NPPs are constructed in developing countries where the threat of terrorism is very high.

4. INHERENT SELF-PROTECTION AND PASSIVE SAFETY OF RF SVBR-100

The main effect in providing a high safety level of the SVBR-100 RF is achieved due to use of fast neutron reactor, heavy liquid-metal coolant, in which there is no stored potential energy (chemical energy, compression energy) that can cause loss of coolant and damage protection barriers, and integral design of the reactor, with total elimination of pipelines with radioactive coolant beyond the monoblock vessel (Fig. 2). That has been verified by realized computations and development works [12].

The reactor possesses a negative void reactivity effect and negative feedbacks, the efficiency of the strongest absorbing rod does not exceed 1 $. And that coupled with technical realization of the control and protection system (CPS) eliminates prompt neutron runaway of the reactor.
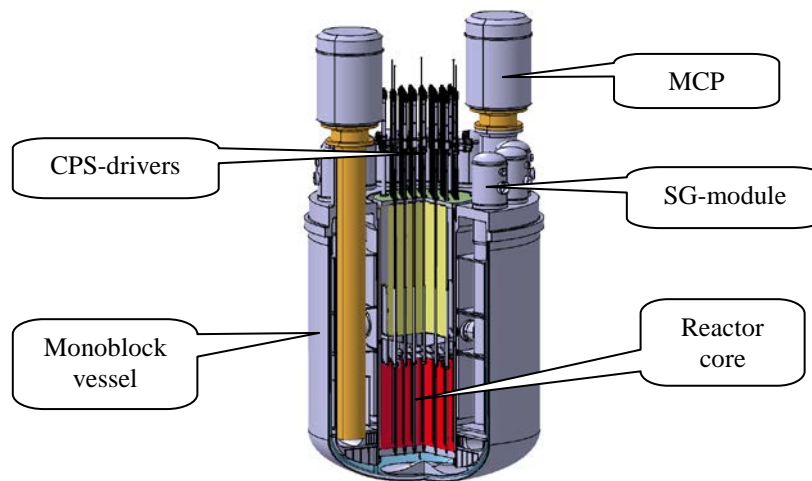
FIG. 2 Reactor monoblock

The high boiling point of coolant heightens reliability of heat removal from the core, and safety due to lack of the heat transfer crisis. Also, being coupled with a provided safeguard casing of the monoblock, that eliminates loss of coolant accidents (LOCA) and high pressure radioactive exhausts.

The low pressure in the primary circuit reduces the risk of its tightness failure and makes possible lessening the thickness of reactor vessel's walls and diminishing the limitations imposed on the rate of temperature change according to thermal-cycling strength conditions.

The RF components do not contain materials releasing hydrogen as a result of thermal and radiation effects and chemical reactions with coolant, water and air. Therefore, in an event of tightness failure in the primary circuit the likelihood of chemical explosions and fires is virtually eliminated.

The circulation scheme of LBC provides elimination of water/steam ingress into the core in an event of SG leak due to effective gravitational separation of steam on a free LBC level in the monoblock.

The RF inherent self-protection properties make it possible to couple realization of much of safety functions and normal operating functions of the RF.

At this point, safety systems do not contain elements, which actuation can be blocked in an event of their failure or under impact of human factors:

— Removal of heat decay is provided passively by natural circulation of LBC in the primary circuit. This is realized by transferring heat over four independent channels in the SG to the secondary circuit water and then to the water tank of the passive heat removal system (PHRS) with removal of generated steam into the atmosphere. (This represents a grace period of about three days long without exceeding the allowed temperature limits);

— In an event of large leak in several SG tubes, localization of SG leak is provided passively while increasing the steam pressure in the gas system over 0.5 MPa. This is provided by using a safeguarding device and discharging steam into the bubbling device. (It should be highlighted that operating experience has revealed that in an event of small leak in the SG, the RF does not need to be shut down at once);

— When LBC temperature is increased over a specified value, the rods of the additional emergency protection system, which are mounted in "dry" channels and are without drivers on the reactor lid, actuate passively by gravity due to fusible locks made of the alloy with a corresponding melting temperature and holding the rods in the upper position at normal temperature modes.

Moreover, in an event of postulated failure of all four channels of the PHRS, it is provided to flood the reactor vault by water from the tank mounted above and transfer heat via the monoblock vessel, air gap and safeguard casing to the water with further removal of generated steam into the atmosphere.

As preliminary computations have revealed, safety potential of RF SVBR-100 is characterized by the following features. No reactor runaway, explosion and fire occurs, even when there is superposition of

such postulated initial events as damage of the protective shell, damage of the reinforced concrete overlapping over the reactor, tightness failure in the primary circuit gas system with direct contact between a LBC surface in the reactor monoblock and atmospheric air, and total "blackout" of the NPP. Radioactivity exhaust into the environment does not reach values requiring population evacuation beyond the NPP fence.

The proposed reactor technology is based on forty-year experience of development and operation of LBC cooled RFs at NSs and ground facilities-prototypes. In the process of mastering this new technology a series of scientific and technical problems has been solved.

First, this is a problem of providing corrosion resistance of structure materials, control and maintenance of coolant quality (coolant technology) in the process of operating. The results of performed works have revealed that assurance of reliable RF operation requires measuring and maintenance of the certain parameter, namely, concentration of oxygen dissolved in LBC, within the specified interval, and this is possible to realize in an automatic mode [13].

The viable problem of providing radiation safety, which was caused by formation of polonium-210 in the process of irradiating bismuth with neutrons, was solved too. The personnel taking part in works were under the periodical medical observations. On the basis of the numerous radiometric investigations of biological samples of the personnel, it was fair determined that there were no events of incorporated polonium intake over the permissible limits. This fact validated a high efficiency of the used individual and collective protection measures, the right choice of the technology and the correct organization of repair and maintenance works [14].

It should be highlighted that because of the monoblock (integral) design of the primary circuit equipment and safeguard casing on the monoblock vessel of RF SVBR-100, coolant leaks have been virtually eliminated. A probability of releasing the radioactive gas has been also reduced much as argon pressure in the gas system approximately equals to the atmospheric one.

The paper published in the USA [15] summarizes the data of the retrospective analysis on mortality among the personnel (about 4500 men) who were dealt with works with Po-210 in 1944-1972 and whose internal intakes of Po-210 were examined. The authors made a conclusion that there was no connection between the doses of internal intake caused by ~1 Sv (100 rem) of incorporated polonium and the death-rate caused by cancer. For the examined personnel almost all trends, which characterized the death-rate caused by various cancer diseases were negative, i.e. the death-rate was even less than that for the control groups of people who were not dealt with polonium.

As operating experience has revealed, the amount of liquid radioactive waste is very low due to lack of the necessity to perform decontamination in the primary circuit.

A problem of multiple "freezing-unfreezing" of LBC while keeping operability of the RF equipment was solved too.

A conservative approach used to design the RF makes it possible to reduce considerably the technical and financial risks, lessen the number of possible errors and failures, which are typical while implementing the innovative nuclear technologies, and predetermines high potential for further improvements in the RF design.

5. CONCLUSION

1. The most expedient way to upgrade the NPP safety and at the same time improve the economic characteristics is use of RFs, in which the value of stored potential energy is the lowest and inherent self-protection and passive safety properties can be realized to the maximal extent.

2. Those RFs cannot amplify the external impacts, therefore, the scale of damages will be only determined by the external impact energy, the exhaust of radioactivity being localized.

3. The innovative nuclear power technology based on multi-purposed standardized modular fast reactors with chemically inert lead-bismuth coolant i.e. SVBR-100, which possess developed inherent self-protection and passive safety properties, will assure a high level of social acceptability for those reactors and widen the area of their application in the NP.

REFERENCES

[1] NUCLEONICS WEEK, Vol. 52, No. 19, May 12 (2011) 6-7.

[2] ORLOV, V.V., AVRORIN, E.N.,ADAMOV, E.O., et al., "Nontraditional Concepts of NPPs with Natural Safety", Atomnaya Energiya, Vol.72, Issue 4 (1992) 317-328.

[3] SPIEVAK, I., WEINBERG, A.M., "Inherently Safe Reactors", Annual Review of Energy, Vol. 10 (1985) 431-462.

[4] FORSBERG, C.W., WEINBERG, A.M., Annual Review of Energy, Vol. 15 (1990) 133-152.

[5] ZRODNIKOV, A.V., TOSHINSKY, G.I., STEPANOV, V.S., et al., "Lead-Bismuth Reactor Technology Conversion: from Nuclear Submarine Reactors to Power Reactors and Ways to Increase the Investment Attractiveness of Nuclear Power Based on Fast-Neutron Reactors", Proc. of IAEA International Conference "Fifty Years of Nuclear Power – the Next Fifty Years", Obninsk, Russia, 27 June-2 July, 2004, Report IAEA-CN-114-A3, (2004) (CD-ROM).

[6] GAT, U., "The Ultimate Safe (U.S.) Reactor", Proceedings of ICENES-4, Madrid, World Sci. Publ. Co. (1987) 584-595.

[7] NOVIKOV, V.M., SLESSAREV, I.S., ALEKSEYEV, P.N., et al., "Nuclear Reactors of Enhanced Safety. The Analysis of Conceptual Designs", Moscow, Energoatomizdat publishers (1993) 52.

[8] INTERNATIONAL ATOMIC ENERGY AGENCY, "Advanced Nuclear Plant Design Options to Cope with External Events", IAEA, February 2006, IAEA-TECDOC-1487, Vienna (2006), http://www-pub.iaea.org/MTCD/publications/PDF/te_1487_web.pdf.

[9] TOSHINSKY, G.I., KOMLEV, O.G., TORMYSHEV, I.V., et al., "Effect of Potential Energy Stored in Reactor Facility Coolant on NPP Safety and Economic Parameters", Proc. of International Congress on Advances in Nuclear Power Plants (ICAPP 2011), Paper 11465, Nice, France, May 2-5, (2011).

[10] NOVIKOVA, N.N., KOMLEV, O.G., TOSHINSKY, G.I., "Neutronic and Physical Characteristics of Reactor SVBR-75/100 with Different Types of Fuel", Proc. of International Congress on Advances in Nuclear Power Plants (ICAPP 2006), Reno, NV, USA, June 4-8, 2006, American Nuclear Society (2006) (CD-ROM), Paper № 6355.

[11] ZRODNIKOV, A.V., TOSHINSKY, G.I., STEPANOV, V.S., et al. "Innovative Nuclear Technology Based on Modular Multi-Purpose Lead-Bismuth Cooled Fast Reactors", Progress In Nuclear Energy, Vol. 50 (2008) 170-178.

[12] TOSHINSKY, G.I., KOMLEV, O.G., STEPANOV, V.S., et al., "Principles of Providing Inherent Self-Protection and Passive Safety Characteristics of the SVBR-75/100 Type Modular Reactor Installation for Nuclear Power Plants of Different Capacity and Purpose", Paper No. 175598, International Conference Advanced Nuclear Fuel Cycles and Systems (GLOBAL'07), September 9-13, 2007, Boise, Idaho, USA (2007).

[13] GROMOV, B.F., ORLOV, Yu.I., MARTYNOV, P.N., GULEVSKY, V.A., "The Problems of Technology of the Heavy Liquid Metal Coolants", Proceeding of the Conference "Heavy Liquid Metal Coolants in Nuclear Technology" (HLMC-98), Obninsk, Russia, Vol. 1 (1999) 87-100.

[14] PANKRATOV, D.V., YEFIMOV, Ye.I., TOSHINSKY, G.I., RYABAYA, L.D., "Analysis of Polonium Hazard in Nuclear Power Installations with Lead-Bismuth Coolant", Proc. of International Congress on Advances in Nuclear Power Plants (ICAPP 2005), CD-ROM, Paper № 5497, Seoul, Korea (2005).

[15] WIGGS, L., VORE, C., VOELZ, G., "Mortality among a Cohort of Workers Monitored for Po-210 Exposure: 1944-1972 y.y. Epidemiology Section Occupational Medicine Group", Los-Alamos National Laboratory, Health physics, Vol. 61, No 1 (1991).

Modelling Validation of Transients and Initial Phase of Accident Scenarios for Sodium Fast Reactors

S. Perez-Martin, W. Pfrang, W. Hering
Institute for Neutron Physics and Reactor Technology (INR)
Karlsruhe Institute of Technology (KIT)
Hermann-von-Helmholtz-Platz 1,
D-76344 Eggenstein-Leopoldshafen
Germany

Abstract. Physical phenomena are presented being of importance in case of transients and / or initial phases of severe accidents in Sodium-cooled Fast Reactors. The CABRI-programmes provided experimental data being characteristic for the physical phenomena and providing information to validate models and parameters used in theoretical simulations. Results of post irradiation examination (PIE), post test examination (PTE) and measurements performed during the experimental tests are presented for transient overpower (TOP), transient undercooling overpower (TUCOP), loss-of-flow tests (LOF) and slow power ramps.

1. Introduction

One important objective of nuclear plant designers is to increase the safety of a plant without forgetting economic feasibility aspects. One key point for achieving that purpose is a computational simulation tool that can predict fuel pin behaviour, thermodynamics, thermo-hydraulics, and the global core behaviour under any type of possible conditions. Code systems can be neither developed nor validated or improved without an adequate set of experimental data that covers the various interfering physical processes and phenomena at different scales.

Beyond normal operation conditions specialists have to understand and master the behaviour of fuel in transients and severe accident conditions and have to presume how the reactor would behave under off-normal situations. This holds especially in case of a loss of inlet coolant flow, a loss of heat sink or an insertion of reactivity. Slow power ramps (caused e.g. by unintended extraction of control rods) should be also considered as they have the potential to lead to an overall core melt accident.

In this work, we present characteristics of the CABRI tests and the transient response of different fuel pins, since a main objective of CABRI programmes was to identify the major physical phenomena, to validate computer codes and to provide guidelines for the development of new models. They were performed in a facility located in Cadarache research centre devoted to fast reactor safety studies. These programmes considered consequences of TOP, LOF, TUCOP transients and power ramp tests. This transient database with various fuel pin designs and pre-irradiation conditions provides relevant information for the understanding of failure mechanisms and subsequent consequences, as well as the failure threshold dependency on power and coolant conditions.

Innovative designs planned for future systems as axial heterogeneous fuel pin designs require experimental data (material properties, fuel pin thermal-mechanical behaviour, coolant natural circulation, etc.) which are presently not available. But to define such experiments adequately, firstly a reference design has to be specified.

2. Physical Phenomena Modelling

Physical phenomena involved in accidental events normally are the result of a complex superposition of individual elements and can hardly be observed separately. This is important when modelling the individual physical mechanisms. One can model separately different physical phenomena, but it will hardly be possible to validate such models in an isolated manner. The validation is global for the coupled models. For instance, fission gas release and fuel and clad geometry are measured in post irradiation examinations (PIE) but not the transient variation of the gap conductance, the fuel temperature, the porosity or crack volumes in the pellet during irradiation. Therefore the validation of models for determination of the gap conductance, fuel restructuring, crack volume, oxygen-to-metal ratio etc. can only be done through the global validation of fission gas release, fuel-clad gap width, clad deformation, etc.

In-pile test programs were designed to study coolant boiling, Pellet Cladding Mechanical Interactions (PCMI), clad melting, pre-failure in-pin fuel motion, fuel pin failure and failure propagation mechanisms, fuel-to-liquid coolant interaction, post-failure materials relocation by achieving specific fuel and cladding thermal conditions and thermal-hydraulic conditions. Such conditions define the fast, slow or structured over-power transients, LOF or LOF + TOP (TUCOP) transients.

This work is intended to focus on experimental evidences of physical phenomena being the only reliable source of information available for understanding and modelling fuel performance, taking into account uncertainties due to applied experimental measurement techniques. The task is to identify relevant parameters, quantify their influence and validate in a consistent manner the analytical models for pre-irradiation and transient.

The way these experimental results are applied to code validation depends on the structure of such codes. They used to be structured with the pin thermo-mechanics module, the coolant thermo-hydraulics and an interface between both. There are codes that only simulate the transient behaviour taking the pre-transient pin status from PIE information or from experimental correlations available to determine the boundary condition (such as the restructuring and gas release). In other codes macroscopic models are considered for both pre-transient and transient theoretical description. For these cases pre-irradiation results are the boundary conditions for the transient calculation, therefore a high accuracy is required for the pre-irradiation calculation. Other codes only study the transient up to pin failure. Every code developer has to decide which experimental data are suitable for validating his code. This phase of demonstration of successful implementation and improvements of physical models in any code systems is of high importance, since they should be able to accurately describe both individual and integral sample cases.

Benchmarks of different fuel pin behaviour codes are sometimes useful for checking models capabilities, but only in-pile experiments can be used as a reference for code qualifications. When using out of pile experiments as source data, it has to be checked carefully, whether the chosen experimental conditions can be quoted to be representative for reactor applications.

The CABRI test sections were well instrumented consisting of flowmeters, pressure transducers, thermocouples, void detectors, microphones, power detectors and the hodoscope to record relevant events during the experiments. Post-test examinations consisted of X-ray, gamma-scanning and neutron radiographs for non-destructive analysis and sublimation technique (for fission gas analysis), EPMA (Electron Probe Microanalysis for isotope repartitions) and metallographic analysis (macrographies and micrographies to see grains, fuel restructuring, molten fuel and cavity extension and un-molten or molten clad) on selected axial and radial cuts in the destructive examinations.

3. Power operation irradiation characterization (pre-transient state)

Characterizing the fuel pin state after steady-state power operation conditions includes fuel thermal condition (oxygen-to-metal ratio, porosity restructuration, grain size, radial and axial stresses, cracks, swelling, fission gas production and release, JOG formation), the gap (conductance, contact pressure, inventory, width), and the clad (swelling and plastic deformation profiles). The state of the fuel pin just before undergoing transient conditions, the so-called t_0-state, has to be known precisely in order to interpret the subsequence physical phenomena correctly. For modelling the transient, the same requirement is necessary for predicting correctly the behaviour during the transient, since the initial gap pressure, clad deformation and gas retention, among other parameters, will influence very much the response of the fuel pin under the transient.

Table 1. Characteristics of the set of pins used in CABRI experiments

	Rig 1/2/3	OPHELIE-6	SCARABIX	VIGGEN-4	QUASAR
Fissile pellet stack height (m)	0,75	0,75	0,75	0,85	0,84
Pellet diameter, inner/outer (mm)	0 / 6,4	2,0 / 7,3	2,0 / 7,1	0 / 5,4	1,7 / 5,4
Smear density (%)	87	83	81	88	80
As fabr. pellet porosity (%)	7.5/7.0	4,5	4	4,5	4,5
As fabr. O/M ratio	1,98	1,97	1,98	1,97	1,96
Peak burn-up (%)	1	4,8	6,4	11,8	12,1
Clad material	316 - CW	316 - CW	15–15 Ti	15–15 Ti	15–15 Ti

CABRI programmes have considered a variety of power operation histories and several fuel pin designs. Table 1 presents the characteristics of the different pins. The Rig 1/2/3 and VIGGEN-4 pins are made by solid pellets. OPHELIE-6, SCARABIX and QUASAR pins have hollow pellets. The smear density is then small (~82%) for annular pellets and larger for the solid ones (~87%). 316-CW cladding pins have burn-ups of ~1 to ~5 at.%. 15-15 Ti cladding pins have higher peak burn-ups, i.e. ~12 at. % for VIGGEN-4 and QUASAR pins, and ~6 at. % for SCARABIX pins. 15-15 Ti stabilized cladding was necessary to reach that high burn-up level without difficulties.

One key magnitude in the characterization of irradiated pins is the fission gas behaviour during power operation. Experimental results of fission gas release and retention are available for all sets of pins after power operation irradiation. The kinetics of fission gas release is a complex process that involves different scales and phenomena. Fuel restructuring due to the temperature gradient influences the grain growth (columnar and elongated grains), porosity migration, plutonium re-distribution, crack volumes, central hole, fuel swelling, etc. Figure 1 shows the phenomena occurring in the fuel pin (this figure was taken from Ref. 1).
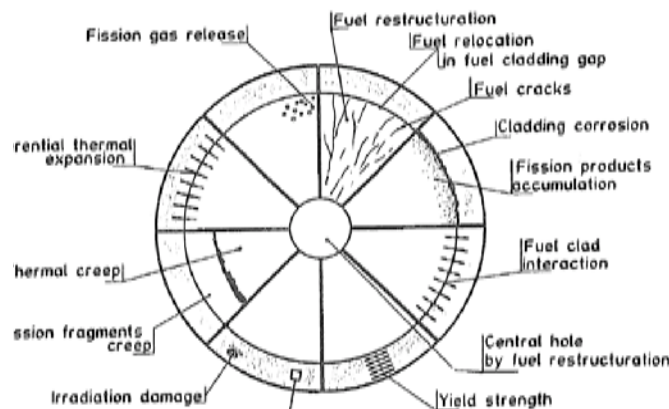

Figure 1. Phenomena affecting the in-pin fuel behaviour (taken from Ref. 1).

For small burn-ups the fission gas concentrations within the fuel is still low, but as soon as the burn-up increases the concentrations enlarge as well (see Figure 2). The fission gas production is proportional to the axial power profile. Though fuel temperatures are elevated around axial peak power position, promoting fission gas release, mostly the gas concentration is larger in the centre than in the edges. Rig 3 pins present an unusual profile of axial concentration. For 5 at. % peak burn-up, the core mid-plane gas concentration was very low compared to the bottom and top parts. Moreover, since the temperature is a bit larger in the top fissile part than in the bottom fissile zone, the gas concentration is coherently lower in the upper part. Most of the gas retained in Rig 3 pins is in the narrow outermost region (0.9-1.0 normalized radius) of the pellet. Rig 2 pins show a very high gas concentration, mostly within the grains due to the low power level during power operation. According to Figure 2 there is a significant difference in quantity and axial distribution of the retained gas for the different type of pins. This will affect their subsequent behaviour during transients.
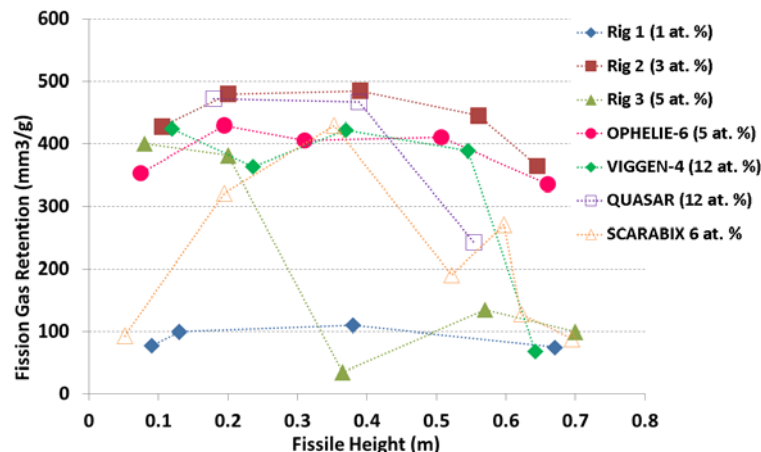

Figure 2. Axial Fission Gas retention profiles for Rig-1/2/3, Ophelie-6, Scarabix, Viggen-4 and Quasar

The global relation between fission gas release fraction and peak burn-up can be seen in Figure 3. For small and medium burn-ups (1-6 at. %) the ratio is approximately linear. However from medium and high ones (6-12 at. %) the relation slightly decreases, ~85% release for 6 at. % and ~70-80% for ~12 at. %. Fission gas retained and the available volumes within the fuel will have opposite contributions to the cavity formation during transient. Thus it is of high priority to model accurately the fission gas behaviour in the fuel as well as the porosity migration and crack volumes. The over-prediction of the amount of retained gas at certain fuel location would induce to over-predict the cavity pressure when the fuel starts to melt.
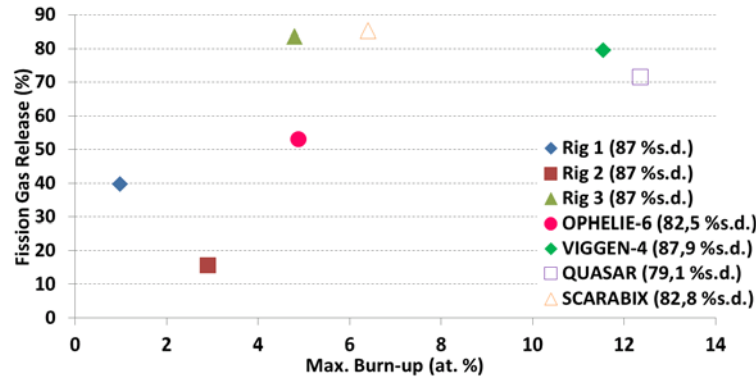

Figure 3. Comparison of FG release vs. burn-up (smear densities are indicated in the legends)

Fission gas induced fuel swelling is dependent on the stress field within the fuel. Therefore under a significant PCMI with fuel swelling, certain compressive stress will appear provided by mechanical constraint from cladding. Clad swelling is also an important feature which may lead to an open fuel-clad gap and then reduces even further the fuel smear density. It can lead to fuel overheating and enhanced gas release as observed in the Rig-3 power operation.

The accumulation of fission products including chemical compounds with U and Pu at the periphery of the fuel pellet (JOG, the French abbreviation for material between fuel and cladding) is a not well-known phenomenon. According to the radial cuts of VIGGEN-4 sibling pin, above the peak corrosion layer (~ 54 cm BFC[1]), fuel-to-clad gap was filled with JOG and fission gas retention at ~64 cm BFC was very low. The low gas retention at this axial level as well as the large columnar grains radius indicated that JOG reduces fuel to cladding gap conductance increasing the fuel temperature and in consequence also the fission gas release. Experimental evidence of JOG induced clad deformation and fission gas release is still scarce since JOG formation has been observed only for high burn-ups (> 10 at. %). Modelling JOG formation and redistribution validation is complex.

4. Transient characterization

CABRI tests serve for: 1) understanding the transient fuel behaviour and the post-failure phenomena occurring during power transients preceded or not by a loss of flow in all kinds of channel conditions at the fuel pin failure time, 2) reflecting all that physical information into analytical code implementation and 3) validating fuel pin thermo-mechanical modelling and the interface with coolant thermo-hydraulics (FCI, Fuel Coolant Interaction).

The CABRI test programmes included different series of test, such as TOP, LOF, TUCOP and slow power ramps. TOP means transient overpower, where power transient half-widths are between few tens to several hundred ms, initiated from typical reactor steady state conditions. LOF transients are tests with sodium flow rate reduction initiated from nominal steady state conditions to simulate reactor conditions during an unprotected pump coast-down. TUCOP transients are undercooling overpower tests where after LOF initiation the TOP can take place prior to sodium boiling or in two-phase coolant condition after cladding dry-out or melting. Transients in all kinds of coolant channel conditions are thus considered: in an unvoided channel (the so-called fully restrained condition), a partially voided channel (semi-restrained condition) and a fully voided channel with molten clad (non-restrained condition).

---

[1] Bottom of the Fissile Column

4

The CABRI tests had particular boundary conditions related to the CABRI driver core and the CABRI test section, e.g. the radial flux depression, the coolant channel width or the radial heat losses, which are different than the realistic reactor core conditions. Moreover, when extending from one-pin test description into a reactor core description, one should be very cautious about the limits of the in-pile tests. For describing a core transient, core scaled tests are needed for modelling a more realistic size and thermo-hydraulic conditions of pin-to-coolant channel interaction.

The CABRI in-pile test results cover a wide range of heating rates corresponding to transient time scales from few ms to few minutes. The transient energy deposition in the test fuel varied between 0.5 kJ/g (partial fuel melting without cladding failure), 1.0 kJ/g (extensive fuel melting leading to clad failure and release of molten fuel into the coolant) and 2.0 kJ/g (fuel vaporization). In Table 2 there is a classification of the pin tests according to the type of transient and the final state of the fuel pin. The colour of the text shows the burn-up (green for fresh and 1 at. %, blue for 3-7 at. %, and red for 11-12 at. %).

Table 2. Classification of CABRI experiments according to transient characteristics and final state of pins

	Slow ramp	Medium TOP	Energetic TOP	LOF + Medium TOP	LOF + Energetic TOP	LOF
No pin failure, partial fuel melting	**PF1 PFX**	**A1 A1R AI1 AGS0 AH1 E4 PF2**	**A5 LT2**			
No pin failure, fuel melting	**E9 E9BIS MF2**	**A2 E5**				
Mechanical Clad Rupture	**E12 BCF1**	**AI2**	**A3 A4 A4R AI3 AGS3 AH3 E7 E6**	**B2**	**B3 BI2 BI4 BI6 E8 E2 E3**	
Clad Melting Rupture				**B4 BGS0 BGS3 BGS4**	**B5 BI3 BI5 E13 E11 LT1 BH3 EFM1 LT4**	**B1 BI1 BG1 BH1**

The importance of time scale was brought to evidence by this experimental set of tests. Different fast, slow TOP's or power ramp transients achieve diverse pre-failure mechanisms and post failure sequences. Therefore not only the total energy injection is important but also the transient energy injection rate. Figure 4 shows the pin energy profile for several overpower experiments where structured and medium TOP's and slow power ramps can be distinguished.
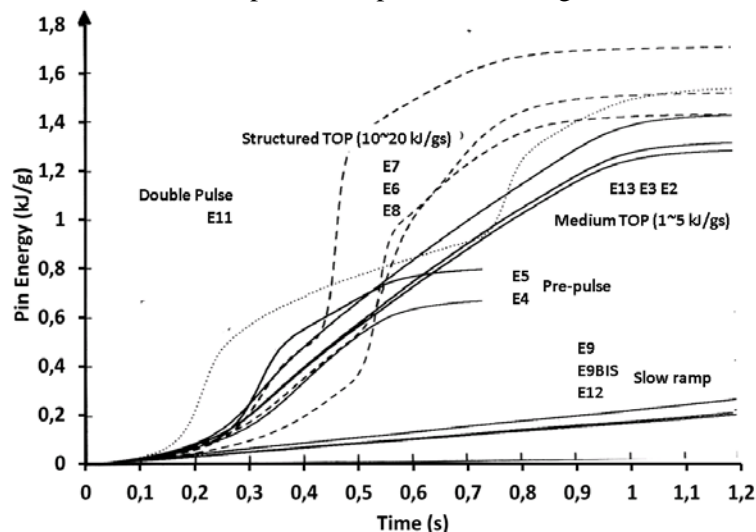

Figure 4. Energy injection of some CABRI-2 experiments (figure taken from Ref. 2).

Fuel elongation during transient

Transient fuel elongation could be measured in CABRI with the hodoscope. Even under the cladding constraint, fuel expansion of ~ 6 mm was observed in medium and fast TOP tests up to failure. In these tests, high fuel temperature was obtained in radially wide region and coherent fuel swelling and thermal expansion have enhanced potential for fuel elongation. During LOF up to coolant boiling, fuel and cladding elongation of ~3 mm was observed with VIGGEN-4 fuel, which is similar to Rig 1/2/3 test results.

Pre-failure, failure and post-failure phenomena

Degradation of cladding properties with increasing temperature dependent on strain rate (as ultimate tensile strength and uniform elongation) are important issues to determine fuel pin disruption during transients. Clad swelling behaviour under irradiation influences the fuel thermal state and has been a limiting factor of fuel performance for achieving high burn-up. PCMI is caused by the different expansion of cladding and solid fuel outer regions and can induce clad failure. This difference can be caused by thermal differential expansion, fuel relocation and cracking or transient fuel swelling. It mainly occurs during the initial phase of a TOP and diminishes when the fuel becomes plastic or melts. The risk for PCMI reduces with decreasing fuel smear density (effective fuel density inside the cladding tube including fuel porosity, gap and central hole volumes). Low and intermediate smear densities provide high failure threshold. In the OPHELIE-6 pins for instance, the already low smear density due to the hollow pellet design is reduced by large swelling of the SS 316 clad up to 5 at. % burn-up level. This mitigates the PCMI effect during power transients.

Table 3. Non-failure tests

Test	P_{max}/P_0	PPN[2] energy injection at scram (kJ/g)	Fuel Pin
A2	318	1.05	solid fresh 316 CW
A5	106	1.56	solid fresh 316 CW
E4	10	0.51	solid 12 at. % 15-15 Ti
E5	26	0.64	hollow 5 at. % 316 CW
PF2	7	0.91	hollow 12 at. % 15-15Ti
LT2	26	1.26	hollow 12 at. % 15-15Ti
E9	1.1 % P_n/s	ramp	hollow 5 at. % 316 CW
E9BIS	1.0 % P_n/s	ramp	hollow 5 at. % 316 CW
PF1	1.4 % P_n/s	ramp	hollow 6 at. % 15-15Ti
PFX	1.3 % P_n/s	ramp	hollow 6 at. % 15-15Ti
MF2	1.2 % P_n/s	ramp	hollow 6 at. % 15-15Ti

When the smear fuel density is high (solid pellets), fuel burn-up and pre-irradiation linear power rating play an important role in fuel swelling which contributes considerably to failure due to the PCMI loading of the clad. With high burn-up as in VIGGEN-4 pins, an important quantity of gases is retained in large bubbles at the grain boundary in the outer radial zone of the fuel pin. Under heat-up, swelling of these bubbles occurs with release to free volume leading to clad deformation if the clad is in constraint condition with residual strength. VIGGEN-4 pins, in spite of high burn-up level, showed a small cladding swelling (1%), which leads to a narrow fuel-clad gap. This small gap promotes PCMI during power transient, however clad mechanical tests from VIGGEN-4 pins showed that sufficient ductility still exits which balances the PCMI loading with regard to failure threshold.

Table 4. TOP tests

Test	P_{max}/P_0	PPN energy injection at failure (kJ/g)	Energy injection rate at failure (kJ/g·s)	Failure time (ms)	Failure location (cm BFC)	Fuel Pin
A3	624	1.04	68	58	48	solid fresh 316 CW
A4	756	1.09	107	56	49	solid fresh 316 CW
A4R	716	1.06	105	57	40	solid fresh 316 CW
AI2	108	0.88	0.9	230	46	solid 1 at. % 316 CW
AI3	250	0.86	36	82	45	solid 1 at. % 316 CW
AGS3	96	0.67	12	524	47	solid 3 at. %316 CW
AH3	398	0.93	47	78	54	solid 5 at. % 316 CW
E7	154	1.06	20	467	53	hollow 5 at. % 316 CW
E6	30	0.82	6	567	54	solid 12 at. % 15-15 Ti

During a TOP there are various mechanisms for cladding loading. Among these are thermal stresses, internal gas pressure, PCMI, molten fuel cavity pressure and axial strain. In irradiated CABRI tests the dominant mode of failure was pressurization of the molten fuel cavity by fission gas while the main contributor to clad deformation in non-failure tests was PCMI. Direct measurements of fuel pressure are not possible in CABRI tests, thus it was important to know clearly the amount of fuel melting and the availability of the fission gas to pressurize the molten fuel. In LOF+TOP tests fuel pressure was also responsible for failure of the weakened clad. The subsequent fuel break-up in both TOP and TUCOP tests was due to fission gas, or to the filling gas in fresh pins. In Table 4 TOP tests with

---

[2] Peak Power Node

mechanical clad failure are described. Time and location of clad failures can be used to validate cavity pressure driven models.

Pure LOF transients or combination of LOF+TOP transients give qualitative information about the single and two phase flow behaviour. Boiling onset, stabilization of bulk boiling, clad dry-out, or the two-phase flow front evolution provides data to validate coolant heat transfer correlations boiling models and FCI models. In Table 5 TUCOP's characteristics are presented.

Table 5. Characteristics of TUCOP tests up to failure

Test	P_{max}/P_0	PPN energy injection (kJ/g)	Boiling onset (s)	Failure time (ms after TOP)	Failure location (cm BFC)	Fuel Pin
B2	396	1.2	-	340	52	solid fresh 316 CW
B3	596	1.4	-	116	52	solid fresh 316 CW
B4	227	0.9	21	87	43-47	solid fresh 316 CW
B5	546	0.8	22	58	22-30;52-69	solid fresh 316 CW
BI2	256	0.8	No	79	52	solid 1 at. % 316 CW
BI3	162	0.5	22	83	36-55	solid 1 at. % 316 CW
BI4	156	0.6	22	88	52	solid 1 at. % 316 CW
BI5	670	0.3	21	60	38-58	solid 1 at. % 316 CW
BI6	578	0.6	24	63	42-56	solid 1 at. % 316 CW
BGS0	19	~0.6	22	500-600	32-60	solid 3 at. % 316 CW
BGS3	86	0.7	21	548	31-55	solid 3 at. % 316 CW
BGS4	74	0.6	22	555	28-64	solid 3 at. % 316 CW
BH3	282	~0.6	22	74	53	solid 5 at. % 316 CW
E8	93	0.5	21	527	56	hollow 5 at. % 316 CW
E2	9	0.7	No	567	50	solid 12 at. % 15-15 Ti
E3	9	0.3	21	370	38-59	solid 12 at. % 15-15 Ti
E13	12	0.2	21	320	38-59	solid 12 at. % 15-15 Ti
E11	36	0.3	21	~200	~ 45-55	solid 12 at. % 15-15 Ti
LT1	24	0.3	No	385	48	hollow 12 at. % 15-15 Ti
LT4	43	1.0	No	621	63	hollow 6 at. % 15-15Ti
EFM1	120	-	23	380-390	41-51	hollow 6 at. % 15-15Ti

Slow power ramps

The influence of the pellet design in the fuel pin behaviour under conditions of control rod withdrawal accident was performed with slow power ramps around 1 % P_0/s starting from nominal conditions. The power to melt resulting from fuel thermal evolution and related fission gases behaviour was studied to determine the risk of molten fuel ejection from an adventitious pin failure with molten volume fraction of 10 to 20 % and the potential for pin to pin propagation inside the subassembly.

In Table 6 the characteristics of the slow ramp tests are presented. Solid pellet at 12 at. % burn-up VIGGEN-4 was used in E12 and BCF1 tests. Annular pellets at 5 at. % burn-up OPHELIE-6 were used in E9 and E9BIS tests. And SCARABIX pins having hollow pellets with 6 at. % and 15-15Ti cladding were used in PF1, PFX and MF2 tests. The difference of fuel smear density in the different pins is important to understand the test results.

Table 6. Slow ramp test

	E9	E9BIS	PF1	PFX	MF2	E12	BCF1
Initial max. linear power P_0 (W/cm)	603	594	414	403	396	474	472
Power ramp (%P_0/s)	1.1	0.95	1.26	1.32	1.2	0.9	2.8
Final max. linear power (W/cm)	1347	1075	883	791	1247	810	840
Initial sodium heat-up (ºC)	180	180	174	176	175	216	219
Time of failure (s)	No failure	No failure	No failure	No failure	No failure	76	28
Location of failure (cm BFC)	-	-	-	-	-	62	~62

The absence of clad deformation and consequently of failure in both tests E9 and E9BIS is explained by the low smear density and the reduction of the cavity pressure due to in-pin fuel motion and gas escape from the molten fuel to plenum. With the solid pellet design of VIGGEN-4 pins and high burn-up level of 12 at. % the solid fuel swelling due to fission gas retained in the outer fuel zone with high grain fragmentation and the cavity pressurization upon fuel melting, resulted in clad deformation and in E12 and BCF1 into failure.

In-pin fuel motion

PTE revealed the occurrence of in-pin fuel motion in E9 and E9BIS (slow power ramp tests) where the central hole in the upper parts was filled with liquid fuel up to the top of the fissile column. In-pin molten fuel relocation along the central hole (fuel squirting) is potentially an important reactivity

feedback mechanism in whole core accident calculations. In Rig 1/2/3 test pins a narrow central hole was formed during the pre-test irradiation and fuel squirting was detected by PTE in some test. In-pin fuel relocation prior to failure was observed by the hodoscope in E5, E9, PF2, MF2, LT2 and E9BIS tests.

Pin failure in restrained conditions

The measured data relevant to the failure and post-failure events are: 1) failure location and time given by the hodoscope signals and acoustic measurements, 2) evolution of sodium temperatures and of sodium voiding obtained by thermocouples, flowmeters and void detectors, 3) in-pin and channel axial fuel motion obtained from the evolution of hodoscope signals, and 4) configuration and morphology of fuel/steel accumulations and final state of fuel pin derived from post-test hodoscope and various PTE examinations (gamma scans, neutrongraphs, radiographs, axial and radial cuts).

Fuel pin failure is accompanied by a significant fuel accumulation within a few ms over a length of some cm around the failure location. The fuel continues to accumulate over the first 10 ms after failure. It then spreads during 25 to 50 ms, faster upwards than downwards because of the difference in the lower an upper sodium inertial lengths and in the inlet and outlet pressures. At the same time voiding of the lower pin parts takes place mostly between 15 ms and 40 ms. The fuel mass increase around the failure location combined with a decrease in the lower part of the pin, shows that the fuel moves axially inside the pin and appears in the channel at the failure location. Voiding of the upper pin parts is less important, since failure location is in the upper part of the fuel melt cavity and for hodoscope detection in-pin motion is shadowed by the upward fuel motion within the coolant channel.

FCI and axial fuel motion in the channel

Pin failure is accompanied by the expulsion of liquid sodium out of the coolant channel in restrained conditions. The failure triggers a large sodium flow divergence which reaches its maximum value within 5 ms. In semi-restrained conditions (BI4, BI6, BH3 tests) the lower liquid sodium slug starts to move soon after failure, the upper slug with some delay.

After the peak flow divergence the sodium flow decreases gradually and the coolant pressure returns to low values of a few bars. This indicates that the fuel-to-sodium heat transfer decreases rapidly after 5 ms, most likely due to fuel fragment blanketing by fission gas and sodium vapour, or by a change of flow regime with decreasing fuel volume fraction.

From hodoscope observations the fuel motion can be separated in two phases: 1) during the first 30 ms, the fuel moves freely, following the liquid sodium interfaces. At 30 to 55 ms after failure a reduction of fuel appears at around the initial failure site. In semi-restrained conditions, the axial fuel motion takes place preferentially upwards into the two-phase sodium zone. 2) After about 50 ms, fuel motion is still noticeable but becomes slower and occurs mainly in the central part of fissile region. Up to around 250 ms, fuel accumulations are built-up; the voiding of sodium continues and drags some fuel with it. Between the two main fuel accumulations significant fuel redistribution occurs, but the leading edges of main fuel accumulations move further by almost 10 cm, often less, except in the experiments with an upward lifting of the upper pin stub.
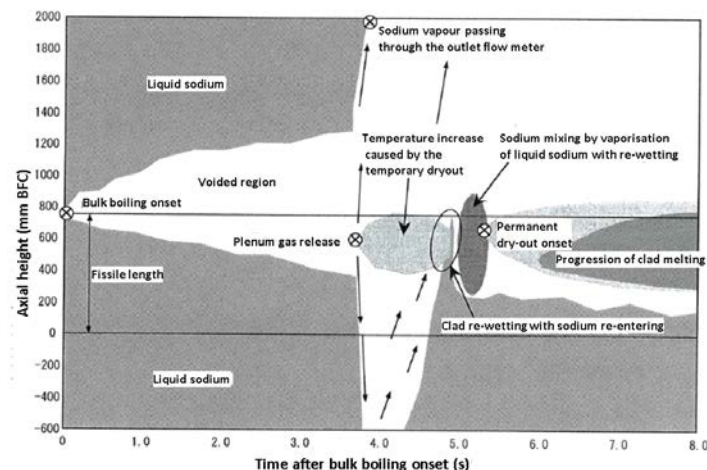

Figure 5. Event sequence during a LOF transient (taken from Ref. 2)

Coolant boiling

Besides in the pure LOF experiments (cf. Table 2) coolant boiling behaviour and clad dry-out was observed in EFM1, E8, BI3 and BGS0 tests. Different patterns of fuel dispersal can be observed in tests BI5, BI6, BGS0, BGS4, E11, EFM1, AI3, AGS3, E6, E7, BI2, LT1, BGS3 and E8. Figure 5 shows a typical sequence of events during a LOF transient.

The E8, E11 and E13 experiments provide sodium thermal-hydraulic results with pin failure occurred after the sodium boiling onset. These tests provide information on local boiling and local boiling duration, superheat, evolution of the boiling interfaces and inlet flow reversal. Figure 6 shows inlet and outlet flow rate of E8 test.
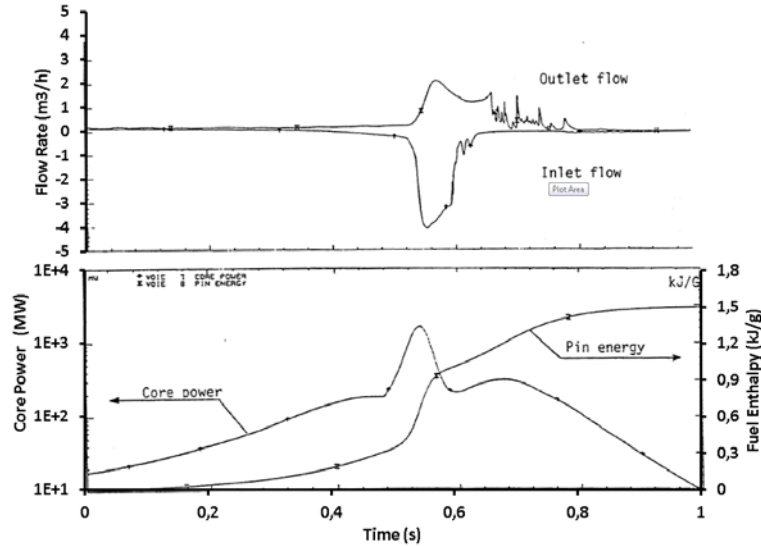
Figure 6. Inlet and outlet flow rate (upper part) and power (lower part) after TOP onset for E8 experiment

Clad melting

Clad melting without fuel melting was observed in B1 test (pure LOF). Clad and fuel melting was observed in BI1 (pure LOF), BG1 (fuel break-up) and BH1 (pure LOF). There are some experiments available where clear indications of molten clad material relocation prior to fuel pin break-up could be deduced from temperature sensors. Those are fresh fuel pin experiments B4 and B5. Clad dry-out was observed in EFM1, E8, BI3, E13 and E11 tests. The coolant flow reversal was a first indication of clad dry-out, resulting in higher clad temperatures. Figure 7 shows the coolant mass flow rate in B4 and B5 tests.
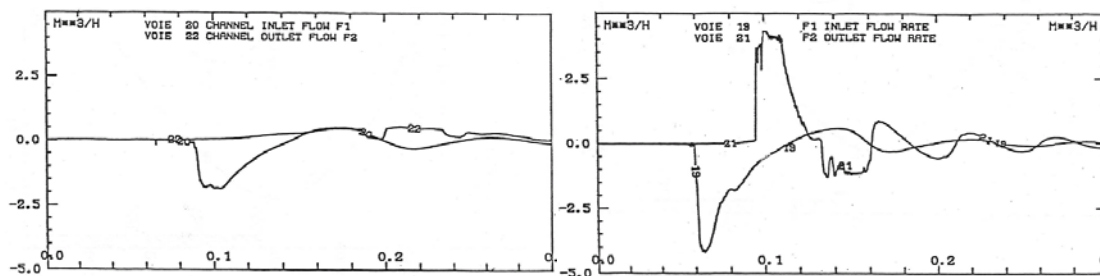

Figure 7. Coolant Mass Flow Rate in B4 test (left) and B5 test (right)

In E13 and E11 tests extended LOF was applied before TOP triggering. TOP was triggered 4.9 and 6.4 s after bulk boiling onset (BBO) respectively. Cladding rupture and plenum gas blowout took place in these tests 3-4 s after BBO when cladding temperature at fissile top increased rapidly with probable cladding dry-out. Fuel disintegration in E11 test took place just after the plenum gas blowout under very weak or molten cladding condition.

Pin lift phenomenon

The pin lift phenomenon occurs generally at most 10 ms after failure on pins with high fission gas retention (e.g. AH3, AGS3) or having reached hot clad conditions (e.g. BH3, BI6) at power pulse onset; it is very pronounced in some semi-restrained tests. This upward directed pin lifting, triggered

by a sufficient internal gas pressure, is enhanced in CABRI because of the lack of obstacles to prevent the pin stub lifting and because of the large channel cross section. However, this phenomenon is not representative of a reactor case.

5. Needs for future validation

In the past, blankets of depleted uranium were used as breeding targets. Nowadays breeder blankets are no longer considered. They are replaced by special layers that improve the void reactivity feedback. It becomes important to define the reactor structure and the pin design for manufacturing such pin designs, irradiating them in a fast spectrum and making afterwards the required experimental tests. This is the sequence used in the past. Currently there is no fast reactor in Europe any more (as Phenix was used in the past) for power operation irradiation of test pins leading to high burn-up and high clad dose. Moreover CABRI test reactor is no longer in operation for fast reactor fuel studies. Thus the second and third phases of the experimental procedure have become critical and a considerable investment should be done to develop in-pile test capability with the same degree of confidence as in the CABRI programmes.

6. Conclusions

An overview of the tests performed in the CABRI programmes has been presented. They cover different fuel pin designs, different irradiation histories and different types of transients. This database can be used for a detailed validation of computer codes.

However, one should have in mind the limits of the non-full validated models. Computational codes are simplified representations of complex real phenomena, and therefore theoretical predictions should be only considered in the framework of validated conditions. When new conditions outside the qualified ones are studied, results are no longer reliable, may become even unphysical responses and have to be checked critically.

REFERENCES

[1]   Fast breeder reactor fuel performances. R. Lallement Phil. Trans. R. Soc. Lond. A 331, 343-354 1990.

[2]   CABRI-2 Project 1986-1994 Results and Achievements. IPSN, KFK, PNC. December 1994

[3]   The CABRI-2 Programme-Overview On Results M. Haessler, D. Struwe et al Proc. Int. Fast Reactor Safety Mtg., Vol. 2. P. 209-221. Snowbird, USA, 1990, American Nuclear Society

[4]   Interpretation of Post Failure Phenomena Observed During CABRI-Top Experiments. J.C. Barescut et al Proc. Int. Conf. Science and Technology of Fast Reactor Safety, St. Peter Port, Guernsey 1986

[5]   Fuel Pin Behaviour Under Conditions Of Control Rod Withdrawal Accident In CABRI-2 Experiments J. Papin et al Proc. Int. Top. Mtg. Sodium Cooled Fast Reactor Safety, Vol. 2, p. 122-133. Obninsk 1994

[6]   The CABRI Project - Overall Status and Achievements. G. Kussmaul et al Pro. Int. Conf. Science and Technology of Fast Reactor Safety, St. Peter Port, Guernsey 1986 Vol. 1 p.103

[7]   Transient Fuel Pin Behaviour And Failure Condition In CABRI-2 In Pile Tests I. Sato et al Proc. Int. Top. Mtg. Sodium Cooled Fast Reactor Safety, Vol. 2, p. 134-145. Obninsk 1994

[8]   Fuel pin behavior under slow-ramp-type transient-overpower conditions in the CABRI-FAST experiments. Y. Fukano et al Journal of Nuclear Science and Technology.Vol 46, Issue 11, 2009, p 1049-1058

Preliminary Safety Analysis of China Lead Alloy Cooled Research Reactor CLEAR-I

Ming Jin, Gang Wang, Yazhou Li, Hao Gong, Pengcheng Long, Liqin Hu, FDS Team

Institute of Nuclear Energy Safety Technology, Chinese Academy of Sciences

Presented by M. JIN

Abstract. CLEAR-I is a pool type reactor cooled by liquid lead bismuth eutectic (LBE). The flow through the primary loop is driven by natural circulation. In this paper, a three dimensional model of the CLEAR-I reactor pool was built. The simulations of several transient-states such as protected loss of heat sink (PLOHS) accident, unprotected loss of heat sink (ULOHS) accident, protected transient overpower (PTOP) accident and unprotected transient overpower (UTOP) accident were carried out by commercial CFD code to investigate the reactor natural circulation capacity and characteristics, and the simulation results of the four transients were analyzed. The analysis results showed that the natural circulation could be achieved, and passive decay heat removal system could cool the reactor effectively. The calculation parameters are under limits and the reactor is safe for all of the four transients.

1. INTRODUCTION

The accelerator driven subcritical system (ADS) is a potential option of a spent fuel transmutation system which is of inherent safety and was credited to Carlo Rubbia [1][2][3]. Since 2011, Chinese Academy of Sciences (CAS) had launched the Strategic Priority Research Program of "the Future Advanced Nuclear Fission Energy-ADS transmutation system" to build ADS system. In the first phase, the ADS research facility consists of a 10MWth lead-bismuth cooled fast reactor (CLEAR-I) will be build. It is developed by FDS Team which has designed a series of lead-alloy cooled sub-critical reactor systems [4][5][6][7][8][9][10][11][12]. The research object of CLEAR-IA is to validate the neutronics, thermal-hydraulics and safety characteristics of lead-bismuth cooled reactor, test the fuel, material technologies and to test the integration technology of ADS system [4].

CLEAR is a pool type reactor in which liquid LBE is used as the primary coolant in natural circulation. As the liquid LBE is driven by the density difference between the hot and cold pools, there are some new characteristics compared to those of pump-driven reactor for transient states. In this contribution, a commercial code FLUENT was employed to investigate the transients of CLEAR-I under typical accident conditions.

2. CLEAR-I REACTOR DESIGN

The preliminary neutronics and thermal-hydraulics design of CLEAR-I has been proposed [4][5][12], and the main parameters of CLEAR-I are presented in Table 1 [4][5][6].The core thermal power is removed by 700 tons of LBE of which the working temperature is between 260℃ and 390℃. The schematic diagram of the CLEAR-I reactor layout is presented in Figure 1. And a Reactor Vessel Air Cooling System (RVACS) [13] is incorporated in CLEAR-I to remove the decay heat in cases that the normal heat removal path involving 4 primary heat exchangers is unavailable. The RVACS is designed to be consisted of 40 U-tubes installed outside the reactor guard vessel to cool the reactor by thermal radiation. The heat removal by the RVACS is continued by means of natural circulation of air. The schematic diagram of the RVACS is presented in Figure 2.

The reasons why the driven force of coolant has been designated to be natural circulation instead of a pump are as follows: (1) As the total thermal power of CLEAR-I is much smaller than most of other ADS designs [14][15][16], the reactor core cooling requirement is very low, which leads to a low

coolant driven force need. (2) The liquid LBE has very good natural circulation characteristics such as a large expansion coefficient and a low kinetic viscosity [17]. (3) As LBE has a strong erosion-corrosion effect on materials, the safety grade LBE mechanical pump is still difficult to be used in CLEAR-I. (4) Besides, a natural circulation ADS design brings several extra benefits, for instance, elimination of loss of flow accident, reducing engineering difficulty, reducing costs of the reactor, etc.

Table 1. Main parameters of CLEAR-I

Parameter		Values
Core	Thermal power (MW)	10
	Activity height (m)	0.8
	Activity diameter (m)	1.05
	Fuel (^{235}U enrichment)	UO$_2$ (19.75%)
Cooling system	Primary coolant	LBE
	Total LBE mass (t)	~530
	Inlet/Outlet temperature（℃）	260/390
	Coolant drive type	Natural circulation
	Second coolant	Water
	Heat sink	Air cooler
Material	Cladding	316 Ti
	Structure	316L

It is assumed that the heat extracted from the vertical surface of reactor vessel only, besides, heat conductivity and heat convection of the gas among main vessel, guard vessel and tube are negligible. Thus, only radiation is considered when the heat transfer between two walls in RVACS is calculated. The relationship between main vessel temperature and wall heat flux density can be obtained by solving the equations of the thermal radiation between walls, thermal conductivity in walls and thermal convection in the air tubes:

$$q''=-2075.8+11.8516T-0.027683T^2+0.000029079T^3 \tag{1}$$

where, q'' is the heat flux density through reactor main vessel (W/m2) and T is temperature of main vessel outer surface (K).
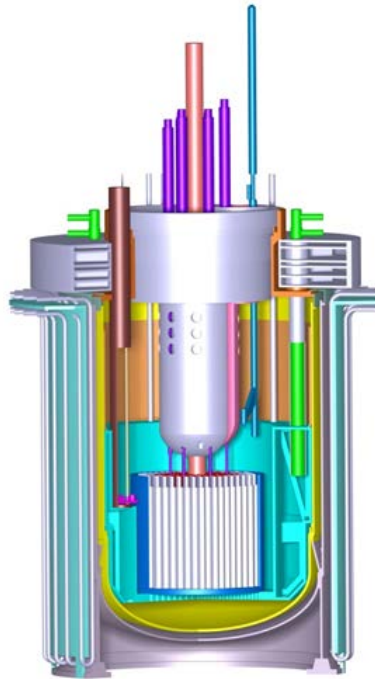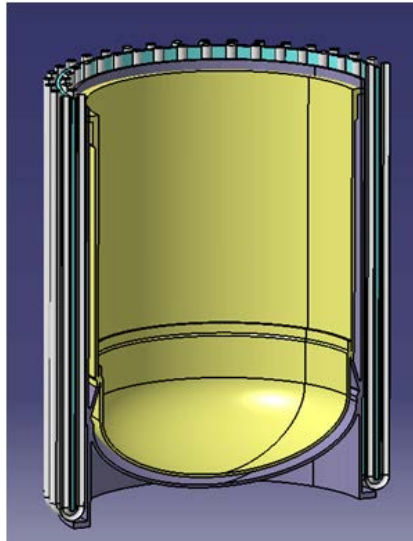

Fig. 1 CLEAR-I reactor layout

Fig. 2 Schematic diagram of RAVCS

3. Calculation Model

A three-dimensional calculation model of CLEAR-I reactor was built to be used for transient simulation, which is presented in Figure 3. The calculation model has been simplified as it's impractical to model the entire geometry in reactor vessel in detail. The model was a quarter of the whole reactor pool and the three-dimensional model of the CLEAR-I reactor includes reactor core, core reflector, hot and cold LBE pools, heat exchanger and heat barrier.

Only one heat exchanger was contained in the calculation model and the two vertical cross sections were treated as symmetry boundary. The reactor core, reflector and heat exchanger were reduced to be a porous medium approximation. The radial power density of the reactor core is not as detailed as the actual conditions, but the uniform heat source was adopted in the vertical direction of the reactor core. The core power and loss heat of heat exchanger for different transient accidents are described by User Defined Function (UDF). The heat loss in each cell was set as proportional to the temperature difference of local temperature and secondary coolant mean temperature.
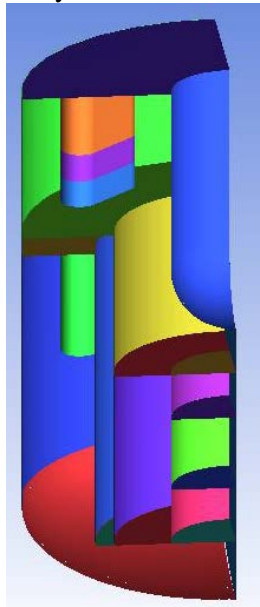

*Fig. 3 Calculation model of CLEAR-I reactor*

## 4. Transient-states simulation

Four transient accidents are considered in this paper, which are protected loss of heat sink (PLOHS) accident, unprotected loss of heat sink (ULOHS) accident, protected transient overpower (PTOP) accident and unprotected transient overpower (UTOP) accident. The protected condition is that some given conditions will initiate the shutdown protecting system, and the unprotected condition is that the shutdown protecting system will never work during the whole transient accident.

4.1. PLOHS

A protected loss of heat sink (PLOHS) scenario has been simulated in order to evaluate the capability of the DHR system for decay heat removal in transient conditions. The initiating event was the total loss of feed water of secondary loops. Reactor scram which was supposed to be leaded by a signal of the protection system was assumed with 10 seconds delay after the water supply flux decreased or the primary heat exchanger ruptured. A conservative assumption that the heat exchangers loss cooling capability completely simultaneously with the accident happens was adopted. Figure 4 presents the simulation results of PLOHS accident.

After LOHS, LBE flow rate decreases rapidly from 520 kg/s to about 60 kg/s in about 160 s. It's caused by the hot LBE flowing into heat exchanger which diminishes the density difference between rise and fall channel and reduces the natural circulation driven force. After 3000 s, the mass flow rate keeps around 56 kg/s. Because of the high thermal conductivity of coolant, the temperature difference between coolant and cladding is less than 10 K under decay heat. Thus, the cladding temperature is under limit after LOHS. For the large thermal inertia of CLEAR-I reactor, the LBE hot pool temperature and hot section of reactor vessel temperature increase very limit before reactor scram and decrease after then, but the cold pool and cold vessel has a large and continuous temperature increase in 5500 s. The core outlet temperature decreased rapidly after 10 s at what time the shutdown signal arrived.
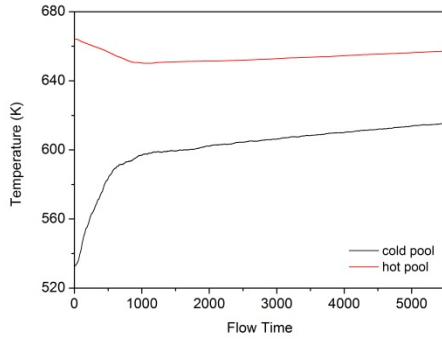

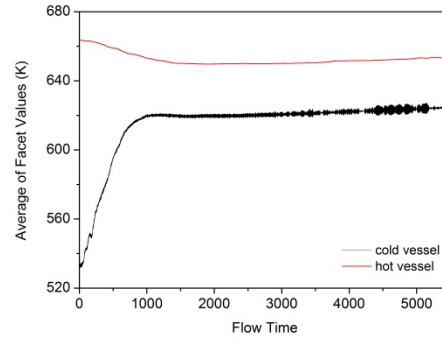(a) (b)

(c) (d)
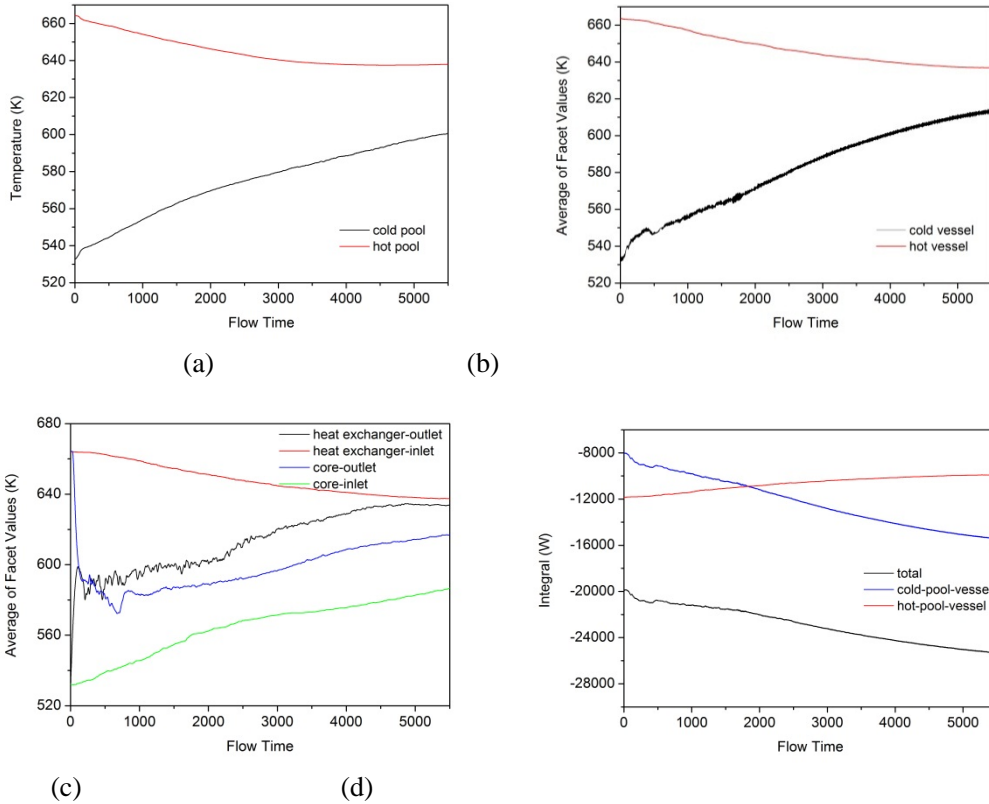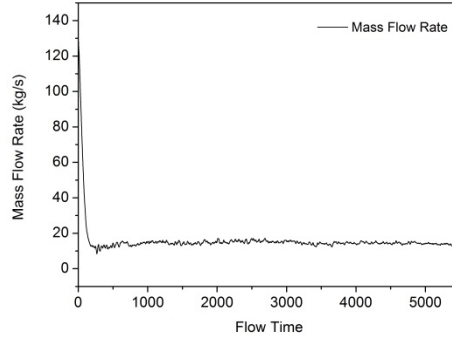
(e)

Fig. 4 Simulation results of PLOHS

(a)Cold pool and hot pool temperatures; (b)Cold vessel and hot vessel temperatures;(c)Core inlet/outlet and heat exchanger inlet/outlet temperatures; (d)Heat loss; (e)Mass flow rate
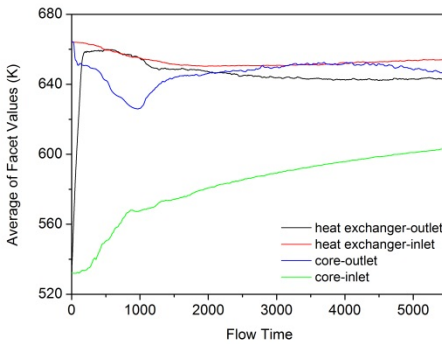
4.2. ULOHS

The unprotected loss of heat sink (ULOHS) accident was also simulated. All the initial conditions of ULOHS accident are the same to those of PLOHS accident. The difference is that neither the water supply flux decrease nor the primary gas pipe rupture can trigger the shutdown protecting system. The simulation results are presented in Figure 5.
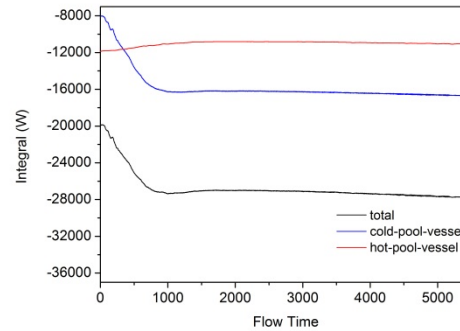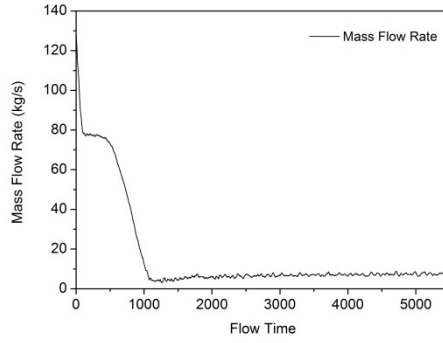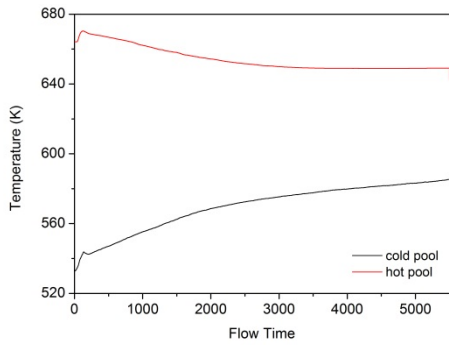

(a)

(b)

(c)

(d)

(e)

Fig. 5 Simulation results of ULOHS

(a)Cold pool and hot pool temperatures; (b)Cold vessel and hot vessel temperatures; (c) Core inlet/outlet and heat exchanger inlet/outlet temperatures; (d)Heat loss; (e)Mass flow rate

We can see from Figure 5 that mass flow rate decreased from 520 kg/s to 80 kg/s at 940s. And after about 20 minute, the mass flow rate turned stable and kept around 16 kg/s. The heat exchanger outlet temperatures both increased first and then decreased. The core outlet temperature decreased after about 30 s, but the decrease rate is not so big as the one of PLHOS. The core outlet temperature touched the bottom at the time of 970 s and the temperature decrease was about 40 K. All the calculation parameter results were under limits.
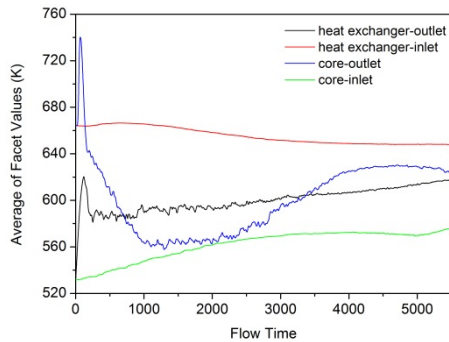
4.3. PTOP

The protected transient overpower (PTOP) accident is assumed that at the initial time, a control rod was out of control and drawn out of the core. The speed of reactivity insertion was 9.33 pcm/s and the total reactivity insertion caused by the runway control rod was 139.95 pcm in 15 s.
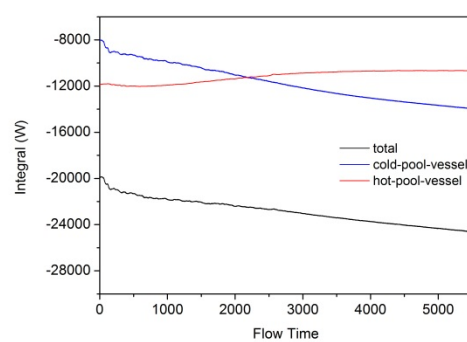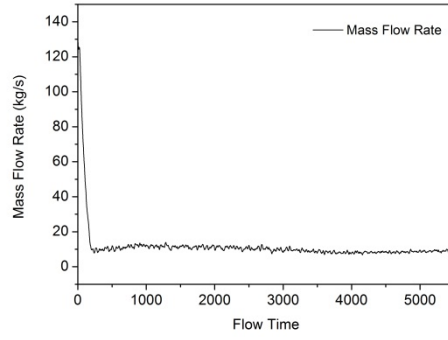

(a)
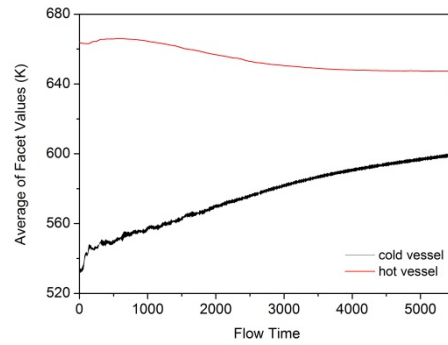
(b)

(c)

(d)

(e)

Fig. 6 Simulation results of PTOP

(a)Cold pool and hot pool temperatures; (b) Cold vessel and hot vessel temperatures; (c) Core inlet/outlet and heat exchanger inlet/outlet temperatures; (d)Heat loss; (e) Mass flow rate

As the rod was drawn and the positive reactivity was inserted, the core power would rise remarkablely Because of the increase of the core power, the core temperature also increased. And as the core temperature increased, a negative reactivity would be inserted and then the core power would decrease. The three parameters influenced each other and when the core outlet temperature was higher than 683 K, the shutdown protecting system worked and the reactor core scrammed. The results are presented in Figure 6.

It can be seen from Fig. 6 that the mass flow rate went down from the start time, after about 2100 s, it became stable and kept about 40 kg/s. The peak of core outlet temperature was about 740 K at the time of 68 s, which was smaller than the clad limited temperature. Both the hot pool and hot vessel had very small temperature increases, but the temperature increases of the cold pool and cold vessel were both large. The temperature difference between coolant and cladding was also less than 10 K.

4.4. UTOP

The unprotected transient overpower (UTOP) accident has the same initial transient conditions as PTOP accident except that the core outlet temperature signal will never trigger the shutdown protecting system. The total positive reactivity insertion caused by the runway control rod was also 139.95 pcm.

The simulation results of UTOP accident are presented in Figure 7. The variation of the mass flow rate in UTOP accident was very small in the first 1000 s. At the time of 1000 s, the mass flow rate was about 436 kg/s. And after 2700 s, the mass flow rate became stable and kept about 460 kg/s. The core outlet temperature increased sharply after the beginning of UTOP. The peak core outlet temperature was about 774K at the time of 291 s. And then the core outlet temperature decreased slowly and became stable after 3000 s. The temperature difference between coolant and cladding is still very small. According to the calculation results, the clad and fuel would not melt and the reactor was safe.

(a)

(b)

(c)

(d)

(e)
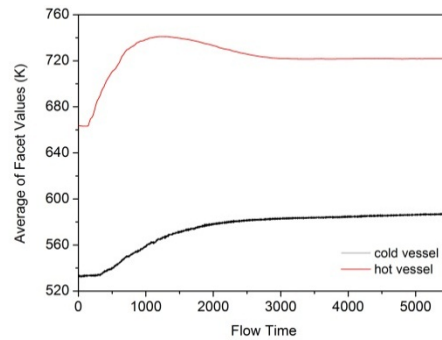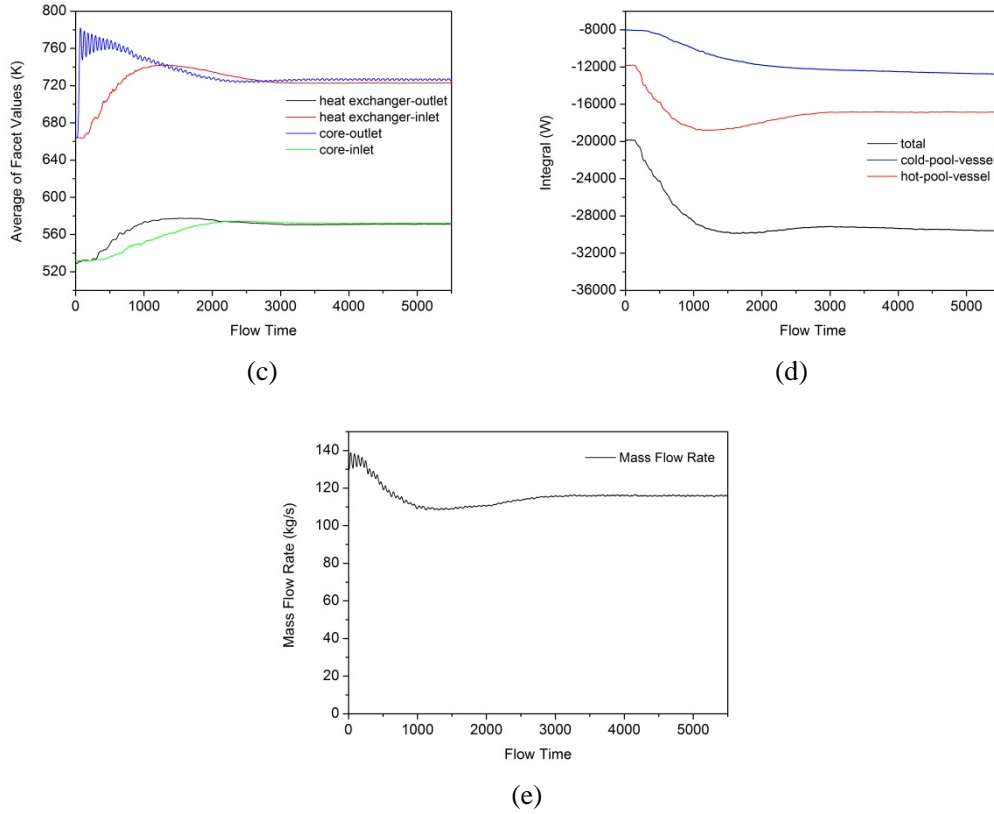
Fig. 7 Simulation results of UTOP

(a)Cold pool and hot pool temperatures; (b) Cold vessel and hot vessel temperatures; (c) Core inlet/outlet and heat exchanger inlet/outlet temperatures; (d)Heat loss; (e) Mass flow rate
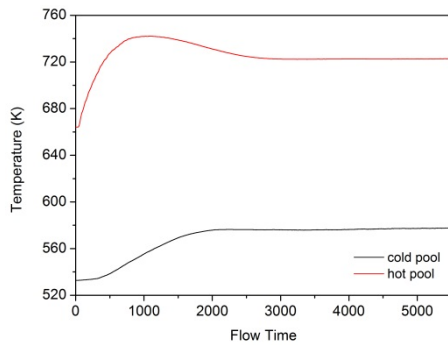
5. Conclusion

Four typical transient accidents of CLEAR-I were simulated and analyzed by FLUENT. The simulation results showed that for all the investigated transient accidents, the key temperatures in the reactor are under limits, the core clad and fuel will not melt. For PLOHS and ULOHS accidents, the core outlet temperatures will decrease rapidly with very small temperature increases and for PTOP and UTOP accidents, core outlet temperatures increases are bigger corresponding to those of PLOHS and ULOHS. The further researches on CLEAR-I primary coolant natural circulation and RVACS are needed and a more detailed CLEAR-I reactor model will be built to meet them.

REFERENCES

[1] A Roadmap for Developing Accelerator Transmutation Accelerator Transmutation of Waste (ATW) Technology, A Report to Congress [R]. USA. October 1999

[2] IAEA-TECDOC--985: Accelerator driven systems: Energy generation and transmutation of nuclear waste. Status report [R]. November 1997.

[3] Won S. Park, et.al. HYPER (Hybrid Power Extraction Reactor): A system for clean nuclear energy [J]. Nuclear Engineering and Design 199 (2000) 155–165

[4] Won S. Park, et.al. HYPER (Hybrid Power Extraction Reactor): A system for clean nuclear energy [J]. Nuclear Engineering and Design 199 (2000) 155–165

[5] Y. BAI et al., "Conceptual Design of Lead-Bismuth Cooled Accelerator Driven Subcritical Reactor (LEBCAR)," presented at the 15th International Conference on Emerging Nuclear Energy Systems (ICENES-15), May 15-19, 2011, San Francisco, USA.

[6] Weihua Wang, et al., "Structure Design and Analysis of Accelerator Driven Subcritical Reactor for China Nuclear Waste Transmutation", presented at the 15th International Conference on Emerging Nuclear Energy Systems (ICENES-15), May 15-19, 2011, San Francisco, USA.

[7] Conceptual Design Activities of FDS Series Fusion Power Plants in China. Y. Wu, FDS Team. Fusion Engineering and Design[J], 2006, 81(23-24): 2713-2718.

[8] Y. Wu, the FDS Team. Design Status and Development Strategy of China Liquid Lithium-Lead Blankets and Related Material Technology. Journal of Nuclear Materials[J], 2007, 367-370, Part B-2: 1410-1415.

[9] Y. Wu, S. Zheng, X. Zhu, et al., Conceptual Design of the Fusion-driven Subcritical System FDS-I. Fusion Engineering and Design[J], 2006, 81, PartB: 1305-1311.

[10] WU Yi-can. A Fusion Neutron Source Driven Sub-critical Nuclear Energy System : A Way for Early Application of Fusion Technology. Plasma Science and Technology, 2001, 3 (6): 1085-1092.

[11] Y. Wu, the FDS Team. Design Status and Development Strategy of China Liquid Lithium-Lead Blankets and Related Material Technology. Journal of Nuclear Materials, 2007, 367-370, Part B-2: 1410-1415.

[12] H. Chen, et al., Preliminary Thermal-hydraulic Design and Analysis of China Lead Alloy Cooled Research Reactor (CLEAR-I), NUTHOS-9, 2012, Taiwan

[13] M. Jin, et al. Natural Circulation Characteristics of China Lead Alloy Cooled Research Reactor CLEAR-I, 2012, Taiwan

[14] Hamid AIT ABDERRAHIM, et al. MYRRHA: A European Experimental ADS for R&D Applications Status at Mid-2005 and Prospective towards Implementation [J]. Journal of NUCLEAR SCIENCE and TECHNOLOGY. Vol. 44, No. 3, p. 491–498 (2007)

[15] Barbensi Andrea, et al., "EFIT: THE EUROPEAN FACILITY FOR INDUSTRIAL TRANSMUTATION OF MINOR ACTINIDES",.

[16] L Cinotti, G Gherardi, "The Pb–Bi cooled XADS status of development", Journal of Nuclear Materials[J].

[17] P. E. MacDonald et al., Design of an Actinide Burning, Lead or Lead-Bismuth Cooled Reactor that Produces Low Cost Electricity Annual Project Status Report, INEEL/EXT-2000-00994

Safety Aspects of Thorium Fuel in Sodium-Cooled Fast Reactors

Carlo Fiorina[a], Fausto Franceschini[b], Matt Memmott[b]

[a] Politecnico di Milano, Milan, Italy

[b] Westinghouse Electric Company, Pittsburgh, United States

Presented by Fausto Franceschini

Abstract. While detrimental to the breeding performance, use of thorium (Th) in Fast Reactors (FRs) has certain positive aspects: in principle, it has better thermal properties and irradiation performance than uranium (U)-based fuels, and it increases the potential burning rate of legacy transuranic waste for a burner design. The impact of thorium on the top-level operational and safety characteristics of a sodium-cooled transuranic-burner FR design is the focus of this paper. Different fuel cycle burning schemes are considered, including the development of a breakeven design to cover the long-term transition to a self-sufficient cycle. For completeness, a comparison with the counterpart U-based cores is also given. Reactivity feedback coefficients and other parameters are employed to predict the impact on the reactor passive-safety features of the various fuel cycle options. Reactivity decomposition techniques are employed to show the key contributors to the reactivity effects of the different fuels. The results show significant safety improvements fostered by implementing thorium fuel, with notable reductions in the reactivity insertion in case of core voiding, ~2$ for the burner designs and ~6$ for the breakeven design (which shows overall negative voids), while preserving a relatively simple core configuration.

1. Introduction

Use of a Th-based fuel in a FR transuranic-(TRU) burning scheme has attractive features. As a result of the more stable fuel matrix, higher thermal conductivity, and higher melting point, use of Th-based fuels is expected to increase irradiation performance and safety margins [1-4]. The inferior breeding performance of Th relative to U in the fast spectrum is advantageous when the main objective is burning surplus Pu or TRU, such as the quantity recovered via the reprocessing of LWR discharged fuel. Under the assumption of full actinide recycle, the ensuing relatively high content of Am and Cm imposes a remote fuel manufacturing requirement regardless of the content of U-232 and the associated gamma-field, thereby making the choice of Th equally penalizing from the standpoint of fuel handling relative to a counterpart U-based burning scheme. Use of Th is also known to foster improved safety, especially with regards to void reactivity insertion [5].

The focus of the present paper is to investigate the impact of Th on the inherent safety features of a sodium-cooled FR, specifically the Toshiba-Westinghouse Advanced Recycling Reactor (ARR) [6]. The safety features are assessed using reactivity feedback coefficients, effective delayed neutron yield (β_{eff}), and burn-up reactivity swing. In addition, a preliminary analysis of the reactor passive safety during main accidental transients is carried out by employing a quasi-static approach. Reactivity decomposition techniques are also applied to identify the isotopes and cross-sections which are responsible for the different responses characterizing the U- and Th-based fuel options.

Section 2 describes the methodology adopted in the paper, focusing on the reactivity decomposition technique adopted. Section 3 presents the core designs and fuel options selected for the analysis. Results are presented in Section 4 while the main conclusions of the work are drawn in Section 5.

2. Methodology

The present paper analyzes the safety parameters characterizing U vs. Th-based TRU burning schemes in the ARR, including the transition to a breakeven core. The differences in the safety parameters are ascribed to the different isotopic compositions characterizing the two schemes and associated nuclear properties using reactivity decomposition techniques. Reactivity decomposition techniques have been developed based on perturbation theory or neutron balances. The latter technique has been adopted in the present paper, based on Ref [7] and the latest formulation from Ref. [8].

Full core flux and burn-up calculations have been performed with ERANOS in the 33 energy-group structure optimized for FR calculation [9]. The multigroup nodal transport theory code VARIANT has been used for flux calculations, employing a P3 approximation with simplified spherical harmonics [10]. The 33-group cross-sections have been obtained from assembly-wise calculations using the collision-probability code ECCO in 1968 energy groups based on the JEFF3.1 library available in ERANOS [11-12].

3. Core designs and fuel inventory

3.1. Core designs

The core designs employed are based on the sodium-cooled Toshiba-Westinghouse ARR [6] and are summarized in Table 1 for the various options. The base core design features a total of 324 driver assemblies split in two regions of respectively 132 (outer core) and 192 (inner core) fuel assemblies. Each hexagonal assembly consists of 271 pins arranged in a triangular array with a 0.65cm outer diameter HT-9 cladding. The axial length of the driver fuel is 60cm. The fuel management consists of 3-batch reloads with annual refuelling intervals.
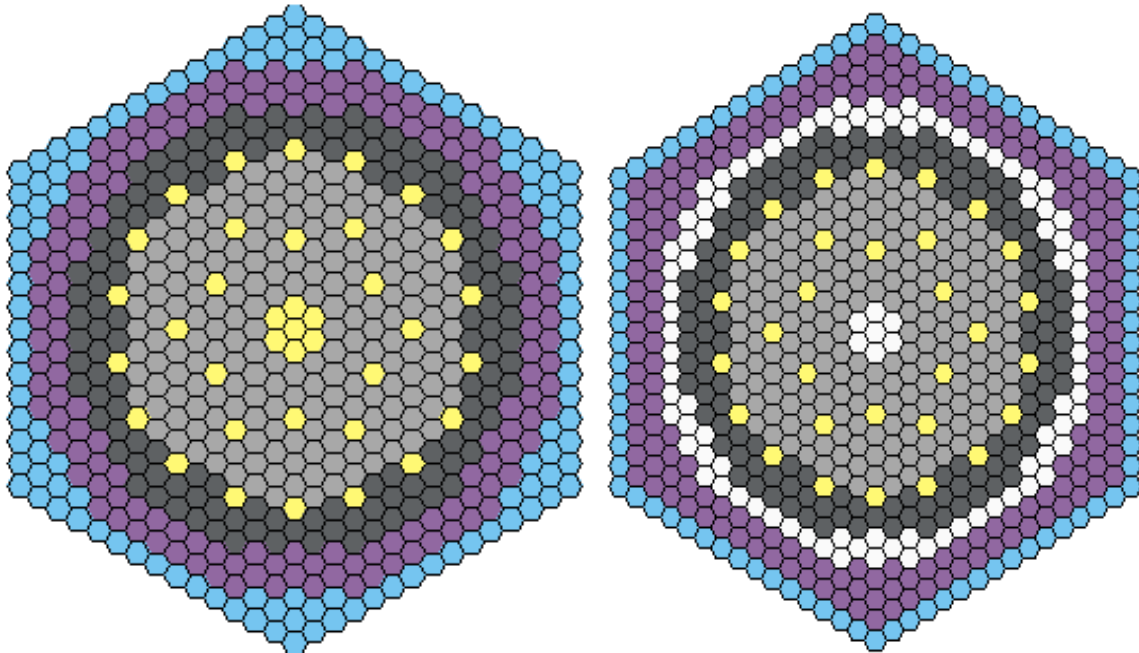

FIG. 1. ARR core layouts for burner (left) and breakeven (right) design. Light grey=inner core; dark grey=outer core; yellow=control rods; violet=steel shield; blue=B$_4$C shield; white=blanket

The main differences between burner and breakeven designs are the presence of radial and axial blankets in the breakeven core (see Fig. 1) and the fuel type chosen. Specifically, the U and Th TRU-burner options intended for the first-wave deployment rely on oxide fuel. The breakeven configurations, with longer time frame deployment, feature Zr-alloyed metallic fuel for the U core and nitride fuel with 95% enriched N-15 in N for the Th core. The rationale for the adoption of metal and nitride in the U and Th breakeven cores is that they foster the best respective breeding performance due to material considerations and neutronic properties [2, 5, 13].

The radial blankets adopted in the breakeven designs consist of a peripheral blanket and one blanket region at the core center. Bottom and top axial blankets are also employed. In order to compensate for the deficit in breeding performance, the Th fuelled design features the same radial blankets, but they are in total nearly 50-cm thicker than the axial blankets in the U fuelled design. Although not optimized, the two breakeven core designs are suitable for a top-level comparison of the core physics performance of U and Th fuels.

Table 1. Main Design Parameters for the ARR Core

	Burner (Th or U-based)	U-based breakeven	Th-based breakeven
Thermal power	1,000 MWth		
Coolant	Na		
Coolant inlet/outlet T	395/550 °C		
Clad/duct material	HT-9		
Assembly type	Hexagonal with duct		
Pin lattice/pitch	Triangular,7.41 mm		
Pins per assembly	271		
Active core height	0.6 m		
Pellet OD; clad ID/OD	4.71; 5.44/6.50 mm		
Fuel/coolant/structure	41.1/32.7/26.2 vol %		
Number of inner/outer FA in the active core	192/132		
Fuel form	Oxide	Metallic (10% Zr alloy)	Nitride (95% N-15 in N)
Upper axial blanket	-	10 cm	30 cm
Lower axial blanket	-	10 cm	36 cm
Number of batches	3		
Refuelling interval	1 year		

3.2. *Fuel inventory*

The cores and fuels investigated in this paper are listed in Table 2 together with the fuel inventory characteristics of each option. The fuel inventories have been obtained by performing multi-cycle core physics simulations using the ERANOS-based EQL3D procedure [14] to simulate a total of 120 Effective Full Power Years (EFPY) of irradiation, at which point practically all isotopes have converged to equilibrium. Cases 1 to 4 listed in Table 2 refer to the TRU-burner design. Case 1 and 2 refer to the U fuel cycle scheme, i.e. natural U is adopted as the fertile carrier, while the external supply of legacy material to burn consists of TRUs recovered via reprocessing of used UO_2 LWR fuel (case 1) or used U-PuO_2 fuel (U-MOX, case 2). Cases 3 and 4 are the counterpart burning schemes in the Th fuel cycle scheme under evaluation, e.g. Th is adopted as the fertile carrier to burn legacy TRUs from used UO_2 LWR fuel (case 3), while the TRUs burned in case 4 are assumed to be recovered from used Th-PuO2 (Th-MOX) PWR fuel and include the U in-bred from Th ("U3" for convenience in Table 2). The legacy supply incinerated in case 2 and case 4 also include the Np, Am, and Cm (MAs) associated to the original Pu recycled in the U-MOX and Th-MOX stages. Table 3

summarizes the external feeds isotopic proportion for Cases 1 through 4. Ref 15 contains a detailed description of the various recycling schemes and mass flows obtained. Cases 5 and 6 relate to the U-based and Th-based breakeven configurations, requiring respectively only natural U and Th feeds, and are self-sufficient in terms of fissile generation.

Table 2 summarizes the main fuel cycle performance parameters for the various options. As expected, Th leads to lower fast-spectrum breeding capabilities from reduced fuel density and higher leakages in Th, lower fission yield of U3 vs. Pu in a fast spectrum, and lower fast-fission fertile contribution (~2% vs ~8% of the total fissions in Th-232 vs. U-238). The lower breeding capability fosters the higher TRU-burning rates shown by Th vs. U burner designs, and leads to the taller axial blankets adopted in the Th breakeven configuration.

The main isotopes characterizing the fuel inventory of the various cores at reactor discharge are shown in the bottom part of Table 2. The smaller fertile proportion of the Th cores is a consequence of the lower neutron economy, which entails higher fissile content to achieve the same cycle length of the U core. The lower Pu content, especially Pu-239, develops from the asbence of the conversion from U-238, replaced by generation of U-233 from Th-232. The higher content of Pu-241, Pu-242, Am and higher actinides is due to the higher feeding rate of TRU to incinerate. Thanks to the asbence of an external TRU feed, the fuel inventory of the Th breakeven configuration is predominantly Th-232 and in-bred U, vs. U-238 and in-bred Pu for the U breakeven core.

Table 2. Summary of the cores and recycling schemes adopted for this study

Case number		1	2	3	4	5	6
Core type		Burner				Breakeven	
Fertile		U	U	Th	Th	U	Th
External fissile supply and source[1]		TRU UO$_2$ LWR	TRU U-MOX LWR	TRU UO$_2$ LWR	TRU+U3 Th-MOX LWR	None	
Smeared density [%TD]		0.85	0.85	0.85	0.85	0.75	0.85
Conversion Ratio[2] [-]		0.47	0.38	0.4	0.31	1	1
TRU burning [kg/Gw$_e$-yr]		494	532	563	644	-	-
Core HM inventory [t]		10.2	10.2	10.2	9.64	13.2	12.1
Blanket HM inventory [t]		-	-	-	-	9.6	20.1
Equilibrium core composition [wt%][3]	**Th-232**	~0	~0	55.81	49.87	~0	77.38
	U-233	~0	~0	5.80	8.49	~0	15.97
	U-234	0.36	0.54	2.17	3.77	0.07	4.40
	U-235	0.10	0.13	0.43	0.79	0.04	0.83
	U-236	0.14	0.18	0.46	0.80	0.07	0.77
	U-238	61.52	56.92	~0	~0	80.54	~0
	Np-237	0.83	1.39	1.10	1.72	0.12	0.15
	Pu-238	1.65	2.44	2.02	2.90	0.23	0.10
	Pu-239	13.11	10.51	8.42	2.33	12.53	0.02
	Pu-240	12.69	13.24	12.26	11.29	5.05	0.11
	Pu-241	1.90	2.22	2.02	2.18	0.43	0.01
	Pu-242	3.62	5.44	4.48	7.03	0.38	0.07
	Am-241	1.82	2.40	2.20	2.92	0.35	0.02
	Am-243	1.11	2.18	1.40	2.89	0.10	0.03
	Cm-244	0.73	1.59	0.86	1.94	0.06	0.02

(1) Fissile composition burned for the various options given in Table 3. (2) Conversion Ratio defined considering Th-232 or U-238 as fertile materials and all other isotopes as fissile (3) Calculated at discharge after 120 EFPY of irradiation

Table 3. External fissile feed [wt%] for the burner configurations in Table 1

	TRU UO$_2$ LWR (Case 1 and 3)	TRU U-MOX LWR[1] (Case 2)	TRU+U3 Th-MOX LWR[1] (Case 4)
U-232	0.00	0.00	0.10
U-233	0.00	0.00	21.20
U-234	0.00	0.00	2.25
U-235	0.00	0.00	0.39
Np-237	4.72	7.73	6.50
Pu-238	2.17	3.56	3.16
Pu-239	47.39	27.17	9.37
Pu-240	22.80	23.52	20.25
Pu-241	8.41	10.88	9.69
Pu-242	6.83	10.87	11.01
Am-241	5.61	8.14	8.15
Am-243	1.55	5.25	5.20
Cm-244	0.45	2.44	2.25
Cm-245	0.04	0.33	0.31

(1): Supplemented with Np, Am and Cm recovered from UOX LWR
fuel providing the Pu for U-MOX fuel (Case 2) or Th-MOX fuel (Case 4)

4. Comparative analysis of main safety parameters

The present section provides a general discussion of the safety aspects related to the different fuel configurations listed in Table 4. The attention is focused on feedback coefficients, β_{eff} and three parameters frequently adopted to assess the passive safety features of sodium-cooled FRs and generally identified as *A, B, C.* [16-17] *A* represents the reactivity variation associated with the fuel temperature increase from the average coolant temperature to the average fuel temperature at nominal conditions. *B* represents the reactivity variation associated with the increase in fuel and coolant temperatures from iso-thermal zero-power conditions (at inlet temperature) to the average coolant temperature. C is the feedback reactivity coefficient associated with the inlet core temperature. Using these parameters, and defining ΔT_c as the operational coolant temperature rise in the core, it is possible to derive sufficient conditions for the reactor passive safety in case of an Unprotected Loss Of Flow (ULOF), an Unprotected Loss Of Heat Sink (ULOHS), a chilled inlet, and an Unprotected Transient OverPower (UTOP), respectively [16]:

$$a)\ \frac{A}{B} < 1 \qquad b)\ \frac{C\Delta T_c}{B} > \frac{1+A/B}{2} \sim 1 \qquad c)\ \frac{C\Delta T_c}{B} < 1.5\left(1+\frac{A}{B}\right)\sim 3 \qquad d)\ \Delta\rho_{ext} < B\left(1+\frac{A}{B}\right) \qquad (1)$$

Application of these conditions is inadequate to characterize the first few tens of seconds of an ULOF transient [16], where the pump coast-down may be quicker than the power reduction as a consequence of the delayed neutron hold-back time. In this case it is possible to demonstrate that the consequences of the increased power-to-flow ratio can be mitigated by minimizing the quantity *(1+(A/B)²)/B/* [16].

Table 4. Safety response for the cases investigated

Case number	1	2	3	4	5	6
Core type	Burner				Breakeven	
Fertile	U	U	Th	Th	U	Th
External fissile supply and source	TRU UOX LWR	TRU U-MOX LWR	TRU UOX LWR	TRU+U3 Th-MOX LWR	None	
Fuel smeared density [%TD]	0.85	0.85	0.85	0.85	0.75	0.85
Conversion Ratio [-]	0.47	0.38	0.40	0.31	1	1
Doppler coeff. [m$/K]	-0.88	-0.93	-0.88	-0.87	-1.03	-1.94
Active core voiding [$]	4.20	5.23	2.66	3.45	4.91	-1.01
Coolant exp. coeff. [m$/K]	1.09	1.36	0.69	0.90	1.28	-0.26
Fuel exp. coeff. [m$/K]	-0.38	-0.43	-0.30	-0.34	-0.51	-0.17
Radial exp. coeff. [m$/K]	-3.00	-3.09	-3.24	-3.18	-2.81	-2.25
A	-668	-720	-624	-636	-351	-479
B	-479	-480	-540	-516	-456	-532
CΔTc	-492	-480	-578	-540	-476	-715
A/B	1.40	1.50	1.16	1.23	0.77	0.90
CΔTc/B	1.03	1.00	1.07	1.05	1.05	1.35
(1+(A/B)^2)|B|	1411	1560	1261	1300	726	963
β_{eff} [pcm]	315	304	285	287	361	342
Reactivity swing [%]	5.1	4.4	5.6	5.2	2.9	4.9
CR[1]'s to limit UTOP power peak	14	12	16	15	7	12
CRs required for passive safety	15	13	17	16	10	15

[1]Number of Control Rod Assemblies

4.1. *TRU-burner core configurations*

The Doppler coefficient for the burner oxide fuels is virtually unaffected by adopting Th, while the most notable impact is a ~40% reduction of void reactivity and coolant expansion coefficient in the Th burning schemes considered vs. the U counterparts. The positive reactivity insertion in case of core voiding is a major concern in sodium-cooled FRs as double-fault accidents like unprotected loss of flow may lead to sodium boiling. Coolant expansion plays a major role during accidental transients, especially when driven by a coolant temperature increase (e.g., ULOHS). It also determines the non-minimum-phase behaviour of FRs, which disturbs the performance of the control system. Th is then expected to foster improved safety and controllability for a burner design, which combines with the increased TRU-burning rate, and makes Th an attractive option in a FR TRU-burning scheme.

The phenomenology underlying this improvement is investigated in the following paragraphs, using the reactivity decomposition technique described in Refs. [7-8]. Fig. 2 reports the isotope-wise decomposition of the void reactivity insertion for Case 1 (U) and Case 3 (Th) in Table 4, employing TRUs from once-through LWR as feed, while Fig. 3 shows capture and fission cross-sections of the main fissile and fertile isotopes characterizing each case.
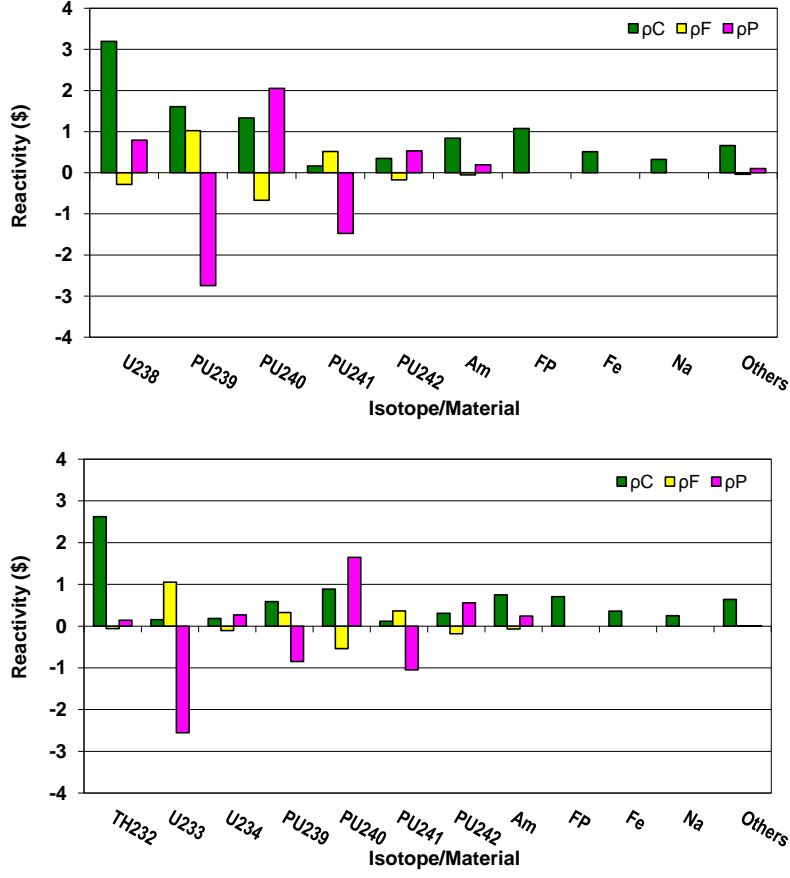
FIG. 2. Isotope-wise decomposition of void reactivity for cases 1 (U, top) and 3 (Th, bottom) in Table 2. ρ_c, ρ_F, and ρ_P are the reactivity contributions from captures, fissions and productions, respectively.
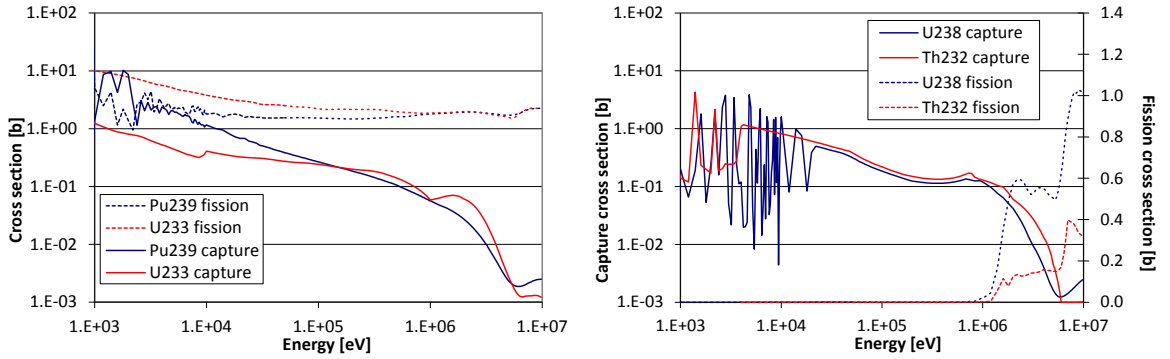
FIG. 3. Cross sections for the main fissile (Pu-239 and U-233, left) and fertile (U-238 and Th-232) isotopes (JEFF3.1 nuclear data library [18])

From an isotopic viewpoint, the direct effect of core voiding is limited to a small reactivity insertion from fewer captures in sodium (Fig. 2). The main reactivity effect is brought about indirectly, through the spectrum hardening that ensues upon voiding. The dominant effect is a reduction of captures, and ensuing increased reactivity, due to the decreasing trend of the capture cross sections with energy (Fig. 3). The main contributors are U-238 and Th-232. As no significant differences are observed in the trend of U-238 and Th-232 capture cross-sections, the Th cores lower reactivity insertion is to be ascribed to the lower relative content of Th in the Th core fuel inventory, compared to the relative content of U in the U core fuel inventory (see Table 2). The absence of the U-238 to Pu-239 breeding

mechanism in Th leads to high destruction rate and low content of Pu-239, with buildup of U-233, which brings additional benefits in case of core voiding due to the flatter capture cross-section of U-233 compared to Pu-239. A substantial contribution to the reactivity insertion is caused by the decreasing captures with energy in Pu-240 and Am isotopes, with a similar content and contribution for the U and Th burners.

A second effect related to spectral hardening is a variation in the fission cross-sections, itself a neutron absorption event but followed by multiple neutrons production. In this case odd and even mass number isotopes show opposite behaviour. In particular, even-mass-number isotopes generally feature threshold fission-cross sections, so that spectral hardening increases fissions, with consequent negative reactivity insertion from increased absorptions but overall positive reactivity insertion from increased neutron production. The higher energy threshold and lower fission cross-section of Th-232 vs. U-238 contributes to its smaller variation in neutron production and negligible positive void reactivity inserted. Odd-mass-number isotopes feature instead a decreasing fission cross section with energy, and decreasing neutron production in case of spectrum hardening. Thanks to a markedly decreasing fission cross-section, U-233 gives a tangible negative contribution to the overall void reactivity. It is interesting to observe that Am, although mainly composed of odd-mass-number isotopes, behaves like an even-mass-number isotope. In fact, the fission cross-sections of Am-241 and Am-243 decrease till ~100 keV, but feature a steep increment at higher energies.

Finally, spectral hardening leads to higher fission neutron yield and increases neutron production with overall reactivity insertions of ~0.4 and 1 $ for the U and Th cases, respectively. The higher value for the Th case is to be ascribed to the steeper increment of the U-233 vs. Pu-239 neutron yield with energy.

It can thus be concluded that Th, primarily from the content of Th-232 and U-233 that it generates, fosters lower reactivity changes following spectral variations. Albeit advantageous to void reactivity and coolant coefficient, such behaviour has negative repercussions in case of spectral softening, such as from fuel axial expansion and core radial expansion, both leading to increased coolant-to-fuel ratio. However, the impact of the fuel expansion coefficient is minimal, while the overall core radial expansion coefficient is comparable due to the higher leakages in the Th case.

The reduced reactivity impact of spectral changes in Th is beneficial to meeting the conditions of the reactor passive safety (1). Condition (1a) for passive safety during an ULOF is not met by the TRU burner concepts due to the high oxide fuel temperature and the ensuing high positive reactivity insertion following a power reduction. However, Th benefits from a higher B value resulting from the reduced coolant effects, leading also to a reduced value of the parameter $(1+(A/B)^2)/B/$ governing the initial increment of the power-to-flow ratio. The condition for passive safety in case of an ULOHS is instead met by all TRU-burner options, with extra margin for Th due to the higher B value. An improved behaviour during an ULOHS implies a worse reactor response in case of chilled-inlet, but condition (1c) shows that this accident is a minor concern for the ARR.

β_{eff} and reactivity swing are penalized by using Th. β_{eff} is driven downward by the relatively high content of TRU, partly counterbalanced in U by the 8% fast-fission contributions in U-238, whereas Th-232 contributes only 2% of the fissions. The lower conversion ratio of Th leads to the higher reactivity swing observed. This combination of a high reactivity swing and a low β_{eff} increases the number of control rods required to meet the typical 0.8 $ limit on the control rods worth [19], or the condition (1d) for passive safety in case of an UTOP.

It is worth noticing that adoption of fissile feed from recycled MOX or Th-MOX LWR fuel (Cases 2 and 4) has a small impact on the safety parameters except a notable degradation in the active core voiding and coolant expansion coefficient, similar in the U and Th cases despite the different feed. This can be ascribed to the increased inventory of Am and Pu-242 compared to the UOX LWR feed, fostering significantly reduced captures, and increased fissions, in case of spectral hardening.

4.2. Breakeven core configurations

As already pointed out, the fission cross-section of U-233 shows a much steeper decrease with energy compared to that of Pu-239, and the capture cross-section is significantly more flat (Fig. 3). As a result, the reactivity contribution from U-233 in case of spectrum hardening is strongly negative, unlike the contribution from Pu-239. The impact of U-233 is limited in the TRU-burner configurations, due to the small U-233 inventory while, with increasing conversion ratio and U-233 production, fissions from U-233 become the dominant contribution. As a result, the negative reactivity insertion of U-233 overcomes the smaller positive contribution of Th-232, leading to an overall negative void reactivity in the breakeven core configuration. The role of the various isotopes and the beneficial impact of U-233 are shown in the isotope-wise decomposition of the void reactivity in Fig. 4. Unlike in the burner configuration, the lower reactivity insertion of Th-232 vs. U-238 plays a minor role compared to the dominant impact of U-233 vs. Pu-239. The coolant expansion coefficient is based on the same phenomenology as the void reactivity insertion, thus showing a similar improvement. On the other hand, fuel and radial expansions cause the coolant-to-fuel ratio to increase, and the spectrum to soften, with an ensuing advantage for the U option. However, similarly to the TRU-burner configurations, the improvements in coolant expansion coefficient and core voiding offset the deterioration of the fuel axial expansion and core radial expansion coefficients.
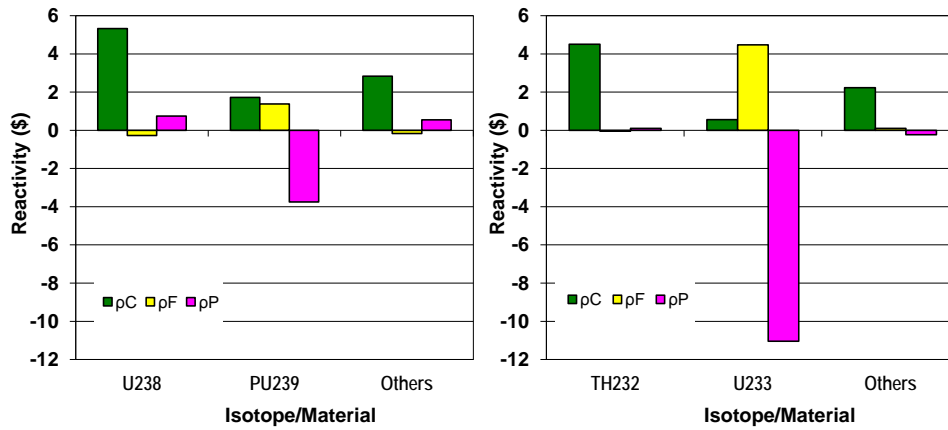

FIG. 4. Isotope-wise decomposition of void reactivity for the
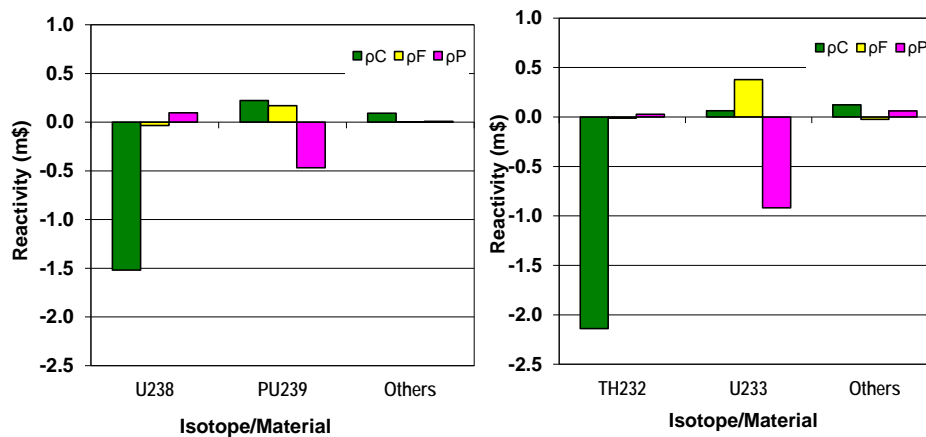*U-based (left) and Th-based (right) breakeven ARR*

FIG. 5. Isotope-wise reactivity decomposition of the Doppler coefficient for the
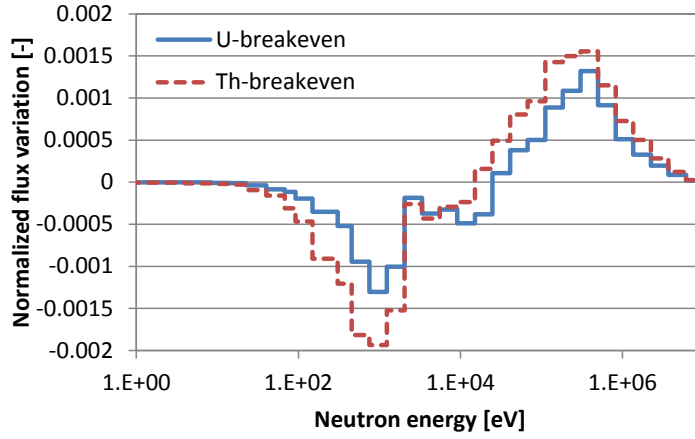*U-based breakeven ARR (left) and Th-based breakeven ARR (right)*

FIG. 6. Flux variation in case of Doppler resonance broadening

Th significantly improves the Doppler coefficient in the breakeven core configuration as well. Fig. 5 indicates that the negative contribution to the Doppler coefficient is dominated by the increased captures in the fertile isotopes, with a 0.5 m$ stronger effect for the Th case. Increased captures in the resonance region cause a suppression of the flux below 10 keV, with a consequent spectrum hardening, as shown in Fig. 6. Spectrum hardening fosters an additional reactivity reduction due to reduced fission in the fissile isotopes, leading to a further advantage for the Th option.

A high Doppler effect is advantageous in terms of load following capabilities and to limit power excursions e.g. in case of an UTOP. As a drawback, there is a larger positive reactivity insertion in case of power reduction, which detracts from passive safety. Specifically, both breakeven cores comply with condition (1a) for passive safety during an ULOF thanks to the low fuel temperature fostered by use of metallic or nitride fuel, but the Th option is much closer to the limiting value of *A/B=1*. Similarly, the parameter *(1+(A/B)²)/|B|* is higher, suggesting worse performance also during the initial power-to-flow increment caused by the ULOF. On the other hand, the dramatic improvement in the coolant coefficient enhances the core capabilities to withstand an ULOHS. As for the TRU-burner options, a chilled inlet transient appears a minor concern.

β$_{eff}$ is higher in the breakeven vs. the TRU-burner core configuration following 1) the higher U-238 content in the U case and 2) the presence of U-233 instead of TRUs as main fissile material in the Th case. The higher β$_{eff}$ combines with a reduced reactivity swing associated to the use of a denser fuel to reduce the required number of control rods necessary to comply with the 0.8 $ limit. Also the required control rods necessary to guarantee the reactor passive safety during an UTOP are reduced thanks to both the reduced reactivity swing and the high value of A, determined by the improved Doppler coefficient. The number of control rods required in the Th case is higher mainly as a consequence of the lower internal breeding and ensuing higher reactivity swing.

5.   Conclusions

The present paper investigates the impact of adopting a Th-based recycling scheme on the safety performance of a sodium-cooled FR, including TRU-burner and breakeven core configurations. The most notable improvements observed regard void reactivity insertion and coolant expansion coefficient. Reactivity decomposition techniques have shown that these improvements are ascribed mainly to the following two aspects, the former being more relevant for the burner design and the latter for the breakeven design: 1) low spectrum sensitivity in Th from the high energy threshold and low fission cross-section of Th-232 relatively to U-238; 2) a markedly negative contribution of U-233 to the delta reactivity ensuing spectral hardening, due to steeply decreasing fission-cross section with increasing neutron energy and relatively flat capture-cross section. Adopting Th in the burner configurations leads to a ~2$ decrease in void reactivity insertion compared to the U burner cores, whereas the synergistic contribution of Th-232 and U-233 in the Th-breakeven configuration yields a

~6$ decrease in void reactivity, leading to an overall negative reactivity insertion in case of core voiding. The reactivity decrement of U-233 following spectral hardening has a significant impact also on the Doppler coefficient, especially for the Th breakeven configuration, where the Doppler is twice as negative as in the U-based counterpart.

As a drawback, the lower sensitivity to spectral hardening fostered by Th deteriorates the reactivity feedbacks related to fuel axial expansion and core radial expansion, both leading to increased coolant-to-fuel ratio and softer spectrum. However the impact is limited compared to the improvements achieved in coolant expansion coefficient and void reactivity (and Doppler coefficient for the breakeven core).

Passive safety features are generally improved by Th. The lower coolant reactivity feedback helps mitigating the consequences of ULOF and ULOHS accidents, especially for the TRU-burner cores. For the breakeven case, the response to an ULOF is instead slightly worsened due to the markedly negative Doppler coefficient and ensuing reactivity gain from a decrease in power. The reactor response to a chilled-inlet transient is potentially worsened by Th but limiting conditions are far from being reached so this accident appears a minor concern for the FR analysed.

A notable disadvantage of Th relatively to U is the higher reactivity swing, caused by higher leakages and lower breeding capability. This results in ~3 additional control rod assemblies for the burner and 5 for the breakeven configurations to meet the standard 0.8 $ control rod worth limit and the condition for passive safety during an UTOP. In this regard, Th use is also penalized relative to U by the lower β_{eff}, which is the result of the much smaller contribution to fission of Th-232 vs. U-238.

REFERENCES

[1] Gruppelaar H., Schapira, J.P., 2006. Thorium as a waste management option. Technical Report. EU 19142 EN.

[2] Rodriguez, P., Sundaram, C. V., 1981. Nuclear and materials aspects of the thorium fuel cycle. J. Nucl. Mater. 100, 227-249.

[3] Bakker, K. at al., "Critical Evaluation of the Thermal Properties of ThO2 and Th1-yUyO2 and a Survey of the Literature Data on Th1-yPuyO2" J.Nucl.Mat. 250 pp1-12 (1997)

[4] Yang J.H. et al., "Fabrication and thermal conductivity of (Th,U)O2 pellets" *Nucl.Tech.* 147 pp113-119 (2004)

[5] Fiorina, C., Franceschini, F., Krepel, J., Mikityuk, K., 2011. Comparative analysis of uranium and thorium fuel cycles in a Lead-cooled Fast Reactor from the perspective of safety and waste management. In: Proc. Int. Conf. GLOBAL 2011, December 11-16, Chiba, Japan.

[6] Dobson, A., 2008. GNEP Deployment Studies Preliminary Conceptual Design Studies. Technical Report. Volume IV - Advanced Recycling Reactor.

[7] Chawla, R., Jatuff, F., Tani, F., 2008. Diagnostic analysis of pin-removal reactivity worth experiments in a SVEA-96+ test lattice. Ann. Nucl. Energy 35, 495-502.

[8] Krepel, J., Saliba, J., Mikityuk, K., Chawla, R., 2011. Comparison of safety related parameters in the equilibrium closed cycle for Generation-IV fast reactors. Proc. Int. Conf. GLOBAL 201,Chiba, Japan.

[9] Rimpault, G., Plisson, D., Tommasi, J., Jacqmin, R., Rieunier, J., Verrier, D., Biron, D., 2002. The ERANOS code and data system for fast reactor neutronic analyses. In: Proc. Int.

Conf. PHYSOR 2002, Seoul, Korea, October 7-10.

[10]   Ruggeri, J.M., 1999. ERANOS : manuel des methodes : reconstruction fine d'un flux nodal. Technical Report. NT-SPRC-LEPH-99-217.

[11]   Rimpault, G., 1997. Physics documentation of eranos the ecco cell code. Technical Report. RT-SPRC-LEPh-97-001.

[12]   Sublet., J.C., Dean., C., Plisson-Rieunier, D., 2005. ECCOLIB-JEFF-3.1 libraries. Technical Report. CEA-R-6100.

[13]   Till, C. E., Chang, Y.I., Kittel, J.H., Fauske, H.K., Lineberry, M.J., Stevenson, M.G., Amundson, P.I., Dance, K.D., 1980. Fast breeder reactor studies. Technical Report. Argonne National Laboratory, ANL-80-40.

[14]   Krepel, J., Pelloni, S., Mikityuk, K., Coddington, P., 2009. EQL3D: ERANOS based equilibrium fuel cycle procedure for fast reactors. Ann. Nucl. Energy 36, 550–561.

[15]   Franceschini, F., Lindley, B., Fiorina, C., Lahoda, E., Wenner, M., 2012. Analysis of a fuel cycle strategy to achieve low-radiotoxicity waste. Proc. Int. Conf. IEMPT. Sept. 24-27 2012, Prague, Czech Republic.

[16]   Wade, D. C., Chang, Y. I., 1987. The Integral Fast Reactor (IFR) Concept: Physics of Operation and Safety. Proc. Int. Topical Meeting on Advances in Reactor Physics Mathematics and Computation, April 17-30, Paris, France.

[17]   Wade, D. C., Hill, R. N., 1997. The design rationale of the IFR. Prog. Nucl. Energ. 3, 1997, 13-42.

[18]   Koning, A., Forrest, R., Kellett, M., Mills, R., Henriksson, H., Rugama, Y., 2006. The JEFF-3.1 Nuclear Data Library. Nuclear Energy Agency. JEFF Report 21.

[19]   Wade, D. C., Wigeland, R.A., Hill, D.J., 1997. The safety of the IFR. Prog. Nucl. Energ. 31(1),63-82.

Coremelt-2D Code for Analysis of Severe Accidents in a Sodium Fast Reactor

I.M. Ashurko, A.V. Volkov, K.F. Raskach

State Scientific Center of the Russian Federation, Institute for Physics and Power Engineering, Obninsk, Russia

Abstract. In the paper there is a description of COREMELT-2D code designed for carrying out coupled two-dimensional analysis of neutronic and thermohydraulic transients, which may occur in the core of sodium cooled fast reactor (SFR), including severe accidents resulting in damage of SFR core and relocation of its components with the change of their aggregative state, namely: boiling and condensation of coolant, damage and melting of fuel element claddings and fuel, relocation of molten core components, thermal interaction of fuel and coolant and freezing of steel and fuel. So, COREMELT-2D code is capable of analyzing all stages of ULOF accident up to expansion phase characterized by the intensive interaction of molten fuel and sodium. Modular structure of COREMELT-2D code consisting of thermohydraulic module COREMELT and neutronic module RADAR is presented. Preservation equations are solved in COREMELT module in two-dimensional cylindrical R-Z geometry in porous body approximation. RADAR module is used for solving multi-group neutron diffusion equation in R-Z and X-Y geometry. Application of the code for solving dynamics tasks with rather rapid changes of neutron constants requires efficient unit for constants preparation. For this purpose, steady state analysis TRIGEX code (HEX-Z geometry) is used, which includes the program of nuclear data preparation CONSYST connected to the ABBN-93 group constants library. In the paper presented are the results of comparative analytical studies on ULOF beyond design severe accident as applied to the BN-1200 reactor design made by COREMELT-2D code and by its previous version based on neutron kinetics point model. The results of analysis make it possible to evaluate the effect of space-time changes of reactor neutronics caused by sodium removal from the core as a result of sodium boiling

1. Introduction

COREMELT-2D code is intended for the fulfillment of coupled calculations of the non-stationary neutronic and thermohydraulic processes in sodium-cooled fast reactor (SFR), including the calculations of severe accidents of the ULOF and UTOP types, which are accompanied by sodium boiling, damage and melting of the fuel pin claddings, fuel meltdown, thermal fuel-coolant interaction, freezing of steel and fuel. At present, application of this code for calculation of the core disruptive accidents (CDA) has been limited by the analysis of the processes where the steel and fuel temperature does not exceed their boiling temperature. In case of complex calculations of the severe accidents, the code is basically applied for the analysis of their initial and transient stages up to the intensive interaction of melted fuel with sodium. In recent time, the code has been used in the calculational analysis of the self-protection level of various options of the BN-1200 reactor core with a sodium plenum in the upper part of the core, where the principal task was in the justification of a possibility of stable sodium boiling under ULOF accident conditions [1], its consequences being limited only by the sodium boiling, without fuel pin melting.

COREMELT-2D is one of the versions of the code developed for analysis of severe accidents, which includes two coupled modules – two-dimensional dynamic thermohydraulic module COREMELT and three-dimensional dynamic neutronic module RADAR.

2. Thermohydraulic module COREMELT

The thermohydraulic module includes the following:

— The 4-velocity model of a multi-component and multi-phase flow in cylindrical R-Z geometry and in the porous body approximation;

— 1D or 2D structural models of the core and reactor elements, where the change of their geometry owing to their melting is accounted;

— The point models of frozen steel or fuel with reference to the main calculational grid.

The module calculates in cylindrical geometry the two-dimensional fields of velocity, pressure, internal energy, and volume fractions of four components – those of sodium (liquid and vapor) and melted particles of steel and fuel. At the first stage of the accident the sodium circulation velocity depends on the pump head, and after cutoff and rundown of the pumps, it is determined by the natural convection forces. For the non-penetrable elements immersed into sodium (such as fuel pins, safety rods, fuel subassembly (FSA) wrappers, heat exchange tubes, etc.) – the conjugate problem of thermal conductivity is solved. The primary circuit sodium transfers heat via the IHX heat exchange tube walls to the secondary circuit sodium, and equation of the sodium heat-and-mass transfer in the IHX is solved separately.

As a rule, the core fuel subassemblies are represented as one-dimensional calculational channels. The most important elements of the primary circuit are modeled, such as heat exchangers, pumps. The fuel pin is described in two-dimensional cylindrical geometry taking into account a possibility of its melting. When the melting takes place, the fuel pin's molten part is carried away by the sodium vapor flow or it flows down. The steel or fuel crusts can be frozen on the surface of not broken fuel pins, and a possibility of their re-melting is taken into account. The geometry of fuel pins and flow cross-section (porosity) of the inter-fuel pin space is changed in all cases. A FSA wrapper is modeled in each calculational channel, which bounds from the external side with the flow of inter-assembly sodium.

The code realizes a multi-component and multi-phase thermohydraulics model. All components are conventionally subdivided in two types: the moving components and stationary (structural) ones. For the moving components, a complete system of differential equations of mass, momentum, and energy conservation is solved. The stationary (structural) components simulating various elements of the reactor core and vessel or the steel and fuel crusts on their surface are described by two differential equations of mass and energy conservation.

The number of components may be different, as dependent on the complication level of the problem to be solved. All moving components are connected mechanically with each other and with the channel walls (structural components). The heat exchange proceeds between all components, described by corresponding relationships which close the basic system of differential equations.

The model of multi-component flow describes two phase transitions – these include the vaporization-condensation v/c and melting-freezing m/f. The equations of mass conservation for the components are written as:

$$\frac{\partial(\alpha_f \varepsilon \rho_f)}{\partial t} + \nabla \cdot (\alpha_f \varepsilon \rho_f u_f) = -\Gamma_e + \Gamma_c,$$

$$\frac{\partial(\alpha_g \varepsilon \rho_g)}{\partial t} + \nabla \cdot (\alpha_g \varepsilon \rho_g u_g) = \Gamma_e - \Gamma_c,$$

$$\frac{\partial(\alpha_{d1} \varepsilon \rho_{d1})}{\partial t} + \nabla \cdot (\alpha_{d1} \varepsilon \rho_{d1} u_{d1}) = S_{Md1} + S_{Md11} - S_{Fd1} - S_{Fd11} + S_{Mw} + S_{Mwd1} - S_{Fwd1},$$

$$\frac{\partial(\alpha_{d2} \varepsilon \rho_{d2})}{\partial t} + \nabla \cdot (\alpha_{d2} \varepsilon \rho_{d2} u_{d2}) = S_{Md2} + S_{Md22} - S_{Fd2} - S_{Fd22} + S_{Mwd2} - S_{Fwd2},$$

where α – the component's volume fraction, Γ_e and Γ_c – intensity of vaporization and condensation of sodium; S_{Md1}, S_{Md2} – intensity of steel and fuel release into the channel owing to fuel pin melting; S_{Mw} – intensity of steel release into the channel owing to FSA wrapper melting; S_{Md11}, S_{Md22}, S_{Fd11}, S_{Fd22} – intensity of melting and freezing of steel and fuel crusts on the fuel pin surface; S_{Mwd1}, S_{Mwd2}, S_{Fwd1}, S_{Fwd2} – intensity of melting and freezing of steel and fuel crusts on the FSA wrapper surface.

The components' volume fractions are in an agreement with the following equation:

$$\alpha_f + \alpha_g + \alpha_{d1} + \alpha_{d2} = 1$$

Equations of the components' momentum conservation are as follows:

$$\frac{\partial(\alpha_f \varepsilon \rho_f u_f)}{\partial t} + \nabla \cdot (\alpha_f \varepsilon \rho_f \mathbf{u}_f \varepsilon u_f) = -\alpha_f \varepsilon \nabla p - \alpha_f \varepsilon \rho_f g - F_{pf} - F_{wf} - F_{ifg} - F_{ifd} - u_f \Gamma_e + u_g \Gamma_c$$

$$\frac{\partial(\alpha_g \varepsilon \rho_g u_g)}{\partial t} + \nabla \cdot (\alpha_g \varepsilon \rho_g \mathbf{u}_g \varepsilon u_g) = -\alpha_g \varepsilon \nabla p - \alpha_g \varepsilon \rho_g g - F_{pg} - F_{wg} - F_{igf} - F_{igd} + u_f \Gamma_e - u_g \Gamma_c$$

$$\frac{\partial(\alpha_{d1} \varepsilon \rho_{d1} u_{d1})}{\partial t} + \nabla \cdot (\alpha_{d1} \varepsilon \rho_{d1} \mathbf{u}_{d1} \varepsilon u_{d1}) = -\alpha_{d1} \varepsilon \nabla p - \alpha_{d1} \varepsilon \rho_{d1} g - F_{pd1} - F_{wd1} - F_{idf} - F_{idg} - \mathbf{u}_{d1} S_{Fd1}$$

$$\frac{\partial(\alpha_{d2} \varepsilon \rho_{d2} u_{d2})}{\partial t} + \nabla \cdot (\alpha_{d2} \varepsilon \rho_{d2} \mathbf{u}_{d2} \varepsilon u_{d2}) = -\alpha_{d2} \varepsilon \nabla p - \alpha_{d2} \varepsilon \rho_{d2} g - F_{pd2} - F_{wd2} - F_{idf} - F_{idg} - \mathbf{u}_{d2} S_{Fd2}$$

where F_{pf}, F_{pf}, F_{pg}, F_{wf}, F_{wg}, F_{pd1}, F_{pd2}, F_{wd1}, F_{wd2} – the components' friction on the core structural elements, F_{igf}, F_{ifg}, F_{idf}, F_{idg}, F_{ifd}, F_{igd} – friction on the inter-component surface.

Equations of the components' energy conservation are as follows:

$$\frac{\partial(\alpha_f \varepsilon \rho_f e_f)}{\partial t} + \nabla \cdot (\alpha_f \varepsilon \rho_f e_f u_f) =$$

$$= -p\left[\frac{\partial \alpha_f \varepsilon}{\partial t} + \nabla \cdot (\alpha_f \varepsilon u_f)\right] + +Q_{kf} + Q_{ifg} + Q_{ifd1} + Q_{ifd2} + Q_{fp} + Q_{fw} + Q_{fwd1} + Q_{fwd2}$$

$$\frac{\partial(\alpha_g \varepsilon \rho_g e_g)}{\partial t} + \nabla \cdot (\alpha_g \varepsilon \rho_g e_g u_g) =$$

$$= -p\left[\frac{\partial \alpha_g \varepsilon}{\partial t} + \nabla \cdot (\alpha_g \varepsilon u_g)\right] + Q_{igf} + Q_{igd1} + Q_{igd2} + Q_{gp} + Q_{gw} + Q_{gwd1} + Q_{gwd2} - S_{Fd1w} e_{wd1}$$

$$\frac{\partial(\alpha_{d1} \varepsilon \rho_{d1} e_{d1})}{\partial t} + \nabla \cdot (\alpha_{d1} \varepsilon \rho_{d1} e_{d1} u_{d1}) = S_{Md1} e_p - S_{Fd1w} e_{wd1} + Q_{kd1} + Q_{id1f} + Q_{id1g} + Q_{id1d2} + Q_{d1p}$$

$$\frac{\partial(\alpha_{d2} \varepsilon \rho_{d2} e_{d2})}{\partial t} + \nabla \cdot (\alpha_{d2} \varepsilon \rho_{d2} e_{d2} u_{d2}) = S_{Md2} e_p - S_{Fd2w} e_{wd2} + Q_{kd2} + Q_{id2f} + Q_{id2g} + Q_{id2d1} + Q_{d2p} + Q_v,$$

where e_f, e_g, e_{d1}, e_{d2} – the components' internal energy; Q_{ifg}, Q_{igf}, Q_{id1f}, Q_{id1g}, Q_{id2f}, Q_{id2g}, Q_{ifd1}, Q_{igd1}, Q_{ifd2}, Q_{igd2}, Q_{id1d2}, Q_{id2d1} – energy exchange on the inter-component surface; Q_{kf}, Q_{kd1}, Q_{kd2} – energy exchange owing to the heat conductance of each component.

The finite-difference method constitutes the basis of technique for the system of conservation equations. The calculation area is covered by the orthogonal difference meshwork: $\left(r_i = i \cdot \Delta r_{i \cdot 1/2}; i = 1,2 \ldots N_r\right) \times \left(z_k = k \cdot \Delta z_{k-1/2}; k = 1,2 \ldots N_z\right)$, which has variable steps over the radius and height. When the difference analogues of the initial equations system are derived, the principle of "displaced meshs" is used, when a part of the unknown variables (energy, pressure) is

determined at the centers of elementary meshs, and projections of the velocity vector **V** are half-step displaced relative thereto by the z and r coordinates.

When the finite-difference approximations are obtained, the equations of mass and energy conservation are integrated over the mesh of the main net, and the momentum conservation equations (velocity projections) – over the mesh of the displaced net. All unknown variables are taken from the upper time step of n+1, and non-linear terms are linearized over the step of iteration process, the time derivatives are approximated by the first-order accuracy differences. The scheme "upwards the flow" is used for approximation of convective terms in the momentum and energy equations.

3. Neutronic module RADAR

Neutronic module RADAR is a network code for solution of non-steady state transport equation in a group diffusion approximation. Two-dimensional module RADAR2D intended for solving the diffusion equation in R-Z- and X-Y- geometry was created in 2011. In 2012, the three-dimensional module RADAR3D was developed, with diffusion equation solved in hexagonal-Z and triangle-Z geometries.

The neutronic module provides solution of two types of problems: the conventionally-critical problem and non-steady state one. Solution of the first problem serves for determining the initial conditions for the second problem. The group equations for the neutron flux are as follows:

$$\frac{1}{v^g}\frac{d\Phi^g}{dt} - \nabla D^{m,g}\nabla\Phi^g + \Sigma_{cfd}^{m,g}\Phi^g = \sum_{h=1}^{g-1}\Sigma_s^{m,h\to g}\Phi^h + Q_p^g + Q_d^g$$

They are solved jointly with the equations for concentrations of the delayed neutrons' precursors:

$$\frac{dC^{n,gd}}{dt} = \frac{1}{k_0}\sum_{h=1}^{ng}\beta^{n,h,gd}v\Sigma_f^{m,n,h}\Phi^h - \lambda^{n,gd}C^{n,gd}$$

In the above equations: Φ^g – the neutron flux in energy group g; $C^{n,gd}$ – concentration of the delayed neutrons' precursors associated with fission of nuclide n and the delay group gd; $D^{m,g}$, $\Sigma_{cfd}^{m,g}$ and $\Sigma_s^{m,h\to g}$ – diffusion coefficient, the withdrawal cross-section and scattering cross-section for material m; $v\Sigma_f^{m,n,g}$ – cross-section of neutron generation for the material m and nuclide n; $\lambda^{n,gd}$ and $\beta^{n,h,gd}$ – decay constant of the precursors and the delayed neutron fraction, v^g – neutron velocity; Q_p^g and Q_d^g – sources of prompt and delayed neutrons respectively.

$$Q_p^g = \frac{1}{k_0}\chi_p^{m,g}\sum_{h=1}^{ng}\mu^{m,h}\Phi^h \; ; \; Q_d^g = \sum_{h=1}^{ng}\sum_{gd=1}^{ngd}\chi_d^{n,g,gd}\lambda_{n,gd}C_{n,gd}$$

$$\mu^{m,g} = \sum_{n=1}^{nn}(1-\overline{\beta}^{n,g})v\Sigma_f^{m,n,g} \; ; \; \overline{\beta}^{n,g} = \sum_{gd=1}^{ngd}\beta^{n,g,gd}$$

The value of k_0 – effective multiplication factor corresponding to the initial steady state condition:

$$\Phi^g(0) = \Phi_0^g,$$

$$C^{n,gd}(0) = \frac{1}{\lambda^{n,gd} k_0} \sum_{h=1}^{ng} \beta^{n,h,gd} \nu\Sigma_f^{m,n,h} \Phi_0^h,$$

where Φ_0^g is in agreement with the equation:

$$-\nabla D^{m,g} \nabla\Phi_0^g + \Sigma_{cfd}^{m,g} \Phi_0^g = \sum_{h=1}^{g-1} \Sigma_s^{m,h\to g} \Phi_0^h + Q_p^g + Q_d^g,$$

where Q_p^g and Q_d^g are estimated by the formulas analogous to those presented above.

In the solution of non-steady state problem, digitization of the time derivative is fulfilled by an implicit pattern. In the solution of non-steady state and conventionally-critical problems, simple external iterations are used. The finite-difference equations are solved by using the method of the upper point relaxation. Description of the delayed neutrons can be provided by using the physical parameters or the effective parameters (in this case the above formulas are simplified in an appropriate way). The module realizes a possibility of control rods relocations by a special algorithm. The approach of geometrical averaging of neutron constants is used for the axial finite-difference layers which coincide with the boundaries (interfaces) of the moving rods' physical zones. To ensure the specified values of control rods' efficiency, a special procedure of their calibration is envisaged. The group neutron macro-constants of diffusion type are calculated by the CONSYST code [2] based on the library of ABBN93 group constants [3].

In the implementation of calculations by the RADAR module within the COREMELT code, the feedbacks in terms of densities and temperatures are accounted for via the macro-constants' variations, which are re-calculated at each time step. The changing of geometrical sizes (axial and radial expansion of the core) is accounted for in another way, namely, via the reactivity coefficients calculated previously, which are estimated before the beginning of time calculation – for the reactor's initial state. If we write the above equation for the neutron flux in a brief operator form ($\hat{L}$, $\hat{S}$ and $\hat{F}$ – operators of absorption, scattering, and fission)

$$\frac{1}{v}\frac{d\Phi}{dt} + \hat{L}\Phi = \hat{S}\Phi + \hat{F}\{\frac{1}{k_0}\nu\Sigma_f\}\Phi$$

then the pattern of accounting, for example, the axial expansion effect will be:

$$\frac{1}{v}\frac{d\Phi}{dt} + \hat{L}\Phi = \hat{S}\Phi + \hat{F}\{\frac{1}{k_0 + \Delta k_{ax}(t)}\nu\Sigma_f\}\Phi$$

where $\Delta k_{ax}(t)$ – additional reactivity recalculated at each time step:

$$\Delta k_{ax}(t) = \alpha \sum_i \rho_i \sum_j h_j (T_{i,j}(t) - T_{i,j}^{(0)})$$

where i – number of thermohydraulic channel, j – number of the layer over the height (axial layer), $h_j = z_{j+1} - z_j$, α – coefficient of linear expansion (for fuel or steel, as dependent on the expansion model accepted), $T_{i,j}(t)$ and $T_{i,j}^{(0)}$ – temperature distributions (for fuel or steel) for time moment t and for the initial steady state.

4. Results of code testing

Figure 1a shows the computational grid of thermohydraulic module COREMELT simulating the primary circuit of the BN-1200 reactor. The core is subdivided into 19 channels. The division of the core fuel subassemblies into channels is in a general agreement with division of the calculational model of RADAR module (Fig. 1b). Sodium flowing through the inter-subassembly space (at the external side of the fuel subassembly wrappers) is modeled by the 20th channel. The heat exchange through the FSA wrappers' walls between the inter-subassembly space and FSAs is modeled. The downcomer region simulates simultaneously the intermediate heat exchangers and pumps of the primary circuit, which allows description of the coolant parameters changing at the inlet to the reactor core (temperature, pressure, flow rate) caused by the primary and secondary circuit pumps' rundown. All structural elements of the primary circuit (fuel pins, absorber rods, fuel subassembly wrappers, IHX tubes, etc.) are described by corresponding calculational grids.
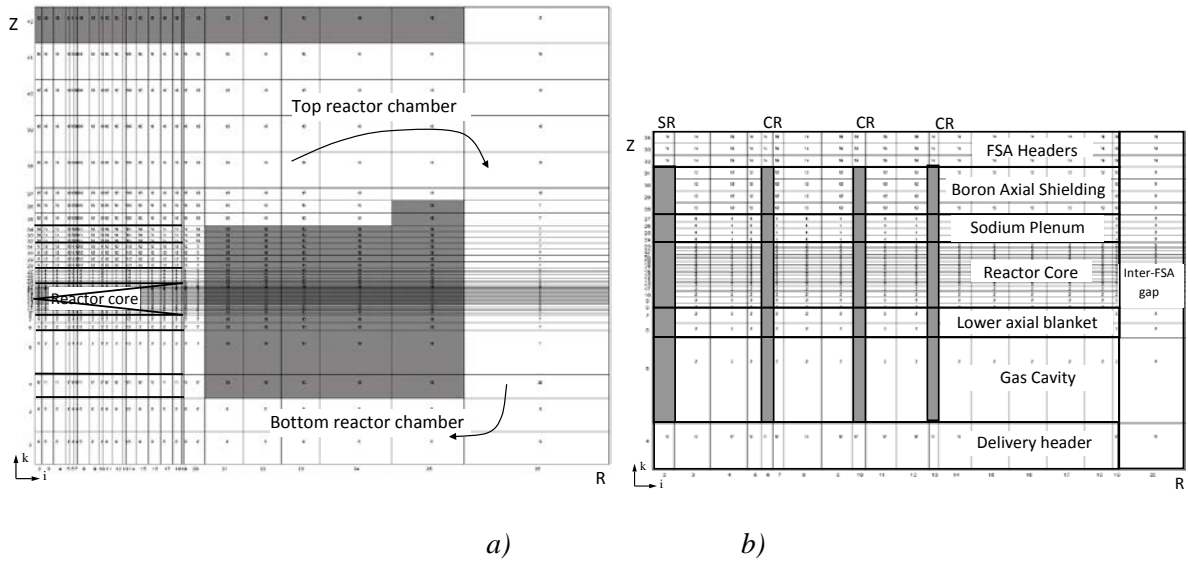

a)   *b)*

FIG. 1. Calculational area of the COREMELT module (Z:R = 1:1) (a), fragment of the calculational area simulating the FSAs of the core (Z:R = 1:3) (b).

A total loss of the grid and emergency power supplies with failure of all reactor shutdown rods, including those of the passive shutdown system (PSS), is considered as the initial event for the ULOF accident. The accident is supposed to occur in the reactor operated at nominal power level at the end of cycle. At the initial time moment, owing to the loss of electric power supply, the main circulation pumps of the primary and secondary circuits are coasted down. The decrease of rotary speeds of the primary and secondary circuit pumps proceeds according to the free rundown law with corresponding rundown constants, and after the pumps' rundown the forced circulation of sodium through the reactor is stopped completely. Since all absorber rods of the reactor, including the PSS rods, are not inserted into the core, the change of reactor power is determined by the temperature reactivity effects.

Comparison of results of the calculations fulfilled by these two code versions (COREMELT-point model of neutron kinetics and COREMELT-2D-space model of neutron kinetics) is illustrated by Fig. 2. The COREMELT-2D calculations did not account for the changes of radial and axial sizes of the core, in the calculation made by COREMELT the computation of reactivity effect caused by change of the radial reactor core sizes was canceled, but the effects of axial expansion of fuel was taken into account. In this connection a minor difference is observed (Fig. 2a) in the rate of power

decrease at the initial stage of the accident, before the onset of sodium boiling in both calculation cases.

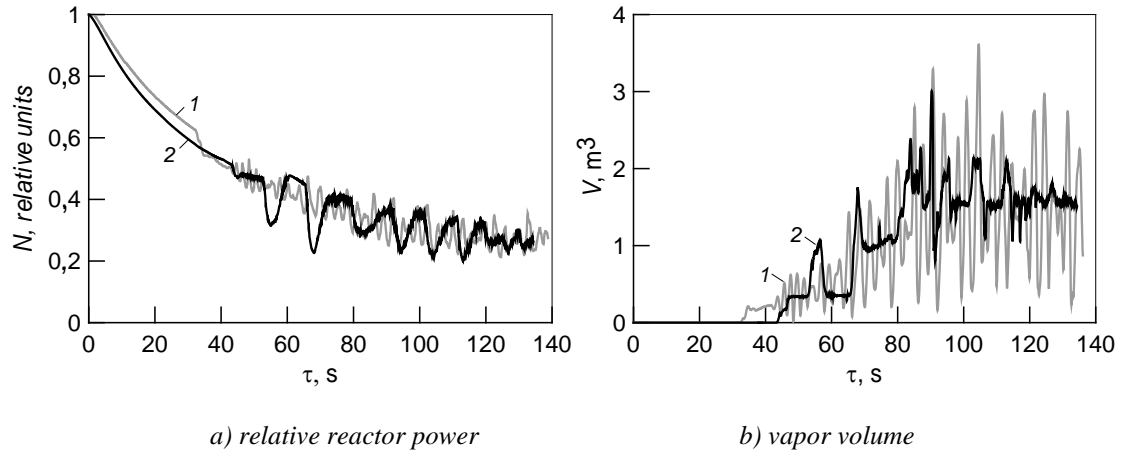*a) relative reactor power*   *b) vapor volume*

FIG. 2. Change of the BN-1200 reactor parameters in the ULOF accident with loss of grid and emergency electric power supplies and simultaneous failure of all reactor shutdown rods, as calculated by the COREMELT-2D (1) and COREMELT (2) codes.

More significant differences in the results appear during the phase of sodium boiling. One of possible explanations of this phenomenon is demonstrated in Figures 3 – 5. Fig. 3 shows the distribution of energy release over the fuel pin's height in different channels at the initial time moment, and Fig. 4 reflects the changes of shape of these distributions relative to the initial distribution at various time moments. It can be seen in the Figures that in the process of coolant heating, a decrease of the energy release at the core outlet takes place (-3%) relative to the initial distribution, and in the bottom part of the core, vice versa, it increases (+1%). The decrease of relative energy release is especially significant in the upper part of the central channels (ch. 3) in the area of vapor bubble (Fig. 4b, time moment 70 s).

At the same time, the change in the energy release profile in radial direction (along the core channels from the center towards periphery) is not so significant. As we can see in Fig. 5, radial distribution of energy release by the core channels relative to the initial distribution varies with time within the range of 1%.

On the whole, results of the calculations by the COREMELT-2D code show that with the removal of sodium from the core channels, a change of the energy release shape is observed, vs. steady-state distribution. This is especially notable in the area of vapor bubbles in the upper part of the boiling channels, where relative energy release is decreasing. In the non-boiling part of channels and in peripheral channels of the core, where no boiling takes place, a minor increase of relative energy release is observed. Presumably, the decrease of boiling intensity at the most hot channels is a consequence of this re-distribution of energy release. As we can see in Fig. 2b, the boiling volume as calculated by COREMELT-2D is nearly the same as in the variant of calculation by the point kinetics model. However, an increased frequence of power oscillations is observed in the process of sodium boiling, which is indicative of an relation of the sodium vaporization dynamics with spatial distribution of energy release in the reactor core.
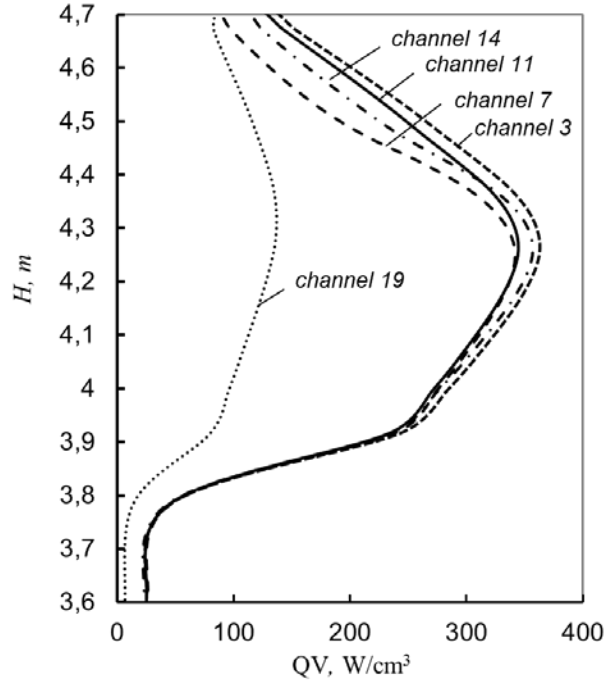
FIG. 3. Distribution of energy release over the channels' height at the initial time moment calculated by COREMELT-2D.
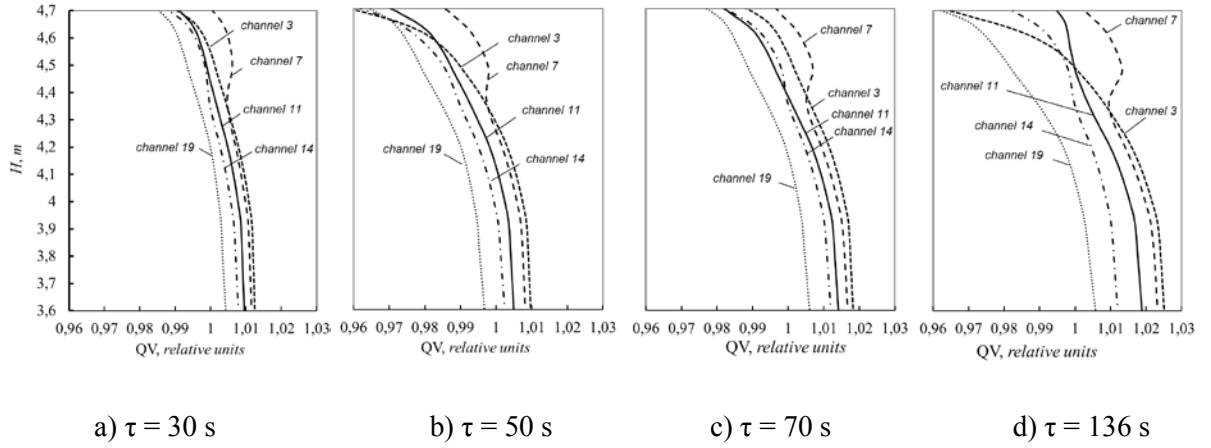

a) τ = 30 s   b) τ = 50 s   c) τ = 70 s   d) τ = 136 s

FIG. 4. Distribution of relative energy release over the channels' height at different time moments as calculated by COREMELT-2D.
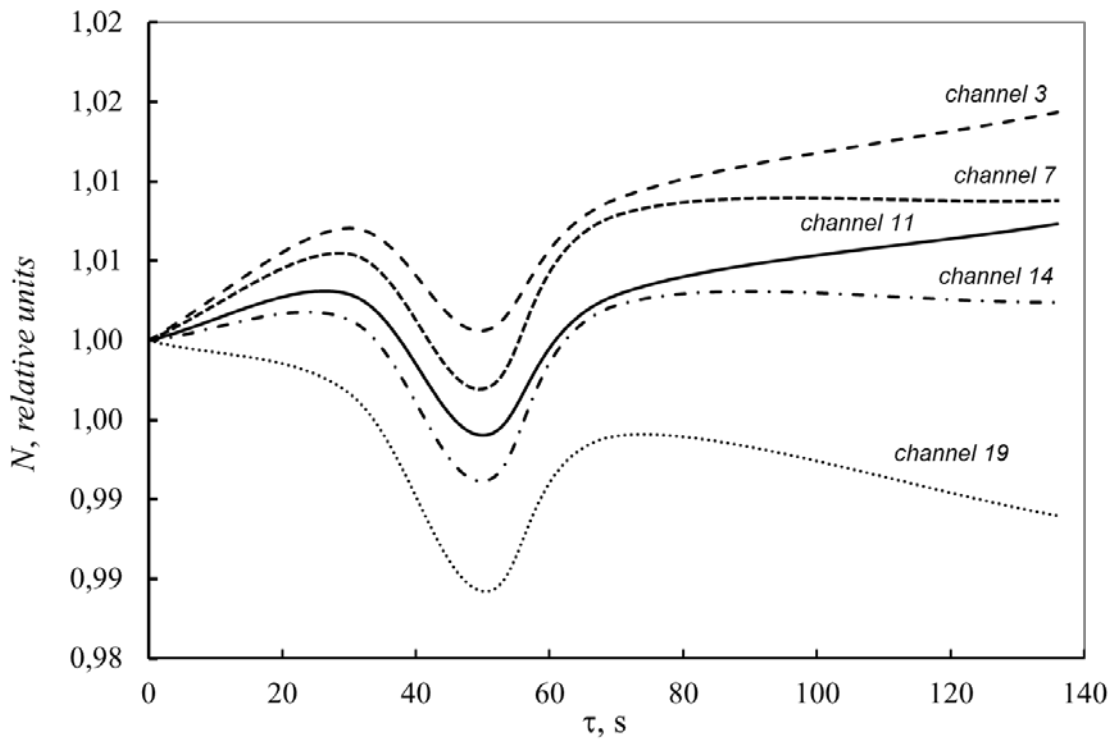
FIG. 5. Change of relative power levels of channels with time, calculated by COREMELT-2D.

5. Conclusion

The results of test calculation of the ULOF accident for the BN-1200 carried out by the COREMELT-2D code complex have been compared with the results of calculation of the same accident obtained earlier by using the COREMELT code version with point model of neutron kinetics. In the general, the results appear to be quite similar for these two codes, however, there have notable differences, caused by the space effects in the neutron kinetics computation, which are arisen during the stage of sodium boiling.

REFERENCES

[1]   POPLAVSKY, V.M., et al., "Studies on Influence of Sodium Void Reactivity Effect on the Concept of the Core and Safety of Advanced Fast Reactor", Journal of Nuclear science and Technology, vol.48, № 4 (2011), pp.538 - 546.

[2]   MANTUROV, G.N., NIKOLAEV, M.N., AND TSIBOULIA, A.M., "ABBN-93 Group Data Library. Part 1: Nuclear Data for the Calculations of Neutron and Photon Radiation Fields," INDC (CCP)-409/L, IAEA (1997), p. 65.

[3]   "Multigroup Constant Set for Calculation of Neutron and Photon Radiation Fields and Functionals, Including the CONSYST2 Program," RSICC DLC-182, ORNL (1995).

Specific Mechanism of Negative Reactivity Feedback

in the Nuclear Burning Wave Reactor

S.P. Fomin[†], O.S. Fomin, Yu.P. Mel'nik, V.V. Pilipenko, N.F. Shul'ga

National Science Center "Kharkov Institute of Physics and Technology", Kharkov, Ukraine

Abstract. The specific mechanism of negative reactivity feedback which is inherent in the innovative fast reactor concept based on the self-sustained regime of nuclear burning wave (NBW) has been studied. This phenomenon has been considered for the case of NBW reactor with metal fuel of the mixed Th–U–Pu cycle and the Pb–Bi coolant. The corresponding calculations have been performed by numerically solving the non-stationary non-linear diffusion equation of neutron transport together with a set of the burn-up equations for fuel components and the equations of nuclear kinetics for the precursor nuclei of delayed neutrons. The temperature effects and heat sink are not taken into account. A notable stability of the NBW regime relative to disturbances of the neutron flux in the system and to possible irregularities of the fuel composition has been shown. This stability is the sequel of the above-mentioned negative reactivity feedback which underlies the intrinsic safety of the NBW reactor.

Keywords: fast reactor, nuclear burning wave, traveling wave reactor, intrinsic safety, negative reactivity feedback, non-stationary diffusion equation

1. INTRODUCTION

Currently, the priority requirement for the development of new concepts of nuclear reactors is to ensure the safety of their operation. One of such promising reactor concepts with a so-called "inherent safety" is a fast reactor that operates in a nuclear burning wave (NBW) regime.

The phenomenon of self-sustained nuclear burning wave (the "neutron-fission wave") in a fast reactor (FR) was discovered and preliminarily studied by Feoktistov [3][4]. The non-linear self-organizing regime of the NBW arises owing to a high conversion ratio from fertile to fissile materials in the FR. The main advantage of this FR type is that it does not require reactivity control and therefore the initial fuel composition of the reactor will evolve according to neutron-nucleus processes without an external intervention and any refueling or fuel shuffling during the entire FR lifetime. In this regime, the FR is automatically sustained in a close-to-critical state.

Further, this concept was developed by several groups of investigators using different approaches and different names for this phenomenon: deflagration wave [15], criticality wave [16], CANDLE [12][13][14], nuclear burning wave [5][6][7][8][9] etc. Lately, the most common name for the concept is the Traveling Wave Reactor due to the TerraPower and Bill Gates activity [10].

To simplify solving the essentially nonlinear non-stationary problem of neutron transport in such a system, Feoktistov [3][4], as well as many authors later (see, e.g., Van Dam, [16]; Sekimoto et al., [12][13]), considered a self-similar solution of this problem. This solution describes only a steady-

---

[†] e-mail: sfomin@kipt.kharkov.ua

state mode in the form of a traveling NBW. This approach does not allow one to investigate the stability of the nuclear burning process in the reactor relative to different external perturbations, as well as to study the behavior of the FR in transient operation modes, such as the reactor start-up, emergency shutting down and restarting, partial coolant loss and so on.

In our previous works [5][6][7][8][9], a deterministic approach for describing the space-time evolution of the self-organizing regime of the NBW in a critical FR has been developed in the framework of multigroup diffusion approximation. This approach is based on solving the non-stationary diffusion equation for neutron transport together with the burn-up equations for the fuel components and the equations of nuclear kinetics for the precursor nuclei of delayed neutrons. This allows us to simulate initiation of the NBW regime and to study its stability relative to distortions of the neutron flux as well as the mechanism of reactivity feedback inherent in this regime. In this approach, a number of studies of the NBW regime behavior were performed for the FR with metal fuel of U-Pu, Th-U and mixed Th-U-Pu cycles with taking into account of typical volume fractions of fuel, constructional material (Fe) and different coolants (Na or Pb-Bi eutectic). These calculations showed, in particular for the metal fuel of U-Pu and mixed Th-U-Pu cycles, a principal possibility of initiating the NBW which then steadily propagates in the breeding zone during a long time period (decades).

In works [5][6][7][8][9], the stability of the NBW regime has been studied in the perturbation of the neutron flux in the system resulting from turning off the external neutron source at the early stages of the NBW initialization. At this stage, the reactor has not yet reached a steady-state mode and has small positive reactivity. So, the damped oscillations of the neutron flux, which are the result of such a perturbation, occur against a background of a slowly increasing neutron flux in this case (see [5][6][7][8][9]).

The paper studies the NBW regime stability at the stage, when the NBW reactor already reaches its steady state with a constant value of the neutron flux in the system and constant value of the NBW propagation velocity. We study the behavior of the NBW reactor in the event of certain external perturbations in the reactor neutron fields and in the event of fuel inhomogeneity in the form of its local initial enrichment by fissile isotopes in the way of the NBW propagation.

2. THE CALCULATION MODEL

We consider a critical FR of the cylindrical form with the metal fuel of Th–U–Pu cycle in which the NBW would propagate along the axial direction. The FR also contains the structural material Fe and the Pb–Bi eutectic coolant.

Following [9], we use an approximate allowance for effects of neutron leakage in the transverse (radial) direction (see, e.g., [7][9]) by using the radial buckling concept [17]. We solve the non-stationary problem under consideration in the so-called effective multigroup approach that was developed by us (see, e.g., [6][7]). In this approach, the non-stationary diffusion equation of neutron transport with allowance for delayed neutrons is written down in the following form:

$$\frac{1}{v}\frac{\partial \Phi}{\partial t} + \frac{\partial V}{\partial z} + DB_r^2\Phi + \Sigma_a\Phi - (1-\overline{\beta})(\nu_f\Sigma_f)\Phi = \sum_l \lambda_l C_l \, , \; V = -D\frac{\partial \Phi}{\partial z} \, , \tag{1}$$

where Φ is the scalar neutron flux; Σ_α, Σ_f are the effective macroscopic absorption and fission cross-sections, and $D = 1/(3\Sigma_{tr})$ is the diffusion coefficient (Σ_{tr} being the effective macroscopic transport cross-section); $\nu_f\Sigma_f = \Sigma_l(\nu_f\sigma_f)_l$, where ν_f is the mean number of neutrons produced at a single nuclear fission event and l is the number of the fissioned nuclide; v is the one-group neutron velocity. In (1), $\beta = \Sigma_l\beta_l(\nu_f\Sigma_f)_l / (\nu_f\Sigma_f)$ is the effective fraction of delayed neutrons, $\lambda_l = \beta_l / \sum_i \beta_l^i \lambda_l^i$ and $\beta_l = \Sigma_l\beta_l^i$; where β_l^i, and λ_l^i are the fraction of delayed neutrons and the decay constant of the precursor nuclei in the i-th group of the l-th fissioned nuclide; C_l is the concentration of the precursor nuclei for the l-th fissioned nuclide in the approximation of one equivalent group of delayed neutrons. The buckling

coefficient is $B_r = 2.405 / (R + \delta_r)$, where δ_r is the extrapolation length. We take $\delta_r = 20$ cm, which corresponds to the case of a thick radial reflector of a heavy material (U, Pb) [17]. The boundary conditions for the flux Φ at the FR ends ($z = 0$ and $z = L$) are: $\left(\Phi + 2V\right)\big|_{z=0} = 2 j_{ex}$, $\left(\Phi - 2V\right)\big|_{z=L} = 0$ (where, j_{ex} is the external neutron flux that initiates the NBW regime and is turned off at a certain time moment at the initial stage of FR operation). Here, we do not consider this initial stage of the NBW reactor operation which was studied in [9], and focus on the effects of the negative reactivity feedback at the stage of steady NBW propagation.

During the FR campaign, the fuel composition in the FR changes with time according to the nuclear transformation chains characteristic of this fuel cycle. For the FR with the mixed Th–U–Pu fuel cycle we involve in the calculations two main nuclear transformation chains, which start from the fertile nuclides ^{238}U and ^{232}Th. Each of these two chains under consideration includes 10 nuclides: $1 - {}^{238}$U, $2 - {}^{239}$U, $3 - {}^{239}$Np, $4 - {}^{239}$Pu, $5 - {}^{240}$Pu, $6 - {}^{241}$Pu, $7 - {}^{242}$Pu, $8 - {}^{243}$Am, $9 - {}^{241}$Am, $10 - FP_U$ (fission products for the U-Pu cycle), and $11 - {}^{232}$Th, $12 - {}^{233}$Th, $13 - {}^{233}$Pa, $14 - {}^{233}$U, $15 - {}^{234}$U, $16 - {}^{235}$U, $17 - {}^{236}$U, $18 - {}^{237}$U, $19 - {}^{237}$Np, $20 - FP_{Th}$ (fission products for the Th-U cycle).

The fission process is considered for six nuclides with numbers 1, 3, 4, 5, 6, 7 for the U-Pu cycle and for seven nuclides numbered 1, 3, 4, 5, 6, 7, 9 for the Th-U cycle. Fission products produced during nuclear fission are considered in the calculation as a single nuclide for each cycle and are denoted by FP$_U$ and FP$_{Th}$ for U-Pu and Th-U cycle respectively as they differ from each other. Note that in our previous calculations [7][9] we neglected intermediate nuclides ^{239}Np and ^{233}Pa burn-up. However this can be noticeable at large values of the neutron flux, especially for ^{233}Pa (Th-U chain) because of greater value of its β-decay half life period.

The fuel nuclide production and burn-up processes are described by the following equations for the nuclide concentrations N_l of the U-Pu transformation chain:

$$\frac{\partial N_1}{\partial t} = -\sigma_{a1}\Phi N_1, \tag{2}$$

$$\frac{\partial N_l}{\partial t} = -\left(\sigma_{al}\Phi + \Lambda_l\right)N_l + \left(\sigma_{c(l-1)}\Phi + \Lambda_{(l-1)}\right)N_{(l-1)} + \sigma_{c3}\Phi N_3 \delta_{l,5}, \quad (l = 2 \div 8) \tag{3}$$

$$\frac{\partial N_9}{\partial t} = \Lambda_6 N_6, \tag{4}$$

$$\frac{\partial N_{10}}{\partial t} = \sum_{l=1,3\div7} \sigma_{fl} N_l \Phi, \tag{5}$$

and the for Th-U transformation chain:

$$\frac{\partial N_{11}}{\partial t} = -\sigma_{a11}\Phi N_{11}, \tag{6}$$

$$\frac{\partial N_l}{\partial t} = -\left(\sigma_{al}\Phi + \Lambda_l\right)N_l + \left(\sigma_{c(l-1)}\Phi + \Lambda_{(l-1)}\right)N_{(l-1)} + \sigma_{c13}\Phi N_{13}\delta_{l,15}, \quad (l = 12 \div 19), \tag{7}$$

$$\frac{\partial N_{20}}{\partial t} = \sum_{l=11,13\div17,19} \sigma_{fl}\Phi N_l, \tag{8}$$

where $\sigma_{al} = \sigma_{cl} + \sigma_{fl}$, σ_{cl}, σ_{fl} are the effective one-group microscopic cross sections of absorption, radiation neutron capture and fission of the l-th nuclide; $\Lambda_l = \ln 2 / T_{1/2}^l$ and $T_{1/2}^l$ are the β-decay constant and the β-decay half-life period. Only Λ_2, Λ_3, Λ_6 and Λ_{12}, Λ_{13}, Λ_{16} are considered as nonzero β-decay constants. For simplicity, we also assume that after neutron capture ^{242}Pu instantly transforms into ^{243}Am and neglect the intermediate nuclide ^{243}Pu. At the initial time moment, certain initial concentrations of these nuclides are chosen $N_l(t=0) = N_{0l}$, $(l = 1 \div 20)$.

We neglect the burn-up of nuclei ^{239}U, ^{241}Am, ^{243}Am ($\sigma_{a2} = \sigma_{a8} = \sigma_{a9} = 0$), as well as the burn-up of ^{233}Th and ^{237}U ($\sigma_{a12} = \sigma_{a18} = 0$) and neutron radioactive capture by ^{237}Np ($\sigma_{c19} = 0$), since the decrease in their concentrations due to these reactions is small in comparison with the processes considered. The changes of FP$_U$ and FP$_{Th}$ due to the neutron absorption are also omitted.

Burn-up equations (2)-(5) and (6)-(8) can be solved by putting effective one-group cross sections and the neutron flux value to constant on each time step τ of the calculation grid, and analytical formulas for the nuclide concentrations can be found at the next time layer $n + 1$ to each node of the spatial grid. Thus, for the U-Pu chain we obtain:

$$N_l^{n+1} = \sum_{m=1}^{l} Z_{lm}^n \exp(-\sigma_{am}^n \Phi^n \tau), \tag{9}$$

$$Z_{lm}^n = \frac{\sigma_{c(l-1)}^n}{\sigma_{al}^n - \sigma_{am}^n} Z_{(l-1)m}^n + \frac{\sigma_{c3}^n}{\sigma_{a5}^n - \sigma_{am}^n} Z_{3m}^n \delta_{l,5} \left(1 - \delta_{m,4}\right), \quad Z_{ll}^n = N_l^n - \sum_{m=1}^{l-1} Z_{lm}^n, \quad (l = 1 \div 8), \tag{10}$$

$$N_9^{n+1} = N_9^n + \frac{\Lambda_6}{\Phi} Q_6^n, \quad N_{10}^{n+1} = N_{10}^n + \sum_{l=1,4\div7} \sigma_{fl}^n Q_l^n, \tag{11}$$

$$Z_{1,1}^n = N_1^n, \quad Q_l^n = \sum_{m=1}^{l} \frac{Z_{lm}^n}{\sigma_{am}^n} \left[1 - \exp(-\sigma_{am}^n \Phi^n \tau)\right]. \tag{12}$$

where: $\sigma_{a2}^n = \sigma_{c2}^n = \Lambda_2 / \Phi^n$, $\sigma_{a3}^n = \sigma_{c3}^n + \sigma_{f3}^n + \Lambda_3 / \Phi^n$, $\sigma_{a6}^n = \sigma_{c6}^n + \sigma_{f6}^n + \Lambda_6 / \Phi^n$; and for Th-U cycle we have:

$$N_l^{n+1} = \sum_{m=11}^{l} Z_{lm}^n \exp(-\sigma_{am}^n \Phi^n \tau), \tag{13}$$

$$Z_{lm}^n = \frac{\sigma_{c(l-1)}^n}{\sigma_{al}^n - \sigma_{am}^n} Z_{(l-1)m}^n + \frac{\sigma_{c3}^n}{\sigma_{a5}^n - \sigma_{am}^n} Z_{3m}^n \delta_{l,15} \left(1 - \delta_{m,14}\right), \quad Z_{ll}^n = N_l^n - \sum_{m=11}^{l-1} Z_{lm}^n \quad (l = 11 \div 19), \tag{14}$$

$$N_{20}^{n+1} = N_{20}^n + \sum_{l=11,13\div17,19} \sigma_{fl}^n Q_l^n, \tag{15}$$

$$Z_{11,11}^n = N_{11}^n, \quad Q_l^n = \sum_{m=11}^{l} \frac{Z_{lm}^n}{\sigma_{am}^n} \left[1 - \exp(-\sigma_{am}^n \Phi^n \tau)\right], \tag{16}$$

where: $\sigma_{a12}^n = \sigma_{c12}^n = \Lambda_{12} / \Phi^n$, $\sigma_{a13}^n = \sigma_{c13}^n + \sigma_{f13}^n + \Lambda_{13} / \Phi^n$, $\sigma_{a18}^n = \sigma_{c18}^n = \Lambda_{18} / \Phi^n$. These analytical expressions for the nuclide concentrations are used in the numerical calculations of the nonstationary problem of the nuclear burning wave regime evolution.

The concentrations of the nuclides included into these transformation chains obey the corresponding sets of burn-up equations, which are described in detail together with the method of their solving in [9]. Since the neutron flux Φ only weakly changes during the decay time of the precursors of delayed neutrons, we describe their concentrations C_l using the kinetics equations in the approximation of one equivalent group of delayed neutrons. The method of solving these equations is analogous to that described in [5].

The diffusion equation (1) is solved numerically using the conservative finite difference method (see, e.g., [11]) and the implicit difference scheme by Crank and Nicolson [2] with a variable time step, as is described in our previous works [5][6][7][8][9]. In the effective multigroup approach, at each time layer we also solve a multigroup stationary criticality problem for the current assembly composition changing with time according to the equations of fuel component burn-up, which is also considered using the radial buckling concept. These calculations are performed in the 26-group approximation, using the group neutron constant library [1]. The found group neutron fluxes are used to calculate the effective one-group microscopic cross-sections in (1) that are corrected at each time step according to the neutron spectrum at each space mesh node. Note that here we do not consider the temperature effects. As for the possible influence of the Dopler reactivity effect due to the neutron capture cross section changes with temperature can be thought to be not very essential for the FR with the metal fuel [11].

3. SIMULATION OF THE NEGATIVE REACTIVITY FEEDBACK EFFECTS

On basis of the above-outlined approach to the simulation of the processes in the FR with a fuel of the mixed Th-U-Pu cycle, we have carried out a series of calculations of the space-time evolution of the NBW regime for different variants of the reactor parameters, which correspond to different compositions and geometrical dimensions of the initial critical FR assembly. In this way, we have performed studies aimed to optimize parameters of the initial FR assembly in order to ensure values of the neutron flux, energy production density and nuclear burning wave velocity that would be acceptable from the practical point of view. As a result of considering a variety of the initial FR assemblies, we have found a number of composition options of the FR with mixed Th-U-Pu fuel cycle that are the most attractive in our view. Below, to illustrate the character of the obtained results, we present some of them. Specifically, here we will show the results for the FR composition with the following parameters: the fuel volume fraction $F_{fuel} = 55$ %, the fuel void fraction $p = 0.2$, the constructional material and coolant volume fractions $F_{Fe} = 15$ % and $F_{cool} = 30$ %, the volume fraction of ^{232}Th in the fuel in the breeding zone $F_{Th} = 62\%$. Note that this value of F_{Th} corresponds to nearly equal concentrations of ^{238}U and ^{232}Th nuclides in the fuel of the breeding zone. In the initial critical FR assembly, we assume that the enrichment level of the uranium fuel in the ignition zone is 10% (here, plutonium isotope content is ^{239}Pu : ^{240}Pu : ^{241}Pu : ^{242}Pu = 0.70 : 0.22 : 0.05 : 0.03). The reactor length is $L = 500$ cm.

In Fig. 1, we present the axial profiles of the neutron flux and main fuel components at different time moments of the reactor cycle in the FR with the cylinder radius $R = 230$ cm and the initial ignition zone size $L_{ig} = 47.8$ cm. This figure shows the process of initiation and propagation of the NBW in the FR under consideration. This option is characterized by a long-term reactor campaign (about 50 years) and the stable NBW regime with values of the neutron flux, total energy production (4.5 GW) and NBW velocity (about 6.5 cm/year). In Fig. 2, we compare the time dependences of the NBW velocity and total power production, and the axial profiles of the final neutron fluence for three options of the FR geometry with different radii and ignition zone size: $R = 215$ cm and $L_{ig} = 48.0$ cm; $R = 230$ cm and $L_{ig} = 47.8$ cm; $R = 250$ cm and $L_{ig} = 47.6$ cm. At the stationary stage of NBW its velocity values for these variants are 1.9, 6.5, and 10.4 cm/year, respectively, and the total FR power is 1.2, 4.5, and 8.5 GW at the energy production density at the NBW front of 160, 440, and 890 W/cm^3, respectively.

We started the study of stability of the NBW regime by simulation of the reactor behavior in the case when the breeding zone contains the axial area, in which the fuel is enriched by isotope ^{235}U. As an example, Fig. 3 shows the results of such calculations for the FR with $F_{Th} = 62\%$ (this corresponds to nearly equal concentrations of ^{238}U and ^{232}Th nuclides in the fuel of the breeding zone), R = 230 cm,

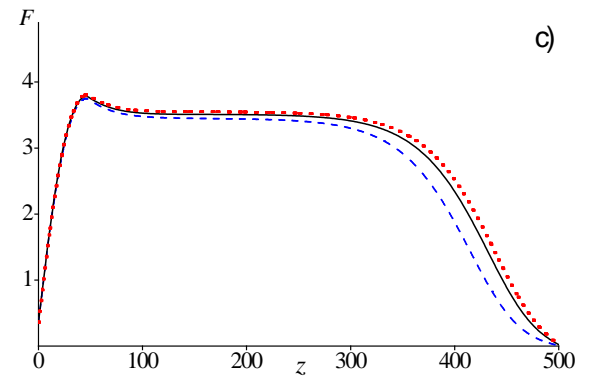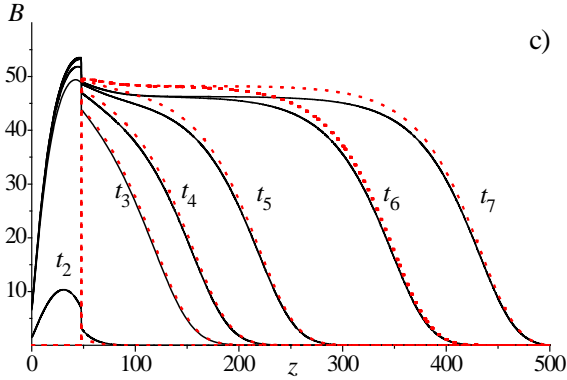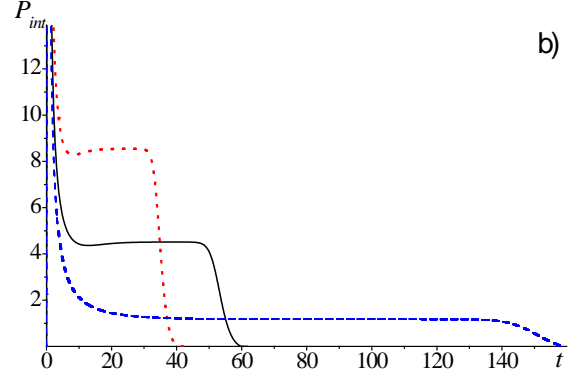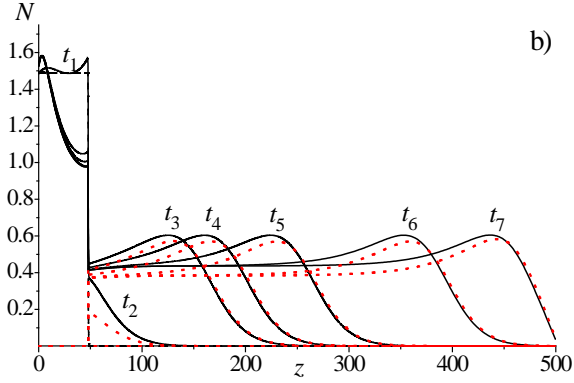when the enriched zone is located at z = 300 ÷ 320 cm, and for two cases of uranium enrichment: 5% and 10%.

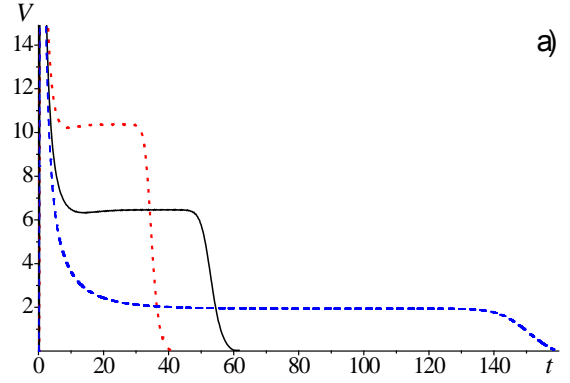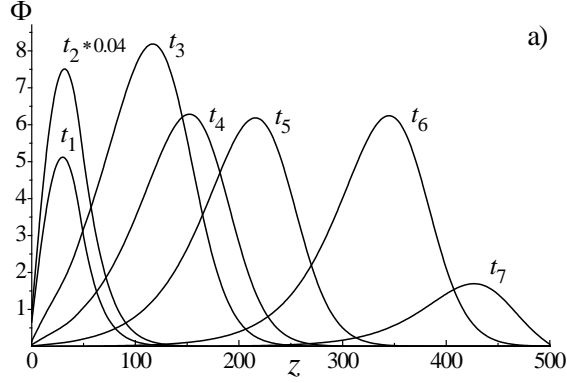Fig.1. (a) The scalar neutron flux Φ ($\times 10^{15}$ cm^{-2} s^{-1}); (b) the concentration N ($\times 10^{21}$ cm^{-3}) for ^{239}Pu (solid curves) and ^{233}U (dots); (c) the fuel burn-up depth B (%) of the U–Pu (solid curves) and Th–U (dots) fuel components versus z (cm) at time moments: $t_1 = 3$, $t_2 = 100$ days, $t_3 = 5$, $t_4 = 10$, $t_5 = 20$, $t_6 = 40$, and $t_7 = 55$ years. The FR radius is $R = 230$ cm.

Fig. 2. (a) The NBW velocity V (cm/year); (b) the total FR power P_{tot} (GW) via time t (years); (c) the neutron fluence F ($\times 10^{24}$ cm^{-2}) for the whole reactor campaign versus z (cm). Dots are for the FR radius $R = 250$ cm, solid curves are for $R = 230$ cm, dashed curves are for $R = 215$ cm.

These results show that at the NBW approaching the area with enriched uranium, the neutron flux and the wave velocity are gradually increased. Accordingly, the reactor power increases significantly too.

Irregularity in velocity V behavior near its peak is apparently due to the fact that at the passage of enriched area, there is distortion of the axial shape of the neutron flux. This means that the definition of the NBW velocity using the position of the neutron flux maximum is not quite accurate. The value of the observed disturbance of the NBW regime strongly depends on the degree of the uranium enrichment. After passing the enriched area, the reactor returns to the previous regime of the NBW propagation with the same parameters as before passing.
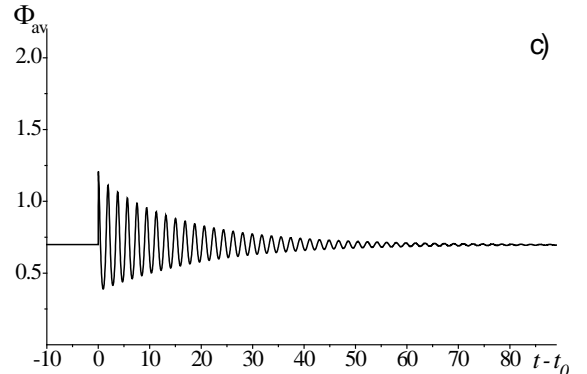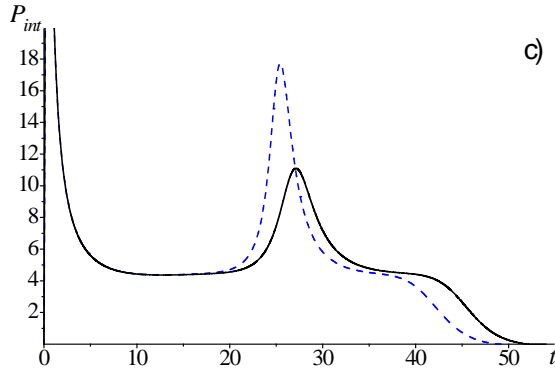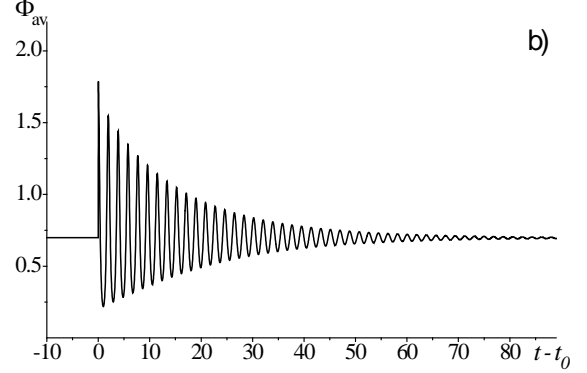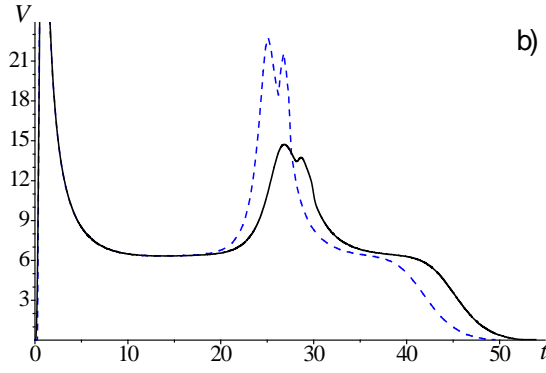

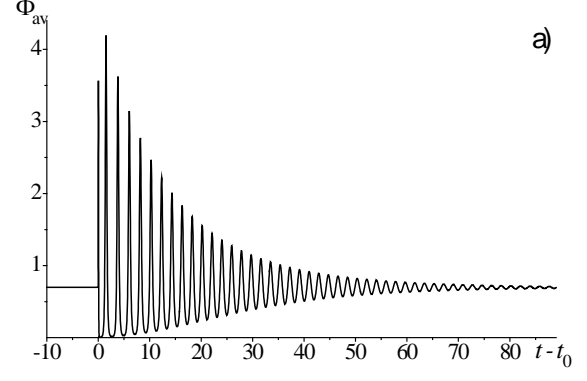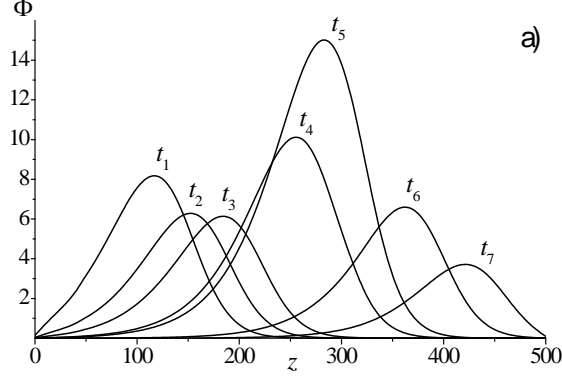Fig. 3. The NBW FR behavior in the case of presence of a uranium layer enriched with ^{235}U at $z = 300 \div 320$ cm. (*a*) The neutron flux Φ ($\times 10^{15}$ см$^{-2}$ с$^{-1}$) for time moments $t_1 = 5$, $t_2 = 10$, $t_3 = 15$, $t_4 = 25$, $t_5 = 27$, $t_6 = 35$, and $t_7 = 45$ years. (*b*) The NBW velocity V (cm/year) and (c) the total FR power P_{int} (GW) versus time t (years). The uranium enrichment is 5% (solid curves) and 10% (dashes).

Fig. 4. The perturbation of volume-average neutron flux Φ_{av} ($\times 10^{15}$ см$^{-2}$ с$^{-1}$) in the NBW FR caused by an external neutron source versus time t (days). The source with intensity $Q_{ex} = 2 \cdot 10^{11}$ (cm^{-3} s^{-1}) starts at $t_0 = 3650$ days, lasts for one hour and is situated at (*a*) $160 < z < 170$ cm, (*b*) $200 < z < 210$ cm, and (*c*) $55 < z < 65$ cm.

Then we carried out a study of the NBW stability relative to the disturbance of the neutron field in the reactor at the stationary stage of the NBW propagation, for example, after ten years from its start. For this purpose, we calculated the behavior of FR in the case of NBW reactor core irradiation by a volumetric neutron source, which operates at a constant intensity during short time (about one hour), and then turns off.

Consideration was given to different cases with varying intensity of such an "external" neutron sources Q_{ex} and its various axial position relative to the NBW front, located at $z = 160$ cm at the moment when the external neutron flux was turned on ($t_0 = 3650$ days). We do not explain the physical nature of the neutron source, and just use such a simple model for simulation of a very powerful sudden external disturbance of the neutron flux in FR. The behavior of the volume-averaged neutron flux in FR with respect to such perturbations in different cases is shown in Fig. 4. This figure shows that the effect of this perturbation depends on the intensity of the source and its axial location. In most cases, as shown in Fig. 4, this perturbation causes severe neutron flux oscillations in FR, which are quickly extinguished by the NBW reactor itself. Increasing the intensity of the neutron source and its approach to the wave front position increases the amplitude of these oscillations, although their period remains unchanged and roughly corresponds to the period of ^{239}Pu production in the fuel U-Pu cycle (about 2 days).

In Fig. 5 we analyze the initial stage of the neutron flux perturbation shown in Fig. 4a in more detail. In order to clarify the mechanism of the negative reactivity feedback, besides the behavior of the neutron flux Φ_{av} averaged over the FR volume, we also present the accompanying variations of the volume-averaged concentrations of the main fissile nuclides ^{239}Pu (N_{Pu}) and ^{233}U (N_U) and main intermediate nuclides ^{239}Np (N_{Np}) and ^{233}Pa (N_{Pa}). For convenience of comparing variations of the volume-averaged concentrations of these nuclides, we have subtracted the difference $N_{Pa} - N_{Np} = 53.1 \cdot 10^{17}$ cm^{-3} in the stationary-wave state ($t = t_0 - 1$) from the current ^{233}Pa concentration $\delta N_{Pa} = N_{Pa} - 53.1 \cdot 10^{17}$ cm^{-3}. This makes it evident that the variations of the concentrations of two intermediate nuclides during the perturbation practically coincide. One can see that the curves for the concentrations of main fissile nuclides ^{239}Pu and ^{233}U also are very close to each other (from N_{Pu} and N_U, we subtract their values a day before the neutron source turning on $\Delta N_{Pu}(t) = N_{Pu}(t) - N_{Pu}(t_0 - 1)$ and $\Delta N_U(t) = N_U(t) - N_U(t_0 - 1)$).
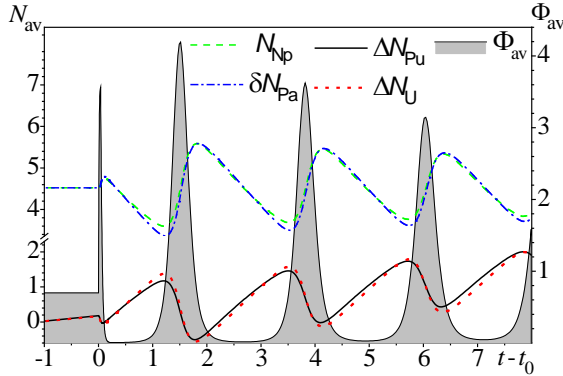
Fig. 5. Evolution of the volume-averaged neutron flux Φ_{av} ($\times 10^{15}$ см$^{-2}$ с$^{-1}$) and concentrations N_{av} ($\times 10^{17}$ cm^{-3}) of the main fissile and intermediate nuclides in the fuel of mixed Th–U–Pu cycle with time t (days) at the initial stage of the neutron flux perturbation shown in Fig. 4a. The values ^{239}Np, δN_{Np}, ΔN_{Pu} and $\Delta N_U(t)$ are described in the text.
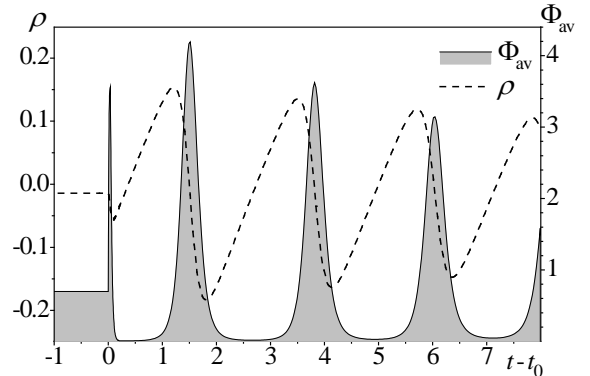
Fig. 6. Variation of the reactivity ρ (dollars) with time t (days) along the variation of the volume-averaged neutron flux Φ_{av} ($\times 10^{15}$ см$^{-2}$ с$^{-1}$) at the initial stage of perturbation shown in Fig. 5.

Fig. 5 shows that the oscillations of the quantities under consideration are completely correlated. The oscillations of concentrations of the fissile nuclides ^{239}Pu and ^{233}U are governed by the variation of the

neutron flux with the same period $\tau \approx 2$ days. When the flux increases (first, due to the action of the external neutron source), their concentrations fall down because of the intensive burning out by neutrons, which brings the FR to a subcritical state and subsequently leads to a quickly decreasing neutron flux. On the contrary, the concentrations of intermediate nuclides ^{239}Np and ^{233}Pa increase with the neutron flux, but when the flux strongly decreases, their concentrations begin to fall down due to the β-decay. This β-decay, in its turn, increases the concentrations of the fissile nuclides ^{239}Pu and ^{233}U, which brings the FR to an supercritical state together with the subsequent increase of the neutron flux in the system. Due to the above-considered processes, the concentrations of the intermediate and fissile nuclides oscillate in antiphase with each other.

This value of τ is close to the half-life of ^{239}Np (≈ 2.34 days), which is an intermediate nuclides in the U-Pu cycle, and an order of magnitude different from the half-life of ^{233}Pa (≈ 27 days), which is an intermediate nuclides in the Th-U cycle. While it may give the impression that ^{239}Np is responsible for the neutron flux oscillations and the stabilization of the NBW regime in the reactor with mixed thorium-uranium fuel, it is not true. ^{233}Pa actually has a greater half-life period than ^{239}Np, however due to this fact, its concentration in the core is about ten times higher than ^{239}Np at the equal value of initial concentrations of the corresponding fertile material. As a result we get approximately equal amounts of the fissile nuclides, ^{239}Pu and ^{233}U (see Fig. 5). So, both intermediate nuclides, ^{239}Np and ^{233}Pa, plays the equivalent role in the NBW stabilizing process.

The described correlated processes are repeated many times with gradually decreasing amplitude of oscillations until the FR damps these oscillations by itself and finally reaches the critical state. The above-discussed alternation of the subcritical and supercritical states of the FR is also illustrated in Fig. 6 which shows the self-consistent variation of the reactivity and the volume-averaged neutron flux caused by the negative reactivity feedback.

Thus, here we have considered different types of distortions of the self-sustained regime in the NBW reactor and showed its outstanding stability. We deliberately used an unrealistically powerful external perturbation of the neutron flux to demonstrate high efficiency of the negative reactivity feedback mechanism, which ensures stability of the NBW regime.

4. CONCLUSION

The analysis of the stability of the NBW regime in FR with mixed Th-U fuel relative to the neutron flux perturbation in the reactor has shown that instantaneous reduction or increase of the neutron flux in the NBW reactor caused by external factors leads to neutron flux oscillations in the reactor. These oscillations are quickly damped down by the reactor itself without any external action. The period of the oscillations is $\tau \approx 2$ days.

There also was studied the stability of the NBW regime relative to the possible non-homogeneity of the fuel in the breeding zone, for example, due to a certain enrichment of the fuel by fissile isotopes. It was shown that when the NBW passes through such an area with the axial size of 20 cm, in which the fuel is enriched to 5% of ^{235}U, the reactor power slowly increases by the factor of two during about 5 years. After passing this area the wave reactor automatically slowly returns to the power production level, which existed prior to the passage of the enriched fuel area in the breeding zone.

Thus, the calculations show remarkable stability of the NBW regime regarding perturbations of the neutron flux and possible non-homogeneity of the fuel. This stability is a manifestation of the specific negative reactivity feedback inherent in the NBW regime. The physical background of this negative feedback mechanism is a significant delay in fissile nuclide production due to beta decay of intermediate nuclides (^{239}Np for the U-Pu cycle and ^{233}Pa for the Th-U cycle) at the neutron flux perturbations.

ACKNOWLEDGEMENTS

REFERENCES

[1]   Bondarenko, I.I., et al., "Group Constants for Nuclear Reactor Calculations" Consultants Bureau Inc., New York (1964).

[2]   Crank, J., Nicolson, P., A practical method for numerical evaluation of solutions of partial differential equations of the heat-conduction type. Proc. Camb. Phil. Soc. 43, (1947) 50–67.

[3]   Feoktistov, L.P., An analysis of a concept of a physically safe reactor. Preprint IAE-4605/4. IAE, Moscow, USSR (1988) (in Russian).

[4]   Feoktistov, L.P., Neutron-induced fission wave. Sov. Phys. Doklady 34, (1989) 1071–1073.

[5]   Fomin, S.P., Mel′nik, Yu.P., Pilipenko, V.V., Shul′ga, N.F., Investigation of self-organization of the non-linear nuclear burning regime in fast neutron reactors. Ann. Nucl. Energy 32, (2005) 1435–1456.

[6]   Fomin, S.P., Mel′nik, Yu.P., Pilipenko, V.V., Shul′ga, N.F., Fast reactor based on the self-sustained regime of nuclear burning wave. In: Cechák, T., et al. (Eds.), Nuclear Science and Safety in Europe. Springer, the Netherlands (2006) 239–251.

[7]   Fomin, S.P., Mel′nik, Yu.P., Pilipenko, V.V., Shul′ga, N.F., Initiation and propagation of nuclear burning wave in fast reactor. Prog. Nucl. Energy 50, (2008) 163–169.

[8]   Fomin, S.P., Fomin, A.S., Mel′nik, Yu.P., Pilipenko, V.V., Shul′ga, N.F., Safe Fast Reactor Based on the Self-Sustained Regime of Nuclear Burning Wave. In CD: Proc. of 1st Int. Conf. "Global 2009", Paris, France (2009) Paper 9456.

[9]   Fomin, S.P., Fomin, O.S., Mel′nik, Yu.P., Pilipenko, V.V., Shul′ga, N.F., Nuclear burning wave in fast reactor with mixed Th-U fuel. Prog. Nucl. Energy 53, (2011) 800–805.

[10]   Gates, Bill, Innovating to zero! Technology, Entertainment, Design (TED), February 12. (2010) http://www.ted.com/talks/bill_gates.html

[11]   Potter, D., Computational Physics. John Wiley & Sons, London - New York - Sydney - Toronto (1973).

[12]   Sekimoto, H., Ryu, K., Yoshimura, Y., CANDLE: the New Burnup Strategy. Nucl. Sci. Engin. 139, (2001) 306–317.

[13]   Sekimoto, H., A Light of CANDLE: New Burnup Strategy. Institute of Technology, Tokyo (2005).

[14]   Sekimoto, H., Miyashita, S., Startup of "Candle" burnup in fast reactor from enriched uranium core. Energy Conv. Manag. 47, (2006) 2772–2780.

[15]   Teller, E., Nuclear Energy for the Third Millennium. Preprint UCRL-JC-129547, LLNL, Livermore, CA, USA (1997).

[16]   Van Dam, H., Self-stabilizing criticality waves. Ann. Nucl. Energy 27, (2000) 1505–1521.

[17]   Waltar, A.E., Reynolds, A.B., Fast Breeder Reactors. Pergamon Press, New York (1981).

Safety features of a power unit with the BREST-OD-300 reactor

Ye.O. Adamov, V.V. Lemekhov, A.V. Lopatkin, V.V. Orlov, V.S. Smirnov, V.V. Tyukov,
A.A. Umanskiy, G.A. Khacheresov, N.G. Chernetsov
Joint Stock Company "N.A. Dollezhal Research and Development Institute of Power
Engineering" (NIKIET), Moscow, Russia

The major requirement to the radiation safety of a new-generation fast reactor in conditions of large-scale NP is that it should exclude severe accidents (fast uncontrolled power growth, loss of coolant and heat removal, fires, and explosions) involving radioactive and toxic emissions that require evacuation and relocation of the public.

A new approach to the selection of principal designs has been employed to ensure safety and remove the contradictions between the safety and cost-effectiveness requirements in the development of new-generation fast reactors. It consists in a progressive implementation of the of the principle of natural (or intrinsic) safety achieved, for the most part, via feedbacks, natural dependencies, the neutron balance in fast reactors, and the inherent physical and chemical behaviors and properties of fuel, coolant and other reactor components.

Two classes of the most severe accidents (with an uncontrolled power growth and with the loss of heat removal) are therefore intrinsically excluded only thanks to the natural regularities of the chain reaction progression in fast reactors, the properties and features of lead and fuel, the major BREST components, and the designs that contribute to their implementation. So it is this approach to addressing the BREST reactor safety in extremely severe accidents that reflects the essence of the ***natural safety*** of this reactor.

The calculation results for the severe scenarios of accidents progression caused by the most hazardous initial events such as positive reactivity insertion up to its full margin (UTOP) and loss of forced coolant circulation without scram (ULOF) will be presented in this paper.

Introduction

Large-scale nuclear power based on innovative fast reactors and their closed nuclear fuel cycle (CNFC) can stop the growth in fossil fuel consumption, take on most of the increase in electricity generation, and offer solutions to problems involved in long-term energy supply for ensuring the sustainable development of the human race, nuclear weapons nonproliferation and rehabilitation of the environment on out planet. Still, nuclear power of such a scale will turn out to be socially acceptable only through excluding the potentiality of severe accidents (power runaway, loss of coolant and heat removal, fires and explosions) with a radioactivity and toxicity release leading to evacuation of the population and formation of exclusion zones, while proving itself to be economically competitive to alternative energy sources. Meeting these requirements will eliminate the limits on the scale of nuclear power development.

It is a common knowledge that high cost of current nuclear power plants is defined primarily by the price of their safety. A novel approach to selection of fundamental technological solutions has been found for overcoming the contradictions between the safety requirements and economic efficiency in the design of new-generation fast reactors. It suggests consistent implementation of the principle of natural (or intrinsic) safety achieved, for the most part, via feedbacks, natural dependencies, the neutron balance in fast reactors, and the inherent physical and chemical behaviors and properties of fuel, coolant and other reactor components rather than thanks to building up expensive engineered barriers and complicated safety systems.

Also important are designs that contribute to the natural safety features of fast reactors being realized as fully as they can be.

An analysis shows that the BREST-OD-300, a pilot demonstration fast reactor with a nitride fuel, a heavy liquid-metal lead coolant and its own CNFC, is the most attractive choice in the range of innovative naturally safe reactor technologies under consideration worldwide.

The BREST reactor was conceived in Russia more than twenty five years ago as the result of the efforts to find a compromise between the growing need for the safety of developing nuclear power and the requirement for its economic efficiency.

1. Design features and characteristics of the naturally safe fast reactor

The development and construction of the BREST-OD-300 reactor is included in the framework of tasks in the "Development Strategy of Nuclear Power in Russia in the First Half of the 21st Century" approved by the Russian Government in 2000, the Federal Target Program "Nuclear Power Technologies of a New Generation for the Period of 2010-2015 and Up to the Year 2020" approved by the Russian Government in 2010, and the "Proryv" Project (2011) that integrates projects on the strategic solution of target tasks in the creation of natural-safety nuclear power technologies based on fast-neutron reactors and a closed nuclear fuel cycle.

The BREST-OD-300 reactor is a pilot demonstration fast reactor of the thermal/electric power 700/300 MW. It includes two heat removal circuits with a subcritical water-steam mixture used as the secondary circuit fluid. The BREST-OD-300 is also viewed as a prototype of future commercial BREST-type reactors for large-scale naturally safe nuclear power. Therefore, the reactor's major designs and performance data, including the BREST-OD-300 power choice, have been targeted not only to demonstrate, through its pilot operation, that this reactor technology is naturally safe and is capable to operate in an equilibrium fuel mode, but also given the requirement for having its key designs continued in future large BREST-type reactors.

1.1 Rationale behind the choice of lead coolant and nitride fuel

The natural safety requirement has been the most important thing to dictate the need for a heavy liquid-metal lead coolant and a dense heat-conducting nitride fuel to be chosen for the reactor concept.

The use in integral design of the BREST reactor of a high-boiling (~2000 K), radiation-resistant, low-activated coolant, which is inert when contacting water and air, does not require high pressure in the primary circuit, and excludes the potentiality of accidents with a loss of coolant and heat removal, fires and explosions in a contact with the environment (water and air).

The use of a dense (γ=14.3 g/cm^3), heat-conducting ($\lambda\approx$20 W/(m·deg.)) nitride fuel, which is compatible with the lead coolant and the fuel cladding steel, permits operation with relatively low working temperatures of the fuel (T<1000°C), small thermal energy store, small release of fission gases from the fuel and their low pressure on the fuel cladding, which contributes to keeping it intact.

In a combination, the properties of the heavy lead coolant and the highly heat-conducting, dense nitride fuel provide conditions for a moderate power of complete plutonium breeding (a core breeding factor of ≥1) to be achieved in the core, which, along with a minor fuel temperature power effect, results in a small total reactivity margin (Table 1) and enables power operation with a small operating reactivity margin (Figure 1) which is lower than effective delayed neutron fraction (β_{eff}) that rules out prompt-neutron reactor power excursions.

Table 1 – Values of reactivity effects in the BREST-OD-300 reactor with (U-Pu)N fuel

Reactivity effect	Value, $\Delta(1/K_{eff})$
Power effect when changing over from N=0 to N=N$_{nom}$	$-4.4 \cdot 10^{-3} / (1.2 \cdot \beta_{eff})$
Power effect when changing over from N=0.3·N$_{nom}$ to N=N$_{nom}$	$-2.2 \cdot 10^{-3} / (0.6 \cdot \beta_{eff})$
Neptunium effect	$-0.7 \cdot 10^{-3} / (0.2 \cdot \beta_{eff})$
Full effect when ascending to N=N$_{nom}$	$-5.1 \cdot 10^{-3} / (1.4 \cdot \beta_{eff})$
Operating reactivity margin at N$_{nom}$	$1.5 \cdot 10^{-3} / (0.4 \cdot \beta_{eff})$
Total reactivity margin at T=380°C	$6.6 \cdot 10^{-3} / (1.8 \cdot \beta_{eff})$
Effective delayed neutron fraction, β_{eff}	$3.68 \cdot 10^{-3}$

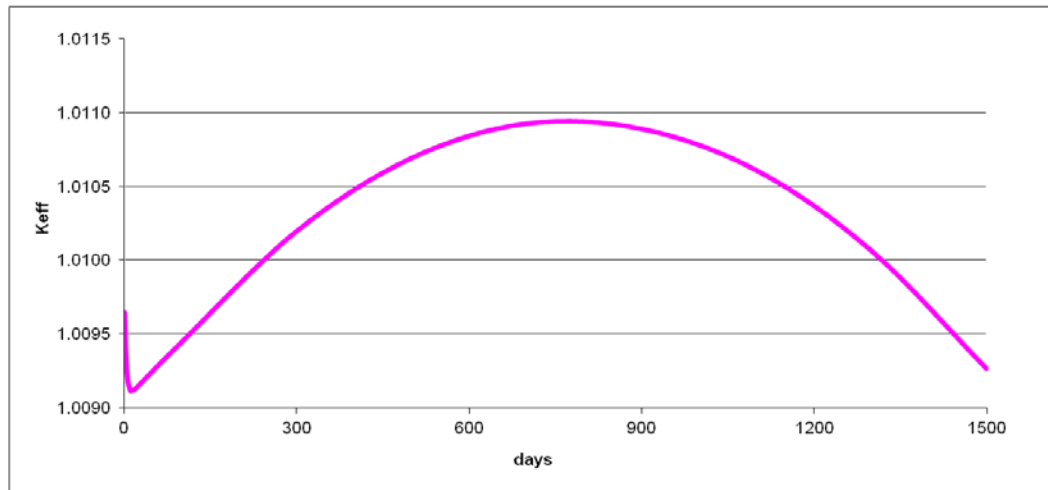Full efficiency of devices of passive feedback (DPFB)– $0.7 \cdot \beta_{eff}$

Figure 1 – Core lifetime reactivity variation versus fuel burnup ($\Delta\rho < 0.5\beta_{eff}$)

A small neutron moderation by the lead makes it possible to expand the fuel element lattice, widen the coolant flow path and increase the amount of heat removed by natural lead circulation during the reactor cooldown without worsening the reactor physical characteristics.

High heat capacity of the lead circuit that accumulates the released heat ensures that emergency and transient processes occur smoothly without a major growth in the circuit temperature. The existing protection features with passive direct-action initiators of response to the coolant flow rate reduction and the coolant temperature increase at the core outlet prevent the safe operation temperature limits from being exceeded when there is an unauthorized power growth or a loss of forced lead circulation. The integral lead circuit with passive and time-unlimited direct residual heat removal from the circuit via natural air circulation with discharge of heat into the atmosphere excludes accidents with fuel and coolant overheating during the reactor cooldown.

Therefore, it is only thanks to the natural dependencies of the chain reaction in fast reactors, the properties and qualities of lead and fuel (the BREST major components), as well as the

designs that help implement these, that two classes of the most severe accidents (caused by an uncontrolled power growth and a loss of heat removal) are excluded in natural manner. And it is in such approach to addressing the problem of the BREST safety in potentially severe accidents that the *natural safety* of this reactor consists in.

This approach to ensuring safety does not however exclude common accidents caused by failures of systems or components or by personnel errors. Still, being limited by the defense-in-depth concept and safety systems, these do not lead to inadmissible radioactivity release that requires evacuation of population and alienation of lands. Such accidents, up to the unit decommissioning for emergency reasons, have an economic dimension, and the damage from these other than exceeding the cost of the NPP unit as such is subject to an insurance coverage.

1.2 – Integral layout of the lead circuit and circulation flowchart

The BREST-OD-300 reactor of a pool-type design has an integral lead circuit accommodated in the central and 4 peripheral cavities of the concrete steel-lined vessel.

The central cavity houses the core barrel together with the side reflector, the CPS rods, the SFA storage and the shell that partitions the hot and the cold lead flows. Four peripheral cavities (according to the loop number) accommodate the SG-RCP units, heat exchangers of the emergency and normal cooldown systems, filters and auxiliary components. The cavities have hydraulic interconnection.

The lead coolant circuit design features a circulation flowchart minimizing the potentiality of steam or gas bubbles getting into the core together with the coolant which results in a positive reactivity introduction that causes a power growth (Figure 2).
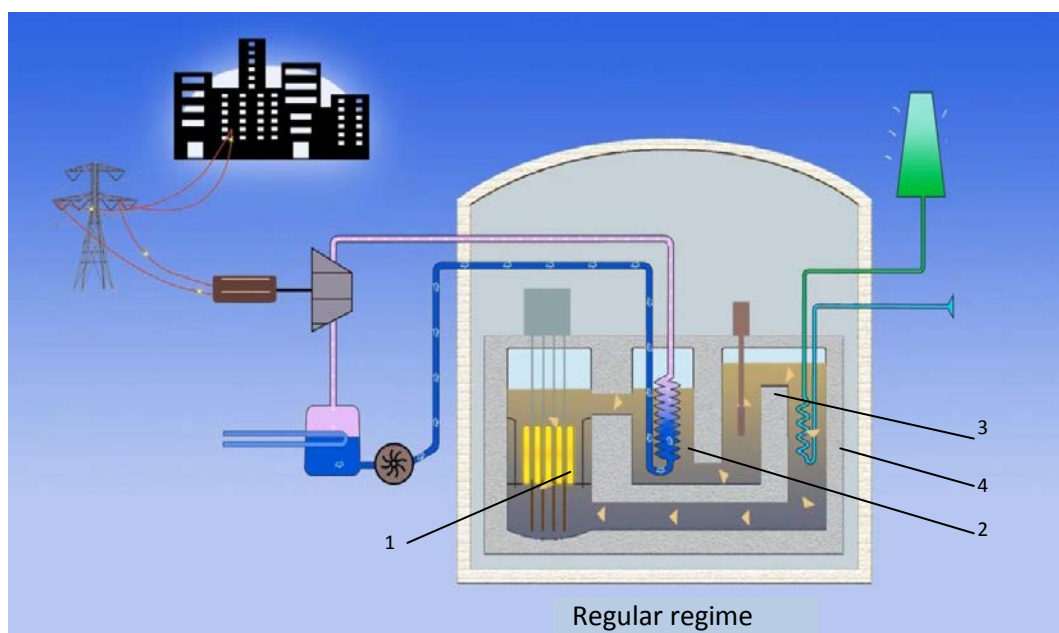
Figure 2 – BREST-OD-300 coolant circulation circuit
1 – core; 2 – steam generator; 3 – reactor coolant pump (RCP); 4 – ECCS channel

The lead circulation through the reactor core and the steam generators is based on the principle of communicating vessels. The pumps pump "cold" lead into the circuit's upper level from where it flows down by gravity to the core inlet, passes through the core flowing upward, and further goes, in a hot state, up to the steam generator inlets, where, while flowing down, it transfers heat to the water and steam and then enters the pump chambers. On its way through the

circuit the lead flow contacts twice the free gas level where exactly the bubbles entrained by the lead flow are separated.

Such circulation flowchart reduces the coolant flow rate irregularity when one or more pumps are tripped and ensures the inertia of the flow rate through the reactor core due to a difference in the levels when all pumps are shut down rapidly.

1.3 – Specific features of the reactor core and CPS member design

The BREST core is composed of shrouded hexagonal fuel assemblies with fuel elements clad in a ferrite-martensite steel but in the future shroudless assemblies will be considered too. For the radial flattening of power density and coolant heat-ups, the reactor core is designed as two radial cores, namely: a central core (CC) and a peripheral core (PC), the fuel assemblies in which differ in just the diameter of the fuel elements (the CC has fuel elements of a smaller diameter and the PC has fuel elements of a larger diameter). The use of the same fuel composition in all fuel assemblies, provided the CBR~1, along with a small reactivity margin, ensures that the FA powers and coolant heat-ups are stable throughout the core lifetime.

Apart from fuel elements, some of the CC fuel assemblies include a control and protection system (CPS) member contained in the vertical channel of the FA central part (Figure 3). In combination, the CPS members form two independent reactor shutdown systems, of which one composed of emergency protection (EP) rods is the emergency shutdown system, while the other one composed of shim rods and automatic reactivity control (AC) rods forms the second system.
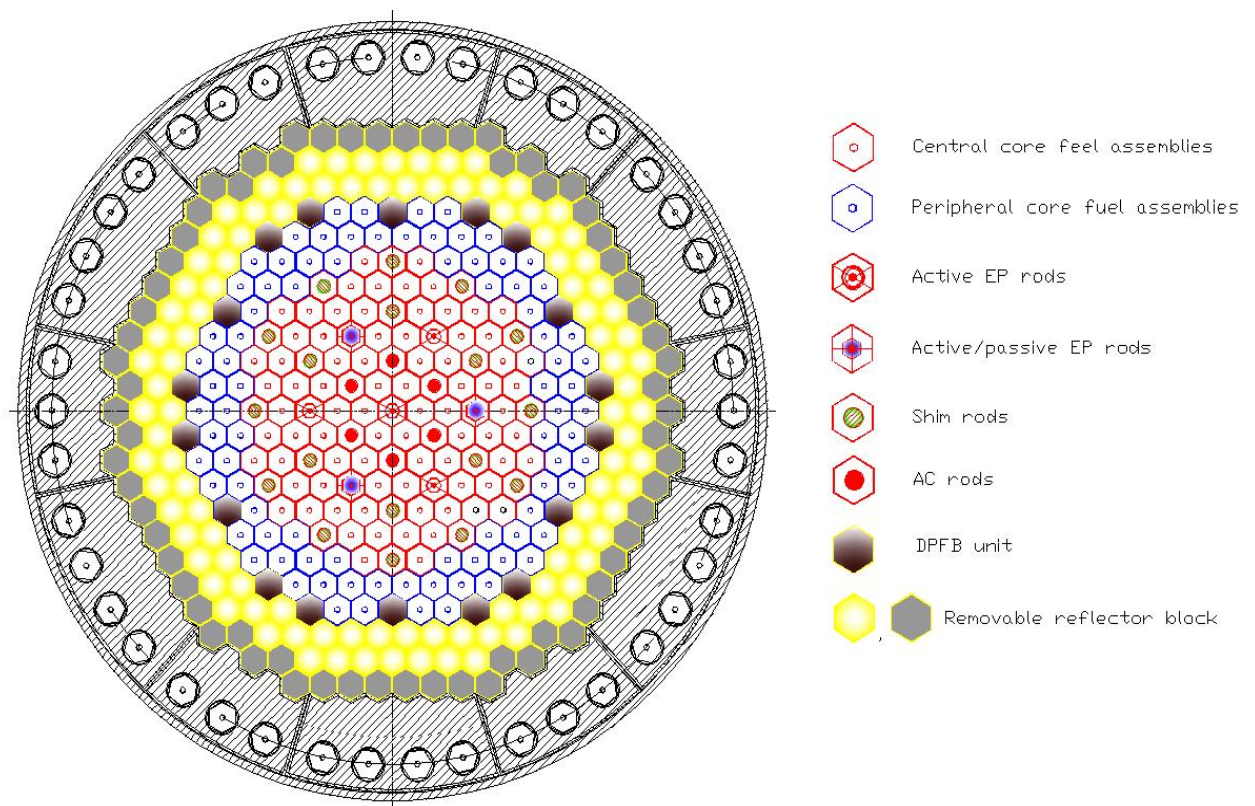

Figure 3 – Core map

The CPS rod drives are installed on the upper rotary plug, while the rods as such are under the core in a withdrawn position. For refueling, the drives are disengaged from the rods which come up into the core by the Archimedes force action and render the reactor deeply subcritical.

Three EP rods are of an active/passive type, that is they operate both actively (in response to the CPS logic signals) and passively (in response to the permissible core coolant temperature (T≥620°C) being exceeded (PEP-T)) when there is an unauthorized coolant flow rate decrease or power growth. The efficiency of two PEP-T rods (a failure of one of three rods is assumed for calculations) is equal to $1.6 \cdot \beta_{eff}$.

The core is surrounded by rows of changeable side lead reflector blocks designed as leak-tight steel hexagonal cans filled with the slow-rate flowing lead coolant. This reflector design ensures that the reactivity decreases monotonically when the in-core lead level goes down and excludes weapon-grade plutonium generation therein. Some of the side reflector blocks that adjoin the core have the form of vertical channels with lead columns plugged at the top. The lead column level follows the coolant pressure (flow rate) and influences the neutron escape. These devices (DPFB) ensure that the reactor reactivity (and power) is passively connected to the in-core coolant flow rate (head), which is an important factor of the reactor safety and control.

As shown by the calculations and measurements in the course of the reactor first criticality and energy startup, the core fuel is arranged in such manner that to have all CPS rods withdrawn from the core when the reactor rises to rated power, except two AC rod groups which compensate the operating reactivity margin ($0.4 \cdot \beta_{eff}$). The minimum time for the AC rods to be withdrawn from the core with the introduction of this reactivity is equal to 30 s.

The devices of passive feedback also regulate and maintain power in the working power range by responding to a coolant flow rate increase or decrease when power is changed for keeping the coolant permanently heated up.

2. Computational study of the most severe accidents

The BREST-OD-300 natural safety properties were demonstrated by results of the computational dynamic studies into severe accident scenarios the initial events for which were assumed to be full positive reactivity margin introduction during power operation of the reactor and full loss of power for all systems also during the reactor power operation.

The following temperature limits for the fuel components were used as the temperature criteria of safety for the calculation:

– maximum fuel cladding temperature of T=650°C – operating limit;

– maximum fuel cladding temperature of T=800°C – safe operation limit;

– maximum fuel temperature of T=2800°C – safe operation limit.

During accidents with a full loss of power for all systems and the failure of forced coolant circulation in the primary and secondary circuits, heat is removed by the ECCS, a passive system that cools the reactor by natural air circulation via the air heat exchangers submerged into the lead coolant, and by heat discharge into the atmosphere. During a postulated failure of 2 out of 4 loops, the power removed by the ECCS is not less than 5 MW.

2.1 – Accidents with full positive reactivity margin introduction

- Accidents with a full positive reactivity margin ($0.4 \cdot \beta$) introduction for 30 s as the result of the AC rod spontaneous movement, when the reactor operates at the rated power level ($N=N_{nom}$) and the rated coolant flow rate is $G=G_{nom}$, were considered for a number of reactivity compensation scenarios:

a) Scram takes place when the setpoint of $N=1.2 \cdot N_{nom}$ is achieved, while the maximum temperatures in the fuel element reach the values of $T_{fuel} \approx 960°C$ and $T_{clad} \approx 650°C$, the asymptotic power is defined by residual heat and is removed by the ECCS, and no safe operation limits are exceeded.

b) Active EP failure. Feedbacks and 2 PEP-T rods are actuated with a delay of 10 s after the core outlet coolant temperature setpoint of $T \geq 620°C$ is reached, the time of the rod insertion into the core being 5 s. $N_{max} \approx 1.60 \cdot N_{nom}$, the maximum temperatures in the fuel element reach the values of $T_{fuel} \approx 1170°C$ and $T_{clad} \approx 720°C$, the asymptotic power is defined by residual heat and is removed by the ECCS, and no safe operation limits are exceeded (Figure 4).
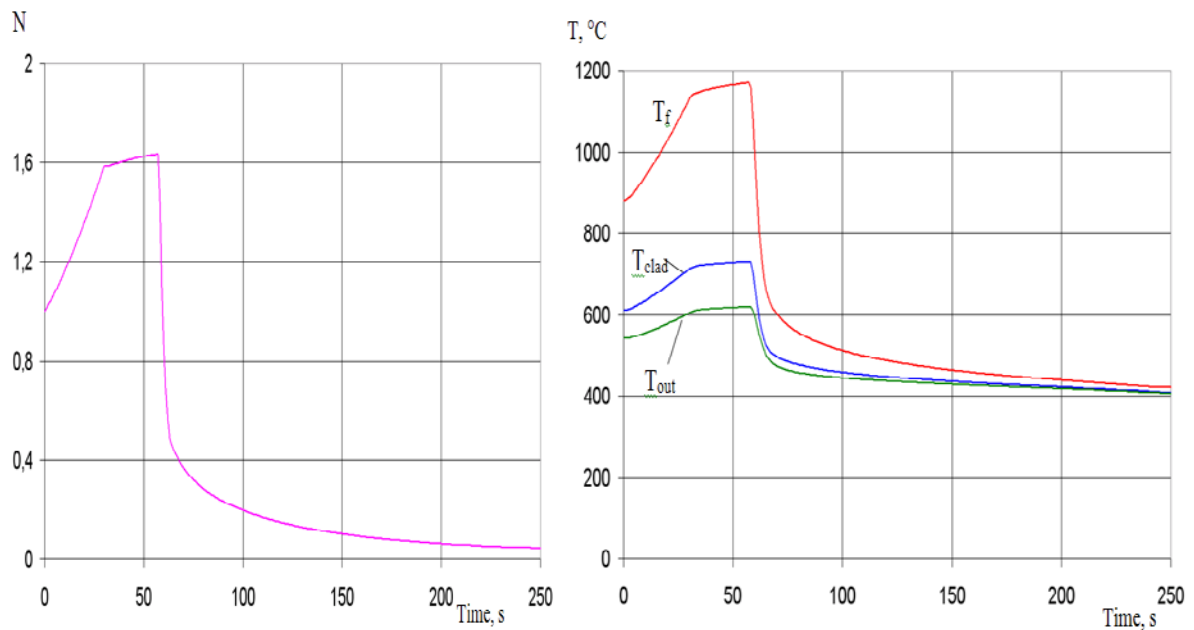

Figure 4 – Relative Power and temperature variation in a full reactivity margin introduction accident

c) Active and passive EP failure. Only temperature feedbacks operate, while $N_{max} \approx 1.65 \cdot N_{nom}$, and the maximum temperatures in the fuel elements reach the values of $T_{fuel} \approx 1200°C$ and $T_{clad} \approx 750°C$, the asymptotic neutron power, together with residual heat, is equal to ~5 MW and is defined by the ECCS heat removal capability, the asymptotic fuel, cladding and coolant temperature practically coincide and are equal to $T \approx 740°C$, and no safe operation limits for the fuel temperatures are exceeded. Temperature level in the lead circuit can be lowered down to $T \approx 700$ °C if defense on exceeding the admitted temperature level at the input to the main circulation pumps ($T \geq 540$ °C) turn off the forced lead circulation, that will put the DPFBs into action, introducing negative reactivity $\Delta\rho \approx 0.6\beta$ and diminishing neutron power.

• Accidents with a full positive reactivity margin ($0.4 \cdot \beta$) introduction for 30 s as the result of the AC rod spontaneous movement when the reactor operates at a partial power of N= $0.3 \cdot N_{nom}$ and the coolant flow rate is G= $0.3 \cdot G_{nom}$:

b) Active EP failure. Feedbacks and 2 PEP-T rods are actuated with a delay of 10 s after the core outlet coolant temperature setpoint of T≥620°C is reached, while $N_{max} \approx 0.65 \cdot N_{nom}$, the maximum temperatures in the fuel element reach the values of $T_{fuel} \approx 840°C$ and $T_{clad} \approx 700°C$, the asymptotic power is defined by residual heat and is removed by the ECCS, and no safe operation limits are exceeded.

c) Active and passive EP failure. Only temperature feedbacks operate, while $N_{max} \approx 0.72 \cdot N_{nom}$, and the maximum temperatures in the fuel element reach the values of $T_{fuel} \approx 900°C$ and $T_{clad} \approx 730°C$, and the asymptotic neutron power, together with residual heat, is equal to ~5 MW and is defined by the ECCS heat removal capability. As the secondary circuit automatics keeps the core inlet coolant temperature at the level of T=420°C, the asymptotic temperatures of fuel, cladding and coolant at core outlet are 900°C, 720°C and 690°C respectively. No safe operation limits for the fuel element temperatures are exceeded.

2.2 – Accidents with a loss of forced heat removal from the core

• Modes with a loss of forced core heat removal as the result of the reactor coolant and feedwater pump trip during blackout. The emergency heat removal is ensured only by the ECCS (power 5 MW). A number of power reduction scenarios were considered:

a) Active EP failure. Two out of three PEP-T rods are actuated with a delay of 10 s when T≥620°C, the time for the introduction of $\Delta\rho=1.6 \cdot \beta$ being 5 s, with DPFB starting to operate as well ($\Delta\rho=0.6 \cdot \beta$). Initially, the flow rate goes down faster than the power decreases and there is an interim (~5 s) growth in the fuel, cladding and coolant temperatures. After the PEP-T introduction, all temperatures go down by the 200th s to the level of T~500-520°C, which is defined by the heat accumulated in the coolant circuit and by the ECCS capacity. The fuel element temperatures do not exceed the respective nominal values (Figure 5).
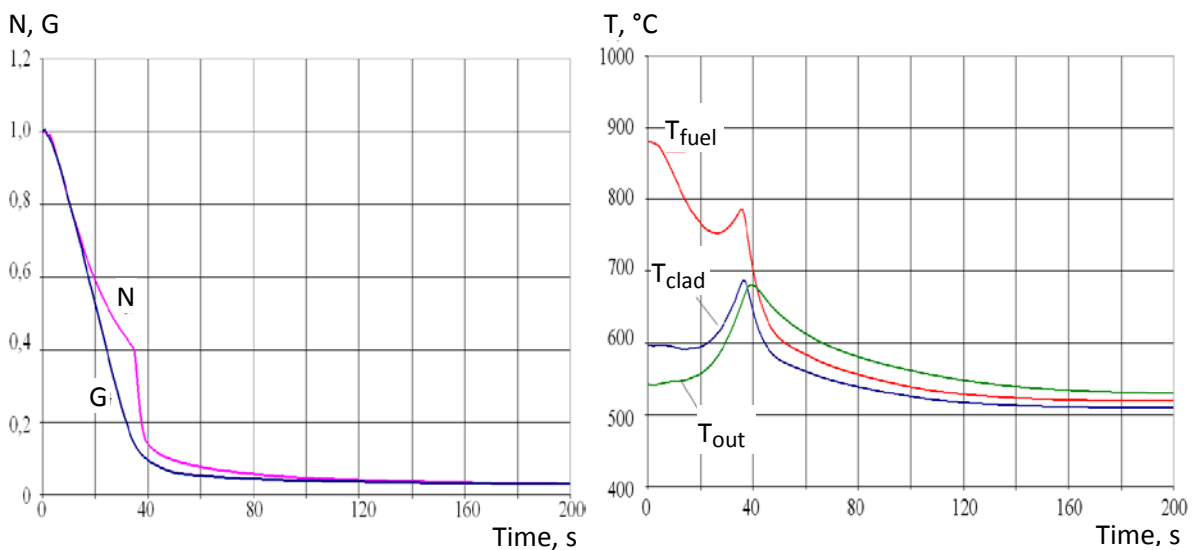

Figure 5 – Power, flow rate and temperature variation for a loss of forced heat removal accident

b) Active and active/passive (PEP-T) protections fail, but the passive feedback device starts to operate ($\Delta\rho=0.7\cdot\beta$). In this accident, the maximum fuel and cladding temperatures ($T_{fuel} \approx 880°C$ and $T_{clad} \approx 780°C$) do not exceed the safe operation limits. With heat removed only through the ECCS, the temperatures in all circuit components level off after ~40 hours at $T\approx650°C$, while tending to go down to $T\approx600°C$ asymptotically.

3. Radiation safety assessment for accidents with a loss of fuel integrity

The radiological consequences from an accident for the initial event leading to a loss of the cladding integrity in all fuel elements in the BREST-OD-300 reactor core have been assessed.

In the initial event the radioactive fission products have escaped through the damaged fuel claddings and entered the reactor gas plenum. In the scenario considered it's believed that the standard system of the accidents localization operates as designed. In this case the fission products release into the environment takes place with a delay in time. The above-ground release height is taken as 100 m. The public exposure doses along the release path axis have been estimated on the ground level.

The assessment of the accident effects on the population on the site boundary with the radius of 0.5 km from the power plant shows that the predicted effective exposure dose for adult public during 1 year after the accident will be about 0.6 mSv, while occupational dose levels won't exceed the established exposure dose limits.

On the INES scale, the accident may be classified as a medium incident of level 2 or as the maximum it will be of level 3 due to radioactive fission products release in the amounts not exceeding five times over the admitted day release.

So no population requires sheltering, preventive iodine administration, evacuation or resettlement.

Severe Accident Scenarios: Indian Perspective

P.Chellapandi and S.C.Chetal
Indira Gandhi Centre for Atomic research, Kalpakkam-603 102, India

Abstract
A parametric study on mechanical energy release values in the range 100 – 1000 MJ has been undertaken for a 500 MWe Pool type Prototype Fast Breeder Reactor (PFBR) to assess the worst possible effects with increase of energy values. The investigation focuses on issues related to structural integrity of primary containment and reactor containment building. Pessimistic assumptions made on mechanical energy release computations have been brought out with appropriate justifications. Fluid and structural dynamics analysis results are presented and discussed in detail depicting the loading sequences and various physical phenomena involved. The analysis indicates that primary containment has high potential to withstand the transient forces generated by energy release even more than 1000 MJ. The sodium ejection into the reactor containment building through top shield penetrations under sodium slug impact phenomenon is limited with higher energy mainly due to large dimensional changes of vessel associated with shorter transient duration. However, it is worth noting that the deformations of decay heat exchangers immersed in the sodium pool could limit the acceptable work potential. For PFBR, this value is found to be 500 MJ from simulated experimental study.

1.0   Introduction

From the Indian context, fast spectrum reactors are essential for realizing the full potential of nuclear energy with the limited availability of natural uranium and vast thorium resources. Hence, India is pursuing the fast reactor programme since 1970. With the successful operation of 40 MWt fast breeder test reactor for about 25 years and R&D results accumulated over about 35 years in various domains of science and technology of fast reactors, India is building a 500 MWe Prototype Fast Breeder Reactor (PFBR), which will be commissioned in this year (2013). The main objective of PFBR is to demonstrate the techno-economic feasibility of a series of sodium cooled fast reactors planned by the Department of Atomic Energy. The PFBR has many inherent and engineered safety features that the probability of occurrence of a severe accident involving melting of whole core, i.e. core disruptive accident (CDA), is very low ($<10^{-6}$/y) that it is categorized under beyond design basis event. The recommended value of mechanical energy release due to CDA is 100 MJ, which was derived from the unprotected loss of flow accident (ULOFA) analysis. For this mechanical energy release by the vapourised portion of the core, called 'core bubble', the important consequences are analysed.

The mechanical consequences are due to rapid expansion of core bubble, releasing high pressure waves. The pressure waves impose direct loading on the surrounding structures, such as main vessel and its internals, causing large deformations. Besides, under the bubble pressure, the sodium slug above the core bubble gets accelerated upward. Once the accelerated sodium impacts at the bottom of the top shield, a high local pressure is developed. Under this pressure, the upper portion of main vessel gets bulged; a portion of the accelerated sodium occupies the available penetrations in the top shield and the cover gas gets compressed at the peripheral region in the vicinity of the top shield bottom. At this state, the core bubble attains a shape with the maximum volume (V_{max}) condition, releasing the maximum mechanical energy, which is the expansion work ($\int P.dV$) integrated over the initial volume to V_{max} with associated pressure ($P_{quasistatic}$) and the vessel has attained the maximum deformed configuration (Fig.1a). The time duration involved to attain this state is generally < 1 s. (It is also customary to define a term called 'work potential' for assessing the maximum possible mechanical energy that could be released by the core bubble by assuming that the core bubble expands till its pressure is equal to the ambient pressure (P_{amb}). P_{amb} is generally taken as a normal atmospheric pressure of one bar. Thus, the work potential quantifies the severity of a CDA). Mechanical consequences further continue with the ejection of sodium present in the gaps out of the top shield under 'pseudo-static pressure' of the core (its initial value is $P_{quasistatic}$). This

pressure drops rapidly, when the core bubble gets cooled by the liquid sodium itself. The event of sodium release continues till $P_{quasistatic}$ reduces to P_{amb}, which could last for 1-2 s typically (Fig.1b). Afterwards the sodium remaining in the top shield penetrations falls back into sodium pool by gravity. The condensation of core bubble reduces pressure inside the vessel, promoting favorable conditions for draining of sodium in the penetrations. The ejected sodium immediately burns on the top surface of the top shield increasing temperature and pressure, which are the design basis loads for the reactor containment building (RCB).

Subsequent to the mechanical consequences, the focus is on the decay heat removal aspects of the core, particularly the relocated molten fuel and structural materials settled on the core catcher in the form of debris after penetrating through the structures below the core (Fig.1c). This event is called post accident heat removal phase, during which the decay heat generated by the core debris is removed continuously, till it becomes insignificant. There are many means to achieve long term coolability of core debris, e.g. incorporation of adequate number of dedicated Safety Grade Decay Heat Removal Heat Exchangers (SGDHX), permanently immersed in the sodium pool within the main vessel. In view of their important role, the functionality of decay heat removal mechanisms should be ensured for the long term coolability of the core debris, for which their structural integrity has also to be assessed under the investigation of mechanical consequences of CDA.
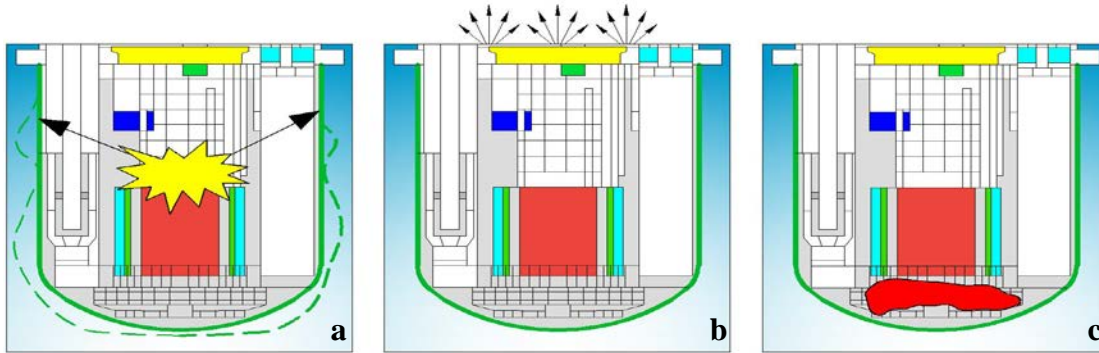

Fig.1 Important consequences of a CDA in SFR

Based on extensive numerical and experimental simulations, the structural integrity of primary containment (main vessel and top shield) and reactor containment building is demonstrated and the functionality of SGDHX has also been ensured with comfortable margins for 100 MJ of work potential. Internationally, the severe accident analysis methodologies of sodium cooled fast reactors are critically re-looked in recent years and several scenarios are postulated. Development of advanced numerical and experimental techniques is carried out with the objective of determining realistic energy release, which is still evolving. In view of this, a parametric study on mechanical energy release values beyond 100 MJ, i.e. in the range 100 – 1000 MJ, has been undertaken for the PFBR, to assess the worst possible effects with increase of energy values. The investigation focuses on issues related to structural integrity of primary containment including RCB and post accident cooling capability. This is the main scope of the present paper.

The paper highlights the PFBR plant details and the main safety systems in section 2, severe accident scenario in section 3, assessment of primary containment potential in section 4 and future perspective in section 5. Section 6 is dedicated to conclusion.

2.0   Safety Features of PFBR

PFBR is a 500 MWe capacity pool type fast reactor with 2 primary and 2 secondary loops with 4 steam generators per loop. The inlet and outlet temperatures of primary sodium are 670 K and 820 K respectively. The sodium from hot pool after transporting its heat to four intermediate heat exchangers (IHX) mixes with the cold pool. The circulation of sodium from cold pool to hot pool is maintained by

two primary sodium pumps and the sodium from hot pool flows through IHX, driven by a level difference (1.5 m of sodium) between the hot and cold pools. The heat from IHX is transported to eight steam generators (SG) by sodium flowing in the secondary circuit. Steam produced in SG is supplied to turbo-generator. In the reactor assembly, the main vessel houses the entire primary sodium circuit including core. Sodium is filled in the main vessel with free surfaces blanketed by argon. The inner vessel separates the hot and cold sodium pools. The reactor core consists of 1757 subassemblies including 181 fuel subassemblies. The control plug, positioned just above the core, houses the 12 absorber rod drive mechanisms and core monitoring thermocouples. The top shield supports the primary sodium pumps, IHX, control plug and fuel handling systems. PFBR uses mixed oxide with both natural and depleted uranium and plutonium oxide as fuel. The structural material for the core components is 20 % cold worked D9 material (15 % Cr- 15 % Ni with Mo and Ti) to have better irradiation resistance. Austenitic stainless steel type 316 LN is the main structural material for the out-of-core components and modified 9Cr-1Mo (grade 91) is for SG. PFBR is designed for a plant life of 40 y with a load factor of 75 %.

The main vessel along with the top shield constitutes primary containment. Accordingly, the vessel is designed to absorb the mechanical energy that could be released under a severe accident condition. The reactor design is based on well established design codes, standards and guides. The sodium components with safety significance are designed as per RCC-MR-2002, the French design code specific to fast reactors. All the probable internal and external events are identified, categorized into 4 Design Basis Events (DBE) and Beyond Design Basis Events (BDBE) and analyzed using validated computer codes. With reference to safety, the temperature and power coefficients of reactivity are negative so that any off-normal increase in temperature or power leads to a reduction in reactivity and the consequent reduction in power. The expansion of coolant and structural steel result in small positive reactivity (+0.241pcm/K). This is compensated by negative and prompt (time constant < 1 ms) reactivity effects like Doppler (-1.320 pcm/K) and fuel expansion (-0.236 pcm/K), which are slow (time constant ~50–100 s). The reactivity feedback resulting from grid plate expansion, spacer pad expansion of core subassemblies (-0.869 pcm/K) and differential control rod expansion (-1 pcm/K) tend to shutdown the reactor for transient under loss of cooling incidents.

Apart from the above features, PFBR has many safety systems to prevent CDA as well as to mitigate its effect. The core is monitored by functionally diverse sensors. Neutron detectors are provided to monitor the power and provide signals for safety action (SCRAM) on parameters like linear power, period and reactivity. These parameters provide protection against transient over power, transient under cooling and anomalous reactivity addition events. Flow delivered by the primary sodium pump is measured and power to flow ratio is also monitored. Pump discharge head and speed are measured and used as trip parameters for protection against pump discharge pipe rupture and pump seizure events respectively. Failure of fuel is detected by monitoring the cover gas fission product activity (alarm parameter) and Delayed Neutron Detection (DND) in the primary coolant. These provisions ensure availability of at least 2 diverse safety parameters as far as possible for each DBE. Based on detailed thermal hydraulics analysis, eight numbers of DND, one on either side of IHX have been finalised, by which pin failure in any fuel subassembly can be detected within 1 minute at any power level. On detection of any abnormality in the reactor, shutdown is assured by two independent, fast acting shut down systems (SDS). Each system consists of sensors, analogue processing circuits, logics, absorber rods and associated drive mechanisms. Reactor cold shutdown is accomplished independently by both the systems by free fall of the B_4C absorber rods even when one rod remains stuck. The response time of shutdown system to initiate rod drop is less than 200 ms and the free fall drop time of rod is < 1 s which is sufficient to protect an incident up to 3 \$/s. Sufficient independence and diversity is provided in the design of sensors, analogue signal processing circuits, SCRAM circuits, SCRAM logic, SCRAM switch, absorber rods and mechanisms of the two systems. With this, the failure frequency of SDS is found to be 6.4×10^{-7}/ reactor-year, which is less than the specified limit ($< 10^{-6}$ /reactor-year). The failure frequency of individual systems is 8×10^{-4}/reactor-year and 4.4×10^{-4}/reactor-year, which is less than the specified limit ($< 10^{-3}$/reactor-year). In the reliability analysis, common cause failures between redundant non-diverse components/systems are accounted appropriately.

Decay heat is about 1.5 % and 0.7 % of nominal power, respectively 1 h and 1 d after reactor shutdown. If off-site power is available, decay heat removal is through the normal heat transport system, i.e., through steam generators and steam-water system. The system is known as Operation Grade Decay Heat Removal System. In case of loss of off-site power, loss of secondary circuit or steam water circuits the decay heat is removed through 4 independent Safety Grade Decay Heat Removal (SGDHR) loops (Fig.2). The SGDHR operation is automatic. Each loop consists of a Decay Heat Exchanger (DHX) of capacity 8 MWt with tube side linked to a intermediate sodium circuit which is connected to sodium-air heat exchanger (AHX). The ultimate heat sink is air. The layout of SGDHR circuit ensures decay heat removal by natural convection in primary sodium, intermediate sodium and air side. Two dampers of diverse design are provided at inlet and outlet of AHX and two diverse designs of DHX and AHX are provided to enhance reliability. Diesel and battery power is also provided to drive the primary pumps at 15 % of the speed for conditions of off-site power failure and station blackout conditions as a defense in depth approach. Reliability analysis is carried out by fault tree method including

Fig.2 Safety grade decay heat removal system

common cause failure between redundant non-diverse components/systems. Passive system failures in the form of sodium leak at loop boundaries, flow blockage and freezing are considered in the analysis. The failure frequency of SGDHR function is found to be 1.5×10^{-7}/reactor-year, which practically meets the specified prescribed limit of 1×10^{-7}/reactor-year, considering the conservatism in the analysis.
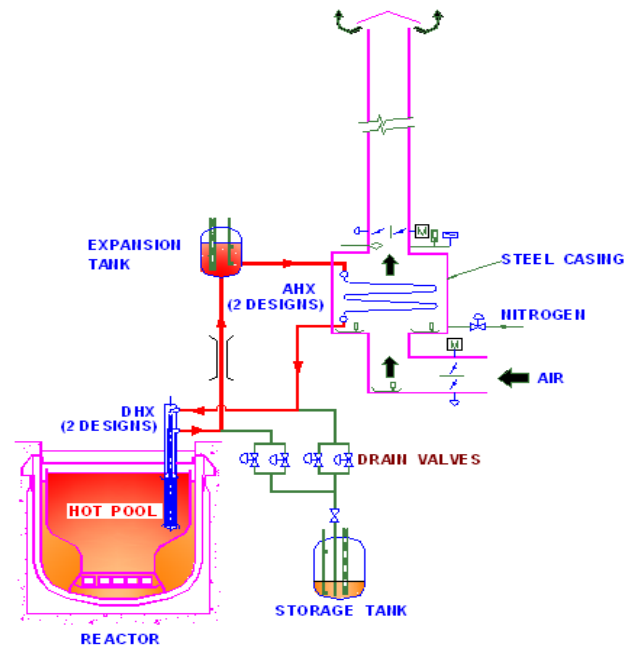
Under the assumption of Total Instantaneous Blockage (TIB), a single subassembly melting progresses at the most to the neighboring six subassemblies. However, if the hot fuel settles at the bottom, the main vessel wall may melt and give way out to the sodium and the molten fuel. Also there is concern for re criticality if the fuel settles down in a more reactive configuration. Therefore, a core catcher is provided below the core support structure to collect the debris resulting from the melting of 7 SA. In order to contain the possible release of radioactive materials during DBE as well as BDBE including severe accident conditions, a rectangular reactor containment building (RCB) is provided. The design pressure of RCB (25 kPa) is derived from the temperature and pressure rise due to burning of sodium in RCB (350 kg) that could eject through the penetrations in the top shield, consequent to a core disruptive accident. More details of PFBR can be found in ref [1].

3.0   Severe Accident Scenario of PFBR

Two initiating events are defined that could lead to a CDA: (1) loss of flow without reactor shutdown leading to Unprotected Loss of Flow Accident (ULOFA) and (2) uncontrolled withdrawal of control rods introducing reactivity ramp leading to Unprotected Transient Overpower Accident (UTOPA). The experimental studies reported in ref [2 and 3] indicate that in the UTOPA scenario, the in-pin motion of molten fuel caused by fission gas pressure, called 'fuel squirting' or 'fuel extrusion', introduces a lot of negative reactivity in the core and hence stabilize the reactor at a higher power level without causing any core melting / boiling / disruption. Hence, UTOPA is not energetic and analysed only for the thermal consequences particularly, the decay heat removal aspects for PFBR. However, ULOFA is analyzed in

detail, since it leads to a CDA that could pose major threat to the structural integrity of primary containment. UTOPA scenario is elaborated in the following paragraph.

ULOFA involves three main phases in sequence: pre-disassembly, transition and disassembly phases. In the pre-disassembly phase, the flow reduction immediately leads to coolant temperature rise in core that gives positive reactivity, which however, is dominated by the negative reactivity due to the radial thermal expansion of core and the net reactivity is negative. This results in decrease in power. However, the power to flow ratio increases subsequently, resulting in high coolant temperature rise and voiding in the upper part of the highly rated fuel channel. The core voiding spreads radially outward and axially downward increasing positive reactivity contribution. When the voiding spreads into the central part of the core, the net reactivity becomes positive, initiating a series of events: power excursion, clad dry out, rapid temperature rise in the fuel and clad and ultimately melting of fuel and clad. The molten materials would be swept out of the core by the shearing force of the coolant vapor (dominant force in the case of fresh fuel) as well as by the accumulated fission gas pressure (dominant in the case of irradiated fuel). If there are sufficient negative reactivity introduced from Doppler and fuel displacement, the core could become subcritical and the accident terminates. Else, with the high rate of positive reactivity addition, the core attains a super prompt critical condition and the core enters into disruptive condition. The consequence is large thermal energy release, causing vaporization of significant portions of fuel and structural materials of the core. Under an idealized condition, a mixture of molten materials at the bottom with vapor phase at the top could be conceived at the end of disassembly phase (Fig.1a).

4.0   Assessment of Primary Containment Potential

In order to raise the confidence on the structural integrity of primary containment as well as RCB, a parametric study on mechanical energy release values in the range 100 – 1000 MJ has been undertaken with some pessimistic assumptions. The highlights of the analysis are given below. More details are presented in ref [4].

4.1   Work potential of core bubble

The mechanical energy release depends upon the reactivity addition rate in the disassembly phase, which in turn depends upon the assumptions made on the sodium void propagation, fuel displacement / slumping characteristics and reactivity feedback mechanisms. This apart, the cross section data, the nature of temperature distributions assumed for the disrupted core and cross section data employed in the analysis decide the work potential value. One of the important parameters influencing the coolant void generation/propagation is flow halving time. With lower flow halving time, the coolant voids could generate below the core top and spread rapidly to the core centre, resulting in high positive reactivity rate in the disassembly phase. With higher flow halving time, the coolant boiling starts at the upper portion of active core, which introduces negative reactivity due to the high neutron leakage. Analysis with pessimistic assumptions: shorter low halving time of 2 s, coherent core lumping, absence of feedbacks, flat temperature distribution across the core at the end of disassembly phase and use of conservative cross section data (CV2M cross section set), yields a pessimistic reactivity addition rate of 200 $/s and associated work potential is ~1000 MJ. Analysis with optimistic assumptions: longer flow halving time of 8 s, incoherent core, presence of all feedbacks, realistic temperature distribution across the core and use of realistic cross section data (ABBN cross section set), yields an optimistic reactivity addition rate of 10.5 $/s and associated work potential is insignificant (< 1 MJ). It is also found that the assumptions made on the fuel dispersion behavior have significant influence on the reactivity addition rate. If a conservative fuel slumping model is employed without considering molten fuel dispersion (incoherent core), higher energy release is possible. As per this, active core zone is divided into three zones axially. The molten fuel from middle one third occupies the core lower portion and fuel from top one third occupies the middle portion. This leads to a reactivity addition rate of 65 $/s and work potential of 100 MJ. In addition, the temperature distribution of the core at the end of disassembly phase can change the work potential value significantly: assumption of a flat temperature distribution can yield the work potential of 268 MJ for the reactivity addition rate of 50 $/s, compared to 100 MJ for the reactivity addition of 65 $/s with the

realistic temperature distributions. The synthesis of above results motivates to investigate the mechanical consequences of a CDA over a wide range of work potentials corresponding to the reactivity addition rates ranging from 25 \$/s to 200 \$/s (Fig.3).

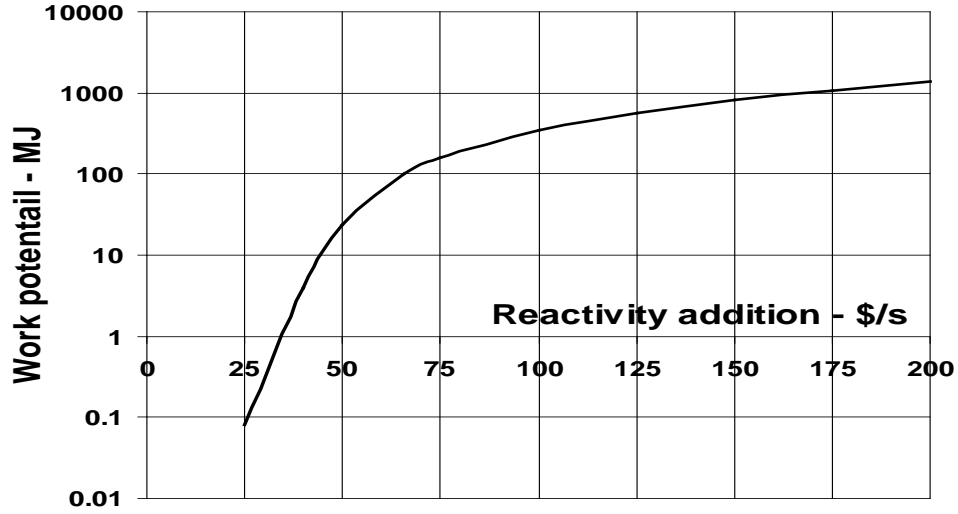Fig.3 Pessimistic energy release in PFBR

4.2   Mechanical Consequences
4.2.1   Sequence of mechanical loadings and energy observations

Rapid expansion of core bubble confined by the liquid sodium, housed in thin vessel, having cover gas space above free level depicts complicated deformation mechanics with the fast transient fluid-structure interaction effects. There are three main phases of the deformations in sequence: (1) bulging of the vessel bottom under direct impact of the pressure waves generated by the bubble, (2) bulk movements of the sodium slug towards top shield compressing the cover gas bulk where in vessel deformations are insignificant and (3) radial local bulging of upper portion of the vessel due to sodium slug impact at the bottom of top shield. The duration of each of these phases and quantum of deformation depend strongly on the work potential of the bubble. These are brought out from the analysis results. Figure 4 depicts the sequence of energy absorbed by the vessel while core has various work potentials. A fraction of work potential absorbed by the upper portion of the vessel is compared with the fraction absorbed by the bottom portion in (Fig.5). While at lower work potentials, the upper portion of vessel as well as cover gas compression absorbs higher fractions of work potential, compared to fraction absorbed by the bottom portion, trend reverses at higher work potentials. Further, it is seen in (Fig.5) that the net fraction of
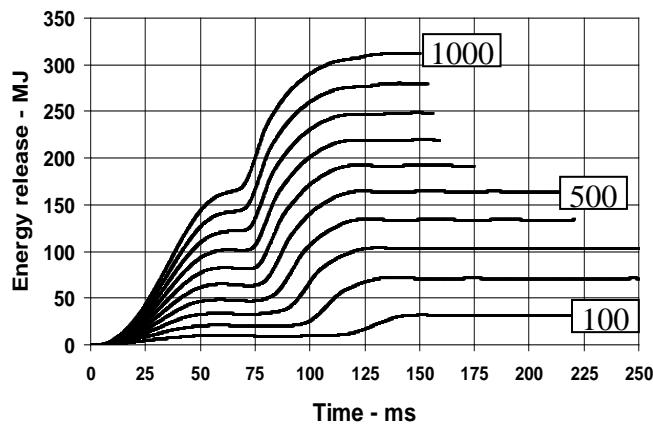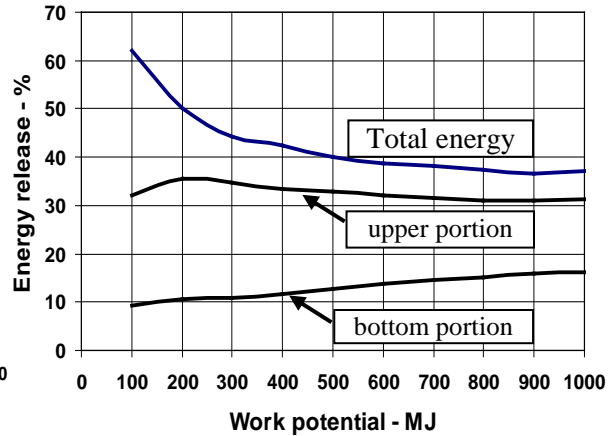

Fig.4 Strain energy absorbed by the vessel

Fig.5 Energy balance in the vessel

6

energy released by the core bubble is decreasing, while the work potential of core bubble increases and tends to stabilize (~36 %). This implies that the impact effects, which cause local deformations, get saturated at high mechanical energy release and the vessel absorbs the energy uniformly, enhancing its energy absorbing potential.

4.2.2   Main vessel deformations

Figure.6 shows the radial deformation profiles along the developed length of the vessel. The absolute values of the downward displacement, radial bulging at middle portion at the elevation of core centre and radial bulging just below top shield junction are quantified in this figure. The values indicate that the main vessel would have mechanical interactions with the safety vessel both at the bottom and at the top, depending upon the inter-vessel space. The safety vessel could contribute in load sharing subsequent to such interactions, which is not simulated in the analysis to preserve conservatism. The local strains at the upper portion as well as averaged strains in the vessel are presented in (Fig.7). The ratio of peak strain to the averaged strain plotted at various work potentials shown in this figure confirms the conclusion derived from the previous subsection, that the deformation becomes more uniform compared to lower work potential cases. This is a favorable feature that the energy absorbing potential is not linear and the vessel can absorb higher energy without undergoing rupture locally upon application of higher energy by the core bubble. It is also shown that the peak strain in the vessel for the work potential of 1000 MJ is 14 %. From the structural integrity consideration, this strain value is acceptable for PFBR main vessel [5]. Simulated tests conducted on the scaled down mockups with low density explosives have demonstrated that the main vessel alone can withstand a work potential of 1200 MJ [6].
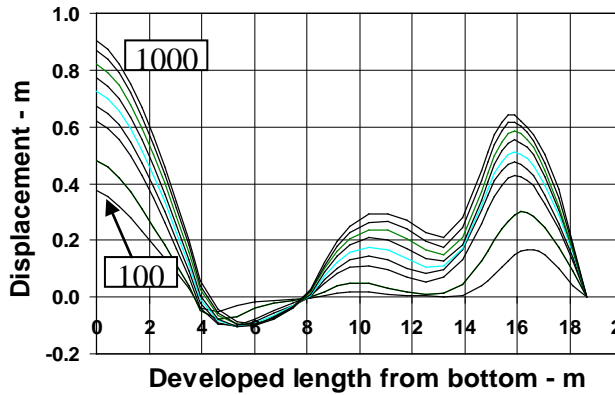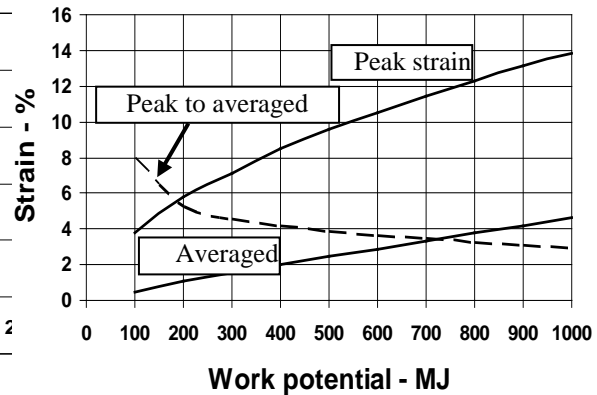

Fig.6 Radial displacement in the vessel   Fig.7 Membrane strains in the vessel

4.2.3   Slug impact loadings and their effects

The evolution of upward velocity values during sodium slug impact phenomenon is shown in (Fig.8) for four specific work potentials (100 MJ, 200 MJ, 500 MJ and 1000 MJ). From this figure, it is brought out that the loading on the top shield is gradual at low work potentials typically at 100 MJ and 200 MJ. Figure 9 shows the impact pressure experienced by the top shield, which shows that at higher work potentials, the top shield is subjected to high impact pressure. The time to initiate sodium slug impact is shorter for higher work potential, which also tends to stabilize in (Fig.9). In view of short duration of impact loadings and high mass inertia of top shield structures, it has high potential to absorb higher impact loads and hence, the integrity of top shield would not be of concern and do not decide the acceptable work potential.
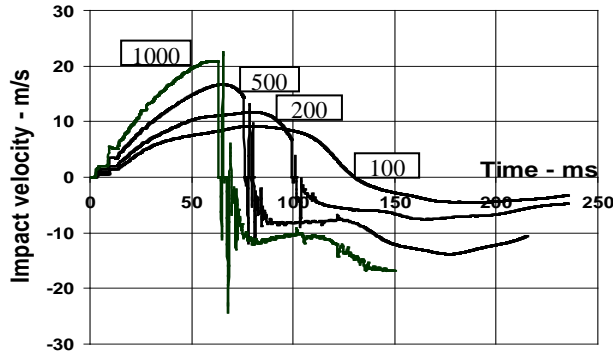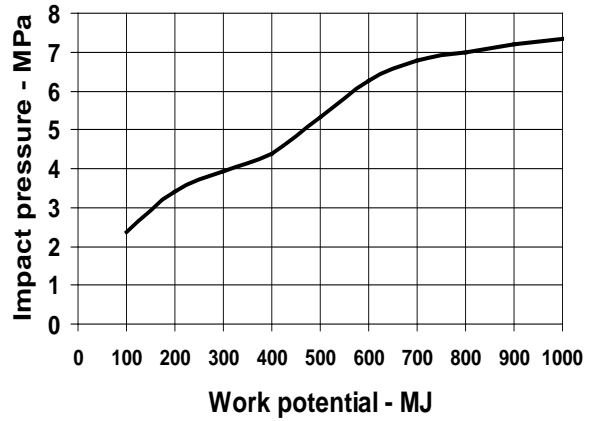
Fig.8 Sodium slug impact scenario

Fig.9 Peak impact pressure on top shield

4.2.4 Sodium leak through top shield and containment design pressure

The peak pressure developed during the sodium slug impact phenomenon causes elongation of the hold down bolts and failure of seals in the top shield, providing leak gaps for the sodium occupied in the penetration. The quasi-static pressure sustaining in the impacted sodium drives this sodium into RCB, which occurs as far as the quasi-static pressure is higher than the ambient pressure above the top shield. To understand further, the status of core bubble at the time of impact is depicted for four work potentials (100 MJ, 200 MJ, 500 MJ and 1000 MJ) in (Fig.10). The status of core bubble as well as cover gas space during quasi-static phase is also depicted in (Fig.10) itself. Due to larger deformations at higher energy levels, the sodium slug decelerates to get separated from the top shield. Hence the quasi-static pressure in the cover gas is tending towards saturation with higher work potential in (Fig.10).

100 MJ   200 MJ   500 MJ   1000

Status of core bubble and cover gas space at instant of slug impact

100 MJ   200 MJ   500 MJ   1000 MJ
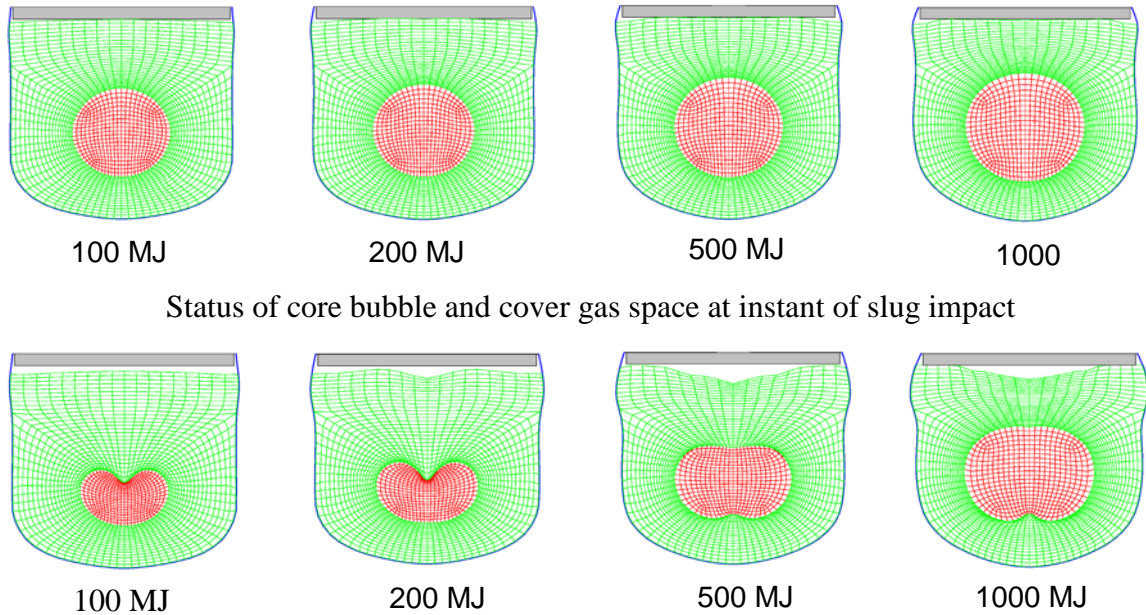
Fig.10 Status of core bubble and cover gas space during quasi-static condition

Starting from the initial quasi-static pressure shown in Fig.10, the decay of bubble pressure while getting cooled by the surrounding colder sodium and the resulting sodium leak rate through all the top shield penetrations are evaluated in ref [7] for the work potential of 100 MJ, the design load for PFBR.

Computation is repeated for other work potentials and corresponding sodium releases are presented in (Fig.11). By postulating a conservative sodium fire scenario in RCB, temperature and pressure rises are computed for 100 MJ of work potential in ref [7]. Computations are repeated to determine the pressure in RCB due to sodium fire in RCB corresponding to higher work potentials and results are presented in (Fig.12). The results indicate that the containment loadings would attain saturation at higher work potentials.
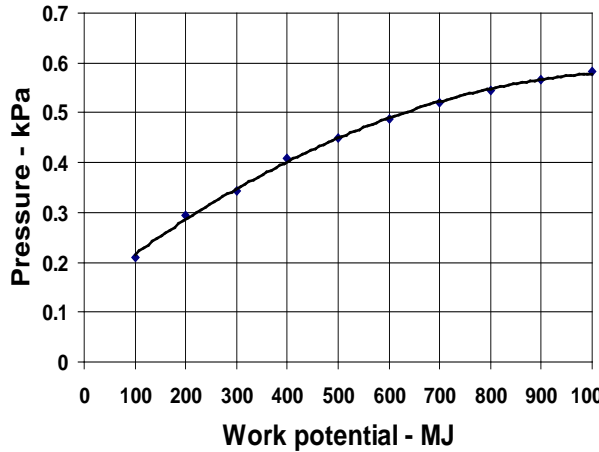
Fig.11   Quasi-static cover gas pressure
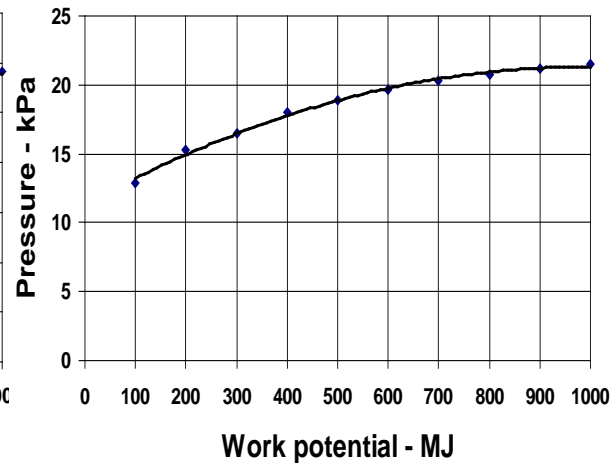
Fig.12 Pressure rise in RCB

5.0   Future Perspective

Innovative and passive shutdown systems are studied for the future reactors beyond PFBR to shutdown the reactor on emergency by using electromagnets without looking for any power if primary pumps stop. In this case, a few backup control rods operated by electromagnets are provided that would get inserted in case of unacceptable temperature increase because of Curie point effect. Further, novel mechanical devices to separate the shutdown rods from the magnet by forces developed by relative thermal expansions, hydraulically suspended absorber rods (Fig.13a), injection of liquid poison (Fig.13b) and stroke limiting device to prevent any possibility of uncontrolled withdrawal of control rods (Fig.13c) are some of the innovative passive features being conceived.

a. Hydraulically suspended rods

b. Liquid poison injection

c. Stroke limiting device

Fig.13 Innovative shutdown systems conceived for future fast reactors

9

With the above mentioned features, the core disruptive accident in a fast reactor may be minimised, even to the extent of elimination. Regardless of the safety provisions made as described, as a 'defense-in-depth', "core catcher" structures are conceived to place below the core for collecting the 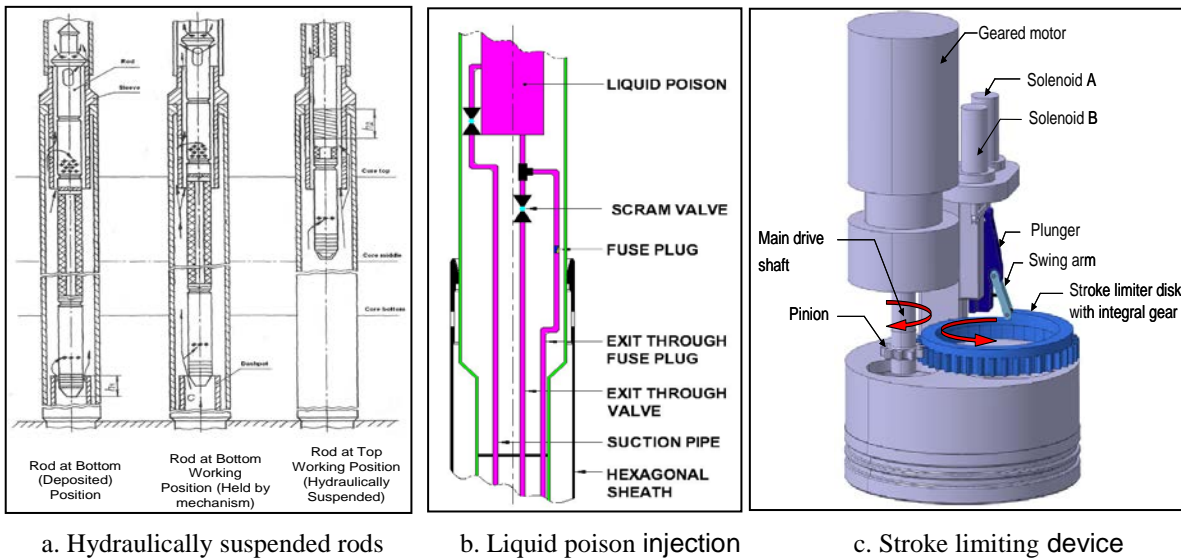molten core thereby preventing the escape of radioactive materials through ground or groundwater contact. These structures are specially configured for facilitating long-term coolability of a molten core if settled on it, by purely natural convection heat sink mechanism.

6.0 Conclusion

PFBR has adequate inherent and engineered safety features. Future reactors would have enhanced and passive safety features. For PFBR, a core disruptive accident having work potential of 100 MJ has been considered as Beyond Design Basis Event. The structural integrity of primary containment has been assured due to mechanical loadings resulting from CDA. Further, temperature and pressure rise in reactor containment building (RCB) following the sodium fire, as a consequence of sodium release under CDA form the design basis loads for RCB. In order to raise the confidence on the structural integrity of primary containment as well as RCB, a parametric study on mechanical energy release values in the range 100 – 1000 MJ has been undertaken with some pessimistic assumptions. The analysis indicates that primary containment has high potential to withstand the transient forces generated by energy release even more than 1000 MJ. The sodium ejection into the reactor containment building through top shield penetrations under sodium slug impact phenomenon is limited with higher energy mainly due to large dimensional changes of vessel associated with shorter transient duration. However, it is worth noting that the deformations of decay heat exchangers immersed in the sodium pool could limit the acceptable work potential. For PFBR, this value is found to be 500 MJ from simulated experimental study.

References

1   P.Chellapandi, P.Puthiyavinayagam, V.Balasubramaniyan, S.Ragupathy, V.Rajanbabu, S.C.Chetal and Baldev Raj, 'Design Concepts for Reactor Assembly Components of 500 MWe Future SFRs', Nuclear Engineering International, Vol. 240, 2010, pp.2948-2956.
2   D. R. Porten et al., "Internal fuel motion as an inherent shut down mechanism" , Topical Meeting on Reactor Safety Aspects of Fuel Behavior, Sun Valley, ID, USA, August 1981.
3   P.Chellapandi. S.C.Chetal and Baldev Raj, 'Structural Integrity Assessment of Reactor Assembly Components of A Pool Type Sodium Fast Reactor under Core Disruptive Accident - Part 1: Development of Computer Code and Validations', Nuclear Technology, Vol. 172 (1), Oct. 2010, pp. 01-15
4   P. Chellapandi, G. S. Srinivasan and S. C. Chetal, 'Primary Containment CFpacity of a Pool Type Sodium Cooled Fast Reactor against Core Disruptive Accident Loadings', Journal of Nuclear Engineering Design, 2012 (in press).
5   H.Kaguchi, et.al, "Strain Limits for Structural Integrity Assessment of Fast Reactors under CDA", 7th Int. Con. Nuclear Engineering (ICONE-7), Tokyo,Japan (April 1999).
6   "Investigation of Mechanical Consequences of a Core Disruptive Accident in Fast Breeder Reactor Based on Simulated Tests on Scaled Down Models", Collaborative Project No-TBRL/IGCAR/TRIG/1997, Terminal Ballistic Research Laboratory. Chandigarh-160 020 (Jan 2002).
7   K. Velusamy, P. Chellapandi, K. Satpathy, Neeraj Verma, G.R. Raviprasan, M. Rajendrakumar and S.C. Chetal, 'Fundamental Approach to Specify Thermal and Pressure Loadings on Containment Buildings of Sodium Cooled Fast Reactors During A Core Disruptive Accident', Annals of Nuclear Energy, Vol. 38, 2011, pp. 2475-2487

* * *

Application of Objective Provision Tree Methodology to Development of Specific Safety Requirement for SFR

Namduk ~~Naduk~~ SUH[a], **Huichang YANG**[b]

[a] Korea Institute of Nuclear Safety ,

[b] TUV Rheinland Korea Ltd

*Corresponding author : k220snd@kins.re.kr

Abstract. *The Objective Provision Tree (OPT) is a methodology to ensure and document the provision of essential "lines of protection" for successful prevention, control or mitigation of phenomena that could potentially damage the nuclear system. The OPT methodology has been developed by International Atomic Energy Agency (IAEA). The OPT is a top-down method with a tree structure for each defense-in-depth level, objectives and barriers, safety functions, challenges to maintain safety functions, mechanisms of safety function degradation, and provisions to each degradation or failure mechanism. The general approach in developing the OPT is to classify challenges based on phenomena, for example, degraded or disruption of heat transfer path, coolant flow blockages in the core, and etc. This approach has benefits in developing further logics for mechanisms and provisions with clear and straight logical paths. Nevertheless, the potential disadvantage lies in that the high complexity might come out during the development of detailed logics considering the plant-specific designs. Considering this, we adopt different approach in that the challenges are defined in terms of system boundaries of primary/intermediate heat transport system and steam generating system. Draft OPT for level 3 of Core Heat Removal safety function is developed for the KALIMER which is conceptually designed by Korea Atomic Energy Research Institute (KAERI). The purpose of our development is basically to apply the developed OPT to confirm whether there is no missing requirements in our safety requirements under development by Korea Institute of Nuclear Safety (KINS).*

1. Introduction

The Objective Provision Tree (OPT) is a methodology to ensure and document the provision of essential "lines of protection" for successful prevention, control or mitigation of phenomena that could potentially damage the nuclear system [1] . The OPT methology was developed mainly by International Atomic Energy Agency (IAEA) and the application of OPT method to development of new reactors such as GEN-IV was strongly recommended by GEN-IV International Forum (GIF) Risk and Safety Working Group (RSWG). Examples of OPT applications during new reactor design can be found in reference [2] and [3] . The OPT is a top-down method with a tree structure for each defense-in-depth level, objectives and barriers, safety functions, challenges to maintain safety functions, mechanisms of safety function degradation, and provisions to each degradation or failure mechanism. The general approach in developing the OPT is to classify challenges mainly based on phenomena, for example, degraded or disruption of heat transfer path, coolant flow blockages in the core, and etc. This approach has benefits in developing further logics for mechanisms and provisions with clear and straight logical paths. But the potential disadvantage of this approach lies in that the high complexity might appear during the development of detailed logics considering the plant-specific designs. We are adopting different approach in a sense that the challenges are defined in terms of system boundaries of primary/intermediate heat transport system and steam generating system.

Draft OPT for defense in depth (DiD) eel3 of Core Heat Removal was developed for the KALIMER reactor which is conceptually designed by Korea Atomic Energy Research Institute (KAERI). The objective of level3 is to control the accidents within the design basis and the engineered features and accident procedures are the essential means to accomsplish to this objective. The OPT is normally

developed by designer to confirm the safety function design but the purpose of our development is basically to apply the developed OPT to confirm whether there is no missing requirements in our regulatory requirements under development by Korea Institute of Nuclear Safety (KINS). Preliminary results are presented in this paper.

2. System Description of KALIMER

2.1. *Overall plant description*

KALIMER-600 is a liquid metal sodium cooled fast reactor plant.[4] The major systems of KALIMER-600 are reactor, reactor coolant system and connected systems, engineered safety features, instrumentaion and control systems, electric power systems, auxiliary systems, and steam and power conversion systems. The overview of the KALIMER-600 plant is shown in Figure 1. Reactor building, which adopts the seismic base isolation system to enhance the structural safety as well as the economics, is separated from both the fuel handling & storage building and the turbine building. For refueling process, a shielded fuel transfer case moves 6 core assemblies between the reactor and the fuel & storage building, and so on.
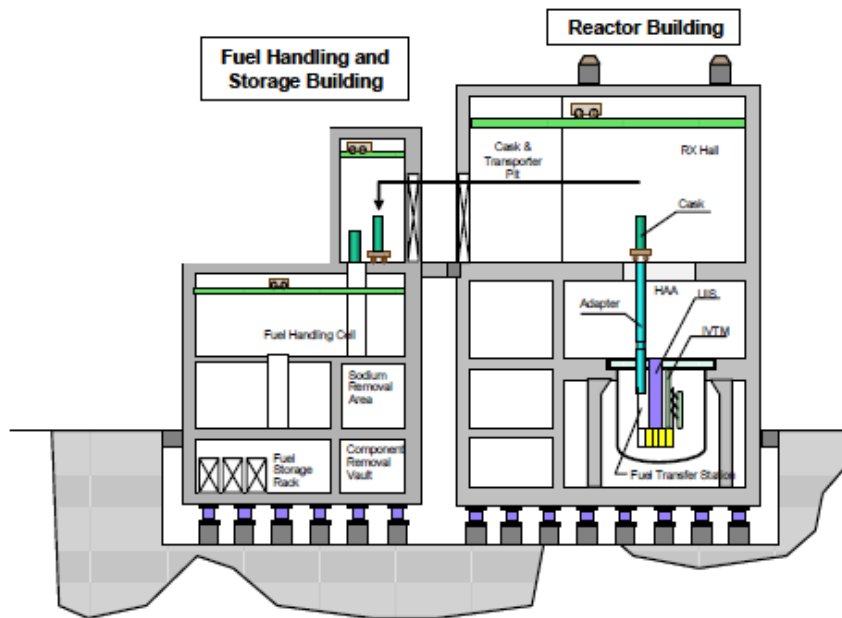

FIG. 1. KALIMER-600 layout

2.2. *Reactor*

The KALIMER-600 breakeven core is designed to generate 1523.4 MWt of power. The core adopts a homogeneous configuration in the radial direction that corporates annular rings of inner, middle, and outer driver assemblies. The core has an active core height of 94.0 cm and a radial equivalent diameter (including control rods) of 367.03 cm. The core structural material is Mod.HT9. The base alloy, ternary (U-TRU-10%Zr) metal fuel is used for the KALIMER-600 breakeven core as the driver fuel. Each fuel assembly includes 271 fuel pins and has a close-packed lattice. All the charged fuels have a single enrichment of TRU nuclides. The cladding thicknesses are different for the fuel rods in the different core regions for the purpose of power flattening under this single enrichment concept. The fuel is immersed in sodium for thermal bonding with the cladding. A fission gas plenum is located above the fuel slug and sodim bond. The bottom of each fuel pin is a solid rod end plug for axial shielding. The active reactivity control and shutdown system consists of fifteen control rods (twelve for primary control system and three for secondary control system) that are used for power control,

burnup compensation and reactor shutdown in response to demands from the plant control or protection systems. The control rod design satisfies both the one rod stuck condition and the unit control rod worth condition against the unprotected transient over power (UTOP) event. The ultimate shutdown system (USS) which drops neutron absorber by gravity is located in the core center as a means to bring the reactor to cold critical conditions in the event of a complete failure of the normal scram system and after the inherent reactivity feedbacks have brought the core to a safe, but critical state at an elevated temperature.

2.3. *Reactor coolant system and connected system*

There are two heat transport systems of Primary Heat Transfer System (PHTS) and Intermediate Heat Transfer System (IHTS), steam generation system Steam Generator System (SGS), and Passive Decay Heat Removal System (PDRS) as the reactor coolant system and connected systems. The overall configuration of the system is shown in Fig.2 below. PHTS mainly delivers the core heat to IHTS and IHTS works as the intermediate system between PHTS where nuclear heat is generated and the SGS where the heat is converted to steam. IHTS consists of two loops and each loop has its own steam generator and related systems. PHTS is a pool type system and this feature provides a large thermal inertia of the primary system. Strong emphasis has been given to the prevention and mitigation of possible sodium-water reaction events to the IHTS piping routing and SG design. For the circulation of PHTS coolant, 2 centrifugal pumps are used. The flow rate and ~~heat~~ can be controlled by varying the rotating speed of the pump impeller. In order to change the rotating speed, two approaches are used. The first one is to change the frequency of the supplied power to the pumps. The other one is to reduce the rotating speed through the fluidic converter. The operating temperature and component size were determined to achieve the net plant thermal efficiency of 39%. In the steam generation system, the feedwater pumps are shared by the two identical steam generation systems but each steam generation system is equipped with its own main and auxiliary flow control valves. In the reactor coolant system and connected systems, the major structures are the reactor vessel, containment vessel, reactor head, reactor internal structures, and reactor support structure. The reactor vessel is the container and support for the reactor core, primary sodium and reactor internal structures. The containment vessel assures that the reactor core will not be uncovered and core cooling can be accomplished even if the reactor vessel leaks. The reactor vessel and containment vessel have neither attachments nor penetration other than the core support structure to improve safety. The reactor head is the common closure for both reactor vessel and containment vessel and provides a cold deck during refueling and maintenance. The reactor internal structures provide mainly the reactor core support, primary sodium flow paths, shielding, seals and restraints for the PHTS pumps and Intermediate Heat Exchangers (IHXs). The reactor structures have been designed based on in-service inspection (ISI) and maintenance approaches to satisfy the safety goals and ensure high plant availability.
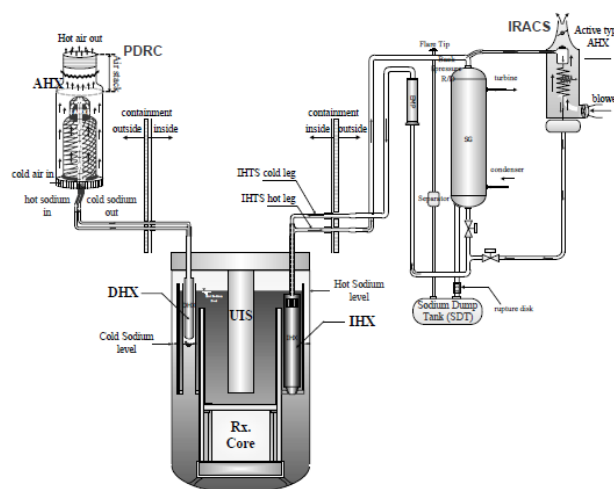

Fig.2 Configuration of KALIMER-600 System

2.4. Engineered safety features

The engineered safety features are the provisions in the plant which are designed to mitigate the consequence of accidents in radioactive material release. The engineered safety features implemented in KALIMER-600 are thPDRC, containment, and the IHTS guard piping.

3. Definition of Level of Defense-in-Depth and Safety Functions

In reference [5], levels of DiD was specified as in Table 1. These definition of DiD levels can be applied to all nuclear facilities including SFRs. Levels of DiD defined in Table 1 is applied to the DiD concept of KALIMER

Table 1. Levels of Defense-in-Depth

Levels of DiD	Objective	Essential Means
Level 1	Prevention of abnormal operation and failures	Conservative design and high quality in construction and operation
Level 2	Control of abnormal operation and detection of failures	Control, limiting and protection systems and other surveillance features
Level 3	Control of accidents within the design basis	Engineered safety features and accident procedures
Level 4	Control of severe plant conditions, including prevention of accident progression and mitigation of the consequences of severe accidents	Complementary measures and accident management
Level 5	Mitigation of radiological consequences of significant releases of radioactive materials	Off-site emergency response

In reference [5], safety functions in general form were specified as following;

- Control of the reactivity
- Core Heat Removal, and
- Confinement of radioactive materials and control of operational discharges, as well as limitation of accident releases.

4. Development of KALIMER OPT

For the development of OPT for KALIMER, level of DiD, objectives and acceptance criteria for Core Heat Removal safety functions are defined as in Table 2. These definitions are adopted from reference [2].

Table 2. Definition of level of DiD, Objectives, Safety Functions and Acceptance Criteria

DiD Level	Objective	Safety Function	Acceptance Criteria
Level 1	Prevention of deviations from normal operation and failure	Core Heat Removal	Transfer the power generated in the core to the BOP respecting allowed temperature ranges on fuel and structures during normal operation
Level 2	Control of abnormal operation and detection of failures	Core Heat Removal	Restore the balance between the heat generated and heat removed in order to comply with the allowed temperature ranges on fuel and structures established

			for anticipated operational occurrences
Level 3	Control of accident within the design basis	Core Heat Removal	Adequate cooling of the fuel, vessel internals, vessel and reactor cavity by active/passive systems, via heat transfer to ultimate heat sink(s), ensuring core geometry, and pressure vessel integrity

Based on the fundamental safety functions suggested in reference [5], safety functions for KALIMER are defined as in Table 3.

Table 3. KALIMER Safety Functions for OPT

Fundamental Safety Functions (IAEA NS-R-1)	KALIMER Safety Functions (draft)	Remarks
Control of reactivity	Reactivity control	Reactivity control function by control rods and other shutdown features
Removal of heat from the core	Core Heat Removal	Heat removal through PHTS
		Heat removal through IHTS
		Heat removal through SGS
		Heat removal in SPFP
Confinement of radioactive materials, control of operational discharges, as well as limitation of accident release	Containment integrity	Function to maintain containment integrity including, - Pressure/temperature control - Combustible gas control - Sodium fire and explosion protection - Radioactive material release control - Spent fuel building integrity

The safety functions, heat removal from core for KALIMR consist of four design-specific sub-safety functions, which can be matched to challenges directly, based on the system boundary definitions. This approach for the definition of core heat removal has several benefits as following;
- Clear logic development for challenges, mechanisms to degrade, and provisions,
- Benefits in verification of OPT integrity and coverage of safety requirements, and
- Reflection of design specificity

In examples of reference [2] and [3], different approaches in defining challenge to safety functions were applied. The benefit of approaches in reference [2] and [3] is that they can ensure the comprehensiveness of OPT by adopting the highly deductive approach. However, there might be potential complexity of OPT logic when the complex design features are considered.

With this philosophy mentioned above and considering the design characteristics, OPT was dveloped for level 3 DiD of core heat removal safety function. For this level of DiD and safety function, focusing is given on the provisions for mitigation. Considering the design status of KALIMER, OPTs were developed in detailed manner based on the physical system classification, for example, PHTS, IHTS and SGS. This enabled the more specific identification of challenges and provisions. The following mechanisms are selected for Level 3 DiD, Core Heat Removal safety function.

- Long-term loss of forced convection,
- Loss of inventory,
- Loss of ultimate heat sinks,
- Loss of vital power (short-term and long-term), and
- Loss of instrumentation and control

The inherent safety features of KALIMER considered during the development of OPT logics are as following;

- High thermal margins to fuel failure,
- High thermal capability of sodium coolant,
- Large pool-type reactor vessel, and
- Passive characteristics of main decay heat removal systems.

The above inherent and passive safety features can remove the many alternative or additional safety features as provisions to specific challenges. Meanwhile, the sodium specific safety features such as Sodium-Water Reaction Pressure Relief System (SWRPRS) and sodium fire suppression system are considered as provisions. The OPTs of level 3 DiD for Core Heat Removal safety function are given in Figures 3,4, and 5 below.
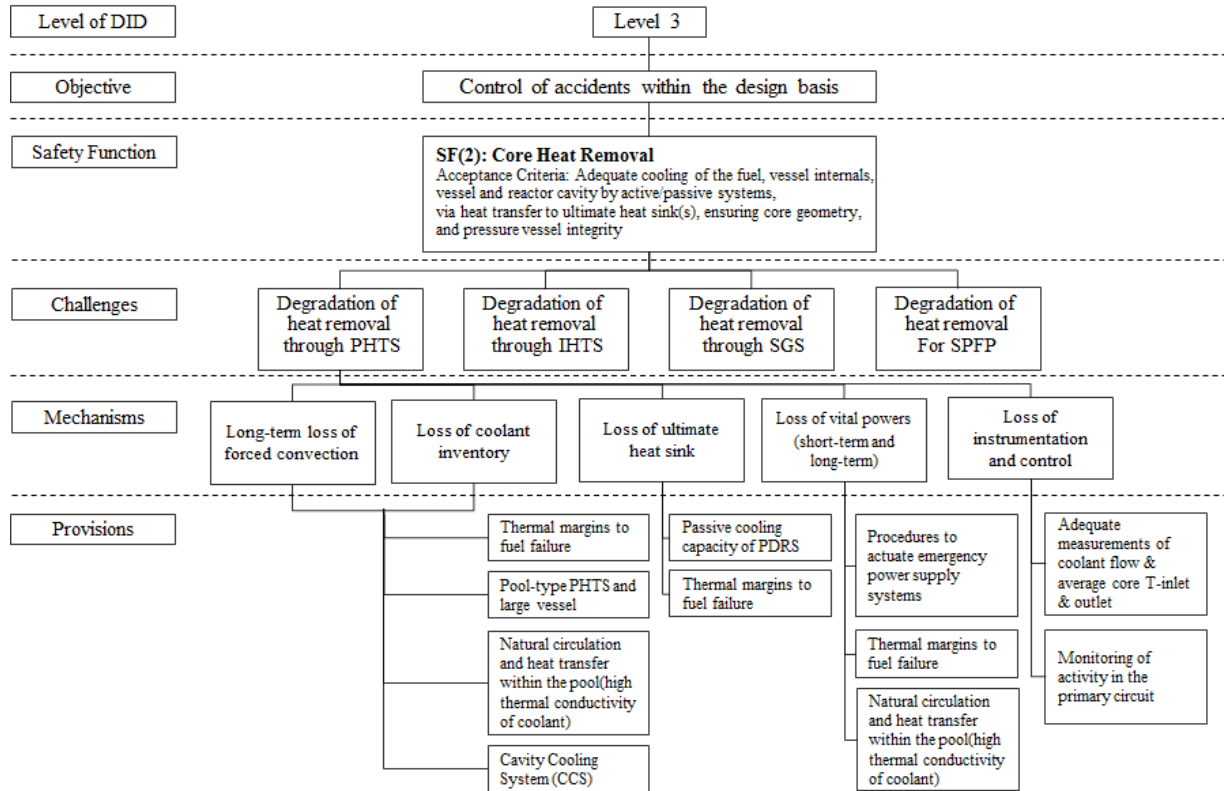

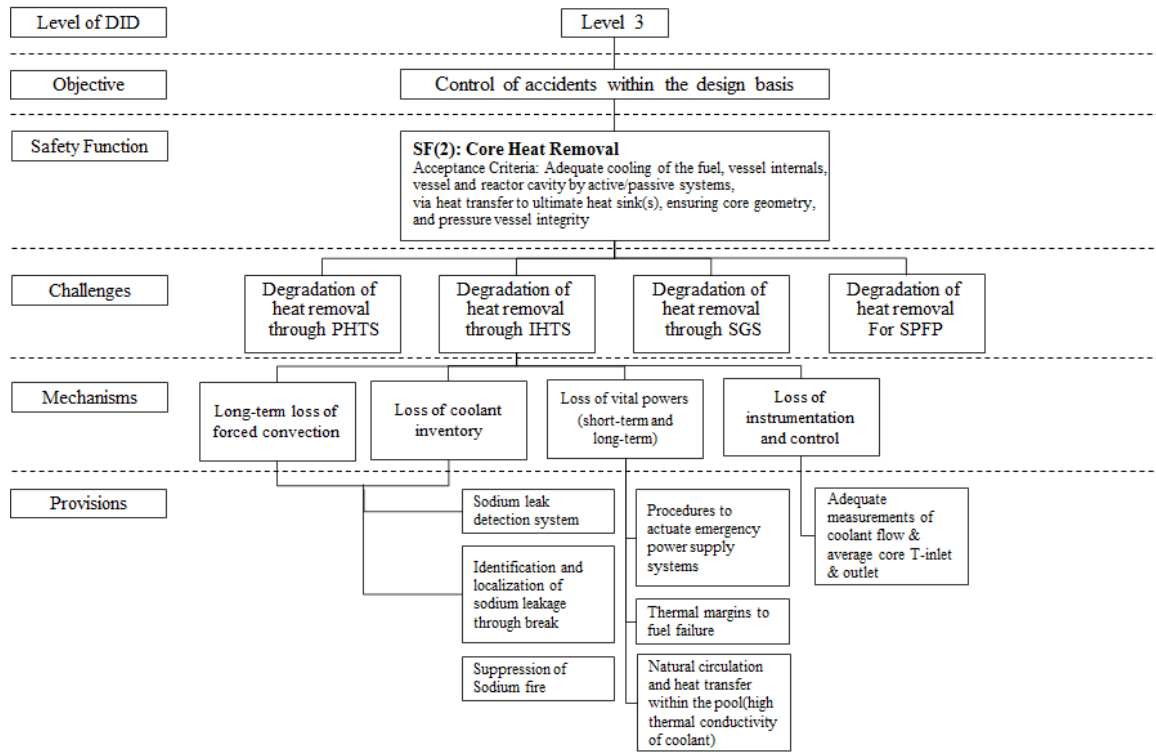FIG. 3. *Level 3 OPT of Core Heat Removal (1)*
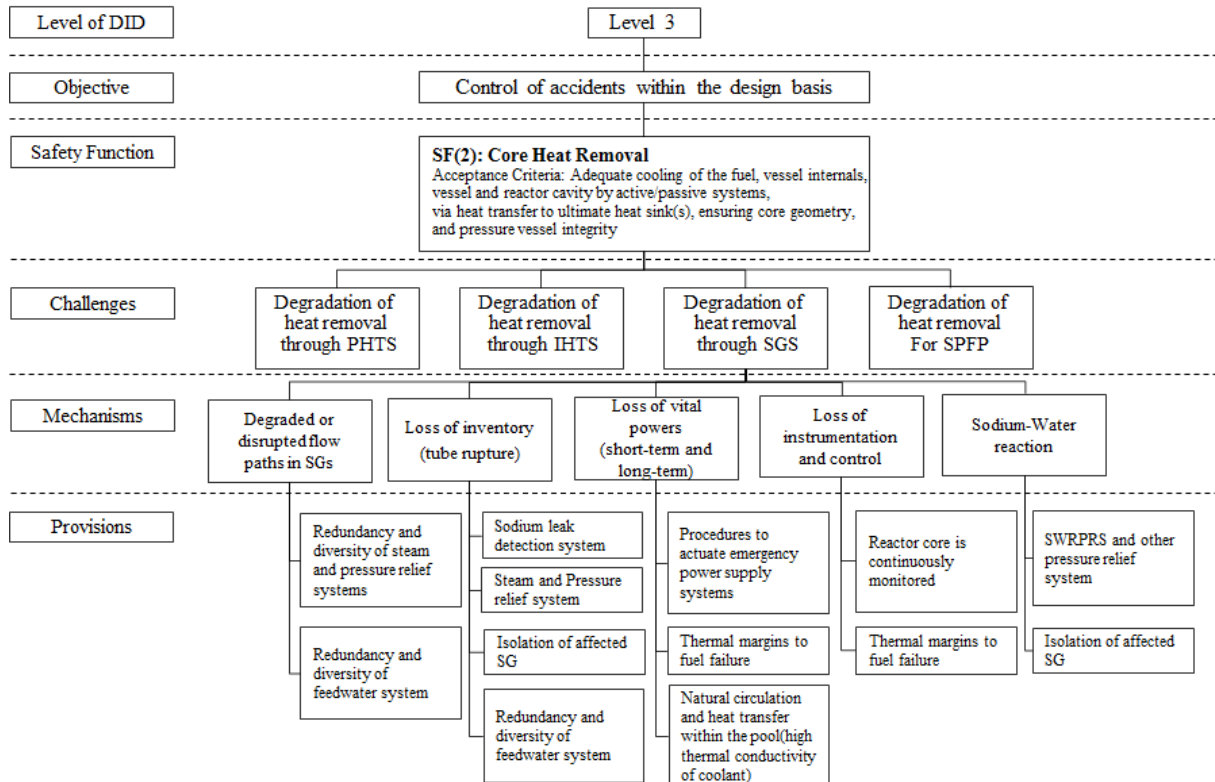
FIG. 4. Level 3 OPT of Core Heat Removal (2)

FIG. 5. Level 3 OPT of Core Heat Removal (3)

5. Conclusion

Draft OPTs for Level 3 of Core Heat Removal safety functions are developed for the KALIMER which is conceptually designed by KAERI. Previously the OPT is developed by designers based on phenomenology. But the potential disadvantage of this approach lies in that the high complexity might apprear during the development of detailed logics considering the plant-specific designs. Thus we used different approach in that the challenges are defined in terms of system boundaries of primary/intermediate heat transport system and steam generating system. The developed OPT provisions will be utilized in confirming whether there is no missing safety requirements. It could be also utilized in developing the Safety Review Plan because the provisions are developed for each system boundaries. Further study is in need to validate the adequacy of the developed OPT and to develop the necessary review guidelines or safety requirements.

REFERENCES

[1] GEN-IV International Forum, Risk and Safety Working Group (RSWG), "An Integrated Safety Assessment Methodology (ISAM) for Generation IV Nuclear System", 2011.

[2] International Atomic Energy Agency, "Consideration in the development of safety requirements for innovative reactors: Application to modular high temperature gas cooled reactors,", IAEA-TECDOC-1366 2003.

[3] G. L. Fiorini and T. Leahy, "Safety approach of Gen-IV systems: Application to SFR," presentation slides, IAEA Workshop on Safety Aspects of Sodium-cooled Fast Reactors, Vienna, 2010.

[4] Korea Atomic Energy Research Institute, "KALIMER-600 Conceptual Design Report," KAERI/TR-3381, 2007

[5] International Atomic Energy Agency, "Safety of Nuclear Power Plants: Design," NS-R-1,2000

Evaluation method of the verification test items for the transient analysis code of sodium cooled fast reactor

S.J. Hong[a], Y.J. Choo[a], N.D. Suh[b], A.D. Shin[b], M.H. Bae[b]

[a] FNC Technology Co., Seoul National University 135-308, Kwanak-ro 1, Kwanak-gu, Seoul, 151-742, S. Korea,

[b] Korea Institute of Nuclear Safety, Gwahak-ro, Yuseong-gu, Daejeon, 305-338, S. Korea

Presented by S.J. Hong

Abstract. GEN-IV reactors as a kind of advanced reactors including SFRs (Sodium Fast Rectors) are now world-widely under development with the aims of highly economical advances and safety enhancement. Together with the development of the advanced reactors, transient and accident analysis method for water reactors has also progressed. However, since the advanced reactors are fundamentally different from the water reactors, regulatory tools (code, data, etc.) may not be further directly applicable to the advanced reactor designs. For the reliable regulatory decision in accident analysis the analysis code should be sufficiently verified and validated. Several code and standards have been applied to light water reactors, for example Reg. Guide 1.157, Reg. Guide 1.203, NUREG-1230, ASME V&V 10.1-2012, and so on. Recently CFD (Computational Fluid Dynamics) has been gradually adopted in nuclear safety analysis and guidelines on the usage have also been suggested such as ECORA (Evaluation of Computational fluid dynamic methods for reactor safety analysis). The critical review of such materials gives insights for the evaluation method for the transient analysis code and this will be discussed in this paper. The key words in these materials are PIRT (Phenomena Identification and Ranking Table) and uncertainty analysis including bias. Another one important feature is that the regulatory bodies do not have the same degree of data as are available for light water reactors. Some proposed an international cooperative research and exploration as only a practical way. KINS (Korea Institute of Nuclear Safety) has devoted much effort in such a problem because Korean nuclear industry are now under pursuance of construction of SFR. As a first research step for the licensing process in SFR accident analysis a phenomena identification table was developed from the intensive research and independent reviews. Ranking process was not performed yet but screening process was conducted. So each item in the table is believed to be worthy while to consider. Such items will be discussed together with the evaluation method of the verification test items for the transient analysis code.

1. Introduction

GEN-IV reactors as a kind of advanced reactors including SFRs (Sodium Fast Rectors) are now world-widely under development with the aims of highly economical advances and safety enhancement [1]. Korea also takes part in that program and plans to construct demonstration reactor of a SFR [2]. To step with the development of the GEN-IV reactors, the safety analysis approach has also gradually advanced. Through the review of the last development of the licensing and safety basis in the advanced reactors, it can be found that one of the most principal issues pertaining to the advanced reactor is surely an accident evaluation. The accident evaluation or accident analysis covers identification of appropriate event categories, associated frequency ranges, evaluation criteria, and analysis of core, system and barrier performances (thermal-hydraulic safety analysis) [3,4]. The identification of appropriate event categories, associated frequency ranges, and evaluation criteria in SFRs are discussed in reference 5, and thermal-hydraulic safety analysis, especially the code accuracy or experiment evaluation, is discussed here.

Together with the development of the advanced reactors, transient and accident analysis method for water reactors has also progressed. However, since the advanced reactors are fundamentally different from the water reactors, regulatory tools (code, data, general design criteria etc.) may not be further directly applicable to the advanced reactor designs. For the reliable regulatory decision in accident analysis the analysis code should be sufficiently verified and validated. In general the reliability of the analysis code is checked through V&V (verification and validation) process, where according to Wikipedia, verification is explained as the evaluation of whether or not a product, service, or system complies with a regulation, requirement, specification, or imposed condition, and validation is explained as the assurance that a product, service, or system meets the needs of the customer and other identified stakeholders [6]. And V&V and evaluation of code uncertainty including bias of the analysis code usually requires the comparison of calculated data with experimental data. Thus, the process or structure of V&V process is of importance for the reliability and confidence of the code. In a similar way, the evaluation of the experiments must be related with the code V&V and uncertainty evaluation.

Several codes and standards have been developed and applied to light water reactors, for example NUREG-1230, Reg. Guide 1.157, Reg. Guide 1.203, and so on [7,8,9,10]. Code V&V methodologies are guided in industrial standards such as ASME V&V 10-2006, ASME V&V 20-2009, ASME V&V 10.1-2012, and so on [11,12,13]. Recently CFD (Computational Fluid Dynamics) has been gradually adopted in nuclear safety analysis, and guidelines on the usage have also been suggested in such as ECORA (Evaluation of computational fluid dynamic methods for reactor safety analysis) and by Bestion et al. [14,15,16,17].

The critical review of such materials gives insights for the evaluation method for the transient analysis code and this will be discussed in this paper. Following the critical review the actual activities of KINS (Korea Institute of Nuclear Safety) is presented.

2. Appraoch of experiment evaluation

US NRC (United Sate Nuclear Regulatory Committee) and industries published several guides on the development of development of thermal hydraulic analysis tools and on the evaluation of uncertainty and bias [7,8,9,10,11,12,13].

- NUREG-1230(1988): Realistic calculation of LOCA (Loss of Coolant Accident)

- Reg. Guide (Regulatory Guide) 1.157(1989): Best estimate of ECCS (Emergency Core Cooling Systeme) performance

- INEL-96/0400(1997): RELAP5/MOD3 evaluation results on AP600 SBLOCA (Small break LOCA)

- Reg. Guide 1.203(2005): Transient and Accident Analysis Methods

- ASME V&V 10-2006(2006): Guide for V&V in Computational Solid Mechanics

- ASME V&V 20-2009 (2009): Standard for V&V in CFD and Heat Transfer

- ASME V&V 10.1-2012 (2012): Illustration of the Concepts of V&V in Computational Solid Mechanics

Study on the guideline of CFD application to nuclear safety analysis has been pursued centering around European nuclear safety analysis researchers [14,15,16,17].

- ECORA (EVOL− ECORA−D01, EVOL−ECORA−D14): Study on the application of CFD to reactor safety

- Bestion, D., et al., (2009, 2012): Study on the guideline of two-phase flow CFD to reactor thermally hydraulic analysis and safety analysis application
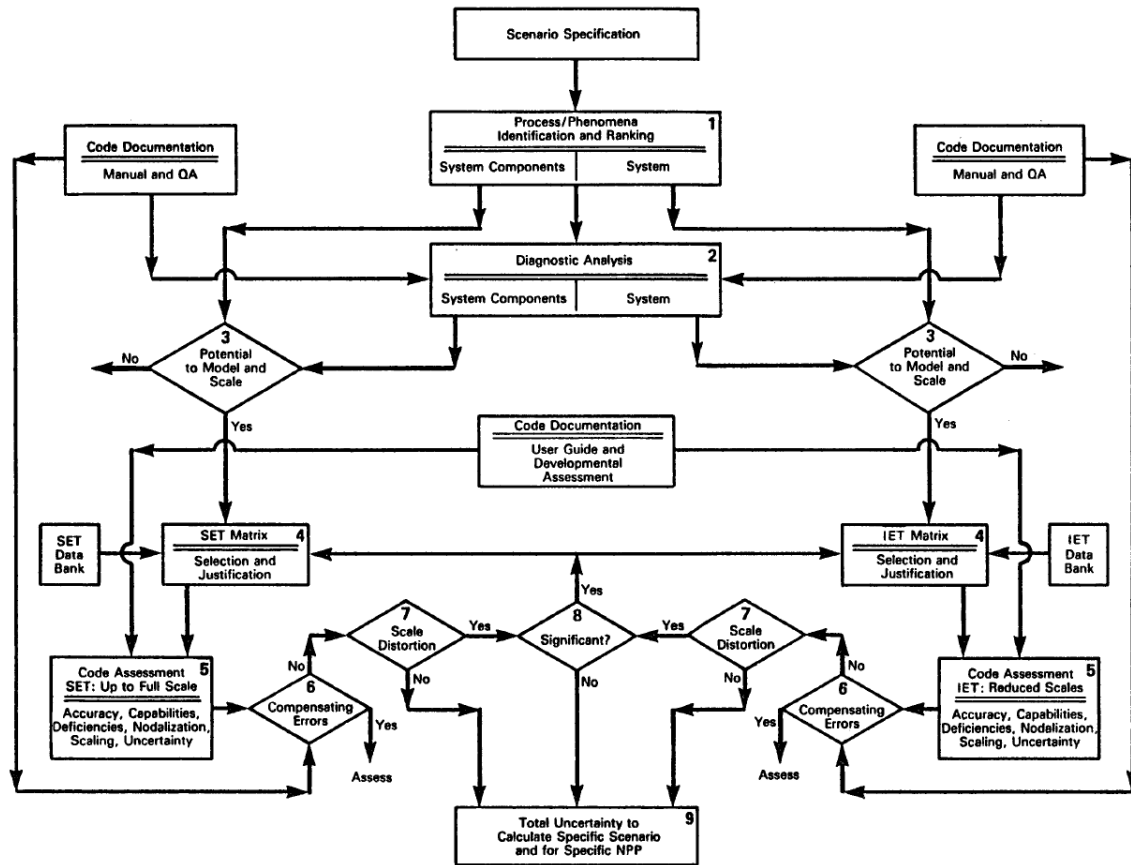

FIG. 1 Flow diagram for the CSAU evaluation method (NUREG-1230)

All of the above approaches discusses on the comparison of analysis code to applicable experimental data of SETs (Separate Effect Tests) and IETs (Integral Effect Tests) in order to decide the overall uncertainty and bias. NUREG-1230, whose flow diagram for the CSAU (Code Scaling, Applicability, and Uncertainty) evaluation method is shown in FIG. 1.

Reg. Guide 1.157 explains the guides of the best estimate calculation of ECCS performance related with LOCA, and the methodology of chapter 4 of NUREG-1230 is endorsed for the evaluation of code uncertainty. This Reg. Guide provides specific procedures in each step of the ECCS performance evaluation in particular. Report of INEL-96/0400 [10] provides the actual analysis of SBLOCA using RELAP5/MOD3 for AP600 power plant and requires the evaluation of SETs and IETs. This is a kind of the top-down concept (Integrated Code Assessments) code assessment. Reg. Guide 1.203 is more general guide on the evaluation model development and assessment process (EMDAP). Outline of the guide is presented in FIG. 2. Elements 1, 2, and 3 are related with the development of evaluation model (EM) and element 4 is related with the adequacy assessment of EM. And the final product of the element 4 is EM bases and uncertainty, and this is used in determination of the adequacy of the EM.
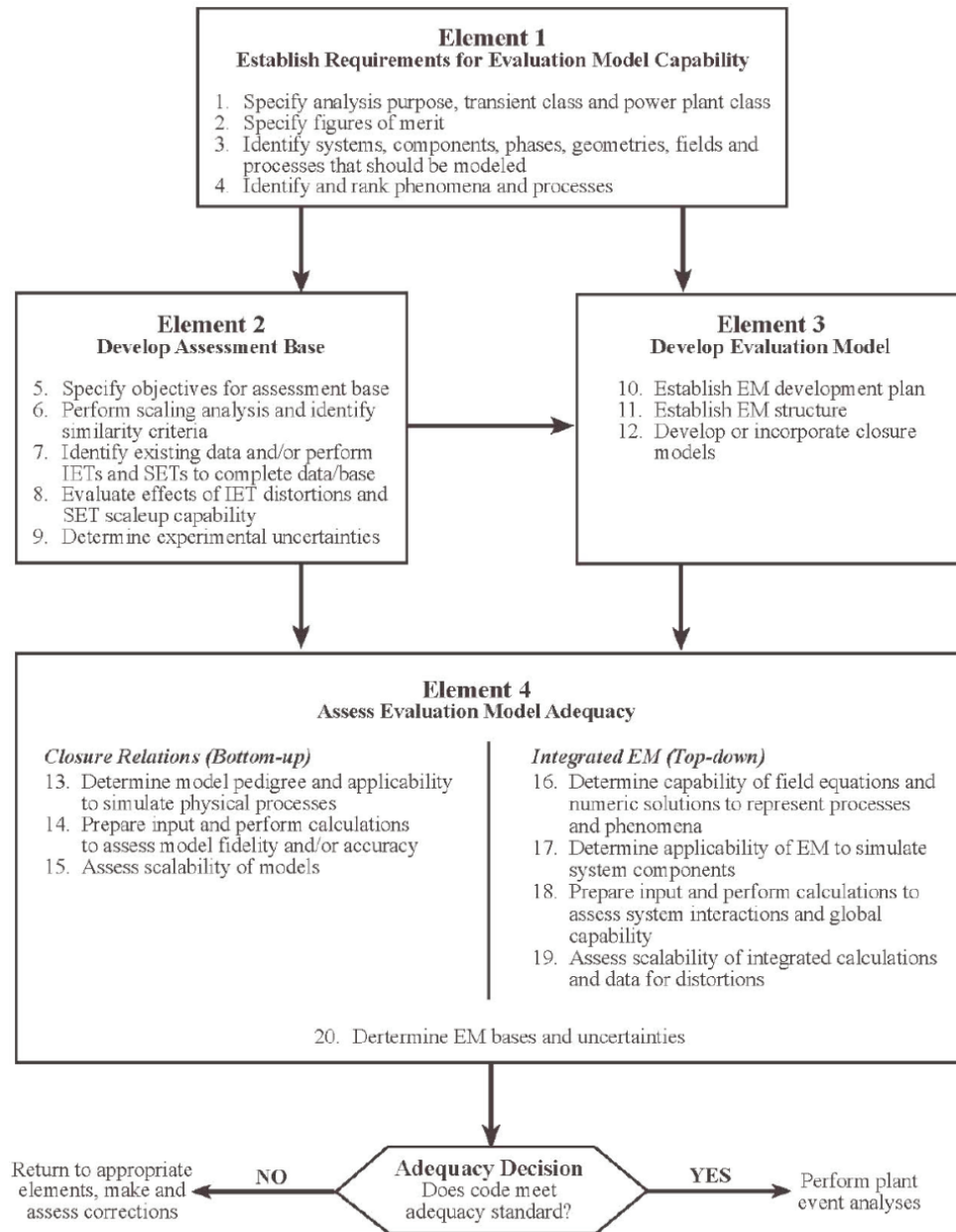
FIG. 2 Overall diagram of the EMDAP (evaluation model development and assessment process) process and the relationships among its elements (Reg. Guide 1.203).

ASME also published several codes and standards on the V&V of computational codes. ASME V&V 10-2006 gives explanation on the element of V&V as modeling activities and experimental activities as shown in FIG. 3. This configuration has some common features with NUREG-1230 and Reg. Guide 1.203, even though this is not on the computational thermo fluid

FIG. 3 Elements of V&V (ASME V&V 10-2006)

dynamics but on computational solid mechanics. ASME V&V 10-2006 also provides guides on V&V activities for realty of interest as FIG. 4. FIG. 4 was reproduced in ASME V&V 10.1-2012. The realty of interest is described as any level of components, subassemblies, assembly, or systems. The term of important phenomena is not used in these codes and standards, and it might be because these are on the solid mechanics which deals with relatively simpler phenomenon of unique in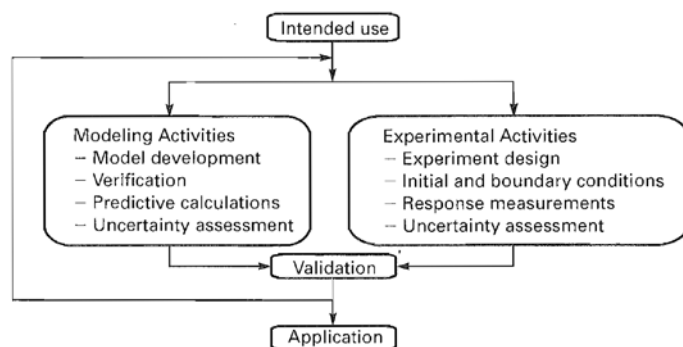terest. FIG. 5 is the validation process with sources of error in ASME V&V 20-2009. Comparison error is simply the difference between simulation and experiment for specified validation variables at a specified set of conditions (validation point). This seems somewhat quantitative, but is thought to be applied to a simple phenomenon.

The overall objective of the ECORA (Evaluation of Computational fluid dynamic methods for reactor safety analysis) project is the evaluation of the capabilities of CFD software packages in relation to simulating flows in the primary system and containment of nuclear reactors. The interest in the application of CFD methods arises from the importance of three-dimensional effects in these flows which cannot be predicted by traditional one-dimensional system codes. ECORA discusses on the selection of experiment for verification, validation, and demonstration step, respectively. This ECORA usually deals with single-phase flow.

FIG. 4 V&V Activities (ASME V&V 10-2006, ASME V&V 10.1-2012)
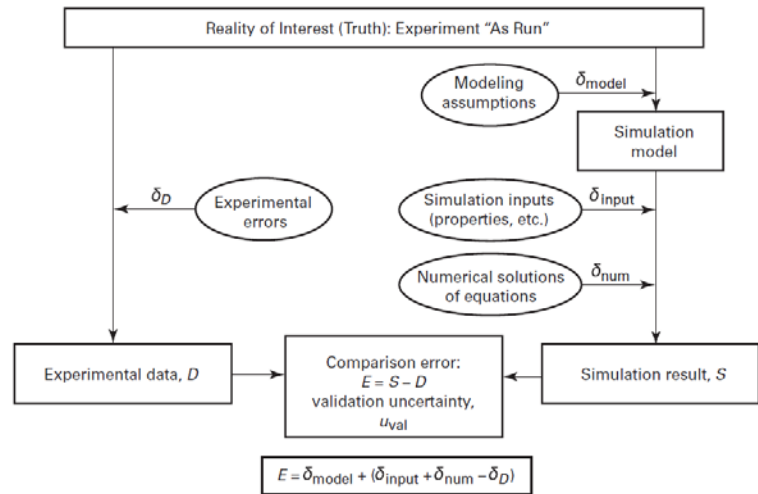
FIG. 5 Overview of the Validation Process With Sources of Error in Ovals (ASME V&V 20-2009)

For two-phase flow application Bestion et al. (2009, 2012) published several study results. They proposed following procedures to apply two-phase CFD to reactor safety analysis.

1. Identification of all important flow processes

2. Main modeling choices
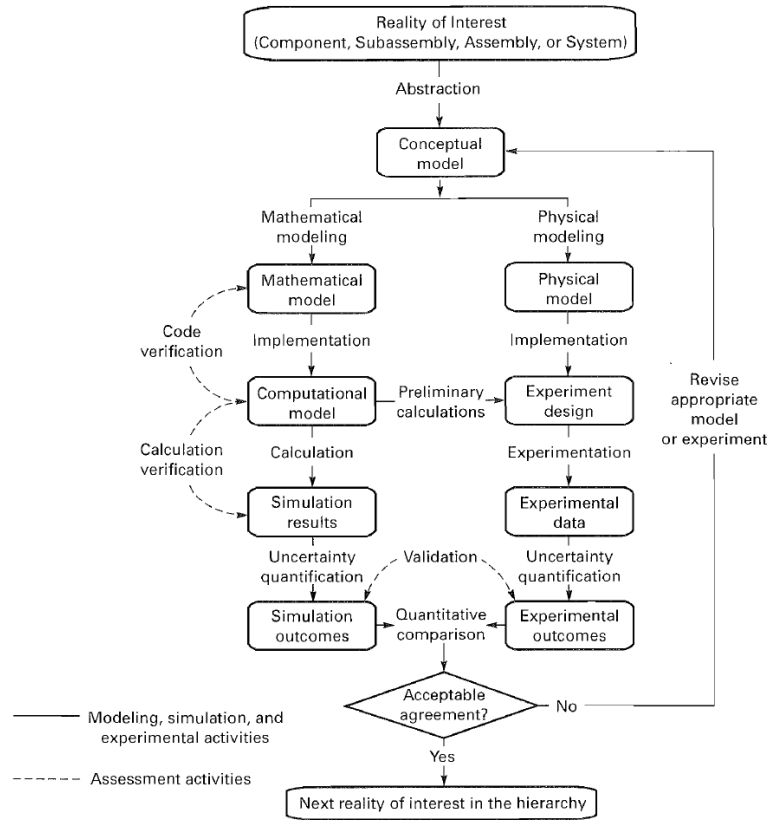
   2.1 Selecting a basic model

2.2 Filtering turbulent scales and two-phase intermittency scales

2.3 Treatment of interfaces

3. Selecting closure laws

    3.1 Modeling interfacial transfers

    3.2 Modeling turbulent transfers

    3.3 Modeling wall transfers

4. Verification

5. Validation

6. Uncertainty evaluation

It is depicted that the identification of all important flow processes is obtained by experiment analysis and/or PIRT (Phenomena Identification and Ranking Table). The methodology for two-phase CFD application to nuclear reactor safety is

FIG. 6 General methodology for two-phase CFD application to Nuclear Reactor Safety (Bestion et al. 2012)

presented in FIG. 6, and it includes V&V and uncertainty evaluations. In the similar way to the previous V&V discussions the verification is more related with model itself and the validation is always related with experiments.
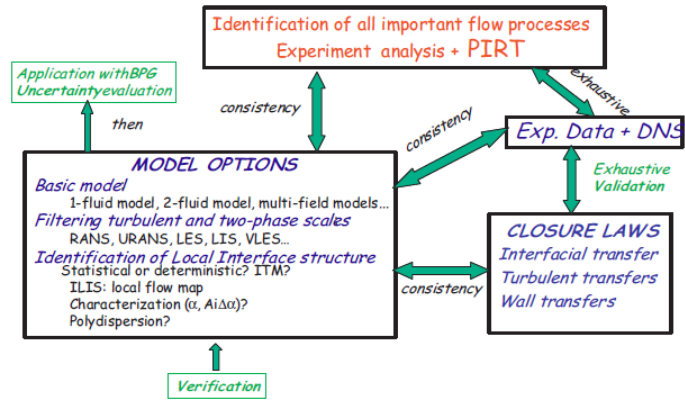
3. Selection of experiment for evaluation

Critical review of above section gives an insight that PIRT [18] must be useful in the selection of experiment for its evaluation or the EM V&V. The PIRT process entails carefully identifying the most demanding scenarios, followed by prioritizing the phenomena that are found in the most demanding scenarios. Key phenomena are those exerting the most influence on the path taken during the most demanding scenarios. Based on the results of PIRT the items and levels of the evaluation model is determined and experiment will be projected. So the selection of experiment for EM evaluation should totally depend on PIRT. Some code and standard such as Reg. Guide 1.157, which guides the best estimate calculation of ECCS performance, explicitly specifies the experiments related with each phenomenon.

EVOL− ECORA−D01 provides interesting guides in selecting and evaluating experimental data. This guide takes graded approaches according to the evaluation step;

- Verification Experiments

- Validation Experiments

- Demonstration Experiments

It is mentioned that the purpose of verification experiment is to ensure the correct implementation of all numerical and physical models in a CFD method. The best verification data would be analytical solutions for simple cases. The requirement for selecting verification experiment is that they allow a judgment of the correct implementation of the code and/or the models. The test suite for model

verification must be diverse enough to check all aspects of the implementation. Verification cases should be selected before the model is implemented. They must be considered an integral part of the model implementation.

The purpose of validation tests is to check the quality of a statistical model for a given flow situation. Validation tests are the only method to ensure that a new model is applicable with confidence to certain types of flows. The goal of validation tests is to minimize and quantify modeling errors. The requirement for selecting validation experiment is that the validation cases are selected to be as close as possible to the intended application of the model. Major features of CFD model for the validation experiments should be clearly identified. And sufficiently detailed data should be provided to evaluate the flow calculation or the CFD methodology. Completeness of information and high quality are key requirements.

The purpose of a demonstration exercise is to build confidence in the ability of a CFD method to simulate complex flows. Typically, the required detail of the experimental data is much lower than for verification or validation cases.

4.   Evaluation of uncertainties and bias

Uncertainty is in general the difference between simulation results by EM and experimental data. And some complicated process using the difference can be taken for the advance assessment of uncertainty.

The meaning that the code calculation result is in good agreement with experimental data is that if the average of code calculation and the average of experimental data are not so much different even though the code predict overly for some experiments and predict underly for the other experiments. It can be said that the accuracy of the code is high if the standard deviation is sufficiently small compared to average and the bias is also sufficiently small compared to standard deviation.

Reference 10 proposes 4 degrees of acceptance criteria as follows:

"Excellent" agreement applies when the code exhibits no deficiencies in modeling a given behavior. Major and minor phenomena and trends are correctly predicted. The calculation will, with few exceptions, lie within the specified or inferred uncertainty bands of the data.

"Reasonable" agreement applies when the code exhibits minor deficiencies. All major trends and phenomena are correctly predicted. Differences between calculation and data are greater than deemed necessary for excellent agreement. The calculation will frequently lie outside but near the specified or inferred uncertainty bands of the data.

"Minimal" agreement applies when the code exhibits significant deficiencies. Overall, the code provides a prediction that is only conditionally acceptable. Some major trends or phenomena are not predicted correctly, and some calculated values lie considerably outside the specified or inferred uncertainty bands of the data.

"Insufficient" agreement applies when the code exhibits major deficiencies. The code provides an unacceptable prediction of the test. Major trends are not predicted correctly. Most calculated values lie outside the specified or inferred uncertainty bands of the data.

For PIRT high-rank phenomena, the minimum standard for acceptability with respect to fidelity is generally "reasonable" agreement.

As a more systematic and quantitative method US NRC developed an uncertainty evaluation methodology called code scaling, applicability, and uncertainty (CSAU). A response surface is developed to act as a surrogate for the computer codes used in estimating the total uncertainty. The response surface can then be extensively Monte Carlo sampled to determine the total uncertainty. The use of limited computer calculations to develop an accurate response surface is followed by sufficient

Monte Carlo sampling of the response surface in an effort to be as thorough as necessary, yet as economical as possible.

D'Auria et al proposed FFTBM (fast Fourier transform based method) to evaluate the uncertainty in frequency domain rather than in time domain [19]. At first the error (difference) of calculation and experiments in time domain for an interesting parameter is calculated, and the experimental data and the errors are Fourier transformed. Then, average amplitude (AA) and weighted frequency (WF) that characterize code accuracy are calculated. For each variable the AA is defined as the sum of error function amplitudes normalized to the sum of experimental signal amplitudes, and the WF is defined as the sum of frequencies multiplied (weighted) by error function amplitudes, normalized to the sum of error function amplitudes. The overall picture of the accuracy for the given code calculation is obtained by defining average performance indices, total weighted AA and total WF, which are the sum of AA_i and WF_i for i-the parameter weighted by weighting factors. Weighting factor is composed of experimental accuracy, safety relevance, and primary pressure normalization. The weighting factor for the i-th parameter is the multiplication of the three items divided by the sum of the multiplication for total concerning parameters. The total AA and total WF can be used as as quantitative indices for the accuracy.

5. Phenomena identification table for SFR in Korea

KINS has devoted much effort in such a problem because Korean nuclear industry are now under pursuance of construction of SFR. As a first research step for the licensing process in SFR accident analysis a phenomena identification table was developed from the intensive researches and independent reviews. Ranking process was not performed yet but screening process was conducted. So each item in the table is believed to be worthwhile to consider. Such items can be discussed together with the evaluation method of the verification test items for the transient analysis code. Table 1 is some of the results. In total, 115 important phenomena were identified.

6. Special features of SFR experiment evaluation

One important feature on the experiment evaluation is that the regulatory bodies do not have the same degree of data as are available for light water reactors. Some proposed an international cooperative research and exploration as only a practical way[20]. For the sufficientness and completeness the international cooperation in SFR experiment project and sharing is thought to be essential.

Table 1 Phenomena identification table for SFR in Korea

No.	Subsystem/Component/SubComponent			Phenomena
1-1	General	-	-	Thermal striping/Stratification
1-2		Sodium	-	Sodium fire
1-3		-	-	Sodium-concrete interaction
1-4		-	-	High thermal diffusivity of sodium
1-5		-	-	Sodium freezing
2-1	Core and Fuel Assemblies	-	-	Pressure loss in core region
2-2		-	-	Natural convection
2-3		-	-	Reactivity feedback
2-4		-	-	Gap conductance between fuel and cladding
2-5		-	-	Heat transfer between cladding and coolant
2-6		-	-	Intra- and inter-assembly flow distribution
2-7		-	-	Radial heat transfer between subassemblies
2-8		-	-	Heat transfer between reflector and coolant
2-9		-	-	Thermal inertia of core assemblies
2-10		-	-	Coolant boiling

7. Conclusion

Experiment evaluation is a part of code V&V and evaluation, and a similar concept can be introduced for experiment evaluation. Several codes and standards and studies are intensively reviewed and some important insight was obtained. PIRT must be useful in the selection of experiment for its evaluation or the EM V&V. The PIRT process entails carefully identifying the most demanding scenarios, followed by prioritizing the phenomena that are found in the most demanding scenarios. Even though the formal PIRT is not used, the identification of important phenomena is very important. Some guide to select experiment for each grade step was also reviewed. The quantification of code uncertainty was also reviewed. CSAU method is reviewed and the other qualitative guides were reviewed. The calculation method of accuracy indices in frequency domain was also reviewed.

Another one important feature related with experiment evaluation is that the regulatory bodies do not have the same degree of data as are available for light water reactors. Some proposed an international cooperative research and exploration as only a practical way. KINS has devoted much effort in such a problem because Korean nuclear industry are now under pursuance of construction of SFR. As a first research step for the licensing process in SFR accident analysis a phenomena identification table was developed from the intensive research and independent reviews. Ranking process was not performed yet but screening process was conducted. So each item in the table is believed to be worth while to consider. Such items will be discussed together with the evaluation method of the verification test items for the transient analysis code.

REFERENCES

[1] U.S. Department of Energy, A Technology Roadmap for Generation IV Nuclear Energy Systems, GIF-002-00, U.S. DOE Nuclear Energy Research Advisory Committee and the Generation IV International Forum, 2002

[2] Y.I. Kim et al., Conceptual Design Report of SFR Demonstration Reactor of 600MWe Capacity, Korea Atomic Energy Research Institute, KAERI/TR-4598/2012, 2012

[3] US NRC, Issues Pertaining to the Advanced Reactor (PRISM, MHTGR, AND PIUS) and CANDU 3 Designs and their Relationship to Current Regulatory Requirements, Unite States Nuclear Regulatory Committee, SECY-93-092, 1993

[4] S.J. Hong et al., Methodology Development for Establishment of Licensing Basis Events and Safety Analysis of GEN-IV Reactors , Fenruary 2010, Korea Institute of Nuclear Safety, KINS/HR-922

[5] S.J. Hong et al., Discussion on a Safety Analysis Approach in The Licensing Process of Pool Type Sodium Fast Reactors in Korea, 2nd International Technical Meeting on Small Reactors, Ottawa, Ontario, Canada, 2012 November 7-9

[6] Wikipedia, http://en.wikipedia.org

[7] NUREG-1230, 1988, Compendium of ECCS Research for Realistic LOCA Analysis,

NUREG-1230, December 1988

[8]   Regulatory Guide 1.157, Best-Estimate Calculations of Emergency Core Cooling System Performance, U.S. Nuclear Regulatory Commission, May 1989

[9]   Regulatory Guide 1.203, 2005, Transient and Accident Analysis Methods, U.S. Nuclear Regulatory Commission, December 2005

[10] C.D. Fletcher, et al., Adequacy Evaluation of RELAP5/MOD3, Version 3.2.1.2 for Simulating AP600 Small Break Loss-of-Coolant Accidents, INEL-96/0400 (nonproprietary version), April 1997

[11] ASME V&V 10-2006, Guide for Verification and Validation in Computational Solid Mechanics

[12] ASME V&V 20-2009, Standard for Verification and Validation in Computational Fluid Dynamics and Heat Transfer

[13] ASME V&V 10.1-2012,An Illustration of the Concepts ofVerification and Validation in Computational Solid Mechanics

[14] EVOL– ECORA–D01, ECORA CONTRACT N° FIKS-CT-2001-00154, CFD Best Practice Guidelines for CFD Code Validation for Reactor-Safety Applications, February, 2002, EVOL– ECORA–D01

[15] EVOL–ECORA–D14, ECORA CONTRACT N° FIKS-CT-2001-00154, Recommendation on Use of CFD Codes for Nuclear Reactor Safety Analysis, September 2004, EVOL–ECORA–D14

[16] D. Bestion, , et al., 2009, Some lessons learned from the use of Two-Phase CFD for Nuclear Reactor Thermalhydraulics. In: 13th International Topical Meeting on Nuclear Reactor Thermal Hydraulics (NURETH-13), Kanazawa City, Japan, September 27–October 2.

[17] D. Bestion, 2012, Applicability of Two-Phase CFD to Nuclear Reactor Thermalhydraulics and Elaboration of Best Practice Guidelines, Nuclear Engineering and Design 253 (2012) 311– 321

[18] Wilson, G..E. & Boyack, B.E., The Role of the PIRT Process in Experiments, Code Development and Code Applications Associated with Reactor Safety Analysis, Nuclear Engineering and Design, Vol. 186, pp 23-37, 1998

[19] A. Prošek et al., Review of quantitative accuracy assessments with fast Fourier transform based method (FFTBM), Nuclear Engineering and Design 217, 2002, pp.179–206

[20] Michael Johnson, Strategic decisions on research for advanced reactors: USNRC perspective, in The Role of Research in a Regulatory Context (RRRC-2), Nuclear Safety NEA/CSNI/R(2008)3, ISBN 978-92-64-99045-6, 2008

Actual Thermophysical investigations in a substantiation of designs and safety of nuclear fast reactors for new generation

A.D. Efanov, F.A. Kozlov, V.M. Poplavsky, A.P. Sorokin

State Scientific Center of Russian Federation – Institute for Physics and Power Engineering named after A.I. Leypunsky, Obninsk, Russia

Bondarenko Sq. 1, 249033, Obninsk, Kaluga Region, Russia
E-mail: sorokin@ippe.ru

Abstract. The results of thermal physical experimental and computation-theoretical investigations executed recently in SSC RF-IPPE with the goal of increasing efficiency and safety of fast reactors of the new generation, including investigations of emergency processes with boiling of the sodium coolant in reactor core, temperature stratification, stratification of coolant and temperature fluctuations in mixing region of the hot pool in a substantiation of decay heat removal systems and passive safety systems, highly effective systems of sodium purifying from the impurity maintaining admissible concentration of impurity etc. which should provide a basis for creation and demonstration of deep level of protection for fast reactors of the new generation with system of barriers and the passive systems preventing development of emergency processes and providing transfer of reactor facility in a condition with a low energy potential are stated and are discussed. Problems further thermal physical investigations are formulated.

1. Introduction

Taking into consideration the gained experience on designing and maintenance of the working NNP and also new more hard safety standards the task of working out of fast reactors with liquid metal coolants of new generation with improved economic and operating characteristics and with raised level of internal security was set. A main direction for solution this task is development and heading of innovative designs and the further development of NNP self-security properties by a combination of safety properties and passive safety systems [1, 2].

For example, the new solutions adopted in the design of advanced fast reactor (BN-1200): updated reactor and SG structure design (lower metal consumption), use of bellows on the secondary piping (lower piping length and metal consumption), accommodation of the primary cold traps in the reactor vessel (elimination of radioactive sodium piping and related auxiliary systems outside reactor vessel), modification of decay heat removal system using independent heat exchangers inside reactor vessel (higher reliability), etc [3].

The wide investigations executed in SSC RF-IPPE in the region of thermal hydraulics, physical-chemical process and coolant technology for a substantiation of projects and safety of fast reactors with sodium coolant, heavy liquid metal coolants, innovative fast reactors projects development, computer codes for numerical modeling of heat and mass transfer process in fast reactors and verification tests systems development [4-5].

2. Studies for justification of projects of advanced fast reactors with sodium coolant

Experimental and analytical studies of accident process development are carried out for justification of projects decision of BN-1200 reactor under severe accident conditions and verification of computer codes used for justification of BN-1200 reactor safety:
- simulation of thermal hydraulics in reactor vessel under normal operation, transient and accidental conditions.
- studies for justification of the emergency decay heat removal system (DHRS) with air heat exchangers (AHX) aimed at increasing its effectiveness;
- studies on sodium boiling in the core fuel subassembly model as applied to reactor severe accident;
- studies on the fuel elements damage rate under coolant leakage conditions;

- studies of efficiency of shut down devices for justification of passive safety systems;
- studies on effectiveness of various methods of sodium leak detection on condition of safety jackets installed on the secondary circuit components;
- studies for justification of hydrogen safety in the steam generator and water pond for spent fuel subassemblies.
- working out of trees for events and failures in SG protection system for definition of probabilistic characteristics of process of hydrogen-air mixes formation in box of SG BN-1200 and numerical analysis of velocity of hydrogen formation and safety in water cooling pond of reactor BN-1200 for justification of hydrogen safety.

2.1. R&D for justification of innovative designs of the main components and systems of NPP with BN-1200 reactor

2.1.1. In-vessel flow. Decay heat removal system

The results of investigations show us that the processes of temperature stratification of coolant, which are not mentioned in the design documents, cause drastic changes of coolant flow structure in upper plenum of fast reactor and temperature mode and formation of stagnation and recirculation zones with large temperature gradients and fluctuations in the interfaces of isothermal areas. Thermal fatigue of material caused by temperature gradients and fluctuations in stratified flow decreases lifetime of in-vessel components [6].

Besides, coolant stratification has strong effect on reactor neutronics, physical and chemical interaction of coolant with structural materials, processes of oxide precipitation in the cold stagnation zones of reactor vessel, and requires justification of installation of standard control system sensors and accommodation of the cold traps in the reactor vessel. Up-to-date computer codes are only capable of evaluating averaged temperature pattern in the coolant flow, but, as a rule, temperature fluctuation characteristics cannot be forecasted by the codes.

In the region with stable stratification above the radial blanket, one or more recirculation zones are formed with the large temperature gradients and fluctuations on the interfaces depending on buoyancy extent which decreases with the decrease of Froude number. In case of reactor scram causing abrupt power decrease the ultimate case of coolant stratification is realized with full suppression of convective transfer on the thin stratified interface involving total cross section of the upper plenum. On the interface between the upper hot and lower cold coolant areas internal waves appear causing temperature fluctuations in the reactor components material.

Experimental model SARH has been mounted on V-200 test facility for simulation of thermal hydraulics in fast reactor vessel under steady state, transient and accident conditions (Figs. 1 and 2). The main objectives of the experimental studies on this model are as follows:
- determination of coolant temperature distribution at the fuel subassembly outlet for the purpose of coolant temperature monitoring above the core and sodium temperature fluctuations influencing mechanical characteristics of structures under the steady state conditions of reactor operation;
- studies on features of stratified flow thermal hydraulics in the elements of coolant flow path in fast reactor operating in various modes;
- working out recommendations on the decrease of temperature non-uniformity and intensification of mixing of non-uniform flow;
- studies on natural flow development in case of ULOF accident and confirmation of design solutions made on passive decay heat removal system with immersed heat exchangers in the upper plenum.

2.1.2. The in-vessel sodium coolant purification system

In view of the main objective of current stage of nuclear power development, i.e. improvement of safety, cost effectiveness and decrease of environmental impact, requirements to all reactor systems would be more rigid [7-8]. In particular, decision has been made to accommodate all radioactive primary sodium systems within the reactor vessel. Therefore, limitations are imposed on the overall dimensions of the

primary sodium purification system. For this reason, positive experience gained earlier on sodium purification systems located outside reactor vessel cannot be used to the full extent.

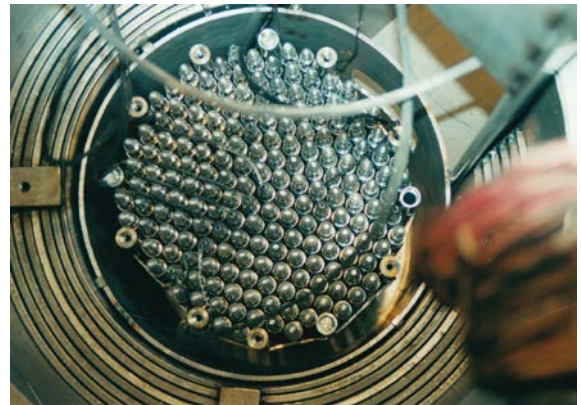*Fig. 1. General view of the upper section of SARH model*

Fig. 2. Top view of dummy fuel subassemblies of SARH model

Engineering system of complex sodium purification from impurity for BN-1200 is executed: studies for justification a new principles of the primary sodium purification system without use of in-vessel cooling system, study of alternative cold trap (CT) designs for primary circuit and monitoring systems of impurity, optimizing of mass transfer calculations in CT, refinement of parameters built-in CT and its units, research of sodium clearing processes with use of new structural materials and filtering and sorption processes at work on the reduced temperature parameters.

Studies have been carried out for justification of sodium purification system of advanced fast reactors taking into account requirements to the in-vessel sodium purification system (IVPS) assuring permissible impurities content in sodium, sufficient volumetric capability in terms of impurities amount, output and elimination of uncontrolled accumulation of impurities in the heat removal loops. Analysis has shown that sodium purification system is mainly based on the cold traps removing both oxygen and hydrogen from sodium coolant in all operating modes of NPP. Besides it is possible to use hot traps (getter – iodine zirconium) under nominal operating conditions, filters for continuous purification of sodium coolant and absorbents for cesium removal.

Demonstration evaluation of heat and mass transfer in the cold traps of advanced fast reactors (Fig. 3 and 4) have shown an intricate pattern of sodium flow including jet flow, recirculation and stagnation regions [9-10].

Sodium flow in the cold trap is strongly influenced by natural flow forces caused by temperature gradients. For instance, in the upper section of working plenum sodium flow on the cooled surface at about -0.2 m/s velocity is directed downwards contrary to the main flow, while the velocity of sodium flowing upwards along hotter surface of supply tube is ~0.3 m/s. According to the calculation results, jet flow velocity decreases down to almost zero at the distance 0.5-1.0 m from the outlet nozzle of supply tube. In the settling chamber region of sodium recirculation at low velocity (1-2 mm/s) is formed. On the periphery of this region sodium flows downwards along outer cooled wall, and in the central area sodium flows upwards.

As researches result on optimization built-in CT BN-1200 (were observed the CT designs with cooling by an argon and sodium in which basis was assumed the design analogous CFT BN-350, BN-600, BOR-60) it is offered:
− to expel hydrogen accumulation in CT primary circuit (the executed estimations have shown, that it can be realized at regimes of CT maintenance of primary and second circuits with outlet temperatures 150 and 120ºC, accordingly);
− to use for cooling of CT primary circuit not argon, and liquid metal coolant, having good thermophysical and corrosive properties, having a firm modular condition at room temperature, not influencing negatively for reactor work at its emergency receipt in the first contour (sodium, an eutectic alloy sodium-lithium are observed).
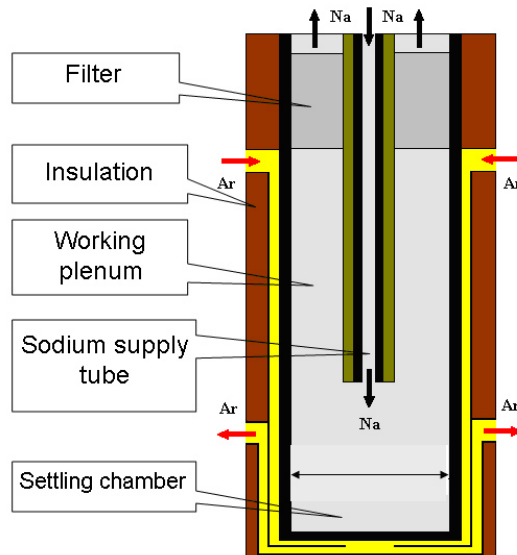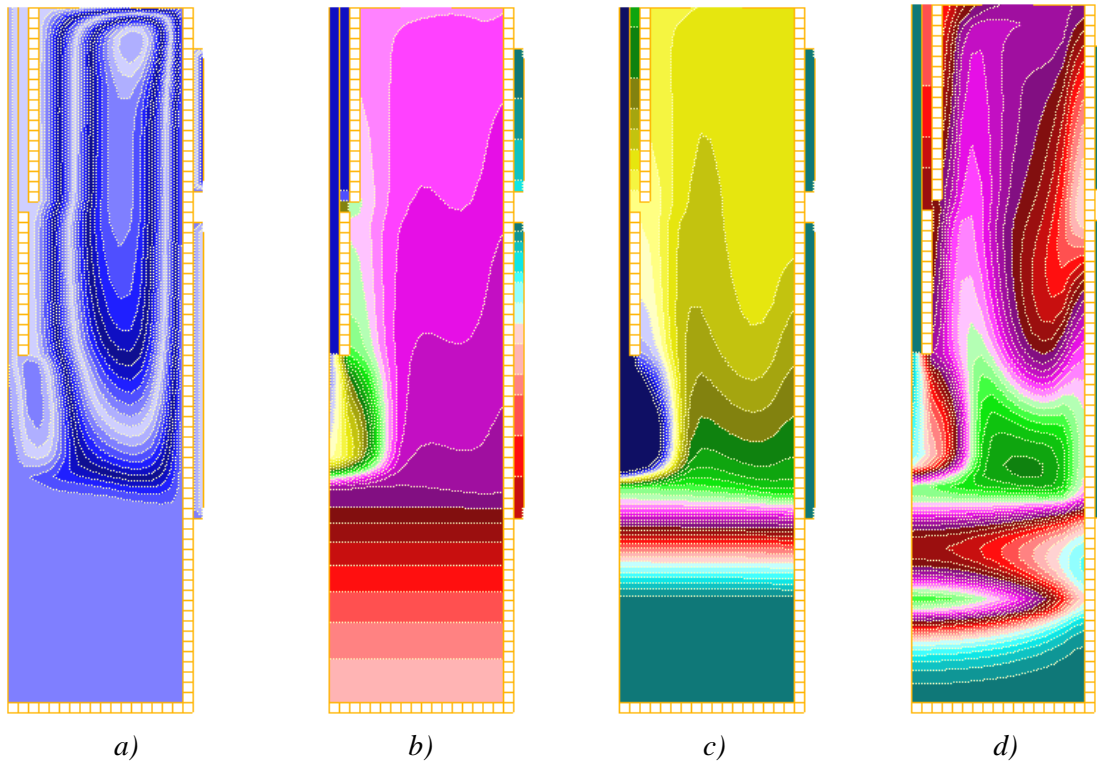
Fig. 3. Diagram showing calculation area of the cold trap model

Filter

Insulation

Working plenum

Sodium supply tube

Settling chamber

a)   b)   c)   d)

Fig. 4. Results of demonstration analytical studies on fast reactor cold trap:
a – flow pattern, b – temperature field, c – dissolved impurities content pattern,
d – crystallized impurities content pattern

Studies have shown that operation of sodium purification system in the mode preventing hydrogen accumulation in the primary circuit would make it possible to decrease the number of replacements of the primary cold traps of fast reactors. Total sodium flow rate in the secondary cold traps should be maintained constant. If IVPS option is chosen, then detailed safety analysis is required concerning operation of the cold traps in all possible modes, as well as storage of the cold traps removed from the reactor vessel. Since there is no IVPS prototype in Russia, extensive analytical, experimental and design work is required for the purpose of justification of the new cold trap design and appropriate auxiliary equipment. The program of further studies has been developed.

2.1.3. Justification for design and safety system of integral steam generator of BN-1200 reactor plant

Extensive R&D work program is implemented for justification of optimum basic design of integral steam generator of BN-1200 reactor plant and its safety system:
−   studies on thermal hydraulics of SG, water chemistry regime and development of technology of sediments removal from SG;
−   studies on SG hydrodynamic stability and carrying out duration tests;
−   studies on structural materials resistance in the area of water leak into sodium;
−   studies on resistance to caustic cracking;
−   studies on the effectiveness of SG safety system in case of water leak into sodium;
−   development of physical and mathematical model of sodium-water reaction zone to be used in LLEAK code designed for simulation of hydrodynamics in the secondary circuit in double-component approximation.

For the large-block steam generator design of the BN-1200 reactor, issues of early leak detection, development of automatic safety system eliminating serious structural damage, and efficient repair important from the standpoint of high load factor are particularly urgent. In order to assure SG safety in case of water (steam) leak to the shell side of module it is planned to carry out tests of updated SG automatic safety system in SAZ test facility which is under construction at the SSC RF-IPPE [11].

SAZ is isothermal test facility simulating full-scale pipelines and components of the BN-800 SG section (Fig. 5). Sodium volume in the loop is about 25 m^3, maximum sodium flow rate is 1200 m^3/h, maximum temperature is 510ºC and electrical supply power is 3000 kW.

Fig. 5. SG safety system test facility SAZ

Failure of SG module tube is simulated by water (steam) injection to the shell side of the module and detected by the leak detection system. It is planned to carry out studies on determination of parameters of efficient detection system operation, minimization of pollution and damages of structures in case of water (steam) leak causing hydrodynamic and temperature effects in the system. Also, mechanisms and equipment of SG safety system will be tested.

2.2. R&D of thermal hydraulics for justification of reactor core safety and main components of advanced fast neutron reactor

2.2.1. Experimental investigations for development of severe accident in fast reactor core

Fast reactor protection against reactivity accidents is provided by inherent safety (self-protection) features of the reactor and by the use of monitoring, control and protection equipment, as well as by reliable heat

removal. Analysis of reactor safety under BDBA conditions performed by calculation of extreme limit states characterized by partial or complete failure of active safety systems and elements resulted in the analysis of core heat removal under conditions of sodium boiling onset.

Earlier studies have shown [12] that due to the high-rate boiling heat transfer continuous FR core cooling can be provided in case of accident. Further studies are focused on boiling progression for the new engineering solution aimed at increasing fast reactor safety, namely: sodium plenum provided above the core [13]. In this regard, studies should be made on conditions of boiling area formation in the fuel subassemblies under accident conditions and sodium boiling characteristics.

Experimental studies on the interaction of core materials with sodium made it possible to formulate a new model of thermal interaction in corium/sodium system based on a stepwise process of successive fragmentation acts of individual corium particles [14].

2.2.2. R&D passive shutdown system for fast reactors

Realization of passive self-controlled shutdown system requires design of subassemblies, boron rod bars and in-vessel structures, which would change their configuration and position, in case of failure of shutdown and heat removal systems resulting in temperature increase, in such a way that the negative reactivity is formed in reactor core ensuring power decrease down to the value sufficiently low to be removed by the natural coolant flow.

From the standpoint of feedback nature the main well known devices can be categorized as those operating on the fuel temperature excess, loss of coolant flow rate or increase of coolant temperature. Development and substantiation of improved passive safety systems (PSS) are carried out in several ways with the use of various technologies: hydrodynamically weighed rod, "magnetic" suspension, "melting", "shape memory" or lyophobic capillary-porous system [15-17].

Self-protection of fast reactor can be successfully achieved by the development of passive (self-adjustable) shutdown system of BN-800 reactor using boron rods hydraulically weighed by sodium flow above the core. Weighting material is removed from shutdown rod, and orifice is installed in the working link. With the flow rate over $0.6Q_{NOM}$ the absorber rod is maintained above the reactor core by a coolant flow. If the flow rate decreases below $0.6Q_{NOM}$, then the rod goes down into the core by gravity and the reactor is shut down. Calculations have shown that the insertion of one safety rod 4 seconds after the main pump failure restricts during ~7 seconds coolant temperature at the reactor core outlet by 700ºC value (with 920ºC boiling temperature).

Advantages of this PSS-G design are as follows: simplicity of principle; wide experience of development of similar hydraulic systems; low time lag of momentum transfer: practically no lag between the time point of achievement of given flow rate and the moment of action of this factor on the absorber rod, thus assuring relatively short time (~ 6 s.) of the absorber rod movement from the upper to the lower position; and the possibility of direct simulation of reactor accident with the purpose of functional check of the device.

The most significant drawbacks of this device are as follows: malfunctioning under BDBA conditions (such as UTOP and ULOHS) if the rated coolant flow rate is maintained in the reactor; unfeasible operation with low flow rates (for instance, if the flow rate is lower $0.67G_{NOM}$ with three heat removal loops); and necessity to control rod position.

Devices operating on the basis of phase transition (melting, sublimation and movement) of nuclear fuel would allow to most effectively ensure fulfillment of safety function. However by now such devices have been purely developed technologically. Rather long and expensive stage of improvement should come before their adaptation. PSS operated on the excess of coolant temperature (PSS-T) are most widely used. These PSS are placed at the reactor core outlet, their sensitive element being bounded by coolant. If max permissible coolant temperature is exceeded, then the element operates causing insertion of the absorber rod to the core and making core subcritical.

The lyophobic capillary-porous system (LCPS) used in the PSS-T consists of a capillary-porous matrix and lyophobic liquid (i.e. non-wetting) matrix. Pressure compensation (stabilization) occurs because of change of LCPS volume with reversible filling/draining of matrix pores by the liquid [4]. The processes in fusible safety devices using lyophobic effect, in contrast to processes in conventional fusible elements, have a series of typical features caused by their nature: stored energy, generation of efforts, and hyper dilatometry with melting.

When simulating conditions of the hottest fuel subassembly in control rod channel, PSS-T operates 9 to 12 seconds (depending on various effects) after the BDBA start. Coolant temperature at the outlet of the hottest fuel subassembly thus makes ~800-850ºC, therefore, significant underheating (about 100ºC) to max permissible temperature (930ºC) and to sodium boiling temperature (960ºC) is assured, i.e. there is practically double time reserve before reaching these temperatures.

3.   R&D for justification of high-temperature fast reactors with the sodium coolant

The executed researches have shown that creation of high-temperature fast reactors with the sodium coolant (BN-VT) is a real technological problem [18, 19]. Reactors of this type have a many potential possibilities. The fast neutron spectrum allows to carry out reproduction of fission materials, to burn out and salvage a considerable part of transuranium elements, and the high temperature gives possibility to develop manufacture of considerable quantities of hydrogen on the basis of one of thermal chemical cycles or a high-temperature electrolysis with high factor of thermal use and the electric power with high efficiency. Relative small overall dimensions, coolant type, sampling of fission substance and structural materials allow to create a reactor with internal properties inherent in it (exclusion runaway of reactor on instantaneous neutron, passive removal of the residual heat release), providing the raised nuclear and radiation safety which is conform the requirements for the future reactors of IV generation.

For design justification is necessary to carry out a numerical and experimental researches of thermal hydraulic characteristics of a reactor core under various conditions, including emergency, to study of working capacity of decay heat removal system of reactor on the basis of thermal pipes, experimental researches of physical and chemical processes in the sodium contours in a temperature range up to 1000ºC, to estimates a mass transfer of corrosion products and tritium, to working out of the advanced concept of the monitoring system of physical and chemical parameters of coolant for NNP with temperatures level in the first contour up to 800-1000ºC.

Preliminary results of working out of complex systems for purification and control of sodium in high-temperature fast reactor with the sodium coolant are obtained. The basic apparatus of purification system is cold traps (CT), providing purification from oxygen, hydrogen and tritium. It is necessary to include in purification system the hot traps, sorbents for purification from caesium and filters. Possibility and reasonability of combination of CT and traps for purification from ^{137}Cs is shown.

For the control of impurity in sodium the electrochemical meshes and pith indicators (oxygen, hydrogen), devices with diffusion membranes (hydrogen, tritium, carbon) can be used.

Purification systems and systems for impurity control should place in the special blocks providing a necessary temperature condition of coolant and its flow rate. Implementation of a highly effective built-in reactor vessel purification system demands special R&D.

Decay Heat Removal Systems (DHRS) of fast reactor can be traditionally built with using of free convection (FC) and on a basis of evaporator-condenser systems (EC) [20]. In case of FC the heat transfer is carried out by sodium natural circulation in a gravitational field. Its deficiencies are the big height of the air heat exchanger (AHE) above reactor, great volume of sodium, constant dump of heat (for readiness maintenance), necessity of the trigger mechanism for an air damper, the big time lag.

In case of EC which use for BN-VT is preferable, heat transfer is carried out in the form of a latent heat of evaporation as a result of evaporation and condensation processes under gravitational field. Its advantages are small height of system, small volume of operating fluid, passivity of start and work (the principle of gas regulated thermal pipe is used), constant readiness practically without heat dump, small time lag.

Updated high-temperature test facility "VTS" with the sodium coolant, intended for researches on thermal hydraulic processes, physical chemistry and technology of high-temperature sodium coolant with reference to working out BN-VT for creation of atomic-hydrogen power engineering is prepared for experimental researches.

4. Thermal hydraulic researches for justification of fast reactors with heavy liquid metal coolant

Thermal hydraulic researches with heavy liquid metal coolant for justification of fast reactor designs consist of:
−   experimental researches of heat exchange and temperature fields in the experimental model which simulation of fuel rods assemblies of central and the peripheral areas of a reactor core;
−   computation and experimental thermal hydraulic researches of twisted steam generation of BREST-OD-300;
−   researches of influence of impurity on heat exchange in liquid lead;
−   numerical modeling of the space three-dimensional non-stationary hydrodynamics, heat and mass transfer processes and processes of formations, removing and sedimentation of impurity in contours with mono phase lead coolant on the basis of code MASKA-LM.

For the first time at test facility "SPRUT" the model of twisted steam generation BREST-OD-300 warmed with lead are conducted: lead temperature on model input – 540ºC, water temperature on model input – 340ºC, a water flow rate – 100%, 80% and 120% from rating value [21].

At test facility work on subcritical pressure (about 18 MPa) steam temperature on outlet from model was (503-509)ºC in all range of flow rate change. At water flow rate (80-120)% from nominal the pulsations of water flow rate on model input are not observed though by calculations for Test facility "SPRUT" on input there should be oscillations of a water flow rate with magnitude from 50 to 150%.

At the supercritical pressure of water (about 25 MPa) tests were conducted at the same operating conditions, as at 18 MPa. Appreciable differences in steam temperature on output from model are not observed, the difference did not exceed (2-3)ºC. Water flow rate pulsations have not been observed (fig. 6).
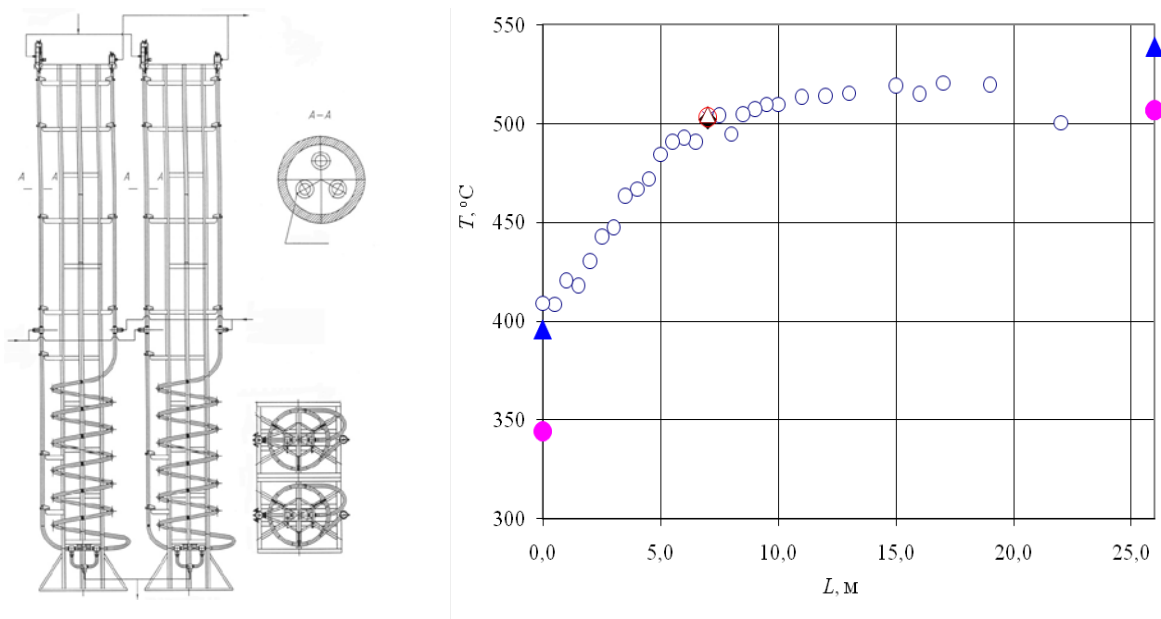

Fig. 6. Experimental model of the steam generator (a) and temperature distribution of an adiabatic wall on model length of the steam generator (b):

▲ – *inlet and outlet temperature of lead;* ● – *inlet and outlet temperature of water (steam);*
○ – *vessel temperature*

Conclusion

Design approaches ensuring the real safety of particular nuclear power plant are governed by its design, characteristics and appropriate knowledge based on accidents. Results of earlier and current studies on the accident processes and development of safety systems would provide the basis for creation and substantiation of defence in depth for reactors of the new generation with a system of barriers and passive systems preventing propagation of accident and bringing reactor facility to the low power potential state.

References

[1]   MATVEEV, V.I., KHOMIAKOV, YU.S., Technical physics of fast reactors with the sodium coolant, Manual under the editorship of corresponding member of the Russian Academy of Sciences V.I. Rachkov, Publishing house MEI, Moscow (2012) (in Russian)

[2]   KUZNETSOV, I.A., POPLAVSKY V.M., Fast reactors safety, Publishing house MEI, Moscow (2012) (in Russian)

[3]   VASILIEV, B.A., Estimation of design solutions efficiency for fast sodium reactors and their development in new designs, Proceedings of reports of the Seventh international scientific and technical conference "Safety, efficiency and atomic engineering economy (MNTK-2010)", VNIIAES, Moscow (2010) (in Russian)

[4]   EFANOV, A.D., KALYAKIN, S.G., SOROKIN, A.P., Thermophysical investigations in a substantiation of designs and safety of nuclear reactors for new generation, Atomnaya Energiya, Moscow (2012), Vol. 112, No. 1, P. 12-18, (in Russian)

[5]   SOROKIN, A.P., EFANOV, A.D., ZARYUGIN, D.G., KALYAKIN, S.G., KAMAYEV, A.A., KIRILOV, P.L., KOZLOV, F.A., ORLOV, Yu.I., TRUFANOV, A.A., CHERNONOG, V.L., Main directions and results of thermophysical researches for new generation NNP. A condition and prospects of works on modernization of experimental base on thermophysics and materials technology in SSC RF-IPPE, Proceedings of scientific and technical conference "Teplofizika-2012" SSC RF-IPPE, Obninsk, (2012), P. 10-12.

[6]   OPANASENKO, A.N, SOROKIN, A.P., ZARYUGIN, D.G. and RACHKOV, M.V., Stratification of coolant in the nuclear power plants, Atomnaya Energiya, Moscow (2011), Vol. 111, No. 3, P. 131-136 (in Russian)

[7]   POPLAVSKY, V.M., EFANOV, A.D., KOZLOV, F.A., ORLOV, Yu.I., SOROKIN, A.P. (IPPE), KOROLKOV, A.S., SHTYNDA, YU.YE. (RIAR), Liquid metal coolants technology for fast reactors, Report on the International Conference on Fast Reactors and Related Fuel Cycles: Challenges and Opportunities (FR09), Kyoto, Japan, December 7-9, 2009, KN-02, 16 p.

[8]   EFANOV, A.D., KOZLOV, F.A., VOLCHKOV, L.G., ALEXEEV, V.V. and SOROKIN, A.P., Issues of creation of primary sodium purification system with cold traps incorporated in the reactor vessel (built-in purification system), Proceedings of Exposition of Innovative Solutions on Implementation of NPP-2006 and New Technological Platform Projects, Rosatom,, Atom-Innovation Center, FSUE TSNIIatominform, Moscow (2007), P. 71–73 (in Russian)

[9]   KUMAEV, V.JA, ALEXEEV, V.V., KOZLOV, F.A., Numerical modelling of impurity mass transfer in cold traps for perspective BN reactors, Scientific and technical proceedings under the editorship of A.D. Efanov, S.G. Kalyakin, A.P. Sorokin, SSC RF-IPPE, Obninsk (2011). P. 101-107 (in Russian)

[10]   SCHERBAKOV, S.I. Numerical research of features of thermohydraulic regime and adjournment of impurity in cold trap of BN-1200, Scientific and technical proceedings under the editorship of A.D. Efanov, S.G. Kalyakin, A.P. Sorokin, SSC RF-IPPE, Obninsk (2011). P. 108-116 (in Russian)

[11]   ALEXEEV, V.V., ARNOLDOV, M.N., BERENSKY, L.L., VOLOV, A.N., DROBYSHEV, A.V., KOVALYOV, YU.P., KOPINA, E.A., MOROZOV, V.A. AND SOROKIN, A.P., Some issues of assurance of operation safety of safety system test facility SAZ, Proceedings of the Interdepartmental Seminar on Technology of Liquid Metal Coolants (Thermophysics-2009), SSC RF-IPPE, Obninsk, 11-13 November 2009, P. 179-189 (in Russian)

[12]   SOROKIN, A.P. Thermal-hydraulic Researches of Safety Problems in Fast Breeder Reactors, Proceedings of The 8th International Topical Meeting on Nuclear Thermal-Hydraulics, Operation and Safety (NUTHOS-8), Shanghai, China, October 10-14 (2010), N8P0154.

[13]   KHAFIZOV, R.R, IVANOV, EU.F., PRIVEZENTSEV, V.V., SOROKIN, A.P., VOLKOV, A.V., Experimental researches in a substantiation of fast reactors safety in accidents with the sodium

coolant boiling, Proceedings of scientific and technical conference "Teplofizika-2012" SSC RF-IPPE, Obninsk, (2012), P. 29-30 (in Russian)

[14] ZAGORUL'KO, YU.I., ZHMURIN, V.G., GANICHEV, N.S., KASCHEYEV, M.V., Experimental modeling of heavy accident development at loss of sodium flow rate on test facility "PLUTON", Scientific and technical proceedings under the editorship of A.D. Efanov, S.G. Kalyakin, A.P. Sorokin, SSC RF-IPPE, Obninsk (2011). P. 232-241 (in Russian)

[15] VOZNESENSKY, R.M., VYUNNIKOV, N.V., KORNILOV, V.P., MALTSEV, V.G., PORTYANOY, A.G., SOROKIN, A.P., The Development of Passive Safety Equipment of Fast Reactor Emergency Protection, Proceedings of International Conference "50 years of Nuclear Power – Prospects for 50 years", SSC RF-IPPE, Obninsk (2004) (in Russian)

[16] SERDUN, E.N., SOROKIN, A.P., PORTYANOY, A.G. et. al., Development and studying of passive accident protection devices for management of beyond the design-basis accident on the basis of hydro-capillary systems, Questions of a nuclear science and engineering, Series: Physics of nuclear reactors, RSC Kurchatov's Institute, Moscow (2000), No. 3, P. 6-13 (in Russian)

[17] BAGDASAROV, Yu.E., KAMAYEV, A.A., Device of passive safety of fast reactors, Atomnaya Energia. Moscow (2012), Vol. 112, No. 1, P. 32-36 (in Russian)

[18] POPLAVSKY, V.M., ZABUDKO, A.N., PETROV, E.Eu., et. al., High-temperature fast sodium reactor as a source of heat high potential for hydrogen manufacture, Proceedings of abstracts of the International Forum "Hydrogen technologies for hydrogen manufacture", President hotel, Moscow (2006), P. 235 (in Russian)

[19] KALYAKIN, S.G., KOZLOV, F.A., SOROKIN, A.P., State and investigation problems on technology of high-temperature sodium coolant Proceedings of the International meeting "High-temperature projects", Indira Gandhi Research centre on fast reactors, Kalpakkam, India (2011)

[20] LOGINOV, N.I., MIKHEEV, A.S. About the concept of evaporator-condenser systems of decay heat removal for fast sodium reactors, // Proceedings of conference "Hydrodynamics and safety of NNP (Thermophysics-1999)", SSC RF-IPPE, Obninsk, (1999), P. 220 (in Russian)

[21] GRABEZHNAYA, V.A, MIKHEEV, A.S., SHTEIN, YU.YU., SEMCHENKOV, A.A., Test of three-tube model of a steam and gas generator for BREST, Proceedings scientific and technical conference "Teplofizika-2012" SSC RF-IPPE, Obninsk, (2012), P. 25-26 (in Russian)